



HAL
open science

Spécificités de la réponse humorale chez le patient transplanté : impact sur la stratégie vaccinale et la survie des greffons

Xavier Charmetant

► To cite this version:

Xavier Charmetant. Spécificités de la réponse humorale chez le patient transplanté : impact sur la stratégie vaccinale et la survie des greffons. Immunologie. Université Claude Bernard Lyon 1, 2022. Français. NNT : 2022LYO1155 . tel-04947299

HAL Id: tel-04947299

<https://hal.science/tel-04947299v1>

Submitted on 14 Feb 2025

HAL is a multi-disciplinary open access archive for the deposit and dissemination of scientific research documents, whether they are published or not. The documents may come from teaching and research institutions in France or abroad, or from public or private research centers.

L'archive ouverte pluridisciplinaire **HAL**, est destinée au dépôt et à la diffusion de documents scientifiques de niveau recherche, publiés ou non, émanant des établissements d'enseignement et de recherche français ou étrangers, des laboratoires publics ou privés.



N°d'ordre NNT : 2022LYO1155

THESE de DOCTORAT DE L'UNIVERSITE DE LYON

opérée au sein de
l'Université Claude Bernard Lyon 1

Ecole Doctorale N° 340
Biologie Moléculaire, Intégrative et Cellulaire

Spécialité de doctorat : Sciences
Discipline : Immunologie

Soutenue publiquement le 20/12/2022, par :
Xavier CHARMETANT

**Spécificités de la réponse humorale
chez le patient transplanté :
impact sur la stratégie vaccinale et la
survie des greffons**

Devant le jury composé de :

Pr Fabienne VENET, PU-PH, Université Claude Bernard Lyon 1
Pr Sophie CANDON, PU-PH, Université Rouen Normandie
Dr Sébastien STORCK, MCU, Université Paris Cité
Pr Olivier THAUNAT, PU-PH, Université Claude Bernard Lyon 1

Présidente
Rapporteuse
Rapporteur
Directeur de thèse

RESUME

La réponse humorale thymo-dépendante est le mécanisme de la réponse immunitaire adaptative qui aboutit à la génération d'anticorps contre les antigènes protéiques, et permet ainsi la défense de l'hôte contre des pathogènes. Elle implique la coopération des lymphocytes T CD4⁺ et des lymphocytes B. Chez les patients transplantés, la réponse humorale dirigée contre les allo-antigènes peut aussi conduire au développement d'anticorps spécifiques du donneur (DSA), responsables du rejet humoral, qui est la première cause de perte des greffons. Les patients transplantés reçoivent donc des traitements immunosuppresseurs pour limiter cette réponse.

Dans la première partie de ce travail, nous avons conduit une étude de vaccinologie contre le SARS-CoV-2. Grâce à l'analyse détaillée des réponses immunitaires d'une cohorte de transplantés rénaux, nous avons démontré que la réponse humorale est au cœur de la protection vaccinale de ces patients. En effet, les anticorps neutralisants dérivés de la réaction de centre germinatif sont associés à la protection contre les infections symptomatiques. Cependant, cette réponse est fortement inhibée par l'immunosuppression. Elle peut être améliorée par des doses supplémentaires de vaccin.

Puisque les immunosuppresseurs inhibent la réaction de centre germinatif, il est nécessaire de comprendre pourquoi les patients continuent malgré tout de générer des DSA. Dans la deuxième partie de ce travail, nous avons donc exploré s'il existait des voies non conventionnelles de production des DSA chez les patients transplantés. Dans un premier travail translationnel, nous avons exploré si les lymphocytes T $\gamma\delta$ pouvaient aider les lymphocytes B lors d'une réponse humorale allo-immune. A partir de l'étude d'une cohorte de transplantés rénaux bien phénotypés, en passant par des expériences in vitro, jusqu'à l'étude d'un modèle murin de transplantation cardiaque, nous avons démontré que les lymphocytes T $\gamma\delta$ n'étaient pas impliqués dans la génération des DSA après transplantation. Enfin, dans un autre travail

translationalnel, nous avons mis en évidence dans un modèle murin une voie d'allorecognition inédite, qui aboutit à la production de DSA précoces. Cette voie, baptisée « directe inversée », implique la reconnaissance, par les lymphocytes T CD4⁺ du donneur dérivés du greffon, des molécules du complexe majeur d'histocompatibilité exprimées par les lymphocytes B alloréactifs du receveur. L'étude de cohortes de patients transplantés rénaux, pulmonaires et intestinaux a permis de montrer que cette voie existe aussi en clinique. Les greffons contiennent effectivement des lymphocytes T CD4⁺ au moment de la transplantation, et particulièrement les poumons et les intestins qui possèdent un tissu lymphoïde associé aux muqueuses. Dans le cas de ces greffons, la détection transitoire des lymphocytes T du donneur dans la circulation du receveur est associée à des DSA et des rejets précoces.

Ce travail explore différents aspects de la réponse humorale des patients transplantés, qui est mise en tension entre la réponse vaccinale bénéfique, souhaitée mais déficiente, et la réponse allo-immune, insuffisamment contrôlée et délétère. De nouvelles stratégies doivent être développées pour améliorer cette balance bénéfice-risque chez les patients transplantés.

Mots-clés : transplantation, réponse humorale, anticorps, immunosuppression, SARS-CoV-2, lymphocytes T CD4⁺, lymphocytes T $\gamma\delta$, rejet.

ABSTRACT

Specificities of the humoral response in transplant patients: impact on vaccination strategy and graft survival

The thymo-dependent humoral response is the mechanism of the adaptive immune response that leads to the generation of antibodies against protein antigens, and thus allows host defense against pathogens. It involves the cooperation of CD4⁺ T cells and B cells. In transplant patients, the humoral response directed against alloantigens can also lead to the development of donor-specific antibodies (DSA), responsible for humoral rejection, which is the primary cause of graft loss. Transplanted patients therefore receive immunosuppressive drugs to limit this response.

In the first part of this work, we conducted a vaccinology study against SARS-CoV-2. Through a comprehensive analysis of the immune responses of a cohort of kidney transplant recipients, we demonstrated that the humoral response is at the heart of the vaccine protection of these patients. Indeed, germinal center-derived neutralizing antibodies are associated with protection against symptomatic infections. However, this response is strongly inhibited by immunosuppression. It can be enhanced by additional doses of vaccine.

Since immunosuppressive drugs inhibit the germinal center response, it is necessary to understand why patients continue to generate DSA. In the second part of this work, we therefore explored whether there are unconventional pathways of DSA production in transplant patients. In a first translational work, we explored whether $\gamma\delta$ T cells could assist B cells during an alloimmune response. From the study of a cohort of well-phenotyped kidney transplant recipients, through in vitro experiments, to the study of a murine model of heart transplantation, we demonstrated that $\gamma\delta$ T cells were not involved in DSA production after transplantation. Finally, in another translational work, we highlighted in a mouse model a novel allorecognition

pathway, which leads to the production of early DSA. This so-called “inverted-direct” pathway involves the recognition of major histocompatibility complex molecules expressed by recipient’s alloreactive B cells by the graft-derived donor CD4⁺ T cells. Studies of cohorts of kidney, lung, and intestine transplant recipients have shown that this pathway also exists in transplant patients. The grafts do contain CD4⁺ T cells at the time of transplantation, particularly the lungs and intestines which have mucosa-associated lymphoid tissue. In these grafts, transient detection of donor T cells in the recipient's circulation is associated with early DSA and rejection.

This work explores different aspects of the humoral response of transplanted patients, which is in tension between the beneficial vaccine response, desired but deficient, and the allo-immune response, insufficiently controlled and deleterious. New strategies must be developed to improve this benefit-risk balance in transplant patients.

Keywords : transplantation, humoral response, antibody, immunosuppression, SARS-CoV-2, CD4⁺ T cells, $\gamma\delta$ T cells, rejection.

Intitulé du laboratoire :

Centre International de Recherche en Infectiologie (CIRI)

INSERM U1111 – CNRS UMR5308 – Equipe “Normal and pathogenic B cell responses”

21 avenue Tony Garnier

69365 Lyon cedex 07

France

REMERCIEMENTS

Au Pr Olivier Thauvat,

Je vous remercie pour votre encadrement et votre confiance tout au long de ces quatre années passées au laboratoire. Vous m'avez offert la possibilité de travailler sur des sujets aussi variés que passionnants. Votre exigence et votre enthousiasme ont été des moteurs pour toujours progresser. Je me réjouis de continuer à travailler avec vous. Veuillez trouver dans cette thèse l'expression de ma reconnaissance.

Au Pr Emmanuel Morelon,

Je vous remercie de m'avoir donné la possibilité de réaliser cette thèse de sciences au milieu de ma formation clinique. Il m'a été précieux de pouvoir compter sur chacun de vos engagements envers moi. Apprendre la transplantation rénale à vos côtés en tant qu'interne a été une chance ; j'espère continuer à progresser dans votre service dans les années qui viennent. Soyez assuré de mon profond respect.

Aux Dr Thierry Defrance et Helena Paidassi,

Merci Thierry de m'avoir accueilli dans ton équipe. Merci à chacun de vous pour les discussions scientifiques que nous avons pu avoir, qui m'ont permis de sortir un peu du cadre de la transplantation et d'aiguiser ma curiosité sur d'autres thématiques, et toutes celles, non scientifiques, qui rendent agréable le travail au laboratoire !

Au Pr Sophie Candon, au Pr Fabienne Venet et au Dr Sébastien Storck, les membres du jury,

Je suis très honoré que vous ayez accepté de faire partie de ce jury. Je vous remercie du temps que vous avez consacré à juger ce travail de thèse. Soyez assurés de ma reconnaissance et de mon profond respect.

Au Pr Julien Zuber et Dr Antoine Marçais, les membres de mon comité de suivi de thèse,

Je vous remercie pour le temps que vous m'avez consacré, pour vos conseils et vos encouragements au cours de cette thèse.

A toutes les personnes qui, de près ou de loin, ont collaboré à la réalisation de ce travail.

A tous les collègues et amis du laboratoire, ceux qui m'ont formé et ceux avec qui j'ai travaillé au long de ces quatre années : Alice, Thomas et Sébastien, vos exemples ont été encourageants ! Katia, Maxime et Sarah, mes co-thésards, merci pour votre soutien au quotidien. Merci Maxime pour tous ces projets menés ensemble, parmi lesquels je compte l'arête des Papillons ! Virginie, Loïc, Véronique (les 2, bien sûr), Floriane, Adrien, Luc, Alan, Carole, Camille, Cyrille, Eline, Morgane, Delphine, et tous les autres ... je reviendrai !

A toute l'équipe du service de Transplantation rénale de l'hôpital Edouard Herriot, et à mes collègues et amis médecins, je suis heureux de vous rejoindre, et de remettre de la clinique dans ma pratique !

A tous mes amis, merci pour votre fidélité et votre soutien au fil des années. Merci pour tout ce que nous partageons, dans les bons moments et les moments plus difficiles.

A mes frères et sœurs, merci pour votre affection et votre soutien infaillibles. Je crois que cette fois-ci, le petit dernier a fini ses études ...

A mes parents, pour tout ce que vous m'avez donné et transmis. Vous m'avez toujours soutenu, de votre affection, de vos conseils. Vous nous avez aidés, Sybille et moi, dans les moments difficiles de cette thèse, et vous vous êtes réjouis avec nous de chacun des accomplissements. Merci.

A ma chère Sybille. Ces quatre années de thèse n'ont pas été de tout repos pour toi ! Et pourtant tu as tenu bon. J'espère que cette nouvelle étape fera naître d'autres rêves et d'autres projets pour notre belle famille qui te doit tant. Je suis heureux d'avancer sur ce chemin avec toi. Merci pour tout !

A mes trois petites blondinettes. L'une après l'autre, vous êtes venues embellir ces dernières années. Avec vous, la déconnexion du boulot est assurée ! Je suis fier de vous, et mes capacités d'émerveillement sont restées intactes ...

TABLE DES MATIERES

<i>Résumé</i>	2
<i>Remerciements</i>	7
<i>Table des matieres</i>	8
<i>Table des illustrations</i>	10
<i>Abréviations</i>	11
<i>Préambule</i>	13
I. INTRODUCTION	14
1. Topographie, déterminants et étapes de la réponse humorale normale	15
1.1. Une architecture lymphoïde structurée pour une réponse efficace	15
1.2. Rencontre entre l'antigène et la cellule adaptative	16
1.3. Mise en place et entretien de la coopération T-B.....	23
1.4. Génération de la mémoire	27
1.5. Fonctions effectrices des anticorps	30
2. Spécificités de la réponse humorale chez le patient transplanté	31
2.1. Les allo-antigènes, spécificité de la transplantation.....	31
2.2. Drainage des allo-antigènes et lieux de production des allo-anticorps	34
2.3. Rôle de la réaction du centre germinatif en transplantation.....	35
2.4. Rôle effecteur des DSA	36
2.5. Voies métaboliques, voies de signalisation, et immunosuppression	37
II. OBJECTIFS	44
III. RESULTATS	46
Article 1 : Infection or a third dose of mRNA vaccine elicit neutralizing antibody responses against SARS-CoV-2 in kidney transplant recipients	47
Article 2 : $\gamma\delta$ T cells cannot replace or synergize with $\alpha\beta$ CD4+ T cells in the production of donor-specific antibodies after solid organ transplantation	68
Article 3 : Inverted direct allorecognition triggers early donor specific antibody responses after transplantation	114

IV. DISCUSSION ET PERSPECTIVES	150
1. Une nécessaire amélioration des stratégies vaccinales du sujet transplanté.....	151
1.1. Limites des stratégies actuelles	151
1.2. Des stratégies non spécifiques pour prévenir la mortalité	153
1.3. Des thérapies cellulaires spécifiques de l'antigène pour prévenir la maladie.....	155
1.4. Un avantage malgré tout pour les patients transplantés ?	158
2. Rôle de l'immunité innée lymphoïde au cours de la réponse allo-immune.....	161
2.1. Le contrôle de l'allorecognition directe inversée.....	161
2.2. Un rôle ambivalent des lymphocytes T $\gamma\delta$?	165
V. CONCLUSIONS.....	167
REFERENCES (articles exclus)	168
ANNEXES	182
1. Publication 1	183
2. Publication 2	199
3. Publication 3	212
4. Publication 4	222
5. Publication 5	232
6. Publication 6	246
7. Publication 7	260

TABLE DES ILLUSTRATIONS

Figure 1. Modalités d'entrée des antigènes au sein du follicule et modalités de reconnaissance des antigènes de grande taille par le lymphocyte B au sein des ganglions.....	20
Figure 2. Amorçage des réponses lymphocytaires T et B et mise en place de la synapse.....	24
Figure 3. Réponse humorale thymo-dépendante.....	29
Figure 4. Les voies de l'alloreconnaissance et leur restriction antigénique.....	33
Figure 5. Régulation de mTORC1 dans le lymphocyte B au cours de la réaction de centre germinatif.....	39
Figure 6. Représentation schématique et simplifiée du rôle de la calcineurine dans le lymphocyte T.....	41
Figure 7. Schéma du concept VAR-T cells.....	156
Figure 8. Evolution de la réponse humorale au temps mémoire.....	158
Figure 9. Schéma de la réponse vaccinale et hypothèse pouvant expliquer le maintien de la réponse dans le temps chez les patients transplantés.....	160
Figure 10. Impact de la perfusion des greffons sur la survenue de DSA de novo après transplantation pulmonaire.....	161
Figure 11. Contrôle de la voie d'alloreconnaissance directe inversée par les lymphocytes NK.....	163
Figure 12. Les lymphocytes T $\gamma\delta$ infiltrent les greffons rénaux au cours du rejet humoral.....	166

ABBREVIATIONS

ADCC	Antibody-dependent cellular cytotoxicity
AID	Activation-induced cytidine deaminase
Akt	Proteine kinase B
ARN	Acide ribonucléique
Ascl2	Achaete-scute homologue 2
Bach2	BTB Domain And CNC Homolog 2
BCL-6	B-cell lymphoma 6
BCR	B-cell receptor
CAR	Chimeric antigen receptor
CCL	C-C motif chemokine ligand
CCR	C-C chemokine motif receptor
CDC	Complement-dependent cytotoxicity
CMH	Complexe majeur d'histocompatibilité
CMV	Cytomégalovirus
COVID-19	COronoVirus Disease-2019
CPA	Cellule présentatrice d'antigène
CR	Récepteur du complément
CRAC	Calcium release-activated Ca ²⁺
CTLA	Cytotoxic T-lymphocyte-associated protein
CXCL	C-X-C chemokine motif ligand
CXCR	C-X-C chemokine receptor
DC-SIGN	Dendritic Cell-Specific Intercellular adhesion molecule-3-Grabbing Non-integrin
DN	Double négatif
DSA	Donor-specific antibody
EBI2	Epstein-Barr virus-induced gene 2
HEV	High endothelial veinule
HLA	Human leukocyte antigen

ICAM	Intercellular adhesion molecule
ICOS	Inducible T-cell costimulator
IL	Interleukine
IMPDH	Inosine-5'-monophosphate déshydrogénase
IQR	Intervalle inter-quartile
IRF4	Interferon regulatory factor 4
ITAM	Immunoreceptor tyrosin-based activation motif
KO	Knock-out
LAG3	Lymphocyte-activation gene 3
LAT	Linker of activated T cells
LFA-1	Lymphocyte function-associated antigen 1
MAC1	Macrophage-1 antigen
MMF	Mycophénolate mofétil
mTOR	Mechanistic target of rapamycin
NFAT	Nuclear factor of activated T cells
NK	Natural killer
PD-1	Programmed cell death-1
PI3K	phosphoinositide 3-kinase
RBD	Receptor-binding domain
SARS-CoV-2	Severe Acute Respiratory Syndrome CoronaVirus 2
SD	Standard deviation
SLAM	Signaling lymphocyte activation molecules
SLP-76	Lymphocyte cytosolic protein 2
STAT3	Signal transducer and activator of transcription 3
TCR	T-cell receptor
T _{FH}	T follicular helper
T _{FR}	T follicular regulator
TIM3	T cell immunoglobulin and mucin domain-containing protein 3
VAR	Vaccine antigen receptor
ZAP-70	Zeta-chain-associated protein kinase 70

PREAMBULE

La transplantation est le seul traitement curatif de la défaillance cardiaque, hépatique et pulmonaire terminale. Elle est aussi la meilleure option thérapeutique pour la prise en charge de l'insuffisance rénale terminale. En raison des différences génétiques qui existent entre le donneur et le receveur, les déterminants antigéniques spécifiques du donneur (allo-antigènes) vont pouvoir activer le système immunitaire du receveur pour conduire au rejet. Pour prévenir cela, les patients prennent quotidiennement des traitements immunosuppresseurs.

Le bras cellulaire de la réponse allo-immune est très efficacement contrôlé par les traitements immunosuppresseurs modernes, et par conséquent l'incidence des rejets cellulaires a nettement diminué au cours des dernières décennies. Au contraire, les patients continuent de développer des anticorps spécifiques du donneur, qui causent les rejets humoraux. Ces rejets humoraux sont considérés comme la première cause de perte des greffons. En conséquence, la survie à long terme des greffons reste limitée par le maintien du bras humoral de la réponse allo-immune sous immunosuppresseurs.

Puisque les immunosuppresseurs sont des traitements non spécifiques des allo-antigènes, ils agissent sur toutes les réponses immunitaires susceptibles d'être montées par le receveur de la greffe, en particulier contre les antigènes infectieux. Ainsi, les complications bactériennes ou virales sont fréquentes chez les patients transplantés. Il est probable que les deux bras de l'immunité adaptative, cellulaire et humoral, soient mis en défaut, avec une importance différente selon le pathogène considéré.

Dans ce travail, nous avons circonscrit notre sujet d'étude à la réponse humorale chez les patients transplantés, qui semble prise en étau entre deux impératifs antagonistes : être limitée pour protéger le greffon du rejet mais suffisante pour protéger le patient des infections.

I. INTRODUCTION

1. Topographie, déterminants et étapes de la réponse humorale normale

1.1. Une architecture lymphoïde structurée pour une réponse efficace

La réponse immunitaire adaptative a lieu au sein de structures spécialisées, les organes lymphoïdes secondaires (ganglions, rate et tissus lymphoïdes associés aux muqueuses). Un défaut structurel de ces derniers peut causer un défaut de réponse humorale, malgré la présence de cellules fonctionnelles (1). Leur architecture a pour but d'augmenter la probabilité de rencontre entre un clone lymphocytaire et son antigène. En leur sein, les cellules immunitaires sont très mobiles à la recherche de leur cible (2). Si la recherche est infructueuse, les cellules quittent le tissu lymphoïde (3) et rejoignent la circulation sanguine via le réseau lymphatique. Elles sont alors réadressées vers d'autres organes lymphoïdes pour poursuivre leur surveillance.

Les ganglions sont entourés d'une capsule, sous laquelle se trouvent le sinus sous-capsulaire puis le cortex. Le cortex contient les follicules et correspond à la zone B. Une couche de macrophages sous-capsulaires sépare le follicule du sinus sous-capsulaire. Le paracortex est adjacent aux follicules et constitue la zone des lymphocytes T. L'architecture des différentes zones est déterminée par des gradients de chimiokines (3). La zone B est composée de cellules folliculaires dendritiques et de lymphocytes B. Ces derniers sont attirés par la sécrétion folliculaire de *C-X-C chemokine motif ligand (CXCL)-13* (4), ligand de *C-X-C chemokine receptor (CXCR)-5* (5). Les lymphocytes T se positionnent dans le paracortex en réponse aux chimiokines *C-C motif chemokine ligand (CCL)-19* et *CCL21*, ligands de *C-C chemokine motif receptor (CCR)-7* (6). Le paracortex contient également des cellules dendritiques et les veinules à endothélium épais (*high endothelial veinules, HEV*). Ces vaisseaux sanguins gèrent les flux de lymphocytes au sein du ganglion. Ils sont reliés au sinus-sous capsulaire par un réseau de canaux, qui peuvent transporter des molécules de faible poids moléculaires (7). Au centre du ganglion se trouve la médulla, qui contient diverses cellules immunitaires (cellules

dendritiques, macrophages, lymphocytes B et T). L'objectif de cette organisation est un échantillonnage efficace des antigènes drainés depuis les tissus par le liquide lymphatique.

L'architecture de la rate est différente, avec une pulpe blanche et une pulpe rouge. La pulpe blanche est organisée de façon similaire aux ganglions avec des zones T et B. En outre, la rate contient une zone marginale, spécialisée dans la réponse aux antigènes thymo-indépendants drainés par le sang (8).

1.2. Rencontre entre l'antigène et la cellule adaptative

1.2.1. Activation du lymphocyte B

1.2.1.1. Nature de l'antigène, déterminant du type de réponse lymphocytaire B

Les antigènes naturels (par opposition aux antigènes artificiels et aux antigènes de synthèse) sont de trois types principaux : polysides, acides nucléiques et protéines.

Les polysides sont majoritairement des antigènes bactériens. Ils portent un grand nombre de motifs épitopiques identiques et répétitifs. Ils sont capables d'induire une réponse chez une souris athymique et sont donc appelés thymo-indépendants. Les acides nucléiques, quant à eux, sont principalement impliqués dans les maladies auto-immunes. Ils ont la particularité de pouvoir déclencher à la fois des réponses thymo-indépendantes et thymo-dépendantes [dépendantes des lymphocytes T dérivés du thymus ; (9,10)]. Enfin, les protéines constituent le troisième groupe des antigènes naturels. Elles entraînent des réponses thymo-dépendantes, qui vont être détaillées ci-après.

1.2.1.2. Antigènes protéiques solubles de petite taille

Les lymphocytes B peuvent acquérir directement des antigènes solubles dans les follicules (11). En effet, les antigènes solubles de petite taille peuvent diffuser librement vers le centre du follicule (Figure 1) ou y entrer par des pores dans le sinus sous-capsulaires (12). Ils peuvent également emprunter des canaux, qui naissent du sinus pour pénétrer les follicules, et activer les lymphocytes B qui se trouvent directement au contact de ces canaux (13).

1.2.1.3. Antigènes protéiques de grande taille

Pour qu'un lymphocyte B soit activé par un antigène de grande taille (antigène particulaire, complexe immun, virus), il faut que celui-ci lui soit présenté (Figure 1). Il ne s'agit pas d'une présentation, par une cellule professionnelle, d'un antigène apprêté au sein d'une molécule du complexe majeur d'histocompatibilité (CMH), mais bien de la présentation d'un antigène sous sa forme native. Trois types cellulaires supportent cette fonction.

La présentation peut être faite par les macrophages du sinus sous-capsulaire CD169⁺, localisés directement sous le sinus. Ils envoient des processus à travers celui-ci pour avoir accès au liquide lymphatique. Ils ont une activité phagocytaire limitée (14) pour prévenir la dégradation de l'antigène. En revanche, ils sont équipés de récepteurs membranaires, tels que des récepteurs du complément [*macrophage-1 antigen*, MAC1, récepteur de C3, (14)], le FcγRIIb (récepteur au fragment cristallisable des immunoglobulines de type IIb) ou le *Dendritic Cell-Specific Intercellular adhesion molecule-3-Grabbing Non-integrin* [DC-SIGN, récepteur aux antigènes glycosylés ; (15)]. Cet équipement permet la présentation de l'antigène sous sa forme native, soit après internalisation sans dégradation et recyclage à la membrane (16), soit en permettant la rétention de l'antigène à la surface de la cellule (14).

Les cellules dendritiques folliculaires sont spécialisées dans la rétention prolongée des complexes immuns et le soutien des centres germinatifs (17). Elles expriment les récepteurs du complément (CR) 1 (CD35) et CR2 (CD21), indispensables à la réaction de centre germinatif (18), ainsi que le Fc γ RIIb (19,20). Les antigènes sous forme de complexes immuns rejoignent le centre du follicule après un transit médié par les lymphocytes B de la zone marginale (21) ou par des lymphocytes B folliculaires (22,23), via des récepteurs membranaires non spécifiques de l'antigène (Figure 1).

Enfin, les cellules dendritiques du paracortex sont également capables de présenter les antigènes aux lymphocytes B. Elles expriment également Fc γ RIIb et DC-SIGN (16). Leur contribution aux réponses humorales n'est pas parfaitement claire, mais elles pourraient servir à activer les lymphocytes B en trafic entre les HEV et les follicules (24) ou à monter les réponses extrafolliculaires.

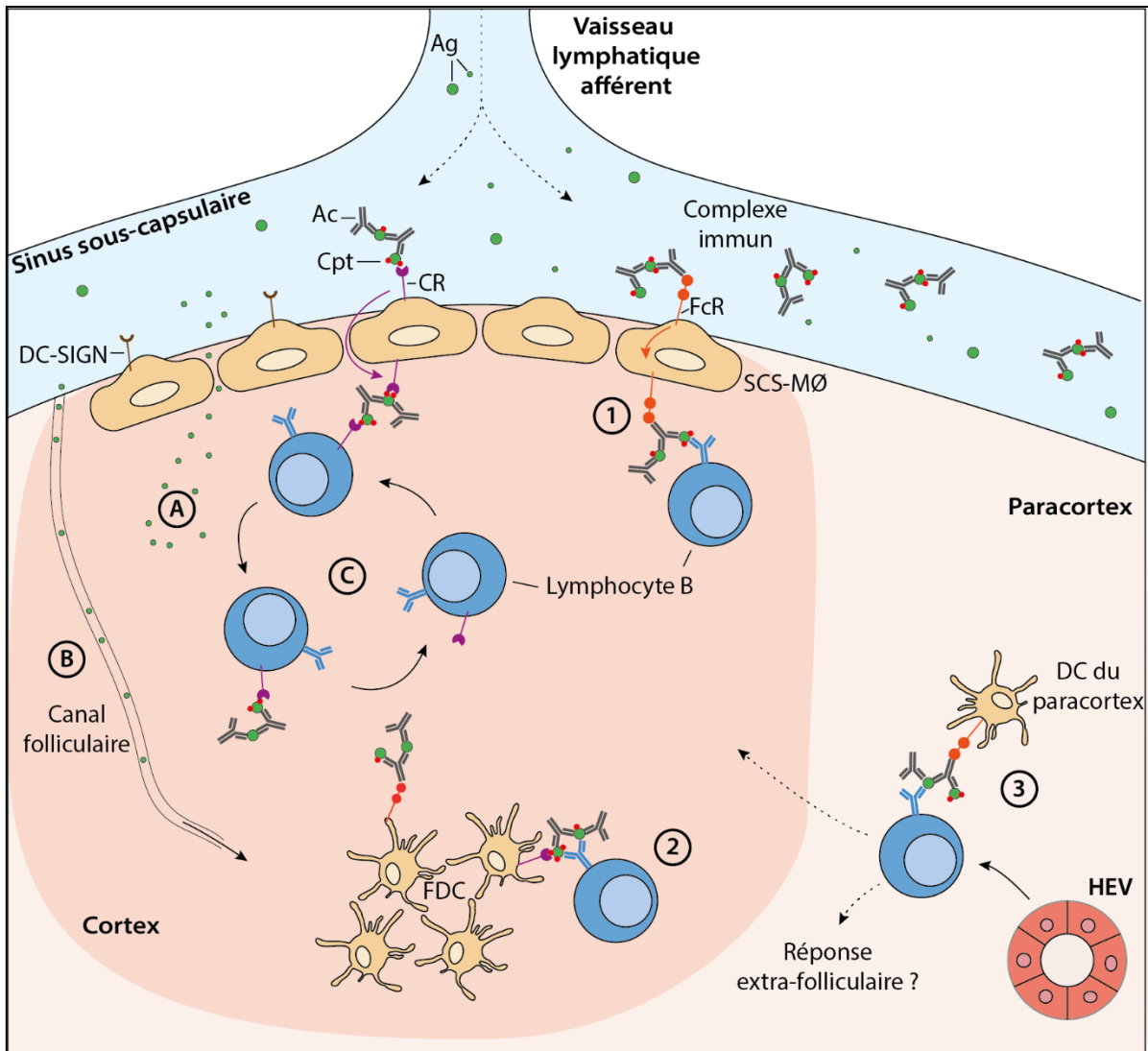


Figure 1. Modalités d'entrée des antigènes au sein du follicule et modalités de reconnaissance des antigènes de grande taille par le lymphocyte B au sein des ganglions

(A à C) Modalités d'entrée des antigènes dans le follicule. Les antigènes de petite taille peuvent diffuser librement au sein du follicule (A) ou être adressés aux lymphocytes B folliculaires par des canaux (B). Il existe aussi un transfert non spécifique des complexes immuns vers le centre du follicule (C).

(1 à 3) Le lymphocyte B peut reconnaître l'antigène au sein de complexes immuns à la surface des macrophages sous-capsulaires (1), des cellules dendritiques folliculaires (2), des cellules dendritiques du paracortex (3).

Abréviations : Ag, antigène ; Ac, anticorps ; Cpt, complément ; FcR : récepteur au fragment Fc des immunoglobulines ; CR, récepteur du complément ; SCS-MΦ, macrophage du sinus sous-capsulaire ; DC, cellule dendritique ; FDC, cellule dendritique folliculaire ; HEV, veinule à endothélium épais.

1.2.2. Capture de l'antigène par le lymphocyte B

La présentation de l'antigène va permettre au lymphocyte B de le reconnaître via son immunoglobuline de surface, et ainsi d'arrêter sa migration pour établir une synapse avec la cellule présentatrice (25,26). L'expression de la molécule d'adhésion *Lymphocyte function-associated antigen 1* (LFA-1) par le lymphocyte B, et son interaction avec son ligand *Intercellular adhesion molecule 1* (ICAM-1) permettent la stabilisation de la synapse et diminuent le seuil d'activation du lymphocyte B (27).

Les récepteurs des lymphocytes B (*B-cell receptor*, BCR) sont composés d'une immunoglobuline associée à des hétérodimères $Ig\alpha$ - $Ig\beta$ qui contiennent des domaines *Immunoreceptor tyrosin-based activation motif* (ITAM). L'agrégation du BCR par l'antigène entraîne la phosphorylation des ITAM par des kinases de la famille Src (Lyn), résultant en un recrutement et une activation de Syk, et en l'induction d'un flux calcique (28). La mise en place de cette signalisation intracellulaire entraîne des modifications du métabolisme cellulaire et du cytosquelette, et induit un programme transcriptionnel d'activation du lymphocyte B (29).

En particulier, ce dernier va dépolymériser le complexe d'actine pour étaler sa membrane autour de la zone initiale d'interaction cellulaire et lever la ségrégation des molécules de signalisation. Ceci augmente les contacts BCR/antigène et permet la formation de microclusters de signalisation (30). D'autres molécules cytosoliques et corécepteurs membranaires (comme CD19) sont recrutés (31). Ensuite, une phase de contraction se met en place pour accumuler l'antigène au centre de la synapse (30). Le lymphocyte B recrute alors, à la synapse, des lysosomes qui libèrent des protéases et permettent de récupérer l'antigène lié à la cellule présentatrice (32). L'extraction de l'antigène peut également se faire par un arrachage de la membrane de la cellule présentatrice (33). Ensuite, l'antigène est internalisé dans les compartiments endosomaux, où il va être dégradé afin d'être présenté au sein des molécules du CMH de classe II.

Quelques heures après la rencontre de l'antigène, le lymphocyte B va exprimer CCR7 et *Epstein-Barr virus-induced gene 2* (EBI2), qui lui permettent de migrer en bordure du follicule vers la zone T [Figure 2, (34,35)]. Un second signal d'activation, délivré par le lymphocyte T, et alors indispensable pour prévenir la mort cellulaire induite par l'activation (36).

1.2.3. Activation du lymphocyte T et induction du programme T_{FH}

Pour être pleinement capable d'aider le lymphocyte B, le lymphocyte T CD4⁺ doit enclencher un programme de différenciation en lymphocyte auxiliaire folliculaire (*T follicular helper*, T_{FH}), qui est un processus en plusieurs étapes (37,38). La première étape de son activation est la reconnaissance d'un complexe CMH-II/peptide par son récepteur de surface (*T-cell receptor*, TCR). Cette reconnaissance a principalement lieu dans la zone T, où le complexe CMH-II/peptide est présenté par une cellule dendritique, au cours d'une interaction stable et prolongée (39). Cependant, elle peut aussi avoir lieu directement à la bordure T-B, par les lymphocytes B activés (40).

Le TCR des lymphocytes T CD4⁺ est composé de deux chaînes α et β , responsables de la spécificité antigénique, associées aux molécules CD3. La reconnaissance du complexe CMH-II/peptide par le lymphocyte T entraîne une agrégation des TCR, des modifications conformationnelles et l'exclusion synaptique des molécules inhibitrices, qui permettent la transduction du signal (41). Les protéines tyrosine kinases Src sont activées et phosphorylent les molécules CD3 ζ au niveau de leurs domaines ITAM, qui recrutent et phosphorylent à leur tour la molécule *Zeta-chain-associated protein kinase 70* [ZAP-70, (41)]. ZAP-70 agit comme une plateforme d'activation de multiples voies de signalisation intracellulaires, via deux molécules adaptatrices, *Linker of activated T cells* (LAT) et *Lymphocyte cytosolic protein 2* (SLP-76) (42,43). L'activation de LAT, la seule que nous détaillerons, conduit à l'augmentation du calcium intracellulaire (initialement relargué depuis le réticulum endoplasmique, puis

importé dans la cellule via les canaux *Calcium release-activated Ca²⁺* [CRAC]), et à l'activation de la calcineurine, une protéine phosphatase dépendante du calcium. La calcineurine active la famille de facteurs de transcription *Nuclear factor of activated T cells* (NFAT) et induit leur translocation nucléaire. NFAT contrôle non seulement la transcription des gènes de l'interleukine (IL)-2 et du récepteur de l'IL-2 (44), mais aussi le programme métabolique qui supporte l'expansion clonale (45).

Comme pour les lymphocytes B, un second signal est nécessaire pour une activation complète du lymphocyte T CD4⁺. Ce signal est délivré par la cellule dendritique. Bien que de nombreux couples de costimulation existent, la stimulation du récepteur CD28 (à la surface du lymphocyte T) par ses ligands CD80 et CD86 (sur la cellule dendritique) est la plus efficace. Le signal CD28 est notamment transduit au sein du lymphocyte T par la voie PI3K/Akt/mTOR (*phosphoinositide 3-kinase/proteine kinase B/mechanistic target of rapamycin*). Il entraîne la prolifération et la survie cellulaires, la production de cytokines et la modification du programme métabolique, et agit également en amplifiant la voie de signalisation du TCR (46).

La décision d'engager spécifiquement le programme T_{FH} est prise au cours des premières divisions cellulaires (47), et implique plusieurs facteurs : le temps de contact TCR/CMH-peptide (48), des cytokines [qui diffèrent entre les espèces, (38)], et le signal CD28 qui est utile pour la différenciation T_{FH} (49). De plus, l'induction des facteurs de transcription *B-cell lymphoma 6* (Bcl-6) et *achaete-scute homologue 2* (Ascl2) est nécessaire (47,50) pour induire l'expression de CXCR5 et la répression de CCR7, et permettre au lymphocyte T de migrer vers la bordure T-B (51) et de poursuivre sa différenciation (Figure 2).

1.3. Mise en place et entretien de la coopération T-B

1.3.1. Etablissement d'une synapse T-B

La rencontre des lymphocytes T et B a lieu à la jonction entre les zones T et B (bordure T-B). Les lymphocytes B vont entrer en compétition pour avoir accès à l'aide des lymphocytes T (52,53). L'établissement d'une synapse T-B stable dépend principalement de trois types d'interaction (Figure 2). Des interactions homophiliques non spécifiques des récepteurs *Signaling lymphocyte activation molecules* (SLAM) se mettent d'abord en place (54,55). La quantité de complexes CMH-II/peptide à la surface des lymphocytes B et leur interaction avec les TCR, ainsi que l'expression d'intégrines (LFA-1 à la surface du T et ICAM-1/2 à la surface du B) permettent ensuite la stabilisation de la synapse (56).

1.3.2. Coopération T-B et orientation de la réponse

Les lymphocytes T délivrent trois signaux principaux aux lymphocytes B (Figure 2). Tout d'abord, la stimulation de CD40 par son ligand CD40L induit la prolifération et la survie du lymphocyte B (57) et le protège de l'apoptose médiée par Fas (58,59). Les lymphocytes T produisent également deux cytokines clés, l'IL-21 et l'IL-4, qui agissent en synergie pour soutenir la réponse B. L'IL-21 favorise la prolifération précoce des B, indépendamment de leur affinité pour l'antigène, et l'induction de Bcl-6, qui détermine le phénotype de B du centre germinatif (60–64). L'IL-4 induit l'expression de l'enzyme *activation-induced cytidine deaminase* [AID ; (65)], dont dépendent la commutation isotypique (changement de classe de l'immunoglobuline de surface) du lymphocyte B et l'hypermutation somatique [permettant la maturation d'affinité de l'immunoglobuline ; (66)].

Le lymphocyte B, quant à lui, délivre un signal *Inducible T-cell costimulator* (ICOS) au lymphocyte T (47) qui poursuit sa différenciation en T_{FH} (Figure 2). Enfin, la sécrétion autocrine et paracrine d'IL-21 par les lymphocytes T CD4⁺ favorise leur prolifération et leur différenciation en T_{FH} (60).

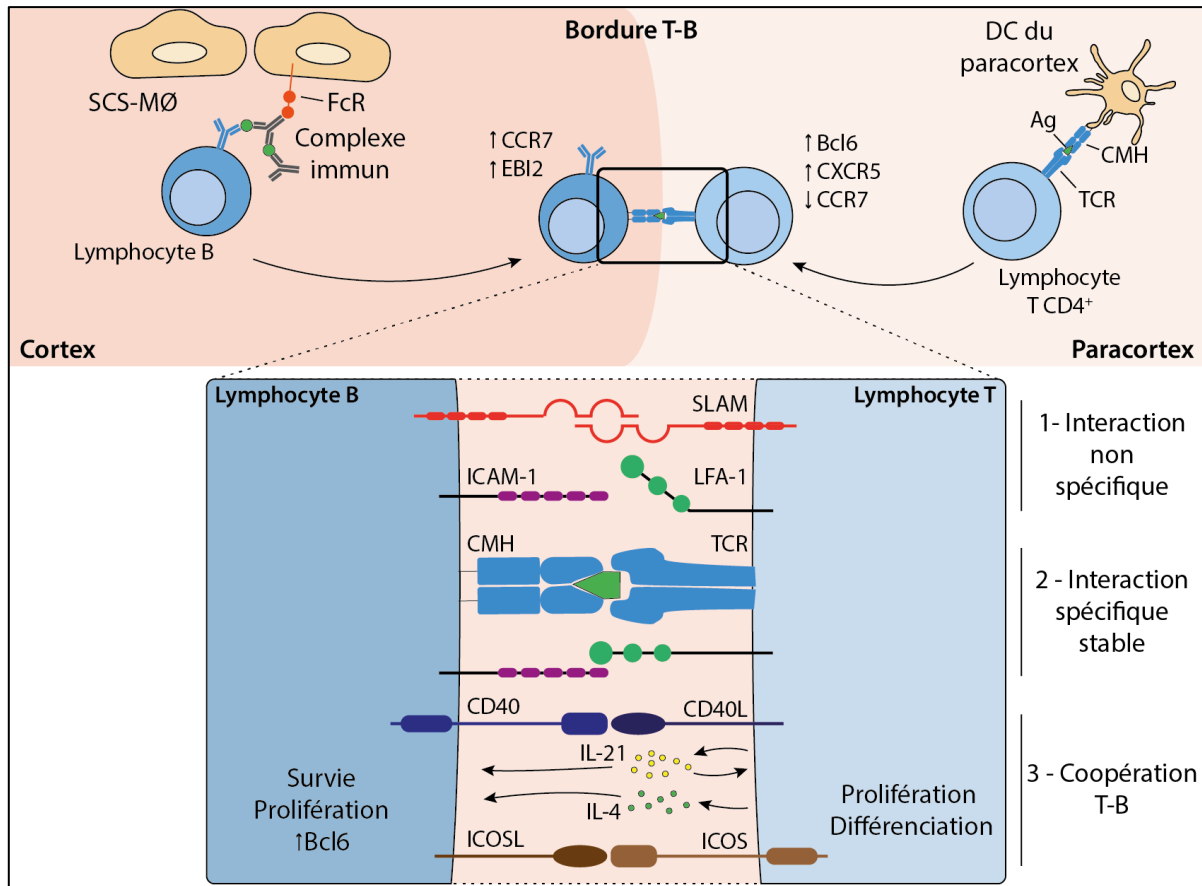


Figure 2. Amorçage des réponses lymphocytaires T et B et mise en place de la synapse

Le lymphocyte B, activé au sein du cortex, et le lymphocyte T, activé au sein du paracortex, migrent à la bordure T-B pour établir une synapse stable. Le contact initial est non spécifique, peu stable (1), puis stabilisé par les interactions spécifiques (2). Une synapse stable permet la coopération entre lymphocyte T et lymphocyte B (3).

Abréviations : Ag, antigène ; FcR : récepteur au fragment Fc des immunoglobulines ; SCS-Mφ, macrophage du sinus sous-capsulaire ; DC, cellule dendritique ; CMH, complexe majeur d'histocompatibilité ; TCR, récepteur des cellules T ; IL, interleukine.

Après sa première rencontre avec le lymphocyte T, le lymphocyte B peut suivre deux destins différents. La première possibilité est la migration vers la zone inter-folliculaire, où il va proliférer, se différencier en plasmablaste à courte durée de vie, et mettre en place une réponse primaire avec sécrétion d'anticorps de faible affinité [réponse extra-folliculaire ; (67,68)]. La deuxième possibilité est la migration concomitante des lymphocytes B et T activés vers le centre du follicule pour former un centre germinatif, qui sera la source des plasmocytes à longue durée de vie et de la majorité des lymphocytes B mémoires (Figure 3).

Les facteurs qui déterminent si la réaction se poursuivra en extra-folliculaire ou dans un centre germinatif ne sont pas parfaitement établis. Une des caractéristiques des réponses extra-folliculaires est la perte de l'architecture lymphoïde, possiblement causée par des signaux inflammatoires [suggéré par (69) ; soutenu par (70–72)], même s'il est probable que des signaux non inflammatoires (68,73), cytokiniques et de costimulation soient également impliqués.

Une fois la réponse résolue, il peut être intéressant de déterminer la voie qu'a empruntée un lymphocyte B. La commutation isotypique et les mutations somatiques ont longtemps été considérées comme spécifiques de la réaction du centre germinatif. Ainsi, lorsque les lymphocytes B présentaient, a posteriori, des arguments en faveur de ces phénomènes, il était admis qu'ils sortaient d'un centre germinatif. Cependant, des données récentes démontrent que la réaction extra-folliculaire peut donner lieu à une maturation d'affinité des immunoglobulines, dans les maladies auto-immunes (69) mais aussi en réponse à des pathogènes (68,74). De plus, la commutation isotypique est un événement précoce de la réaction thymo-dépendante, qui intervient le plus souvent avant que le lymphocyte B n'entre dans le centre germinatif (75), et concerne donc également les réponses extra-folliculaires. Ce dernier mécanisme est sous le contrôle conjoint d'ICOS et CD40L (76,77), mais aussi de l'environnement cytokinique [IL-4, TFG β ; (78,79)].

1.3.3. Réaction du centre germinatif

Après leur première collaboration à la bordure T-B, les lymphocytes B et T peuvent donc migrer conjointement dans le follicule pour former un centre germinatif. Le lymphocyte B entre alors dans un premier cycle de prolifération (zone sombre du centre germinatif). A l'issue de celui-ci, les clones expandus entrent dans la zone claire du centre germinatif pour y subir une sélection, sous le contrôle des lymphocytes T_{FH}. A ce stade, les lymphocytes B du centre germinatif expriment le récepteur de mort Fas (80), et ont perdu l'expression de la molécule anti-apoptotique Bcl-2 (81), réprimée par Bcl-6 (82). Le destin par défaut du lymphocyte B est donc la mort par apoptose. Pour poursuivre la réaction du centre germinatif, les clones vont entrer en compétition pour les signaux de survie (83).

Tout d'abord, les lymphocytes B vont capturer l'antigène présenté par les cellules dendritiques folliculaires. Plus le BCR est affin, plus le lymphocyte B internalise une grande quantité d'antigènes (84). Par conséquent, la quantité de complexes CMH-II/peptide qu'il présente ensuite en surface est le reflet direct de l'affinité du BCR. Puis, les différents clones vont entrer en compétition pour l'aide T_{FH}. Les clones peu affins expriment peu de complexes CMH-II/peptide, et sont incapables d'entrer en compétition pour l'aide T_{FH}. Ils ne reçoivent pas de signal de survie et entrent alors en apoptose (83). Au contraire, les clones les plus affins expriment une grande quantité de complexes CMH-II/peptide, et interagissent avec les T_{FH} (85). Ces derniers fournissent alors des cytokines [IL-4 et IL-21 ; (64,86)] et des signaux de costimulation [ICOS et CD40L ; (87)], qui contrebalancent les signaux pro-apoptotiques et permettent la survie des lymphocytes B du centre germinatif.

Au total, cette aide T_{FH} sélectionne les clones B les plus affins (88) pour un second cycle de prolifération dans la zone sombre. L'intensité de l'aide T_{FH} reçue détermine directement le nombre de divisions que vont subir les clones B sélectionnés (89). Dans la zone sombre, les lymphocytes B expriment AID (90) qui introduit, au gré des divisions, des mutations ponctuelles dans les gènes des chaînes variables des immunoglobulines, dans le but d'augmenter l'affinité de ces dernières pour l'antigène (66,91). Si les mutations compromettent la structure des immunoglobulines, les cellules entrent en apoptose avant de quitter la zone sombre (92) ; si, au contraire, les lymphocytes B conservent un BCR fonctionnel, ils entrent à nouveau dans la zone claire où ils subissent le contrôle par les T_{FH} . Au cours de cette réaction en boucle, les lymphocytes B peuvent être exportés pour former des lymphocytes B mémoires ou des plasmocytes à longue durée de vie.

1.4. Génération de la mémoire

1.4.1. Mémoire cellulaire

Certains travaux proposent que la réaction extrafolliculaire produise des lymphocytes B mémoires d'un phénotype particulier (DN2, double négatifs de type 2, à savoir $IgD^+CD27^-CD11c^+CD21^-$). Ces données reposent sur l'étude, chez l'humain, de maladies auto-immunes et d'infections sévères (72,93).

Au cours de la réaction du centre germinatif, les lymphocytes B mémoires sont exportés précocement (94), préférentiellement à partir de clones de faible affinité exprimant CCR6 et *BTB Domain And CNC Homolog 2* (Bach2) (95,96). En conséquence, le compartiment B mémoire est polyclonal, avec une grande capacité de cross-réactivité (97–99), et contient également de nombreuses cellules ayant une très faible affinité pour l'antigène initial (100).

Plusieurs études témoignent également de la persistance des T_{FH} à distance d'une réponse primaire, à la fois dans les organes lymphoïdes secondaires et le sang (101–103). Des travaux récents démontrent que les T_{FH} persistent dans le follicule après la résolution du centre germinatif, avec deux phénotypes distincts. Le premier compartiment a un profil transcriptionnel compatible avec des fonctions régulatrices. Le profil du second suggère une programmation pour la persistance et la capacité à répondre à une deuxième exposition antigénique, caractéristiques des compartiments mémoires (104). Ces T_{FH} mémoires ont été caractérisés par leur capacité à aider un lymphocyte B lors d'une nouvelle exposition à l'antigène (105–107).

1.4.2. Mémoire sérologique

Les mécanismes qui permettent l'export et la différenciation d'un lymphocyte B du centre germinatif en plasmocytes sont majoritairement inconnus. Ce processus s'accompagne de la répression de Bcl-6 par l'induction conjointe d'*Interferon regulatory factor 4* (IRF4) et de *B-lymphocyte-induced maturation protein 1* (Blimp1) dans le lymphocyte B au sein du centre germinatif (108,109). A nouveau, les signaux BCR et CD40 ont été suggérés comme prenant part à ce mécanisme. Le compartiment plasmocytaire est sélectionné pour des BCR de haute affinité (110,111). Après leur export, les plasmocytes vont nicher dans la moelle osseuse ou dans la muqueuse, selon que la réponse immunitaire était systémique ou muqueuse (112). Ils y sécrètent des anticorps indépendamment de la persistance de l'antigène (113).

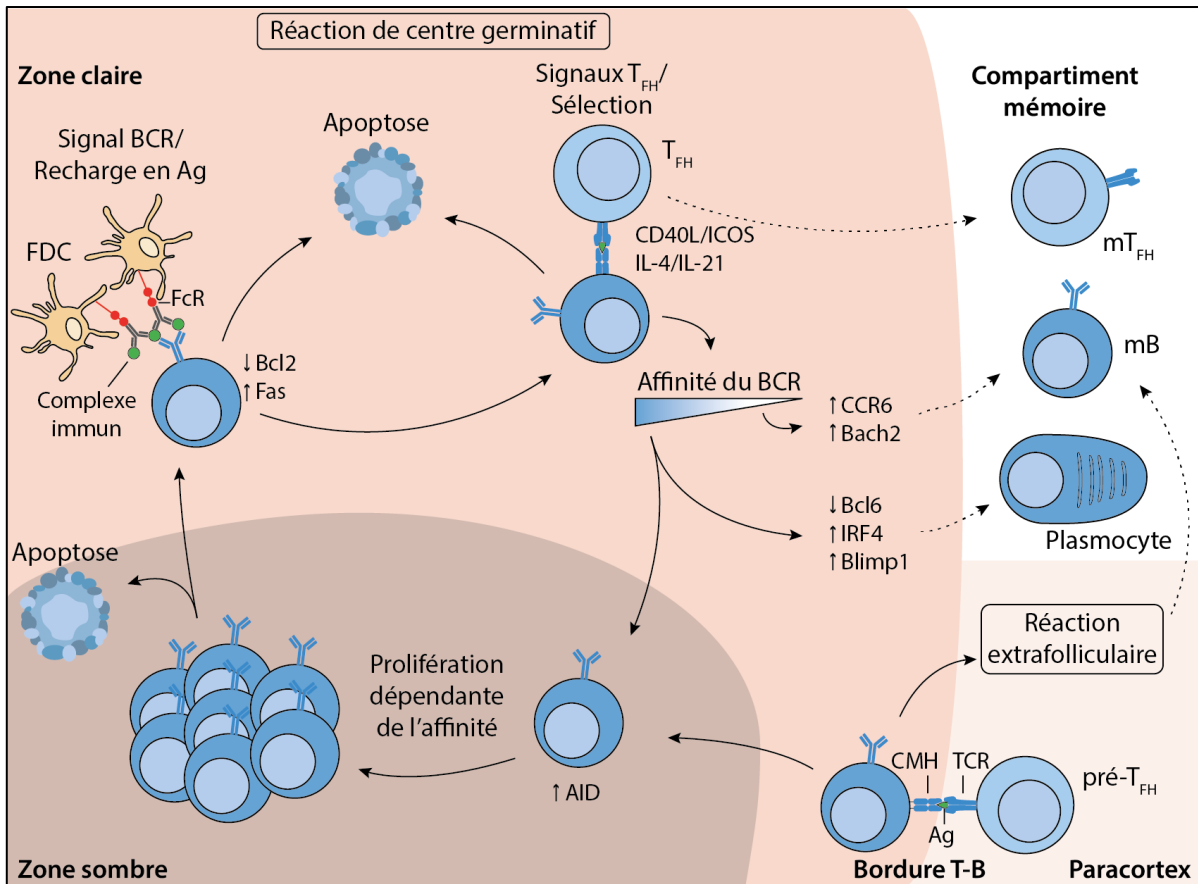


Figure 3. Réponse humorale thymo-dépendante

Après l'amorçage des réponses T et B, un premier dialogue T-B se met en place à la bordure T-B. A partir de là, deux réactions peuvent avoir lieu : la réaction extra-folliculaire et la réaction du centre germinatif. Au sein du centre germinatif, le lymphocyte B alterne des phases de prolifération (zone sombre) et des phases de sélection. Un contingent mémoire émerge à différents moments de la réaction.

Abréviations : Ag, antigène ; FcR : récepteur au fragment Fc des immunoglobulines ; FDC, cellule dendritique folliculaire ; CMH, complexe majeur d'histocompatibilité ; TCR, récepteur des cellules T ; BCR, récepteur des lymphocytes B ; T_{FH}, lymphocyte auxiliaire folliculaire ; AID, activation-induced cytidine deaminase ; IL, interleukine ; mT_{FH}, lymphocyte T_{FH} mémoire ; mB, lymphocyte B mémoire .

1.5. Fonctions effectrices des anticorps

Après leur production par les plasmocytes, les anticorps peuvent être sécrétés dans les muqueuses pour la protection contre les antigènes aéro-digestifs. Ils peuvent également être sécrétés dans le compartiment vasculaire, dans lequel ils restent alors majoritairement séquestrés [hors transfert materno-fœtal et périnatal via le placenta et le lait maternel ; (112)]. Après la rencontre de leur antigène cible, ils peuvent avoir différentes fonctions effectrices. Tout d'abord, ils peuvent se fixer à des pathogènes ou des toxines et neutraliser leur interaction avec leur récepteur sur la cellule eucaryote. Ensuite, le recouvrement des pathogènes par les anticorps (opsonisation) permet également de faciliter leur phagocytose par les cellules spécialisées. Enfin, les anticorps peuvent recruter des effecteurs de l'immunité innée à la surface du pathogène pour entraîner sa destruction. Il existe deux mécanismes : l'activation du complément par sa voie classique (*complement-dependent cytotoxicity*, CDC) et le recrutement de cellules équipées d'un récepteur au fragment cristallisable des immunoglobulines (FcR ; *antibody-dependent cellular cytotoxicity*, ADCC). Ces différentes fonctionnalités peuvent varier selon l'isotype de l'immunoglobuline sécrétée (114).

Au-delà de ces fonctions bénéfiques dans la lutte contre les infections, les anticorps peuvent aussi avoir des effets délétères [maladies auto-immunes, aggravation de certaines maladies infectieuses (*antibody-dependent enhancement*), allergie] que nous ne détaillerons pas ici.

2. Spécificités de la réponse humorale chez le patient transplanté

2.1. Les allo-antigènes, spécificité de la transplantation

Les patients transplantés sont exposés à tous les antigènes que peuvent rencontrer les sujets non transplantés. Ils sont, en plus, exposés aux allo-antigènes, les antigènes du donneur portés par le greffon. Il existe deux classes d'antigènes d'histocompatibilité : les antigènes majeurs et mineurs. Les antigènes majeurs sont les molécules du CMH (*Human Leukocyte Antigen*, HLA, chez l'homme). Cela représente peu de molécules, mais elles ont une variabilité extrême. A ce jour, plus de 34000 allèles sont connus, pour un peu plus de 22500 variants protéiques (hla.alleles.org). Les antigènes mineurs d'histocompatibilité sont tous les antigènes qui diffèrent entre le donneur et le receveur mais qui ne sont pas des molécules du CMH : variants liés à des polymorphismes, ou protéines exprimées par le donneur mais absentes chez le receveur (115). La variabilité de ces antigènes mineurs est très faible, mais cela concerne énormément de protéines. Au total, on estime que le poids des deux classes d'allo-antigènes, majeurs et mineurs, est équivalent dans la réponse allo-immune (116).

Tous les allo-antigènes vont être capables d'induire une réponse humorale thymo-dépendante. Ils vont alors être apprêtés par les cellules présentatrices d'antigènes du receveur pour être présentés au sein du CMH de classe II aux lymphocytes T CD4⁺. Dans le contexte de la transplantation, ce processus est appelé « allorecognition indirecte » (117,118). Il s'oppose à l'« allorecognition directe », propre à la transplantation et spécifique des antigènes majeurs d'histocompatibilité. Dans tous les contextes autres que la transplantation, le TCR, suite à la sélection thymique, est restreint aux peptides présentés par le CMH du soi. La fréquence des clones qui en résulte est comprise entre 10⁻⁴ et 10⁻⁵. Lors de l'allorecognition directe, le TCR est capable de reconnaître une molécule de CMH allogénique intacte. Il existe deux théories mécanistiques pour expliquer ce phénomène (117–119). Selon la première théorie, le TCR reconnaît directement le polymorphisme du CMH, indépendamment de

l'antigène présenté. La densité antigénique à la surface d'une cellule allogénique est telle qu'elle permet d'activer un lymphocyte T malgré une faible affinité TCR/ligand (120). Selon la seconde théorie, les différences moléculaires entre les molécules du CMH du donneur et du receveur vont affecter principalement le sillon de fixation des peptides, et modifier la présentation des antigènes du soi (bien que ces antigènes puissent être communs entre donneur et receveur). Ces antigènes, présentés différemment, apparaîtront alors comme étrangers pour le receveur (119,121).

Les lymphocytes T de spécificité directe vont reconnaître le CMH allogénique directement à la surface d'une cellule du donneur dérivée du greffon [reconnaissance directe, (122)], ou à la surface d'une cellule syngénique [reconnaissance semi-directe, (123)] qui aura acquis des allo-antigènes intacts après contact cellulaire (124) ou via des vésicules extracellulaires (125,126). La fréquence des clones de spécificité directe est très élevée [environ 1 à 10% (122)]. A ce jour, la voie d'alloreconnaissance directe n'est pas impliquée dans la réponse humorale, car le dogme prévalent considère que seul un lymphocyte T de spécificité indirecte peut aider un lymphocyte B à produire des DSA.

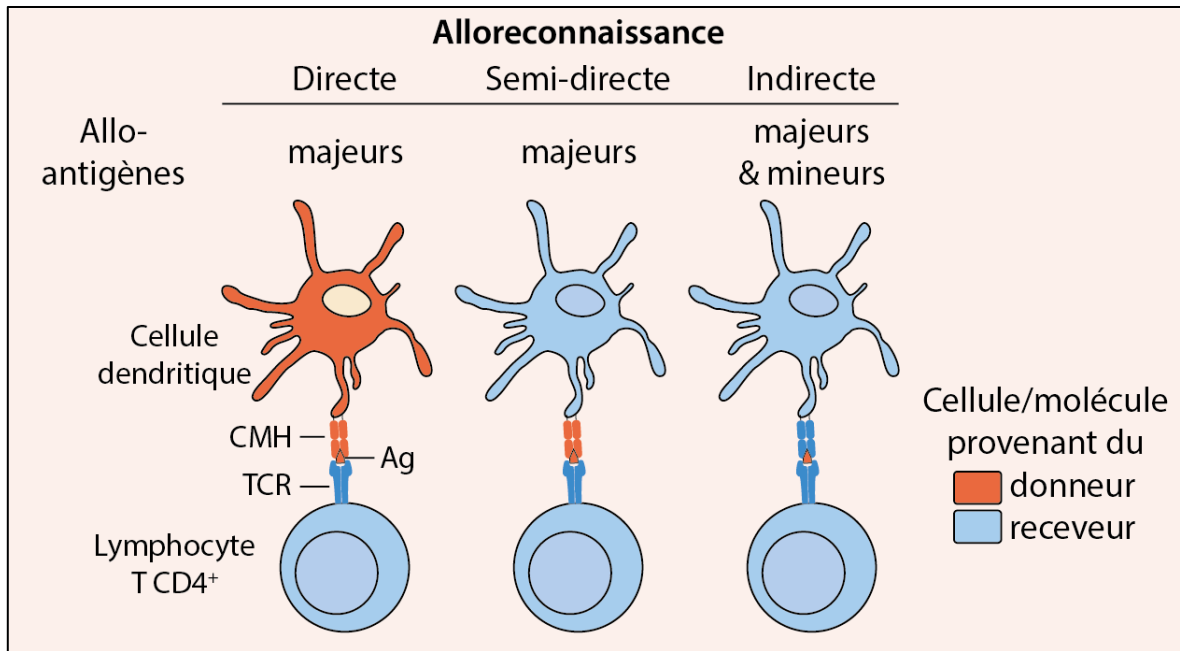


Figure 4. Les voies de l'alloreconnaissance et leur restriction antigénique

Abréviations : CMH, complexe majeur d'histocompatibilité ; TCR, récepteur des cellules T ; Ag, antigène.

2.2. Drainage des allo-antigènes et lieux de production des allo-anticorps

2.2.1. Les ganglions périphériques et la rate

Après transplantation, seuls les vaisseaux sanguins sont anastomosés : il n'y a pas de suture lymphatique. Le rétablissement du flux sanguin est donc immédiat, alors que le rétablissement du flux lymphatique prend plusieurs jours (127,128). En conséquence, le drainage des allo-antigènes est d'abord sanguin puis lymphatique.

L'utilisation de modèles de transplantation chez des souris *aly/aly* (absence de ganglions et de plaques de Peyer) et *Hox11^{-/-}* (asplénique) ont permis de déterminer l'importance respective des organes lymphoïdes secondaires dans la réponse allo-immune. Ces travaux démontrent que les ganglions ou la rate sont nécessaires mais suffisants pour monter une réponse allo-immune contre un greffon vascularisé (129).

2.2.2. Les organes lymphoïdes tertiaires

La persistance chronique d'un antigène au sein d'un tissu dans des conditions inflammatoires est responsable du développement d'organes lymphoïdes tertiaires. C'est le cas au cours des infections chroniques, des cancers ou des maladies auto-immunes (130,131).

La transplantation d'organe résume aussi ces deux conditions (persistance de l'antigène et inflammation) à l'intérieur du greffon. Ainsi, les organes lymphoïdes tertiaires ont été largement décrits dans ce contexte [examiné dans (132)], et ce, quel que soit l'organe transplanté [de façon non exhaustive, après transplantation rénale (133,134), cardiaque (135), pulmonaire (136)].

Leur développement dépend probablement de mécanismes partagés avec les organes lymphoïdes secondaires et de mécanismes propres aux structures tertiaires [examiné dans (132,137)]. Ces structures reproduisent localement, de façon plus ou moins complète, la microarchitecture d'un organe lymphoïde : ségrégation des zones T et B, néovaisseaux lymphatiques et HEV (138). Des centres germinatifs peuvent alors se développer au sein de l'organe transplanté (138), avec une production locale autonome d'anticorps spécifiques du donneur (DSA), en quantité plus importante et avec un répertoire plus large que dans les organes lymphoïdes secondaires (139).

2.3. Rôle de la réaction du centre germinatif en transplantation

Après transplantation, les allo-antigènes sont drainés dans les organes lymphoïdes secondaires par différents moyens. Les cellules dendritiques du donneur peuvent quitter le greffon pour rejoindre le ganglion drainant (140). Le greffon peut également relarguer des vésicules extracellulaires couvertes de CMH du donneur. Ces vésicules sont capturées par les macrophages du sinus sous-capsulaire dans les ganglions (ou leurs équivalents dans la rate) pour une présentation aux lymphocytes B allo-spécifiques (141). En parallèle, les cellules dendritiques du receveur, après avoir acquis l'antigène localement ou au sein même du greffon, vont le présenter aux lymphocytes T CD4⁺ de spécificité indirecte (142), pour initier le développement d'un centre germinatif (143).

Il est intéressant de noter que les traitements immunosuppresseurs parfois utilisés en induction de greffe, qui visent à dépléter les lymphocytes T, entraînent une disparition des centres germinatifs : cette disparition est transitoire et les organes lymphoïdes se repeuplent en lymphocytes T dans les semaines qui suivent la déplétion (144).

Ainsi, la réponse humorale aux allo-antigènes dépend des centres germinatifs. Pour tous les autres antigènes protéiques auxquels pourraient être exposés les patients transplantés, il est probable que l'orientation de la réponse entre voie extrafolliculaire et centre germinatif dépende des mêmes facteurs que ceux discutés plus haut, mais cela n'est pas documenté.

2.4. Rôle effecteur des DSA

Après la différenciation et l'export des plasmocytes allo-spécifiques au cours de la réaction du centre germinatif, des DSA vont être sécrétés. Ces DSA, du fait de leur nature, sont des macromolécules qui sont majoritairement séquestrées dans le secteur vasculaire (145). En conséquence, leur cible est l'endothélium des greffons, et le rejet humoral dont ils sont la cause est une maladie vasculaire.

Après avoir reconnu leur cible à la surface de la cellule endothéliale, les DSA peuvent léser le greffon par deux mécanismes (146). Premièrement, ils peuvent recruter des cellules de l'immunité innée via leur récepteur au fragment cristallisable des immunoglobulines. Ces cellules, activées au contact de l'endothélium du greffon, vont relarguer localement des enzymes lytiques [ADCC, (147)]. Ce phénomène conduit à un rejet infraclinique ou chronique (148). Deuxièmement, s'ils sont en concentration suffisante, ils peuvent activer la voie classique de la cascade du complément (CDC) et entraîner un rejet plus aigu (149).

Le rejet humoral est une problématique majeure en transplantation, car il est considéré aujourd'hui comme la première cause de perte des greffons (150,151).

2.5. Voies métaboliques, voies de signalisation, et immunosuppression

Afin de limiter la production de DSA et le rejet humoral, les patients transplantés reçoivent des traitements immunosuppresseurs. Nous ne décrivons ici que les voies métaboliques et les voies de signalisation ciblées par les principaux immunosuppresseurs qui sont utilisés au long cours : corticostéroïdes à faible dose, inhibiteurs de la calcineurine, inhibiteur de l'inosine-5'-monophosphate déshydrogénase (IMPDH), inhibiteurs de mTOR (*mechanistic target of rapamycin*) et bloqueurs de la costimulation.

2.5.1. Rôle des glucocorticoïdes dans l'initiation de la réponse immune

A faible dose, les corticostéroïdes agissent sur les cellules de l'immunité innée et peuvent inhiber l'initiation de la réponse immune. Ainsi, ils inhibent la maturation des cellules dendritiques et diminuent leur sécrétion de cytokines pro-inflammatoires (152). Le récepteur aux glucocorticoïdes active également des inhibiteurs de NF- κ B au sein des macrophages (153).

2.5.2. Activation et prolifération du lymphocyte B

Lors de l'activation du lymphocyte B, le BCR et le corécepteur CD19 activent ensemble la voie de signalisation PI3K/Akt/mTOR (154). En conséquence, une expression génétiquement inhibée de mTOR chez la souris, en plus d'entraîner un phénotype global hypomorphe, affecte le compartiment lymphocytaire B : les lymphocytes B sont hypotrophiques, prolifèrent moins et produisent moins d'anticorps (155). Ainsi, après une immunisation, la formation des centres germinatifs et la maturation d'affinité des anticorps est fortement diminuée chez ces souris (156). Lorsqu'un knock-out (KO) complet de mTOR est appliqué spécifiquement aux lymphocytes B, les mêmes résultats sont observés (156).

Le blocage pharmacologique de mTOR par la rapamycine reproduit in vivo le blocage de la réponse humorale obtenu par l'inhibition génétique (156). La rapamycine est également efficace in vitro sur des cellules humaines pour inhiber l'activation, la progression dans le cycle cellulaire, et donc la prolifération des lymphocytes B (157–159).

Des études plus récentes ont permis de préciser le rôle de mTOR au cours de la réponse thymo-dépendante. L'activité de mTORC1 est modulée dans le lymphocyte B au cours de la réaction du centre germinatif. La sélection positive des lymphocytes B du centre germinatif par les T_{FH} induit l'activation de mTORC1 de façon dépendante de CD40 : mTORC1 est nécessaire pour accompagner les changements métaboliques (croissance cellulaire) qui accompagnent le passage de la zone claire à la zone sombre. Ensuite, l'activité mTORC1 diminue au fil des proliférations jusqu'au retour du lymphocyte B dans la zone claire [Figure 5 ; (160)]. En conséquence, l'inhibition précoce de mTORC1 après une immunisation bloque l'expansion clonale des lymphocytes B du centre germinatif, tandis qu'un blocage plus tardif, une fois que l'expansion a débuté, a un effet nettement moins important sur l'issue de la réaction du centre germinatif (160,161). Enfin, mTOR contrôle la traduction de l'ARN messager *Aicda* (codant pour AID), et donc la commutation isotypique du lymphocyte B (162).

L'IMPDH est une enzyme impliquée dans la voie de synthèse de novo des purines. Son expression cellulaire est non spécifique, et de nombreuses cellules immunitaires peuvent en transcrire le gène (163). Cependant, l'expression protéique est majoritaire dans les lymphocytes T et B (164). L'inhibition de l'IMPDH par l'acide mycophénolique inhibe la prolifération et la différenciation des lymphocytes B humains in vitro, et donc la formation des plasmocytes (165–167).

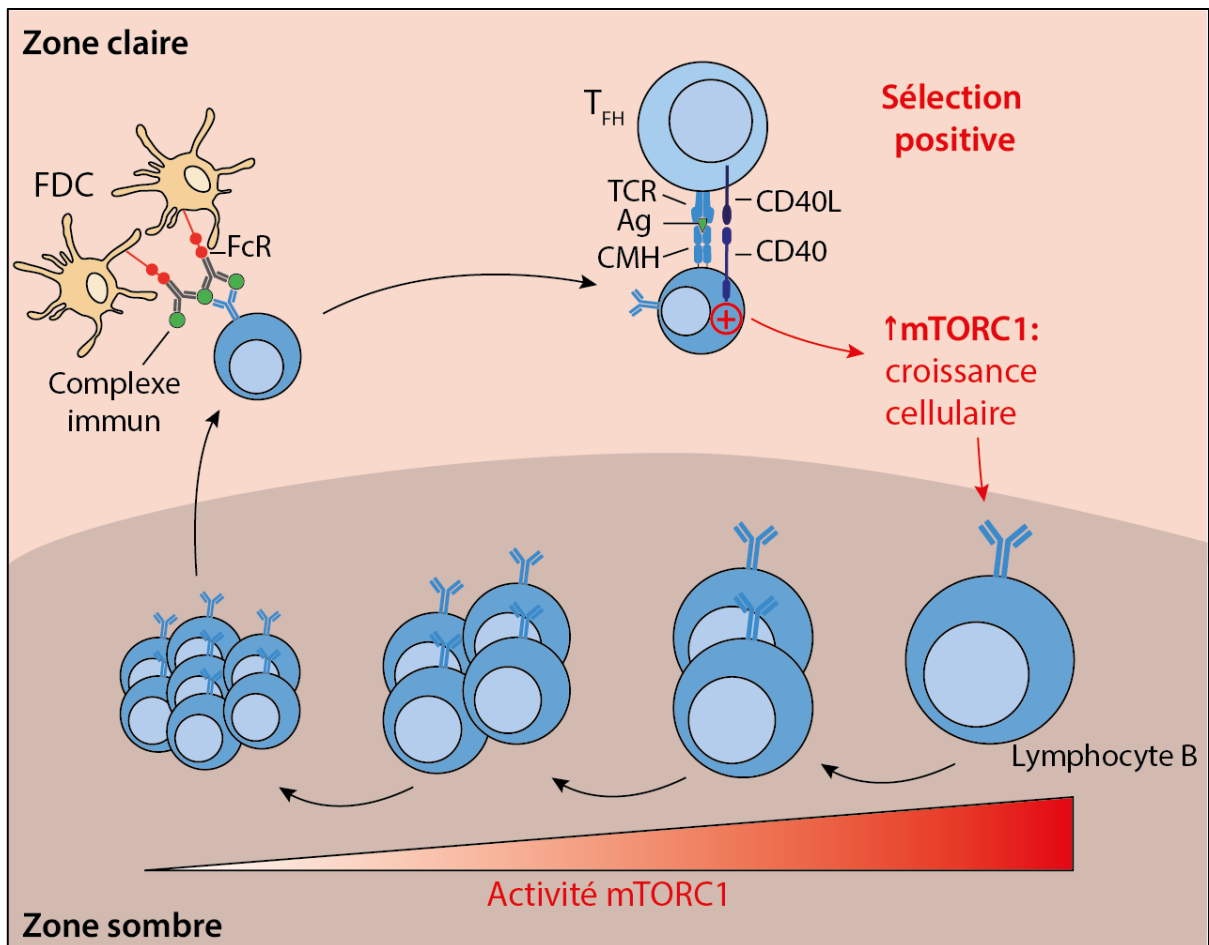


Figure 5. Régulation de mTORC1 dans le lymphocyte B au cours de la réaction de centre germinatif [d'après (160)]

mTORC1 est induit par le signal CD40 au cours de la sélection positive des lymphocytes B du centre germinatif. mTORC1 accompagne les changements métaboliques qui permettent la croissance cellulaire en vue de la prolifération. Une fois la prolifération débutée, l'activité mTORC1 n'est plus essentielle et diminue.

Abréviations : FDC, cellules folliculaires dendritiques ; FcR, récepteur au fragment Fc des immunoglobulines ; CMH, complexe majeur d'histocompatibilité ; TCR, récepteur des cellules T ; Ag, antigène ; T_{FH}, lymphocyte T auxiliaire folliculaire.

2.5.3. Activation du lymphocyte T, différenciation T_{FH} et prolifération

Si la molécule mTOR est indispensable au bon fonctionnement des lymphocytes B du centre germinatif, elle est également cruciale pour la réponse T_{FH}. Cela a bien été démontré dans un modèle de transplantation cardiaque chez la souris. La délétion spécifique de mTOR dans les lymphocytes T CD4⁺ inhibe la formation des centres germinatifs en bloquant la réponse effectrice T_{FH}, et en conséquence augmente la survie des greffons (168). Des travaux récents précisent la mécanistique : mTOR est indispensable pour faire le lien entre les signaux de costimulation du lymphocyte T et l'induction du programme métabolique qui soutient la différenciation en T_{FH} (169). mTORC1 permet les premières divisions cellulaires nécessaires à la réponse T_{FH}, et mTORC1 et mTORC2 soutiennent conjointement la polarisation T_{FH} (169,170) plutôt que T_{H1} (171).

Au cours de la réponse humorale, la calcineurine est activée à la fois dans le lymphocyte T et le lymphocyte B (41,172). Cependant, des études *in vitro* sur cellules humaines ont permis de montrer que, chez le patient transplanté, l'inhibition de la calcineurine pour bloquer la coopération T-B agit principalement sur le blocage de la réponse lymphocytaire T, plutôt que B (173). Le rôle le mieux connu de la calcineurine est de faire le lien entre flux calcique et NFAT (cf ci-dessus). Mais il existe un autre mode d'action décrit plus récemment, et indépendant de NFAT. Dans le lymphocyte T activé, la calcineurine est recrutée par le TCR pour déphosphoryler Lck, une kinase associée à la molécule CD4. Lck déphosphorylée permet de maintenir active la phosphorylation de ZAP-70 par CD3 ζ , promouvant ainsi l'adhésion synaptique via LFA-1 et l'amplification de la signalisation TCR (174). Par conséquent, les inhibiteurs de la calcineurine agissent immédiatement en aval du signal TCR pour bloquer la translocation nucléaire de NFAT, mais également en inhibant la boucle d'amplification de la réponse T [Figure 6, (175)]. Enfin, une étude récente suggère que le tacrolimus aurait une action spécifique sur les T_{FH} circulants et résidents dans les ganglions, et ciblerait donc

particulièrement la réponse humorale (176). Quoiqu'il en soit, ces voies d'activation sont finement régulées in vivo, et une inhibition pharmacologique est différente d'une invalidation d'un gène dans un modèle murin. Des travaux récents sur un modèle de transplantation rénale chez le rat confirme l'intuition selon laquelle le blocage plus ou moins efficace des interactions T-B dépend de la dose d'inhibiteur de calcineurine utilisée (177).

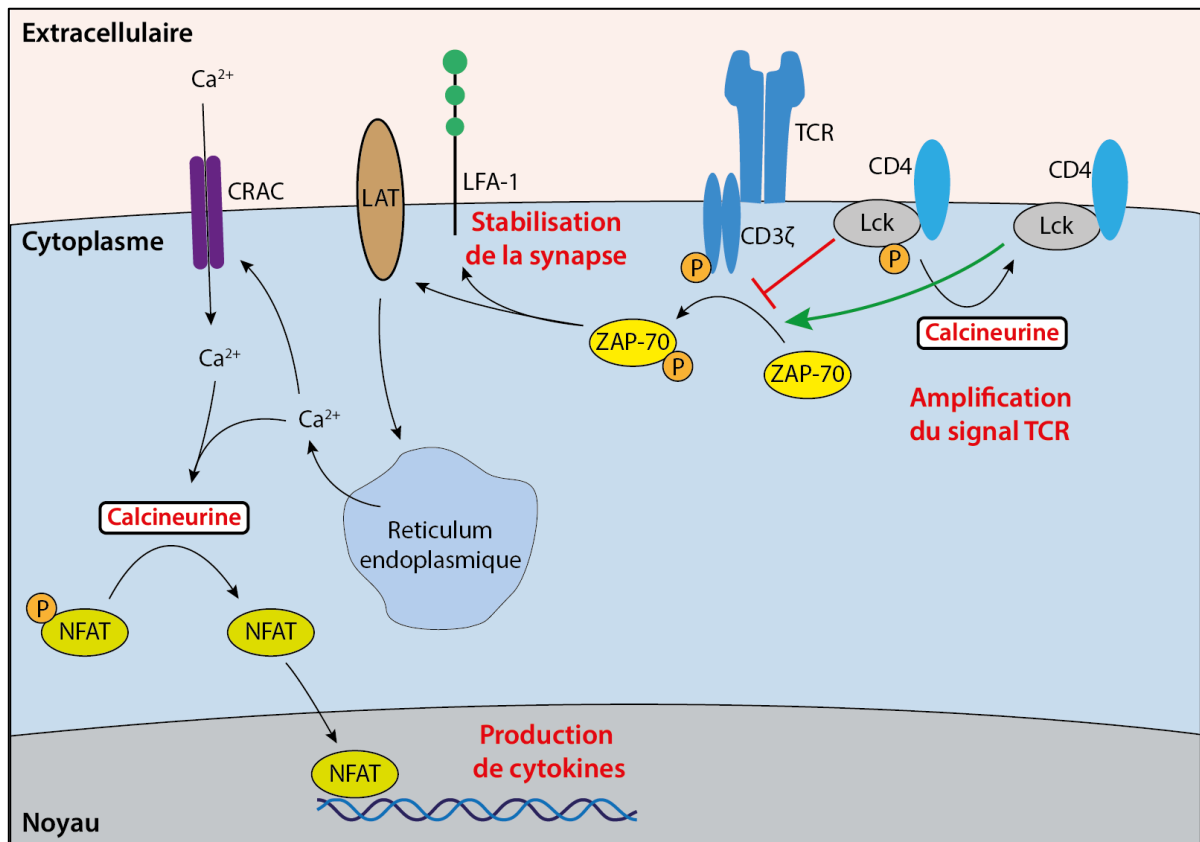


Figure 6. Représentation schématique et simplifiée du rôle de la calcineurine dans le lymphocyte T

La calcineurine agit à deux niveaux distincts. Elle déphosphoryle NFAT pour permettre sa translocation nucléaire. Mais elle déphosphoryle également Lck pour lever un rétrocontrôle négatif sur la signalisation TCR et stabiliser la synapse.

Abréviations : CRAC, Calcium release-activated Ca^{2+} ; LAT, linker of activated T cells ; LFA-1, Lymphocyte function-associated antigen 1 ; TCR, récepteur des cellules T ; ZAP-70, Zeta-chain-associated protein kinase 70 ; NFAT, Nuclear factor of activated T cells.

Ensuite, comme nous l'avons expliqué plus haut, les lymphocytes T expriment l'enzyme IMPDH pour la synthèse d'ADN au cours des phases prolifératives. Or, la prolifération des lymphocytes T est indispensable, puisque la quantité d'aide T_{FH} est un facteur qui contrôle à la fois l'entrée des lymphocytes B dans le centre germinatif (53) et leur expansion dans la zone sombre (89). Par conséquent, l'inhibition de l'IMPDH dans le lymphocyte T inhibe la réponse humorale en inhibant efficacement la prolifération des lymphocytes T activés (178).

Enfin, les lymphocytes T sont la principale cible des glucocorticoïdes [détaillé dans (179)]. L'activation du récepteur des glucocorticoïdes dans les lymphocytes T régule la transcription de nombreux gènes, et en particulier diminue l'expression des molécules de costimulation CD28 et 4-1BB, augmente l'expression des checkpoints inhibiteurs *Programmed cell death-1* (PD1), *Cytotoxic T-lymphocyte-associated protein 4* (CTLA-4), *T cell immunoglobulin and mucin domain-containing protein 3* (TIM3) et *Lymphocyte-activation gene 3* (LAG3), et diminue la production de cytokines et chimiokines.

2.5.4. Costimulation des lymphocytes T

Comme nous l'avons décrit, l'activation des lymphocytes T nécessite deux signaux: le signal TCR et un signal de costimulation. Parmi les différents signaux de costimulation, l'activation de CD28 par ses ligands CD80 et CD86 a un rôle prépondérant. CD80 et CD86 ont un autre récepteur (inhibiteur cette fois-ci) à la surface du lymphocyte T, qui est CTLA-4. La molécule de fusion CTLA4-Ig (Belatacept) a été développée pour se fixer à CD80 et CD86 sur la cellule présentatrice d'antigène, et ainsi bloquer la costimulation des lymphocytes T. Pourtant, son utilisation et son étude approfondie ont montré qu'elle a aussi une action directe sur sa cellule cible par le fait de sa liaison à CD80 et CD86.

Le traitement de cellules dendritiques par CTLA-4 in vitro inhibe leurs fonctions pro-inflammatoires et diminue leur capacité à faire proliférer des lymphocytes T CD4⁺ allogéniques (180). Ce mécanisme est dépendant de l'induction de *Signal transducer and activator of transcription* (STAT) 3 en aval de CD80 (180), qui a aussi été observée après traitement de lymphocytes B par la molécule CTLA4-Ig (181). Sur les B activés, CTLA4-Ig diminue l'expression des molécules de costimulation et inhibe la différenciation en plasmablastes et la commutation isotypique (181). Par son action directe sur les lymphocytes B et par l'inhibition du signal CD28, CTLA4-Ig diminue l'activation et la différenciation des T_{FH} (182,183) ainsi que leur prolifération induite par les B (181). L'action de CTLA4-Ig sur la synapse T-B est confortée par le maintien de son efficacité sur des réponses humorales en cours, même quand la molécule est administrée après l'activation des lymphocytes T alloréactifs (184,185).

2.5.5. Génération de la mémoire

Nous avons décrit de nombreux mécanismes et voies métaboliques qui contrôlent l'activation, la prolifération ou la différenciation des lymphocytes T et B, et qui sont accessibles à des traitements immunosuppresseurs. A ce jour, on ne connaît pas de phénomène qui soit impliqué exclusivement dans la génération de la mémoire humorale, sans être impliqué en amont. Cependant, il est raisonnable de penser que le ciblage de la production des cellules mémoires n'est pas la méthode la plus efficace pour contrôler une réponse humorale primaire, et qu'il est préférable de cibler l'activation des cellules en amont, comme cela a été fait jusqu'à présent.

II. OBJECTIFS

Après avoir fait un état des lieux des modalités de la réponse humorale normale, et des spécificités de celle-ci chez les patients transplantés, de nombreuses questions demeurent.

D'un part, on ne sait pas si les immunosuppresseurs sont susceptibles de modifier l'orientation de la réponse aux antigènes infectieux et vaccinaux vers la voie extra-folliculaire ou vers le centre germinatif, et en conséquence, d'affecter les aspects quantitatifs et qualitatifs des réponses vaccinales des patients transplantés. La pandémie de SARS-CoV-2 nous a offert l'occasion de documenter cette question dans la première partie de ce travail.

D'autre part, il reste à comprendre pourquoi certains patients continuent de développer des DSA sous traitement immunosuppresseur. Ainsi, avant d'évoquer un défaut d'observance par les patients (qui reste bien sûr possible), il faut être certain qu'il n'existe pas des voies immunologiques qui permettent de produire des DSA en dehors du cadre décrit jusqu'à présent. Ainsi, puisque les immunosuppresseurs ont été développés principalement pour bloquer l'activation des lymphocytes T conventionnels, nous avons cherché à savoir, dans la deuxième partie de ce travail, si les lymphocytes T $\gamma\delta$ (non conventionnels) pouvaient être impliqués dans la production de DSA. Enfin, il ne faut pas oublier que la transplantation est une situation inédite qui peut mettre en contact des cellules immunitaires allogéniques. Peu de travaux documentent les collaborations qui peuvent, en théorie, se mettre en place lorsque des cellules allogéniques se rencontrent. La troisième partie de ce travail s'intéresse à cette situation.

Ce travail de thèse a donc trois principaux objectifs.

1. Etudier la production d'anticorps contre les antigènes infectieux et vaccinaux chez les sujets transplantés, ainsi que l'impact de l'immunosuppression sur ces mécanismes.
2. Explorer si la prévention du développement des allo-anticorps par l'inhibition pharmacologique des voies canoniques n'est pas mise en défaut par l'existence de voies non conventionnelles.
3. Etudier si des situations inédites engendrées par la transplantation permettent d'aboutir à la production de DSA.

III. RESULTATS

Article 1 : Infection or a third dose of mRNA vaccine elicit neutralizing antibody responses against SARS-CoV-2 in kidney transplant recipients

La survenue de la pandémie de COVID-19 a entraîné la suspension de nombreux projets qui n'étaient pas directement liés à l'infection au SARS-CoV-2.

Or, il y a eu très rapidement des alertes relatives à la gravité de cette infection chez les patients transplantés. Afin de mieux comprendre pourquoi les sujets transplantés avaient des formes si sévères de la maladie, et dans le but d'améliorer leur prise en charge, nous nous sommes organisés pour collecter des échantillons biologiques afin d'étudier les réponses immunitaires déclenchées par l'infection par le SARS-CoV-2 et la vaccination par vaccin à ARNm chez les patients transplantés. Nous souhaitons ainsi caractériser l'immunité cellulaire et humorale de nos patients en réponse à ce virus inconnu et à ce vaccin utilisant une technologie utilisée pour la première fois à large échelle.

Dans le même temps, notre groupe faisait partie d'un réseau national de surveillance épidémiologique de la maladie chez les patients transplantés. En lien avec ce réseau, nous avons alors fait une observation très importante : les patients transplantés rénaux qui avaient survécu à une première infection ne se réinfectaient jamais au cours du temps, alors qu'un nombre non négligeable de patients vaccinés développaient un COVID-19 symptomatique dans les semaines suivant la vaccination.

Nous avons alors en main tous les éléments nécessaires pour étudier si cette observation clinique avait un substratum immunologique. Par l'analyse des échantillons biologiques nous avons alors cherché à mettre en évidence un corrélât de protection chez les sujets transplantés.

CORONAVIRUS

Infection or a third dose of mRNA vaccine elicits neutralizing antibody responses against SARS-CoV-2 in kidney transplant recipients

Xavier Charmetant^{1†}, Maxime Espi^{1†}, Ilies Benotmane^{2,3,4†}, Véronique Barateau¹, Françoise Heibel², Fanny Buron⁵, Gabriela Gautier-Vargas², Marion Delafosse⁵, Peggy Perrin², Alice Koenig^{1,5,6}, Noëlle Cognard², Charlene Levi⁵, Floriane Gallais^{3,4}, Louis Manière⁵, Paola Rossolillo⁷, Eric Soulier⁴, Florian Pierre⁴, Anne Ovize⁸, Emmanuel Morelon^{1,5,6}, Thierry Defrance¹, Samira Fafi-Kremer^{3,4}, Sophie Caillard^{2,3,4‡}, Olivier Thauinat^{1,5,6*‡}

Copyright © 2022 The Authors, some rights reserved; exclusive licensee American Association for the Advancement of Science. No claim to original U.S. Government Works. Distributed under a Creative Commons Attribution License 4.0 (CC BY).

Transplant recipients, who receive therapeutic immunosuppression to prevent graft rejection, are characterized by high coronavirus disease 2019 (COVID-19)-related mortality and defective response to vaccines. We observed that previous infection with severe acute respiratory syndrome coronavirus 2 (SARS-CoV-2), but not the standard two-dose regimen of vaccination, provided protection against symptomatic COVID-19 in kidney transplant recipients. We therefore compared the cellular and humoral immune responses of these two groups of patients. Neutralizing anti-receptor-binding domain (RBD) immunoglobulin G (IgG) antibodies were identified as the primary correlate of protection for transplant recipients. Analysis of virus-specific B and T cell responses suggested that the generation of neutralizing anti-RBD IgG may have depended on cognate T-B cell interactions that took place in germinal center, potentially acting as a limiting checkpoint. High-dose mycophenolate mofetil, an immunosuppressive drug, was associated with fewer antigen-specific B and T follicular helper (T_{FH}) cells after vaccination; this was not observed in patients recently infected with SARS-CoV-2. Last, we observed that, in two independent prospective cohorts, administration of a third dose of SARS-CoV-2 mRNA vaccine restored neutralizing titers of anti-RBD IgG in about 40% of individuals who had not previously responded to two doses of vaccine. Together, these findings suggest that a third dose of SARS-CoV-2 mRNA vaccine improves the RBD-specific responses of transplant patients treated with immunosuppressive drugs.

INTRODUCTION

In December 2019, an outbreak of apparently viral pneumonia of unknown etiology emerged in the city of Wuhan in the Chinese province of Hubei (1). On 9 January 2020, the World Health Organization (WHO) announced the discovery of a novel coronavirus officially named severe acute respiratory syndrome coronavirus 2 (SARS-CoV-2), which is the pathogen responsible for coronavirus disease 2019 (COVID-19). The disease quickly disseminated from Wuhan, and as of 13 January 2022, more than 307 million cases have been confirmed in 218 countries (2), leading the WHO to consider COVID-19 as the first pandemic triggered by a coronavirus.

Among the various alarms raised by the pandemic was its impact on the population of patients receiving organ transplants, whose COVID-19-related mortality was estimated at about 20%, several

magnitudes higher than that of the general population (3–7). This vulnerable population of patients was therefore prioritized for vaccination against SARS-CoV-2 by health authorities (8). However, prevention of allograft rejection requires lifelong immunosuppression regimens, which nonspecifically inhibit T and B cells in transplant recipients, resulting in reduced response rates to vaccines in general (9, 10). As expected, several recent publications have documented that immunosuppressed transplant recipients develop mitigated immune responses following the standard two-dose regimen of vaccination with either of the two approved SARS-CoV-2 mRNA vaccines (11–15).

Although insufficiency of vaccinal protection in transplant recipients has emerged as a concern due to accumulating reports of severe COVID-19 in vaccinated patients (16, 17), the underlying immune mechanisms explaining this problem are still elusive (15, 18). In an attempt to determine the relative contribution of humoral and T cell immunity in conferring protection against COVID-19 and understand immunosuppression-induced defects after SARS-CoV-2 vaccination, we undertook a prospective translational study that compared recently infected and vaccinated transplant recipients.

RESULTS

Infection conferred increased protection against symptomatic COVID-19 to transplant recipients relative to vaccination

The incidence of COVID-19 was monitored in all 873 renal transplant recipients of Strasbourg University Hospital and compared

¹CIRI, INSERM U1111, Université Claude Bernard Lyon I, CNRS UMR5308, Ecole Normale Supérieure de Lyon, Univ. Lyon, 21 avenue Tony Garnier, 69007 Lyon, France. ²Department of Nephrology and Transplantation, Strasbourg University Hospital, 67000 Strasbourg, France. ³Department of Virology, Strasbourg University Hospital, 67000 Strasbourg, France. ⁴Inserm UMR S1109, LabEx Transplantex, Fédération de Médecine Translationnelle de Strasbourg (FMTS), Université de Strasbourg, 67000 Strasbourg, France. ⁵Department of Transplantation, Nephrology, and Clinical Immunology, Hospices Civils de Lyon, Edouard Herriot Hospital, 5, place d'Arsonval, 69003 Lyon, France. ⁶Claude Bernard University (Lyon 1), 43 boulevard du 11 Novembre 1918, 69622 Villeurbanne, France. ⁷Institut de Génétique et de Biologie Moléculaire et Cellulaire (IGBMC), Centre National de la Recherche Scientifique (CNRS), UMR 7104, Institut National de la Santé et de la Recherche Médicale (INSERM), U1258, Université de Strasbourg, 67400 Illkirch, France. ⁸Eurofins Biomnis Laboratory, 69007 Lyon, France.

*Corresponding author. Email: olivier.thauinat@chu-lyon.fr

†These authors contributed equally to this work.

‡These authors contributed equally to this work.

between those with previous history of infection with SARS-CoV-2 (group “infected,” $n = 137$) and those who received the standard two-dose regimen of vaccination with mRNA-1273 (group “vaccinated,” $n = 736$). The clinical characteristics of this large epidemiological cohort are provided in table S1. Strikingly, whereas none of the recently infected patients developed symptomatic reinfection, 20 vaccinated patients developed COVID-19 (Fig. 1; log-rank test, $P = 0.0286$). Of note, this observation was made during the follow-up period of recently infected patients, which was significantly longer than that of vaccinated patients [289 days, interquartile range (IQR) [119; 333] versus 79 days, IQR [56; 210]; $P < 0.0001$, Mann-Whitney test].

The total absence of symptomatic reinfection in renal transplant recipients with previous history of COVID-19 is unexpected and conflicts with the results of previously published studies in the general population (19–22). However, in contrast with the previously published studies, of which two were conducted in health care workers (highly exposed to SARS-CoV-2) using systematic PCR (polymerase chain reaction) screening to define reinfection, our approach only allowed to capture symptomatic reinfections in a population particularly prone to strictly comply to social distancing rules (23). We concluded that SARS-CoV-2 infection confers protection against symptomatic COVID-19 to immunocompromised transplant recipients.

Mechanistic study population details

Comparison of cellular and humoral immune responses developed by recently infected and vaccinated transplant patients offers a unique opportunity to determine which immune effector(s) is associated with protection against COVID-19 in this vulnerable population (3–7). The COVATRHUS cohort (Covid-19 Vaccine in Transplant Recipients, Hopitaux Universitaires de Strasbourg) was therefore established to prospectively collect synchronous serum and peripheral blood mononuclear cell (PBMC) samples from renal transplant recipients diagnosed with COVID-19 in the absence of previous

vaccine injection (group infected, $n = 21$; mean sampling time: 30.6 ± 6.9 days after the onset of symptoms) or vaccinated with two doses of mRNA-1273 (group vaccinated, $n = 29$; mean sampling time: 14.7 ± 3.7 days after the second dose, or 42.8 ± 3.8 days after initial contact with the antigen). This time point for analysis was chosen on the basis of previous studies, which reported that, in recently infected renal transplant patients, both the cellular and humoral responses against SARS-CoV-2 were clearly detectable between 25 and 37 days, although cell functionality (especially cytokine secretion) could still evolve thereafter (24).

The clinical characteristics of the COVATRHUS cohort are presented in table S1. With the exception of a shorter time after transplantation in infected patients and a slightly different comorbidity profile of vaccinated patients, the rest of the clinical characteristics of COVATRHUS patients are similar to that of the epidemiological cohort. Recently infected and vaccinated patients from the COVATRHUS cohort had similar clinical profiles (table S1). Of note, the severity of COVID-19 in infected patients was mainly mild/moderate (16 of 21, 76%), and most of them did not require hospitalization (14 of 21, 67%).

SARS-CoV-2-specific cellular immunity is comparable in previously infected and vaccinated transplant recipients

Virus-specific CD8⁺ T cells reduce disease severity and promote recovery in many respiratory infections, including those driven by coronaviruses (25, 26), by eliminating infected cells. Optimal generation of these cytotoxic effectors depends upon the help provided by the T helper 1 (T_H1) CD4⁺ T cells (27). We observed that no difference in the total count of CD4⁺ and CD8⁺ T cells was observed between vaccinated and recently infected patients (Fig. 2, A and B). Cytotoxic CD8⁺ T cells directed against the spike protein of SARS-CoV-2, identified by the coexpression of CD69 and CD137 (28), could be detected in the circulation of both vaccinated and recently infected patients (Fig. 2C). However, only recently infected patients had CD8⁺ T cells directed against the other proteins of the virus (nucleocapsid and membrane). This finding was expected because nucleocapsid and membrane proteins are not included in the vaccine formulation (Fig. 2, C and D). There was no difference in spike protein-specific CD8⁺ T cells in the circulation of patients with recent infection versus vaccinated patients (Fig. 2D). The result remained the same when all specificities (spike, nucleocapsid, and membrane) were added together to better take into account the difference of repertoire between the two groups (Fig. 2E). The functionality of these SARS-CoV-2-specific CD8⁺ T cells was demonstrated by their ability to produce interferon- γ (IFN- γ) upon in vitro stimulation (Fig. 2F). The frequency of IFN- γ -producing SARS-CoV-2-specific CD8⁺ T cells was similar between vaccinated and recently infected patients (Fig. 2G).

SARS-CoV-2-specific CD4⁺ T cell responses were monitored using the same approach as above (28); OX40 and CD137 were used as surface activation-induced markers on CD4⁺ T cells (Fig. 2H). Comparison of CD4⁺ and T_H1 responses of vaccinated and recently infected patients resulted in the same conclusions as for CD8⁺ T cell responses (Fig. 2, I to L).

Thus, although the repertoire of the cellular immune response directed against SARS-CoV-2 is wider in recently infected patients (Fig. 2, C, D, H, and I), the minimal increase in cellular effectors ($P = 0.240$ for CD8⁺ T cells, Fig. 2E; $P = 0.158$ for CD4⁺ T cells, Fig. 2J) is unlikely to account alone for the marked advantage in

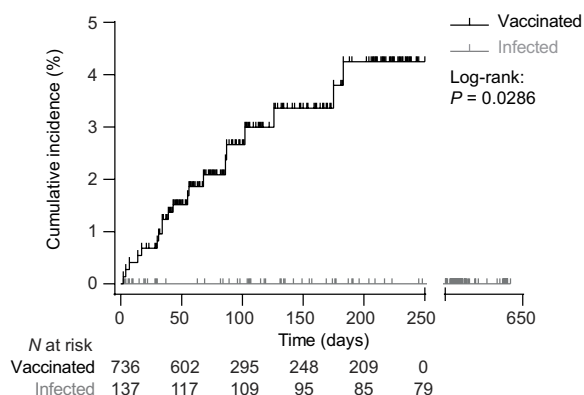
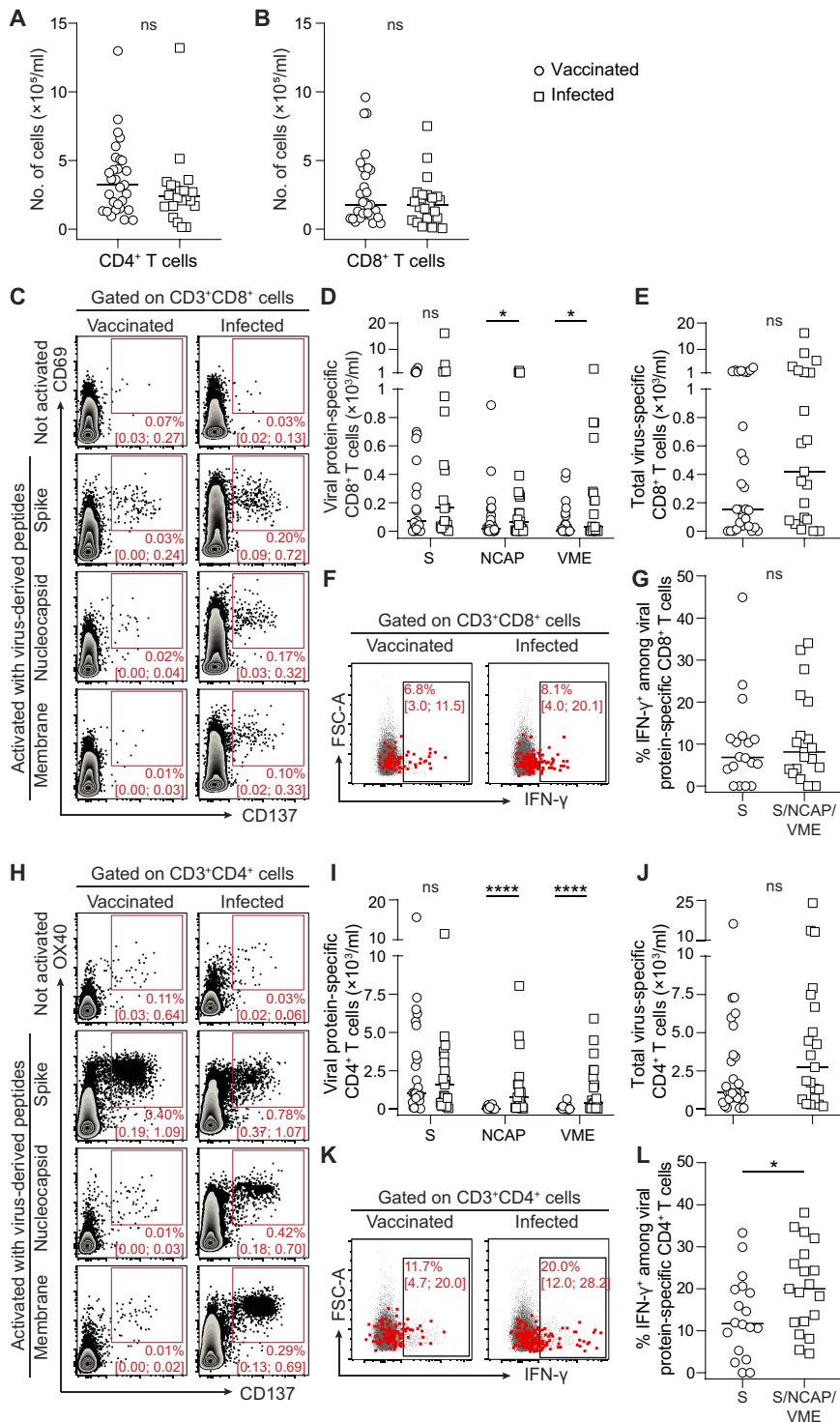


Fig. 1. Infection confers better protection against symptomatic COVID-19 than vaccination in transplant recipients. Protection against COVID-19 was compared between renal transplant recipients with previous history of infection with SARS-CoV-2 (group “infected,” gray curve) and those who received the standard two-dose regimen of mRNA-1273 (group “vaccinated,” black curve). The follow-up started at the time of COVID-19 symptom onset for infected patients and at the time of the second vaccine administration for the vaccinated patients. Cumulative incidence in the two groups was plotted using the Kaplan-Meier method. Data were analyzed by a log-rank test; $P = 0.0286$.

Fig. 2. SARS-CoV-2-specific cellular immunity was comparable in previously infected and vaccinated transplant recipients. (A and B) CD4⁺ (A) and CD8⁺ (B) T cells were enumerated in the circulation of recently infected ($n=21$; open squares) and vaccinated ($n=29$; open circles) transplant recipients. (C to L) CD8⁺ T cells (C to G) and CD4⁺ T_H1 cells (H to L) directed against the spike (S), nucleocapsid (NCAP), and membrane (VME) proteins of SARS-CoV-2 were enumerated in the circulation of recently infected and vaccinated transplant recipients. Data were background-subtracted against DMSO-negative control. (C) Flow cytometry profiles of a representative patient of each group. Median percentage and IQR are indicated. (D) The count of CD8⁺ T cells specific to each viral protein is plotted for each patient. (E) For each patient, the total number of virus-specific CD8⁺ cytotoxic T cells is plotted. (F) Concatenated flow cytometry profiles of the two groups of patients. Median percentage and IQR are indicated. FSC-A, forward scatter area. (G) The proportion of IFN- γ -producing SARS-CoV-2-specific CD8⁺ cytotoxic T cells is plotted for each patient (infected patients, $n=7$; vaccinated patients, $n=18$). (H) Flow cytometry profiles of a representative patient of each group. Median percentage and IQR are indicated. (I) The count of T_H1-polarized CD4⁺ T cells specific to each viral protein is plotted for each patient. (J) For each patient, the total number of virus-specific T_H1-polarized CD4⁺ T cells is plotted. (K) Concatenated flow cytometry profiles of the two groups of patients. Median percentage and IQR are indicated. (L) The proportion of IFN- γ -producing SARS-CoV-2-specific T_H1 CD4⁺ T cells is plotted for each patient (infected patients, $n=7$; vaccinated patients, $n=18$). The bars indicate the median. Data were analyzed using a Mann-Whitney test; not significant (ns), $P > 0.05$; * $P \leq 0.05$; **** $P < 0.0001$.



terms of protection against symptomatic COVID-19 observed in this group as compared with vaccinated transplant recipients. Another argument in favor of this hypothesis is the fact that some recently infected patients had barely detectable virus-specific T cells, suggesting that their protection was due to other types of immune effectors, a hypothesis also supported by a recently published experimental study (29).

Presence of neutralizing IgG correlates with protection against COVID-19 in transplant recipients

Beside cellular effectors, the adaptive immune system also generates antibodies against SARS-CoV-2. As expected, antibodies directed against viral nucleocapsid (not included in the vaccine formulation) were exclusively detected in patients from the recent infection group (Fig. 3A), but only in half of them (11 of 19, 58%). In contrast, almost all (20 of 21, 95%) recently infected transplant recipients developed anti-RBD (receptor-binding domain) IgG (immunoglobulin G) (Fig. 3B). The spike glycoprotein mediates virus entry

into target cells using the angiotensin-converting enzyme 2 (ACE2) receptor, and it has been shown that antibodies directed against the RBD can block viral infection of human cells in vitro and counter viral replication in vivo (30–34). Despite the fact that anti-RBD IgG titers were lower than those observed in a cohort of 30 vaccinated healthy volunteers (35), serum isolated from recently infected transplant recipients still efficiently block pseudo-virus entry in human cells in vitro (Fig. 3C). A positive correlation between anti-RBD IgG

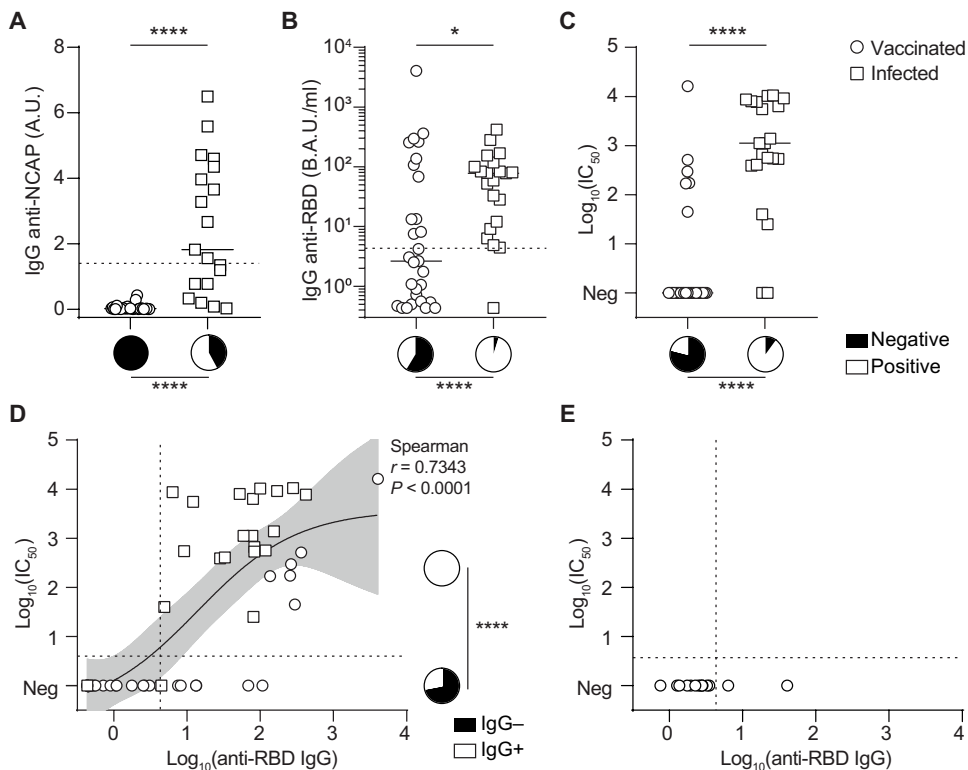


Fig. 3. Anti-SARS-CoV-2-specific humoral immunity elicited by infection and vaccination differs in transplant recipients. (A and B) The titers of IgG antibodies directed against the nucleocapsid protein (A) or receptor-binding domain (B) of SARS-CoV-2 were measured in the circulation of recently infected ($n = 21$; open squares) and vaccinated ($n = 29$; open circles) transplant recipients. A.U., arbitrary units; B.A.U., binding antibody units. (C) The neutralizing capacity of patients' serum was compared between recently infected ($n = 21$; open squares) and vaccinated ($n = 29$; open circles) transplant recipients. Neutralizing titers are presented as the \log_{10} of the dilution inhibiting 50% of target infection [$\log_{10}(\text{IC}_{50})$]. Neg indicates no evidence of neutralizing antibodies. For (A) to (C), the bars indicate median values. Pie charts are used to compare proportions. (D and E) The values of anti-RBD IgG titers and neutralizing capacity of the serum were log-transformed and plotted. (D) Results for the patients of the COVATRHUS cohort who were infected ($n = 21$; open squares) or vaccinated ($n = 29$; open circles) are plotted. The relation between the two variables was analyzed with a nonlinear regression model using a four-parameter slope. The result of Spearman correlation test is shown on the graph. The pie charts represent the proportion of patients with (white) anti-RBD IgG among those with or without neutralizing humoral response. (E) Results for the 14 patients from the epidemiological cohort, who developed COVID-19 after vaccination, are plotted. Dotted lines indicate the threshold of positivity of each assay. Mann-Whitney tests were used to compare antibody or neutralizing titers in (A) to (C), and Fisher's exact test was used to compare proportions in (A) to (D); $*P \leq 0.05$ and $****P < 0.0001$.

titer and the result of the in vitro neutralization assay was demonstrated (Fig. 3D). In contrast with recently infected patients, the humoral response of the vaccinated group against RBD was heterogeneous, and most patients (17 of 29, 59%) failed to generate detectable anti-RBD IgG after two doses of vaccine (Fig. 3B). This defect was even more clear in the context of a pseudo-virus neutralization assay, in which only 21% of vaccinated patients had neutralizing antibody response against the pseudo-virus (6 of 29; Fig. 3C).

These findings led us to hypothesize that the lack of protection against COVID-19 in some vaccinated transplant recipients may be due to insufficient generation of neutralizing anti-RBD antibodies. To test this theory, we retrieved the 14 available serum samples collected after the two doses of mRNA-1273 but before COVID-19 diagnosis for the vaccinated patients of the epidemiological cohort. In line with our hypothesis, only 2 of 14 (14%) patients had detectable circulating anti-RBD IgG antibodies after the standard scheme of vaccination and none of these serum samples were able to block

the entry of pseudo-virus in human cells in vitro (Fig. 3E). Thus, the 29 vaccinated transplant recipients were distributed into the group "responder" ($n = 6$ of 29, 21%) or "nonresponder" ($n = 23$ of 29, 79%) to vaccine according to whether or not serum collected after two doses of mRNA-1273 vaccine showed neutralizing capacity against pseudo-virus in vitro. Clinical and biological characteristics of these two groups are similar and presented in Table 1.

Generation of neutralizing antibodies after vaccination is associated with evidence of germinal center-derived B cell responses

The immunologic dogma has long held that the generation of IgG against protein antigen was dependent upon complex interactions between antigen-specific B cells and cognate CD4^+ T follicular helper (T_{FH}) cells that take place in specialized structures of secondary lymphoid organs called germinal centers (36, 37). However, this has been challenged by a number of studies (38–41). It is now clear that IgG can be generated during extrafollicular responses (which are sometimes independent of T cells).

To characterize where IgG response to COVID-19 mRNA vaccine develops, RBD-specific B cells were enumerated in the circulation of vaccinated patients and their expression of CD21, CD11c, CD27, and IgD was determined by flow cytometry (Fig. 4, A to C). Previous studies have demonstrated that the extrafollicular differentiation pathway generates an atypical population of antigen-experienced B cells that is referred to as type 2 double-negative ($\text{IgD}^- \text{CD27}^-$). The latter is characterized by high expression of CD11c and low to negative expression of CD21 (42, 43). As such, they differ from their conventional germinal center-derived counterparts, which are mostly CD27^+ . As expected, RBD-specific B cells were found in both higher proportion and number in the circulation of responders than non-responders to vaccine (Fig. 4B). B cells expressing a germinal center-associated phenotype represented the vast majority (about 90%) of RBD-specific B cells in the circulation of responders to vaccine (Fig. 4C). Furthermore, their number correlated well with both the anti-RBD IgG titers (Fig. 4D) and the in vitro viral neutralization capacity of their serum (Fig. 4E).

Generation of neutralizing antibodies after vaccination is associated with circulating spike protein-specific T_{FH} cells

Because the humoral response to SARS-CoV-2 correlated with abundance of B cells expressing a germinal center-associated phenotype,

Table 1. Characteristics of vaccinated patients. IQR, interquartile range; BMI, body mass index; NA, not available; CNl, calcineurin inhibitor; MMF/MPA, mycophenolate mofetil/mycophenolic acid; imTOR, inhibitor of the mechanistic target of rapamycin; CRP, C-reactive protein.

n (%) or median [IQR]	Nonresponders	Responders	P*
	N = 23	N = 6	
Age (years)	61.2 [45.8; 70.1]	47.7 [41.2; 61.7]	0.254
Male	14 (61)	4 (67)	>0.999
BMI	24.9 [23.8; 29.4]	23.8 [20.2; 24.5]	0.138
Comorbidities			
Cardiopathy	15 (65)	6 (100)	0.138
Diabetes	3 (13)	0 (0)	>0.999
Time since transplantation (years)	7.0 [1.6; 15.9]	10.4 [3.5; 24.6]	0.414
Donor type			
Deceased	20 (87)	5 (83)	
Living	3 (13)	1 (17)	
Induction therapy			
Anti-thymocyte globulins	13 (57)	4 (67)	0.453
Basiliximab	8 (35)	1 (17)	
No induction	1 (4)	1 (17)	
NA	1 (4)	0 (0)	
Maintenance immunosuppression			
CNl (yes)	22 (96)	6 (100)	>0.999
MMF/MPA (mg/day)	1000 [500; 1000]	250 [0; 625]	0.014
Steroids (mg/day)	5.0 [0.0; 5.0]	2.5 [0.0; 5.0]	0.358
imTOR (yes)	1 (4)	2 (33)	0.100
Belatacept (yes)	1 (4)	0 (0)	>0.999
Biological data			
Lymphocytes (G/liter)	1.16 [0.99; 1.38]	1.99 [1.45; 2.66]	0.069
Monocytes (G/liter)	0.55 [0.41; 0.79]	0.51 [0.44; 0.70]	0.723
CRP (mg/liter)	4.0 [4.0; 5.8]	4.5 [4; 10.6]	0.570
Albumin (g/liter)	43 [42; 46]	44 [43; 45]	0.874
Creatinine (μ M)	134 [97; 183]	131 [97; 237]	0.859

*Qualitative variables were compared using a Fisher or chi-square test, and quantitative variables were compared using a Mann-Whitney test.

we speculated that a T_{FH} defect may be contributing to the lack of generation of neutralizing antibodies observed in some vaccinated transplant recipients, a hypothesis justified by the detrimental impact of maintenance immunosuppression on T_{FH} functions (9, 36, 44). Although T_{FH} cells act within germinal centers in secondary lymphoid organs, recent studies have demonstrated that human blood $CXCR5^+CD4^+$ T cells are counterparts of T_{FH} . This population contains specific subsets that differentially support antibody secretion and can be identified on the basis of their profile of chemokine receptor expression (45). In line with these studies, the three subsets of T_{FH} , T_{FH1} ($CXCR3^+CCR6^-$), T_{FH2} ($CXCR3^-CCR6^-$), and T_{FH17} ($CXCR3^-CCR6^+$) could be identified and enumerated by flow cytometry in the circulation of vaccinated patients (Fig. 5A). No difference was observed regarding the total count of $CD4^+$ T cells, T_{FH} , or any of the T_{FH} subsets between responders and nonresponders (Fig. 5B). However, in line with our hypothesis, all subsets of spike protein-specific $CD4^+$ T cells were found in higher quantity in the

circulation of responders than nonresponders (Fig. 5, C and D). Moreover, a positive correlation between the total number of spike protein-specific T_{FH} and the neutralizing capacity of the sera was observed (Fig. 5E). This observation remained true when subanalyses were conducted separately with the three different subsets of T_{FH} (fig. S1). Last, a strong positive correlation was also observed between the number of germinal center-derived RBD-specific B cells and that of cognate T_{FH} cells (Fig. 5F), further emphasizing the importance of bidirectional interactions between these partners within the germinal center for an efficient response to SARS-CoV-2 vaccine.

High mycophenolate mofetil dose was associated with reduced vaccine response in vaccine recipients

The dynamic of germinal center reactions, in which antigen-specific B and T cells proliferate, is the major determinant controlling the humoral immune response after vaccination against SARS-CoV-2 in healthy volunteers (46, 47). The reduced count in both spike

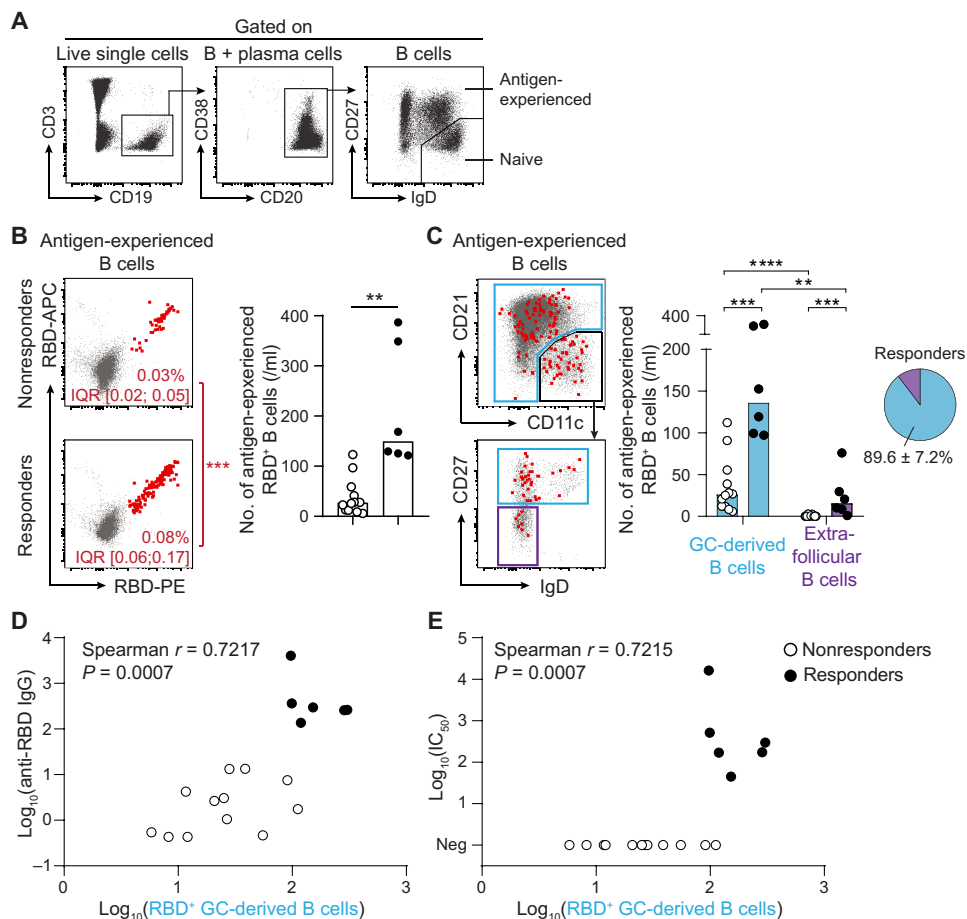


Fig. 4. Generation of neutralizing IgG antibodies after vaccination is associated with evidence of a germinal center reaction. (A) Gating strategy used for flow cytometry analysis of RBD-specific B cell response. (B) RBD-specific cells were enumerated among antigen-experienced B cells in the circulation of vaccinated renal transplant recipients. Left: Concatenated flow cytometry profiles of nonresponders (upper thumbnail) and responders (lower thumbnail) to vaccine. Median percentage and IQR are indicated. Proportions of RBD-specific B cells were compared. Right: The numbers of RBD-specific antigen-experienced B cells of nonresponders ($n = 12$; open circles) and responders ($n = 6$; black circles) were compared. (C) The site in which the humoral response against the vaccine developed was indirectly analyzed on the basis of the phenotype of RBD-specific B cells. Extrafollicular responses are characterized by the generation of type 2 double-negative ($CD11c^{high} CD21^{low} IgD^{+} CD27^{-}$) B cells (purple gate). The rest of antigen-experienced B cells (blue gates) are thought to be derived from the germinal center. Left: Concatenated flow cytometry profiles of all vaccinated patients, together with the gating strategy used for analysis. Right: Bar graphs (left) show the number of RBD-specific antigen-experienced B cells likely derived from germinal centers (GC; blue) or extrafollicular (purple) responses for nonresponders ($n = 12$; open circles) and responders ($n = 6$; black circles) to vaccine. The proportions of RBD-specific antigen-experienced B cells derived from germinal center and extrafollicular responses in responders to vaccine are shown in the pie chart (right). Data in (B) and (C) were analyzed using a Mann-Whitney test. $**P < 0.01$; $***P < 0.001$; $****P < 0.0001$. (D and E) Correlation between the number of germinal center–derived RBD-specific antigen-experienced B cells and the titer of anti-RBD IgG (D) or the viral neutralization capacity of the serum (E). The results of Spearman correlation test are shown on the graphs.

protein-specific B and T_{FH} cells observed in nonresponders to vaccine therefore provides a potential explanation for the defect of generation of anti-RBD IgG and, in turn, the lack of viral neutralization capacity of their serum. We next asked what distinguished nonresponders from responders in our vaccinated cohort. Among the immunosuppressive drugs used in maintenance regimen, some block the activation of T cells (calcineurin inhibitor), whereas others, such as mycophenolate mofetil, act by blocking the proliferation of adaptive immune effectors. Although responders and nonresponders to vaccine were similarly exposed to calcineurin inhibitors, nonresponders

received significantly more mycophenolate mofetil (250 mg/day, IQR [0; 625] versus 1000 mg/day, IQR [500; 1000] in responders versus nonresponders; $P = 0.014$; Fig. 6A).

This result suggests that the antiproliferative effect of high-dose mycophenolate mofetil may impede germinal center reaction and thereby be the cause of the lack of response after two doses of mRNA-1273 vaccine observed in some transplant recipients. However, despite the fact that recently infected patients received the same (high) dose of mycophenolate mofetil at the time of infection as nonresponders to vaccine (Fig. 6A), they generated higher numbers of virus-specific germinal center–derived B cells (Fig. 6B) and T_{FH} (Fig. 6C), and consequently neutralizing anti-RBD IgG antibodies, as do responders to vaccine (Fig. 6, D and E).

A third dose of mRNA vaccine improved neutralizing anti-RBD IgG responses in a subset of prior vaccine nonresponders

Our last observation led us to ask whether the potential negative impact of high-dose mycophenolate mofetil could be overcome by further immunogenic stimulation than the standard vaccination scheme, such as the one provided to the patients by infection with live virus. In line with this hypothesis, vaccinated patients without neutralizing anti-RBD IgG after two doses of mRNA-1273 did generate neutralizing anti-RBD IgG after infection (Fig. 7, A and B). On the basis of these results, we tested the impact of an additional dose of vaccine on the humoral response of 17 of the 23 transplant patients that were nonresponders to the standard two-dose vaccine regimen for mRNA-1273. In accordance with our hypothesis, not only we observed an increase in anti-RBD IgG titers after the third dose of vaccine (Fig. 7C) but also 41% of the serum

samples (7/17) efficiently block pseudo-virus entry in human cells in vitro (Fig. 7D).

We next validated these findings in an independent, external cohort. A third dose of the other currently approved mRNA SARS-CoV-2 vaccine (BNT162b2) was administered to a cohort of 62 renal transplant recipients from Lyon University Hospital that did not have neutralizing anti-RBD IgG after two doses of vaccine. In accordance with our previous results with mRNA-1273, we observed a similar increase in anti-RBD IgG titers in these nonresponders after the third dose of vaccine (Fig. 7E), and serum from 39% (24 of 62)

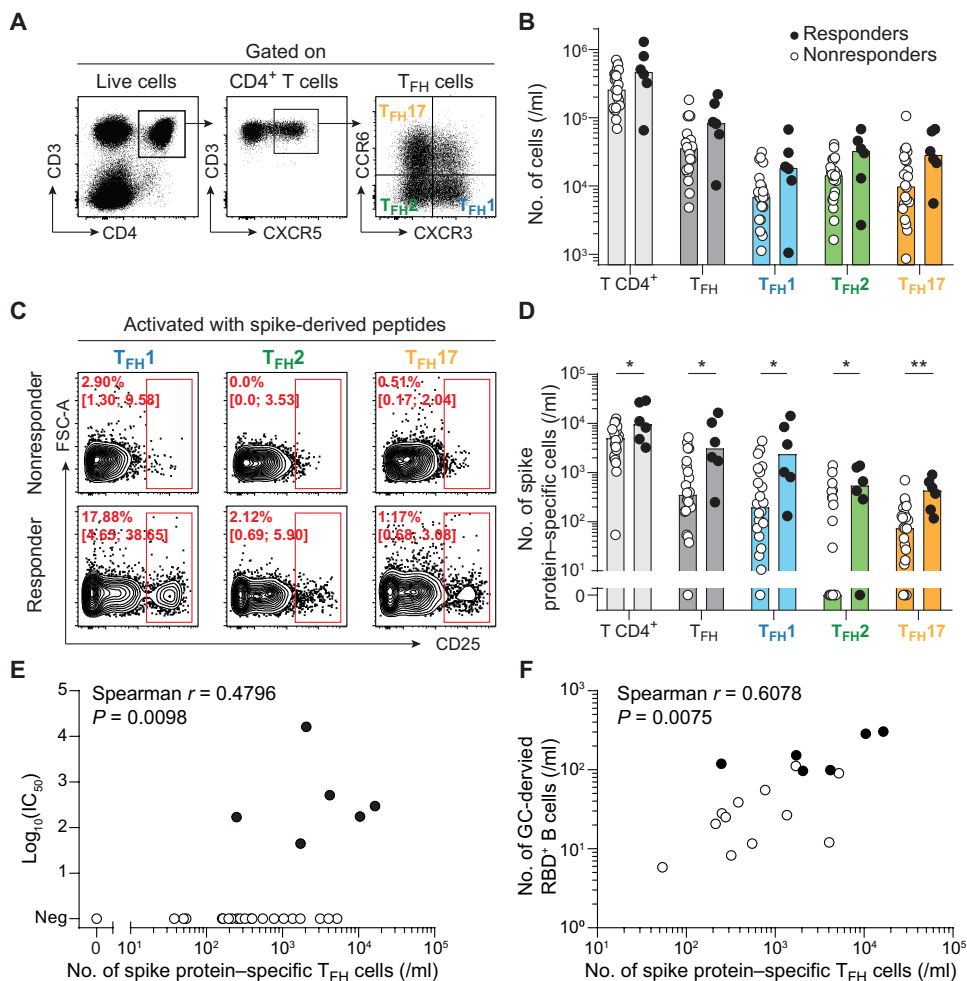


Fig. 5. Generation of neutralizing antibodies after vaccination correlates with the number of spike protein-specific T_{FH} cells. Follicular helper T (T_{FH}) cells were enumerated in the circulation of responders ($n = 6$; black circles) and nonresponders ($n = 22$; open circles) after two doses of SARS-CoV-2 mRNA vaccine. (A) Representative flow cytometry profiles with the gating strategy used to identify the three subsets of T_{FH} cells: T_{FH1} (blue), T_{FH2} (green), and T_{FH17} (orange). (B) The counts of circulating $CD4^+$ T cell subsets are plotted for each patient. (C and D) Spike protein-specific cells were enumerated among each $CD4^+$ T cell subset for each vaccinated patient. Data were background-subtracted against a DMSO-only negative control. (C) Representative flow cytometry profiles of nonresponders (upper row) and responders (lower row). Median percentage and IQR are indicated. (D) The counts of circulating spike protein-specific $CD4^+$ T cell subsets are plotted for each patient. Bars indicate median values. Data in (D) were compared using Mann-Whitney tests. * $P < 0.05$; ** $P < 0.01$. (E) Correlation between the number of spike protein-specific T_{FH} cells and viral neutralization capacity of the serum. The result of Spearman correlation test is shown on the graph. (F) Correlation between the number of spike protein-specific T_{FH} cells and germinal center-derived RBD-specific antigen-experienced B cells. The result of Spearman correlation test is shown on the graph.

of recipients efficiently blocked pseudo-virus entry in human cells in vitro (Fig. 7F).

DISCUSSION

Although antibody titers and their ability to neutralize the virus are emerging as correlates of protection against COVID-19 in healthy individuals (48–50), there is still an urgent need to understand the relative contribution of humoral and T cell immunity in conferring protection to immunosuppressed populations (18), in particular transplant patients, who are both at high risk of death due to COVID-19 (3–7) and poor responders to mRNA vaccines (11–14, 51).

Taking advantage of the observation that a previous infection by SARS-CoV-2, but not the standard two-dose scheme of vaccination, provided protection against symptomatic COVID-19 to transplant recipients, we designed a translational study to compare the adaptive immune responses of these two groups of patients. The results of this study suggest that germinal center-derived anti-SARS-CoV-2-neutralizing IgG may be a critical component of the adaptive immune response associated with protection against symptomatic COVID-19 in transplant recipients. Our data also suggest that the negative impact of mycophenolate mofetil on response to vaccine may be overcome by increasing antigen exposure with a third dose.

Newer studies have challenged a long-standing dogma in immunology, which considered switched antibodies directed against protein antigens (such as spike protein) a hallmark of germinal center reactions. For example, recent experimental works have demonstrated that T cell-independent IgG class switching can also occur, in particular against certain outer membrane proteins of pathogens (39, 40). Additional studies have shown that, during T cell-dependent humoral response, IgG class switching is triggered before differentiation into germinal center B cells (38). Last, it has been demonstrated that IgG class switching can also take place during an extrafollicular (and thus germinal center-independent) differentiation pathway that is promoted by inflammatory conditions (41), including in the particular setting of severe COVID-19 (52). Our observation that the generation of virus-neutralizing IgG in responders to vaccination correlated with both the number of antigen-specific germinal center B cells and T_{FH} cells may indicate that the

response to SARS-CoV-2 mRNA vaccine requires germinal center reactions in renal transplant recipients, as has been recently reported for immunocompetent healthy volunteers (46).

Interestingly, serum neutralization capacity and antigen-specific germinal center B cells after vaccination correlate not only with the number of antigen-specific T_{FH1} cells, the subset predominantly produced after vaccination in healthy participants (53, 54), but also with the two other T_{FH} subsets (T_{FH2} and T_{FH17}). These populations are thought to be the most efficient to drive antibody generation (9, 45). This latter finding, which conflicts with the negative correlation recently reported after infection between the number of T_{FH17} cells and the neutralizing antibody response (55), could

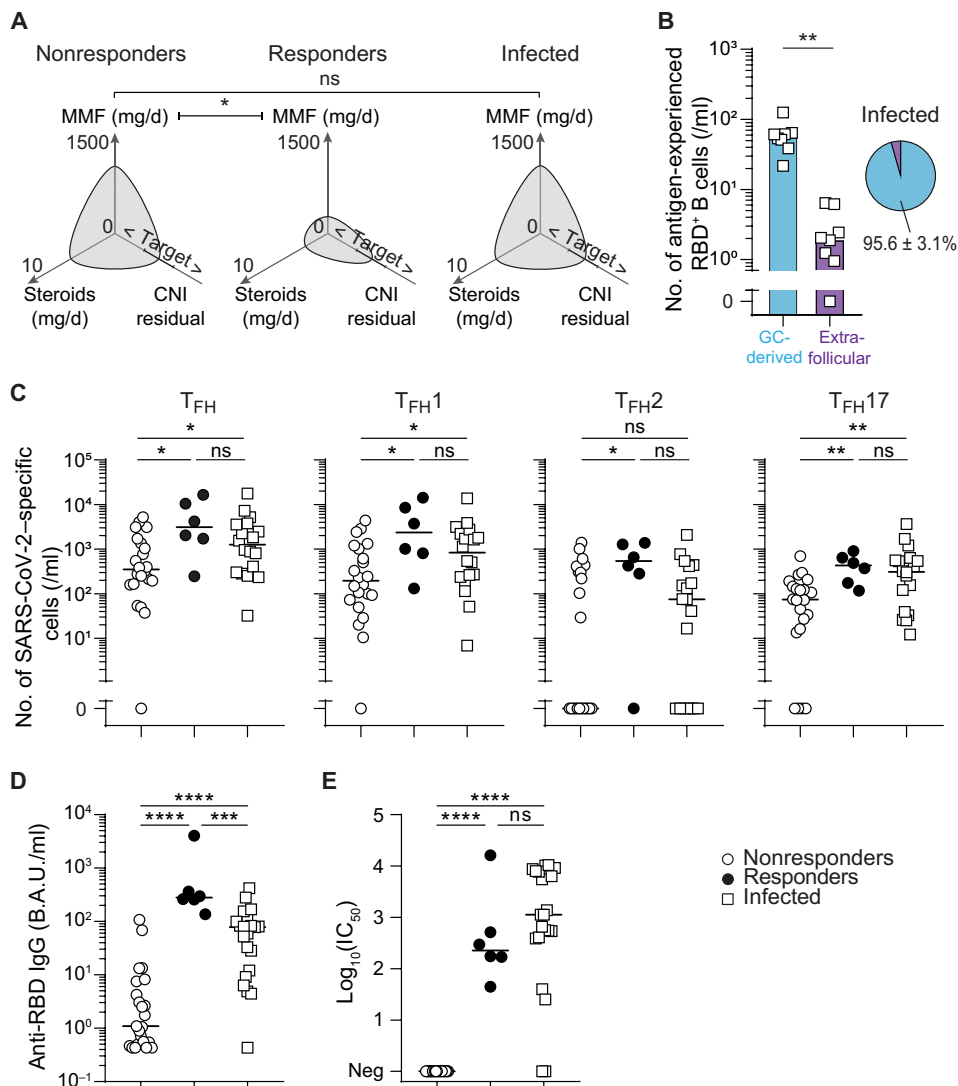


Fig. 6. High mycophenolate mofetil dose was associated with evidence of poorer vaccination-induced germinal center reactions. (A) Polar plots were used to compare maintenance immunosuppression regimens for nonresponders ($n = 23$; left) and responders ($n = 6$; middle) to two doses of SARS-CoV-2 mRNA vaccine, and patients previously infected with SARS-CoV-2 ($n = 21$; right). Median values are plotted. MMF, mycophenolate mofetil; CNI, calcineurin inhibitor. Target indicates the target residual blood concentration of calcineurin inhibitor. < and > symbols indicate residual blood concentrations of calcineurin inhibitor below or above the target, respectively. (B) The bar graph (left) shows the number of RBD-specific antigen-experienced B cells thought to be derived from germinal center (blue) and extra-follicular (purple) responses of each recently infected patient ($n = 8$; open squares). The proportions of RBD-specific antigen-experienced B cells likely derived from germinal center and extrafollicular responses in recently infected patients are shown in the pie chart (right). (C) SARS-CoV-2-specific T_{FH} subsets were enumerated in the circulation of nonresponders ($n = 22$; open circles) and responders ($n = 6$; black circles) to two doses of SARS-CoV-2 mRNA vaccine, as well as for patients recently infected with SARS-CoV-2 ($n = 18$; open squares). (D) The titers of anti-RBD antibodies were measured in the circulation for nonresponders ($n = 23$; open circles) and responders ($n = 6$; black circles) to two doses of SARS-CoV-2 mRNA vaccine, as well as for patients recently infected with SARS-CoV-2 ($n = 21$; open squares). (E) The neutralizing capacity of patients' serum was compared for nonresponders ($n = 23$; open circles) and responders ($n = 6$; black circles) to two doses of SARS-CoV-2 mRNA vaccine, as well as for patients recently infected with SARS-CoV-2 ($n = 21$; open squares). Neutralizing titers are presented as $\log_{10}(IC_{50})$. Bars indicate the median. Data were analyzed by Mann-Whitney tests; ns, $P > 0.05$; * $P \leq 0.05$; *** $P < 0.01$; **** $P < 0.001$; ***** $P < 0.0001$.

indicate that efficient germinal center response to infection and vaccination requires different T_{FH} subpopulations.

It is not clear what factors impair germinal center reaction in nonresponders to SARS-CoV-2 mRNA vaccine. We observed that

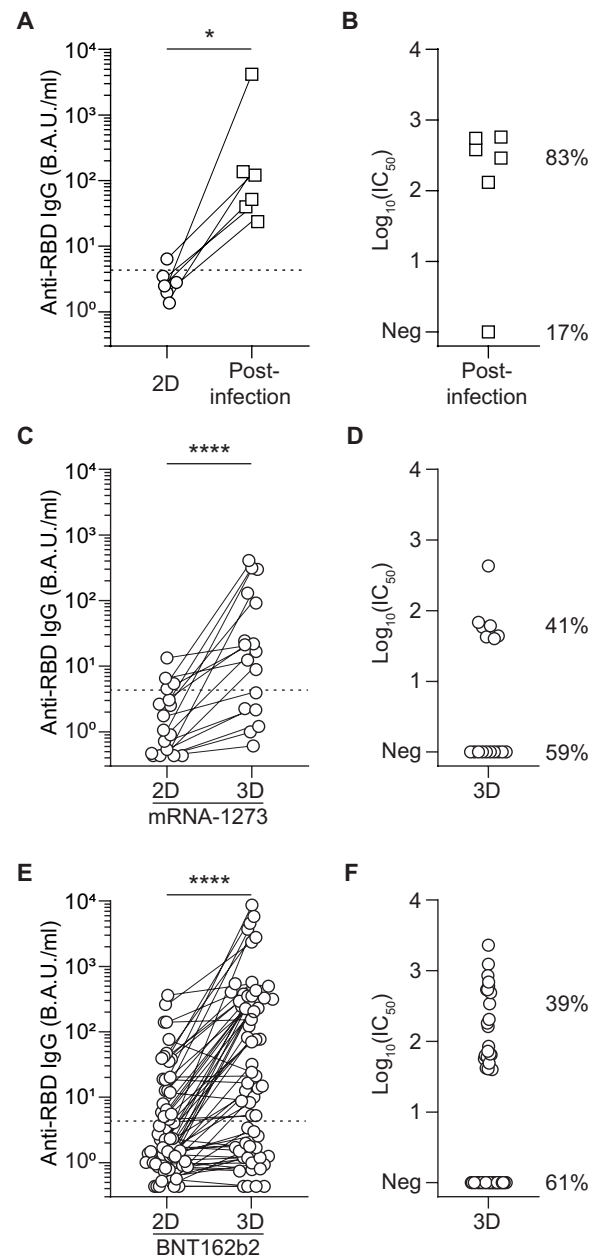
transplant patients without viral neutralizing IgG after two doses of vaccine were exposed to a higher dose of mycophenolate mofetil, an immunosuppressive drug that acts by blocking proliferation of activated B and T lymphocytes (56, 57). This observation is supported by other independent studies, which have also reported an association between exposition to mycophenolate mofetil and lower antibody responses (44, 58, 59), including to SARS-CoV-2 vaccines (11, 14). On the basis of these findings, it is tempting to speculate that a reduction (or suspension) of the maintenance dose of mycophenolate mofetil before vaccination might help obtain better response rates. On the other hand, this non-antigen-specific attitude might increase the risk of generation of donor-specific antibodies (9), which is the first cause of late allograft loss (60) through accelerated chronic vascular rejection (61, 62).

On the basis of the observation that recently infected patients successfully generated viral neutralizing IgG despite a high dose of mycophenolate mofetil, similar to that of nonresponders, we hypothesized that an additional exposure to viral antigen in the form of a third dose of vaccine could improve a patient's protection without requiring the reduction of maintenance immunosuppression. In line with this hypothesis, administration of a third dose of mRNA vaccine resulted in the generation of neutralizing anti-RBD IgG in about 40% of individuals who did not respond to the standard two-dose course of vaccination. This result was further validated in a larger independent prospective cohort with the other approved SARS-CoV-2 mRNA vaccines and has been reported by independent groups (15, 63–66). Furthermore, our group recently reported that a fourth dose of an mRNA-based vaccine produces a satisfactory antibody response in some kidney transplant recipients who did not respond adequately after three previous doses (67).

In addition to increasing the number of vaccinations, another possibility to increase vaccine immunogenicity is to increase the amount of antigen provided

in each dose. This strategy has been successfully tested in transplant recipients with protein-based vaccines against influenza (68, 69). In this regard, note that several studies have already reported higher antibody titers in healthy patients vaccinated with

Fig. 7. Infection after vaccination or a third dose of mRNA vaccination improves SARS-CoV-2-specific antibody responses. (A) Anti-RBD IgG titers were measured before and after SARS-CoV-2 infection in individuals who received two doses (2D) of mRNA vaccine ($n = 6$). (B) Virus neutralization capacity of the serum was measured after SARS-CoV-2 infection in transplant recipients who did not respond to two doses of mRNA vaccine ($n = 6$). Percentages indicate the fraction of individuals with (83%) or without (17%) measurable neutralizing titers after two doses of vaccine and SARS-CoV-2 infection. (C) A discovery cohort (mRNA-1273 vaccine; $n = 17$) was used to compare anti-RBD IgG titers after the second (2D) and third (3D) dose of mRNA vaccine in those who were nonresponders after two doses of mRNA-1273 vaccine. (D) Virus neutralization capacity of the patients' serum was measured after the third dose ($n = 17$). Percentages indicate the fraction of individuals with (41%) or without (59%) measurable neutralizing titers after three doses of mRNA-1273 vaccine. (E) An external validation cohort (BNT162b2 vaccine; $n = 62$) was used to compare anti-RBD IgG titers after the second (2D) and third (3D) dose of mRNA vaccine in those who were nonresponders to two doses of BNT162b2 mRNA vaccine. (F) Virus neutralization capacity of the patients' serum was measured after the third dose ($n = 62$). Percentages indicate the fraction of individuals with (39%) or without (61%) measurable neutralizing titers after three doses of BNT162b2 vaccine. Wilcoxon test, $*P < 0.05$ and $****P < 0.0001$.



mRNA-1273 (which contains 100 μg of mRNA) than in those that received BNT162b2 (30 μg of mRNA) (70), although whether one vaccine is more effective than the other in this cohort remains to be evaluated.

The process of adapting vaccination regimens has limits. A fraction of transplanted patients will likely not be able to generate an efficient antibody response whatever the vaccination scheme. In this cohort, protection against COVID-19 might depend on infusion of cocktails of therapeutic or prophylactic monoclonal antibodies (mAbs). This primary prevention strategy has been successfully tested in people with household exposure to SARS-CoV-2 with the combination of casirivimab and imdevimab (REGEN-COV) (71). In this study, mAb infusion reduced the risk of developing symptomatic and asymptomatic COVID-19 and also reduced the duration of symptoms. Further studies evaluating this strategy of passive immunization in organ transplant recipients are essential to protecting this at-risk population.

This study has several limitations. First, only a limited number of patients were enrolled ($n = 50$), the immune response of whom was analyzed at only a single time point. Second, the impact of vaccination or infection on the various immune cell subsets was analyzed in peripheral blood instead of the secondary lymphoid organs (spleen and lymph nodes), where immune responses actually develop. This limitation made it impossible to directly evaluate the formation of germinal centers in responders to vaccines and during mild-to-moderate COVID-19 disease. Third, these data were collected before the emergence of the omicron variant, which is currently the dominant circulating variant of concern. Last, we did not directly test the hypothesis that stopping mycophenolate mofetil would allow for better expansion of antigen-specific B and T cells and thereby an improved response rate to vaccination. Thus, future studies to investigate causal relationships between these parameters are needed.

In conclusion, our study suggests that the protection of renal transplant recipients against severe COVID-19 depends upon the

germinal center-dependent generation of virus-neutralizing IgG antibodies. In contrast with SARS-CoV-2 infection, which efficiently drives protective humoral response, the standard two-dose regimen of mRNA vaccine might be insufficient in some transplant patients treated with immunosuppressive drugs. Thus, these patients may require additional booster dose(s) of mRNA vaccine.

MATERIALS AND METHODS

Study design

A monocentric epidemiological cohort of kidney transplant patients was used to retrospectively compare the incidence of symptomatic

SARS-CoV-2 infections in patients vaccinated against SARS-CoV-2 with two doses of mRNA vaccine versus patients with a previous history of COVID-19. A cohort of 50 patients (21 recently infected and 29 vaccinated, COVATRHUS cohort) was extracted from this initial cohort for in-depth retrospective analysis of their cellular and humoral immune responses against SARS-CoV-2. The impact of a third dose of mRNA vaccine was first evaluated in the nonresponders of COVATRHUS cohort ($n = 23$) and then in an external validation cohort ($n = 62$) in a prospective observational study.

Characteristics of study populations

The incidence of SARS-CoV-2 infections was monitored since the beginning of the pandemic, in the entire cohort of kidney transplant recipients at the University Hospital of Strasbourg, France, and compared between patients with a previous history of COVID-19 and those who received the two doses of mRNA-1273. The follow-up started at the time of COVID-19 symptom onset for the infected patients. For vaccinated transplant recipients, because the protection conferred by mRNA vaccine is operant as early as 12 days after the first injection in the general population (72), the follow-up started at the date of the second dose of vaccine. The Kaplan-Meier method was used to compare COVID-19 incidence in the two populations. Data were censored at either date of death or 10 October 2021. Furthermore, to ensure the accuracy of the comparison, infected patients who did not develop reinfection before immunization were censored at the time of their first mRNA vaccine injection. Also, because in France a systematic third vaccine dose was proposed to all transplant recipients from April 11th onward, vaccinated patients who did not develop COVID-19 before their third dose of vaccine were censored at the time of the third vaccine injection.

The COVATRHUS cohort was used to analyze immune mechanisms involved in protection against COVID-19. Twenty-nine patients, naive for SARS-CoV-2 infection, were prospectively recruited from the cohort of kidney transplant recipients of the University Hospital of Strasbourg. According to the recommendations of the French health authority, they received two doses of mRNA-1273 (Moderna) SARS-CoV-2 vaccine. A third vaccine injection of mRNA-1273 SARS-CoV-2 vaccine was offered to all patients who did not develop viral neutralizing IgG after the second dose.

Vaccinated patients were compared to 21 patients retrospectively recruited among adult kidney transplant recipients of the University Hospital of Strasbourg, who were diagnosed with COVID-19 between 1 November 2020 and 31 January 2021. The diagnosis of COVID-19 was based on positive testing of nasopharyngeal swabs by reverse transcription PCR (RT-PCR). The study protocol complied with the tenets of the Helsinki Declaration and was approved by the Institutional Review Board (approval number: 18/21 03, Comité de Protection des Personnes Ouest IV Nantes) and registered on clinicaltrials.gov as NCT04757883. Clinical, demographic, and laboratory data were collected at the time of the first vaccine injection or at the time of the COVID-19 diagnosis. Severity of COVID-19 was graded as asymptomatic, mild, moderate, severe, critical, or death following the first WHO recommendations dated 27 May 2020. The immune response after vaccination or infection was assessed at day 14 after the second dose of vaccine or 1 month after symptom onset, respectively.

An external validation cohort consisted of nonresponders to two doses of BNT162b2 vaccine (Pfizer-BioNtech). These individuals were part of a cohort of kidney transplant recipients of

Lyon University Hospital, France. The study protocol was approved by the local Institutional Review Board (approval number: 2020-A02918-31).

Assessment of cellular immune responses directed against SARS-CoV-2

PBMCs were collected and isolated by centrifugation on a Ficoll density gradient. The cells were then frozen in fetal calf serum supplemented with 10% dimethyl sulfoxide (DMSO; Sigma-Aldrich). SARS-CoV-2-specific CD8⁺ T cells and CD4⁺ T cells were identified as previously described (9, 28). Briefly, after thawing, cells were concentrated at 10⁷ cells/ml in complete medium [RPMI 1640 GlutaMAX medium (Invitrogen) supplemented with 10% fetal calf serum, 25 mM Hepes (Invitrogen), and penicillin/streptomycin (10 U/ml; Invitrogen)] and left to rest overnight at 37°C and 5% CO₂ in a 96-well round-bottom plate at 10⁶ cells per well. The next day, the RPMI 1640 medium was changed, and the cells were cultured for 24 hours in the presence of peptide pools derived from the viral spike, nucleocapsid, and membrane proteins (PepMix, JPT Peptides Technologies GmbH). The pools contained overlapping peptides covering the entire sequence of the indicated viral protein antigens. The final concentration of the peptides was 1 µg/ml. Cells cultured with DMSO (Sigma-Aldrich) alone (1:250) were used as negative controls. Cells were then rinsed and incubated at room temperature with the relevant fluorescent antibodies for 30 min: CD3 (UHCT1, Brilliant Violet 421, dilution 1:80, BD Biosciences, catalog no. 562426, RRID: AB_11152082), CD8 [SK1, allophycocyanin (APC)-H7, dilution 1:80, BD Biosciences, catalog no. 560179, RRID: AB_1645481], CXCR3 (1C6, Alexa Fluor 488, dilution 1:10, BD Biosciences, catalog no. 558047, RRID: AB_397008), CXCR5 (RF8B2, Alexa Fluor 647, dilution 1:80, BD Biosciences, catalog no. 558113, RRID: AB_2737606), CCR6 [11A9, phycoerythrin (PE)-cyanine (Cy) 7, dilution 1:80, BD Biosciences, catalog no. 560620, RRID: AB_1727440], CD25 (2A3, PE, dilution 1:50, BD Biosciences, catalog no. 341011, RRID: AB_2783790), CD4 [SK3, peridinin-chlorophyll-protein (PerCP)-Cy5.5, dilution 1:20, BD Biosciences, catalog no. 332772, RRID: AB_2868621, or Alexa Fluor 488, dilution 1:10, BioLegend, catalog no. 344604, RRID: AB_1937227], CD69 (FN50, PE/Dazzle 594, dilution 1:150, BioLegend, catalog no. 310942, RRID: AB_2564277), CD137 (4B4-1, Alexa Fluor 647, dilution 1:20, BioLegend, catalog no. 309824, RRID: AB_2566258), and a Fixable Viability Dye (eBioscience, eFluor 510, dilution 1:500). Cells were fixed with 2% methanol-free formaldehyde.

For IFN-γ staining, surface antigen-stained cells were incubated for 30 min at 4°C in Fixation/Permeabilization buffer (Foxp3/Transcription Factor Staining Buffer Set from eBioscience). The cells were then rinsed and incubated with anti-IFN-γ fluorescent antibody (4S.B3, PE, dilution 1:10, BD Biosciences, catalog no. 554552, RRID: AB_395474) in the permeabilization buffer according to manufacturer instructions. Of note, these experiments were performed without brefeldin A. Samples were acquired on a BD LSR Fortessa 4L flow cytometer (BD Biosciences).

Assessment of humoral immune responses directed against SARS-CoV-2

IgGs directed against the receptor-binding domain (anti-RBD IgG) of the spike glycoprotein of the SARS-CoV-2 were detected by a chemiluminescence technique, using the Maglumi SARS-CoV-2S-RBD IgG test (Snibe Diagnostic) on a Maglumi 2000 analyzer

(Snibe Diagnostic), according to the manufacturer's instructions. This test displays clinical sensitivity and specificity of 100 and 99.6%, respectively. Following WHO recommendation (73), titers are expressed as binding antibody units per milliliter (BAU/ml); the correction factor for Maglumi was 4.33.

The Abbott anti-nucleocapsid (N) IgG assay is an automated chemiluminescence microparticle immunoassay (CMIA) conducted and interpreted according to manufacturer guidelines. A sample-to-calibrator relative light unit index of ≥ 1.4 is considered positive, an index of ≥ 0.49 to < 1.40 is considered borderline, and an index of < 0.49 is considered negative. This CMIA displays clinical sensitivity and specificity of 96.5 and 99.2%, respectively (74).

Neutralization assays were performed as follows: 3×10^4 293T-ACE2 (provided by O. Schwartz laboratory, Institut Pasteur) were plated in 96-well plates. Serum samples were sequentially diluted and incubated with D614G spike-pseudotyped lentiviral particles (provided by Rossolillo laboratory, Institut de Génétique et de Biologie Moléculaire et Cellulaire) for 1 hour at 37°C. The mixes were then added to cells. After 72 hours, the intracellular luciferase signal was measured with Bright-Glo luciferase assay system using a luminescence Counter MicroBetaTriLux 1450LSC (PerkinElmer). The percentage of neutralization was calculated as follows: $100 \times (1 - (\text{mean}(\text{luciferase signal in sample duplicate}) / (\text{mean}(\text{luciferase signal in virus alone}))))$. The results are reported as the \log_{10} of the dilutions that inhibit 50% of the infection of the targets [$\log_{10}(\text{IC}_{50})$].

SARS-CoV-2 RBD-specific B cells were identified as previously reported (75). Briefly, biotinylated recombinant RBD domain of SARS-CoV-2 RBD (Miltenyi Biotec) was tetramerized with either streptavidin-PE (BD Biosciences) or streptavidin-APC (BioLegend). Cryopreserved PBMCs were centrifuged, suspended in PEB buffer (phosphate-buffered saline plus 0.5% bovine serum albumin and 2 mM EDTA), and incubated with Fc receptor block (Miltenyi Biotec) for 15 min at 4°C (dilution 1:10). Next, cells were washed in PEB and stained for 30 min in brilliant stain buffer at 4°C in the dark using the following antibodies: anti-CD3 (clone SK7, APC-Fire810, dilution 1:25, BioLegend, catalog no. 344858, RRID: AB_2860895), anti-CD11c (clone 3.9, Brilliant Violet 785, dilution 1:20, BioLegend, catalog no. 301644, RRID: AB_2565779), anti-IgD (clone IA6-2, Brilliant Violet 605, dilution 1:50, BioLegend, catalog no. 348232, RRID: AB_2563337), anti-CD19 (clone LT19, PE-Vio770, dilution 1:50, Miltenyi Biotec, catalog no. 130-113-170, RRID: AB_2733209), anti-CD27 (clone M-T271, PerCP-Vio700, dilution 1:50, Miltenyi Biotec, catalog no. 130-113-632, RRID: AB_2784096), anti-CD38 (clone REA572, VioBright fluorescein isothiocyanate, dilution 1:25, Miltenyi Biotec, catalog no. 130-113-433, RRID: AB_2726165), anti-CD20 (clone 2H7, Brilliant Violet 421, dilution 1:25, BD Biosciences, catalog no. 562873, RRID: AB_2737857), and anti-CD21 (clone B-ly4, Brilliant Ultra-Violet 496, dilution 1:100, BD Biosciences, catalog no. 750614, RRID: AB_2874746), together with both PE- and APC-conjugated recombinant RBD tetramers. Cells were washed in PEB and resuspended in a PEB dilution (1:500) of the fixable viability dye eFluor 780 (eBioscience, eFluor 780, dilution 1:500). They were next washed and fixed at 4% paraformaldehyde for 20 min at 4°C in the dark before a final wash and resuspension for analysis. Samples were then acquired on a Cytex Aurora spectral flow cytometer equipped with five lasers operating on 355, 405, 488, 561, and 640 nm using the SpectroFlo V2.2.0 (Cytex) software. Data were analyzed using FlowJo10.6.1 software (Becton Dickinson). Because our interest was on the ongoing humoral immune response

(antigen-experienced B cells), we excluded naive B cells ($\text{CD}19^+ \text{CD}20^+ \text{IgD}^+ \text{CD}27^-$) from analysis.

Statistical analysis

Raw, individual-level data for experiments where $n < 20$ are presented in data file S1. All the analyses were carried out using GraphPad Prism v8.0. Qualitative variables were expressed as percentages and compared with the chi-square test or Fisher's exact test when the conditions of application of chi-square were not met. Because of the lack of normal distribution of some variables in the epidemiological cohort or small sample size in the mechanistic cohort, quantitative variables were all expressed as median \pm IQR and compared using Mann-Whitney test. Paired data were compared using Wilcoxon test. All tests were two-sided. Incidence data were analyzed by Kaplan-Meier plot and compared using a log-rank test. Nonlinear regression was performed to study the correlation of continuous quantitative variables.

SUPPLEMENTARY MATERIALS

www.science.org/doi/10.1126/scitranslmed.abl6141

Fig. S1

Table S1

Data file S1

MDAR Reproducibility Checklist

[View/request a protocol for this paper from Bio-protocol.](#)

REFERENCES AND NOTES

1. N. Zhu, D. Zhang, W. Wang, X. Li, B. Yang, J. Song, X. Zhao, B. Huang, W. Shi, R. Lu, P. Niu, F. Zhan, X. Ma, D. Wang, W. Xu, G. Wu, G. F. Gao, W. Tan; China Novel Coronavirus Investigating and Research Team, A novel coronavirus from patients with pneumonia in China, 2019. *N. Engl. J. Med.* **382**, 727–733 (2020).
2. European Centre for Disease Prevention and Control, COVID-19 situation update worldwide, as of week 1, updated 13 January 2022; www.ecdc.europa.eu/en/geographical-distribution-2019-ncov-cases.
3. E. J. Williamson, A. J. Walker, K. Bhaskaran, S. Bacon, C. Bates, C. E. Morton, H. J. Curtis, A. Mehrkar, D. Evans, P. Inglesby, J. Cockburn, H. I. McDonald, B. MacKenna, L. Tomlinson, I. J. Douglas, C. T. Rentsch, R. Mathur, A. Y. S. Wong, R. Grieve, D. Harrison, H. Forbes, A. Schultze, R. Croker, J. Parry, F. Hester, S. Harper, R. Perera, S. J. W. Evans, L. Smeeth, B. Goldacre, Factors associated with COVID-19-related death using OpenSAFELY. *Nature* **584**, 430–436 (2020).
4. S. Caillard, D. Anglicheau, M. Maignon, A. Durrbach, C. Greze, L. Frimat, O. Thauinat, T. Legris, V. Moal, P. F. Westeel, N. Kamar, P. Gatault, R. Snanoudj, A. Sicard, D. Bertrand, C. Colosio, L. Couzi, J. M. Chemouny, C. Masset, G. Blanco, J. Bamouli, A. Duveau, N. Bouvier, N. Chavarot, P. Grimbert, B. Moulin, Y. Le Meur, M. Hazzan; French SOT COVID Registry, An initial report from the French SOT COVID Registry suggests high mortality due to COVID-19 in recipients of kidney transplants. *Kidney Int.* **98**, 1549–1558 (2020).
5. K. J. Jager, A. Kramer, N. C. Chesnaye, C. Couchoud, J. E. Sánchez-Álvarez, L. Garneata, F. Collart, M. H. Hemmeler, P. Ambühl, J. Kerschbaum, C. Legeai, M. D. Del Pino Y Pino, G. Mircescu, L. Mazzoleni, T. Hoekstra, R. Winzeler, G. Mayer, V. S. Stel, C. Wanner, C. Zoccali, Z. A. Massy, Results from the ERA-EDTA Registry indicate a high mortality due to COVID-19 in dialysis patients and kidney transplant recipients across Europe. *Kidney Int.* **98**, 1540–1548 (2020).
6. O. Thauinat, C. Legeai, D. Anglicheau, L. Couzi, G. Blanco, M. Hazzan, M. Pastural, E. Savoye, F. Bayer, E. Morelon, Y. Le Meur, O. Bastien, S. Caillard; French nationwide Registry of Solid Organ Transplant Recipients with COVID-19, IMPact of the COVID-19 epidemic on the mortality of kidney transplant recipients and candidates in a French Nationwide registry sTudy (IMPORTANT). *Kidney Int.* **98**, 1568–1577 (2020).
7. S. Caillard, N. Chavarot, H. Francois, M. Maignon, C. Greze, N. Kamar, P. Gatault, O. Thauinat, T. Legris, L. Frimat, P. F. Westeel, V. Goutaudier, M. Jdidou, R. Snanoudj, C. Colosio, A. Sicard, D. Bertrand, C. Mousson, J. Bamouli, C. Masset, A. Thierry, L. Couzi, J. M. Chemouny, A. Duveau, V. Moal, G. Blanco, P. Grimbert, A. Durrbach, B. Moulin, D. Anglicheau, Y. Ruch, C. Kaeuffer, I. Benotmane, M. Solis, Y. LeMeur, M. Hazzan, F. Danion; French SOT COVID Registry, Is COVID-19 infection more severe in kidney transplant recipients? *Am. J. Transplant.* **21**, 1295–1303 (2021).
8. Haute Autorité de Santé, Vaccins Covid-19: Quelle stratégie de priorisation à l'initiation de la campagne?; www.has-sante.fr/jcms/p_3221237/fr/vaccins-covid-19-quelle-strategie-de-priorisation-a-l-initiation-de-la-campagne.

9. S. Dahdal, C. Saison, M. Valette, E. Bachy, N. Pallet, B. Lina, A. Koenig, G. Monneret, T. Defrance, E. Morelon, O. Thanaat, Residual activatability of circulating Tfh17 predicts humoral response to thymodependent antigens in patients on therapeutic immunosuppression. *Front. Immunol.* **9**, 3178 (2019).
10. A. Duchini, J. A. Goss, S. Karpen, P. J. Pockros, Vaccinations for adult solid-organ transplant recipients: Current recommendations and protocols. *Clin. Microbiol. Rev.* **16**, 357–364 (2003).
11. B. J. Boyarsky, W. A. Werbel, R. K. Avery, A. A. R. Tobian, A. B. Massie, D. L. Segev, J. M. Garonzik-Wang, Antibody response to 2-dose SARS-CoV-2 mRNA vaccine series in solid organ transplant recipients. *JAMA* **325**, 2204–2206 (2021).
12. H. Rincon-Arevalo, M. Choi, A.-L. Stefanski, F. Halleck, U. Weber, F. Szelinski, B. Jahrsdörfer, H. Schrezenmeier, C. Ludwig, A. Sattler, K. Kotsch, A. Potekhin, Y. Chen, G. R. Burmester, K.-U. Eckardt, G. M. Guerra, P. Durek, F. Heinrich, M. Ferreira-Gomes, A. Radbruch, K. Budde, A. C. Lino, M.-F. Mashreghi, E. Schrezenmeier, T. Dörner, Impaired humoral immunity to SARS-CoV-2 BNT162b2 vaccine in kidney transplant recipients and dialysis patients. *Sci. Immunol.* **6**, eabj1031 (2021).
13. A. Sattler, E. Schrezenmeier, U. A. Weber, A. Potekhin, F. Bachmann, H. Straub-Hohenbleicher, K. Budde, E. Storz, V. Proß, Y. Bergmann, L. M. Thole, C. Tizian, O. Hölsken, A. Diefenbach, H. Schrezenmeier, B. Jahrsdörfer, T. Zemojtel, K. Jechow, C. Conrad, S. Lukassen, D. Stauch, N. Lachmann, M. Choi, F. Halleck, K. Kotsch, Impaired humoral and cellular immunity after SARS-CoV2 BNT162b2 (Tozinameran) prime-boost vaccination in kidney transplant recipients. *J. Clin. Invest.* **131**, e150175 (2021).
14. I. Benotmane, G. Gautier-Vargas, N. Cognard, J. Olagne, F. Heibel, L. Braun-Parvez, J. Martzloff, P. Perrin, B. Moulin, S. Fafi-Kremer, S. Caillard, Low immunization rates among kidney transplant recipients who received 2 doses of the mRNA-1273 SARS-CoV-2 vaccine. *Kidney Int.* **99**, 1498–1500 (2021).
15. S. Caillard, O. Thanaat, COVID-19 vaccination in kidney transplant recipients. *Nat. Rev. Nephrol.* **17**, 785–787 (2021).
16. S. Caillard, N. Chavarot, D. Bertrand, N. Kamar, O. Thanaat, V. Moal, C. Masset, M. Hazzan, P. Gatault, A. Sicard, J. M. Chemouny, J. P. Rerolle, C. Colosio, H. Francois, J. Bamoulid, N. Bouvier, A. Duveau, D. Anglicheau, G. Blanco; French Society of Transplantation, Occurrence of severe COVID-19 in vaccinated transplant patients. *Kidney Int.* **100**, 477–479 (2021).
17. N. M. Ali, N. Alnazari, S. A. Mehta, B. Boyarsky, R. K. Avery, D. L. Segev, R. A. Montgomery, Z. A. Stewart, Development of COVID-19 infection in transplant recipients after SARS-CoV-2 vaccination. *Transplantation* **105**, e104–e106 (2021).
18. P.-S. Heeger, C. P. Larsen, D. L. Segev, Implications of defective immune responses in SARS-CoV-2 vaccinated organ transplant recipients. *Sci. Immunol.* **6**, eabj6513 (2021).
19. C. H. Hansen, D. Michlmayr, S. M. Gubbels, K. Molbak, S. Ethelberg, Assessment of protection against reinfection with SARS-CoV-2 among 4 million PCR-tested individuals in Denmark in 2020: A population-level observational study. *Lancet* **397**, 1204–1212 (2021).
20. V. J. Hall, S. Foulkes, A. Charlett, A. Atti, E. J. M. Monk, R. Simmons, E. Wellington, M. J. Cole, A. Saei, B. Oguti, K. Munro, S. Wallace, P. D. Kirwan, M. Shrotri, A. Vusirikala, S. Rokadiya, M. Kall, M. Zambon, M. Ramsay, T. Brooks, C. S. Brown, M. A. Chand, S. Hopkins; SIREN Study Group, SARS-CoV-2 infection rates of antibody-positive compared with antibody-negative health-care workers in England: A large, multicentre, prospective cohort study (SIREN). *Lancet* **397**, 1459–1469 (2021).
21. S. F. Lumley, D. O'Donnell, N. E. Stoesser, P. C. Matthews, A. Howarth, S. B. Hatch, B. D. Marsden, S. Cox, T. James, F. Warren, L. J. Peck, T. G. Ritter, Z. de Toledo, L. Warren, D. Axten, R. J. Cornell, E. Y. Jones, D. I. Stuart, G. Scream, D. Ebner, S. Hoosdally, M. Chand, D. W. Crook, A.-M. O'Donnell, C. P. Conlon, K. B. Pouwels, A. S. Walker, T. E. A. Peto, S. Hopkins, T. M. Walker, K. Jeffery, D. W. Eyre, Antibody status and incidence of SARS-CoV-2 infection in health care workers. *N. Eng. J. Med.* **384**, 533–540 (2021).
22. L. J. Abu-Raddad, H. Chemaitelly, P. Coyle, J. A. Malek, A. A. Ahmed, Y. A. Mohamoud, S. Younus-kunju, H. H. Ayoub, Z. A. Kanaani, E. A. Kuwari, A. A. Butt, A. Jeremijenko, A. H. Kaleeckal, A. N. Latif, R. M. Shaik, H. F. A. Rahim, G. K. Nasrallah, H. M. Yassine, M. G. A. Kuwari, H. E. A. Romaihi, M. H. Al-Thani, A. A. Khal, R. Bertollini, SARS-CoV-2 antibody-positivity protects against reinfection for at least seven months with 95% efficacy. *EClinicalMedicine* **35**, 100861 (2021).
23. L. Couzi, M. Manook, S. Caillard, É. Épailly, B. Barrou, D. Anglicheau, M. Buchler, S. Musso, J. Dumortier, O. Thanaat, L. Sebbag, G. Blanco, Y. Le Meur, Y. A. Patel, M. Samoylova, L. McElroy, B. I. Shaw, S. Sanoff, M. Hazzan, Impact of Covid-19 on kidney transplant and waiting list patients: Lessons from the first wave of the pandemic. *Nephrol. Ther.* **17**, 245–251 (2021).
24. A. Favà, L. Donadeu, N. Sabé, V. Pernin, J. González-Costello, L. Lladó, M. Meneghini, X. Charmetant, E. García-Romero, A. Cacher, A. Torija, R. Rodríguez-Urquía, E. Crespo, I. Teubel, E. Mellili, N. Montero, A. Manonelles, R. Preyer, K. Strecker, A. Ovize, J. J. Lozano, J. Sidorova, J. M. Cruzado, M. Le Quintrec, O. Thanaat, O. Bestard, SARS-CoV-2-specific serological and functional T cell immune responses during acute and early COVID-19 convalescence in solid organ transplant patients. *Am. J. Transplant.* **21**, 2749–2761 (2021).
25. R. A. Seder, P. A. Darrah, M. Roederer, T-cell quality in memory and protection: Implications for vaccine design. *Nat. Rev. Immunol.* **8**, 247–258 (2008).
26. R. Channappanavar, C. Fett, J. Zhao, D. K. Meyerholz, S. Perlman, Virus-specific memory CD8 T cells provide substantial protection from lethal severe acute respiratory syndrome coronavirus infection. *J. Virol.* **88**, 11034–11044 (2014).
27. M. J. Bevan, Helping the CD8⁺ T-cell response. *Nat. Rev. Immunol.* **4**, 595–602 (2004).
28. A. Grifoni, D. Weiskopf, S. I. Ramirez, J. Mateus, J. M. Dan, C. R. Moderbacher, S. A. Rawlings, A. Sutherland, L. Premkumar, R. S. Jardi, D. Marrama, A. M. de Silva, A. Frazier, A. F. Carlin, J. A. Greenbaum, B. Peters, F. Krammer, D. M. Smith, S. Crotty, A. Sette, Targets of T cell responses to SARS-CoV-2 coronavirus in humans with COVID-19 disease and unexposed individuals. *Cell* **181**, 1489–1501.e15 (2020).
29. B. IsraeLOW, T. Mao, J. Klein, E. Song, B. Menasche, S. B. Omer, A. Iwasaki, Adaptive immune determinants of viral clearance and protection in mouse models of SARS-CoV-2. *Sci. Immunol.* **6**, eabl4509 (2021).
30. X. Chen, R. Li, Z. Pan, C. Qian, Y. Yang, R. You, J. Zhao, P. Liu, L. Gao, Z. Li, Q. Huang, L. Xu, J. Tang, Q. Tian, W. Yao, L. Hu, X. Yan, X. Zhou, Y. Wu, K. Deng, Z. Zhang, Z. Qian, Y. Chen, L. Ye, Human monoclonal antibodies block the binding of SARS-CoV-2 spike protein to angiotensin converting enzyme 2 receptor. *Cell. Mol. Immunol.* **17**, 647–649 (2020).
31. R. Shi, C. Shan, X. Duan, Z. Chen, P. Liu, J. Song, T. Song, X. Bi, C. Han, L. Wu, G. Gao, X. Hu, Y. Zhang, Z. Tong, W. Huang, W. J. Liu, G. Wu, B. Zhang, L. Wang, J. Qi, H. Feng, F.-S. Wang, Q. Wang, G. F. Gao, Z. Yuan, J. Yan, A human neutralizing antibody targets the receptor-binding site of SARS-CoV-2. *Nature* **584**, 120–124 (2020).
32. Y. Wu, F. Wang, C. Shen, W. Peng, D. Li, C. Zhao, Z. Li, S. Li, Y. Bi, Y. Yang, Y. Gong, H. Xiao, Z. Fan, S. Tan, G. Wu, W. Tan, X. Lu, C. Fan, Q. Wang, Y. Liu, C. Zhang, J. Qi, G. F. Gao, F. Gao, L. Liu, A noncompeting pair of human neutralizing antibodies block COVID-19 virus binding to its receptor ACE2. *Science* **368**, 1274–1278 (2020).
33. E. Seydoux, L. J. Homad, A. J. MacCamy, K. R. Parks, N. K. Hurlburt, M. F. Jennewein, N. R. Akins, A. B. Stuart, Y.-H. Wan, J. Feng, R. E. Whaley, S. Singh, M. Boeckh, K. W. Cohen, M. J. McElrath, J. A. Englund, H. Y. Chu, M. N. Pancera, A. T. McGuire, L. Stamatatos, Analysis of a SARS-CoV-2-infected individual reveals development of potent neutralizing antibodies with limited somatic mutation. *Immunity* **53**, 98–105.e5 (2020).
34. B. Ju, Q. Zhang, J. Ge, R. Wang, J. Sun, X. Ge, J. Yu, S. Shan, B. Zhou, S. Song, X. Tang, J. Yu, J. Lan, J. Yuan, H. Wang, J. Zhao, S. Zhang, Y. Wang, X. Shi, L. Liu, J. Zhao, X. Wang, Z. Zhang, L. Zhang, Human neutralizing antibodies elicited by SARS-CoV-2 infection. *Nature* **584**, 115–119 (2020).
35. M. Espi, X. Charmetant, T. Barba, L. Koppe, C. Pelletier, E. Kalbacher, E. Chalencon, V. Mathias, A. Ovize, E. Cart-Tanneur, C. Bouz, L. Pellegrina, E. Morelon, D. Fouque, L. Juillard, O. Thanaat, The ROMANOV study found impaired humoral and cellular immune responses to SARS-CoV-2 mRNA vaccine in virus unexposed patients receiving maintenance hemodialysis. *Kidney Int.* **100**, 928–936 (2021).
36. C.-C. Chen, A. Koenig, C. Saison, S. Dahdal, G. Rigault, T. Barba, M. Taillardet, D. Charatoire, M. Ovize, E. Morelon, T. Defrance, O. Thanaat, CD4⁺ T cell help is mandatory for naive and memory donor-specific antibody responses: Impact of therapeutic immunosuppression. *Front. Immunol.* **9**, 275 (2018).
37. A. Lanzavecchia, Antigen-specific interaction between T and B cells. *Nature* **314**, 537–539 (1985).
38. J. A. Roco, L. Mesin, S. C. Binder, C. Nefzger, P. Gonzalez-Figueroa, P. F. Canete, J. Ellyard, Q. Shen, P. A. Robert, J. Cappello, H. Vohra, Y. Zhang, C. R. Nowosad, A. G. Schiepers, L. M. Corcoran, K.-M. Toellner, J. M. Polo, M. Meyer-Hermann, G. D. Victoria, C. G. Vinuesa, Class-switch recombination occurs infrequently in germinal centers. *Immunity* **51**, 337–350.e7 (2019).
39. C. Gil-Cruz, S. Bobat, J. L. Marshall, R. A. Kingsley, E. A. Ross, I. R. Henderson, D. L. Leyton, R. E. Coughlan, M. Khan, K. T. Jensen, C. D. Buckley, G. Dougan, I. C. M. MacLennan, C. López-Macias, A. F. Cunningham, The porin OmpD from nontyphoidal *Salmonella* is a key target for a protective B1b cell antibody response. *Proc. Natl. Acad. Sci. U.S.A.* **106**, 9803–9808 (2009).
40. A. E. Schager, C. C. Dominguez-Medina, F. Necchi, F. Micoli, Y. S. Goh, M. Goodall, A. Flores-Langarica, S. Bobat, C. N. L. Cook, M. Arcuri, A. Marini, L. D. W. King, F. C. Morris, G. Anderson, K.-M. Toellner, I. R. Henderson, C. López-Macias, C. A. MacLennan, A. F. Cunningham, IgG responses to porins and lipopolysaccharide within an outer membrane-based vaccine against nontyphoidal *Salmonella* develop at discordant rates. *mBio* **9**, e02379–17 (2018).
41. J. H. Lam, F. L. Smith, N. Baumgarth, B cell activation and response regulation during viral infections. *Viral Immunol.* **33**, 294–306 (2020).
42. S. A. Jenks, K. S. Cashman, E. Zumaquero, U. M. Marigorta, A. V. Patel, X. Wang, D. Tomar, M. C. Woodruff, Z. Simon, R. Bugrovsky, E. L. Blalock, C. D. Scharer, C. M. Tipton, C. Wei, S. S. Lim, M. Petri, T. B. Niewold, J. H. Anolik, G. Gibson, F. E.-H. Lee, J. M. Boss, F. E. Lund, I. Sanz, Distinct effector B cells induced by unregulated toll-like receptor 7 contribute to pathogenic responses in systemic Lupus Erythematosus. *Immunity* **49**, 725–739.e6 (2018).
43. I. Sanz, C. Wei, S. A. Jenks, K. S. Cashman, C. Tipton, M. C. Woodruff, J. Hom, F. E.-H. Lee, Challenges and opportunities for consistent classification of human B cell and plasma cell populations. *Front. Immunol.* **10**, 2458 (2019).

44. S. Heidt, D. L. Roelen, C. Eijnsink, M. Eikmans, C. van Kooten, F. H. J. Claas, A. Mulder, Calcineurin inhibitors affect B cell antibody responses indirectly by interfering with T cell help. *Clin. Exp. Immunol.* **159**, 199–207 (2010).
45. R. Morita, N. Schmitt, S.-E. Benteibibel, R. Ranganathan, L. Bourdery, G. Zurawski, E. Foucat, M. Dullaers, S. Oh, N. Sabzghabaei, E. M. Lavecchio, M. Punaro, V. Pascual, J. Banchereau, H. Ueno, Human blood CXCR5(+)CD4(+) T cells are counterparts of T follicular cells and contain specific subsets that differentially support antibody secretion. *Immunity* **34**, 108–121 (2011).
46. J. S. Turner, J. A. O'Halloran, E. Kalaidina, W. Kim, A. J. Schmitz, J. Q. Zhou, T. Lei, M. Thapa, R. E. Chen, J. B. Case, F. Amanat, A. M. Raouf, A. Haile, X. Xie, M. K. Klebert, T. Suessen, W. D. Middleton, P.-Y. Shi, F. Krammer, S. A. Teefey, M. S. Diamond, R. M. Presti, A. H. Ellebedy, SARS-CoV-2 mRNA vaccines induce persistent human germinal centre responses. *Nature* **596**, 109–113 (2021).
47. B. J. Laidlaw, A. H. Ellebedy, The germinal centre B cell response to SARS-CoV-2. *Nat. Rev. Immunol.* **22**, 7–18 (2022).
48. S. Feng, D. J. Phillips, T. White, H. Sayal, P. K. Aley, S. Bibi, C. Dold, M. Fuskova, S. C. Gilbert, I. Hirsch, H. E. Humphries, B. Jepson, E. J. Kelly, E. Plested, K. Shoemaker, K. M. Thomas, J. Vekemans, T. L. Villafana, T. Lambe, A. J. Pollard, M. Voysey; Oxford COVID Vaccine Trial Group, Correlates of protection against symptomatic and asymptomatic SARS-CoV-2 infection. *Nat. Med.* **27**, 2032–2040 (2021).
49. D. S. Khoury, D. Cromer, A. Reynaldi, T. E. Schlub, A. K. Wheatley, J. A. Juno, K. Subbarao, S. J. Kent, J. A. Triccas, M. P. Davenport, Neutralizing antibody levels are highly predictive of immune protection from symptomatic SARS-CoV-2 infection. *Nat. Med.* **27**, 1205–1211 (2021).
50. M. Bergwerk, T. Gonen, Y. Lustig, S. Amit, M. Lipsitch, C. Cohen, M. Mandelboim, E. G. Levin, C. Rubin, V. Indenbaum, I. Tal, M. Zavitan, N. Zuckerman, A. Bar-Chaim, Y. Kreiss, G. Regev-Yochay, Covid-19 breakthrough infections in vaccinated health care workers. *N. Eng. J. Med.* **385**, 1474–1484 (2021).
51. M. Miele, R. Busà, G. Russell, M. C. Sorrentino, M. Di Bella, F. Timoneri, A. Mularoni, G. Panarello, P. Vitulo, P. G. Conaldi, M. Bulati, Impaired anti-SARS-CoV-2 humoral and cellular immune response induced by Pfizer-BioNTech BNT162b2 mRNA vaccine in solid organ transplanted patients. *Am. J. Transplant.* **21**, 2919–2921 (2021).
52. M. C. Woodruff, R. P. Ramonell, D. C. Nguyen, K. S. Cashman, A. S. Saini, N. S. Haddad, A. M. Ley, S. Kyu, J. C. Howell, T. Ozturk, S. Lee, N. Suryadevara, J. B. Case, R. Bugrovsky, W. Chen, J. Estrada, A. Morrison-Porter, A. Derrico, F. A. Anam, M. Sharma, H. M. Wu, S. N. Le, S. A. Jenks, C. M. Tipton, B. Staitieh, J. L. Daiss, E. Ghosn, M. S. Diamond, R. H. Carnahan, J. E. Crowe, W. T. Hu, F. E.-H. Lee, I. Sanz, Extrafollicular B cell responses correlate with neutralizing antibodies and morbidity in COVID-19. *Nat. Immunol.* **21**, 1506–1516 (2020).
53. S. A. Apostolidis, M. Kakara, M. M. Painter, R. R. Goel, D. Mathew, K. Lenzi, A. Rezk, K. R. Patterson, D. A. Espinoza, J. C. Kadri, D. M. Markowitz, C. E. Markowitz, I. Mexhitaj, D. Jacobs, A. Babb, M. R. Betts, E. T. L. Prak, D. Weiskopf, A. Grifoni, K. A. Lundgreen, S. Gouma, A. Sette, P. Bates, S. E. Hensley, A. R. Greenplate, E. J. Wherry, R. Li, A. Bar-Or, Cellular and humoral immune responses following SARS-CoV-2 mRNA vaccination in patients with multiple sclerosis on anti-CD20 therapy. *Nat. Med.* **27**, 1990–2001 (2021).
54. K. Lederer, E. Bettini, K. Parvathaneni, M. M. Painter, D. Agarwal, K. A. Lundgreen, M. Weirick, K. Muralidharan, D. Castano, R. R. Goel, X. Xu, E. M. Drapeau, S. Gouma, J. T. Ort, M. Awofolaj, A. R. Greenplate, C. Le Coz, N. Romberg, J. Trofe-Clark, G. Malat, L. Jones, M. Rosen, D. Weiskopf, A. Sette, B. Besharatian, M. Kaminiski, S. E. Hensley, P. Bates, E. J. Wherry, A. Najj, V. Bhoj, M. Locci, Germinal center responses to SARS-CoV-2 mRNA vaccines in healthy and immunocompromised individuals. *Cell* **185**, 1–17 (2022).
55. J. A. Juno, H.-X. Tan, W. S. Lee, A. Reynaldi, H. G. Kelly, K. Wragg, R. Esterbauer, H. E. Kent, C. J. Batten, F. L. Mordant, N. A. Gherardin, P. Pymm, M. H. Dietrich, N. E. Scott, W.-H. Tham, D. I. Godfrey, K. Subbarao, M. P. Davenport, S. J. Kent, A. K. Wheatley, Humoral and circulating follicular helper T cell responses in recovered patients with COVID-19. *Nat. Med.* **26**, 1428–1434 (2020).
56. O. Thunat, A. Koenig, C. Leibler, P. Grimbert, Effect of immunosuppressive drugs on humoral allo-sensitization after kidney transplant. *J. Am. Soc. Nephrol.* **27**, 1890–1900 (2016).
57. A. C. Allison, E. M. Eugui, Immunosuppressive and other effects of mycophenolic acid and an ester prodrug, mycophenolate mofetil. *Immunol. Rev.* **136**, 5–28 (1993).
58. K. G. Smith, N. M. Isbel, M. G. Catton, J. A. Leydon, G. J. Becker, R. G. Walker, Suppression of the humoral immune response by mycophenolate mofetil. *Nephrol. Dial. Transplant.* **13**, 160–164 (1998).
59. G. H. Struijk, R. C. Minnee, S. D. Koch, A. H. Zwinderman, K. A. M. I. van Donselaar-van der Pant, M. M. Idu, I. J. M. ten Berge, F. J. Bemelman, Maintenance immunosuppressive therapy with everolimus preserves humoral immune responses. *Kidney Int.* **78**, 934–940 (2010).
60. R. S. Gaston, J. M. Cecka, B. L. Kasiske, A. M. Fieberg, R. Leduc, F. C. Cosio, S. Gourishankar, J. Grande, P. Halloran, L. Hunsicker, R. Mannon, D. Rush, A. J. Matas, Evidence for antibody-mediated injury as a major determinant of late kidney allograft failure. *Transplantation* **90**, 68–74 (2010).
61. E. Pouliquen, A. Koenig, C. C. Chen, A. Sicard, M. Rabeyrin, E. Morelon, V. Dubois, O. Thunat, Recent advances in renal transplantation: Antibody-mediated rejection takes center stage. *F1000Prime Rep.* **7**, 51 (2015).
62. O. Thunat, Humoral immunity in chronic allograft rejection: Puzzle pieces come together. *Transpl. Immunol.* **26**, 101–106 (2012).
63. N. Kamar, F. Abravanel, O. Marion, C. Couat, J. Izopet, A. Del Bello, Three doses of an mRNA Covid-19 vaccine in solid-organ transplant recipients. *N. Engl. J. Med.* **385**, 661–662 (2021).
64. W. A. Werbel, B. J. Boyarsky, M. T. Ou, A. B. Massie, A. A. R. Tobian, J. M. Garonzik-Wang, D. L. Segev, Safety and immunogenicity of a third dose of SARS-CoV-2 vaccine in solid organ transplant recipients: A case series. *Ann. Intern. Med.* **174**, 1330–1332 (2021).
65. I. Benotmane, G. Gautier, P. Perrin, J. Olagne, N. Cognard, S. Fafi-Kremer, S. Caillard, Antibody response after a third dose of the mRNA-1273 SARS-CoV-2 vaccine in kidney transplant recipients with minimal serologic response to 2 doses. *JAMA* **326**, 1063 (2021).
66. V. G. Hall, V. H. Ferreira, T. Ku, M. Ierullo, B. Majchrzak-Kita, C. Chaparro, N. Selzner, J. Schiff, M. McDonald, G. Tomlinson, V. Kulasingam, D. Kumar, A. Humar, Randomized trial of a third dose of mRNA-1273 vaccine in transplant recipients. *N. Eng. J. Med.* **385**, 1244–1246 (2021).
67. S. Caillard, O. Thunat, I. Benotmane, C. Masset, G. Blancho, Antibody response to a fourth messenger RNA COVID-19 vaccine dose in kidney transplant recipients: A case series. *Ann. Intern. Med.* , (2022).
68. Y. Natori, M. Shiotsuka, J. Slomovic, K. Hoschler, V. Ferreira, P. Ashton, C. Rotstein, L. Lilly, J. Schiff, L. Singer, A. Humar, D. Kumar, A double-blind, randomized trial of high-dose vs standard-dose influenza vaccine in adult solid-organ transplant recipients. *Clin. Infect. Dis.* **66**, 1698–1704 (2018).
69. M. Mombelli, N. Rettby, M. Perreau, M. Pascual, G. Pantaleo, O. Manuel, Immunogenicity and safety of double versus standard dose of the seasonal influenza vaccine in solid-organ transplant recipients: A randomized controlled trial. *Vaccine* **36**, 6163–6169 (2018).
70. D. Steensels, N. Pierlet, J. Penders, D. Mesotten, L. Heylen, Comparison of SARS-CoV-2 antibody response following vaccination with BNT162b2 and mRNA-1273. *JAMA* **326**, 1533–1535 (2021).
71. M. P. O'Brien, E. Forleo-Neto, B. J. Musser, F. Isa, K.-C. Chan, N. Sarkar, K. J. Bar, R. V. Barnabas, D. H. Barouch, M. S. Cohen, C. B. Hurt, D. R. Burwen, M. A. Marovich, P. Hou, I. Heirman, J. D. Davis, K. C. Turner, D. Ramesh, A. Mahmood, A. T. Hooper, J. D. Hamilton, Y. Kim, L. A. Purcell, A. Baum, C. A. Kyrtatos, J. Krainson, R. Perez-Perez, R. Mohseni, B. Kowal, A. T. DiCiccio, N. Stahl, L. Lipsich, N. Braunstein, G. Herman, G. D. Yancopoulos, D. M. Weinreich; Covid-19 Phase 3 Prevention Trial Team, Subcutaneous REGEN-COV antibody combination to prevent Covid-19. *N. Eng. J. Med.* **385**, 1184–1195 (2021).
72. L. R. Baden, H. M. El Sahly, B. Essink, K. Kotloff, S. Frey, R. Novak, D. Diemert, S. A. Spector, N. Roupchal, C. B. Creech, J. McGittigan, S. Khetan, N. Segall, J. Solis, A. Brosz, C. Fierro, H. Schwartz, K. Neuzil, L. Corey, P. Gilbert, H. Janes, D. Follmann, M. Marovich, J. Mascola, L. Polakowski, J. Ledgerwood, B. S. Graham, H. Bennett, R. Pajon, C. Knightly, B. Leav, W. Deng, H. Zhou, S. Han, M. Ivarsson, J. Miller, T. Zaks; COVE Study Group, Efficacy and safety of the mRNA-1273 SARS-CoV-2 vaccine. *N. Eng. J. Med.* **384**, 403–416 (2021).
73. G. Mattiuzzo, E. M. Bentley, E. S. Rountley, V. Bernasconi, P. Kristiansen, H. Harvala, D. Roberts, G. Semple, L. C. Turtle, P. J. Openshaw, K. Baillie, C. Investigators, L. S. H. Nissen-Meyer, A. B. Brants, E. Atkinson, P. Rigby, D. Padley, N. Almond, N. J. Rose, M. Page, *Establishment of the WHO International Standard and Reference Panel for Anti-SARS-CoV-2 Antibody* (World Health Organization, 2020).
74. H. Wang, D. Wirejia, L. Yang, P. L. Bulterys, C. Costales, K. Röltgen, J. Manalac, J. Yee, J. Zehnder, R. Z. Shi, S. D. Boyd, B. A. Pinsky, Case-control study of individuals with discrepant nucleocapsid and spike protein SARS-CoV-2 IgG results. *Clin. Chem.* **67**, 977–986 (2021).
75. B. Pozzetto, V. Legros, S. Djebali, V. Barateau, N. Guibert, M. Villard, L. Peyrot, O. Allatif, J.-B. Fassier, A. Massardier-Pilonchéry, K. Brengel-Pesce, M. Yaugel-Novoa, S. Denolly, B. Boson, T. Bourlet, A. Bal, M. Valette, T. Andrieu, B. Lina, F.-L. Cosset, S. Paul, T. Defrance, J. Marvel, T. Walzer, S. Trouillet-Assant, Immunogenicity and efficacy of heterologous ChadOx1–BNT162b2 vaccination. *Nature* **600**, 701–706 (2021).

Acknowledgments: We thank A. Kochman and the members of the Groupe de Recherche Clinique (GREC: C. Dagot, F. Pauwels, F. M'Raiagh, and D. Sperandio) for excellent technical assistance during the collection of the samples. O.T. is thankful to L. Siard, C. Lecuelle, and P. Favre from Eurofins Biomnis for their help during the conduction of the study. **Funding:** The study was supported by funding from the Société Francophone de Transplantation (to X.C.), the Hospices civils de Lyon (to M.E.), INSERM (to M.E. and S.F.-K.), the Etablissement Français du Sang (to O.T.), the Fondation pour la Recherche Médicale (PME20180639518 to O.T.), the Strasbourg University Hospital (SeroCoV-HUS; PRI 7782 to S.F.-K.), Programme Hospitalier de Recherche Clinique (PHRC N 2017-HUS no. 6997 to S.F.-K.), the Agence Nationale de la Recherche (ANR-18-CE17-0028 to S.F.-K.), and the Laboratoire d'Excellence TRANSLANTEX (ANR-11-LABX-0070_TRANSPLANTEX to S.F.-K.). **Author contributions:** X.C., M.E., and O.T. conceptualized and designed experiments. X.C., M.E., I.B., F.H., F.B., G.G.-V., M.D., P.P., A.K., N.C.,

C.L., L.M., E.M., S.C., and O.T. acquired the clinical samples. X.C., M.E., I.B., V.B., F.G., P.R., E.S., F.P., and A.O. performed the experiments (X.C. and M.E.: T cell response; I.B., F.G., P.R., E.S., and F.P.: neutralization and anti-nucleocapsid IgG assays; V.B.: B cell response; A.O.: anti-RBD IgG assay). X.C., M.E., I.B., A.O., S.F.-K., S.C., and O.T. analyzed the data. X.C. and O.T. wrote the original draft. X.C., F.H., F.B., G.G.-V., M.D., P.P., A.K., N.C., C.L., F.G., L.M., P.R., E.M., T.D., S.F.-K., S.C., and O.T. reviewed and edited the manuscript. **Competing interests:** O.T. participated in advisory boards for Biotech, Novartis, and AstraZeneca and received research grants from Immucor, Biomerieux, and BMS. All other authors declare that they have no competing interests. **Data and materials availability:** All data associated with this study are present in the paper or the Supplementary Materials. This work is licensed under a Creative Commons Attribution 4.0 International (CC BY 4.0) license, which permits unrestricted use, distribution, and

reproduction in any medium, provided the original work is properly cited. To view a copy of this license, visit <http://creativecommons.org/licenses/by/4.0/>. This license does not apply to figures/photos/artwork or other content included in the article that is credited to a third party; obtain authorization from the rights holder before using this material.

Submitted 25 July 2021
Resubmitted 15 November 2021
Accepted 25 January 2022
Published First Release 1 February 2022
Published 16 March 2022
10.1126/scitranslmed.abl6141

Infection or a third dose of mRNA vaccine elicits neutralizing antibody responses against SARS-CoV-2 in kidney transplant recipients

Xavier CharmetantMaxime Espillies BenotmaneVéronique BarateauFrancoise HeibelFanny BuronGabriela Gautier-VargasMarion DelafossePeggy PerrinAlice KoenigNoëlle CognardCharlène LeviFloriane GallaisLouis ManièrePaola RossolilloEric SoulierFlorian PierreAnne OvizeEmmanuel MorelonThierry DefranceSamira Fafi-KremerSophie CaillardOlivier Thauinat

Sci. Transl. Med., 14 (636), eabl6141. • DOI: 10.1126/scitranslmed.abl6141

Protecting transplant recipients

Recipients of kidney transplants are placed on immunosuppressive drugs, which, while prevent rejection of their graft, also put them at increased risk of infections with viruses such as SARS-CoV-2. Here, the authors compared the immune response elicited by SARS-CoV-2 infection and vaccination in kidney transplant recipients. Infection elicited a broader response to SARS-CoV-2 associated with fewer cases of reinfection. The authors also observed a subset of individuals that did not respond to two doses of mRNA vaccine, potentially due to exposure to the immunosuppressive drug, mycophenolate mofetil. A subset of nonresponders who received a third dose of mRNA vaccine developed antibodies comparable to responders to two doses, suggesting that populations with immunosuppression should be prioritized for booster vaccine doses.

View the article online

<https://www.science.org/doi/10.1126/scitranslmed.abl6141>

Permissions

<https://www.science.org/help/reprints-and-permissions>

Use of this article is subject to the [Terms of service](#)

Supplementary Materials for
Infection or a third dose of mRNA vaccine elicits neutralizing antibody responses against SARS-CoV-2 in kidney transplant recipients

Xavier Charmetant *et al.*

Corresponding author: Olivier Thauvat, olivier.thauvat@chu-lyon.fr

Sci. Transl. Med. **14**, eabl6141 (2022)
DOI: 10.1126/scitranslmed.abl6141

The PDF file includes:

Fig. S1
Table S1

Other Supplementary Material for this manuscript includes the following:

Data file S1
MDAR Reproducibility Checklist

Supplementary materials

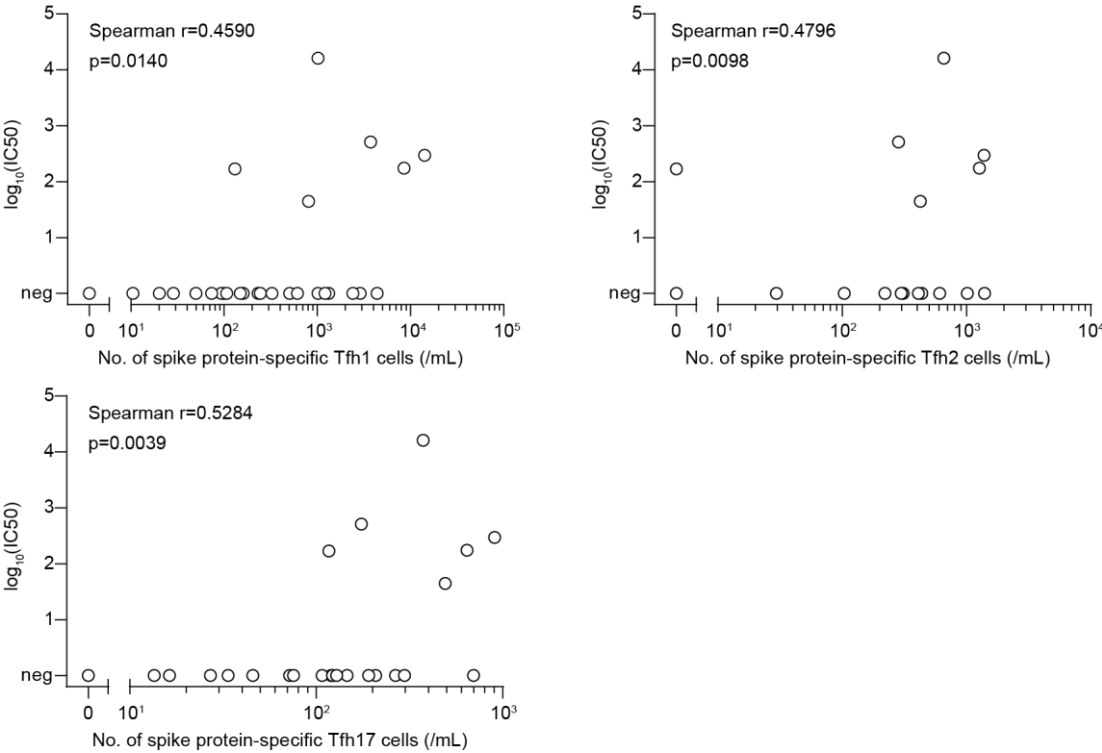


Fig. S1. Correlations between Tfh subpopulations and the viral neutralization capacity of the serum. The correlations between the number of spike protein-specific Tfh1, Tfh2, or Tfh17 cells and the viral neutralization capacity of the serum are shown. The results of Spearman correlation test are shown on the graphs. Tfh, T follicular helper. Neg indicates absence of neutralizing antibodies.

Table S1. Clinical characteristics of epidemiological and COVATRHUS cohorts.

n (%) or median [IQR]	Epidemiological cohort		p ¹	COVATRHUS cohort		p ²	Inf p ³	Vac p ⁴
	Infected n= 137	Vaccinated n= 736		Infected n=21	Vaccinated n=29			
Age (y)	59.9 [49.7-68.9]	57.7 [49.1-67.3]	0.219	54.9 [36.9-60.4]	56.4 [43.4-69.6]	0.314	0.057	0.819
Male	88 (64)	439 (60)	0.361	12 (57)	18 (62)	0.726	0.530	0.794
BMI (kg/m²)	26.0 [23.0-31.0]	26.0 [22.6-30.0]	0.404	25.0 [22.5-30.0]	24.2 [23.4-27.5]	0.603	0.543	0.259
Time since transplantation (y)	6.18 [2.14-12.6]	6.41 [2.94-13.1]	0.176	2.0 [1.35-7.53]	7.04 [2.19-16.2]	0.017	0.027	0.846
Donor type			0.652			0.08	0.140	0.544
Deceased	106 (77)	602 (82)		13 (62)	25 (86)			
Living	27 (20)	134 (18)		7 (33)	4 (14)			
NA	4 (3)	0		1 (5)	0			
Comorbidities								
Cardiovascular disease	48 (35)	226 (31)	0.367	4 (19)	21 (72)	<0.001	0.146	<0.001
Diabetes	58 (42)	263 (36)	0.169	7 (33)	3 (10)	0.045	0.435	0.005
Induction			<0.001			0.087	0.797	0.743
Anti-thymocyte globulins	47 (34)	418 (57)		8 (38)	17 (59)			
Basiliximab	80 (58)	254 (34)		12 (57)	9 (31)			
No induction	7 (5)	38 (5)		0	0			
NA	3 (2)	26 (4)		1 (5)	1 (3)			
Immunosuppressive drugs								
CNI	126 (92)	659 (90)	0.385	19 (90)	28 (97)	0.372	0.817	0.221
MMF/MPA	109 (80)	582 (80)	0.898	19 (90)	22 (76)	0.184	0.235	0.677
Steroids	89 (65)	493 (67)	0.645	14 (67)	19 (66)	0.932	0.879	0.869
imTOR	22 (16)	126 (17)	0.751	1 (5)	3 (10)	0.472	0.172	0.336
Belatacept	3 (2)	24 (3)	0.506	2 (10)	1 (3)	0.372	0.074	0.956
Imurel	3 (2)	16 (2)	0.991	0	0	NA	NA	NA

Qualitative variables were compared using a Chi-square test, quantitative variables were compared using a Mann Whitney test.

Significant p-values are in bold. p¹ was the comparison between infected (Inf) and vaccinated (Vac) patients from the epidemiological

cohort; p^2 was the comparison between infected and vaccinated patients from the biological cohort; p^3 was the comparison between infected patients from the epidemiological and biological cohorts; p^4 was the comparison between vaccinated patients from the epidemiological and biological cohorts. IQR, interquartile range; BMI, body mass index; SD, standard deviation; y, years; NA, not available; CNI, calcineurin inhibitor; MMF/MPA, mycophenolate mofetil/mycophenolic acid; imTOR, inhibitors of the mechanistic target of rapamycin.

DISCUSSION

Ce travail, qui constitue la première partie de cette thèse, a permis de mettre en évidence un corrélat de protection contre l'infection symptomatique à SARS-CoV-2 chez les patients transplantés rénaux, similaire à celui identifié chez les patients immunocompétents : les IgG neutralisantes anti-RBD. Bien que ceci ait été évalué de façon indirecte par l'analyse des cellules circulantes, et non par l'analyse directe des cellules ganglionnaires, nous avons montré que ces anticorps étaient la conséquence d'une réaction de centre germinatif. Bien que les effectifs soient faibles, nous avons aussi montré que la prise de mycophénolate mofétil (MMF), un immunosuppresseur inhibiteur de l'inosine-monophosphate déshydrogénase, impliqué dans la voie de synthèse de novo des bases puriques, était négativement associée à la réponse IgG.

Ainsi, nous confirmons que la réaction de centre germinatif est bien la voie canonique de réponse humorale contre les antigènes thymo-dépendants exogènes chez le patient transplanté. Ce travail donne également des informations sur le rôle du traitement immunosuppresseur dans le contrôle de la réponse humorale. L'absence d'association de l'exposition aux anti-calcineurine avec le défaut de réponse humorale semble indiquer que l'activation lymphocytaire T n'est pas le mécanisme majeur de contrôle du bras humoral chez le patient transplanté. Le traitement qui semble jouer le plus grand rôle dans le contrôle de la réponse humorale est le MMF, qui agit en bloquant la prolifération des lymphocytes B et T activés.

Dans la deuxième partie de cette thèse, nous quittons la vaccinologie pour nous concentrer sur la réponse allo-immune. Compte-tenu de l'efficacité des traitements immunosuppresseurs pour contrôler la réponse humorale, nous nous sommes posé la question de l'existence de voies « non conventionnelles » de production de DSA, pour expliquer l'apparition de DSA chez des patients sous traitement immunosuppresseur. Cette deuxième partie englobe deux travaux indépendants.

Article 2 : $\gamma\delta$ T cells cannot replace or synergize with $\alpha\beta$ CD4⁺ T cells in the production of donor-specific antibodies after solid organ transplantation

La production d'anticorps ne peut pas être dissociée du lymphocyte B. Si une voie non conventionnelle de production des DSA existe, elle implique une tierce cellule qui viendrait soit remplacer le lymphocyte T CD4⁺ du receveur, soit soutenir le couple T CD4⁺/B pour l'aider à être opérationnel malgré la contrainte immunosuppressive. Dans ce travail, nous avons étudié si les lymphocytes T $\gamma\delta$ pourraient jouer l'un de ces deux rôles.

$\gamma\delta$ T cells cannot replace or synergize with $\alpha\beta$ CD4⁺ T cells in the production of donor-specific antibodies after solid organ transplantation

Xavier Charmetant^{1,*}, Guillaume Rigault^{1,*}, Chien-Chia Chen², Hannah Kaminski^{3,4}, Jonathan Visentin^{4,5}, Benjamin Taton³, Gabriel Marseres⁴, Alice Koenig^{1,6,7}, Thomas Barba^{1,7,8}, Jean-Paul Duong van Huyen⁹, Pierre Merville^{3,4}, Emmanuel Morelon^{6,7}, Julie Déchanet-Merville⁴, Valérie Dubois¹⁰, Lionel Couzi^{3,4}, Olivier Thaunat^{1,6,7}.

¹ CIRI, INSERM U1111, Université Claude Bernard Lyon I, CNRS UMR5308, Ecole Normale Supérieure de Lyon, Univ. Lyon, 21, avenue Tony Garnier, 69007 Lyon, France.

² Department of Surgery, National Taiwan University Hospital, Taipei, Taiwan

³ Department of Nephrology, Transplantation, Dialysis and Apheresis, Pellegrin Hospital, Bordeaux, France.

⁴ Univ. Bordeaux, CNRS, Immunoconcept, UMR 5164, Bordeaux, France

⁵ Laboratory of Immunology et Immunogenetics, Pellegrin Hospital, Bordeaux, France

⁶ Hospices Civils de Lyon, Edouard Herriot Hospital, Department of Transplantation, Nephrology and Clinical Immunology, 69003 Lyon, France.

⁷ Claude Bernard University (Lyon 1), Villeurbanne, France.

⁸ Department of Internal Medicine, Edouard Herriot Hospital, Lyon, France

⁹ Pathology Department, Assistance Publique-Hôpitaux de Paris, Necker Hospital, Paris, France

¹⁰ French National Blood Service (EFS), HLA Laboratory, Décines, France

* These two authors contributed equally to this work

Abstract

The generation of donor-specific antibodies (DSA) after transplantation requires that alloreactive B cells receive help from T follicular helper (T_{FH}) cells, a subset of α/β T cells. In certain situations, it has been reported that γ/δ T cells could also help B cells in a T_{FH}-like manner or contribute to the humoral response by priming α/β T_{FH}, but nothing is known about their role in DSA generation. In this translational work, we studied a cohort of 331 kidney transplant recipients in whom the alloimmune humoral response was the same regardless of the number of circulating γ/δ T cells two years after transplantation. Experiments on human cells confirmed that activated γ/δ T cells cannot acquire simultaneously CXCR5 and CD40L, two key functional molecules for T_{FH} cells. In fact, histological analysis revealed that γ/δ T cells preferentially localize outside the follicles in lymph nodes, suggesting instead an “antigen-presenting cell” (APC)-like role for the priming of T_{FH} response. However, γ/δ T cells also failed to acquire APC features after stimulation. Finally, γ/δ T cells neither made B cells proliferate nor synergized with α/β T cells in proliferation assays. These results were confirmed in vivo. Wild-type and TCR δ KO C57BL/6 (H-2^b) mice developed similar DSA responses against a Balb/c (H-2^d) heart allograft, which goes against a “T_{FH}-helper” role for γ/δ T cells. On the contrary, TCR α KO recipients did not develop any DSA, which discredits a “T_{FH}-like” role. These results demonstrate that γ/δ T cells are not involved in the generation of DSA.

Introduction

Organ transplantation is the best (sometimes the only) therapeutic option to treat vital organ failure. Despite recent advances made in the field of therapeutic immunosuppression, that have helped controlling the cellular arm of the adaptive immunity and the subsequent cellular rejections (1), many patients still develop de novo donor-specific antibodies (DSA) (2, 3). The generation of DSA requires that B cells receive help from a CD4⁺ T cell, either syngeneic by the canonical indirect pathway of allorecognition (4, 5), or allogeneic by the recently described inverted direct pathway (6, 7). This cooperation between T and B cells allows B cell differentiation into DSA-producing plasma cells. Those DSAs are sequestered in the recipients' circulation (8) and can encounter their targets at the surface of the graft endothelium. Once bound to their target, they can either activate the classical pathway of the complement cascade, or recruit innate immune cells through their Fc receptors (9). These two mechanisms are responsible for the microvascular inflammation that damages the graft and accounts for the majority of the graft losses (10, 11).

Although insufficiently effective in controlling the humoral arm of the alloimmune response, immunosuppression still exposes transplant patients to viral infections (12). Among them, cytomegalovirus (CMV) infection is very frequent and can occur despite anti-viral pre-emptive treatment or prophylaxis (13, 14). It deserves special attention because CMV infection leaves a lasting imprint on the immune system. The response to CMV involves several subsets of lymphoid cells [NK cells, CD8⁺ T cells (15)] but compelling evidence demonstrate a particular role for a subset of $\gamma\delta$ T cells (16) in viral clearance and the prevention of recurrences (17). Those cells expand specifically after CMV encountering (18), in particular in solid organ transplant recipients (19, 20). This expansion of $\gamma\delta$ T cells is long-lasting and oligoclonal, arguing for antigen-induced proliferation (18, 21).

$\gamma\delta$ T cells are innate-like immune cells equipped with a clonally rearranged TCR that is for the vast majority of them not restricted to MHC molecules, but recognizes phospho-antigens or stress-induced antigens. They also express a large range of receptors found mainly on innate cells, such as natural killer receptors (22) or toll-like receptors (23, 24). They are mainly involved in anti-infectious and anti-tumor defense, via effector functions of cytotoxicity and cytokine secretion.

However, beyond these innate functions, $\gamma\delta$ T cells have also been implicated in adaptive immune responses. Several studies demonstrate that they could help B cell responses, induce germinal centers and switched antibody responses directly (25, 26) or by supporting the T_{FH} program in $CD4^+$ T cells (27). Furthermore, a recent study demonstrated that $\gamma\delta$ T cells recognizing tumor antigen in an HLA-I restricted manner could be generated in vitro and found in the naïve normal repertoire (28). Given the particular profile of the $\gamma\delta$ T cells in transplant patients, and their capacity to participate in adaptive responses, we undertook this translational study to evaluate whether $\gamma\delta$ T cells could be involved in the production of DSA after solid organ transplantation.

Results

The numbers of circulating $\gamma\delta$ T cells are not correlated with de novo DSA incidence after kidney transplantation in humans

In humans, $\gamma\delta$ T cells are divided into two groups based on their phenotypic and functional characteristics. The V δ 2 chain associates preferentially with the V γ 9 chain, resulting in the V δ 2⁺V γ 9⁺ (hereafter referred to as V δ 2⁺) subpopulation. These cells are activated by endogenous or bacterial phosphoantigens in a butyrophilin-dependent manner (29–31). The other group of $\gamma\delta$ T cells mainly encompasses V δ 1⁺ or V δ 3⁺ cells (hereafter referred to as V δ 2⁻), and is thought to be sensitive to a broad panel of stress-induced antigens, most of which are unknown.

To assess the potential involvement of the two subgroups of $\gamma\delta$ T cells in DSA production after kidney transplantation, we took advantage of a cohort of kidney transplant recipients (KTRs) whose $\gamma\delta$ T cell were measured after transplantation. Among 921 patients who had undergone kidney transplantation at Bordeaux University Hospital between January 1, 2004, and December 31, 2011, 628 had phenotyping of their circulating $\gamma\delta$ T cells. We excluded 240 KTRs who received a depleting induction therapy, and another 57 who had prior DSA or no serologic follow-up. Finally, a total of 331 patients fulfilled inclusion criteria (Supplementary Figure 1). In this cohort, 62 patients developed de novo DSA during the ten years post transplantation (Figure 1A). The clinical characteristics of the patients are summarized in Supplementary Table 1. In these patients, the numbers of V δ 2⁺ and V δ 2⁻ $\gamma\delta$ T cells were measured in the circulation by flow cytometry at baseline and two years after transplantation (Figure 1B). Overall, the total number of $\gamma\delta$ T cells significantly increased between the day of the transplantation and two years later (Supplementary Figure 2A). This increase was entirely explained by the expansion of the V δ 2⁻ $\gamma\delta$ T cells (Supplementary Figure 2). Indeed, after transplantation, KTRs who are infected (or reinfected) with cytomegalovirus (CMV) show an

expansion of a CMV-specific V δ 2⁻ oligoclonal population (18, 19). Given that i) most CMV infections occur early (before 6 months) after transplantation (32, 33) and ii) the pool of expanded V δ 2⁻ $\gamma\delta$ T cells remains stable over time (19), we considered only the measurement performed two years after the transplantation to study the impact of $\gamma\delta$ T cells on DSA production during the period from 2 to 10 years post-transplantation. The 22 KTRs who developed DSA during the first two years were consequently excluded from the analysis.

To compare patients with high or low circulating $\gamma\delta$ T cells, we first determined thresholds to divide the cohort into two groups. Receiver operating characteristics (ROC) curves correlating the numbers of total, V δ 2⁺ or V δ 2⁻ $\gamma\delta$ T cells and the occurrence of DSA during follow-up did not allow us to determine a relevant threshold (Supplementary Figure 2B). We therefore set arbitrary thresholds at 85, 40 and 55 cells/volume unit, using the distribution of total, V δ 2⁺ and V δ 2⁻ $\gamma\delta$ T cell counts, respectively (Supplementary Figure 2C). We consequently divided our cohort into patients with low or high numbers of total, V δ 2⁺ or V δ 2⁻ $\gamma\delta$ T cells (Supplementary Figure 2D). Thus, whether we consider the total number of $\gamma\delta$ T cells, the number of V δ 2⁺ or V δ 2⁻ $\gamma\delta$ T cells, the incidence of DSA is strictly comparable between the two groups of patients (low versus high, p=0.82, p=0.77, p=0.86, log-rank test, for the total number of $\gamma\delta$ T cells, V δ 2⁺ and V δ 2⁻ $\gamma\delta$ T cells, respectively; Figure 1C). Furthermore, $\gamma\delta$ T cells have no impact on the titers (Figure 1D), targets (Figure 1E) or repertoire (Figure 1F) of the DSA response.

This clinical study does not demonstrate a role for $\gamma\delta$ T cells, either V δ 2⁺ or V δ 2⁻, in the anti-donor humoral response following renal transplantation. However, this study is very indirect, attempting to correlate a rare event that occurs in the secondary lymphoid organs (i.e., DSA production) with a circulating cell count performed at a single time point. In order to strengthen these results we conducted a set of mechanistic experiments.

Figure 1

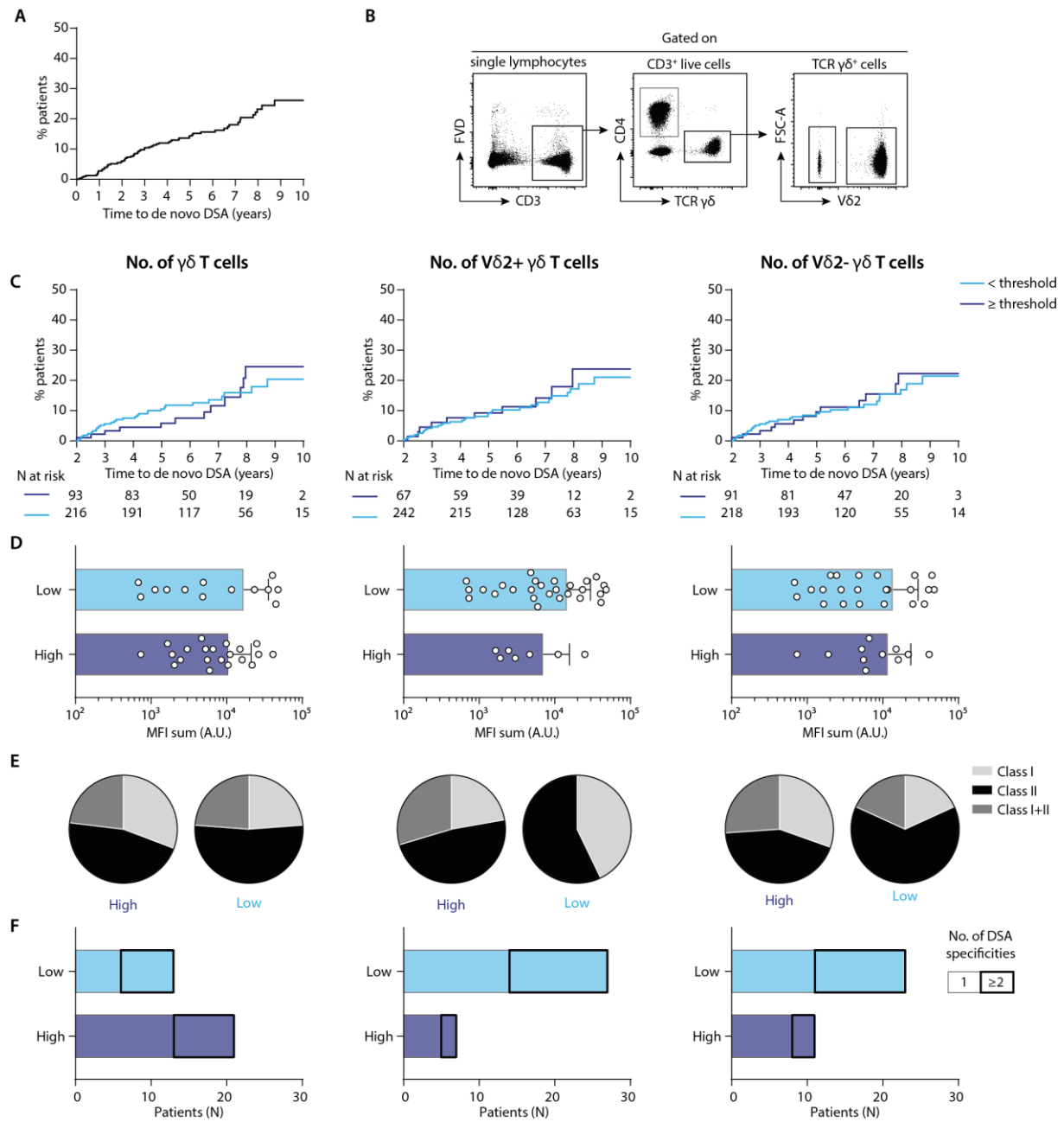


Figure 1. Circulating $\gamma\delta$ T cells are not correlated with de novo DSA incidence after kidney transplantation.

(A) Kaplan-Meier curve of DSA-free survival after kidney transplantation in the complete cohort.

(B) Representative flow cytometry profiles of the gating strategy used to assess the numbers of the different $\gamma\delta$ T cells subtypes.

(C to F). For each analysis, the cohort was divided in patients with high numbers (dark blue) or low numbers (light blue) of TCR $\gamma\delta$ T cells (left column), V δ 2⁺ $\gamma\delta$ T cells (middle column) or V δ 2⁻ $\gamma\delta$ T cells (right column) at two years after transplantation.

(C) Kaplan-Meier curves of de novo DSA incidence after kidney transplantation, from the second year of follow-up.

(D) The titers of de novo DSA were quantified by solid phase assay in kidney transplant recipients. The sum of MFI is plotted. Individual values and mean +/- SD.

(E) The specificities of the de novo DSA were compared between each group of patients.

(F) The repertoire of the de novo DSA response was compared between each group of patients.

Assessment of the ability of human $\gamma\delta$ T cells to play a follicular helper role

Several studies have reported that $\gamma\delta$ T cells have the ability to interact with B cells in germinal centers and to support the production of class-switched auto-antibodies in mouse models (25, 34).

To test if human $\gamma\delta$ T cells could also play a role of T follicular helper (T_{FH}) cells and support DSA (allo-antibodies) production after transplantation, we first studied the distribution of T cells in secondary lymphoid tissues, where the alloimmune response takes place after solid organ transplantation (35). To this end, we stained lymph nodes with either an anti-TCR β or an anti-TCR δ antibody. The density of TCR β^+ cells in the secondary follicles (i.e., the germinal centers) was much higher than that of TCR δ^+ cells, even if some rare TCR δ^+ could be found in some follicles (median density of cells: 7.2, interquartile range (IQR) 5.7 to 9.6 versus 0.3, IQR 0.1 to 0.8 for TCR β^+ and TCR δ^+ cells, respectively; $p=0.0002$; Figure 2A). As a consequence, TCR β^+ cells represent around 95% of T cells in the germinal centers (Figure 2A), suggesting that their role in helping germinal center B cells is more crucial than that of $\gamma\delta$ T cells.

To further assess the ability of $\gamma\delta$ T cells to acquire T_{FH} features after activation, we moved to in vitro experiments. Peripheral blood mononuclear cells (PBMCs) from 4 healthy volunteers were either left to rest or stimulated with beads coated with anti-CD3 and anti-CD28 mAbs, which allow to deliver both TCR and costimulating signals, regardless the specificity of the TCR. After stimulation, the expression of CXCR5 [a chemokine receptor allowing cell migration towards B-cell rich zones in secondary lymphoid organs, (36)] and CD40L [a key costimulatory molecule for B cells responses to T-dependent antigens, (37)] on $\gamma\delta$ T cells was assessed by flow cytometry (Figure 2C). CD4 $^+$ T cells, which encompass the professional subset of T_{FH} cells that specialize in helping B cells, were used as reference. First, to ensure that all the cells had the same capacity to react to stimulating signals and did not have exhausted profiles, we measured the upregulation of CD69, a non-specific activation marker, which

confirmed that all the cells had the same capacity to get activated (Figure 2C). The expression of CXCR5 by $\gamma\delta$ T cells was low or null at steady state and did not increase after activation, whereas a median of 19.3% (IQR 15.6 to 21.2) of $CD4^+$ T cells expressed CXCR5 after activation. This result is consistent with the literature (38) and mirrors the observation in the figure 2A that $CD4^+$ T cells are more prone than $\gamma\delta$ T cells to localize to germinal centers.

In contrast however, and as it has already been described (26), the $V\delta 2^+$ subset of $\gamma\delta$ T cells was able to significantly upregulate CD40L after activation as compared with $V\delta 2^-$ cells, but in lower proportions than $CD4^+$ T cells (47.8%, IQR 36.1 to 62.3 versus 89.2%, IQR 83.6 to 94.1, $p=0.0286$). Furthermore, the median fluorescence intensity (MFI) of CD40L of $V\delta 2^+CD40L^+$ T cells was much lower than that of $CD4^+CD40L^+$ T cells (5688, IQR 4596 to 7037 versus 21861, IQR 15139 to 32121, $p=0.0286$, Figure 2F). It should be noted that the cells that express CD40L the most ($V\delta 2^+$ cells) are those that have the least capacity to express CXCR5, which makes it unlikely that they are involved in DSA production.

Since $\gamma\delta$ T cells are innate-like lymphoid cells, which also depend on “innate” immune signaling such as cytokine stimulation, interleukin(IL)-18 or a combination of IL-2 and IL-15 was added to the bead signal in some culture conditions. These cytokines have indeed been shown to potentiate $\gamma\delta$ TCR-induced activation (39) and proliferation (40). However, the addition of cytokines did not change the expression profiles of CD69, CXCR5 or CD40L after activation (Supplementary Figure 3, A to D).

To confirm these results in a functional assay, we next performed T and B cell cocultures. The canonical sequence that leads to DSA production is as follows: i) a B cell is activated by an allo-antigen via its cognate BCR (signal 1), after what the antigen is internalized and processed for presentation at the surface as a peptide within MHC-II molecules; ii) a $CD4^+$ T cell of indirect specificity is then activated by recognition, by its cognate TCR, of the complex consisting of self-MHC and the allogeneic MHC-derived peptide, and in turn delivers a

costimulatory signal (signal 2) to the B cell. The sum of these two signals allows the proliferation of B cells and their differentiation into DSA-producing plasma cell (4, 5, 41, 42). This cooperation can be easily reproduced in vitro, provided that two tricks are used to overcome the barrier of antigen specificity of T and B cells: i) in order to activate a sufficient number of B cell, signal 1 can be delivered by the use of an anti-IgM antibody that will cross-link the BCR and activate the cell regardless of its specificity (6), and ii) to ensure that sufficient numbers of T cells will support B cell activation, allogeneic CD4⁺ T and B cells are used, so that T cells can be activated by direct recognition of MHC-II molecules [which means ~1-10% of T cells able to react (43)]. This coculture, which was used as a reference in our experiments (Figure 2G), leads to efficient proliferation of B cells (as assessed by dilution of a proliferation dye and calculation of the B cell division index, Figure 2H). Moreover, the importance of trogocytosis [the phenomenon by which a cell extracts surface molecules from the cell with which it interacts and expresses them on its own surface, (44)] under these conditions is indicative of the intensity of the T-B dialogue within the immune synapses: after 6 days of coculture, around 70% of B cells express CD4 and CD3 (Figure 2I). In contrast, when CD4⁺ T cells were replaced by $\gamma\delta$ T cells in the same coculture (Figure 2G), B cells were unable to proliferate (Figure 2H), and no trogocytosis was observed (Figure 2I). These cocultures demonstrate that the TCR of $\gamma\delta$ T cells is not able to interact with MHC-II molecules expressed at the surface of B cells, and that BCR-activated B cells do not upregulate any surface antigen capable of activating $\gamma\delta$ T cells. Thus, we conclude that $\gamma\delta$ T cells are not able to perform “T_{FH}-like” functions.

Figure 2

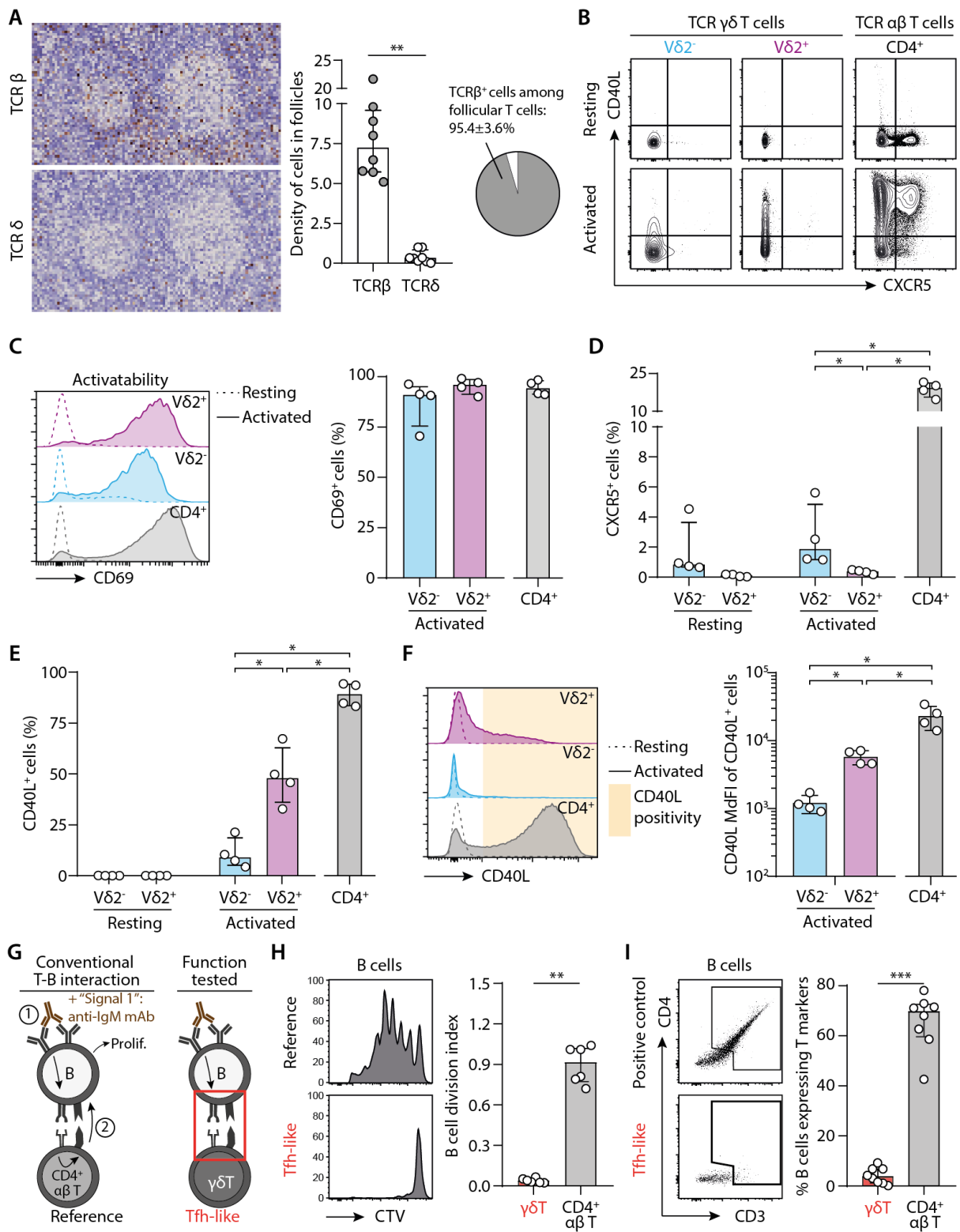


Figure 2. Assessment of the ability of human $\gamma\delta$ T cells to play a follicular helper role

(A) Left: immunohistochemical study of a peripheral lymph node section, stained for TCR β (up) and TCR δ (down). Middle: density of TCR β^+ and TCR δ^+ cells in the follicles quantified by computer-assisted morphometry. Right: pie-chart representing the proportion of TCR β^+ and TCR δ^+ cells among follicular T cells.

(B to F) PBMCs were cultured in the presence or absence of beads coated with anti-CD3 and anti-CD28 mAbs.

(B) Representative flow cytometry profiles for the expression of CD40L and CXCR5 in resting (upper row) and activated (lower row) T cells.

(C) Left: Representative histograms for the expression of CD69 in resting (dotted line) or activated (full line) V δ^+ (up, purple), V δ^- (middle, blue) or control CD4 $^+$ T cells (down, grey). Right: individual values for percentages of CD69 $^+$ cells.

(D and E) Individual values for percentages of **(D)** CXCR5 $^+$ and **(E)** CD40L $^+$ cells.

(F) Left: Representative histograms for the expression of CD40L in resting (dotted line) or activated (full line) V δ^+ (up, purple), V δ^- (middle, blue) or control CD4 $^+$ T cells (down, grey). Right: individual MdfI values for CD40L $^+$ cells.

(G to I) Human B cells were cocultured with allogeneic CD4 $^+$ T or $\gamma\delta$ T cells in the presence of IgM F(ab')₂ (signal 1), and **(H)** the percentage of divided cells among alive B cells was evaluated by flow cytometry, as well as **(I)** the trogocytosis between B and T cells.

(G) Schematic representation of the experiment.

(H) Left: Representative histograms. Right: Individual coculture values.

(I) Left: The flow cytometry gating strategy for the assessment of trogocytosis. Right: percentage of B cells that have experienced trogocytosis in each coculture.

Data are presented as median \pm IQR. Data were analyzed by Mann-Whitney test. *P < 0.05, **P < 0.01 and ***P < 0.001.

Assessment of the ability of human $\gamma\delta$ T cells to support $CD4^+$ T_{FH}

If $\gamma\delta$ T cells are not able to directly help B cells for the production of DSA, they could however indirectly act by supporting T_{FH} functions. This hypothesis is supported by i) histological findings demonstrating that the majority of gamma-delta T cells are located outside germinal centers in lymph nodes, where they form a network intertwined with that of the $\alpha\beta$ T cells (Figure 3A), and ii) previously published studies showing that $\gamma\delta$ T cells may present antigenic peptides within MHC-II (27, 45) or assist $CD4^+$ T cells in initiating the T_{FH} program [in mouse, (27)].

To test this hypothesis, we performed the same experiments as describe above. This time, B cells, which are professional antigen-presenting cells (APC), were used as reference. First, to assess the ability of $\gamma\delta$ T cells to present antigens, we measured the expression of HLA-DR at steady state and after activation. The MdFI of HLA-DR barely increased after activation in $V\delta^+$ cells, and remained much lower than that observed in B cells (MdFI=196, IQR 170 to 268; 549, IQR 427 to 840 and 35030, IQR 32506 to 36168 for resting $V\delta^+$, activated $V\delta^+$ and B cells, respectively; $p=0.0286$ for both resting versus activated $V\delta^+$ cells and activated $V\delta^+$ versus B cells comparisons; Figure 3B). We then evaluated the expression of costimulatory molecules (CD80 and CD86; Figure 3C). The results obtained with the expression of costimulatory markers are very similar to those obtained with HLA-DR: activation has an extremely modest effect on the increase in the expression of CD80 and CD86 molecules by $\gamma\delta$ T cells, and the expression remains much lower than that observed on a professional APC like B cells (Figure 3, D and E). Of note, similar results were obtained when cytokines were added to the culture medium (Supplementary figure 3, E to G).

Finally, to test the ability of $\gamma\delta$ T cells to act as APCs in a more functional assay, we replicated the coculture described above, adding $\gamma\delta$ T cells to the reference condition (Figure 3F). Under these conditions, B cells proliferate efficiently, as in the reference condition (Figure 3G), but the presence of $\gamma\delta$ T cells does not increase the number of dividing B cells (B cell division index, Figure 3G) or the number of divisions of those dividing B cells (B cell proliferation index, Figure 3G).

Overall, these data do not indicate a role for $\gamma\delta$ in supporting CD4⁺ T_{FH} function.

Figure 3

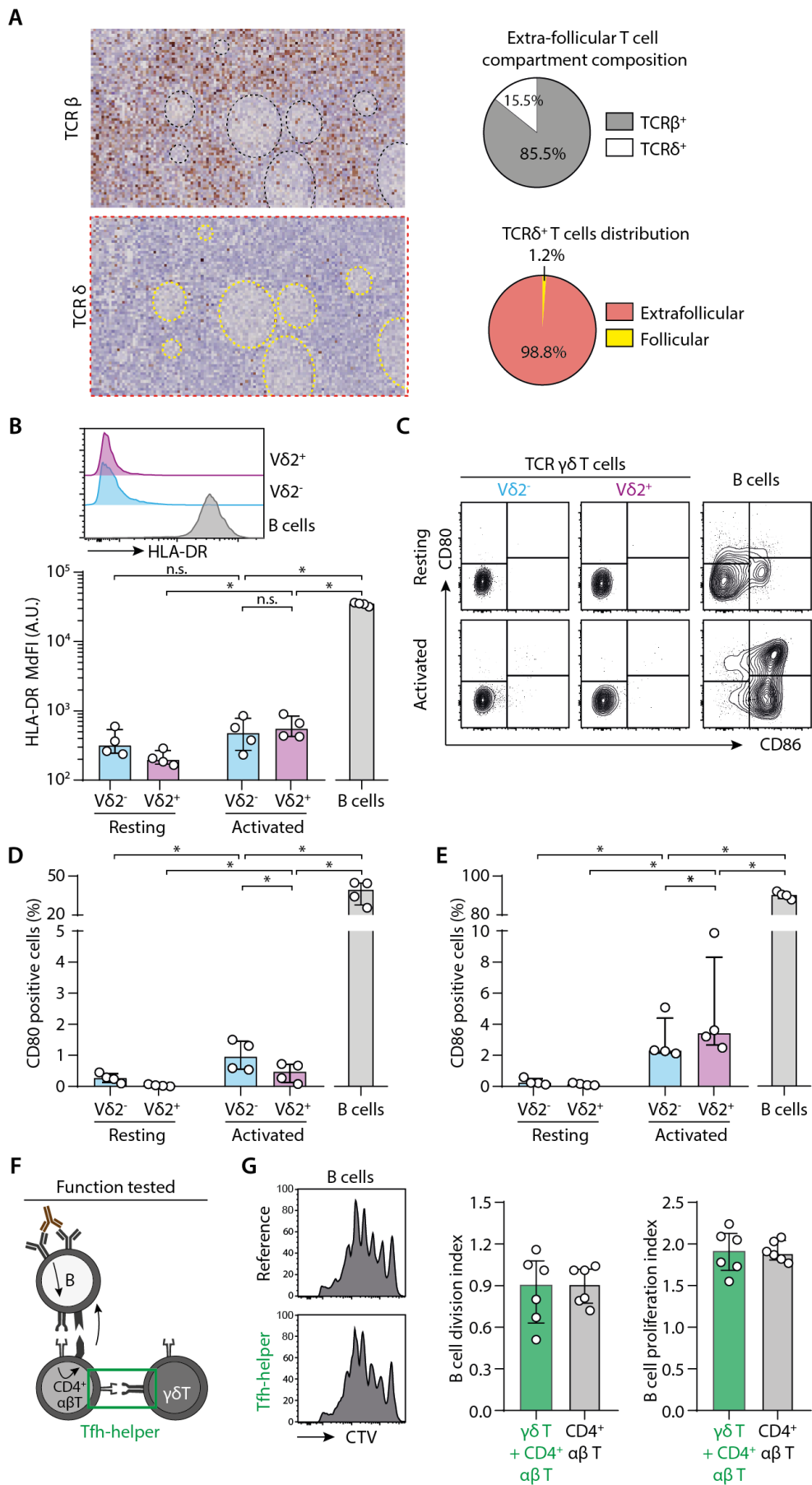


Figure 2. Assessment of the ability of $\gamma\delta$ T cells to support $CD4^+$ T_{FH}

(A) Left: immunohistochemical study of a peripheral lymph node section, stained for TCR β (up) and TCR δ (down). Middle: density of TCR β^+ and TCR δ^+ cells in the follicles quantified by computer-assisted morphometry. Right: density of TCR β^+ and TCR δ^+ cells in the follicles were quantified by computer-assisted morphometry. Pie-chart representing the proportion of TCR β^+ and TCR δ^+ cells among extra-follicular T cells (up) and the distribution of TCR δ^+ T cells (down).

(B to F) PBMCs were cultured in the presence or absence of beads coated with anti-CD3 and anti-CD28 mAbs.

(B) Up: Representative histograms for the expression of HLA-DR in V $\delta 2^+$ (up, purple), V $\delta 2^-$ (middle, blue) $\gamma\delta$ T cells or control B cells (down, grey). Down: individual MdfI values for HLA-DR $^+$ cells.

(C) Representative flow cytometry profiles for the expression of CD80 and CD86 in resting (upper row) and activated (lower row) T cells.

(D and E) Individual values for percentages of **(D)** CD80 $^+$ and **(E)** CD86 $^+$ cells.

(F and G) Signal 1-primed human B cells were cocultured with allogeneic CD4 $^+$ T in the presence or absence of syngeneic $\gamma\delta$ T cells.

(F) Schematic representation of the experiment.

(G) The percentage of divided cells among alive B cells was evaluated by flow cytometry. Left: Representative histograms. Middle: individual B cell division index values. Right: individual B cell proliferation index values.

Data are presented as median \pm IQR. Data were analyzed by Mann-Whitney test. *P < 0.05.

Confirmation of human clinical and experimental results in a mouse model of heart transplantation

Finally, to confirm our human data in an unbiased in vivo model, we moved to mouse experiments. We performed full mismatch heterotopic heart transplantation as a model of solid organ transplantation. Different recipient mice on C57BL/6 (H-2^b) background were used, namely i) wild-type mice (concomitant presence of $\alpha\beta$ and $\gamma\delta$ T cells, positive controls), ii) TCR α KO mice (absence of $\alpha\beta$ T cells), iii) TCR δ KO mice (absence of $\gamma\delta$ T cells), and iv) CD3 ϵ KO mice (complete absence of T lymphocytes, negative controls; Figure 4A). In the absence of the TCR α chain, positive selection in the thymus cannot occur, and TCR α KO mice have no $\alpha\beta$ T lymphocytes in the periphery. In contrast, $\gamma\delta$ T cells do not undergo thymic selection against MHC molecules, but the deletion of the delta chain prevents the development of $\gamma\delta$ T cells (46). Finally, the knock-out of CD3 ϵ arrests thymocyte development and residual thymocytes are totally immature. As a consequence, CD3 ϵ KO mice have no T cells at all (Supplementary Figure 4, A to C). Since the $\alpha\beta$ compartment is dominant in wild-type mice (Supplementary Figure 4, A & C), TCR δ KO mice have an overall normal T cell count in the spleen, composed exclusively of $\alpha\beta$ T cells (Supplementary Figure 4, A to C) whereas TCR α KO mice have a very restricted T cell population, composed exclusively of $\gamma\delta$ T cells (Supplementary Figure 4, A to C). In contrast, the genetic manipulations in these three mouse strains have no effect on B cell physiology, and all these mice consequently have normal numbers of B cells in the spleen (Supplementary Figure 4B).

These mice were used as recipients of a full mismatch heart graft from Balb/c (H-2^d) donors (Figure 4B). We used nude donors because grafts from these athymic mice do not contain T cells (Figure 4B). Indeed, we and others have recently demonstrated that donor T cells could be involved in DSA production after transplantation by the inverted direct allorecognition pathway (6, 7). Overall, this mouse models provides a unique opportunity to study the role of $\gamma\delta$ T cells in DSA production after transplantation: TCR α KO mice are used to study the ability of $\gamma\delta$ to perform T_{FH} functions, and TCR δ KO are used to see if the absence of $\gamma\delta$ T cells impacts antibody production.

Whereas wild-type mice develop a detectable DSA response as early as day 7 and peaking at day 28 (Figure 4C), CD3 ϵ KO and TCR α KO mice produce no DSA after heart transplantation (Figure 4C). This lack of response is not explained by a defect in B-cell functionality in the recipient mice as these mice develop normal antibody titers after immunization with the thymo-independent antigen 4-hydroxy-3-nitrophenyl acetyl(NP)-Dextran (Supplementary Figure 4D). This rules out any possibility for $\gamma\delta$ T cells to play a T_{FH} role in DSA production. In contrast, TCR δ KO mice produce DSA with the same kinetics as wild-type mice (Figure 4C) and reach a comparable peak (Figure 4D). Furthermore, the quality of the DSA response is not affected by the absence of $\gamma\delta$ T cells, because the affinity of the DSAs, as evaluated by their residual binding capacity on a target after incubation in the presence of a chaotropic agent (urea, Figure 4E), and their isotypes (Figure 4F), are strictly the same in wild-type and TCR δ KO mice. This suggests that $\gamma\delta$ T cells have no impact on T_{FH} priming or on ongoing germinal center responses. In conclusion, in the context of solid organ transplantation, $\gamma\delta$ T cells are not able to assist B cells in DSA production, and do not act in support of CD4⁺ T_{FH} as their absence does not affect the kinetics, intensity or affinity of the DSA response.

Figure 4

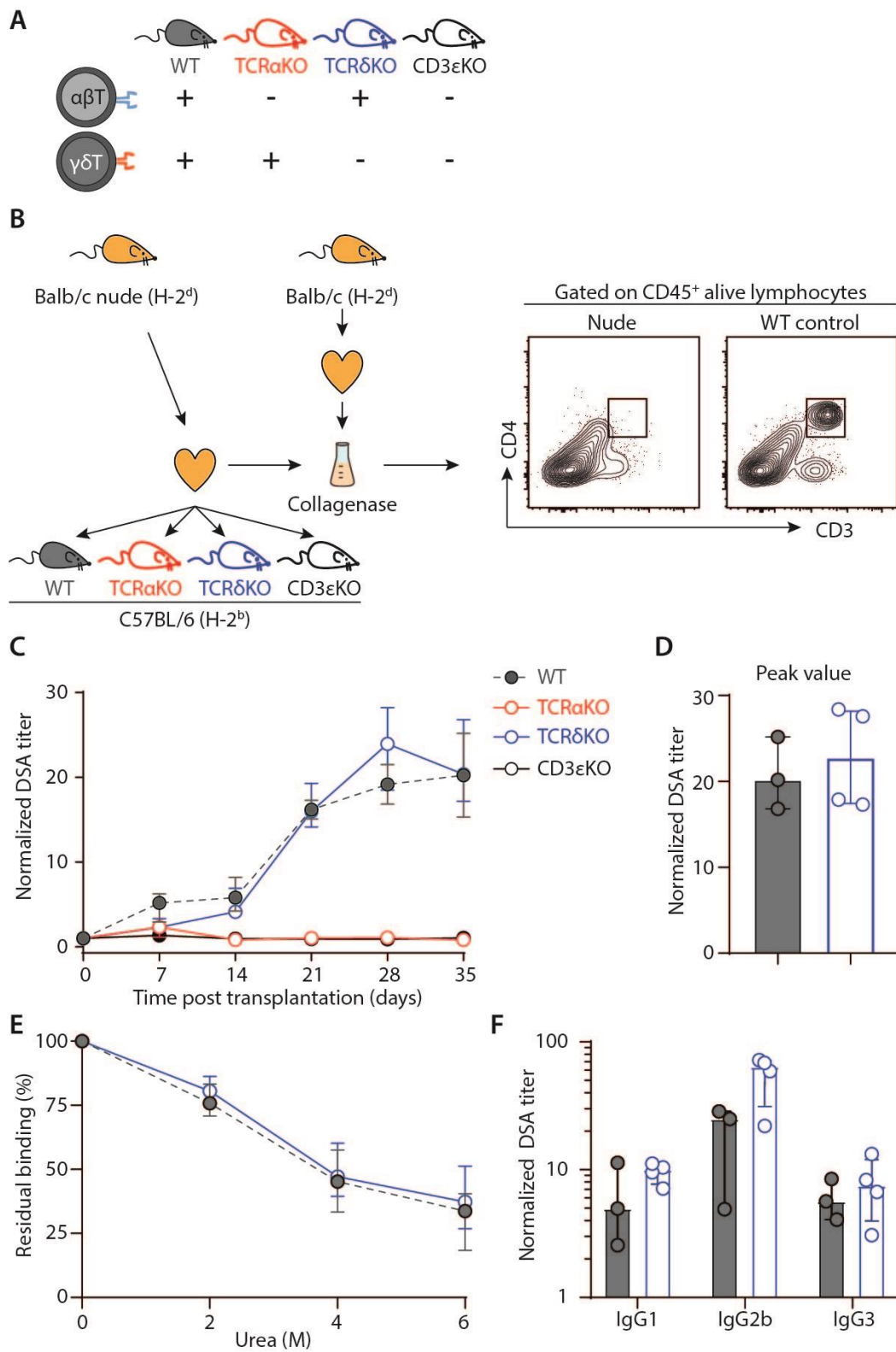


Figure 4. Assessment of the role of $\gamma\delta$ T cells in a mouse model of heart transplantation

(A) Schematic representation of the mouse strains used and their $\alpha\beta$ and $\gamma\delta$ T cells compartments.

(B) Presentation of the mouse model. Allogeneic Balb/c nude (H-2^d) hearts were transplanted to wild-type (WT), TCR α KO, TCR δ KO or CD3 ϵ KO C57BL/6 (H-2^b) recipient mice. Results are from one experiment. Heart grafts were harvested from Balb/c nude and Balb/c WT donors and digested with collagenase. Heart graft cell suspensions were analyzed by flow cytometry. Representative flow cytometry profiles are shown.

(C) Evolution of normalized DSA titers in the circulation of recipients is shown for wild-type (grey, n=3), TCR α KO (red, n=4), TCR δ KO (blue, n=4) and CD3 ϵ KO (black, n=5) C57BL/6 mice.

(D) DSA titers were compared at the peak of the response between wild-type (grey, n=3) and TCR δ KO (blue, n=4) C57BL/6 mice.

(E) The avidity of DSA produced by wild type (grey, n=2) and TCR δ KO (blue, n=4) C57BL/6 recipients were compared at day 28 by assessing the stability of DSA binding to Balb/c splenocytes in the presence of increasing concentrations of urea.

(F) DSA isotypes were tested at the peak of the response for wild-type (grey, n=2) and TCR δ KO (blue, n=4) C57BL/6 mice. Data are presented as mean \pm SD.

Data are presented as median \pm IQR.

Abbreviations: TCR, T-cell receptor; WT, wild-type.

Discussion

It is known that it is essential for B cells to receive T-cell help to develop into DSA-producing plasma cells after transplantation. Here, from the analysis of a cohort of KTRs up to in vivo mouse model of heart transplantation, we demonstrate that $\gamma\delta$ T cells, a kind of innate-like lymphoid cells, cannot provide help to B cells, either directly by replacing T_{FH} $CD4^+$ T cells or indirectly by priming the T_{FH} response.

Although the results of this study were negative, recent literature confirms that the field of study of the role of innate cells in allorecognition phenomena is worth exploring. On the one hand, the work of the Lakkis group has demonstrated that certain myeloid cells are capable of allorecognition (47, 48). This work, although yet to be confirmed in humans, represents a paradigm shift in understanding the role of myeloid innate immunity in transplantation. On the other hand, innate lymphoid cells, although not directly involved in DSA production to date, have been studied for their role in supporting or controlling antibody production (49). Among those processes, we can mention the role of NK cells, which are able to control the alloimmune responses by eliminating the graft-derived antigen presenting cells (50–52) or $CD4^+$ T cells (7). More recently, they have been involved in chronic vascular rejection, in a way independent of (53–55) or synergizing with DSA (56). Indeed, NK cells can get activated directly at the surface of the graft endothelium by a phenomenon called the missing-self, which is an innate allorecognition process that is totally independent of the adaptive immune system. Finally, all innate-like T cells other than $\gamma\delta$ T cells were involved in antibody production in different studies, although with a very restricted TCR repertoire (57, 58).

Regarding the ability of $\gamma\delta$ T cells to directly help B cells, our results are perfectly consistent with what is described in the literature. Indeed, it has been demonstrated that mice lacking $\alpha\beta$ T cells can produce autoantibodies (25, 34), but never antibodies against an exogenous protein antigen (27). A single study has highlighted the existence of tonsillar $V\delta 2^+V\gamma 9^+$ T cells

expressing CXCR5, CD40L and ICOS, that do not exist in periphery. In vitro $V\delta 2^+V\gamma 9^+CXCR5^+$ T cells were able to help B cell in antibody production (59). However, while their phenotype is indicative of their ability to migrate to B zones in vivo, it is not indicative of their ability to establish an immunological synapse with them. The difference in behavior between self and exogenous (including allo-) antigens described in the literature and confirmed in this work remains to be explained. It is now known that the response to self-antigens (in particular nucleic acids) depends to a large extent on the joint ligation of the BCR and TLRs in B cells (60), which is not the case for the response to exogenous antigens, which use only the BCR. It can be hypothesized that the TLR signal induces a phenotype of the B cell that would enable it to interact with $\gamma\delta$ T cells, via the membrane expression of stress antigens for example (61). The response against self-antigens was not the focus of this study, but given the high incidence of autoantibodies that have been reported in transplanted patients (62–64), it would be worthwhile to test the role of $\gamma\delta$ T cells in this context.

The results we obtained when studying the role of $\gamma\delta$ T cells in priming the $CD4^+$ T_{FH} cells in response to allo-antigens are also not contradictory with previously published data. Indeed, a recently published study reported a crucial role of $\gamma\delta$ T cells in the response to an exogenous antigen, through the induction of T_{FH} differentiation (27). However, in this work, $\gamma\delta$ T cells were involved in the response against ovalbumin only when it was adjuvanted with CFA (and not with alum), meaning that T-cell helping capacity is highly context dependent. We show that the context of transplantation does not allow $\gamma\delta$ T cells to prime $CD4^+$ T_{FH} cells.

Finally, this study has limitations. First, the analysis of the cohort of KTRs relies on T cell phenotypes performed on PBMCs, and clinical data are correlative. The demonstration that $\gamma\delta$ T cells are not involved in DSA production would have required to perform invasive biopsies of the graft-draining secondary lymphoid organs, without any certainty to catch the germinal center reaction responsible for DSA production. In addition, the analysis of T cell phenotypes was rendered complex by the difficulty of establishing a threshold to split the cohort in two, which ultimately relied on an arbitrarily defined cut-off based on the distribution of patients. However, given the results obtained, we doubt that any method would have allowed us to establish a more relevant threshold and lead to different results. Second, one could argue that, in the in vitro experiments, the stimulation combining CD3 and CD28 is not adapted to stimulate $\gamma\delta$ T cells, since the majority of $V\delta 2^-$ $\gamma\delta$ T cells are $CD28^-$ in patients with a history of CMV infection (65). However, these cells, once activated express the same level of CD69 than their $V\delta 2^+$ counterparts, and the addition of cytokines, used to counteract a hypothetical costimulation defect, did not change the outcome of the experiment. Moreover, this upregulation of CD69, similar in all T cell populations, shows that the absence of CXCR5/CD40L expression on the one hand, and HLA-DR/CD80/CD86 on the other hand, are not related to the an exhausted state of the $\gamma\delta$ T cells that we obtained from PBMCs.

In conclusion, we demonstrate here that $\gamma\delta$ T cells are not involved in the first stage of antibody-mediated rejection, namely DSA production. However, it should be kept in mind that this does not exclude them from being involved in AMR, as some of these cells express CD16 (66), enabling them to be secondarily recruited by the endothelium-bound DSA to cause microvascular inflammation of the graft (67).

Materials and methods

Cohort of transplanted patients

The study was carried out in accordance with French legislation on biomedical research and the Declaration of Helsinki. All patients gave written informed consent for the utilization of clinical data and biological samples for research purpose (written consent collected in RAN, regional computerized file; Commission Nationale de l'Informatique et des Libertés (CNIL) final agreement, decision 2009-413, n° 1357154). The patients were followed at least 2 years post-transplantation with peripheral blood immunophenotyping and serological follow-up.

Flow cytometry analyses for the monitoring of $\gamma\delta$ T cells

V δ ⁻ and V δ ⁺ $\gamma\delta$ T cells counts were obtained by flow cytometry at day 0 of the graft and 2 years post transplantation. Immunophenotypic characterization was carried out on 100 μ l anticoagulated whole blood taking into account at least 5000 total lymphocytes stained with anti-CD45, antipan- δ (clone IMMU 510; Beckman Coulter, Krefeld, Germany), and anti-TCR V δ 2 (clone 15D; Thermo Fisher Scientific, Rockford, IL). Percentages of cell populations were obtained using CELLQUEST software (BD Bioscience), and absolute counts of lymphocytes were obtained using the Single-Platform Lyse/No-Wash Trucount (BD Bioscience).

Anti-HLA antibody detection and characterization

Collected sera samples were analyzed using Single-antigen Bead Assay (One Lambda, Canoga Park, CA) according to the manufacturer's instructions. DSA were defined as positive by a mean fluorescence intensity (MFI)>500.

Lymph node histology

The samples analyzed by histology were normal peripheral lymph nodes. Staining of formalin-fixed paraffin-embedded (FFPE) sections was performed by automated immunohistochemistry

(LEICA BOND-III, Leica Biosystems) using anti-human TCR β (anti-T-cell receptor [TCR] β antibody; clone G11; Santa Cruz Biotechnology) and TCR δ (anti-T-cell receptor [TCR] δ antibody; clone H41; Santa Cruz Biotechnology) mAbs. Computer-assisted morphometric quantifications were performed using FIJI software (68).

$\gamma\delta$ T cell activation

Human Peripheral Blood Mononuclear Cells (PBMC) were collected from the French National Blood Service (Etablissement Français du Sang, EFS) and isolated by centrifugation on a Ficoll density gradient. Cells were cultured overnight in complete RPMI medium at 37°C and 5% CO₂, with or without Dynabeads™ Human T-activator CD3/CD28 (ThermoFisher Scientific), IL-18 (50ng/mL) or IL-2 (100IU/mL) + IL-15 (10ng/mL). In some conditions, anti-CD40L (TRAP1) antibody was added to the culture medium. After removal of the Dynabeads, cells were incubated at 4°C with relevant antibodies: CD3 (UCHT1, BD Biosciences), CD4 (SK3, BD Biosciences), TCR $\gamma\delta$ (REA-591, Miltenyi Biotec), V δ 2 (REA-771, Miltenyi Biotec), CD19 (HIB19, BD Biosciences), CXCR5 (RF8B2, BD Biosciences), CD69 (FN50, BD Biosciences), MHC-II (G46-6, BD Biosciences), CD80 (2D10, Biolegend), CD86 (FUN-1, BD Biosciences), and a fixable viability dye (ThermoFisher Scientific). Samples were acquired on a BD LSRFortessa flow cytometer (BD Biosciences). Data were analyzed with FlowJo software (Tree Star).

Cocultures

For B cell proliferation assay, B cells, CD4⁺ and $\gamma\delta$ T cells were purified (up to 95% purity) from PBMCs by negative selection with magnetic enrichment kits (Stemcell). B cells were stained with a proliferation dye (CellTrace Violet, ThermoFisher Scientific) according to the manufacturer's instructions. 4x10⁴ B cells were cocultured either with 4x10⁵ allogeneic CD4⁺ T cells or 3.2x10⁵ allogeneic CD4⁺ T cells plus 8x10⁴ syngeneic $\gamma\delta$ T cells. A soluble anti-human IgM F(ab')₂ (5 μ g/mL, Jackson Immunoresearch) was added to the culture medium.

After 6 days, cells were incubated at 4°C with fluorescent antibodies: CD3 (UHCT1), CD4 (SK3), CD19 (HIB19), CD20 (2H7), all from BD Biosciences, and a Fixable Viability Dye (eBiosciences). Sample acquisitions were made on a BD LSR Fortessa flow cytometer (BD Biosciences). Data were analyzed with FlowJo software (Tree Star).

Mice

Wild-type C57BL/6 (H-2^b) mice and wild-type or nude Balb/c (H-2^d) mice were purchased from Charles River Laboratories (Saint Germain sur l'Arbresle, France). TCR α (69) on C57BL/6 genetic background (TCR α KO) were obtained from the Centre de Distribution, Typage et Archivage animal (Orléans, France). TCR δ knock out (46) mice on C57BL/6 genetic background (TCR δ KO) were provided by B. Malissen. CD3 ϵ KO mice on C57BL/6 genetic background were purchased from The Jackson Laboratory (Bar Harbor, ME, USA).

All mice were maintained under EOPS (Exemption of Specific Pathogenic Organisms) conditions in our animal facility: Plateau de Biologie Expérimentale de la Souris (<http://www.sfr-biosciences.fr/plateformes/animal-sciences/AniRA-PBES>; Lyon, France). All studies and procedures were performed in accordance with EU guidelines and were approved by the local ethical committee for animal research (CECCAPP Lyon, registered by the French National Ethics Committee of Animal Experimentation under No. C2EA15, <http://www.sfr-biosciences.fr/ethique/experimentation-animale/ceccapp>).

Characterization of the immune phenotype of the different mouse strains

Before staining, murine cells from spleen, lymph nodes, heart or blood were incubated with a blocking anti-mouse Fc receptor antibody (2.4G2, home-made hybridoma). Cells were then incubated at 4°C with fluorescent antibodies: CD3 (145-2C11), CD19 (1D3), TCR β (H57-597, BD Biosciences) and TCR δ (GL3), all from BD Biosciences. Before analysis by flow cytometry, DAPI (4',6-diamidino-2-phenylindole dihydrochloride, Sigma-Aldrich) was added

to the cell suspension to exclude dead cells. Sample acquisitions were made on a BD LSR II flow cytometer (BD Biosciences).

Functional evaluation of the B cell compartment of the different mouse strains

Mice were immunized intraperitoneally with 200 µg NP-Dextran. Sera were tested for IgM anti-NP antibodies. Maxisorp plates (Nunc) were coated with NP 23-conjugated BSA. Serially diluted serum samples were added for 1 h 30 at room temperature. NP-specific antibodies were detected with alkaline phosphatase conjugated goat anti-mouse IgM Abs (1/2,000 dilution) followed by phosphatase substrate (Sigma-Aldrich). The plates were read at 405 nm/490 nm with an automatic reader (Zeiss VERSAmax). We used standard curves to convert OD to concentration using a four-parameter logistic equation (Softmax Pro 5.3 software; Molecular Devices).

Heterotopic heart transplantation in mice

Heterotopic heart transplantations were performed as previously described (8, 70). DSA titer was determined using a custom flow cross match assay as in Chen et al (8). Briefly, Balb/c CD4⁺ T cells were incubated with the sera of sensitized recipients. Binding of DSA to Balb/c cells was revealed using an anti-kappa light chain (187.1, BD Biosciences), anti-IgG1 (A85-1, BD Biosciences), anti-IgG2b (SouthernBiotech) or anti-IgG3 (R40-82, BD Biosciences) secondary antibody. Syngeneic C57BL/6 CD4⁺ T cells were used as controls. The titer of anti-donor antibodies at each time point (dx) was calculated with the following formula: normalized DSA titer = [MFI Balb/c (dx)/ MFI C57BL/6 (dx)]/ [MFI Balb/c (d0)/ MFI C57BL/6 (d0)]. Avidity of DSA was estimated by measuring the stability of preformed antigen-antibody complexes in the presence of increasing concentrations of a chaotropic agent (urea).

Statistical analysis

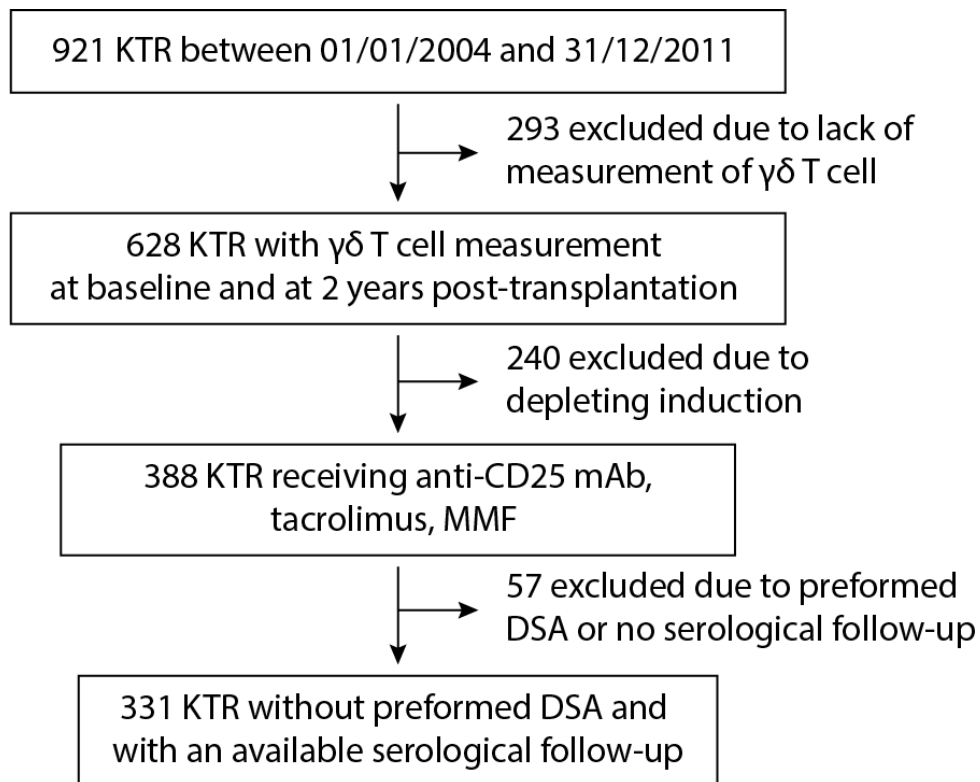
Statistical analysis and graphs were performed using Prism software (GraphPad). Quantitative variables were expressed as median \pm IQR and compared using Mann-Whitney test. All tests were two-sided. Incidence and survival data were analyzed by Kaplan-Meier plot and compared using a log-rank test. Statistical significance was considered for a p-value <0.05 .

Supplementary Table 1. Baseline kidney recipients characteristics

N (%) or mean±SD	Whole cohort n=331	De novo DSA within 10 years n=62	No DSA n=269
Age at time of transplantation (y)	50±15	45±18	51±14
Male	223 (67%)	38 (61%)	185 (69%)
Blood group			
O	132 (40%)	21 (34%)	111 (41%)
A	157 (47%)	34 (55%)	123 (46%)
B	26 (8%)	4 (6%)	22 (8%)
AB	16 (5%)	3 (5%)	13 (5%)
Cause of renal failure			
Glomerulonephritis	82 (25%)	20 (32%)	62 (23%)
Diabetes mellitus	27 (8%)	4 (6%)	23 (9%)
Vascular	16 (5%)	3 (5%)	13 (5%)
Hereditary	73 (22%)	10 (16%)	63 (23%)
Uropathy	30 (9%)	6 (10%)	24 (9%)
Others	103 (31%)	19 (31%)	84 (31%)
Donor			
Age	48±17	46±20	48±16
Living	23 (7%)	3 (5%)	20 (7%)
Deceased	308 (93%)	59 (95%)	249 (93%)
Transplantation condition			
First transplantation	320 (97%)	59 (95%)	261 (97%)
No. of HLA A/B/DR/DQ mismatches	4.9±1.5	5.5±1.5	4.8±1.5
CMV status			
D ⁻ /R ⁻	79 (24%)	14 (23%)	65 (24%)
D ⁺ /R ⁻	75 (23%)	11 (18%)	64 (24%)
R ⁺	177 (53%)	37 (60%)	140 (52%)
CMV < 2 years			
Disease	48 (15%)	10 (16%)	38 (14%)
DNAemia	92 (28%)	18 (29%)	74 (28%)

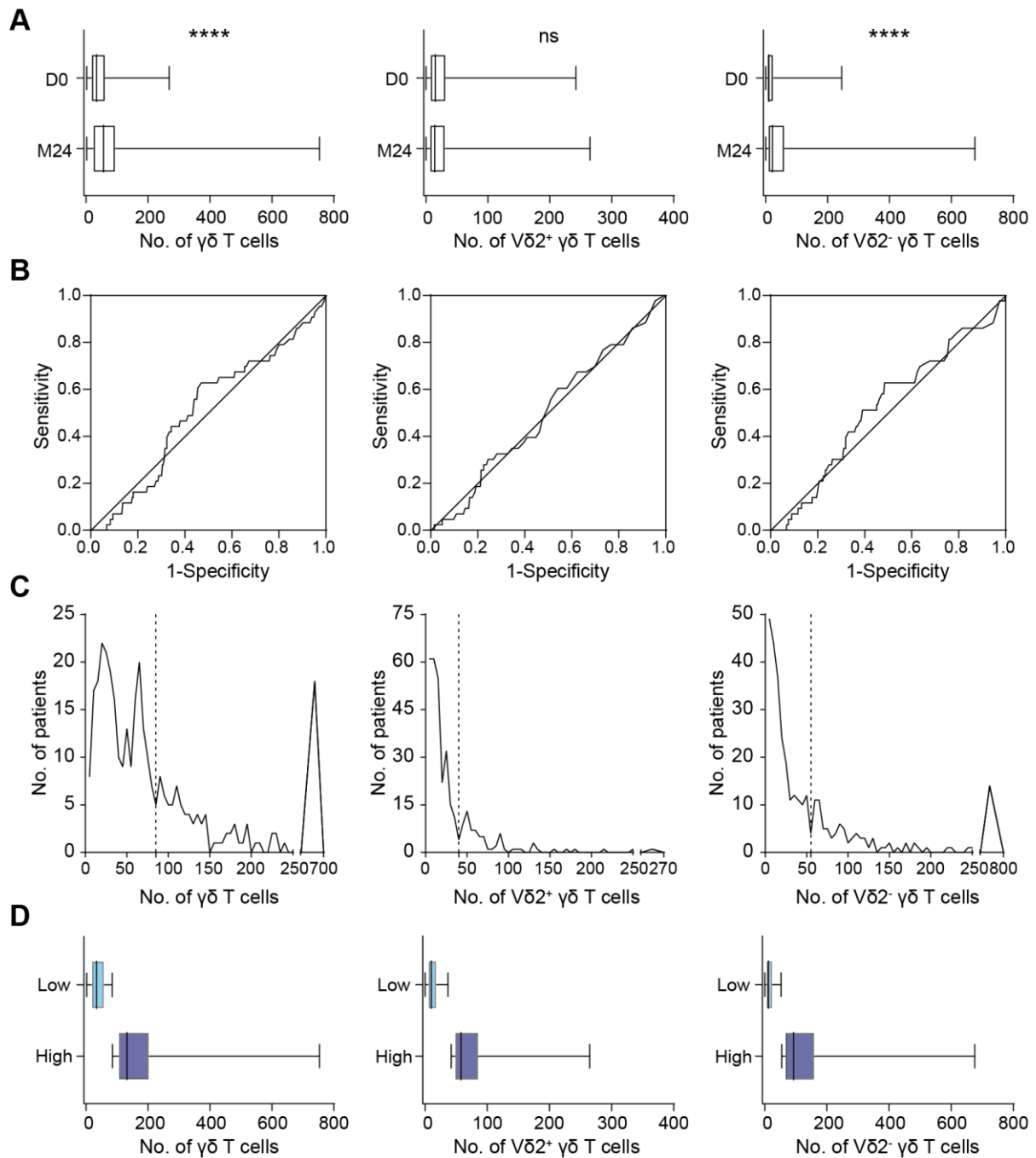
Abbreviations: DSA, donor-specific antibodies; y, years; No., number; CMV, cytomegalovirus; D/R, donor/recipient.

Supplementary Figure 1. Flow-chart of the study



Abbreviations: KTR: kidney transplant recipients; mAb: monoclonal antibody; MMF: mycophenolate mofetil; DSA: donor-specific antibody.

Supplementary Figure 2



Supplementary Figure 2. Methods used to determine the threshold to discriminate patients with low or high numbers of $\gamma\delta$ T cells

(A) Kidney transplant recipients T cells were phenotyped the day of the transplantation (D0) and two years later (M24). The number of TCR $\gamma\delta$ T cells (left panel), V δ 2⁺ $\gamma\delta$ T cells (middle panel) or V δ 2⁻ $\gamma\delta$ T cells (right panel) were compared between the day of the transplantation (J0) and M24. Median; box, 25th and 75th percentiles; whiskers, minimum to maximum. Mann-Whitney test, ****P<0,0001.

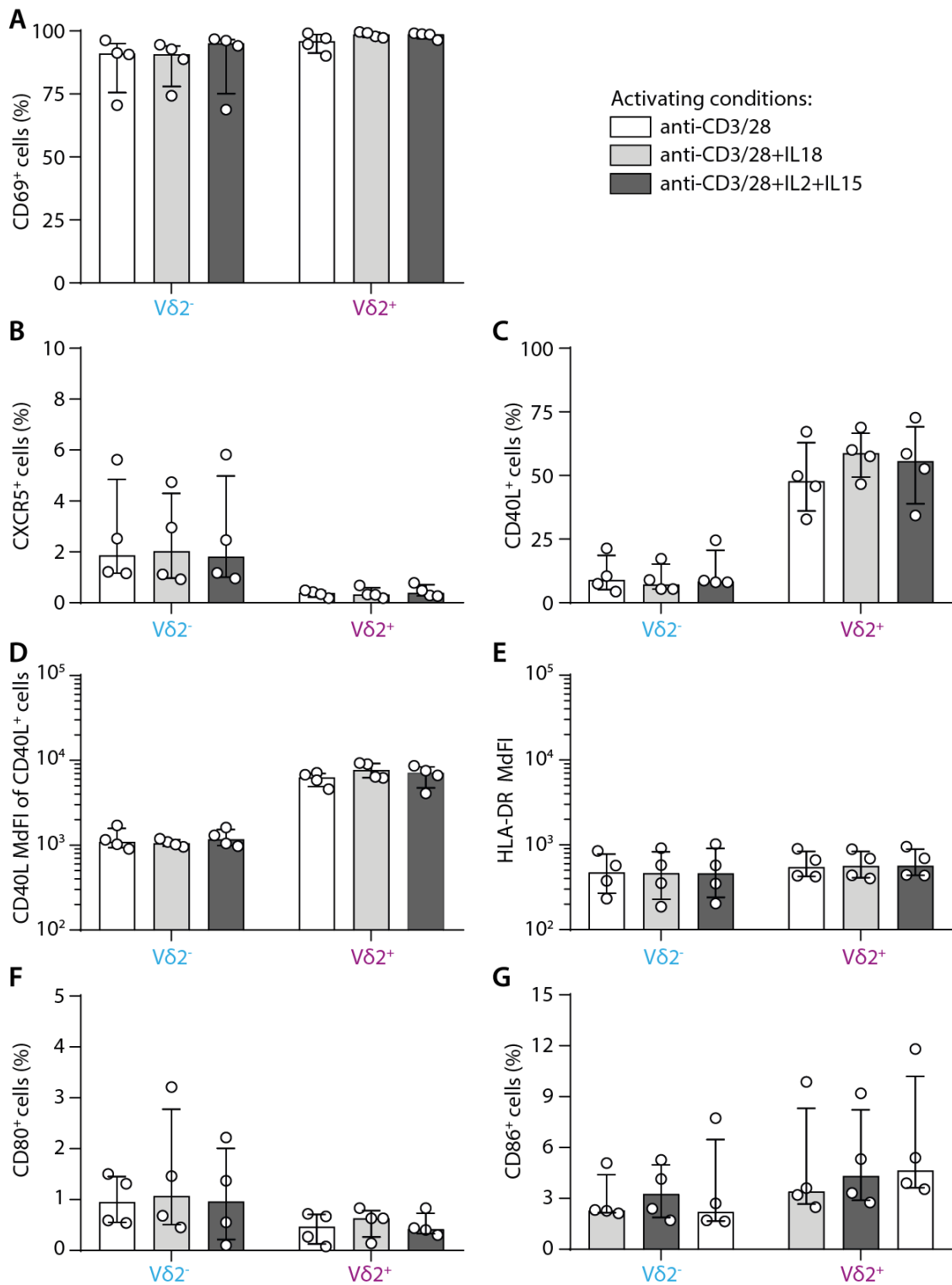
(B) Receiver-operating characteristic curves were constructed to determine the ability of TCR $\gamma\delta$ T cells (left panel), V δ 2⁺ $\gamma\delta$ T cells (middle panel) or V δ 2⁻ $\gamma\delta$ T cells (right panel) quantification at M24 to predict de novo DSA until 10 years after the transplantation.

(C) The distribution of patients according to the number of TCR $\gamma\delta$ T cells (left panel), V δ 2⁺ $\gamma\delta$ T cells (middle panel) or V δ 2⁻ $\gamma\delta$ T cells (right panel) quantification at M24 was analyzed. The vertical dashed line represents the threshold used in Figure 5.

(D) The patients were grouped according to whether they had high (dark blue) or low (light blue) numbers of TCR $\gamma\delta$ T cells (left panel), V δ 2⁺ $\gamma\delta$ T cells (middle panel) or V δ 2 $\gamma\delta$ T cells (right panel). The threshold used was determined in panel C. Median; box, 25th and 75th percentiles; whiskers, minimum to maximum.

Abbreviations: No., number.

Supplementary Figure 3



Supplementary Figure 3. Comparison of different activation cocktails

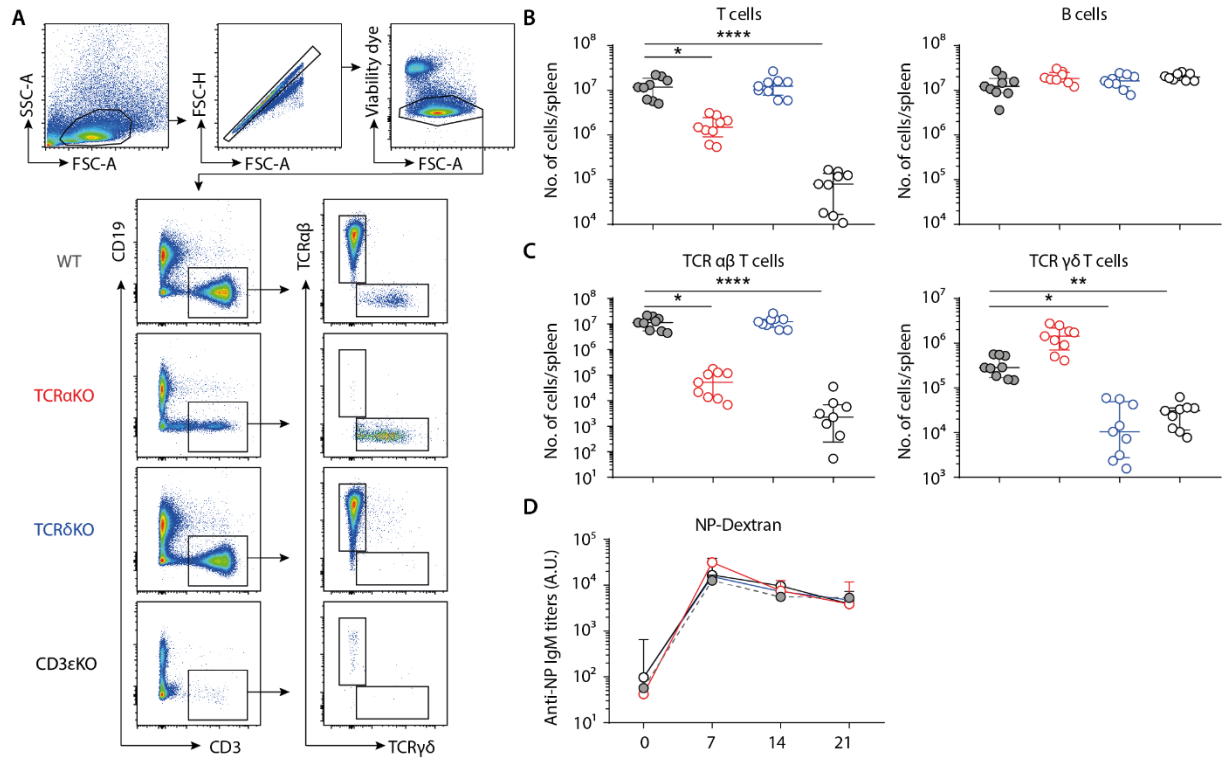
PBMCs were activated with beads coated with anti-CD3 and anti-CD28 mAbs, in the presence or absence of IL-18 or IL-2+IL-15.

(A to C) Individual values for percentages of **(A)** CD69⁺, **(B)** CXCR5⁺ and **(C)** CD40L⁺ cells.

(D and E) Individual MdfI values for **(D)** CD40L⁺ and **(E)** HLA-DR⁺ cells.

(F and G) Individual values for percentages of **(F)** CD80⁺ and **(G)** CD86⁺ cells.

Supplementary Figure 4



Supplementary Figure 4. Phenotypic and functional assessment of the four murine strains

(A) Flow cytometry gating strategy.

(B) Absolute number of T cells (left panel) and B cells (right panel) contained in the spleen of wild-type (WT, grey, n=9), TCR α KO (red, n=8), TCR δ KO (blue, n=9) and CD3 ϵ KO (black, n=8) C57BL/6 mice.

(C) Absolute number of TCR $\alpha\beta$ T cells (left panel) and TCR $\gamma\delta$ T cells (right panel) contained in the spleen of wild-type (WT, grey, n=9), TCR α KO (red, n=8), TCR δ KO (blue, n=9) and CD3 ϵ KO (black, n=8) C57BL/6 mice.

(D) Animals were immunized with the thymo-independent model antigen NP-Dextran and IgM titers were measured. Comparison over time of anti-NP antibody titres of wild-type C57BL/6 (grey, n=3), TCR α KO (red, n=3), TCR δ KO (blue, n=3) and CD3 ϵ KO (black, n=3).

Data are presented as median \pm IQR. Kruskal-Wallis test with Dunn's multiple comparisons.

*P<0.05; **P<0.01; ****P<0,0001.

Abbreviations:; TCR, T-cell receptor; No., number; WT, wild-type.

References

1. P. F. Halloran, J. Chang, K. Famulski, L. G. Hidalgo, I. D. R. Salazar, M. Merino Lopez, A. Matas, M. Picton, D. de Freitas, J. Bromberg, D. Serón, J. Sellarés, G. Einecke, J. Reeve, Disappearance of T Cell-Mediated Rejection Despite Continued Antibody-Mediated Rejection in Late Kidney Transplant Recipients. *J. Am. Soc. Nephrol. JASN*. **26**, 1711–1720 (2015).
2. M. J. Everly, L. M. Rebellato, C. E. Haisch, M. Ozawa, K. Parker, K. P. Briley, P. G. Catrou, P. Bolin, W. T. Kendrick, S. A. Kendrick, R. C. Harland, P. I. Terasaki, Incidence and Impact of De Novo Donor-Specific Alloantibody in Primary Renal Allografts: *Transplant. J.* **95**, 410–417 (2013).
3. C. Wiebe, I. W. Gibson, T. D. Blydt-Hansen, M. Karpinski, J. Ho, L. J. Storsley, A. Goldberg, P. E. Birk, D. N. Rush, P. W. Nickerson, Evolution and Clinical Pathologic Correlations of De Novo Donor-Specific HLA Antibody Post Kidney Transplant. *Am. J. Transplant.* **12**, 1157–1167 (2012).
4. T. M. Conlon, K. Saeb-Parsy, J. L. Cole, R. Motallebzadeh, M. S. Qureshi, S. Rehakova, M. C. Negus, C. J. Callaghan, E. M. Bolton, J. A. Bradley, G. J. Pettigrew, Germinal Center Alloantibody Responses Are Mediated Exclusively by Indirect-Pathway CD4 T Follicular Helper Cells. *J. Immunol.* **188**, 2643–2652 (2012).
5. C.-C. Chen, A. Koenig, C. Saison, S. Dahdal, G. Rigault, T. Barba, M. Taillardet, D. Chartoire, M. Ovize, E. Morelon, T. Defrance, O. Thaunat, CD4+ T Cell Help Is Mandatory for Naive and Memory Donor-Specific Antibody Responses: Impact of Therapeutic Immunosuppression. *Front. Immunol.* **9**, 275 (2018).
6. X. Charmetant, C.-C. Chen, S. Hamada, D. Goncalves, C. Saison, M. Rabeyrin, M. Rabant, J.-P. Duong van Huyen, A. Koenig, V. Mathias, T. Barba, F. Lacaille, J. le Pavec, O. Brugière, J.-L. Taupin, L. Chalabreysse, J.-F. Mornex, L. Couzi, S. Graff-Dubois, R. Jeger-Madiot, A. Tran-Dinh, P. Mordant, H. Paidassi, T. Defrance, E. Morelon, L. Badet, A. Nicoletti, V. Dubois, O. Thaunat, Inverted direct allorecognition triggers early donor-specific antibody responses after transplantation. *Sci. Transl. Med.* **14**, eabg1046 (2022).
7. I. G. Harper, J. M. Ali, S. J. F. Harper, E. Wlodek, J. Alsughayyir, M. C. Negus, M. S. Qureshi, R. Motalleb-Zadeh, K. Saeb-Parsy, E. M. Bolton, J. A. Bradley, M. R. Clatworthy, T. M. Conlon, G. J. Pettigrew, Augmentation of Recipient Adaptive Alloimmunity by Donor Passenger Lymphocytes within the Transplant. *Cell Rep.* **15**, 1214–1227 (2016).
8. C.-C. Chen, E. Pouliquen, A. Broisat, F. Andreatta, M. Racapé, P. Bruneval, L. Kessler, M. Ahmadi, S. Bacot, C. Saison-Delaplace, M. Marcaud, J.-P. D. Van Huyen, A. Loupy, J. Villard, S. Demuylder-Mischler, T. Berney, E. Morelon, M.-K. Tsai, M.-N. Kolopp-Sarda, A. Koenig, V. Mathias, S. Ducreux, C. Ghezzi, V. Dubois, A. Nicoletti, T. Defrance, O. Thaunat, Endothelial chimerism and vascular sequestration protect pancreatic islet grafts from antibody-mediated rejection. *J. Clin. Invest.* **128**, 219–232 (2018).

9. E. Pouliquen, A. Koenig, C. C. Chen, A. Sicard, M. Rabeyrin, E. Morelon, V. Dubois, O. Thauinat, Recent advances in renal transplantation: antibody-mediated rejection takes center stage. *F1000prime Rep.* **7**, 51 (2015).
10. R. S. Gaston, J. M. Cecka, B. L. Kasiske, A. M. Fieberg, R. Leduc, F. C. Cosio, S. Gourishankar, J. Grande, P. Halloran, L. Hunsicker, R. Mannon, D. Rush, A. J. Matas, Evidence for Antibody-Mediated Injury as a Major Determinant of Late Kidney Allograft Failure. *Transplantation.* **90**, 68–74 (2010).
11. J. Sellarés, D. G. de Freitas, M. Mengel, J. Reeve, G. Einecke, B. Sis, L. G. Hidalgo, K. Famulski, A. Matas, P. F. Halloran, Understanding the causes of kidney transplant failure: the dominant role of antibody-mediated rejection and nonadherence. *Am. J. Transplant. Off. J. Am. Soc. Transplant. Am. Soc. Transpl. Surg.* **12**, 388–399 (2012).
12. S. Karuthu, E. A. Blumberg, Common Infections in Kidney Transplant Recipients. *Clin. J. Am. Soc. Nephrol.* **7**, 2058–2070 (2012).
13. A. Humar, Y. Lebranchu, F. Vincenti, E. A. Blumberg, J. D. Punch, A. P. Limaye, D. Abramowicz, A. G. Jardine, A. T. Voulgari, J. Ives, I. A. Hauser, P. Peeters, The efficacy and safety of 200 days valganciclovir cytomegalovirus prophylaxis in high-risk kidney transplant recipients. *Am. J. Transplant. Off. J. Am. Soc. Transplant. Am. Soc. Transpl. Surg.* **10**, 1228–1237 (2010).
14. O. Witzke, I. A. Hauser, M. Bartels, G. Wolf, H. Wolters, M. Nitschke, VIPP Study Group, Valganciclovir prophylaxis versus preemptive therapy in cytomegalovirus-positive renal allograft recipients: 1-year results of a randomized clinical trial. *Transplantation.* **93**, 61–68 (2012).
15. N. Terrazzini, F. Kern, Cell-mediated immunity to human CMV infection: a brief overview. *F1000Prime Rep.* **6** (2014) (available at <https://facultyopinions.com/prime/reports/b/6/28>).
16. H. Kaminski, L. Couzi, M. Eberl, Unconventional T cells and kidney disease. *Nat. Rev. Nephrol.* **17**, 795–813 (2021).
17. H. Kaminski, I. Garrigue, L. Couzi, B. Taton, T. Bachelet, J.-F. Moreau, J. Déchanet-Merville, R. Thiébaud, P. Merville, Surveillance of $\gamma\delta$ T Cells Predicts Cytomegalovirus Infection Resolution in Kidney Transplants. *J. Am. Soc. Nephrol. JASN.* **27**, 637–645 (2016).
18. J. Déchanet, P. Merville, F. Bergé, G. Bone-Mane, J. L. Taupin, P. Michel, P. Joly, M. Bonneville, L. Potaux, J. F. Moreau, Major expansion of gammadelta T lymphocytes following cytomegalovirus infection in kidney allograft recipients. *J. Infect. Dis.* **179**, 1–8 (1999).
19. J. Déchanet, P. Merville, A. Lim, C. Retière, V. Pitard, X. Lafarge, S. Michelson, C. Méric, M.-M. Hallet, P. Kourilsky, L. Potaux, M. Bonneville, J.-F. Moreau, Implication of $\gamma\delta$ T cells in the human immune response to cytomegalovirus. *J. Clin. Invest.* **103**, 1437–1449 (1999).
20. L. Couzi, X. Lafarge, V. Pitard, M. Neau-Cransac, C. Dromer, M.-A. Billes, F. Lacaille, J.-F. Moreau, P. Merville, J. Déchanet-Merville, Gamma-delta T cell expansion is closely

associated with cytomegalovirus infection in all solid organ transplant recipients. *Transpl. Int. Off. J. Eur. Soc. Organ Transplant.* **24**, e40-42 (2011).

21. M. S. Davey, C. R. Willcox, S. Hunter, S. A. Kasatskaya, E. B. M. Remmerswaal, M. Salim, F. Mohammed, F. J. Bemelman, D. M. Chudakov, Y. H. Oo, B. E. Willcox, The human V δ 2 + T-cell compartment comprises distinct innate-like V γ 9 + and adaptive V γ 9 - subsets. *Nat. Commun.* **9**, 1760 (2018).
22. D. V. Correia, A. Lopes, B. Silva-Santos, Tumor cell recognition by $\gamma\delta$ T lymphocytes: T-cell receptor vs. NK-cell receptors. *Oncoimmunology.* **2**, e22892 (2013).
23. K. Pietschmann, S. Beetz, S. Welte, I. Martens, J. Gruen, H.-H. Oberg, D. Wesch, D. Kabelitz, Toll-like receptor expression and function in subsets of human gammadelta T lymphocytes. *Scand. J. Immunol.* **70**, 245–255 (2009).
24. D. Wesch, C. Peters, H.-H. Oberg, K. Pietschmann, D. Kabelitz, Modulation of $\gamma\delta$ T cell responses by TLR ligands. *Cell. Mol. Life Sci. CMLS.* **68**, 2357–2370 (2011).
25. L. Wen, W. Pao, F. S. Wong, Q. Peng, J. Craft, B. Zheng, G. Kelsoe, L. Dianda, M. J. Owen, A. C. Hayday, Germinal center formation, immunoglobulin class switching, and autoantibody production driven by non alpha/beta T cells. *J. Exp. Med.* **183**, 2271–2282 (1996).
26. A. A. Horner, H. Jabara, N. Ramesh, R. S. Geha, $\gamma\delta$ T lymphocytes express CD40 ligand and induce isotype switching in B lymphocytes. *J. Exp. Med.* **181**, 1239–1244 (1995).
27. R. M. Rezende, A. J. Lanser, S. Rubino, C. Kuhn, N. Skillin, T. G. Moreira, S. Liu, G. Gabriely, B. A. David, G. B. Menezes, H. L. Weiner, $\gamma\delta$ T cells control humoral immune response by inducing T follicular helper cell differentiation. *Nat. Commun.* **9**, 3151 (2018).
28. P. M. Benveniste, S. Roy, M. Nakatsugawa, E. L. Y. Chen, L. Nguyen, D. G. Millar, P. S. Ohashi, N. Hirano, E. J. Adams, J. C. Zúñiga-Pflücker, Generation and molecular recognition of melanoma-associated antigen-specific human $\gamma\delta$ T cells. *Sci. Immunol.* **3**, eaav4036 (2018).
29. A. Sandstrom, C.-M. Peigné, A. Léger, J. E. Crooks, F. Konczak, M.-C. Gesnel, R. Breathnach, M. Bonneville, E. Scotet, E. J. Adams, The Intracellular B30.2 Domain of Butyrophilin 3A1 Binds Phosphoantigens to Mediate Activation of Human V γ 9V δ 2 T Cells. *Immunity.* **40**, 490–500 (2014).
30. M. Rigau, S. Ostrouska, T. S. Fulford, D. N. Johnson, K. Woods, Z. Ruan, H. E. G. McWilliam, C. Hudson, C. Tutuka, A. K. Wheatley, S. J. Kent, J. A. Villadangos, B. Pal, C. Kurts, J. Simmonds, M. Pelzing, A. D. Nash, A. Hammet, A. M. Verhagen, G. Vairo, E. Maraskovsky, C. Panousis, N. A. Gherardin, J. Cebon, D. I. Godfrey, A. Behren, A. P. Uldrich, Butyrophilin 2A1 is essential for phosphoantigen reactivity by $\gamma\delta$ T cells. *Science.* **367** (2020), doi:10.1126/science.aay5516.
31. M. M. Karunakaran, C. R. Willcox, M. Salim, D. Paletta, A. S. Fichtner, A. Noll, L. Starick, A. Nöhren, C. R. Begley, K. A. Berwick, R. A. G. Chaleil, V. Pitard, J. Déchanet-Merville, P. A. Bates, B. Kimmel, T. J. Knowles, V. Kunzmann, L. Walter, M. Jeeves, F. Mohammed, B. E. Willcox, T. Herrmann, Butyrophilin-2A1 Directly Binds Germline-

- Encoded Regions of the V γ 9V δ 2 TCR and Is Essential for Phosphoantigen Sensing. *Immunity*. **52**, 487-498.e6 (2020).
32. E. Cordero, C. Casasola, R. Ecarma, R. Danguilan, Cytomegalovirus disease in kidney transplant recipients: incidence, clinical profile, and risk factors. *Transplant. Proc.* **44**, 694–700 (2012).
 33. D. Giakoustidis, A. Antoniadis, I. Fouzas, A. Sklavos, A. Giakoustidis, N. Ouzounidis, D. Gakis, K. Koubanagiti, G. Myserlis, A. Tsitlakidis, I. Gerogiannis, A. Papagiannis, P. Christoforou, T. Deligiannidis, F. Solonaki, G. Imvrios, V. Papanikolaou, Prevalence and Clinical Impact of Cytomegalovirus Infection and Disease in Renal Transplantation: Ten Years of Experience in a Single Center. *Transplant. Proc.* **44**, 2715–2717 (2012).
 34. L. Wen, S. J. Roberts, J. L. Viney, F. S. Wong, C. Mallick, R. C. Findly, Q. Peng, J. E. Craft, M. J. Owen, A. C. Mayday, Immunoglobulin synthesis and generalized autoimmunity in mice congenitally deficient in $\alpha\beta$ (+) T cells. *Nature*. **369**, 654–658 (1994).
 35. F. G. Lakkis, A. Arakelov, B. T. Konieczny, Y. Inoue, Immunologic ‘ignorance’ of vascularized organ transplants in the absence of secondary lymphoid tissue. *Nat. Med.* **6**, 686–688 (2000).
 36. M. D. Gunn, V. N. Ngo, K. M. Ansel, E. H. Ekland, J. G. Cyster, L. T. Williams, A B-cell-homing chemokine made in lymphoid follicles activates Burkitt’s lymphoma receptor-1. *Nature*. **391**, 799–803 (1998).
 37. J. Gordon, A. Katira, M. Holder, I. MacDonald, J. Pound, Central role of CD40 and its ligand in B lymphocyte responses to T-dependent antigens. *Cell. Mol. Biol. Noisy--Gd. Fr.* **40 Suppl 1**, 1–13 (1994).
 38. M. Brandes, K. Willmann, A. B. Lang, K.-H. Nam, C. Jin, M. B. Brenner, C. T. Morita, B. Moser, Flexible migration program regulates $\gamma\delta$ T-cell involvement in humoral immunity. *Blood*. **102**, 3693–3701 (2003).
 39. F. Guerville, S. Daburon, R. Marlin, L. Lartigue, S. Loizon, V. Pitard, L. Couzi, J.-F. Moreau, J. Déchanet-Merville, B. Faustin, TCR-dependent sensitization of human $\gamma\delta$ T cells to non-myeloid IL-18 in cytomegalovirus and tumor stress surveillance. *OncImmunity*. **4**, e1003011 (2015).
 40. H. Kaminski, C. Ménard, B. El Hayani, A.-N. Adjibabi, G. Marsères, M. Courant, A. Zouine, V. Pitard, I. Garrigue, S. Burrel, J.-F. Moreau, L. Couzi, J. Visentin, P. Merville, J. Déchanet-Merville, Characterization of a Unique $\gamma\delta$ T-Cell Subset as a Specific Marker of Cytomegalovirus Infection Severity. *J. Infect. Dis.* **223**, 655–666 (2021).
 41. D. J. Steele, T. M. Laufer, S. T. Smiley, Y. Ando, M. J. Grusby, L. H. Glimcher, H. Auchincloss, Two levels of help for B cell alloantibody production. *J. Exp. Med.* **183**, 699–703 (1996).
 42. S. Dahdal, C. Saison, M. Valette, E. Bachy, N. Pallet, B. Lina, A. Koenig, G. Monneret, T. Defrance, E. Morelon, O. Thauinat, Residual Activatability of Circulating Tfh17 Predicts Humoral Response to Thymodependent Antigens in Patients on Therapeutic Immunosuppression. *Front. Immunol.* **9**, 3178 (2018).

43. E. J. Suchin, P. B. Langmuir, E. Palmer, M. H. Sayegh, A. D. Wells, L. A. Turka, Quantifying the Frequency of Alloreactive T Cells In Vivo: New Answers to an Old Question. *J. Immunol.* **166**, 973–981 (2001).
44. E. Joly, D. Hudrisier, What is trogocytosis and what is its purpose? *Nat. Immunol.* **4**, 815–815 (2003).
45. M. Brandes, K. Willmann, B. Moser, Professional Antigen-Presentation Function by Human $\gamma\delta$ T Cells. *Science.* **309**, 264–268 (2005).
46. S. Itohara, P. Mombaerts, J. Lafaille, J. Iacomini, A. Nelson, A. R. Clarke, M. L. Hooper, A. Farr, S. Tonegawa, T cell receptor δ gene mutant mice: Independent generation of $\alpha\beta$ T cells and programmed rearrangements of $\gamma\delta$ TCR genes. *Cell.* **72**, 337–348 (1993).
47. H. Dai, P. Lan, D. Zhao, K. Abou-Daya, W. Liu, W. Chen, A. J. Friday, A. L. Williams, T. Sun, J. Chen, W. Chen, S. Mortin-Toth, J. S. Danska, C. Wiebe, P. Nickerson, T. Li, L. R. Mathews, H. R. Turnquist, M. L. Nicotra, S. Gingras, E. Takayama, H. Kubagawa, M. J. Shlomchik, M. H. Oberbarnscheidt, X. C. Li, F. G. Lakkis, PIRs mediate innate myeloid cell memory to nonself MHC molecules. *Science.* **368**, 1122–1127 (2020).
48. H. Dai, A. J. Friday, K. I. Abou-Daya, A. L. Williams, S. Mortin-Toth, M. L. Nicotra, D. M. Rothstein, W. D. Shlomchik, T. Matozaki, J. S. Isenberg, M. H. Oberbarnscheidt, J. S. Danska, F. G. Lakkis, Donor SIRP α polymorphism modulates the innate immune response to allogeneic grafts. *Sci. Immunol.* **2** (2017), doi:10.1126/sciimmunol.aam6202.
49. X. Charmetant, T. Bachelet, J. Déchanet-Merville, T. Walzer, O. Thaunat, Innate (and Innate-like) Lymphoid Cells: Emerging Immune Subsets With Multiple Roles Along Transplant Life. *Transplantation.* **105**, e322 (2021).
50. J. N. Beilke, N. R. Kuhl, L. V. Kaer, R. G. Gill, NK cells promote islet allograft tolerance via a perforin-dependent mechanism. *Nat. Med.* **11**, 1059–1065 (2005).
51. G. Yu, X. Xu, M. D. Vu, E. D. Kilpatrick, X. C. Li, NK cells promote transplant tolerance by killing donor antigen-presenting cells. *J. Exp. Med.* **203**, 1851–1858 (2006).
52. S. Laffont, C. Seillet, J. Ortaldo, J. D. Coudert, J.-C. Guéry, Natural killer cells recruited into lymph nodes inhibit alloreactive T-cell activation through perforin-mediated killing of donor allogeneic dendritic cells. *Blood.* **112**, 661–671 (2008).
53. A. Koenig, C.-C. Chen, A. Marçais, T. Barba, V. Mathias, A. Sicard, M. Rabeyrin, M. Racapé, J.-P. Duong-Van-Huyen, P. Bruneval, A. Loupy, S. Dussurgey, S. Ducreux, V. Meas-Yedid, J.-C. Olivo-Marin, H. Paidassi, R. Guillemain, J.-L. Taupin, J. Callemeyn, E. Morelon, A. Nicoletti, B. Charreau, V. Dubois, M. Naesens, T. Walzer, T. Defrance, O. Thaunat, Missing self triggers NK cell-mediated chronic vascular rejection of solid organ transplants. *Nat. Commun.* **10**, 5350 (2019).
54. S. Hamada, O. Thaunat, A. Koenig, Un nouveau type de rejet de greffe induit par les lymphocytes natural killer : le rejet chronique vasculaire « inné ». *médecine/sciences.* **36**, 984–987 (2020).
55. J. Callemeyn, A. Senev, M. Coemans, E. Lerut, B. Sprangers, D. Kuypers, A. Koenig, O. Thaunat, M.-P. Emonds, M. Naesens, Missing Self-Induced Microvascular Rejection of

- Kidney Allografts: A Population-Based Study. *J. Am. Soc. Nephrol. JASN.* **32**, 2070–2082 (2021).
56. A. Koenig, S. Mezaache, J. Callemeyn, T. Barba, V. Mathias, A. Sicard, B. Charreau, M. Rabeyrin, F. Dijoud, C. Picard, V. Meas-Yedid, J.-C. Olivo-Marin, E. Morelon, M. Naesens, V. Dubois, O. Thauinat, Missing Self-Induced Activation of NK Cells Combines with Non-Complement-Fixing Donor-Specific Antibodies to Accelerate Kidney Transplant Loss in Chronic Antibody-Mediated Rejection. *J. Am. Soc. Nephrol.* (2020), doi:10.1681/ASN.2020040433.
 57. O. Jensen, S. Trivedi, J. D. Meier, K. C. Fairfax, J. S. Hale, D. T. Leung, A subset of follicular helper-like MAIT cells can provide B cell help and support antibody production in the mucosa. *Sci. Immunol.* **7**, eabe8931 (2022).
 58. P.-P. Chang, P. Barral, J. Fitch, A. Pratama, C. S. Ma, A. Kallies, J. J. Hogan, V. Cerundolo, S. G. Tangye, R. Bittman, S. L. Nutt, R. Brink, D. I. Godfrey, F. D. Batista, C. G. Vinuesa, Identification of Bcl-6-dependent follicular helper NKT cells that provide cognate help for B cell responses. *Nat. Immunol.* **13**, 35–43 (2011).
 59. N. Caccamo, L. Battistini, M. Bonneville, F. Poccia, J. J. Fournié, S. Meraviglia, G. Borsellino, R. A. Kroczek, C. L. Mendola, E. Scotet, F. Dieli, A. Salerno, CXCR5 Identifies a Subset of V γ 9V δ 2 T Cells which Secrete IL-4 and IL-10 and Help B Cells for Antibody Production. *J. Immunol.* **177**, 5290–5295 (2006).
 60. S. Fillatreau, B. Manfroi, T. Dörner, Toll-like receptor signalling in B cells during systemic lupus erythematosus. *Nat. Rev. Rheumatol.* **17**, 98–108 (2021).
 61. S. Rajagopalan, C. Mao, S. K. Datta, Pathogenic autoantibody-inducing gamma/delta T helper cells from patients with lupus nephritis express unusual T cell receptors. *Clin. Immunol. Immunopathol.* **62**, 344–350 (1992).
 62. O. Thauinat, S. Graff-Dubois, N. Fabien, A. Duthey, V. Attuil-Audenis, A. Nicoletti, N. Patey, E. Morelon, A stepwise breakdown of B-cell tolerance occurs within renal allografts during chronic rejection. *Kidney Int.* **81**, 207–219 (2012).
 63. T. S. Win, G. J. Pettigrew, Humoral Autoimmunity and Transplant Vasculopathy: When Allo is Not Enough. *Transplantation.* **90**, 113–120 (2010).
 64. G. Mieli-Vergani, D. Vergani, De novo autoimmune hepatitis after liver transplantation. *J. Hepatol.* **40**, 3–7 (2004).
 65. L. Couzi, V. Pitard, S. Netzer, I. Garrigue, M.-E. Lafon, J.-F. Moreau, J.-L. Taupin, P. Merville, J. Déchanet-Merville, Common features of gammadelta T cells and CD8(+) alphabeta T cells responding to human cytomegalovirus infection in kidney transplant recipients. *J. Infect. Dis.* **200**, 1415–1424 (2009).
 66. L. Couzi, V. Pitard, X. Sicard, I. Garrigue, O. Hawchar, P. Merville, J.-F. Moreau, J. Déchanet-Merville, Antibody-dependent anti-cytomegalovirus activity of human $\gamma\delta$ T cells expressing CD16 (Fc γ RIIIa). *Blood.* **119**, 1418–1427 (2012).
 67. T. Bachelet, L. Couzi, V. Pitard, X. Sicard, C. Rigotherier, S. Lepreux, J.-F. Moreau, J.-L. Taupin, P. Merville, J. Déchanet-Merville, Cytomegalovirus-Responsive $\gamma\delta$ T Cells:

- Novel Effector Cells in Antibody-Mediated Kidney Allograft Microcirculation Lesions. *J. Am. Soc. Nephrol.* **25**, 2471–2482 (2014).
68. J. Schindelin, I. Arganda-Carreras, E. Frise, V. Kaynig, M. Longair, T. Pietzsch, S. Preibisch, C. Rueden, S. Saalfeld, B. Schmid, J.-Y. Tinevez, D. J. White, V. Hartenstein, K. Eliceiri, P. Tomancak, A. Cardona, Fiji: an open-source platform for biological-image analysis. *Nat. Methods.* **9**, 676–682 (2012).
69. P. Mombaerts, A. R. Clarke, M. A. Rudnicki, J. Iacomini, S. Itohara, J. J. Lafaille, L. Wang, Y. Ichikawa, R. Jaenisch, M. L. Hooper, S. Tonegawa, Mutations in T-cell antigen receptor genes α and β block thymocyte development at different stages. *Nature.* **360**, 225–231 (1992).
70. Z. H. Chen, A technique of cervical heterotopic heart transplantation in mice. *Transplantation.* **52**, 1099–1101 (1991).

Article 3 : Inverted direct allorecognition triggers early donor specific antibody responses after transplantation

L'allorecognition directe inversée est une histoire ancienne de mon équipe d'accueil qui découle de ses premiers travaux.

Puisque les molécules HLA sont des protéines, l'aide lymphocytaire T CD4⁺ est cruciale pour permettre aux lymphocytes B allospécifiques de se différencier en plasmocytes producteurs de DSA. Le maintien d'une production de DSA sous immunosuppresseurs (qui ciblent plus particulièrement les lymphocytes T) serait donc une situation paradoxale, qui soulève l'hypothèse d'une production de DSA indépendante de l'aide T.

Cette hypothèse était soutenue par des travaux de Zinkernagel (186), qui démontrent qu'une infection virale peut induire une réponse humorale chez une souris dépourvue de lymphocytes T, et que cette T-indépendance est corrélée à une accumulation d'antigènes dans la rate. Or, après transplantation, le premier site d'adressage des allo-antigènes est la rate. Les travaux initiaux de l'équipe visaient donc à tester cette hypothèse : l'accumulation d'alloantigènes dans la rate après transplantation permettrait une production de DSA indépendante de l'aide T CD4⁺.

Ainsi, un modèle de transplantation cardiaque chez la souris a été mis au point. Une souris receveuse A β KO (KO de la chaîne I-A β du MHC de la souris) a été utilisée comme modèle de déplétion génétique des lymphocytes T CD4⁺. Cette souris ne développe aucun DSA après transplantation d'un cœur allogénique, malgré une accumulation documentée des allo-antigènes dans la rate. Ces résultats ont fait l'objet d'une publication de l'équipe en 2018 (187).

L'hypothèse de l'indépendance des réponses DSA à l'aide T CD4⁺ semblait définitivement réfutée, jusqu'à ce que d'autres expériences soient réalisées.

En effet, un autre modèle permet l'étude de la déplétion génétique des lymphocytes T chez la souris : le modèle CD3 ϵ KO (KO de la chaîne ϵ du TCR ; fond génétique H-2^b). D'autres transplantations ont été réalisées chez ces souris, et contre toute attente, ces souris ont généré des DSA après transplantation d'un cœur allogénique CBA (H-2^k). Après multiplication des expériences pour éliminer toute erreur liée à la manipulation, l'observation se confirme. Ce résultat aurait probablement pu être rapidement expliqué s'il n'avait pas été mis d'emblée face à une contradiction forte : la production de DSA n'a pas lieu si la souris CD3 ϵ KO reçoit un cœur Balb/c (H-2^d).

Ces observations sont malheureusement restées sans explication, alors même que l'équipe avait les yeux rivés sur la cellule responsable de ce phénomène : le lymphocyte NK, étudié en parallèle pour son rôle dans le rejet vasculaire chronique des greffons, en raison de ses capacités d'allorecognition innée.

Ceci jusqu'à la publication de travaux par une équipe indépendante, rapportant une observation tout à fait similaire et donnant la clé de la différence entre les deux modèles (cœur CBA et Balb/c) : les lymphocytes T du donneur sont directement impliqués dans la production de DSA en aidant les B allospécifiques du receveur (modèle cœur CBA), à moins qu'ils ne soient éliminés précocement par les NK du receveur [modèle cœur Balb/c ; (188)].

Ainsi, à mon arrivée au laboratoire, cette thématique se retrouvait à nouveau parmi les sujets brûlants de l'équipe avec un enjeu supplémentaire : faire la translation de la preuve de concept expérimentale vers la clinique.

TRANSPLANTATION

Inverted direct allorecognition triggers early donor-specific antibody responses after transplantation

Xavier Charmetant^{1†}, Chien-Chia Chen^{2†}, Sarah Hamada³, David Goncalves¹, Carole Saison³, Maud Rabeyrin⁴, Marion Rabant⁵, Jean-Paul Duong van Huyen⁵, Alice Koenig^{1,6,7}, Virginie Mathias³, Thomas Barba¹, Florence Lacaille⁸, Jérôme le Pavec⁹, Olivier Brugière¹⁰, Jean-Luc Taupin^{11,12}, Lara Chalabreysse⁴, Jean-François Mornex^{13,14}, Lionel Couzi¹⁵, Stéphanie Graff-Dubois¹⁶, Raphaël Jeger-Madiot¹⁶, Alexy Tran-Dinh¹⁷, Pierre Mordant¹⁸, Helena Paidassi¹, Thierry Defrance¹, Emmanuel Morelon^{1,6,7}, Lionel Badet^{6,19}, Antonino Nicoletti¹⁷, Valérie Dubois³, Olivier Thauinat^{1,6,7*}

Copyright © 2022 The Authors, some rights reserved; exclusive license American Association for the Advancement of Science. No claim to original U.S. Government Works

The generation of antibodies against donor-specific major histocompatibility complex (MHC) antigens, a type of donor-specific antibodies (DSAs), after transplantation requires that recipient's allospecific B cells receive help from T cells. The current dogma holds that this help is exclusively provided by the recipient's CD4⁺ T cells that recognize complexes of recipient's MHC II molecules and peptides derived from donor-specific MHC alloantigens, a process called indirect allorecognition. Here, we demonstrated that, after allogeneic heart transplantation, CD3ε knockout recipient mice lacking T cells generate a rapid, transient wave of switched alloantibodies, predominantly directed against MHC I molecules. This is due to the presence of donor CD4⁺ T cells within the graft that recognize intact recipient's MHC II molecules expressed by B cell receptor-activated allospecific B cells. Indirect evidence suggests that this inverted direct pathway is also operant in patients after transplantation. Resident memory donor CD4⁺ T cells were observed in perfusion liquids of human renal and lung grafts and acquired B cell helper functions upon in vitro stimulation. Furthermore, T follicular helper cells, specialized in helping B cells, were abundant in mucosa-associated lymphoid tissue of lung and intestinal grafts. In the latter, more graft-derived passenger T cells correlated with the detection of donor T cells in recipient's circulation; this, in turn, was associated with an early transient anti-MHC I DSA response and worse transplantation outcomes. We conclude that this inverted direct allorecognition is a possible explanation for the early transient anti-MHC DSA responses frequently observed after lung or intestinal transplantations.

INTRODUCTION

The best therapeutic option for patients with end-stage vital organ failure is organ transplantation, which restores essential physiologic functions through the surgical substitution of the defective organ by a functioning graft retrieved from a donor. However, the antigenic determinants that differ between the donor and the recipient (alloantigens), particularly the highly polymorphic molecules from major histocompatibility complex (MHC) molecules [or human leukocyte antigens (HLA) in human], are inevitably targeted by the adaptive immune system of the recipient. This leads to the failure of the transplanted organ, a process named rejection, which still currently represents the first cause of graft failure (1, 2). Depending on the nature of the adaptive immune effectors responsible for graft destruction, a distinction is made between (i) T cell-mediated rejection

(TCMR), in which recipient's T cells infiltrate graft interstitium and destroy the epithelial cells, and (ii) antibody-mediated rejection (AMR) that results from the binding of donor-specific antibodies (DSAs) sequestered in recipient's circulation to directly accessible donor-specific MHC molecules expressed on graft vasculature (3, 4).

This dichotomic vision of the immunopathology of rejection has long been thought to be the consequence of a unique feature of transplantation: antigen-presenting cells (APCs) can have two origins, donor or recipient, leading to two distinct pathways for allorecognition, direct and indirect (5–7). Direct allorecognition of donor-specific MHC molecules expressed as intact complexes on the surface of passenger APCs activates up to 10% of a recipient's T cells (8), which triggers TCMR. Disappearance of donor bone marrow-derived passenger

¹CIRI, Centre International de Recherche en Infectiologie, Université de Lyon, INSERM U1111, Université Claude Bernard Lyon 1, CNRS, UMR5308, ENS de Lyon, 69007 Lyon, France. ²Department of Surgery, National Taiwan University Hospital, Taipei 100, Taiwan. ³French National Blood Service (EFS), HLA Laboratory, 69150 Décines, France. ⁴Department of Pathology, Hospices Civils de Lyon, Groupement Hospitalier Est, 69500 Bron, France. ⁵Pathology Department, Assistance Publique-Hôpitaux de Paris, Hôpital Necker, 75015 Paris, France. ⁶Lyon-Est Medical Faculty, Claude Bernard University (Lyon 1), 69008 Lyon, France. ⁷Department of Transplantation, Nephrology and Clinical Immunology, Hospices Civils de Lyon, Edouard Herriot Hospital, 69003 Lyon, France. ⁸Pediatric Gastroenterology-Hepatology-Nutrition Unit, Hôpital Universitaire Necker-Enfants malades, 75015 Paris, France. ⁹Department of Pulmonology and Lung Transplantation, Marie Lannelongue Hospital, 92350 Le Plessis Robinson, France. ¹⁰Pulmonology Department, Adult Cystic Fibrosis Centre and Lung Transplantation Department, Foch Hospital, 92150 Suresnes, France. ¹¹Laboratory of Immunology and Histocompatibility, Hôpital Saint-Louis APHP, 75010 Paris, France. ¹²INSERM U976 Institut de Recherche Saint-Louis, Université Paris Diderot, 75010 Paris, France. ¹³Université de Lyon, Université Lyon 1, INRAE, IVPC, UMR754, 69000 Lyon, France. ¹⁴Department of Pneumology, GHE, Hospices Civils de Lyon, 69000 Lyon, France. ¹⁵Department of Nephrology, Transplantation, Dialysis, Apheresis, Pellegrin Hospital, 33000 Bordeaux, France. ¹⁶Sorbonne Université, INSERM, Immunology-Immunopathology-Immunotherapy (i3), 75013 Paris, France. ¹⁷Université de Paris, LVTS, INSERM U1148, 75018 Paris, France. ¹⁸Department of Vascular and Thoracic Surgery, Assistance Publique-Hôpitaux de Paris, Bichat-Claude Bernard Hospital, 75018 Paris, France. ¹⁹Department of Urology and Transplantation Surgery, Hospices Civils de Lyon, Edouard Herriot Hospital, 69003 Lyon, France.

*Corresponding author. Email: olivier.thauinat@inserm.fr

†These authors equally contributed to this work.

APCs, which cannot be replenished, provides the explanation to the decay of TCMR incidence reported with time after transplantation (9). In contrast, the indirect recognition of allogeneic peptides processed from donor-specific MHC molecules by recipient's APCs and presented within MHC II molecules on their surface activates a smaller number of CD4⁺ T cells; however, these cells are critically important for the differentiation of allospecific B cells into DSA-producing plasma cells (10–13). Persistence of indirect response would explain why AMR is the major threat to long-term transplant survival (1, 14–21).

Although this dogma provides a general frame compatible with most of the rejection episodes observed in transplant recipients, it fails to explain why some transplant recipients develop episodes of TCMR several years after transplantation (22–24), at a time when the last donor-derived APC has been eliminated and the direct pathway of allorecognition should be inoperant. This discrepancy led to the discovery in the early 2000s of the semidirect pathway of allorecognition (25), by which a recipient's cytotoxic T cells of "direct specificity" can recognize intact allogeneic MHC molecules displayed on recipient APCs (MHC cross-dressing) after their transfer through cell-cell contact (26) or through extracellular vesicles (27, 28). Persistence of this pathway for the life of the transplant explains the sustained activation of direct-pathway T cells and the occurrence of late TCMR episodes (29, 30). Recent reevaluations of the respective contribution of direct and semidirect pathways suggest that it is the latter that is the dominant mechanism triggering TCMR, including immediately after transplantation (27, 31).

Inspired by the progress made in the understanding of TCMR pathophysiology and by another recent study (32), we initiated this translational study aiming at reassessing the importance of the indirect pathway in the pathophysiological sequence leading to AMR. Combining murine experimental models with the analysis of renal, lung, and intestine recipients, we confirmed that CD4⁺ T cell help is indeed mandatory for DSA generation. However, when the grafted organ contains a high number of donor CD4⁺ T cells (which is the case for graft containing professional secondary lymphoid tissue), these passenger CD4⁺ T cells can interact with recipient's B cells through direct allorecognition of intact recipient's MHC molecule and provide help for DSA generation. This transient, inverted direct pathway is responsible for the early onset of DSA generation, which can have a detrimental impact on graft survival.

RESULTS

CD3ε knockout recipient mice develop alloantibodies after heart transplantation

Current dogma in transplant immunology holds that the generation of alloantibody against donor-specific MHC proteins depends on a prototypical T cell-dependent humoral response. After the binding of donor-specific MHC molecules to their B cell receptor (BCR) that delivers the first signal of activation, recipient allospecific B cells indeed need a second signal of activation that is thought to come from cognate interactions with recipient's CD4⁺ T cells. This implies that the T cells involved in the alloantibody response are of indirect specificity, meaning that their T cell receptor (TCR) is specific for the complexes consisting of a recipient's MHC and a peptide derived from a donor's MHC molecule.

Aiming at testing the dependency of alloantibody response to recipient's T cells, we used CD3ε knockout (KO) mice. CD3ε is a

signaling component of the TCR complex, the genetic ablation of which impedes the positive selection of T cells in the thymus. Thus, CD3εKO mice showed complete elimination of CD3⁺ T lymphocytes in their spleen, lymph nodes, and peripheral blood mononuclear cells (PBMCs; fig. S1A). Because this genetic manipulation has no impact on B cell ontogeny, CD3εKO mice exhibited a normal CD19⁺ B cell count (fig. S1A). To further document the lack of T cell help and the functionality of B cell compartment in this strain, CD3εKO mice were immunized with either the thymo-independent or the thymo-dependent forms of the model hapten 4-(hydroxy-3-nitro-phenyl) acetyl (NP) antigen. Whereas CD3εKO and wild-type (WT) C57BL/6 mice developed similar anti-NP immunoglobulin M (IgM) response after immunization with NP-dextran (a known thymo-independent antigen due to its polysaccharide structure), only WT mice developed anti-NP IgG after immunization with the thymo-dependent NP-keyhole limpet hemocyanin (KLH) antigen (fig. S1B).

To specifically address the question of the dependency of the alloantibody response to recipient's T cell help, a fully allogeneic (CBA; H-2^k) heart graft was transplanted heterotopically into WT or CD3εKO C57BL/6 (H-2^b) recipients (Fig. 1A). The donor-specific antibody (DSA) responses against the donor's MHC molecules were assessed by flow cross-match using CBA (H-2^k) CD4⁺ T cells. As expected, WT recipients developed DSAs, which became detectable from day 14 onward and reached a peak around day 28 (Fig. 1B). However, unexpectedly, T cell-deficient CD3εKO recipients also generated DSAs (Fig. 1B).

The alloantibody response of CD3εKO recipients is early and transient

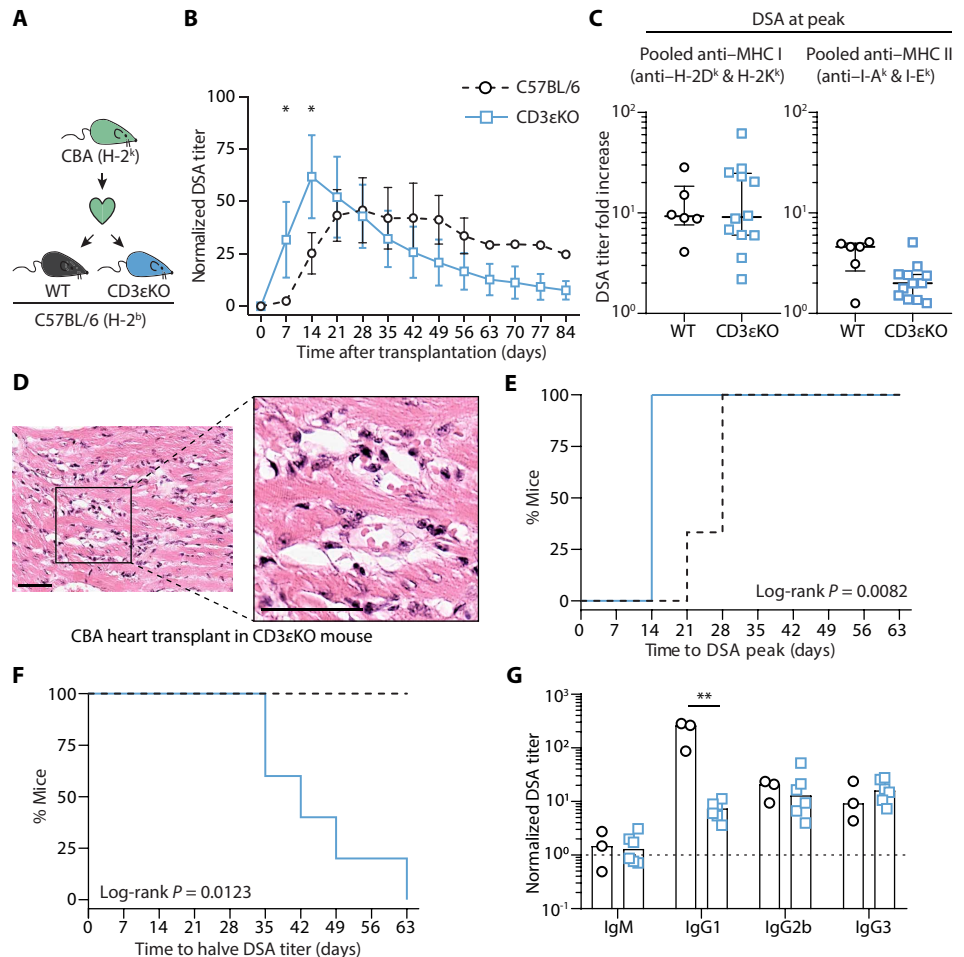
A custom single-antigen bead assay, similar to the one used in routine clinical practice, was used to compare the specificity and intensity of the DSA response of the two groups of recipient mice. Although CD3εKO recipients generated the same concentration of anti-MHC I alloantibodies as WT controls, the former produced much less DSAs directed against donor-specific MHC II (Fig. 1C). DSAs generated by CD3εKO recipients were, nevertheless, deleterious because they were able to trigger the development of microvascular inflammatory lesions in the heart allograft (Fig. 1D).

Analyzing the kinetics of the alloimmune humoral response more precisely revealed that CD3εKO recipients developed DSAs with faster kinetics as compared with WT recipients ($P = 0.0082$, log-rank test; Fig. 1, B and E) but their DSA titers rapidly decayed after the peak ($P = 0.0123$, log-rank test; Fig. 1, B and F). Because these two features are evocative of a T cell-independent B cell response, which are exclusively made of IgM and IgG3, we next analyzed the heavy chain isotype of the DSAs generated by WT and CD3εKO recipients. At the peak of the antibody response, the DSAs generated by CD3εKO recipients were not predominantly IgM and IgG3 (Fig. 1G). Except a lower amount of IgG1, the profile of the heavy chain isotypes of DSAs generated by CD3εKO recipients was similar to that of WT recipients (Fig. 1G).

Together with the fact that donor MHC molecules are proteins and not sugar antigens, this suggested that DSA response in CD3εKO recipients did not result from a T cell-independent humoral response. This therefore raised the intriguing question of how CD3εKO recipients develop T cell-dependent DSA responses when they have no T cells (fig. S1A) to provide help to their alloreactive B cells.

Fig. 1. CD3 ϵ KO recipient mice develop alloantibodies after transplantation.

(A) Presentation of the mouse model. Allogeneic CBA (H-2^k) hearts were transplanted to wild-type (WT) or CD3 ϵ KO C57BL/6 (H-2^b) recipient mice. Results are from two independent experiments. **(B)** Development of normalized anti-MHC I DSA titers in the circulation of recipients is shown for WT C57BL/6 ($n = 3$; black circles) and CD3 ϵ KO ($n = 6$; blue squares). Data are presented as means \pm SD. Data were analyzed by multiple t tests. $*P < 0.05$. **(C)** DSAs were analyzed in WT (black circles) and CD3 ϵ KO (blue squares) recipients between day 14 (D14) and D28 after transplantation. Serum samples were screened for the presence of anti-MHC I (left) or anti-MHC II (right) antibodies using a custom single-antigen bead assay. Bars indicate the median and interquartile ranges (IQR). **(D)** Representative histological findings of an allogeneic CBA (H-2^k) heart graft after transplantation to a CD3 ϵ KO recipient. Hematoxylin and eosin staining is shown. Scale bars, 50 μ m. Kaplan-Meier curves of **(E)** the delay between transplantation and DSA peak or **(F)** the peak and the time to halve DSA titers for WT ($n = 3$; dashed black line) and CD3 ϵ KO ($n = 6$; blue line) recipients. **(G)** Anti-MHC DSA isotypes were tested at the peak of the response. Individual values (and median value) of normalized titers are represented. The horizontal dashed line indicates the positivity threshold. Data were analyzed by Mann-Whitney test. $**P < 0.01$.

**DSAs can be generated with the help of CD4⁺ T cells from the donor**

To further examine the role of CD4⁺ T cells in the generation of DSAs in CD3 ϵ KO recipients, we conducted a series of experiments, in which the recipients were treated with depleting anti-CD3 (clone 17A2) or anti-CD4 (clone GK1.5) monoclonal antibodies (mAbs). Treatment with both depleting mAbs drastically reduced DSA response of CD3 ϵ KO recipients (Fig. 2A). This result demonstrates that the interaction of CD4⁺ T cells with B cells is essential to generate DSA, including in CD3 ϵ KO recipients.

Because CD3 ϵ KO recipients completely lack T cells (fig. S1A) and fail to mount T cell-dependent humoral response upon immunization with a model protein antigen (fig. S1B), we hypothesized that the CD4⁺ T cells providing help to recipient's alloreactive B cells could originate from the graft. In support of this theory, around 4500 CD4⁺ T cells were observed in the cell suspensions obtained after collagenase digestion of heart grafts (Fig. 2, B and C). To further demonstrate the role of these passenger CD4⁺ T cells in the DSA response of CD3 ϵ KO recipients, anti-CD3- or anti-CD4-depleting mAbs were administered to the donor animals before harvesting of the heart. CD4⁺ T cells were efficiently depleted with both mAbs, both in the heart and the periphery of donor mice, albeit with slightly different kinetics (Fig. 2C). Heart grafts were collected at the nadir of CD4⁺ T cell count (day 1 after anti-CD3 injection and day 7 after anti-CD4 injection; Fig. 2C) and transplanted into CD3 ϵ KO recipients. CD3⁺ or CD4⁺ T cell depletion in the donor not only abrogated DSA response in recipients (Fig. 2D) but also drastically reduced microvascular inflammatory lesions within the graft (Fig. 2E), thus suggesting that donor's CD4⁺ T cells present within the graft are able

to provide the help required by recipient's alloreactive B cells to differentiate into DSA-producing plasma cells.

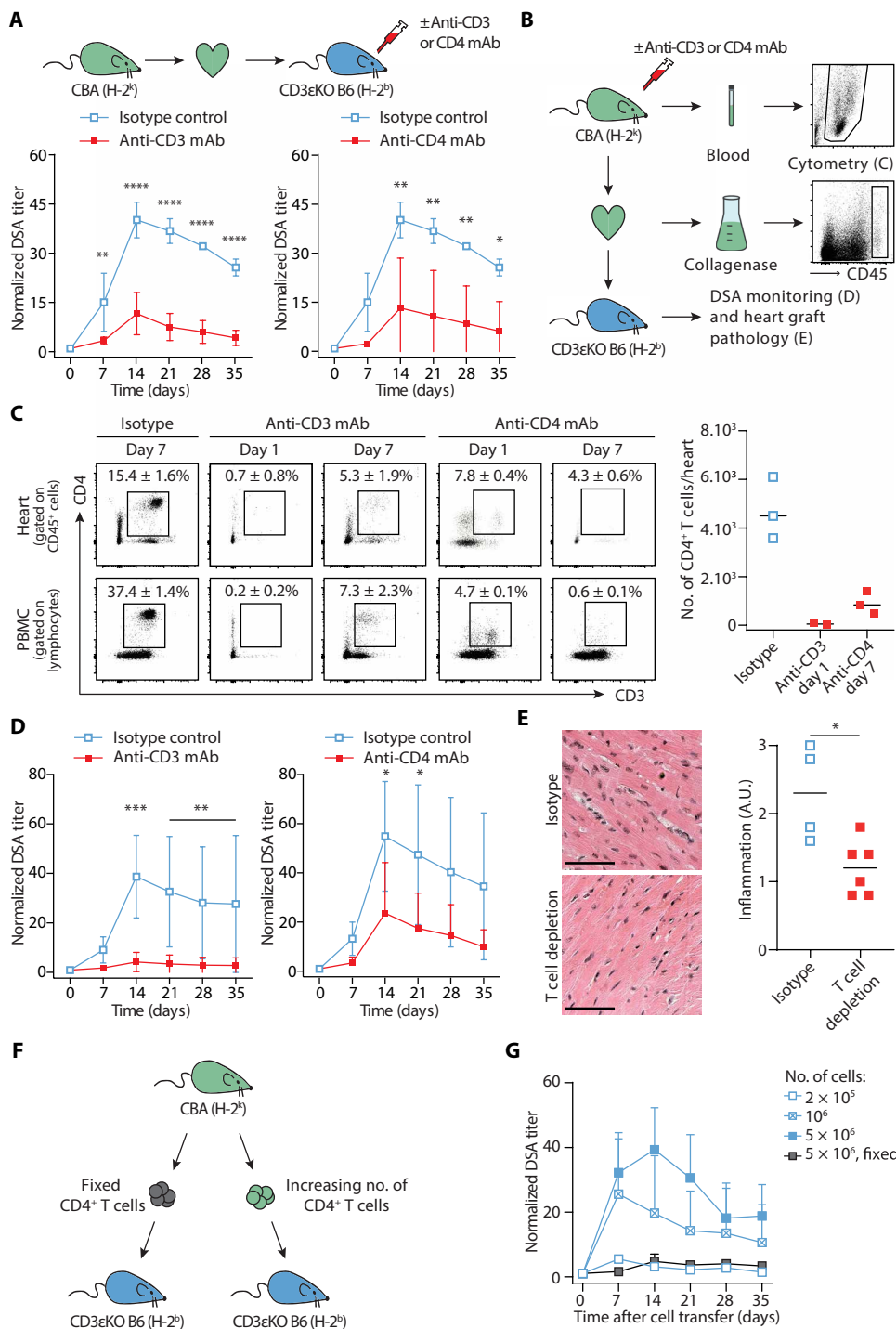
The existence of this allorecognition pathway, distinct from the canonical indirect pathway but capable of triggering the generation of deleterious DSAs, was later confirmed by the demonstration that the mere transfer of allogeneic CBA (H-2^k) CD4⁺ T cells was sufficient to trigger the generation of DSAs in C57BL/6 (H-2^b) CD3 ϵ KO mice (Fig. 2F). Furthermore, using this simplified model, we highlighted that this allorecognition pathway was critically dependent on the number of allogeneic CD4⁺ T cells injected in the circulation of the recipient (Fig. 2G). Furthermore, because no DSA was generated (even with the higher number of allogeneic CD4⁺ T cells) when cells were fixed before the transfer (Fig. 2G), we concluded that this allorecognition pathway requires that the allogeneic CD4⁺ T cells are functional.

Donor's CD4⁺ T cells recognize allogeneic MHC II on the surface of the recipient's B cells

The sequence leading to the generation of DSA through the canonical indirect pathway is well known (Fig. 3A). The recognition of donor-specific MHC molecules by the BCR delivers the first signal of activation to recipient allospecific B cells and induces the internalization of the alloantigen. To complete their differentiation, allospecific B cells need to present alloantigen-derived peptides within surface MHC II molecules. Only when these complexes are recognized by

Fig. 2. DSA generation requires CD4⁺ T cells, which can originate from the donor. (A to E) Allogeneic CBA (H-2^k) hearts were transplanted to CD3εKO C57BL/6 (H-2^b) recipient mice.

(A) Recipient mice were injected intravenously after transplantation with either a depleting anti-CD3 mAb (left; red curve; *n* = 4), a depleting anti-CD4 mAb (right; red curve; *n* = 4), or an isotype control (blue curve). Evolution of normalized anti-MHC DSA titers is shown (means ± SD). Data were analyzed by multiple *t* tests. **P* < 0.05, ***P* < 0.01, and *****P* < 0.0001. (B) Donor CBA mice were injected intravenously with either a depleting anti-CD3 mAb, a depleting anti-CD4 mAb, or an isotype control before flow cytometry analysis or heart transplantation. (C) Heart grafts were harvested 1 or 7 days after mAb injection and digested with collagenase. Heart graft cell suspension (top rows) and PBMCs (bottom rows) were analyzed by flow cytometry. Representative flow cytometry profiles. The far-right plot shows the absolute number of CD4⁺ T cells isolated from murine heart grafts from the three groups. Horizontal bars indicate the median. (D) Evolution of normalized anti-MHC DSA titers (means ± SD) was measured in CD3εKO recipients of a CBA heart harvested either after anti-CD3 treatment (top row; red curve; *n* = 4), anti-CD4 treatment (bottom row; red curve; *n* = 4), or isotype control treatment (blue curve; *n* = 3). Data were analyzed by multiple *t* tests. **P* < 0.05, ***P* < 0.01, and ****P* < 0.001. (E) CBA (H-2^k) heart grafts harvested from mice previously injected intravenously with either an isotype control (*n* = 4; top image, blue) or a T cell-depleting mAb (*n* = 6; bottom image, red) were transplanted into CD3εKO C57BL/6 (H-2^b) recipients. Left: Representative hematoxylin and eosin staining. Scale bars, 50 μm. Right: The intensity of microvascular inflammatory lesions, which was graded on a semiquantitative scale (score 0 to 3). Horizontal bars indicate the median. Data were analyzed by Mann-Whitney test. **P* < 0.05. A.U., arbitrary units. (F and G) Purified allogeneic CBA (H-2^k) CD4⁺ T cells were injected intravenously to CD3εKO (H-2^b) recipient mice. Evolution of normalized anti-MHC DSA titers was measured (means ± SD). (F) Schematic representation of the experiments. (G) Indicated numbers of alive (blue curves) or alcohol-fixed (black curve) purified allogeneic CBA CD4⁺ T cells (2 × 10⁵ to 5 × 10⁶) were injected intravenously to WT C57BL/6 (H-2^b) recipient mice, and DSA titers were analyzed at the indicated times after cell transfer.



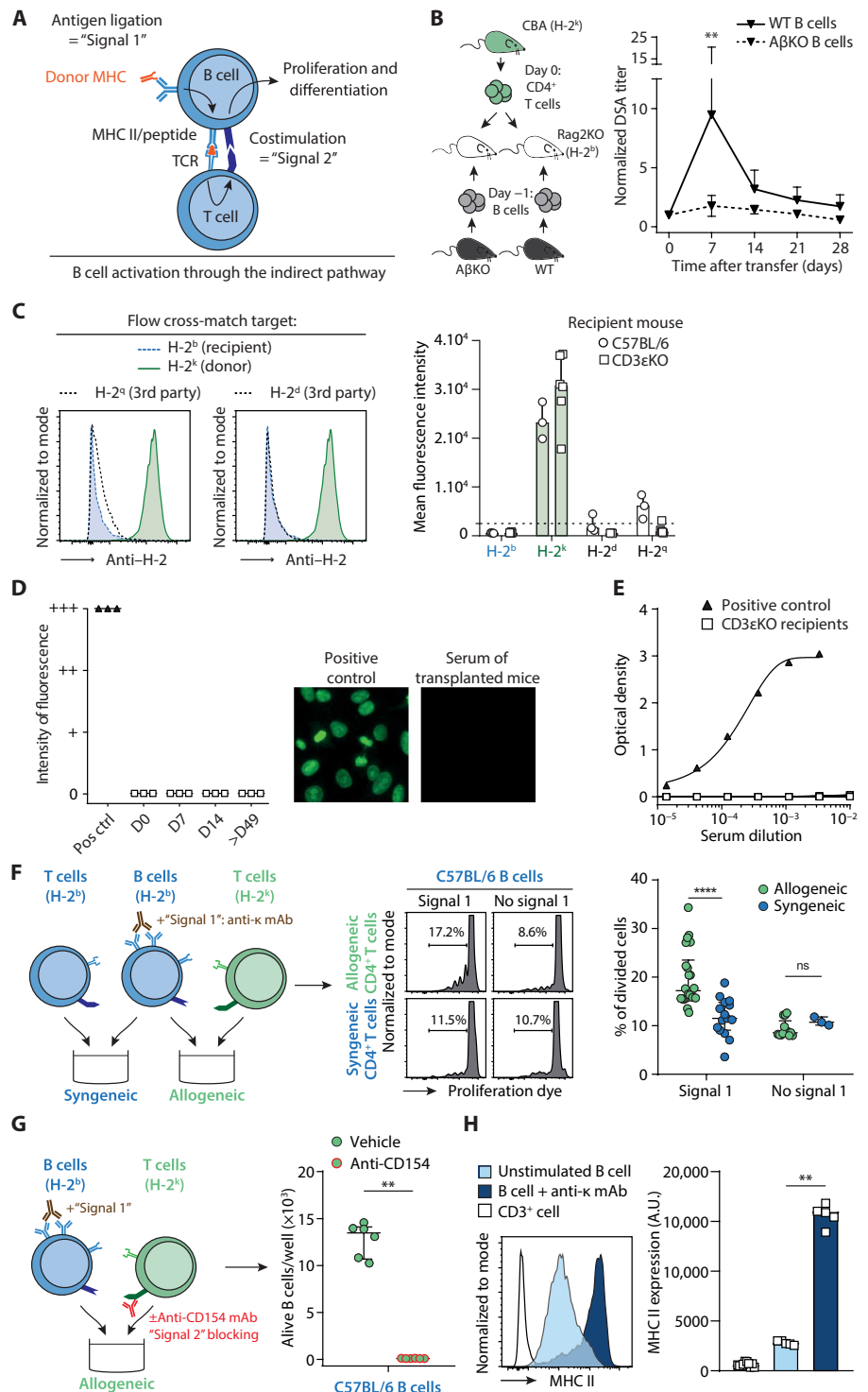
Downloaded from <https://www.science.org at INSERM> on September 22, 2022

the recipient's cognate CD4⁺ T cells can the latter deliver the "second" signal of activation to allo-specific B cells.

To test whether MHC II expression on recipient's B cells was also important for their interaction with donor's CD4⁺ T cells, we transferred purified allogeneic (CBA; H-2^k) CD4⁺ T cells to C57BL/6 (H-2^b) recombination activating gene 2 (Rag2) KO recipient mice that had been previously replenished by adoptive transfer of syngeneic B cells purified from either WT (controls) or MHC class II I-A β chain KO

(referred to as "AβKO") C57BL/6 mice. As the result of the genetic ablation of the I-A β chain, none of the cells of AβKO mice, including B cells, expresses MHC II molecules. This lack of MHC II expression in the thymus also disrupts positive selection of CD4⁺ T cells, which are totally absent from the PBMCs, the spleen, and the lymph nodes of these animals (fig. S1A). As expected, AβKO mice can therefore neither generate antibody after immunization with the T cell-dependent antigen NP-KLH (fig. S1B) nor generate DSA through

Fig. 3. Donor CD4⁺ T cells recognize allogeneic MHC II on the surface of antigen-activated recipient allo-specific B cells. (A) Schematic representation of the molecular requirements for B cell activation through the canonical indirect pathway. (B) Purified allogeneic CBA (H-2^k) CD4⁺ T cells were injected intravenously to Rag2KO C57BL/6 (H-2^b) mice. The day before the T cell transfer, 5 × 10⁶ B cells were purified from WT (black curve; n = 6) or AβKO (dashed black curve; n = 4) mice (H-2^b) and were injected intravenously to Rag2KO mice. Data were analyzed by multiple t tests. Data are presented as means ± SD. **P < 0.01. (C) Serum samples from WT and CD3εKO recipients were collected at the peak of the DSA response and incubated with different cells expressing recipient (H-2^b), donor (H-2^k), or third-party (H-2^d) MHC molecules. Left: Representative histograms. Right: Mean fluorescence intensity values. Data are presented as median ± IQR. The horizontal dashed line indicates negative controls. (D) Serum from CD3εKO mice transplanted with allogeneic CBA hearts (n = 3) were screened for the presence of autoantibodies by indirect immunofluorescence on Hep-2 cells; representative images are shown on the right. Individual semiquantitative evaluations are shown. Serum from three mice with lupus was used as positive controls. (E) Serum from CD3εKO mice transplanted with allogeneic CBA hearts (n = 6) was screened for the presence of anti-NP antibodies by enzyme-linked immunosorbent assay. Curves representing the optical density as a function of the sample's concentration are shown. Serum from one WT mouse immunized with NP-KLH was used as a positive control. (F) C57BL/6 (H-2^b) B cells, activated or not by BCR cross-linking with anti-κ mAb (signal 1), were cocultured with syngeneic or allogeneic (CBA; H-2^k) CD4⁺ T cells. Left: The schematic representation of the experiments. Middle: Representative flow cytometry histograms. The median percentage of divided B cells is shown. Right: Individual coculture values. Data are presented as median ± IQR. Data were analyzed by Mann-Whitney tests. ****P < 0.0001. ns, nonsignificant. (G) BCR-activated C57BL/6 B cells were cocultured with CBA CD4⁺ T cells in the presence or absence of blocking anti-CD154 mAb. The number of alive B cells was measured by flow cytometry. Left: A schematic representation of the experimental cocultures. Right: Individual coculture values. Data are presented as median ± IQR. Data were analyzed by Mann-Whitney test. **P < 0.01. (H) MHC II expression was quantified on the surface of B cells before and after BCR cross-linking with anti-κ mAb. Left: Representative histograms. Right: Individual mean fluorescence intensity values. Bars indicate median values. Data were analyzed by Mann-Whitney test. **P < 0.01.



the canonical indirect pathway. However, because the genetic manipulation has no impact on B cell ontogeny, AβKO mice exhibited normal CD19⁺ B cell count (fig. S1A) and mounted an antibody response after immunization with the T cell-independent antigen NP-dextran (fig. S1B). In contrast with Rag2KO mice replenished with WT B cells, those injected with AβKO B cells did not generate DSA after the transfer of allogeneic CBA (H-2^k) CD4⁺ T cells (Fig. 3B).

Furthermore, the same lack of DSA generation was obtained when AβKO recipients were transplanted with an allogeneic CBA heart (fig. S2). This demonstrates that the expression of MHC II molecules on the surface of the recipient's B cells is mandatory for their interaction with the donor's CD4⁺ T cells. We therefore called this pathway of allorecognition the "inverted direct pathway" because T cells recognize intact allogeneic MHC molecules on the surface of

the APC, as in canonical direct allorecognition. However, in this case, the origin of the interacting cells is “inverted” as compared with canonical direct allorecognition: T cells come from the donor and recognize intact recipient’s MHC class II molecules on allo-specific B cells.

The humoral response triggered by the inverted direct pathway is allospecific

Because B cells are professional APCs, they constitutively express MHC II on their surface. This implies that alloreactive donor’s CD4⁺ T cells could theoretically interact with any recipient’s B cell, regardless its BCR specificity, and, therefore, that the control of the specificity of the B cell response might be lost in the inverted direct pathway. In disagreement with this hypothesis, however, we did not detect any antibody directed against third-party (H-2^d and H-2^g) MHC molecules in the serum of CD3εKO recipients (H-2^b) of an allogeneic CBA (H-2^k) heart (Fig. 3C). Screening for autoantibodies (Fig. 3D) or antibodies directed against an irrelevant model antigen (Fig. 3E) was equally negative. The humoral alloimmune response of CD3εKO recipients, in which only the inverted direct pathway is functional, targeted exclusively donor-specific MHC molecules, exactly similar to that of WT controls, except for a quantitative bias toward MHC I (Fig. 1C). These results raise the intriguing question of what molecular mechanisms maintain the alloantigen specificity in the antibody response triggered by this inverted direct pathway.

Inverted direct allorecognition requires BCR and costimulatory signals

To dissect the molecular requirements for the dialog between recipient’s B cells and donor’s CD4⁺ T cells and shed light on how this unconventional T cell help manages to maintain the antigen specificity of the antibody response, we moved to *in vitro* models. To deliver the first (BCR-mediated) signal of activation to purified WT murine B cells in culture, we used an anti-κ light chain mAb. By cross-linking surface BCRs, the latter triggers downstream signaling in a high proportion of polyclonal B cells (fig. S3, A and B) with an intensity similar to that observed when the cognate antigen binds to the BCR of specific B cell clone (fig. S3, A and B). This strategy therefore allowed us to test the importance of the first signal of activation independently of the alloantigen itself and its subsequent presentation within the MHC II molecules of activated B cells.

After 3 days, B cells proliferated more when cocultured with allogeneic than syngeneic CD4⁺ T cells [17.2%, interquartile range (IQR) 15.7 to 23.5 versus 11.5%, IQR 9.1 to 14.8 divided B cells, $P < 0.0001$; Fig. 3F]. However, this difference was only observed if B cells were previously activated with anti-κ mAb. When the same B cell–T cell cocultures were performed with resting B cells, the amount of divided B cells was low and not different between the two coculture conditions (8.6%, IQR 8.1 to 11.0 versus 10.7%, IQR 10.1 to 11.8 $P = 0.182$; Fig. 3F). In line with the results shown in Fig. 3B and fig. S2A, signal 1–primed B cells from AβKO mice (which do not express MHC II) did not proliferate, regardless of whether they were cocultured with allogeneic or syngeneic CD4⁺ T cells (fig. S4). Last, we investigated the molecular nature of the second signal of activation delivered by donor T cells to the recipient’s B cells. Given the importance of CD154 (also known as CD40L)/CD40 costimulation in canonical B cell responses to T cell–dependent antigens (33), we hypothesized that it could also be crucial in this allorecognition pathway. To test this hypothesis, C57BL/6 B cells were primed with anti-κ light chain

mAb and were then cocultured with allogeneic CBA CD4⁺ T cells with or without anti-CD154 blocking mAb. In line with our hypothesis, blocking anti-CD154 mAb in the coculture resulted in the death of activated B cells (Fig. 3G).

We next asked why BCR stimulation was critical for the recipient’s B cells to interact with the cognate donor’s CD4⁺ T cells if the antigen is dispensable and MHC II and CD40 are expressed on the surface of unstimulated B cells. It has been shown previously that concurrent engagement of BCR and CD40 provides B cells with a critical advantage and protects them from Fas-mediated apoptosis (34, 35). Furthermore, the cross-linking of surface BCR induced a strong up-regulation of MHC II expression on the surface of B cells (15891, IQR 14678 to 16432 versus 2748, IQR 2630 to 3005 $P = 0.0079$; Fig. 3H), hence increasing the number of molecular targets that can be directly recognized by the TCR of donor T cells of direct specificity. The BCR stimulation that makes B cells fit to interact with donor T cells is not provided by artificial anti-κ mAb *in vivo* but by alloantigens coming from the graft, the most abundant of which is donor-specific MHC I molecules (which are expressed by all the cells of the graft). We hypothesize that this could be the reason why the antibody response triggered through the inverted direct pathway is restricted to alloantigen and biased toward donor-specific MHC I (Fig. 1C).

Human allogeneic T cells provide help to B cells *in vitro*

To test whether inverted direct allorecognition pathway could be of clinical importance, we adapted the murine *in vitro* model described above to human T and B cells. Similar to what was observed in mice, BCR cross-linking with anti-IgM F(ab')₂ resulted in up-regulation of MHC II expression by purified human B cells in culture (fig. S5). Furthermore, BCR-mediated stimulation also resulted in up-regulation of several key costimulatory molecules (including CD40, CD80, and CD86) involved in T cell activation (fig. S5). In line with this observation, as in mice, only signal 1–primed human B cells proliferated when cocultured with allogeneic human CD4⁺ T cells (Fig. 4A).

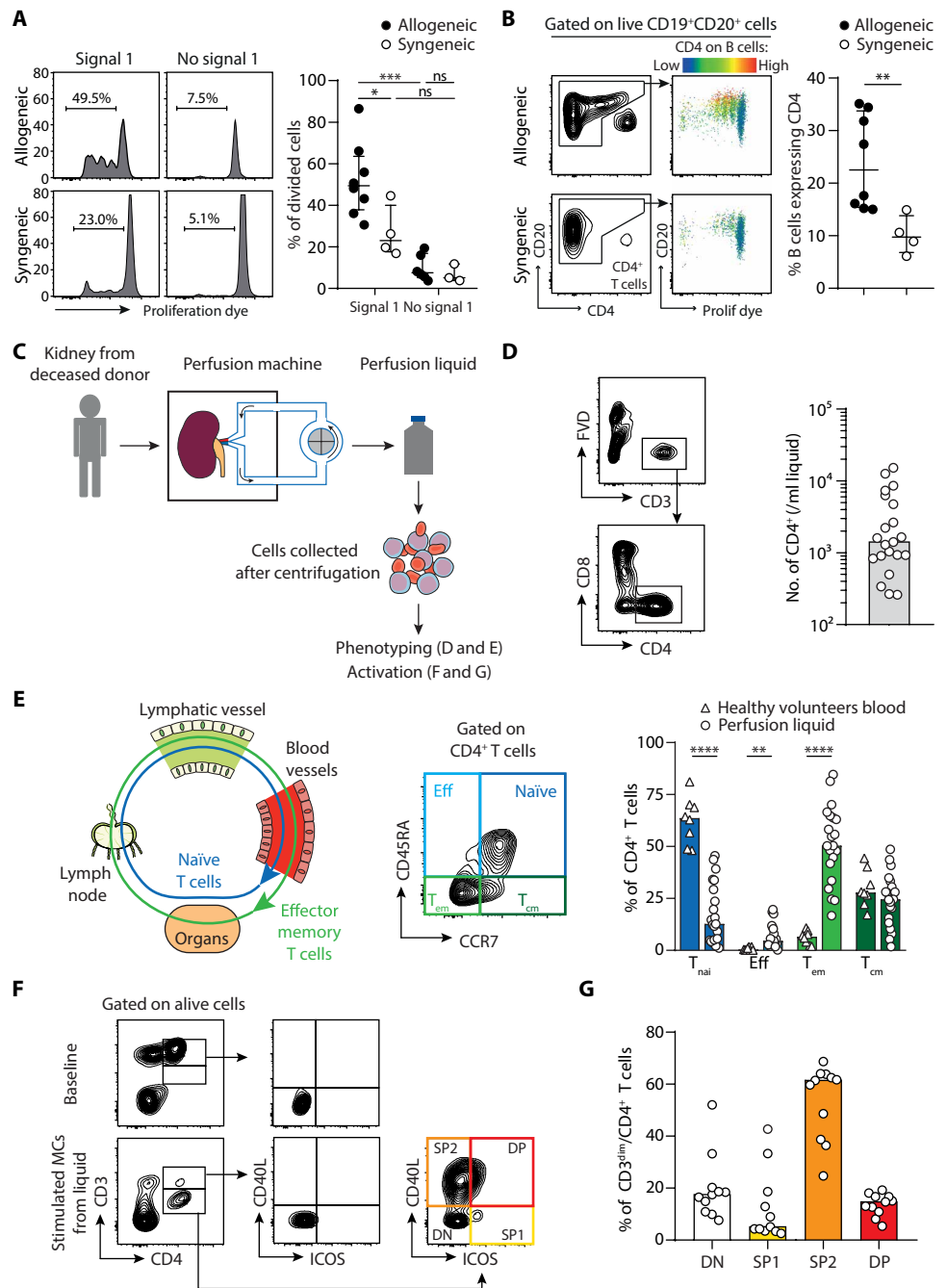
To further demonstrate that human B cells and allogeneic T cells establish cognate interactions in cocultures, we analyzed trogocytosis, which corresponds to an active transfer of surface molecules between cellular partners closely interacting, such as in the case of immunological synapse formation (36). We observed that B cells cocultured with allogeneic T cells captured significantly more CD4 molecules (22.5%, IQR 15.4 to 33.8 versus 9.8%, IQR 6.8 to 13.8 $P = 0.004$; Fig. 4B). Therefore, we concluded that human B cells require the same conditions as murine B cells to proliferate efficiently. These results suggest that the production of early DSA by the inverted direct allorecognition pathway could occur in patients after organ transplantation, provided that donor CD4⁺ T cells are present in human transplants.

Passenger T cells present within kidney graft acquire costimulation capabilities upon activation

Machine perfusion is a technique used in transplantation to preserve the organs after their removal from the donor (Fig. 4C). Briefly, the grafts are rinsed from the donor’s blood before being connected to a machine that generates a controlled recirculating flow of the preservation solution at 4°C. To investigate the presence of donor CD4⁺ T cells within kidney grafts, we took advantage of this procedure and prospectively collected 37 kidney graft perfusion liquids. The perfusion liquids were collected right at the end of the procedure (median

Fig. 4. Human allogeneic T cells present in kidney grafts can provide help to B cells in vitro.

(A) Human B cells were cocultured with syngeneic or allogeneic CD4⁺ T cells in the presence or not of IgM F(ab')₂ (signal 1), and the percentage of divided cells among alive B cells was evaluated by flow cytometry. Left: Representative histograms with median value for each condition. Right: Individual coculture values. Data are presented as median ± IQR. Data were analyzed by Mann-Whitney test. **P* < 0.05 and ****P* < 0.001. **(B)** Human B cells activated with IgM F(ab')₂ were cocultured with syngeneic or allogeneic CD4⁺ T cells. Left: The flow cytometry gating strategy for the assessment of trogocytosis. Right: The percentage of B cells that have experienced trogocytosis in each coculture. Data are presented as median ± IQR. Data were analyzed by Mann-Whitney test. ***P* < 0.01. **(C)** Perfusion fluids of renal allograft were collected (*n* = 37) at the end of procedure, and the phenotype of the immune cells that passed from the graft to the fluid was determined by flow cytometry. **(D)** Representative flow profiles and the flow cytometry gating strategy are shown for the analysis of renal allograft perfusion fluids (left). The number of CD4⁺ T cells that contained per milliliter of perfusion fluid was quantified (right). FVD, fixable viability dye. **(E)** Left: A schematic representation of the circulation behavior of the different T cell subsets. Middle: A representative flow profile for T cell phenotyping. Right: The percentages of naïve (T_{naï}), effector (Eff), effector memory (T_{em}), and central memory (T_{cm}) CD4⁺ T cells found in renal allograft perfusion fluids (open circles) as compared with those observed in the blood of eight healthy volunteers (triangles). Bars indicate median values. Data were analyzed by Mann-Whitney test. ***P* < 0.01 and *****P* < 0.0001. **(F and G)** Mononuclear cells (MCs) isolated from renal allograft perfusion fluids were stimulated (or not) with anti-CD3/anti-CD28 nanoparticles. Flow cytometry was used to measure the surface expression of CD40L and ICOS. **(F)** The flow cytometry gating strategy is shown. SP, single positive; DP, double positive; DN, double negative. **(G)** The percentages of the various CD4⁺ T cell subsets observed after activation are plotted for the 11 renal allograft perfusion fluids analyzed. Bars indicate median values.



perfusion length 630 min; range, 245 to 1195) and centrifugated to isolate the cells, which were then analyzed by flow cytometry (Fig. 4D). Kidney grafts did contain passenger mononuclear cells, including CD4⁺ T cells (Fig. 4D).

Although kidneys are rinsed before being connected to the perfusion machine, contamination with the donor's blood remains possible. To evaluate the importance of this potential bias, we compared the ratios of red and white blood cells in paired blood and perfusion liquid samples. We observed that white blood cells were 34.4-fold more abundant in the perfusion liquid than in the blood. In addition, the distribution between the various CD4⁺ T subsets in

perfusion liquid was different from that observed in the blood of healthy volunteers (Fig. 4E). Perfusion liquids were largely enriched with CCR7⁻CD45RA⁻CD4⁺ effector memory T cells, a subset localized within tissue, and were deprived of circulating CCR7⁺CD45RA⁺CD4⁺ naïve T cells (Fig. 4E). These results suggest that cell populations identified in perfusion liquids reflect the cellular content of human kidney grafts. Although passenger CD4⁺ T cells did not express the surface molecules typically associated with B helper function at baseline, a strong up-regulation of CD40L expression [and, to a lesser extent, inducible T cell costimulatory (ICOS)] was observed on their surface after TCR stimulation (Fig. 4, F and G).

Early DSA generation depends on the graft content in donor's T cells in humans

Recipient's B cells are located within secondary lymphoid organs: lymph nodes and spleen. The lymphatic vasculature of the graft is not anastomosed to that of the recipient during the surgical procedure, and reestablishment of the lymphatic outflow takes several days (37, 38). In line with this, it has been shown that after the transplantation of a vascularized organ, donor passenger leukocytes are found in the recipient's spleen (homing through blood) rather than in lymph nodes (homing through lymph) (39). We therefore reasoned that passenger CD4⁺ T cells should be detectable in recipient's circulation immediately after transplantation if they were to reach the spleen and interact with the recipient's B cells to generate a first early wave of DSAs. Chimerism analysis of the circulating CD3⁺ compartment was performed during the first 3 days after kidney transplantation in nine consecutive recipients. Despite the fact that kidney grafts contain passenger T cells (Fig. 4), T cells of donor origin could only be detected (and at very low abundance) in the circulation of a single patient (Fig. 5A). This is likely explained by the fact that (i) kidney grafts contain relatively few passenger T cells and (ii) 6 of 15 tested kidney recipients received thymoglobulin as induction therapy (but not the one with positive chimerism).

In contrast with the kidney, the lung contains a professional lymphoid tissue [bronchus-associated lymphoid tissue (BALT)]. Computer-assisted morphometric quantification showed that a lung contains on average 11.5-fold more CD4⁺ T cell per surface unit than a kidney (Fig. 5B). This difference does not take into account the size difference between the two organs (a lung weighs about 420 g versus only about 130 g for a kidney), and most of the time, two lungs are transplanted together to the recipients. In total, we estimated that lung recipients receive about 74-fold more donor T cells than kidney recipients. Together with the fact that depleting induction is rarely used in thoracic transplantation centers, these differences likely explain why all lung recipients tested had high amounts (up to 20%) of CD3⁺ T cells from donor origin detectable in their circulation the day after transplantation (Fig. 5A). Although a clear trend for diminution was noted afterward, this chimerism persisted for several days (Fig. 5A).

The phenotype of the passenger CD4⁺ T contained in the perfusion liquids of lung transplants was analyzed by flow cytometry as

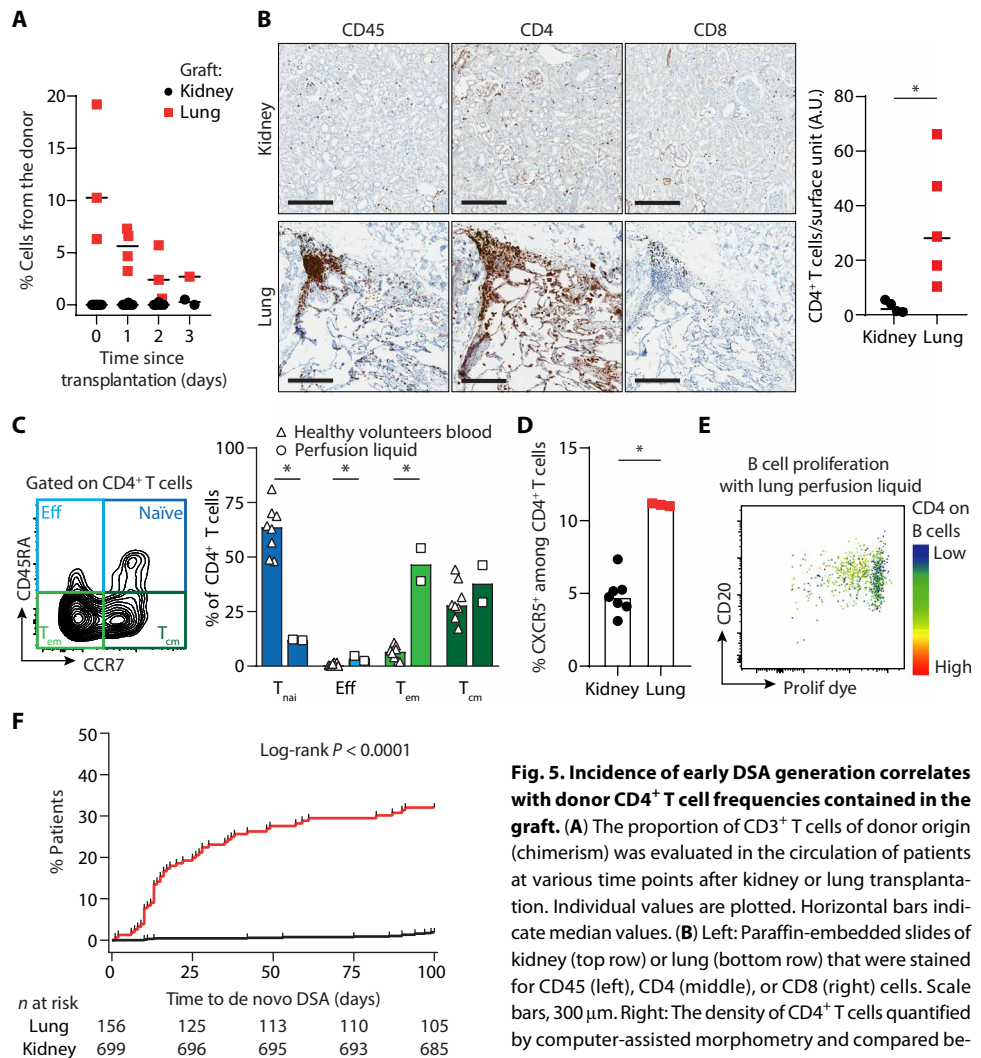


Fig. 5. Incidence of early DSA generation correlates with donor CD4⁺ T cell frequencies contained in the graft. (A) The proportion of CD3⁺ T cells of donor origin (chimerism) was evaluated in the circulation of patients at various time points after kidney or lung transplantation. Individual values are plotted. Horizontal bars indicate median values. (B) Left: Paraffin-embedded slides of kidney (top row) or lung (bottom row) that were stained for CD45 (left), CD4 (middle), or CD8 (right) cells. Scale bars, 300 μm. Right: The density of CD4⁺ T cells quantified by computer-assisted morphometry and compared between kidney and lung. Horizontal bars indicate median values. Data were analyzed by Mann-Whitney test. **P* < 0.05. (C) Lung graft perfusion fluids were collected at the end of the procedure, and their cell content was analyzed by flow cytometry. Left: A representative flow profile for T cell phenotyping in lung perfusion liquid. Right: The percentages of T_{naïv}, Eff, T_{em}, and T_{cm} CD4⁺ T cells detected in lung allograft perfusion fluids (open squares), which were compared with those observed in the blood of healthy volunteers (triangles). Bars indicate median values. Data were analyzed by Mann-Whitney test. **P* < 0.05. (D) Kidney and lung graft perfusion fluids were collected at the end of the procedure, and their cell content was analyzed by flow cytometry. The percentage of T_{FH} (CXCR5⁺ cells) among CD4⁺ T cells is compared. Bars indicate median values. Data were analyzed by Mann-Whitney test. **P* < 0.05. (E) The cells collected in a lung perfusion liquid were cocultured with allogeneic B cells stained with a proliferation dye. The flow cytometry plot shows the proliferation of the CD20⁺ population. A color scale is used to code the proportion of B cells that acquired CD4 molecules by trogocytosis. (F) A Kaplan-Meier curve for DSA-free survival after kidney (black curve) and lung (red curve) transplantation is shown.

for kidney grafts (Fig. 5C). Beyond the mere quantitative aspect mentioned above, there was also a difference in the nature of the passenger T cells between the two types of grafts. BALT is a professional secondary lymphoid tissue, which contains T follicular helper cells (T_{FH}), a subset of CD4⁺ T cells specialized in providing help to B cells (11, 12, 40). T_{FH} are constitutively equipped with CXCR5, a chemokine receptor that allows T_{FH} to migrate efficiently in B cell areas (11, 12, 40). As expected, up to 10% of passenger CD4⁺ T cells were CXCR5⁺ T_{FH} in lungs, whereas they represented only 5% in the kidneys (Fig. 5D).

To evaluate whether passenger CD4⁺ T cells could help the recipient's B cells to differentiate into DSA-producing plasma cells, the cells contained in a lung perfusion liquid were cocultured with allogeneic B cells from a healthy volunteer. As expected, T cells contained in the lung perfusion liquid interacted with B cells and efficiently promoted their proliferation (Fig. 5E). These data led us to hypothesize that, in the clinic (as in the murine model; Fig. 2G), there is a direct relationship between the amount of donor T cells found in the circulation after transplantation, the intensity of inverted direct allorecognition, and the risk to develop a first early wave of DSA. To test this, we compared the incidence of DSAs in two cohorts of lung ($n = 156$) and kidney ($n = 699$) recipients in the early phase (first 100 days) after transplantation. Patients' characteristics are summarized in table S1. As expected, lung recipients, in which inverted direct allorecognition is most likely to occur, were also much more prone to generate de novo DSA within the first 100 days ($P < 0.0001$, log-rank test; Fig. 5F).

Early onset of de novo DSAs occurs frequently after intestinal transplantation

To further evaluate the robustness of the relationship between the amount of donor T cells in the graft and the risk of developing a first early wave of DSAs, we focused our interest on intestinal transplantation. This rare procedure is currently the only therapeutic option for patients with intestinal failure with irreversible complications associated with the long-term use of parenteral nutrition (41). Intestinal grafts include gut-associated lymphoid tissue (GALT; Fig. 6A), a professional secondary lymphoid tissue that contains as many lymphocytes as the spleen (42), and germinal centers enriched in T_{FH} (Fig. 6A). We therefore hypothesized that intestinal graft recipients could experience a very strong inverted direct stimulation of their alloreactive B cells and should be at extremely high risk of developing an

early DSA response. Twenty-six intestine recipients transplanted between 1 May 2009 and 30 November 2014 were retrospectively enrolled (the clinical characteristics of the patients are presented in table S1). Two patients who died within the first week after the procedure were excluded because they had no DSA screening available. In agreement with our hypothesis, 20 of 24 (83%) intestine recipients developed de novo DSAs within the first 30 days after transplantation, with a higher incidence and faster kinetics than what observed in any other types of transplantation ($P < 0.0001$ for intestine versus lung and intestine versus kidney, log-rank test; Fig. 6B).

Early DSA responses in humans are transient

We then compared the early (<100 days; supposed to be mediated by the inverted direct pathway) and late (≥ 100 days; supposed to be mediated by the indirect pathway) DSA responses in our three cohorts of transplant recipients (kidney, lung, and intestine). The amount of DSAs generated was higher (fig. S6A) and the repertoire was more diverse (fig. S6B) in early than in late DSA responses. Furthermore, reminiscent of the mouse model, in which the DSA response induced by the inverted direct pathway was biased toward the donor's MHC I (Fig. 1C), the proportion of patients with anti-MHC I DSA was higher in early than in late DSA responses (fig. S6C). Another similarity with the murine model (Fig. 1, B and F) was the fact that early DSA responses exhibited a rapid decay of alloantibodies titers, whereas late DSA responses persisted over time. This observation, first made by the comparison of the early DSA responses of intestine recipients and the late DSA responses of kidney recipients (fig. S6D), held true in a homogeneous population of lung transplant recipients (fig. S6E).

Complement-binding early DSAs impair graft survival

The fact that early DSA responses are transient does question their pathogenicity for the graft and, therefore, their relevance for clinicians. There are two processes by which DSAs could damage the graft. First, the binding of circulating DSAs to graft endothelium can recruit Fc γ receptor-expressing innate immune effectors, which, in turn, promote damage to graft endothelial cells through the release of lytic enzymes (43). This process is slow and leads to subclinical or chronic AMR (2, 44, 45). Second, whenever the titer is sufficient, DSAs can activate the classical complement pathway, thereby accelerating the rejection process (2, 14). Given the transient nature of early DSA responses, we hypothesized that the latter could affect graft survival if complement-binding DSAs were generated. We tested this hypothesis in the two cohorts of lung and intestine recipients, in which the ability of DSAs generated within the first 100 days to bind C1q in ex vivo assay was assessed. Occurrence of severe chronic lung allograft dysfunction (CLAD 3; in lung recipients; Fig. 7A) or graft survival (in intestine recipients; Fig. 7B) was compared between three groups of recipients: with non-complement-binding DSAs, with complement-binding DSAs, and without DSA. In line with our hypothesis, early DSA responses did affect intestinal graft survival only for recipients with DSAs able to activate the classical complement cascade ($P = 0.0019$ and $P = 0.0135$ for lung and intestine recipients, respectively, log-rank test).

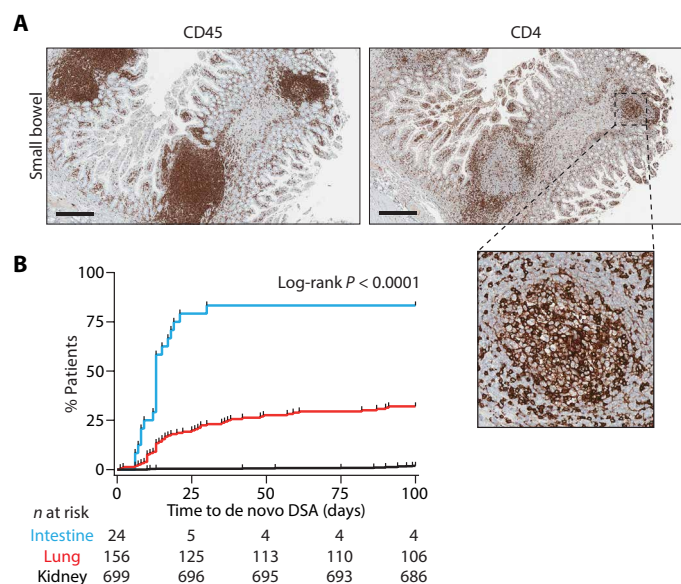


Fig. 6. Early onset of de novo DSAs is observed after intestinal transplantation.

(A) Paraffin-embedded slides of small intestine were stained for CD45⁺ (left) or CD4⁺ (right) cells. The magnified image highlights the CD4⁺ T_{FH} cell population in a germinal center. Scale bars, 500 μ m. (B) Kaplan-Meier curves of DSA-free survival after kidney (black), lung (red), and intestinal (blue) transplantation are shown.

DISCUSSION

CD4⁺ T cell help is known to be mandatory for the differentiation of the recipient's allospecific B cells into DSA-producing plasma cells

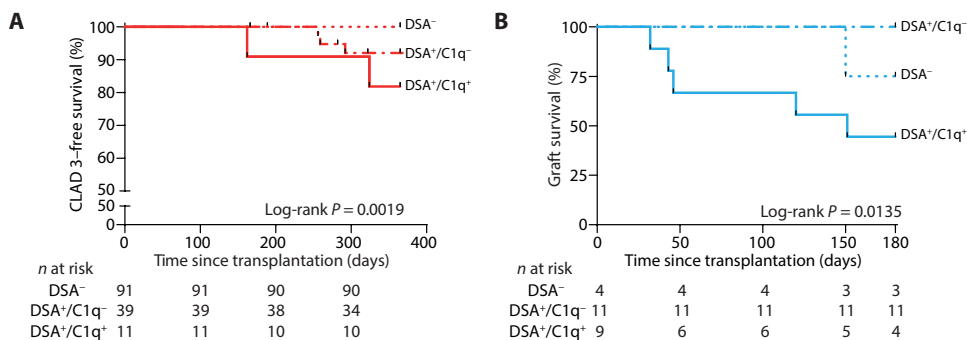


Fig. 7. Early onset of de novo DSAs has a detrimental impact on transplantation outcome. Kaplan-Meier curves for (A) severe chronic lung allograft dysfunction (CLAD 3)–free survival or (B) intestinal graft survival are shown according to the presence of early DSAs (DSA⁺ or DSA⁻) and their ability to bind complement (C1q⁺ or C1q⁻).

(10–13). However, we here demonstrate that when graft contains sufficient number of passenger CD4⁺ T cells, these cells migrate into the recipient's circulation and can provide help to the recipient's allo-specific B cells; this was associated with an early wave of transient DSAs directed predominantly against donor-specific MHC I alloantigens. We named this pathway of allorecognition “inverted direct” because, as in canonical direct pathway, it involves recognition of allogeneic MHC molecules by the TCR of CD4⁺ T cells in a peptide-degenerate manner. However, in this case, the T cells are from the donor, whereas the APCs (the allospecific B cells) come from the recipient. The origins of the cells are therefore inverted. The results from our murine models are aligned with experimental data reported by Harper *et al.* (32), and our translational approach allowed the validation of these findings in the clinical setting, suggesting that inverted direct pathway also exists in patients and might have a detrimental impact on graft survival.

The interactions between lymphohematopoietic cells from two genetically distinct patients have been previously reported in bone marrow transplantation (46). Although the threat of lymphohematopoietic graft-versus-host disease (47) is well known, other studies have also documented the beneficial impact of the bidirectional alloreactivity (graft-versus-host and host-versus-graft reactivity, due to micro- or macrochimerism) in the induction and maintenance of transplant tolerance (48–50). Even if the interaction reported here can be considered belonging to the same family of immune mechanisms, it stands out because, in contrast with previously discussed situations (47) in which the donor's T cells invariably destroy the recipient's cells, the inverted direct pathway instead provides functional help to the recipient's B cells.

Our results challenge the prevailing dogma that the indirect pathway is the only mechanism involved in DSA generation. In the indirect pathway, binding of donor MHC molecules to the BCR activates allospecific B cells of recipient, which, in turn, present alloantigen-derived peptides within surface MHC II molecules. Only when these complexes are recognized by the recipient's cognate CD4⁺ T cells can the latter deliver the second signal of activation to allospecific B cells. In the inverted direct pathway, this control of the specificity of the B cell response is expected to be lost. It is the recipient MHC II molecules (expressed on all B cells irrespective of their antigen specificity) that are directly recognized by the donor's CD4⁺ T cells of direct allospecificity. However, no massive polyclonal antibody response was observed, neither in experimental models nor in transplant

recipients. The results of our experiments indicate instead that the alloantigen specificity of the response triggered by the inverted direct pathway is maintained through the requirement for BCR signal, which provides the allospecific B cell clones with a decisive advantage to interact with alloreactive donor T cells.

A notable feature of the DSA response generated through the inverted direct pathway is its transient nature. The number of CD4⁺ T cells available to provide help being a critical factor for the development of germinal centers (11), it is likely that the rapid diminution in the help provided to allospecific B cells due to the elimination of donor's T cells could ex-

plain the decay in DSA titer. This hypothesis is supported by a recent experimental study, which has reported that, at 7 weeks after heart transplantation, no germinal center could be detected in the secondary lymphoid organs of recipients in which only the inverted direct pathway was operant (51). Pushing this line of thinking forward, the authors demonstrated that, in this murine model, the antibody response depended primarily on an extrafollicular B cell response (51).

The inverted direct pathway of allorecognition provides a possible molecular explanation for the early transient onset of anti-MHC I DSA sometimes observed in naïve recipients within days after transplantation, a delay too short to be the consequence of the indirect pathway. Early onset of DSA, which is rare after kidney transplantation (16), has been much more frequently observed in other types of transplantation, including lung (52, 53) and intestinal transplantations (21, 54, 55). This is in agreement with the fact that, if passenger CD4⁺ T cells with a tissue-resident memory phenotype can be found in almost all organs (56), including kidney graft (57, 58), then the inverted direct pathway is much stronger when the transplanted organ contains mucosa-associated lymphoid tissue (MALT), such as BALT in the lung and GALT in the intestine. We found a correlation between the number of passenger CD4⁺ T cells in the graft, the presence of donor CD4⁺ T cells in the recipient's circulation, and the risk of early DSA response. Beyond the mere quantitative difference, the nature of the CD4⁺ T cells present within the graft might also have an influence on the process. Although tissue-resident memory CD4⁺ T cells can acquire B cell helper functions upon TCR stimulation, MALT contains a large amount of T_{FH}, a subset specialized in providing help to B cell, which constitutively express the chemokine receptor CXCR5, which is required to efficiently migrate to the recipient's B cell areas. The development of ectopic lymphoid tissue (named “tertiary” lymphoid structures) has been reported upon chronic inflammation in numerous organs normally devoid of developmentally programmed secondary lymphoid tissue (59–61). It is reasonable to speculate that such organs, when transplanted, induce inverted direct allorecognition.

Strategies to target the inverted direct pathway, and therefore limit the early generation of DSA, are needed to promote graft survival. We found passenger CD4⁺ T cells in cold perfusion liquid; however, normothermic perfusion could be more efficient at clearing tissue-resident T cells from the graft by mobilizing them in the perfusion liquid (62). This technique alone is, however, likely to be insufficient to achieve adequate T cell depletion of the graft, a goal that may require

adding T cell-depleting (or T cell-attracting) drugs to the perfusion fluid (63). Last, it should be kept in mind that passenger CD4⁺ T cells can only provide help to B cells if they reach the recipient's secondary lymphoid organs. In this regard, induction by thymoglobulin appears as the most straightforward option to reduce the intensity of inverted direct pathway by destroying all passenger CD4⁺ T cells whenever they enter the recipient's circulation.

Our study has some limitations. First, the data obtained in patients, although consistent with the existence of the inverted direct pathway of allorecognition in the clinic, remain purely correlative. The demonstration that interactions between the allogeneic donor's T cells and the recipient's B cells occur in patients would have required performing invasive biopsies of secondary lymphoid organs, which are not devoid of side effects and were difficult to justify. Second, the reason why the inverted direct pathway of allorecognition triggered selectively the activation of recipient's allospecific B cells remains incompletely understood. This result is in disagreement with the data reported by Harper *et al.*, who observed the generation of autoantibodies in a murine experimental model of inverted direct allorecognition (32). Although we did not detect autoantibodies in our model, we cannot exclude that the difference in the molecular mechanisms controlling the specificity of B cell clones able to differentiate into plasma cells might be more leaky in the case of the inverted direct pathway and therefore responsible for the higher incidence of autoantibodies sometimes reported in transplant recipients (64–66). Last, this study did not explore what mechanisms could influence the interactions between donor and recipient hematopoietic cells toward DSA production, tolerance promotion, or graft-versus-host disease, a fascinating topic that will require future dedicated studies.

In conclusion, we describe here a mechanism of allorecognition that we named the inverted direct pathway, in which intragraft passenger CD4⁺ T cells of donor origin provide help to the recipient's allospecific B cells. The inverted direct pathway is prominent when transplanted organs contain MALT. This mechanism thus provides a possible explanation for the particularly high incidence of early transient onset of anti-MHC I DSAs reported after transplanting such organs.

MATERIALS AND METHODS

Study design

Transplanting allogeneic heart grafts in recipient mice devoid of T cells, we observed the unexpected generation of DSAs. This murine experimental model was used to perform a mechanistic study, which led to the identification of the inverted direct allorecognition pathway. The murine model was then adapted and combined with *in vitro* approaches to dissect the molecular mechanisms involved in the inverted direct allorecognition pathway. When applicable, mice were randomly assigned to the different groups. The follow-up of the mice and most of the analyses were not blinded. Only the pathological analysis of the heart grafts was blinded. Sample sizes were not based on power analysis. Each experiment was performed at least twice, and data describe biological replicates. No outliers were excluded from the analysis. Aiming at evaluating the clinical validity of these experimental findings, we next analyzed perfusion liquids of renal and lung grafts to characterize their content in immune cells from donor origin and thus provide indirect clues regarding the existence of the inverted direct allorecognition pathway in patients. Three independent cohorts of patients living with a transplant (kidney, lung, or intestine) were then retrospectively analyzed to study the relation

between graft's content in donor CD4⁺ T cells and the incidence of early DSAs and graft survival.

Mice

WT C57BL/6 (H-2^b) and CBA (H-2^k) mice were purchased from Charles River Laboratories. MHC II KO (A β KO) mice on C57BL/6 genetic background were provided by C. Benoist and D. Mathis (67). CD3eKO mice on C57BL/6 genetic background were purchased from the Jackson Laboratory. Rag2KO mice on a C57BL/6 background were obtained from the Cryopreservation Distribution Typage et Archivage Animal. All mice were maintained under EOPS (Exemption of Specific Pathogenic Organisms) conditions in our animal facility: Plateau de Biologie Expérimentale de la Souris (www.sfr-biosciences.fr/plateformes/animal-sciences/AniRA-PBES). All studies and procedures were performed in accordance with European Union guidelines and were approved by the local ethical committee for animal research (CECCAPP Lyon, registered by the French National Ethics Committee of Animal Experimentation under no. C2EA15; www.sfr-biosciences.fr/ethique/experimentation-animale/ceccapp).

Heterotopic heart transplantation in mice

Heart transplantations were performed as previously described (3, 68). We used intravenous administration of 17A2 (20 μ g), an anti-murine CD3 mAb (69), and GK1.5 (32 μ g), an anti-murine CD4 mAb (70) (both rat IgG2b antibodies), to deplete CD3⁺ or CD4⁺ T cells in mice. The injections were given to the donors 2 days in a row, just before the transplantation (17A2) or 1 week before the transplantation (GK1.5). The recipients were depleted by two injections, the day of the transplantation and the following day. DSA titers were determined using a single antigen bead assay or a custom flow cross-match assay as in the study by Chen *et al.* (3). For further details, see Supplementary Methods and fig. S7.

Pathological analyses

Cardiac transplants were collected for the histological assessment of the DSA-mediated lesions. Recipient mice were euthanized by cervical dislocation after general anesthesia. Heart transplants were fixed in 4% buffered formalin for 24 hours and embedded in paraffin for hematoxylin and eosin staining. The slides were scanned before analysis (NanoZoomer S60 digital slide scanner, Hamamatsu Photonics). Regions for analysis were randomly selected in the left ventricle.

Intravenous allogeneic cell injection

Purified allogeneic CBA (H-2^k) CD4⁺ T cells (2×10^5 to 5×10^6) were injected intravenously to CD3eKO, Rag2KO, or WT C57BL/6 (H-2^b) mice. The day before the T cell transfer, 5×10^6 B cells purified from WT or A β KO mice (H-2^b) were injected intravenously to Rag2KO mice. CD4⁺ T cells and B cells were isolated using negative selection kits (STEMCELL Technologies and R&D Systems), according to the manufacturer's instructions. For some experiments, CD4⁺ T cells were fixed with 35% ethanol before injection.

Cocultures

To perform murine cell cultures, spleens were harvested from C57BL/6, CBA, and A β KO mice. B cells from C57BL/6 or A β KO mice and T cells from C57BL/6 and CBA mice were isolated, using B and T cell negative selection kits (R&D Systems), respectively, according to the manufacturer's instructions. For B cell proliferation assays, B cells were stained with a proliferation dye (CellTrace Violet, Thermo

Fisher Scientific) according to the manufacturer's instructions. B cells (10^5) were cocultured with 10^5 syngeneic or allogeneic T cells in the presence or absence of a soluble anti- κ mAb (1 μ g for 10^6 cells; see Supplementary Methods). When indicated, an anti-CD154 mAb was added (clone MR1, BD Biosciences; 10 μ g/ml).

For MHC expression assays, 10^6 B cells from C57BL/6 mice were cultured overnight at 37°C and 5% CO₂ in complete medium [for mouse: RPMI 1640 GlutaMAX medium (Invitrogen) supplemented with 10% fetal calf serum, 50 μ M β -mercaptoethanol (Sigma-Aldrich), 25 mM Hepes (Invitrogen), and penicillin/streptomycin (10 U/ml; Invitrogen)], with a soluble anti- κ mAb (1 μ g for 10^6 cells).

Before staining, murine cells were incubated with a blocking anti-mouse Fc receptor antibody (2.4G2; homemade hybridoma). Cells were then incubated at 4°C with the following fluorescent antibodies: CD3 [dilution 1:200; 145-2C11, Brilliant Violet 421 (BV421), BD Biosciences, catalog no. 562600, RRID:AB_11153670], CD19 [dilution 1:200; 1D3, phycoerythrin (PE)–CF594, BD Biosciences, catalog no. 562291, RRID:AB_11154223], B220 (dilution 1:200; RA3-6B2, allophycocyanin, BD Biosciences, catalog no. 553092, RRID:AB_398531), and MHC II [dilution 1:250; 2G9, fluorescein isothiocyanate (FITC), BD Biosciences, catalog no. 553623, RRID:AB_394958]. Before analysis by flow cytometry, DAPI (4',6-diamidino-2-phenylindole dihydrochloride; Sigma-Aldrich) was added to the cell suspension to exclude dead cells. Samples were analyzed on a BD LSR II flow cytometer (BD Biosciences).

Human PBMCs were collected from the French National Blood Service (Etablissement Français du Sang, EFS) and isolated by centrifugation on a Ficoll density gradient. B cells and T cells were isolated, using B and T cell negative selection kits (R&D Systems), respectively, according to the manufacturer's instructions. For MHC, CD40, CD86, and CD80 expression assays, 5×10^5 PBMC cells were cultured overnight at 37°C and 5% CO₂ in complete medium [for human: RPMI 1640 GlutaMAX medium (Invitrogen) supplemented with 10% fetal calf serum, 25 mM Hepes (Invitrogen), and penicillin/streptomycin (10 U/ml; Invitrogen)], with a soluble anti-human IgM F(ab')₂ (5 μ g/ml). Cells were then processed as described above for murine samples.

For human B cell proliferation assays, T cells and B cells were purified (up to 95% purity) from PBMCs by negative selection with magnetic enrichment kits (R&D Systems). B cells were stained with a proliferation dye (CellTrace Violet or carboxyfluorescein succinimidyl ester, Thermo Fisher Scientific) according to the manufacturer's instructions. B cells (4×10^5) were cocultured with 4×10^4 syngeneic or allogeneic T cells in the presence or absence of a soluble anti-human IgM F(ab')₂ (5 μ g/ml; Jackson ImmunoResearch).

Cells were then incubated at 4°C with the following fluorescent antibodies: CD3 [dilution 1:20; UHCT1, PE, BD Biosciences, catalog no. 555333, RRID:AB_395740 or peridinin-chlorophyll-protein (PerCP)–cyanin 5.5 (Cy5.5), BD Biosciences, catalog no. 560835, RRID:AB_2033956], CD4 (dilution 1:40; SK3, PE-Cy7, BD Biosciences, catalog no. 557852, RRID:AB_396897), CD19 (dilution 1:40; HIB19, allophycocyanin-R700, BD Biosciences, catalog no. 564977, RRID:AB_2744308), CD20 (2H7; dilution 1:5; FITC, BD Biosciences, catalog no. 555622, RRID:AB_395988; or dilution 1:40; BV421, BD Biosciences, catalog no. 562873, RRID:AB_2737857), MHC II (dilution 1:20; G46-6, allophycocyanin-H7, BD Biosciences, catalog no. 561358, RRID:AB_10611876), CD40 (dilution 1:20; 5C3, Alexa Fluor 488, BioLegend, catalog no. 334318, RRID:AB_1501188), CD86 (dilution 1:20; FUN-1, BV650, BD Biosciences, catalog no.

563411, RRID:AB_2744456), CD80 (dilution 1:20; 2D10, PE/Dazzle 594, BioLegend, catalog no. 305230, RRID:AB_2566489), and a Fixable Viability Dye (dilution 1:500; eBioscience, eFluor506). Samples were analyzed on a BD LSRFortessa 4L flow cytometer (BD Biosciences).

Cohorts of transplant recipients

The renal and lung transplant cohort studies were carried out in accordance with French legislation on biomedical research and the Declaration of Helsinki. All patients gave informed consent for the utilization of clinical data [Données Informatiques Validées en Transplantation (DIVAT)] and biological samples for research purpose. For DIVAT, a declaration was made to the CCTIRS (Comité consultatif sur le Traitement de l'Information en matière de Recherche dans le domaine de la Santé) and the CNIL (Commission nationale de l'Informatique et des Libertés). For the biocollection, an authorization (nos. of biocollection: AC-2011-1375 and AC-2016-2706) was obtained from the French Ministry of Higher Education and Research (direction générale pour la recherche et l'innovation, cellule bioéthique). For the study of the early incidence of DSAs after transplantation, all patients over 16 years who underwent a first lung transplantation at Bichat (Paris, France), Foch (Suresnes, France), or Marie-Lannelongue (le Plessis-Robinson, France) hospitals between 1 May 2008 and 30 June 2012 or a first kidney transplantation at Lyon University Hospital (Lyon, France) between 1 January 2013 and 31 December 2017 were enrolled. The analysis compared the period of the first 100 days with the subsequent period. This period allows for the inclusion of the anti-HLA antibody testing carried out in the third month after transplantation, which corresponds to the first sampling for many patients. For the lung transplant survival study, the outcome considered the onset of severe CLAD 3. For the intestine transplant cohort, all patients who underwent intestinal transplantation at Necker University Hospital (Paris) between 1 May 2009 and 30 November 2014 were enrolled. For the intestinal transplant survival study, the outcome considered both graft and patient survival.

Analysis of graft perfusion liquids

The renal and lung perfusion liquids (from Lyon University Hospital and Bichat University Hospital, Paris, respectively) were collected after the organ was removed from the machine. The cells were isolated as follows: after a first wash in phosphate-buffered saline (PBS), leukocytes and red blood cells were counted before red blood cell lysis in ammonium-chloride-potassium (ACK) lysis buffer (for renal perfusion liquids only). After a second wash in PBS, cells were frozen and kept at –80°C until their analysis. After thawing, the cells were cultured for 12 hours in complete RPMI 1640 at 37°C and 5% CO₂ before staining, with or without human T-activator CD3/CD28 Dynabeads (Thermo Fisher Scientific). Cells were then incubated at 4°C with relevant antibodies: CD3 (dilution 1:100; UCHT1, BV421, BD Biosciences, catalog no. 562426, RRID:AB_11152082), CD4 (dilution 1:80; SK3, PerCP-Cy5.5, BD Biosciences, catalog no. 332772, RRID:AB_2868621), CD8 (dilution 1:100; SK1, allophycocyanin-H7, BD Biosciences, catalog no. 560179, RRID:AB_1645481), CXCR5 (dilution 1:80; RF8B2, Alexa Fluor 647, BD Biosciences, catalog no. 558113, RRID:AB_2737606), CD40L (dilution 1:20; TRAP1, PE, BD Biosciences, catalog no. 561720, RRID:AB_10924597), CD45RA (dilution 1:100; L48, PE-Cy7, BD Biosciences, catalog no. 337186, RRID:AB_2828012), CCR7 (dilution 1:40; 150503, FITC, BD Biosciences,

catalog no. 561271, RRID:AB_10561679; or dilution 1:20; 3D12, BV605, BD Biosciences, catalog no. 563711, RRID:AB_2738385), ICOS (dilution 1:20; ISA-3, FITC, Thermo Fisher Scientific, catalog no. 11-9948-41, RRID:AB_10667883), and a viability dye LIVE/DEAD Aqua (1:1000; Invitrogen). Cells were then fixed using Cytofix/Cytoperm (BD Biosciences) according to the manufacturer's instructions. Samples were acquired on a BD FACSAria II flow cytometer (BD Biosciences) or a BD LSRFortessa 4L flow cytometer (BD Biosciences). Data were analyzed with FlowJo software (Tree Star).

Kidney, lung, and intestinal graft histology

The samples analyzed by histology were kidneys that were discarded for transplantation or lungs and intestines from cancer excision surgery. In the latter case, the samples tested were distant from any tumor lesions. CD45, CD4, and CD8 staining were performed by automated immunohistochemistry (System BenchMark ULTRA IHC/ISH, Roche) using anti-human CD45 (dilution 1:100; 2B11 and PD7/26, Dako), CD4 (dilution 1:100; SP35, Cell Marque), and CD8 (dilution 1:20; 4B11, Novocastra) mAbs and the ultraView Universal DAB Detection Kit (Ventana Medical Systems). Computer-assisted morphometric quantifications were performed using FIJI software (71).

Analysis of PBMC chimerism after transplantation

Donor and recipient leukocyte chimerism was evaluated in PBMCs isolated from kidney and lung transplant recipients. Samples were taken on day 0 just after transplantation surgery and at day 1, day 2, and day 3 after transplantation. Chimerism was performed on genomic DNA extracted from CD3 cells after cell sorting (MACSprep Chimerism CD3 MicroBeads, human, Miltenyi Biotec) using quantitative real-time polymerase chain reaction associated with TaqMan technology. Before quantification, the donor and recipient were genotyped using primers and probes specific for 34 genetic markers (QTRACE Assays, JETA Molecular). An allele was considered informative when positive on recipient DNA and negative on donor DNA or conversely negative on recipient DNA and positive on donor DNA. Then, quantification was performed, and the result was given as a percentage of donor cells on patient posttransplantation samples, based on the donor informative system as reference. Mixed chimerism was defined by the presence of at least 0.2% of donor cells.

Anti-HLA antibody detection and characterization

Collected serum samples were analyzed using a single-antigen bead assay (Immucor or One Lambda). DSAs were defined as positive by a mean fluorescence intensity (MFI) greater than 500. The C1q-fixing capacity of posttransplantation DSAs was measured using the C1q-Screen kit (One Lambda), according to the manufacturer's recommendations. The ability of antibodies to bind C1q is correlated to their titers (fig. S8A). A receiver operating characteristic curve was constructed with all available C1q assays (area under the curve = 0.929; 95% confidence interval 0.876 to 0.983; fig. S8B). Given this high value, these data were used to define a test threshold above which DSAs were considered as complement fixing (MFI = 3040; see fig. S8, A and B). This threshold was used to extrapolate the results of the C1q assay for the patients whose serum samples were not available for the retrospective C1q analysis.

Statistical analysis

All raw, individual-level data for experiments where $n < 20$ are presented in data file S1. Statistical analysis and graphs were performed

using Prism software (GraphPad). Quantitative DSA titers were compared using multiple unpaired t tests. All other quantitative variables were expressed as median \pm IQR and compared using Mann-Whitney tests. All tests were two-sided. Incidence and survival data were analyzed by Kaplan-Meier plot and compared using a log-rank test. Statistical significance was considered for a P value of <0.05 .

SUPPLEMENTARY MATERIALS

stm.sciencemag.org/cgi/content/full/14/663/eabg1046/DC1

Methods

Figs. S1 to S8

Table S1

Data file S1

MDAR Reproducibility Checklist

[View/request a protocol for this paper from Bio-protocol.](#)

REFERENCES AND NOTES

1. J. Sellarés, D. G. de Freitas, M. Mengel, J. Reeve, G. Einecke, B. Sis, L. G. Hidalgo, K. Famulski, A. Matas, P. F. Halloran, Understanding the causes of kidney transplant failure: The dominant role of antibody-mediated rejection and nonadherence. *Am. J. Transplant.* **12**, 388–399 (2012).
2. E. Pouliquen, A. Koenig, C. C. Chen, A. Sicard, M. Rabeyrin, E. Morelon, V. Dubois, O. Thauat, Recent advances in renal transplantation: Antibody-mediated rejection takes center stage. *F1000prime Rep.* **7**, –51 (2015).
3. C.-C. Chen, E. Pouliquen, A. Broisat, F. Andreatta, M. Racapé, P. Bruneval, L. Kessler, M. Ahmadi, S. Bacot, C. Saison-Delaplace, M. Marcaud, J.-P. D. Van Huyen, A. Loupy, J. Villard, S. Demuylder-Mischler, T. Berney, E. Morelon, M.-K. Tsai, M.-N. Kolopp-Sarda, A. Koenig, V. Mathias, S. Ducreux, C. Ghezzi, V. Dubois, A. Nicoletti, T. Defrance, O. Thauat, Endothelial chimerism and vascular sequestration protect pancreatic islet grafts from antibody-mediated rejection. *J. Clin. Invest.* **128**, 219–232 (2018).
4. O. Thauat, Humoral immunity in chronic allograft rejection: Puzzle pieces come together. *Transpl. Immunol.* **26**, 101–106 (2012).
5. J. H. Y. Siu, V. Surendrakumar, J. A. Richards, G. J. Pettigrew, T cell allorecognition pathways in solid organ transplantation. *Front. Immunol.* **9**, 2548 (2018).
6. B. Afzali, G. Lombardi, R. I. Lechler, Pathways of major histocompatibility complex allorecognition. *Curr. Opin. Organ Transplant.* **13**, 438–444 (2008).
7. F. G. Lakkis, R. I. Lechler, Origin and biology of the allogeneic response. *Cold Spring Harb. Perspect. Med.* **3**, a014993 (2013).
8. E. J. Suchin, P. B. Langmuir, E. Palmer, M. H. Sayegh, A. D. Wells, L. A. Turka, Quantifying the frequency of alloreactive T cells in vivo: New answers to an old question. *J. Immunol.* **166**, 973–981 (2001).
9. P. F. Halloran, J. Chang, K. Famulski, L. G. Hidalgo, I. D. R. Salazar, M. Merino Lopez, A. Matas, M. Picton, D. de Freitas, J. Bromberg, D. Serón, J. Sellarés, G. Einecke, J. Reeve, Disappearance of T cell-mediated rejection despite continued antibody-mediated rejection in late kidney transplant recipients. *J. Am. Soc. Nephrol.* **26**, 1711–1720 (2015).
10. D. J. Steele, T. M. Laufer, S. T. Smiley, Y. Ando, M. J. Grusby, L. H. Glimcher, H. Auchincloss Jr., Two levels of help for B cell alloantibody production. *J. Exp. Med.* **183**, 699–703 (1996).
11. C.-C. Chen, A. Koenig, C. Saison, S. Dahdal, G. Rigault, T. Barba, M. Taillardet, D. Charoitte, M. Ovize, E. Morelon, T. Defrance, O. Thauat, CD4+ T cell help is mandatory for naive and memory donor-specific antibody responses: Impact of therapeutic immunosuppression. *Front. Immunol.* **9**, 275 (2018).
12. S. Dahdal, C. Saison, M. Valette, E. Bachy, N. Pallet, B. Lina, A. Koenig, G. Monneret, T. Defrance, E. Morelon, O. Thauat, Residual activatability of circulating Tfh17 predicts humoral response to thymodependent antigens in patients on therapeutic immunosuppression. *Front. Immunol.* **9**, 3178 (2019).
13. T. M. Conlon, K. Saeb-Parsy, J. L. Cole, R. Motalebzadeh, M. S. Qureshi, S. Rehakova, M. C. Negus, C. J. Callaghan, E. M. Bolton, J. A. Bradley, G. J. Pettigrew, Germinal center alloantibody responses are mediated exclusively by indirect-pathway CD4 T follicular helper cells. *J. Immunol.* **188**, 2643–2652 (2012).
14. A. Sicard, S. Ducreux, M. Rabeyrin, L. Couzi, B. McGregor, L. Badet, J. Y. Scoazec, T. Bachelet, S. Lepreux, J. Visentin, P. Merville, V. Fremeaux-Bacchi, E. Morelon, J.-L. Taupin, V. Dubois, O. Thauat, Detection of C3d-binding donor-specific anti-HLA antibodies at diagnosis of humoral rejection predicts renal graft loss. *J. Am. Soc. Nephrol.* **26**, 457–467 (2015).
15. R. S. Gaston, J. M. Cecka, B. L. Kasiske, A. M. Fieberg, R. Leduc, F. C. Cosio, S. Gourishankar, J. Grande, P. Halloran, L. Hunsicker, R. Mannon, D. Rush, A. J. Matas, Evidence for antibody-mediated injury as a major determinant of late kidney allograft failure. *Transplantation* **90**, 68–74 (2010).

16. C. Wiebe, I. W. Gibson, T. D. Blydt-Hansen, M. Karpinski, J. Ho, L. J. Storsley, A. Goldberg, P. E. Birk, D. N. Rush, P. W. Nickerson, Evolution and clinical pathologic correlations of de novo donor-specific HLA antibody post kidney transplant. *Am. J. Transplant.* **12**, 1157–1167 (2012).
17. L. J. Lobo, R. M. Aris, J. Schmitz, I. P. Neuringer, Donor-specific antibodies are associated with antibody-mediated rejection, acute cellular rejection, bronchiolitis obliterans syndrome, and cystic fibrosis after lung transplantation. *J. Heart Lung Transplant.* **32**, 70–77 (2013).
18. R. D. Yusen, L. B. Edwards, A. I. Dipchand, S. B. Goldfarb, A. Y. Kucheryavaya, B. J. Levvey, L. H. Lund, B. Meiser, J. W. Rossano, J. Stehlik; International Society for Heart and Lung Transplantation, The Registry of the International Society for Heart and Lung Transplantation: Thirty-third Adult Lung and Heart-Lung Transplant Report-2016; Focus theme: Primary diagnostic indications for transplant. *J. Heart Lung Transplant.* **35**, 1170–1184 (2016).
19. K. M. Abu-Elmagd, G. Wu, G. Costa, J. Lunz, L. Martin, D. A. Koritsky, N. Murase, W. Irish, A. Zeevi, Preformed and de novo donor specific antibodies in visceral transplantation: Long-term outcome with special reference to the liver. *Am. J. Transplant.* **12**, 3047–3060 (2012).
20. E. Y. Cheng, M. J. Everly, H. Kaneku, N. Banuelos, L. J. Wozniak, R. S. Venick, E. A. Marcus, S. V. McDiarmid, R. W. Busuttill, P. I. Terasaki, D. G. Farmer, Prevalence and clinical impact of donor-specific alloantibody among intestinal transplant recipients. *Transplantation* **101**, 873–882 (2017).
21. M. Rabant, M. Racapé, L.-M. Petit, J. L. Taupin, O. Aubert, J. Bruneau, P. Barbet, O. Goulet, C. Suberbielle, F. Lacaille, D. Canioni, J.-P. D. V. Huyen, Antibody-mediated rejection in pediatric small bowel transplantation: Capillaritis is a major determinant of C4d positivity in intestinal transplant biopsies. *Am. J. Transplant.* **18**, 2250–2260 (2018).
22. X. Zhao, G. Huang, S. Randhawa, G. Zeng, J. Lunz, P. Randhawa, Rejection of the renal allograft in the absence of demonstrable antibody and complement. *Transplantation* **101**, 395–401 (2017).
23. L. R. Solomon, S. Martin, C. D. Short, W. Lawler, R. Gokal, R. W. G. Johnson, N. P. Mallick, Late cellular rejection in renal transplant recipients. *Transplantation* **41**, 262–264 (1986).
24. H. P. Brunner-La Rocca, J. Schneider, A. Künzli, M. Turina, W. Kiowski, Cardiac allograft rejection late after transplantation is a risk factor for graft coronary artery disease. *Transplantation* **65**, 538–543 (1998).
25. O. B. Herrera, D. Golshayan, R. Tibbott, F. S. Ochoa, M. J. James, F. M. Marelli-Berg, R. I. Lechler, A novel pathway of alloantigen presentation by dendritic cells. *J. Immunol.* **173**, 4828–4837 (2004).
26. V. Russo, D. Zhou, C. Sartirana, P. Rovere, A. Villa, S. Rossini, C. Traversari, C. Bordignon, Acquisition of intact alloantigenic human leukocyte antigen molecules by human dendritic cells. *Blood* **95**, 3473–3477 (2000).
27. J. Marino, M. H. Babiker-Mohamed, P. Crosby-Bertorini, J. T. Paster, C. LeGuern, S. Germana, R. Abdi, M. Uehara, J. I. Kim, J. F. Markmann, G. Tocco, G. Benichou, Donor exosomes rather than passenger leukocytes initiate alloreactive T cell responses after transplantation. *Sci. Immunol.* **1**, aaf8759 (2016).
28. Q. Liu, D. M. Rojas-Canales, S. J. Divito, W. J. Shufesky, D. B. Stolz, G. Erdos, M. L. G. Sullivan, G. A. Gibson, S. C. Watkins, A. T. Larregina, A. E. Morelli, Donor dendritic cell-derived exosomes promote allograft-targeting immune response. *J. Clin. Invest.* **126**, 2805–2820 (2016).
29. L. A. Smyth, R. I. Lechler, G. Lombardi, Continuous acquisition of MHC:peptide complexes by recipient cells contributes to the generation of anti-graft CD8+ T cell immunity. *Am. J. Transplant.* **17**, 60–68 (2017).
30. S. J. F. Harper, J. M. Ali, E. Wlodek, M. C. Negus, I. G. Harper, M. Chhabra, M. S. Qureshi, M. Mallik, E. Bolton, J. A. Bradley, G. J. Pettigrew, CD8 T-cell recognition of acquired alloantigen promotes acute allograft rejection. *Proc. Natl. Acad. Sci.* **112**, 12788–12793 (2015).
31. A. D. Hughes, D. Zhao, H. Dai, K. I. Abou-Daya, R. Tieu, R. Rammal, A. L. Williams, D. P. Landsittel, W. D. Shlomchik, A. E. Morelli, M. H. Oberbarnscheidt, F. G. Lakkis, Cross-dressed dendritic cells sustain effector T cell responses in islet and kidney allografts. *J. Clin. Invest.* **130**, 287–294 (2020).
32. I. G. Harper, J. M. Ali, S. J. F. Harper, E. Wlodek, J. Alsughayyir, M. C. Negus, M. S. Qureshi, R. Motaleb-Zadeh, K. Saeb-Parsy, E. M. Bolton, J. A. Bradley, M. R. Clatworthy, T. M. Conlon, G. J. Pettigrew, Augmentation of recipient adaptive alloimmunity by donor passenger lymphocytes within the transplant. *Cell Rep.* **15**, 1214–1227 (2016).
33. J. Gordon, A. Katira, M. Holder, I. MacDonald, J. Pound, Central role of CD40 and its ligand in B lymphocyte responses to T-dependent antigens. *Cell. Mol. Biol. (Noisy-le-grand)* **40** (Suppl. 1), 1–13 (1994).
34. C. Lagresle, P. Mondière, C. Bella, P. H. Krammer, T. Defrance, Concurrent engagement of CD40 and the antigen receptor protects naive and memory human B cells from APO-1/Fas-mediated apoptosis. *J. Exp. Med.* **183**, 1377–1388 (1996).
35. T. Rothstein, J. Wang, D. Panka, L. Foote, Z. Wang, B. Stanger, H. Cui, S. Ju, A. Marshak-Rothstein, Protection against Fas-dependent Th1-mediated apoptosis by antigen receptor engagement in B cells. *Nature* **374**, 163–165 (1995).
36. E. Joly, D. Hudrisier, What is trogocytosis and what is its purpose? *Nat. Immunol.* **4**, 815–815 (2003).
37. R. J. Scothorne, Lymphatic repair and the genesis of homograft immunity. *Ann. N. Y. Acad. Sci.* **73**, 673–675 (1958).
38. P. Málek, J. Vruble, J. Kolc, Lymphatic aspects of experimental and clinical renal transplantation. *Bull. Soc. Int. Chir.* **28**, 110–114 (1969).
39. C. P. Larsen, P. J. Morris, J. M. Austyn, Migration of dendritic leukocytes from cardiac allografts into host spleens. A novel pathway for initiation of rejection. *J. Exp. Med.* **171**, 307–314 (1990).
40. M. D. Gunn, V. N. Ngo, K. M. Ansel, E. H. Ekland, J. G. Cyster, L. T. Williams, A B-cell-homing chemokine made in lymphoid follicles activates Burkitt's lymphoma receptor-1. *Nature* **391**, 799–803 (1998).
41. D. Grant, K. Abu-Elmagd, G. Mazariegos, R. Vianna, A. Langnas, R. Mangus, D. G. Farmer, F. Lacaille, K. Iyer, T. Fishbein, Intestinal Transplant Registry Report: Global activity and trends. *Am. J. Transplant.* **15**, 210–219 (2015).
42. C. A. Janeway, P. Travers, M. Walport, M. J. Shlomchik, The mucosal immune system, in *Immunobiology: The Immune System in Health and Disease* (Garland Science, ed. 5, 2001).
43. T. Hirohashi, C. M. Chase, P. Della Pelle, D. Sebastian, A. Alessandrini, J. C. Madsen, P. S. Russell, R. B. Colvin, A novel pathway of chronic allograft rejection mediated by NK cells and alloantibody. *Am. J. Transplant. Off. J. Am. Soc. Transplant. Am. Soc. Transpl. Surg.* **12**, 313–321 (2012).
44. T. Hirohashi, S. Uehara, C. M. Chase, P. DellaPelle, J. C. Madsen, P. S. Russell, R. B. Colvin, Complement independent antibody-mediated endarteritis and transplant arteriopathy in mice. *Am. J. Transplant.* **10**, 510–517 (2010).
45. G. Guidicelli, F. Guerville, S. Lepreux, C. Wiebe, O. Thauinat, V. Dubois, J. Visentin, T. Bachelet, E. Morelon, P. Nickerson, P. Merville, J.-L. Taupin, L. Couzi, Non-complement-binding de novo donor-specific anti-HLA antibodies and kidney allograft survival. *J. Am. Soc. Nephrol. JASN.* **27**, 615–625 (2016).
46. M. Sykes, M. A. Sheard, D. H. Sachs, Graft-versus-host-related immunosuppression is induced in mixed chimeras by alloresponses against either host or donor lymphohematopoietic cells. *J. Exp. Med.* **168**, 2391–2396 (1988).
47. K. Vincent, D.-C. Roy, C. Perreault, Next-generation leukemia immunotherapy. *Blood* **118**, 2951–2959 (2011).
48. W. J. Burlingham, G. Benichou, Bidirectional alloreactivity. *Chimerism* **3**, 29–36 (2012).
49. J. Zuber, S. Rosen, B. Shonts, B. Sprangers, T. M. Savage, S. Richman, S. Yang, S. P. Lau, S. DeWolf, D. Farber, G. Vlad, E. Zorn, W. Wong, J. Emond, B. Levin, M. Martinez, T. Kato, M. Sykes, Macrochimerism in intestinal transplantation: Association with lower rejection rates and multivisceral transplants, without GVHD. *Am. J. Transplant.* **15**, 2691–2703 (2015).
50. J. Fu, J. Zuber, M. Martinez, B. Shonts, A. Obradovic, H. Wang, S. Lau, A. Xia, E. E. Waffarn, K. Frangaj, T. M. Savage, M. T. Simpson, S. Yang, X. V. Guo, M. Miron, T. Senda, K. Rogers, A. Rahman, S. Ho, Y. Shen, A. Griesemer, D. L. Farber, T. Kato, M. Sykes, Human intestinal allografts contain functional hematopoietic stem and progenitor cells that are maintained by a circulating pool. *Cell Stem Cell.* **24**, 227–239.e8 (2019).
51. M. S. Qureshi, J. Alsughayyir, M. Chhabra, J. M. Ali, M. J. Goddard, C. A. Devine, T. M. Conlon, M. A. Linterman, R. Motalebzadeh, G. J. Pettigrew, Germinal center humoral autoimmunity independently mediates progression of allograft vasculopathy. *J. Autoimmun.* **98**, 44–58 (2019).
52. F. Ius, W. Sommer, I. Tudorache, C. Kühn, M. Avsar, T. Siemeni, J. Salman, M. Hallensleben, D. Kieneke, M. Greer, J. Gottlieb, A. Haverich, G. Warnecke, Early donor-specific antibodies in lung transplantation: Risk factors and impact on survival. *J. Heart Lung Transplant.* **33**, 1255–1263 (2014).
53. R. R. Hachem, M. Kamoun, M. M. Budev, M. Askar, V. N. Ahya, J. C. Lee, D. J. Levine, M. S. Pollack, G. S. Dhillon, D. Weill, K. B. Schechtman, L. E. Leard, J. A. Golden, L. Baxter-Lowe, T. Mohanakumar, D. B. Tyan, R. D. Yusen, Human leukocyte antigens antibodies after lung transplantation: Primary results of the HALT study. *Am. J. Transplant.* **18**, 2285–2294 (2018).
54. C. Kubal, R. Mangus, R. Saxena, A. Lobashevsky, N. Higgins, J. Fridell, A. J. Tector, Prospective monitoring of donor-specific anti-HLA antibodies after intestine/multivisceral transplantation: Significance of de novo antibodies. *Transplantation* **99**, e49 (2015).
55. J. Zuber, B. Shonts, S.-P. Lau, A. Obradovic, J. Fu, S. Yang, M. Lambert, S. Coley, J. Weiner, J. Thome, S. DeWolf, D. L. Farber, Y. Shen, S. Caillat-Zucman, G. Bhagat, A. Griesemer, M. Martinez, T. Kato, M. Sykes, Bidirectional intra-graft alloreactivity drives the repopulation of human intestinal allografts and correlates with clinical outcome. *Sci. Immunol.* **1**, eaah3732 (2016).
56. D. L. Turner, C. L. Gordon, D. L. Farber, Tissue-resident T cells, in situ immunity and transplantation. *Immunol. Rev.* **258**, 150–166 (2014).

57. J. Zuber, O. Boyer, B. Neven, I. Jollet, V. Renac, R. Berthaud, R. Levy, B. Lamarthée, J. Visentin, A. Marchal, N. Gouge-Biebuyck, A. Godron-Dubrasquet, N. Aladjidi, M. O. Rabah, S. Winter, J. Léon, M. Dussiot, M. Rabant, S. Krid, P. Krug, M. Charbit, F. Lacaille, I. André, M. Cavazzana, B. Llanas, L. Allard, F. Pirenne, S. Gross, R. Djoudi, P. Tiberghien, J.-L. Taupin, S. Blanche, R. Salomon, Donor-targeted serotherapy as a rescue therapy for steroid-resistant acute GVHD after HLA-mismatched kidney transplantation. *Am. J. Transplant.* **20**, 2243–2253 (2020).
58. B. J. Stewart, J. R. Ferdinand, M. D. Young, T. J. Mitchell, K. W. Loudon, A. M. Riding, N. Richoz, G. L. Frazer, J. U. L. Staniforth, F. A. V. Braga, R. A. Botting, D.-M. Popescu, R. Vento-Tormo, E. Stephenson, A. Cagan, S. J. Farrdon, K. Polanski, M. Efreanova, K. Green, M. D. C. Velasco-Herrera, C. Guzzo, G. Collord, L. Mamanova, T. Aho, J. N. Armitage, A. C. P. Riddick, I. Mushtaq, S. Farrell, D. Rampling, J. Nicholson, A. Filby, J. Burge, S. Lisgo, S. Lindsay, M. Bajenoff, A. Y. Warren, G. D. Stewart, N. Sebire, N. Coleman, M. Haniffa, S. A. Teichmann, S. Behjati, M. R. Clatworthy, Spatiotemporal immune zonation of the human kidney. *Science* **365**, 1461–1466 (2019).
59. A. Koenig, O. Thauinat, Lymphoid neogenesis and tertiary lymphoid organs in transplanted organs. *Front. Immunol.* **7**, 646 (2016).
60. O. Thauinat, A.-C. Field, J. Dai, L. Louedec, N. Patey, M.-F. Bloch, C. Mandet, M.-F. Belair, P. Bruneval, O. Meilhac, B. Bellon, E. Joly, J.-B. Michel, A. Nicoletti, Lymphoid neogenesis in chronic rejection: Evidence for a local humoral alloimmune response. *Proc. Natl. Acad. Sci.* **102**, 14723–14728 (2005).
61. A. Kratz, A. Campos-Neto, M. S. Hanson, N. H. Ruddle, Chronic inflammation caused by lymphotoxin is lymphoid neogenesis. *J. Exp. Med.* **183**, 1461–1472 (1996).
62. J. P. Stone, A. L. Ball, W. R. Critchley, T. Major, R. J. Edge, K. Amin, M. J. Clancy, J. E. Fildes, Ex vivo normothermic perfusion induces donor-derived leukocyte mobilization and removal prior to renal transplantation. *Kidney Int. Rep.* **1**, 230–239 (2016).
63. Y. Brewer, D. Taube, M. Bewick, G. Hale, F. Dische, A. Palmer, K. Welsh, C. Bindon, H. Waldmann, V. Parsons, S. Snowden, Effect of graft perfusion with two CD45 monoclonal antibodies on incidence of kidney allograft rejection. *The Lancet.* **334**, 935–937 (1989).
64. O. Thauinat, S. Graff-Dubois, N. Fabien, A. Duthey, V. Attuail-Audenis, A. Nicoletti, N. Patey, E. Morelon, A stepwise breakdown of B-cell tolerance occurs within renal allografts during chronic rejection. *Kidney Int.* **81**, 207–219 (2012).
65. T. S. Win, G. J. Pettigrew, Humoral autoimmunity and transplant vasculopathy: When allo is not enough. *Transplantation* **90**, 113–120 (2010).
66. G. Mieli-Vergani, D. Vergani, De novo autoimmune hepatitis after liver transplantation. *J. Hepatol.* **40**, 3–7 (2004).
67. D. Cosgrove, D. Gray, A. Dierich, J. Kaufman, M. Lemeur, C. Benoist, D. Mathis, Mice lacking MHC class II molecules. *Cell* **66**, 1051–1066 (1991).
68. Z. H. Chen, A technique of cervical heterotopic heart transplantation in mice. *Transplantation* **52**, 1099–1101 (1991).
69. G. C. Miescher, M. Schreyer, H. R. MacDonald, Production and characterization of a rat monoclonal antibody against the murine CD3 molecular complex. *Immunol. Lett.* **23**, 113–118 (1989).
70. D. P. Dialynas, Z. S. Quan, K. A. Wall, A. Pierres, J. Quintáns, M. R. Loken, M. Pierres, F. W. Fitch, Characterization of the murine T cell surface molecule, designated L3T4, identified by monoclonal antibody GK1.5: Similarity of L3T4 to the human Leu-3/T4 molecule. *J. Immunol.* **131**, 2445–2451 (1983).
71. J. Schindelin, I. Arganda-Carreras, E. Frise, V. Kaynig, M. Longair, T. Pietzsch, S. Preibisch, C. Rueden, S. Saalfeld, B. Schmid, J.-Y. Tinevez, D. J. White, V. Hartenstein, K. Eliceiri, P. Tomancak, A. Cardona, Fiji: An open-source platform for biological-image analysis. *Nat. Methods* **9**, 676–682 (2012).

Acknowledgments: We thank the staff of the flow cytometry platform (AniRA, SFR BioSciences, UMS34444/US8) and the staff of the animal facility (PBES, SFR BioSciences). We thank the NIH Tetramer Core Facility (Emory University) for providing tetramers. Servier Medical Art illustrations (under Creative Commons Attribution 3.0 Unported License) were used and modified to produce the figures (<https://smart.servier.com/>). **Funding:** The study was supported by funding from the Hospices Civils de Lyon (to X.C.), the Société Francophone de Transplantation (to X.C.), the Institut Hospitalo-Universitaire–Organ Protection and Replacement (IHU-OPeRa; ANR-10-IBHU-004 to C.-C.C.), the Agence Nationale pour la Recherche (ANR-12-PDOC-0019.01 and ANR-16-CE17-0007-01 to O.T.), the Fondation pour la Recherche Médicale (PME20180639518 to O.T.), and the Etablissement Français du Sang (to O.T.). **Author contributions:** X.C., C.-C.C., and O.T. conceived and designed the experiments. X.C., C.-C.C., S.H., D.G., C.S., M. Rabeyrin, M. Rabant, J.-P.D.v.H., A.K., V.M., L. Chalabreyse, S.G.-D., R.J.-M., A.T.-D., and J.-L.T. performed the experiments (X.C. performed cellular flow cross-match and single-antigen bead assay, mouse experiments, and analysis of perfusion liquids; X.C., S.G.-D., and R.J.-M. performed human cocultures; C.-C.C. performed heart transplantations, cellular flow cross-match, and mouse cocultures; S.H. performed CD3⁺ chimerism in recipient's circulation; D.G. performed autoantibody test; C.S. and A.T.-D. performed collection and analysis of perfusion liquids; M. Rabeyrin, M. Rabant, J.-P.D.v.H., and L. Chalabreyse performed collection and analysis of mouse and human histopathological samples; A.K. performed imaging flow cytometry; V.M. and V.D. performed collection of HLA typing and anti-HLA immunization data; and J.-L.T. performed collection of HLA typing and anti-HLA immunization data and C1q assays). X.C., F.L., O.B., P.M., and J.I.P. acquired the clinical samples. X.C., C.-C.C., S.H., D.G., C.S., A.K., T.B., and O.T. analyzed the data. X.C. and O.T. wrote the original draft. J.-F.M., F.L., S.G.-D., P.M., L. Couzi, H.P., T.D., E.M., L.B., A.N., and V.D. revised the manuscript. **Competing interests:** O.T. participated in advisory boards for Biotech, Novartis, and AstraZeneca and received research grants from Immucor, bioMérieux, and BMS. The other authors declare that they have no competing interests. **Data and materials availability:** All data associated with this study are present in the paper or the Supplementary Materials.

Submitted 14 December 2020
 Resubmitted 2 May 2022
 Accepted 19 August 2022
 Published 21 September 2022
 10.1126/scitranslmed.abg1046

Inverted direct allorecognition triggers early donor-specific antibody responses after transplantation

Xavier CharmetantChien-Chia ChenSarah HamadaDavid GoncalvesCarole SaisonMaud RabeyrinMarion RabantJean-Paul Duong van HuyenAlice KoenigVirginie MathiasThomas BarbaFlorence LacailleJérôme le PavecOlivier BrugièreJean-Luc TaupinLara ChalabreysseJean-François MornexLionel CouziStéphanie Graff-DuboisRaphaël Jeger-MadiotAlexy Tran-DinhPierre MordantHelena PaidassiThierry DeFranceEmmanuel MorelonLionel BadetAntonino NicolettiValérie DuboisOlivier Thauvat

Sci. Transl. Med., 14 (663), eabg1046. • DOI: 10.1126/scitranslmed.abg1046

Inverting immunity

A canonical pathway has been implicated in the development of donor-specific antibodies (DSAs) after transplantation. This pathway, called indirect allorecognition, occurs when a recipient's B cells target alloantigens on the graft, such as donor major histocompatibility complex (MHC) molecules. This is thought to rely on the recipient's CD4 T cells providing help to the alloreactive B cells. However, Charmetant *et al.* found, using murine models, that development of DSAs can occur in the absence of recipient CD4 T cells. Instead, donor-derived CD4 T cells recognizing recipient MHC II molecules were capable of activating recipient B cells, a process the authors term "inverted direct allorecognition." The authors further showed that, in patients receiving allografts, transplant of tissues with higher passenger CD4 T cell abundance correlated with early anti-MHC DSA responses, suggesting that this pathway is intact in humans as well.

View the article online

<https://www.science.org/doi/10.1126/scitranslmed.abg1046>

Permissions

<https://www.science.org/help/reprints-and-permissions>

Use of this article is subject to the [Terms of service](#)

Supplementary Materials for
**Inverted direct allorecognition triggers early donor-specific antibody
responses after transplantation**

Xavier Charmetant *et al.*

Corresponding author: Olivier Thauvat, olivier.thauvat@inserm.fr

Sci. Transl. Med. **14**, eabg1046 (2022)
DOI: 10.1126/scitranslmed.abg1046

The PDF file includes:

Methods
Figs. S1 to S8
Table S1
Legend for data file S1

Other Supplementary Material for this manuscript includes the following:

Data file S1
MDAR Reproducibility Checklist

List of Supplementary Materials

Supplementary Methods

Fig. S1

Fig. S2

Fig. S3

Fig. S4

Fig. S5

Fig. S6

Fig. S7

Fig. S8

Table S1

Supplementary methods

Characterization of the immune phenotype of the different murine strains

Before staining, murine cells from spleen, lymph nodes, heart or blood were incubated with a blocking anti-mouse Fc receptor antibody (2.4G2, in-house made hybridoma). Cells were then incubated at 4°C with fluorescent antibodies: CD45 (30-F11, Alexa Fluor 700, dilution 1:200, BD Biosciences, catalog no. 560510, RRID:AB_1645208), CD3 (145-2C11, phycoerythrin (PE)-CF594, 1:400, BD Biosciences, catalog no. 562286, RRID:AB_11153307), CD4 (RM4-4, peridinin-chlorophyll-protein (PerCP)-cyanine (Cy) 5.5, 1:200, BD Biosciences, catalog no. 550954, RRID:AB_393977), CD8 (53-6.7, allophycocyanin (APC), 1:200, BD Biosciences, catalog no. 553035, RRID:AB_398527), and CD19 (1D3, fluorescein isothiocyanate (FITC), 1:200, BD Biosciences, catalog no. 553785, RRID:AB_395049). Before analysis by flow cytometry, DAPI (4',6-diamidino-2-phenylindole dihydrochloride, Sigma-Aldrich) was added to the cell suspension to exclude dead cells. Sample acquisitions were made on a BD LSR II flow cytometer (BD Biosciences).

Functional evaluation of the B cell compartment of the different murine strains

Mice were immunized intraperitoneally with 75 µg 4-(hydroxy-3-nitro-phenyl) acetyl (NP)-keyhole limpet hemocyanin (KLH) mixed with 100 µL Inject Alum Adjuvant (Thermo Fisher Scientific) or 200 µg NP-Dextran. Serum samples were tested for concentrations of IgM and IgG anti-NP antibodies. Maxisorp plates (Nunc) were coated with NP 23-conjugated bovine serum albumin (BSA). Serially diluted serum samples were added for 1 hour and 30 minutes at room temperature. NP-specific antibodies were detected with alkaline phosphatase-conjugated goat anti-mouse IgM or IgG Abs (1:2,000 dilution) followed by phosphatase substrate (Sigma-Aldrich). The plates were read at 405 nm/490 nm with an automatic reader (Zeiss VERSAmax). We used standard curves to convert optical densities (OD) to concentration using a four-parameter logistic equation (Softmax Pro 5.3 software; Molecular Devices).

Characterization of the donor-specific antibody (DSA) response after heart transplantation

A single antigen bead assay was designed to analyze the repertoire of the DSA response (**fig. S7**). Briefly, 1×10^5 polystyrene beads of $4.95 \mu\text{m}$ diameter coated with streptavidin (Bangs Laboratories) were incubated for 15 minutes at room temperature with $0.1 \mu\text{g}$ of biotinylated H-2, I-A or I-E monomers (provided by the NIH Tetramer Core Facility, Emory University) in phosphate-buffered saline supplemented with 1% of BSA. The beads were then rinsed and incubated with the serum of recipient mice for 30 minutes at 4°C . DSA binding was then measured using an anti- κ light chain secondary antibody (187.1, PE, 1:200, BD Biosciences, catalog no. 559940, RRID:AB_397384). The mean fluorescence intensity (MFI) obtained at the peak of the response was normalized over the value obtained with the serum collected at day 0.

For the monitoring of the kinetic of DSA response, CD4^+ T cells from CBA mice were incubated with serum isolated from sensitized recipients. Binding of DSA to cells from CBA mice was measured using an anti- κ light chain (187.1, PE, 1:200, BD Biosciences, catalog no. 559940, RRID:AB_397384), anti-IgM (R6-60.2, PE-Cy7, 1:200, BD Biosciences, catalog no. 552867, RRID:AB_394500), anti-IgG1 (A85-1, APC, 1:200, BD Biosciences, catalog no. 560089, RRID:AB_1645625), anti-IgG2b (FITC, 1:200, SouthernBiotech, 1090-02, RRID:AB_2794518) or anti-IgG3 (R40-82, FITC, 1:200, BD Biosciences, catalog no. 553403, RRID:AB_394840) secondary antibody. Syngeneic C57BL/6 CD4^+ T cells were used as controls, as well as BALB/c and FVB CD4^+ T cells in some experiments. The titer of anti-human leukocyte antigen (HLA) antibodies at each time point (dx) was calculated with the following formula: normalized DSA titer = $[\text{MFI CBA (dx)} / \text{MFI C57BL/6 (dx)}] / [\text{MFI CBA (d0)} / \text{MFI C57BL/6 (d0)}]$ (3).

Imaging flow cytometry

Phosphoflow analysis were performed as previously described (70), using the phospho-epitopes exposure kit (Beckman Coulter). Briefly, prewarmed B cells were cultured in the presence or not (negative control) of a soluble rat anti-mouse κ light chain (clone 187.1, BD Biosciences, 15 μ g/mL) monoclonal antibody (mAb) for 3 minutes. Prewarmed B cells from a B1.8 mouse cultured in the presence of soluble NP-BSA for 3 minutes were used as positive controls. They were then incubated for 10 minutes at room temperature with fixative reagent and then for 5 minutes at 37°C with permeabilizing reagent. Before incubation with anti- λ light chain (JC5-1, FITC, 1:200, Abcam, catalog no. ab99623, RRID:AB_10675830), anti-B220 (RA3-6B2, APC-H7, 1:200, BD Biosciences, catalog no. 565371, RRID:AB_2739208) and mouse anti-phosphorylated B-cell linker protein [(pBLNK), J117-1278, PE, 1:2.5, BD Biosciences, catalog no. 558442, RRID:AB_647182] mAbs (30 minutes at room temperature), permeabilized cells were incubated for 15 minutes with κ light chain-positive mouse IgG isotype control (clone X40, BD Biosciences) in order to avoid reactivity between anti- κ mAb present in the medium and mouse phycoerythrin (PE) anti-pBLNK mAb. Data were collected on a four laser ImageStream X Mark II (Amnis-EMD Millipore) with 60X magnification and analyzed with IDEAS software (v6.0).

Supplementary Figures

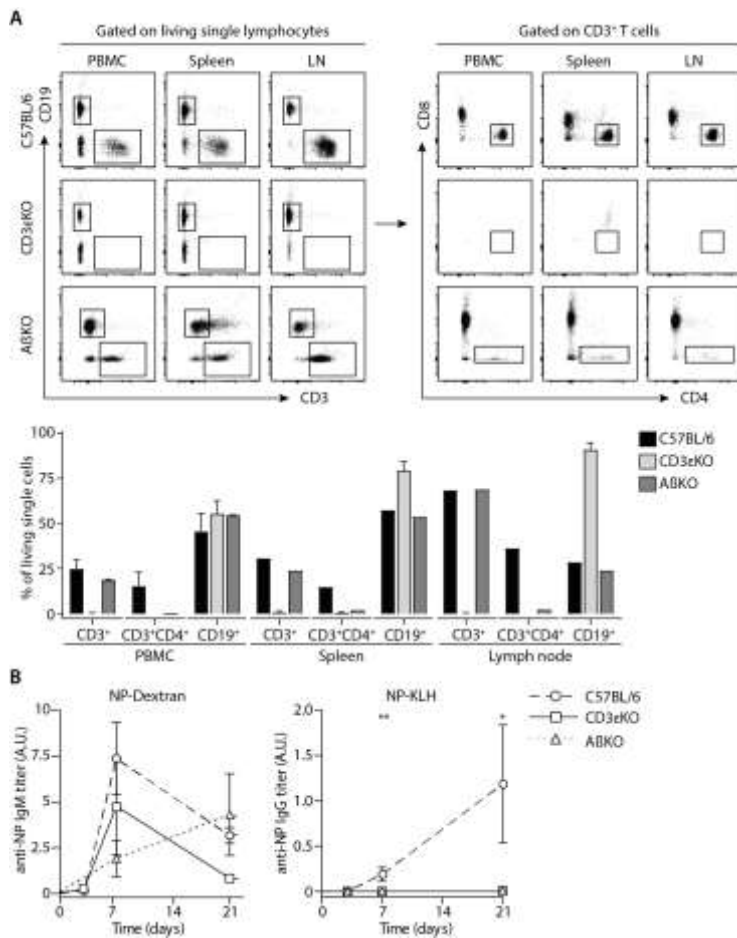


Fig. S1. Phenotypic and functional assessment of the three murine strains.

(A) Flow cytometry analysis of the lymphocyte population in peripheral blood mononuclear cells (PBMC) and secondary lymphoid organs (SLO; spleen and lymph nodes [LN]) of wild-type (WT) C57BL/6 (PBMC, n=2; SLO, n=1), CD3ε knockout (KO; PBMC, n=6; SLO, n=2), and AβKO (PBMC, n=2; SLO, n=1) mice. Upper panels show representative flow cytometry profiles. The lower plot shows quantification (mean + standard deviation). **(B)** A comparison of anti-NP antibody titers is shown over time between WT C57BL/6 (n=4, circles, dashed line), CD3εKO (n=4, squares, black line) and AβKO (n=4, triangles, dotted line). Data are presented as mean ± standard deviation. The left panel shows titers from animals immunized with the thymo-independent model antigen, NP-Dextran; IgM titers were measured. The right panel

shows titers from animals immunized with the thymo-dependent model antigen, NP-KLH; IgG titers were measured. Data were analyzed by multiple t-tests. * $p < 0.05$; ** $p < 0.01$.

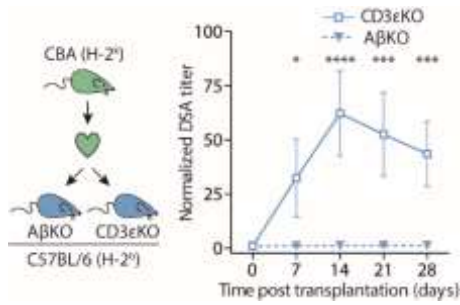


Fig. S2. MHC II expression on the B cell surface is mandatory for inverted direct allorecognition in vivo.

Allogeneic CBA (H-2^k) heart was transplanted to AβKO or CD3εKO C57BL/6 (H-2^b) recipient mice. The evolution of normalized anti-MHC DSA titers were measured in AβKO (dashed curve, n=3) and CD3εKO (solid curve, n=5) recipients. Data are presented as mean ± standard deviation. Data were analyzed by multiple t tests. *p<0.05; ***p<0.001; ****p<0.0001.

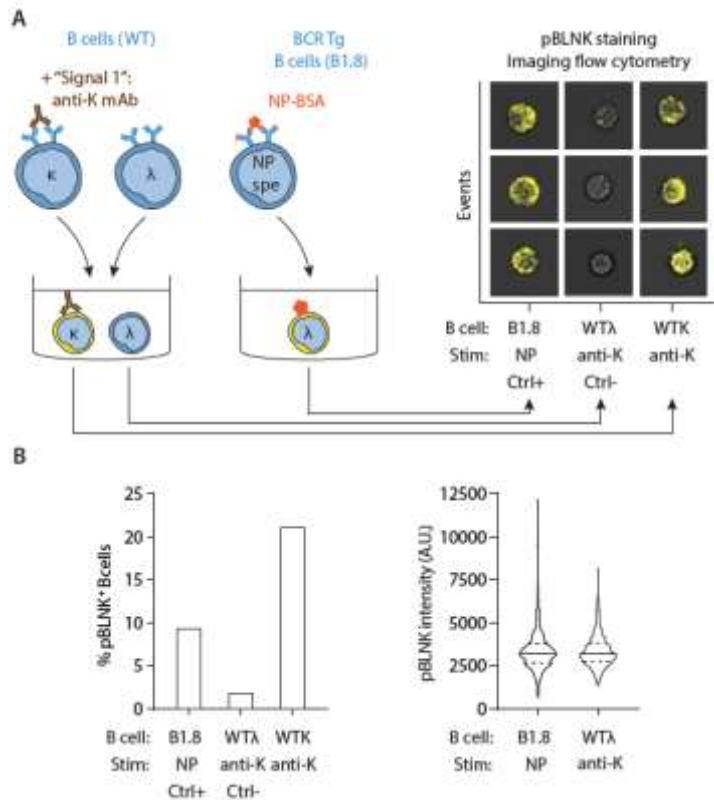


Fig. S3. Anti- κ monoclonal antibody treatment triggers BLNK phosphorylation.

(A) Purified murine B cells from WT C57BL/6 or BCR transgenic (Tg) B1.8 mice (whose BCR is specific for NP antigen) were stimulated (Stim) with either anti- κ mAb or NP coupled to BSA. Imaging flow cytometry was used to identify B cells (B220⁺), determine the isotype of BCR light chain (κ or λ), and to detect the phosphorylated form of the B-cell linker protein (pBLNK). The left panel shows the schematic representation of the experiment. The right panel shows representative imaging flow cytometry pictures merging brightfield and pBLNK signals.

(B) A histogram representing the percentage of the pBLNK positive B cells in each condition is shown on the left. The right panel shows a violin plot comparing the pBLNK signal intensity measured in transgenic B1.8 B cells stimulated with NP and wild-type κ^+ B cells stimulated with anti- κ mAb, respectively. Ctrl, control; A.U., arbitrary units.

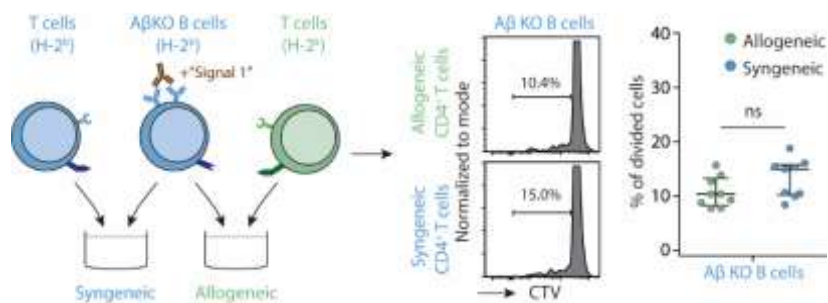


Fig. S4. MHC II expression on the B cell surface is mandatory for inverted direct allorecognition in vitro.

Purified AβKO B cells were activated through their B cell receptors (BCR) and cocultured with syngeneic (C57BL/6, H-2^b, blue) or allogeneic (CBA, H-2^k, green) purified CD4⁺ T cells. The percentage of divided cells among alive B cells was measured by flow cytometry. The left panel shows a schematic representation of the experimental cocultures. The middle panel shows representative flow cytometry histograms; CTV indicates cell trace violet. The right panel shows the % of divided cells for individual cocultures. Data are presented as median ± IQR. Data were analyzed by Mann-Whitney test. ns, p>0.05.

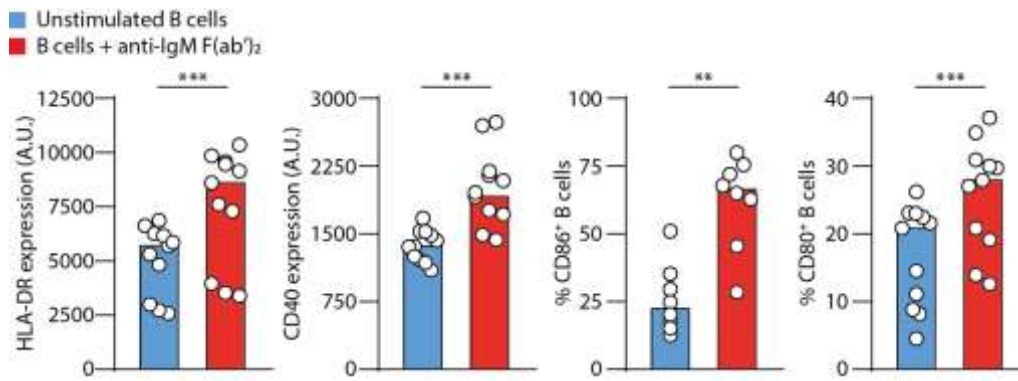


Fig. S5. BCR-stimulated human B cells upregulate their expression of MHC II and costimulatory molecules.

Human PBMCs were incubated in presence or not of anti-human IgM F(ab')₂. The expression of HLA-DR (MHC II) or CD40 and the percentage of CD80 or CD86 positive cells were measured in the B cell population (CD19⁺CD20⁺CD3⁻) by flow cytometry. Individual sample values are shown. Data were analyzed by Wilcoxon tests. **p<0.01; ***p<0.001.

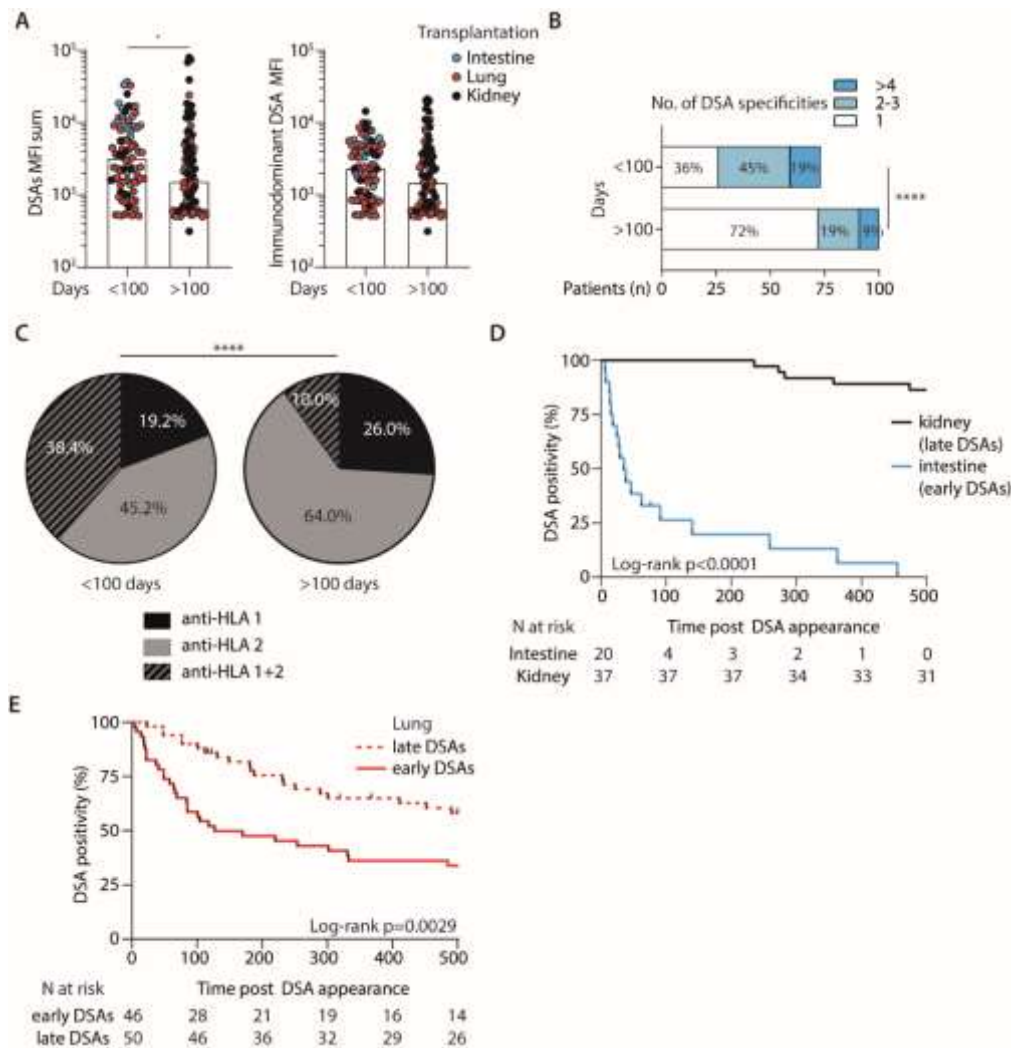


Fig. S6. The early DSA wave in human transplant recipients is transient and biased toward anti-MHC I.

(A) The titers of the early (<100 days) and late (>100 days) de novo DSA were quantified by a solid phase assay in serum collected from intestine (blue), lung (red), and kidney (black) transplant recipients. The sum of the MFI (left panel) or the MFI of the immunodominant DSA (right panel) are plotted. Individual values and median are shown. Data were analyzed by a Mann-Whitney test. * $p < 0.05$.

(B) The repertoires of the early and late de novo DSA response were compared. Data were analyzed by a Chi-square test. **** $p < 0.0001$.

(C) The specificities of the early and late de novo DSA were analyzed. Data were analyzed by a Chi-square test. **** $p < 0.0001$.

(D and E). Kaplan-Meier curves of the delay between the first detection of de novo DSA and their disappearance in solid phase assay are shown. Early DSA responses after intestinal transplantation (blue) were compared to late DSA responses after kidney transplantation (black) (E), or early and late DSA responses were compared after lung transplantation (F).

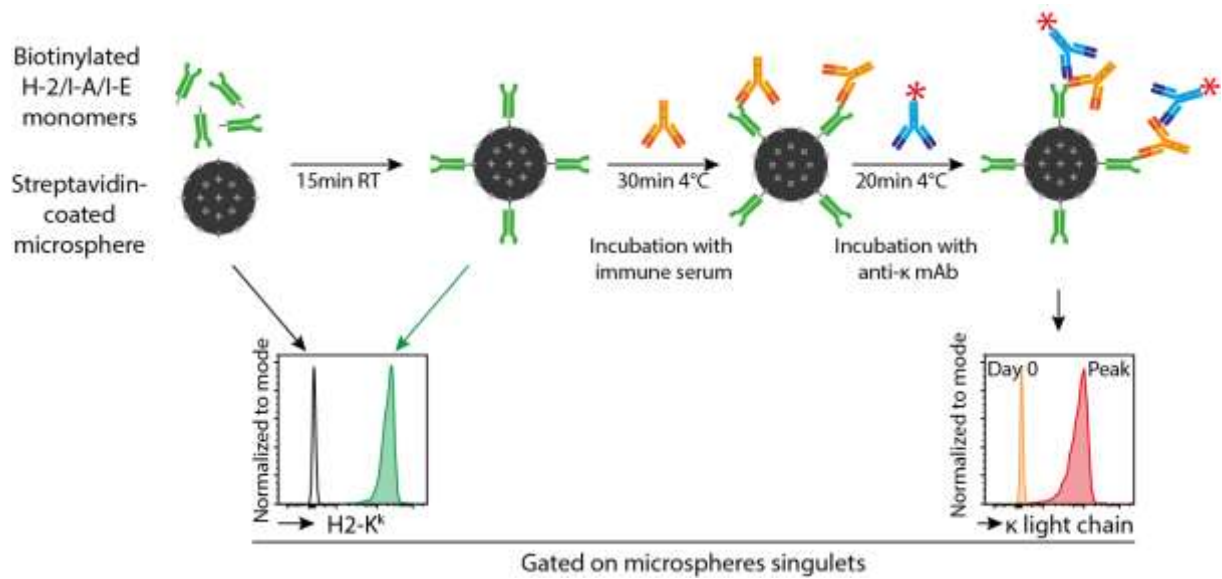


Fig. S7. Single antigen bead assay used to determine the specificity of the DSA response.

The upper row shows a schematic representation of the assay. Polystyrene microspheres covered with streptavidin were coated with biotinylated MHC I or MHC II monomers and incubated with the serum of sensitized recipient mice. Binding of DSA to microspheres was revealed using a PE (red asterisk)-conjugated secondary antibody directed against κ light chains. The lower row shows representative flow cytometry histograms.

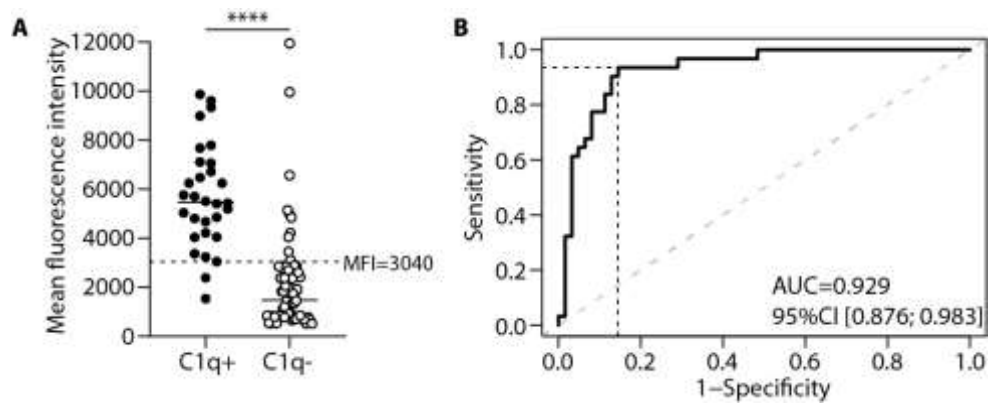


Fig. S8. DSA MFI closely correlates with the results of the C1q binding assay.

(A) The MFI of DSA responses were compared between the groups of patients with a positive (left) and negative (right) C1q binding assay. Individual values are shown. Data were analyzed by a Mann-Whitney test. **** $p < 0.0001$.

(B) A receiver-operating curve was constructed to determine the threshold of MFI above which the C1q binding assay is positive. This cutoff (MFI=3040) was used to extrapolate the result of the C1q test for all patients whose serum was no longer available. AUC, area under the curve; CI, confidence interval.

Table S1. Patient characteristics (n (%)) or mean ± standard deviation).

	Kidney recipients n=699	Lung recipients n=156	Intestine recipients n=24
Age at transplantation	53.0 ± 14.9	44.7 ± 14.2	5.3 ± 2.6
Males	422 (60.3)	66 (42.3)	15 (62.5)
Cause of vital organ failure	Glomerulonephritis: 185 (26.5)	COPD/AAT def.: 38 (24.4)	Congenital: 12 (50.0)
	Diabetes mellitus: 79 (11.3)	CF/bronchiectasis: 37 (23.7)	Short bowel synd.: 7 (29.2)
	Vascular: 58 (8.3)	PF/interstitial dis.: 46 (29.5)	Motility disorder: 5 (20.8)
	Hereditary: 120 (17.2)	PH: 27 (17.3)	
	Uropathy: 58 (8.3)	Others: 8 (5.1)	
	Others: 199 (28.5)		
Transplantation type			Isolated intestine: 11 (45.8)
			Intestine + liver: 13 (54.2)
Blood group			
O	280 (40.1)	67 (43.5)	8 (33.3)
A	313 (44.7)	63 (40.9)	9 (37.5)
B	81 (11.6)	20 (13.0)	5 (20.8)
AB	25 (3.6)	4 (2.6)	2 (8.3)
Donor age	54.4 ± 17.8	45.1 ± 14.1	10.7 ± 14.0
Male donors	393 (56.2)	81 (53.3)	10 (41.7)
Donor type			
Living donor	92 (13.2)	0 (0)	0 (0)
DBD	548 (78.4)	117 (76.5)	24 (100)
DCD	59 (8.4)	36 (23.5)	0 (0)
No. of HLA-A/B/DR mismatch	3.6 ± 1.4	4.8 ± 1.0	4.7 ± 1.1

Ischemia time*	768 ± 403	304 ± 90	NA
Perfusion machine			
Yes	329 (47.1)	7 (4.6)	0 (0)
Induction treatment			
Anti-thymocyte globulins	446 (63.8)	11 (7.1)	6 (25.0)
Anti-IL-2R	271(38.8)	7 (4.5)	18 (75.0)
No induction	0 (0)	138 (88.4)	0 (0)
Maintenance immunosuppression			
Cyclosporin	106 (15.2)	70 (44.9)	0 (0)
Tacrolimus	641 (91.7)	84 (53.8)	24 (100)
mTORi	52 (7.4)	10 (6.4)	0 (0)

*Cold ischemia for kidneys and total ischemia for lungs. ESRD: end-stage renal disease; COPD: chronic obstructive lung disease; AAT def.: alpha-1 antitrypsin deficiency; CF: cystic fibrosis; PF: pulmonary fibrosis; interstitial dis.: interstitial lung disease; PH: Pulmonary hypertension; synd.: syndrome; DCD: donation after circulatory death; DBD: donation after brain death; NA: data not available; IL: interleukin; mTORi: mechanistic target of rapamycin inhibitor.

Data File S1. Raw, individual-level data for experiments where $n < 20$.

IV. DISCUSSION ET PERSPECTIVES

1. Une nécessaire amélioration des stratégies vaccinales du sujet transplanté

1.1. Limites des stratégies actuelles

1.1.1. Limites liée à la définition des corrélats de protection

La mise en évidence d'un corrélat de protection a été l'objet de nombreuses recherches après les premières études vaccinales, afin de savoir qui était protégé contre l'infection par le SARS-CoV-2 et qui ne l'était pas. Notre étude chez les patients transplantés s'inscrit dans ce contexte. Ainsi, nous avons pu montrer que les IgG anti-receptor binding domain (RBD) étaient associées à la protection contre les formes symptomatiques de l'infection par le SARS-CoV-2 chez les patients transplantés, comme chez les sujets non transplantés (189). Cependant, mise à l'épreuve du temps, la définition des corrélats de protection se heurte à de nombreuses limites. Tout d'abord, les tests de neutralisation virale sont compliqués à réaliser en routine. Ce sont des tests coûteux, nécessitant des cultures cellulaires de plusieurs jours, du personnel qualifié, dans des laboratoires spécialisés dans la manipulation des agents infectieux, et donc impossibles à faire à grande échelle. De plus, ces tests doivent être sans cesse réadaptés aux nouveaux variants, et un sérum caractérisé comme neutralisant un jour, peut ne plus l'être le lendemain lors de la rencontre d'un variant. Par conséquent, il est difficile de suivre le titre d'anticorps neutralisants d'un patient au cours du temps. Dans les premières études de vaccinologie, il a été proposé d'utiliser un test substitutif, le dosage des anticorps anti-RBD ou anti-Spike. Compte-tenu de la forte corrélation entre anticorps post-vaccinaux et capacité de neutralisation virale (190), un titre d'anticorps « seuil » avait été proposé, au-delà duquel tous les sérums étaient neutralisants (191). Ainsi, le corrélat de protection était accessible avec un test automatisé et disponible à grande échelle. Cependant, ce seuil est variable selon la modalité de rencontre de l'antigène (vaccinale ou infectieuse ; données personnelles chez les sujets transplantés) et le variant considéré. A mesure que les gens sont vaccinés et que les vagues de COVID-19 se

succèdent avec de nouveaux variants, les situations individuelles deviennent très hétérogènes en termes d'exposition antigénique. Un seuil unique n'est donc pas généralisable.

Finalement, l'utilisation des corrélats de protection a focalisé l'attention sur la mémoire sérologique de la réponse vaccinale et infectieuse, et masque le rôle essentiel que peut jouer l'immunité cellulaire contre les formes graves de la maladie (192). En effet, la mémoire humorale compte aussi les compartiments lymphocytaires B et T_{FH} mémoires. Dans les cohortes de patients transplantés, nous avons pu mettre en évidence, à distance de la vaccination anti-SARS-CoV-2, que les sujets répondeurs au vaccin, contrairement aux non-répondeurs, avaient des lymphocytes B et T_{FH} mémoires. Nous avons aussi montré i) que ces cellules avaient une cross-réactivité bien plus importante que les anticorps contre les variants et ii) que la présence d'une mémoire cellulaire semblait être corrélée à une moindre incidence de formes sévères de la maladie (données personnelles). Ainsi, l'analyse du compartiment cellulaire offre également des opportunités de suivi de la protection effective des patients. Cependant, elle se heurte aux mêmes limites que l'analyse de la capacité de neutralisation des sérums (coût, durée, technicité, difficulté à transposer à la routine). Cela nécessite donc de développer des tests plus accessibles. En ce sens, une étude a démontré la performance d'une PCR sur sang total pour quantifier la réactivité cellulaire T contre le SARS-CoV-2 (193). Dans ce test, les lymphocytes T activés par les peptides dérivés du virus sécrètent de l'interféron- γ , qui stimule à son tour la production de CXCL10 par les monocytes (amplification de la réponse primaire). L'ARNm CXCL10 est alors quantifié, comme témoin de l'activation T. Ce test est rapide, entièrement automatisable et peu sensible aux variants (193). Malheureusement, l'exploration du versant lymphocytaire B de la mémoire reste aujourd'hui limitée à la technique de référence qu'est l'ELISpot. Le développement d'un test substitutif nécessiterait d'identifier une signature moléculaire spécifique des B mémoires (transcriptomique, boucle d'amplification cytokinique), qui n'est pas connue à ce jour.

1.1.2. Limites du schéma vaccinal chez le sujet transplanté

Notre travail a montré un rôle délétère de l'immunosuppression dans la réponse vaccinale. En particulier, nous avons montré que l'utilisation de mycophénolate mofétil (MMF) était associée à une moindre réponse vaccinale, probablement liée au blocage de l'expansion clonale des lymphocytes B et T spécifiques de l'antigène vaccinal. Ces résultats ont été largement confirmés par d'autres études indépendantes (194–196).

Dans notre cohorte, nous n'avons qu'un patient traité par inhibiteur de la costimulation (CTLA4-Ig ou Belatacept), qui était non-répondeur au vaccin. Plusieurs études ont rapporté que ce traitement était associé aux plus faibles taux de réponse vaccinale, avec un taux de séroconversion inférieur à 10% après deux doses de vaccin (197,198).

Au total, après transplantation rénale, les études ont rapporté des taux de séroconversion de 4 à 48% après un schéma vaccinal standard en 2 doses (199), contre près de 100% chez des sujets sains. Cette stratégie vaccinale est donc très insuffisante et a, pour conséquence directe, la survenue de cas de COVID-19 sévères chez des patients transplantés rénaux complètement vaccinés (200).

1.2. Des stratégies non spécifiques pour prévenir la mortalité

Il apparaît donc indispensable de développer des stratégies pour rendre le schéma vaccinal plus immunogène et améliorer la réponse vaccinale des patients transplantés. Ces stratégies pourraient comporter, entre autres, l'augmentation de la dose d'antigène administrée à chaque injection, l'augmentation du nombre de doses de vaccin, la modification de l'adjuvantation, la modulation de l'immunosuppression de l'hôte.

Ainsi, nous avons proposé, ainsi que d'autres groupes indépendants, d'administrer une troisième, voire une quatrième dose de vaccin. Cette stratégie est efficace et permet à chaque étape de « rattraper » une partie des non répondeurs. Elle a cependant des limites. Tout d'abord, certains patients ne répondent pas, malgré de nombreuses injections vaccinales [50% des transplantés non immunisés après trois doses ne répondent pas à la quatrième dose, (201)]. De plus, en période de forte circulation virale, les injections répétées correspondent à de nombreuses semaines au cours desquelles les patients ne sont pas protégés et donc exposés au risque de maladie sévère.

Ils peuvent alors bénéficier d'une immunisation passive par l'injection d'anticorps monoclonaux. Il est très intéressant de noter qu'une étude a rapporté la possibilité d'une réponse humorale efficace à un vaccin administré dans les semaines qui suivent un traitement par anticorps monoclonaux (202). Les anticorps pré-formés peuvent avoir différents rôles au cours d'une réaction humorale : soit un rôle inhibiteur, soit un rôle activateur. En particulier, les anticorps peuvent capturer les antigènes pour former des complexes immuns. Il est tout à fait possible que ces complexes facilitent la capture de l'antigène vaccinal par les cellules immunitaires et permettent une meilleure présentation aux lymphocytes B et T, augmentant ainsi l'immunogénicité du vaccin. Il serait alors intéressant de tester cette hypothèse dans des modèles murins, car nous avons montré dans notre étude qu'une immunogénicité plus grande permettait parfois de surpasser l'effet de l'immunosuppression. Cette étude incite également à poursuivre la vaccination des patients transplantés qui reçoivent un traitement prophylactique par anticorps monoclonaux.

Enfin, certains groupes ont proposé de suspendre le traitement par MMF pendant la période encadrant la vaccination (203). Cette approche est très prometteuse en terme de réponse vaccinale. Malgré l'absence d'immunisation après 3 doses de vaccin, environ trois quarts des patients ont développé une réponse humorale et cellulaire après la 4^{ème} dose. Cependant, la levée de l'immunosuppression étant globale, cette stratégie expose au risque de s'immuniser contre le greffon. Les auteurs ne rapportent pas d'immunisation anti-HLA chez leurs patients dans cette étude, mais les effectifs sont faibles et le suivi est court.

1.3. Des thérapies cellulaires spécifiques de l'antigène pour prévenir la maladie

La méthode la plus prometteuse pour augmenter la réponse vaccinale des sujets transplantés (suspension du MMF) est aussi la plus risquée vis-à-vis du greffon, car non spécifique de l'antigène.

Les thérapies spécifiques d'antigènes peuvent être abordées sous deux angles différents en transplantation. Afin de se passer de l'immunosuppression, de nombreux groupes travaillent sur des stratégies dérivées des *Chimeric antigen receptor* (CAR) T cells, sous la forme de CAR-Tregs (régulateurs). L'objectif est d'induire une tolérance spécifique vis-à-vis des antigènes du greffon et de se passer de l'immunosuppression. Ainsi, le risque infectieux des patients transplantés serait le même que celui des sujets non transplantés. Cette stratégie, quoique séduisante, pose de nombreuses questions de faisabilité, que nous n'aborderons pas ici, mais qui incitent à regarder sous un autre angle. Si l'on admet que l'on ne peut pas se passer de l'immunosuppression, on peut alors envisager le développement d'une autre thérapie cellulaire spécifique d'antigène, à visée vaccinale : les *Vaccine antigen receptor* (VAR)-T cells. Cette thématique est actuellement en cours d'exploration au sein de mon équipe d'accueil, sous l'impulsion du chef d'équipe, d'une ingénieure et d'une thésarde.

Le principe est de développer un lymphocyte T CD4⁺ portant un CAR dont le domaine extracellulaire est l'antigène vaccinal (RBD par exemple). La portion intracellulaire, comme dans un CAR « classique », associerait un domaine CD3ζ et un domaine de costimulation (CD28 ou 4-1BB). Ainsi, cette cellule modifiée serait capable d'interagir avec un lymphocyte B spécifique de l'antigène vaccinal, en lui présentant l'antigène et en lui délivrant dans le même temps les signaux de costimulation (Figure 7).

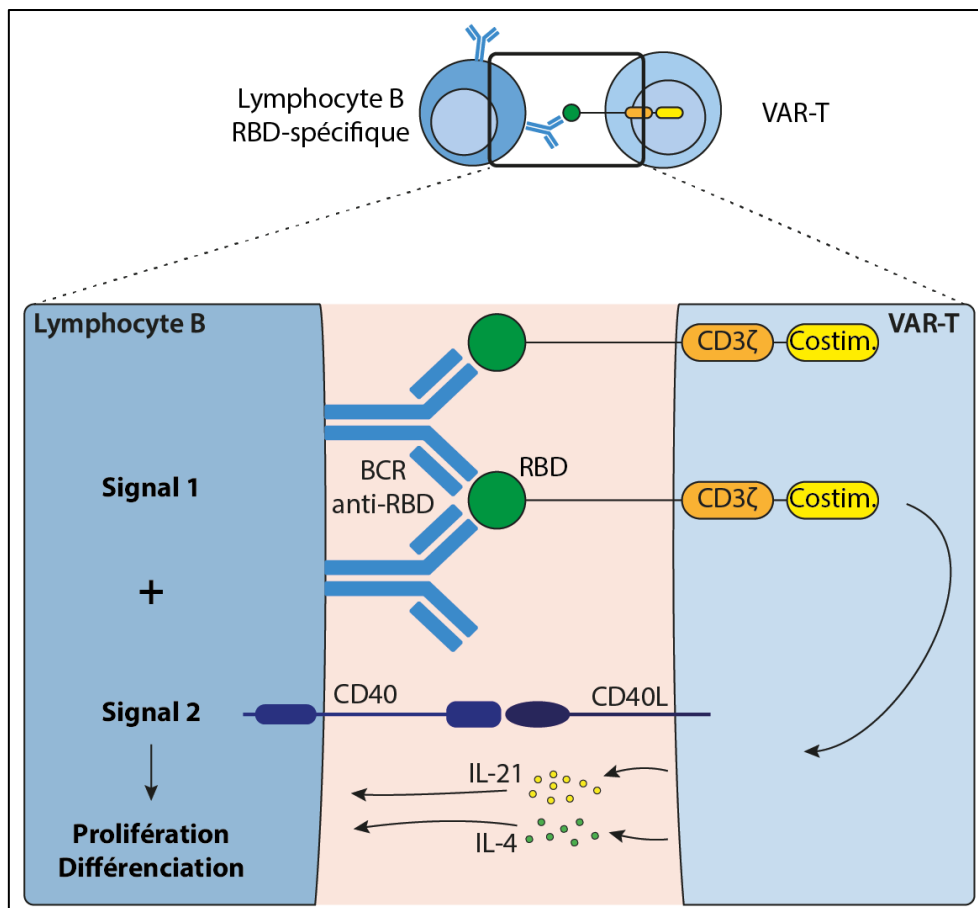


Figure 7. Schéma du concept VAR-T cells

Abréviations : BCR, récepteur des lymphocytes B ; RBD, receptor-binding domain ; VAR, vaccine antigen receptor ; Costim., costimulation.

Bien évidemment, il ne faut pas oublier que cette stratégie serait utilisée chez des patients sous immunosuppresseurs. Cependant, le concept présente justement de nombreux avantages vis-à-vis de l'immunosuppression. Tout d'abord, il est possible que le MMF ait peu d'effet sur cette thérapie, car le traitement consistera en l'administration d'une population clonale, pré-expandue. De plus, la stimulation du VAR déclenche simultanément des signaux TCR-like via le CD3 (dépendants de la calcineurine) et des signaux de costimulation (indépendants de la calcineurine). On peut penser que la synergie d'action des deux signaux diminuera la sensibilité de la cellule aux inhibiteurs de la calcineurine. Si, malgré cela, la thérapie s'avérait être très sensible à l'inhibition de la calcineurine, un gène de résistance pourrait être introduit au moment de la modification génétique.

Tous les éléments discutés ici sont spéculatifs, et nécessitent d'être rigoureusement démontrés.

1.4. Un avantage malgré tout pour les patients transplantés ?

De façon inattendue, le suivi de la réponse humorale au temps mémoire a mis en évidence un avantage des patients transplantés (répondeurs au vaccin) par rapport aux sujets non transplantés, en terme de maintien des titres d'anticorps et de la capacité de neutralisation (Figure 8).

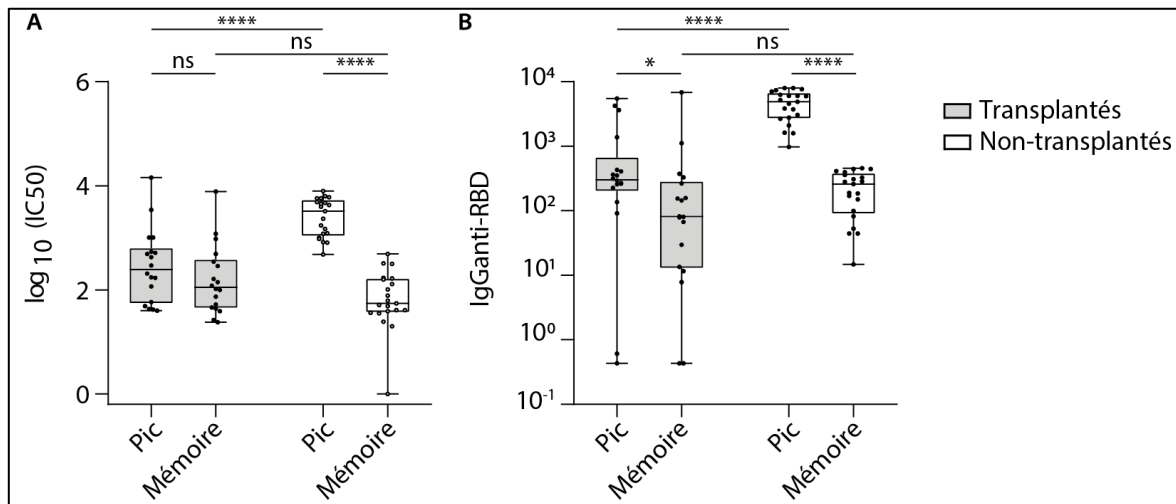


Figure 8. Evolution de la réponse humorale au temps mémoire

Evolution (A) des capacités de neutralisation et (B) des titres d'anticorps anti-RBD entre le pic de la réponse et le temps mémoire, chez des sujets transplantés ou non. Test de Mann-Whitney. ns, non significatif ; *P<0.05 ; ****P<0.0001.

Cette observation peut être mise en parallèle avec des données récemment publiées en vaccinologie, montrant que le maintien du titre d'anticorps peut être directement lié au maintien dans le temps du centre germinatif (204). Nous pouvons donc supposer que les patients transplantés, une fois que le seuil d'immunogénicité a été atteint et permet une réponse, maintiennent des centres germinatifs plus persistants que les volontaires sains.

L'hypothèse que nous avons formulée pour expliquer ce phénomène est directement liée au mode de fonctionnement des vaccins à ARN messager (ARNm). La nanoparticule vaccinale a besoin d'une cellule hôte (probablement cellule musculaire) pour produire l'antigène à partir de l'ARNm. L'antigène est alors pris en charge par le système immunitaire pour développer une réponse humorale, mais aussi une réponse cellulaire cytotoxique. Il est tout à fait possible que la cellule musculaire productrice d'antigènes et exprimant des peptides dérivés de la Spike au sein de son CMH de classe I, soit la première cible des effecteurs cytotoxiques. Ceci interromprait alors l'approvisionnement du centre germinatif en antigène, entraînant sa résolution. Or, nous avons observé que chez les patients transplantés qui développaient une réponse humorale après vaccination, la réponse cellulaire T CD8⁺ spécifique du vaccin était très inférieure à celle des sujets sains. Nous faisons donc l'hypothèse qu'un défaut de réponse cytotoxique soutient une production prolongée d'antigènes et le maintien dans le temps du centre germinatif (Figure 9). On pourrait y opposer le fait que la demi-vie d'un ARNm au sein d'une cellule est très court et ne permet donc pas une production prolongée de l'antigène. Cependant, l'ARNm vaccinal a été modifié pour augmenter sa stabilité, et en conséquence a été détecté jusqu'à 37 jours post vaccination dans des organes lymphoïdes secondaires (205).

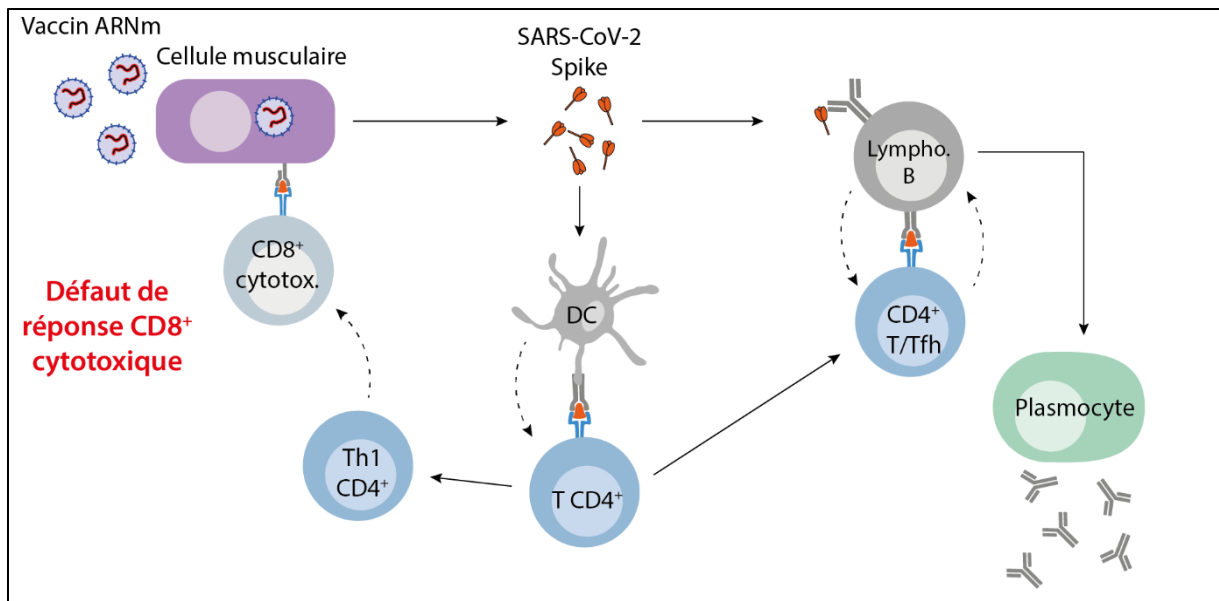


Figure 9. Schéma de la réponse vaccinale et hypothèse pouvant expliquer le maintien de la réponse dans le temps chez les patients transplantés

Abréviations : cytotox., cytotoxique ; lympho., lymphocyte ; Tfh, T auxiliaire folliculaire ; DC, cellule dendritique.

2. Rôle de l'immunité innée lymphoïde au cours de la réponse allo-immune

2.1. Le contrôle de l'alloreconnaissance directe inversée

Nous avons montré que des cellules allogéniques pouvaient coopérer pour aboutir à la production de DSA précoces chez des sujets transplantés. Cette vague de DSA précoces implique la coopération des T CD4⁺ dérivés du greffon et des B alloréactifs du receveur selon une modalité de reconnaissance directe inversée. Elle n'est pas observée chez tous les patients. Nous avons pu discuter de facteurs de contrôle de cette voie liés au temps de la transplantation. En particulier, la déplétion des cellules résidentes du greffon par l'utilisation de machines de perfusion semblait être une technique attrayante, car déjà utilisée en routine. Malheureusement, dans une étude rétrospective cas-témoin, nous n'avons observé aucune différence en termes d'incidence de DSA précoces chez des transplantés pulmonaires ayant reçu un greffon perfusé (n = 20) ou non (n = 39 ; Log-rank p=0.4508 ; Figure 10).

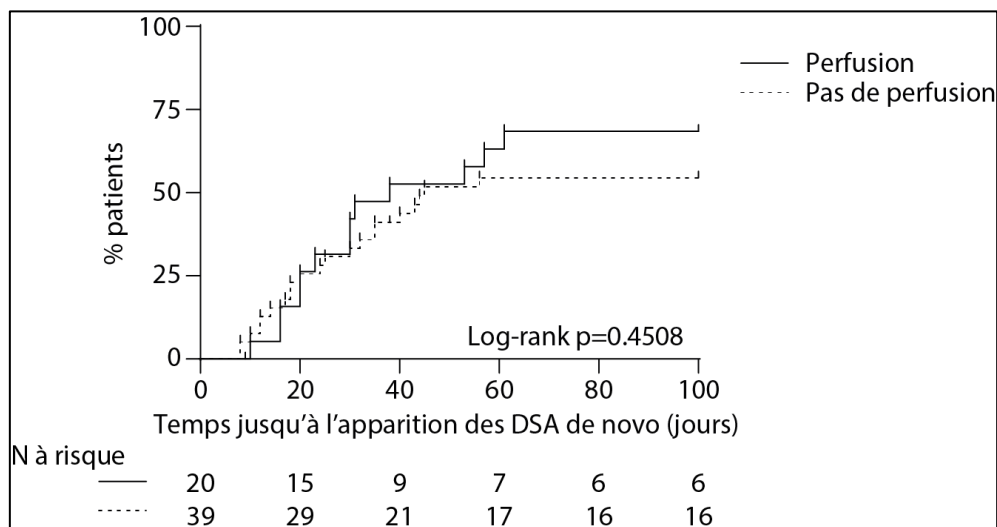


Figure 10. Impact de la perfusion des greffons sur la survenue de DSA de novo après transplantation pulmonaire

Courbe de Kaplan-Meier de la survie sans DSA des patients transplantés pulmonaires ayant reçu un greffon perfusé (trait plein) ou non (trait pointillé).

Cela ne discrédite pas pour autant la technique, qui pourrait être améliorée par l'ajout d'agents déplétants dans le liquide de perfusion, ou de chimiokines permettant de mobiliser les cellules du greffon. Cette stratégie est probablement plus réaliste que la généralisation des traitements d'induction qui déplètent les lymphocytes T. Ces derniers risqueraient d'exposer les patients transplantés pulmonaires à de graves complications infectieuses.

Cependant, il existe probablement d'autres facteurs qui contrôlent la voie d'alloreconnaissance directe inversée, et qui impliquent l'appariement génétique entre donneur et receveur. La voie d'alloreconnaissance directe inversée a été mise en évidence dans un modèle de transplantation d'un cœur de souris CBA (H-2^k) chez une souris CD3εKO de fond génétique C57BL/6 (H-2^b). Or, quand on change de modèle, en transplantant cette fois un cœur Balb/c (H-2^d) chez une même receveuse CD3εKO, on n'observe pas de DSA précoce (Figure 11A). Pourtant, le greffon Balb/c est bien immunogénique chez une souris sauvage (Figure 11B), et les lymphocytes T de la souris Balb/c ont la même capacité que les CBA à faire proliférer les lymphocytes B d'une souris C57BL/6 (Figure 11C). Inspirés par les premiers travaux qui ont mis en évidence la voie directe inversée (188), nous avons fait l'hypothèse qu'il existait un mécanisme immunologique qui empêchait les lymphocytes T Balb/c d'interagir avec les B alloréactifs de la receveuse. Compte-tenu de la précocité du phénomène d'alloreconnaissance directe inversée (dès J7 post transplantation), nous avons exploré le rôle de l'immunité innée. Nous avons alors transféré des lymphocytes T CD4⁺ provenant de souris CBA, Balb/c ou C57BL/6 (contrôles) à des souris Rag2^{-/-} de fond C57BL/6, dépourvues d'immunité adaptative. Nous avons observé que contrairement aux cellules d'origine CBA, qui s'expandaient après injection, les cellules Balb/c étaient éliminées dès le premier jour après transfert (Figure 11D). Les lymphocytes Natural Killer (NK) sont des candidats crédibles pour réagir face à des cellules allogéniques car capables d'alloreconnaissance. Nous avons alors testé leur implication en répétant l'expérience, mais après avoir déplété les NK dans un groupe de souris à l'aide d'un anticorps anti-NK1.1.

La déplétion des NK a restauré la survie des lymphocytes T Balb/c chez la receveuse Rag2^{-/-} (Figure 11D). Finalement, la déplétion des NK d'une souris CD3εKO restaure la production de DSA après transfert de lymphocytes T de souris Balb/c (modèle simplifié d'allorecognition directe inversée ; Figure 11E). Ainsi, nos travaux confirment les résultats du travail pionnier (188) et renforcent ainsi leur robustesse.

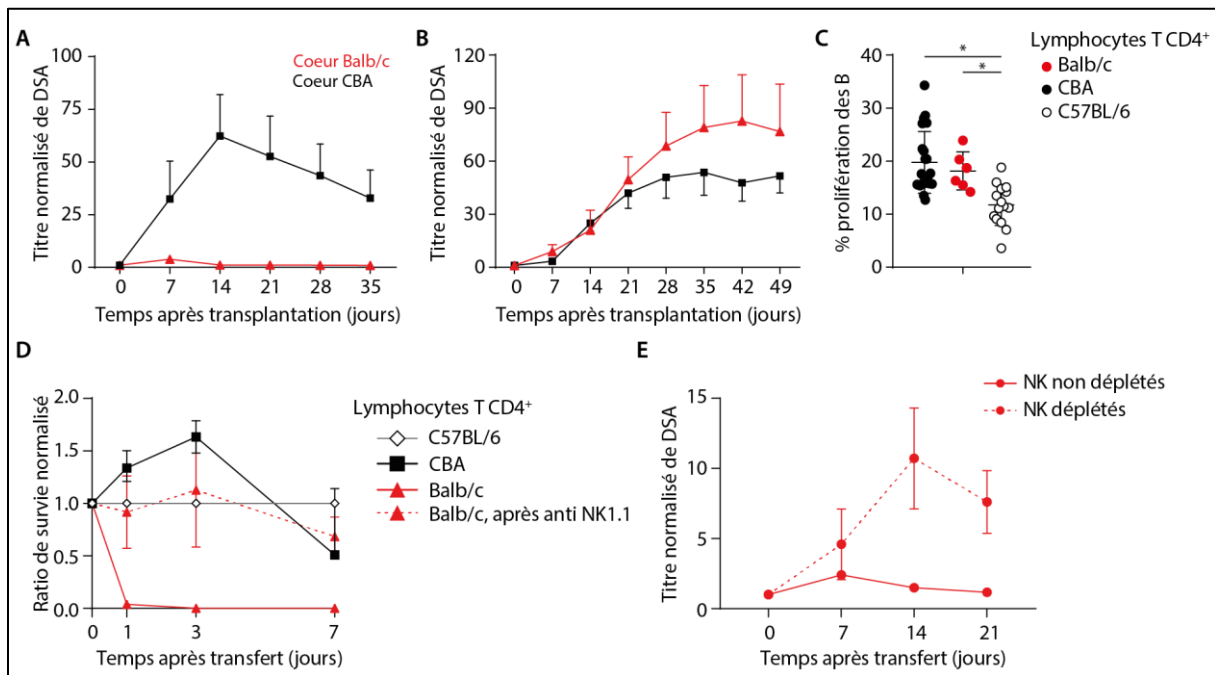


Figure 11. Contrôle de la voie d'allorecognition directe inversée par les lymphocytes NK

(A et B). Des souris (A) CD3εKO ou (B) sauvages de fond génétique C57BL/6 (H-2^b) ont été transplantées avec un cœur de souris Balb/c (H-2^d) ou CBA (H-2^k). Evolution au cours du temps du titre normalisé de DSA. Moyenne ± SD. (C) Des lymphocytes B C57BL/6 (H-2^b), activés par cross-linking du BCR avec un anticorps anti-κ, ont été cultivés avec des lymphocytes T CD4⁺ syngéniques ou allogéniques (CBA, H-2^k ou Balb/c, H-2^d). Le pourcentage de B ayant proliféré dans chaque coculture est présenté. Médiane ± IQR. Test de Mann-Whitney. *P < 0.05. (D) Des lymphocytes T CD4⁺ syngéniques ou allogéniques (CBA, H-2^k ou Balb/c, H-2^d) ont été injectés par voie intraveineuse à des souris Rag^{-/-} de fond C57BL/6, sans (lignes pleines) ou avec (ligne pointillée) déplétion préalable des lymphocytes NK. Après récolte des rates, la survie des cellules allogéniques a été normalisée sur le nombre de cellules syngéniques co-transférées. Moyenne ± SD. (E) Des lymphocytes T CD4⁺ de souris Balb/c (H-2^d) ont été injectés par voie intraveineuse à des souris CD3εKO de fond C57BL/6 (H-2^b), sans (ligne pleine) ou avec (ligne pointillée) déplétion préalable des lymphocytes NK. Evolution au cours du temps du titre normalisé de DSA. Moyenne ± SD.

Un mécanisme similaire a été décrit dans le contrôle de la survie des cellules présentatrices d'antigènes dérivées du greffon : les NK alloréactifs du receveur peuvent éliminer les cellules dendritiques du donneur. Ceci inhibe l'activation des T alloréactifs de spécificité directe (206,207). Il existe deux mécanismes potentiels pour expliquer cela. Les NK possèdent un arsenal de récepteurs activateurs et inhibiteurs, dont une partie a pour ligand des molécules du CMH de classe I. Ainsi, en face d'une cellule allogénique, les NK peuvent s'activer soit par la rencontre d'un ligand CMH-I activateur, soit en raison de l'absence d'un ligand CMH-I inhibiteur (soi-manquant, ou « missing-self »). Nous souhaitons, à l'aide d'expériences in vitro et in vivo, essayer de disséquer les mécanismes moléculaires impliqués.

La question qui se pose maintenant est celle de la pertinence clinique de ces résultats, que nous allons nous efforcer de mettre en lumière. Pour cela, nous sommes en train d'étudier une cohorte de transplantés pulmonaires. Nous souhaitons démontrer que les patients qui ont des NK réactifs vis-à-vis de leur donneur font moins de DSA précoces par la voie directe inversée que ceux dont les NK ne sont pas réactifs. Pour cela, nous utiliserons une approche génétique, avec typage des récepteurs NK activateurs et inhibiteurs des patients transplantés. Le résultat sera confronté au typage HLA de classe I du donneur, pour évaluer la capacité des NK du receveur à s'activer face à un lymphocyte T du donneur. Cette approche, bien qu'indispensable, a des limites. Tout d'abord, l'expression des récepteurs des NK est variée. En conséquence, l'analyse génétique ne donne pas un panorama réel des populations potentiellement alloréactives du sujet. De plus, certains de ces récepteurs, pour être actifs, nécessitent une primo-activation des NK [infection virale par le cytomégalovirus (CMV), par exemple], que nous ne pourrions pas capturer par le génotypage.

Si nous parvenons à mettre en évidence un rôle bénéfique de l'alloreconnaissance NK dans le contrôle de la voie directe inversée chez les patients transplantés, une autre question en découlera : est-ce susceptible de modifier les modalités d'attribution des greffons afin de prévenir les DSA précoces ? Cela est peu probable, étant donné que notre groupe a mis en évidence un autre effet de l'alloréactivité des NK, mais délétère cette fois-ci. En effet, les NK peuvent s'activer par « missing-self » en regard des cellules endothéliales du greffon et causer des lésions de rejet vasculaire chronique (208). Cette observation, validée en transplantation rénale, est en cours d'exploration dans le contexte de la transplantation pulmonaire. L'approche la plus prometteuse serait alors probablement le développement de thérapies visant à moduler l'activité des NK en fonction du contexte.

2.2. Un rôle ambivalent des lymphocytes T $\gamma\delta$?

Les lymphocytes T $\gamma\delta$ se situent à l'interface entre immunité innée et immunité adaptative. Les ligands de leurs TCR sont majoritairement inconnus. Il a été rapporté que certains clones étaient capables de reconnaître un peptide tumoral présenté au sein du CMH (209). Ceci soutient un rôle potentiel des lymphocytes T $\gamma\delta$ dans la réponse adaptative, ce que nous avons testé dans notre étude. Nos résultats ne confirment pas la participation des lymphocytes T $\gamma\delta$ à la réponse humorale allo-immune : nous avons démontré qu'après transplantation, les lymphocytes T $\gamma\delta$ n'étaient pas impliqués dans la production des DSA.

Si la génération des DSA est indispensable au développement des lésions de rejet humoral, elle n'en constitue que la première étape. Après leur production, les DSA circulent dans les vaisseaux pour trouver leur cible à la surface de l'endothélium du greffon. Une fois fixés, un de leur mécanismes effecteurs est le recrutement de cellules de l'immunité innée via leurs récepteurs au fragment cristallisable des immunoglobulines. Ce phénomène a été démontré en premier avec les lymphocytes NK, recrutés via le CD16/Fc γ RIIIa (147).

Or, chez les patients transplantés, les lymphocytes T $\gamma\delta$ qui s'expandent après infection par le CMV expriment également le CD16 (210). Il a été montré que des lignées dérivées de ces cellules étaient capables de cytotoxicité contre des cibles endothéliales (211). Nous souhaitons donc étudier si les lymphocytes T $\gamma\delta$ sont impliqués en aval de la production des DSA, en tant qu'effecteurs dans le rejet humoral. Ainsi, nous avons pu identifier ces cellules dans des biopsies de rejet humoral (Figure 12). Nous sommes en train d'analyser des jeux de données transcriptomiques (RNAseq et single-cell RNAseq) obtenues à partir de biopsies de rejets humoraux, pour i) confirmer la présence des lymphocytes T $\gamma\delta$ au sein de l'infiltrat inflammatoire, et ii) préciser leur état d'activation. L'objectif est ensuite d'étudier si cet infiltrat est associé à un pronostic plus péjoratif. De tels résultats conforteraient la notion évoquée ci-dessus, selon laquelle le développement de thérapies ciblant les cellules innées pourrait être une approche prometteuse pour la prise en charge des patients transplantés.

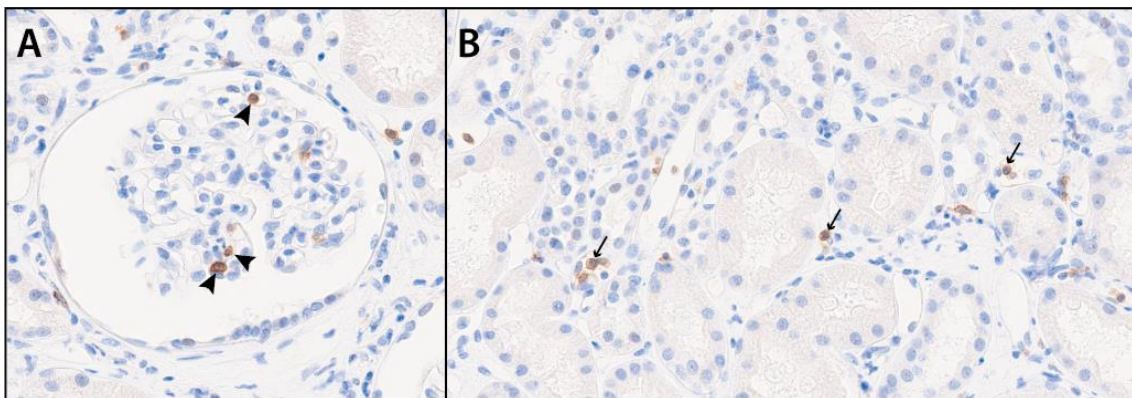


Figure 12. Les lymphocytes T $\gamma\delta$ infiltrent les greffons rénaux au cours du rejet humoral

Etude immunohistochimique de sections de greffon rénal présentant les lésions caractéristiques du rejet humoral, colorée pour le TCR δ . (A) Focus sur un glomérule rénal avec lésions de glomérulite. Les têtes de flèches désignent les lymphocytes T $\gamma\delta$. (B) Tissu interstitiel rénal avec lésions de capillarite péri-tubulaire. Les flèches désignent les lymphocytes T $\gamma\delta$.

V. CONCLUSIONS

Ces travaux ont permis d'étudier différents aspects de la réponse humorale chez les sujets transplantés, ainsi que son impact sur les stratégies vaccinales et la survie des greffons.

Tout d'abord, dans une étude de vaccinologie, nous avons montré que les patients transplantés répondaient insuffisamment aux vaccins à ARNm contre le SARS-CoV-2. Certains immunosuppresseurs ont un impact particulièrement néfaste sur la réponse vaccinale. Nous avons proposé des stratégies d'urgence efficaces pour améliorer la protection des patients en augmentant les doses de vaccin. Mais ces stratégies sont imparfaites, et certains patients restent exposés aux formes graves de la maladie.

Puis, nous avons exploré des voies non conventionnelles de réponse humorale allo-immune. Nous avons confirmé l'importance des lymphocytes T CD4⁺ pour la production des DSA, et démontré que les lymphocytes T $\gamma\delta$ n'étaient pas impliqués dans ce processus. Ces données sont rassurantes, mais elles sont à considérer avec prudence. En effet, les lymphocytes T $\gamma\delta$ pourraient être des effecteurs d'aval au cours du rejet humoral, mais ceci reste à démontrer. Enfin, nous avons mis en lumière une voie d'allorecognition qui implique les lymphocytes T CD4⁺ du donneur, et aboutit à des DSA et rejets précoces. Il reste à préciser les mécanismes immunologiques qui contrôlent cette voie chez le receveur.

En conclusion, ce travail explore différents aspects de la réponse humorale des patients transplantés, qui est mise en tension entre la réponse vaccinale bénéfique, souhaitée mais déficiente, et la réponse allo-immune, insuffisamment contrôlée et délétère. De nouvelles stratégies doivent être développées pour améliorer cette balance bénéfice-risque chez les patients transplantés.

REFERENCES (articles exclus)

1. Karrer U, Althage A, Odermatt B, Roberts CWM, Korsmeyer SJ, Miyawaki S, et al. On the Key Role of Secondary Lymphoid Organs in Antiviral Immune Responses Studied in A lymphoplastic (aly/aly) and Spleenless (Hox11^{-/-}) Mutant Mice. *J Exp Med*. 16 juin 1997;185(12):2157-70.
2. Miller MJ, Wei SH, Parker I, Cahalan MD. Two-Photon Imaging of Lymphocyte Motility and Antigen Response in Intact Lymph Node. *Science*. 7 juin 2002;296(5574):1869-73.
3. von Andrian UH, Mempel TR. Homing and cellular traffic in lymph nodes. *Nat Rev Immunol*. nov 2003;3(11):867-78.
4. Legler DF, Loetscher M, Roos RS, Clark-Lewis I, Baggiolini M, Moser B. B Cell-attracting Chemokine 1, a Human CXC Chemokine Expressed in Lymphoid Tissues, Selectively Attracts B Lymphocytes via BLR1/CXCR5. *J Exp Med*. 16 févr 1998;187(4):655-60.
5. Förster R, Mattis AE, Kremmer E, Wolf E, Brem G, Lipp M. A Putative Chemokine Receptor, BLR1, Directs B Cell Migration to Defined Lymphoid Organs and Specific Anatomic Compartments of the Spleen. *Cell*. 13 déc 1996;87(6):1037-47.
6. Zlotnik A, Yoshie O. Chemokines: A New Classification System and Their Role in Immunity. *Immunity*. 1 févr 2000;12(2):121-7.
7. Batista FD, Harwood NE. The who, how and where of antigen presentation to B cells. *Nat Rev Immunol*. janv 2009;9(1):15-27.
8. Bohnsack JF, Brown EJ. The role of the spleen in resistance to infection. *Annu Rev Med*. 1986;37:49-59.
9. Rawlings DJ, Schwartz MA, Jackson SW, Meyer-Bahlburg A. Integration of B cell responses through Toll-like receptors and antigen receptors. *Nat Rev Immunol*. avr 2012;12(4):282-94.
10. Fillatreau S, Manfroi B, Dörner T. Toll-like receptor signalling in B cells during systemic lupus erythematosus. *Nat Rev Rheumatol*. févr 2021;17(2):98-108.
11. Pape KA, Catron DM, Itano AA, Jenkins MK. The Humoral Immune Response Is Initiated in Lymph Nodes by B Cells that Acquire Soluble Antigen Directly in the Follicles. *Immunity*. 27 avr 2007;26(4):491-502.
12. Gretz JE, Norbury CC, Anderson AO, Proudfoot AEI, Shaw S. Lymph-Borne Chemokines and Other Low Molecular Weight Molecules Reach High Endothelial Venules via Specialized Conduits While a Functional Barrier Limits Access to the Lymphocyte Microenvironments in Lymph Node Cortex. *J Exp Med*. 13 nov 2000;192(10):1425-40.
13. Roozendaal R, Mempel TR, Pitcher LA, Gonzalez SF, Verschoor A, Mebius RE, et al. Conduits Mediate Transport of Low-Molecular-Weight Antigen to Lymph Node Follicles. *Immunity*. 20 févr 2009;30(2):264-76.
14. Phan TG, Green JA, Gray EE, Xu Y, Cyster JG. Immune complex relay by subcapsular sinus macrophages and noncognate B cells drives antibody affinity maturation. *Nat Immunol*. juill 2009;10(7):786-93.
15. Koppel EA, Wieland CW, van den Berg VCM, Litjens M, Florquin S, van Kooyk Y, et al. Specific ICAM-3 grabbing nonintegrin-related 1 (SIGNR1) expressed by marginal

- zone macrophages is essential for defense against pulmonary *Streptococcus pneumoniae* infection. *Eur J Immunol*. oct 2005;35(10):2962-9.
16. Bergtold A, Desai DD, Gavhane A, Clynes R. Cell Surface Recycling of Internalized Antigen Permits Dendritic Cell Priming of B Cells. *Immunity*. 1 nov 2005;23(5):503-14.
 17. Heesters BA, Myers RC, Carroll MC. Follicular dendritic cells: dynamic antigen libraries. *Nat Rev Immunol*. juill 2014;14(7):495-504.
 18. Fischer MB, Goerg S, Shen L, Prodeus AP, Goodnow CC, Kelsoe G, et al. Dependence of Germinal Center B Cells on Expression of CD21/CD35 for Survival. *Science*. 24 avr 1998;280(5363):582-5.
 19. Qin D, Wu J, Vora KA, Ravetch JV, Szakal AK, Manser T, et al. Fc gamma receptor IIB on follicular dendritic cells regulates the B cell recall response. *J Immunol Baltim Md 1950*. 15 juin 2000;164(12):6268-75.
 20. Yoshida K, van den Berg TK, Dijkstra CD. Two functionally different follicular dendritic cells in secondary lymphoid follicles of mouse spleen, as revealed by CR1/2 and FcR gamma II-mediated immune-complex trapping. *Immunology*. sept 1993;80(1):34-9.
 21. Gray D, Kumararatne DS, Lortan J, Khan M, MacLennan IC. Relation of intra-splenic migration of marginal zone B cells to antigen localization on follicular dendritic cells. *Immunology*. août 1984;52(4):659-69.
 22. Phan TG, Grigorova I, Okada T, Cyster JG. Subcapsular encounter and complement-dependent transport of immune complexes by lymph node B cells. *Nat Immunol*. sept 2007;8(9):992-1000.
 23. Heinen E, Braun M, Coulie PG, Van Snick J, Moeremans M, Cormann N, et al. Transfer of immune complexes from lymphocytes to follicular dendritic cells. *Eur J Immunol*. févr 1986;16(2):167-72.
 24. Qi H, Egen JG, Huang AYC, Germain RN. Extrafollicular Activation of Lymph Node B Cells by Antigen-Bearing Dendritic Cells. *Science*. 16 juin 2006;312(5780):1672-6.
 25. Carrasco YR, Batista FD. B Cells Acquire Particulate Antigen in a Macrophage-Rich Area at the Boundary between the Follicle and the Subcapsular Sinus of the Lymph Node. *Immunity*. 27 juill 2007;27(1):160-71.
 26. Junt T, Moseman EA, Iannaccone M, Massberg S, Lang PA, Boes M, et al. Subcapsular sinus macrophages in lymph nodes clear lymph-borne viruses and present them to antiviral B cells. *Nature*. nov 2007;450(7166):110-4.
 27. Carrasco YR, Fleire SJ, Cameron T, Dustin ML, Batista FD. LFA-1/ICAM-1 Interaction Lowers the Threshold of B Cell Activation by Facilitating B Cell Adhesion and Synapse Formation. *Immunity*. 1 mai 2004;20(5):589-99.
 28. Reth M, Wienands J. Initiation and processing of signals from the B cell antigen receptor. *Annu Rev Immunol*. 1997;15:453-79.
 29. Kwak K, Akkaya M, Pierce SK. B cell signaling in context. *Nat Immunol*. août 2019;20(8):963-9.
 30. Fleire SJ, Goldman JP, Carrasco YR, Weber M, Bray D, Batista FD. B Cell Ligand Discrimination Through a Spreading and Contraction Response. *Science*. 5 mai 2006;312(5774):738-41.
 31. Depoil D, Fleire S, Treanor BL, Weber M, Harwood NE, Marchbank KL, et al. CD19 is essential for B cell activation by promoting B cell receptor-antigen microcluster formation in response to membrane-bound ligand. *Nat Immunol*. janv 2008;9(1):63-72.

32. Yuseff MI, Reversat A, Lankar D, Diaz J, Fanget I, Pierobon P, et al. Polarized Secretion of Lysosomes at the B Cell Synapse Couples Antigen Extraction to Processing and Presentation. *Immunity*. 23 sept 2011;35(3):361-74.
33. Suzuki K, Grigorova I, Phan TG, Kelly LM, Cyster JG. Visualizing B cell capture of cognate antigen from follicular dendritic cells. *J Exp Med*. 8 juin 2009;206(7):1485-93.
34. Reif K, Ekland EH, Ohl L, Nakano H, Lipp M, Förster R, et al. Balanced responsiveness to chemoattractants from adjacent zones determines B-cell position. *Nature*. mars 2002;416(6876):94-9.
35. Pereira JP, Kelly LM, Xu Y, Cyster JG. EB12 mediates B cell segregation between the outer and centre follicle. *Nature*. août 2009;460(7259):1122-6.
36. Akkaya M, Traba J, Roesler AS, Miozzo P, Akkaya B, Theall BP, et al. Second signals rescue B cells from activation-induced mitochondrial dysfunction and death. *Nat Immunol*. août 2018;19(8):871-84.
37. Crotty S. T follicular helper cell differentiation, function, and roles in disease. *Immunity*. 16 oct 2014;41(4):529-42.
38. Crotty S. T Follicular Helper Cell Biology: A Decade of Discovery and Diseases. *Immunity*. 21 mai 2019;50(5):1132-48.
39. Stoll S, Delon J, Brotz TM, Germain RN. Dynamic Imaging of T Cell-Dendritic Cell Interactions in Lymph Nodes. *Science*. 7 juin 2002;296(5574):1873-6.
40. Hong S, Zhang Z, Liu H, Tian M, Zhu X, Zhang Z, et al. B Cells Are the Dominant Antigen-Presenting Cells that Activate Naive CD4⁺ T Cells upon Immunization with a Virus-Derived Nanoparticle Antigen. *Immunity*. 16 oct 2018;49(4):695-708.e4.
41. Smith-Garvin JE, Koretzky GA, Jordan MS. T Cell Activation. *Annu Rev Immunol*. 2009;27(1):591-619.
42. Wardenburg JB, Fu C, Jackman JK, Flotow H, Wilkinson SE, Williams DH, et al. Phosphorylation of SLP-76 by the ZAP-70 Protein-tyrosine Kinase Is Required for T-cell Receptor Function*. *J Biol Chem*. 16 août 1996;271(33):19641-4.
43. Zhang W, Sloan-Lancaster J, Kitchen J, Tribble RP, Samelson LE. LAT: The ZAP-70 Tyrosine Kinase Substrate that Links T Cell Receptor to Cellular Activation. *Cell*. 9 janv 1998;92(1):83-92.
44. Lee JU, Kim LK, Choi JM. Revisiting the Concept of Targeting NFAT to Control T Cell Immunity and Autoimmune Diseases. *Front Immunol* [Internet]. 2018 [cité 22 sept 2022];9. Disponible sur: <https://www.frontiersin.org/articles/10.3389/fimmu.2018.02747>
45. Vaeth M, Maus M, Klein-Hessling S, Freinkman E, Yang J, Eckstein M, et al. Store-Operated Ca²⁺ Entry Controls Clonal Expansion of T Cells through Metabolic Reprogramming. *Immunity*. 17 oct 2017;47(4):664-679.e6.
46. Acuto O, Michel F. CD28-mediated co-stimulation: a quantitative support for TCR signalling. *Nat Rev Immunol*. déc 2003;3(12):939-51.
47. Choi YS, Kageyama R, Eto D, Escobar TC, Johnston RJ, Monticelli L, et al. ICOS Receptor Instructs T Follicular Helper Cell versus Effector Cell Differentiation via Induction of the Transcriptional Repressor Bcl6. *Immunity*. 24 juin 2011;34(6):932-46.
48. Tubo NJ, Pagán AJ, Taylor JJ, Nelson RW, Linehan JL, Ertelt JM, et al. Single Naive CD4⁺ T Cells from a Diverse Repertoire Produce Different Effector Cell Types during Infection. *Cell*. 9 mai 2013;153(4):785-96.

49. Linterman MA, Denton AE, Divekar DP, Zvetkova I, Kane L, Ferreira C, et al. CD28 expression is required after T cell priming for helper T cell responses and protective immunity to infection. *Powrie FM, éditeur. eLife.* 27 oct 2014;3:e03180.
50. Liu X, Chen X, Zhong B, Wang A, Wang X, Chu F, et al. Transcription factor achaete-scute homologue 2 initiates follicular T-helper-cell development. *Nature.* mars 2014;507(7493):513-8.
51. Haynes NM, Allen CDC, Lesley R, Ansel KM, Killeen N, Cyster JG. Role of CXCR5 and CCR7 in Follicular Th Cell Positioning and Appearance of a Programmed Cell Death Gene-1High Germinal Center-Associated Subpopulation. *J Immunol.* 15 oct 2007;179(8):5099-108.
52. Yeh CH, Nojima T, Kuraoka M, Kelsoe G. Germinal center entry not selection of B cells is controlled by peptide-MHCII complex density. *Nat Commun.* 2 mars 2018;9(1):928.
53. Schwickert TA, Victora GD, Fooksman DR, Kamphorst AO, Mugnier MR, Gitlin AD, et al. A dynamic T cell-limited checkpoint regulates affinity-dependent B cell entry into the germinal center. *J Exp Med.* 16 mai 2011;208(6):1243-52.
54. Schwartzberg PL, Mueller KL, Qi H, Cannons JL. SLAM receptors and SAP influence lymphocyte interactions, development and function. *Nat Rev Immunol.* janv 2009;9(1):39-46.
55. Biram A, Davidzohn N, Shulman Z. T cell interactions with B cells during germinal center formation, a three-step model. *Immunol Rev.* 2019;288(1):37-48.
56. Zaretsky I, Atrakchi O, Mazor RD, Stoler-Barak L, Biram A, Feigelson SW, et al. ICAMs support B cell interactions with T follicular helper cells and promote clonal selection. *J Exp Med.* 22 sept 2017;214(11):3435-48.
57. Gordon J, Katira A, Holder M, MacDonald I, Pound J. Central role of CD40 and its ligand in B lymphocyte responses to T-dependent antigens. *Cell Mol Biol Noisy--Gd Fr.* 1 janv 1994;40 Suppl 1:1-13.
58. Lagresle C, Mondière P, Bella C, Krammer PH, Defrance T. Concurrent engagement of CD40 and the antigen receptor protects naive and memory human B cells from APO-1/Fas-mediated apoptosis. *J Exp Med.* 1 avr 1996;183(4):1377-88.
59. Rothstein T, Wang J, Panka D, Foote L, Wang Z, Stanger B, et al. Protection against Fas-dependent Th1-mediated apoptosis by antigen receptor engagement in B cells [Internet]. *Nature.* 1995 [cité 13 nov 2020]. Disponible sur: <https://pubmed.ncbi.nlm.nih.gov/7533263/>
60. Quast I, Dvorscek AR, Pattaroni C, Steiner TM, McKenzie CI, Pitt C, et al. Interleukin-21, acting beyond the immunological synapse, independently controls T follicular helper and germinal center B cells. *Immunity.* 9 août 2022;55(8):1414-1430.e5.
61. Zotos D, Coquet JM, Zhang Y, Light A, D'Costa K, Kallies A, et al. IL-21 regulates germinal center B cell differentiation and proliferation through a B cell-intrinsic mechanism. *J Exp Med.* 8 févr 2010;207(2):365-78.
62. Linterman MA, Beaton L, Yu D, Ramiscal RR, Srivastava M, Hogan JJ, et al. IL-21 acts directly on B cells to regulate Bcl-6 expression and germinal center responses. *J Exp Med.* 8 févr 2010;207(2):353-63.
63. Dvorscek AR, McKenzie CI, Robinson MJ, Ding Z, Pitt C, O'Donnell K, et al. IL-21 has a critical role in establishing germinal centers by amplifying early B cell proliferation. *EMBO Rep.* 5 sept 2022;23(9):e54677.

64. Weinstein JS, Herman EI, Lainez B, Licona-Limón P, Esplugues E, Flavell R, et al. TFH cells progressively differentiate to regulate the germinal center response. *Nat Immunol.* oct 2016;17(10):1197-205.
65. Zhou C, Saxon A, Zhang K. Human activation-induced cytidine deaminase is induced by IL-4 and negatively regulated by CD45: implication of CD45 as a Janus kinase phosphatase in antibody diversification. *J Immunol Baltim Md 1950.* 15 févr 2003;170(4):1887-93.
66. Muramatsu M, Kinoshita K, Fagarasan S, Yamada S, Shinkai Y, Honjo T. Class switch recombination and hypermutation require activation-induced cytidine deaminase (AID), a potential RNA editing enzyme. *Cell.* 1 sept 2000;102(5):553-63.
67. Cunningham AF, Gaspal F, Serre K, Mohr E, Henderson IR, Scott-Tucker A, et al. Salmonella Induces a Switched Antibody Response without Germinal Centers That Impedes the Extracellular Spread of Infection. *J Immunol.* 15 mai 2007;178(10):6200-7.
68. Di Niro R, Lee SJ, Vander Heiden JA, Elsner RA, Trivedi N, Bannock JM, et al. Salmonella Infection Drives Promiscuous B Cell Activation Followed by Extrafollicular Affinity Maturation. *Immunity.* 21 juill 2015;43(1):120-31.
69. Elsner RA, Shlomchik MJ. Germinal Center and Extrafollicular B Cell Responses in Vaccination, Immunity, and Autoimmunity. *Immunity.* 15 déc 2020;53(6):1136-50.
70. St John AL, Abraham SN. Salmonella disrupts lymph node architecture by TLR4-mediated suppression of homeostatic chemokines. *Nat Med.* nov 2009;15(11):1259-65.
71. Popescu M, Cabrera-Martinez B, Winslow GM. TNF- α Contributes to Lymphoid Tissue Disorganization and Germinal Center B Cell Suppression during Intracellular Bacterial Infection. *J Immunol Baltim Md 1950.* 1 nov 2019;203(9):2415-24.
72. Woodruff MC, Ramonell RP, Nguyen DC, Cashman KS, Saini AS, Haddad NS, et al. Extrafollicular B cell responses correlate with neutralizing antibodies and morbidity in COVID-19. *Nat Immunol.* déc 2020;21(12):1506-16.
73. Hastey CJ, Ochoa J, Olsen KJ, Barthold SW, Baumgarth N. MyD88- and TRIF-Independent Induction of Type I Interferon Drives Naive B Cell Accumulation but Not Loss of Lymph Node Architecture in Lyme Disease. *Infect Immun.* avr 2014;82(4):1548-58.
74. Trivedi N, Weisel F, Smita S, Joachim S, Kader M, Radhakrishnan A, et al. Liver Is a Generative Site for the B Cell Response to *Ehrlichia muris*. *Immunity.* 17 déc 2019;51(6):1088-1101.e5.
75. Roco JA, Mesin L, Binder SC, Nefzger C, Gonzalez-Figueroa P, Canete PF, et al. Class-Switch Recombination Occurs Infrequently in Germinal Centers. *Immunity.* 20 août 2019;51(2):337-350.e7.
76. Tafuri A, Shahinian A, Bladt F, Yoshinaga SK, Jordana M, Wakeham A, et al. ICOS is essential for effective T-helper-cell responses. *Nature.* janv 2001;409(6816):105-9.
77. McAdam AJ, Greenwald RJ, Levin MA, Chernova T, Malenkovich N, Ling V, et al. ICOS is critical for CD40-mediated antibody class switching. *Nature.* janv 2001;409(6816):102-5.
78. Stavnezer J. Immunoglobulin class switching. *Curr Opin Immunol.* 1 avr 1996;8(2):199-205.
79. Reinhardt RL, Liang HE, Locksley RM. Cytokine-secreting follicular T cells shape the antibody repertoire. *Nat Immunol.* avr 2009;10(4):385-93.

80. Martinez-Valdez H, Guret C, de Bouteiller O, Fugier I, Banchereau J, Liu YJ. Human germinal center B cells express the apoptosis-inducing genes Fas, c-myc, P53, and Bax but not the survival gene bcl-2. *J Exp Med*. 1 mars 1996;183(3):971-7.
81. Liu YJ, Mason DY, Johnson GD, Abbot S, Gregory CD, Hardie DL, et al. Germinal center cells express bcl-2 protein after activation by signals which prevent their entry into apoptosis. *Eur J Immunol*. 1991;21(8):1905-10.
82. Ci W, Polo JM, Cerchiatti L, Shaknovich R, Wang L, Yang SN, et al. The BCL6 transcriptional program features repression of multiple oncogenes in primary B cells and is deregulated in DLBCL. *Blood*. 28 mai 2009;113(22):5536-48.
83. Victora GD, Nussenzweig MC. Germinal centers. *Annu Rev Immunol*. 2012;30:429-57.
84. Batista FD, Arana E, Barral P, Carrasco YR, Depoil D, Eckl-Dorna J, et al. The role of integrins and coreceptors in refining thresholds for B-cell responses. *Immunol Rev*. 2007;218(1):197-213.
85. Thauvat O, Granja AG, Barral P, Filby A, Montaner B, Collinson L, et al. Asymmetric segregation of polarized antigen on B cell division shapes presentation capacity. *Science*. 27 janv 2012;335(6067):475-9.
86. Shulman Z, Gitlin AD, Weinstein JS, Lainez B, Esplugues E, Flavell RA, et al. Dynamic signaling by T follicular helper cells during germinal center B cell selection. *Science*. 29 août 2014;345(6200):1058-62.
87. Liu D, Xu H, Shih C, Wan Z, Ma X, Ma W, et al. T-B-cell entanglement and ICOSL-driven feed-forward regulation of germinal centre reaction. *Nature*. janv 2015;517(7533):214-8.
88. Victora GD, Schwickert TA, Fooksman DR, Kamphorst AO, Meyer-Hermann M, Dustin ML, et al. Germinal center dynamics revealed by multiphoton microscopy with a photoactivatable fluorescent reporter. *Cell*. 12 nov 2010;143(4):592-605.
89. Gitlin AD, Shulman Z, Nussenzweig MC. Clonal selection in the germinal centre by regulated proliferation and hypermutation. *Nature*. mai 2014;509(7502):637-40.
90. Cattoretti G, Büttner M, Shaknovich R, Kremmer E, Alobeid B, Niedobitek G. Nuclear and cytoplasmic AID in extrafollicular and germinal center B cells. *Blood*. 15 mai 2006;107(10):3967-75.
91. Di Noia JM, Neuberger MS. Molecular mechanisms of antibody somatic hypermutation. *Annu Rev Biochem*. 2007;76:1-22.
92. Stewart I, Radtke D, Phillips B, McGowan SJ, Bannard O. Germinal Center B Cells Replace Their Antigen Receptors in Dark Zones and Fail Light Zone Entry when Immunoglobulin Gene Mutations are Damaging. *Immunity*. 18 sept 2018;49(3):477-489.e7.
93. Jenks SA, Cashman KS, Zumaquero E, Marigorta UM, Patel AV, Wang X, et al. Distinct Effector B Cells Induced by Unregulated Toll-like Receptor 7 Contribute to Pathogenic Responses in Systemic Lupus Erythematosus. *Immunity*. 16 oct 2018;49(4):725-739.e6.
94. Weisel FJ, Zuccarino-Catania GV, Chikina M, Shlomchik MJ. A Temporal Switch in the Germinal Center Determines Differential Output of Memory B and Plasma Cells. *Immunity*. 19 janv 2016;44(1):116-30.
95. Suan D, Kräutler NJ, Maag JLV, Butt D, Bourne K, Hermes JR, et al. CCR6 Defines Memory B Cell Precursors in Mouse and Human Germinal Centers, Revealing Light-Zone

- Location and Predominant Low Antigen Affinity. *Immunity*. 19 déc 2017;47(6):1142-1153.e4.
96. Shinnakasu R, Inoue T, Kometani K, Moriyama S, Adachi Y, Nakayama M, et al. Regulated selection of germinal-center cells into the memory B cell compartment. *Nat Immunol*. juill 2016;17(7):861-9.
 97. Kaku CI, Bergeron AJ, Ahlm C, Normark J, Sakharkar M, Forsell MNE, et al. Recall of preexisting cross-reactive B cell memory after Omicron BA.1 breakthrough infection. *Sci Immunol*. 12 mai 2022;7(73):eabq3511.
 98. Sokal A, Broketa M, Barba-Spaeth G, Meola A, Fernández I, Fourati S, et al. Analysis of mRNA vaccination-elicited RBD-specific memory B cells reveals strong but incomplete immune escape of the SARS-CoV-2 Omicron variant. *Immunity*. 14 juin 2022;55(6):1096-1104.e4.
 99. Kotaki R, Adachi Y, Moriyama S, Onodera T, Fukushi S, Nagakura T, et al. SARS-CoV-2 Omicron-neutralizing memory B cells are elicited by two doses of BNT162b2 mRNA vaccine. *Sci Immunol*. 3 févr 2022;7(70):eabn8590.
 100. Viant C, Weymar GHJ, Escolano A, Chen S, Hartweger H, Cipolla M, et al. Antibody Affinity Shapes the Choice between Memory and Germinal Center B Cell Fates. *Cell*. 25 nov 2020;183(5):1298-1311.e11.
 101. Chevalier N, Jarrossay D, Ho E, Avery DT, Ma CS, Yu D, et al. CXCR5 expressing human central memory CD4 T cells and their relevance for humoral immune responses. *J Immunol Baltim Md 1950*. 15 mai 2011;186(10):5556-68.
 102. Morita R, Schmitt N, Bentebibel SE, Ranganathan R, Bourdery L, Zurawski G, et al. Human blood CXCR5(+)CD4(+) T cells are counterparts of T follicular cells and contain specific subsets that differentially support antibody secretion. *Immunity*. 28 janv 2011;34(1):108-21.
 103. Locci M, Havenar-Daughton C, Landais E, Wu J, Kroenke MA, Arlehamn CL, et al. Human Circulating PD-1+CXCR3-CXCR5+ Memory Tfh Cells Are Highly Functional and Correlate with Broadly Neutralizing HIV Antibody Responses. *Immunity*. 17 oct 2013;39(4):758-69.
 104. Robinson AM, Higgins BW, Shuparski AG, Miller KB, McHeyzer-Williams LJ, McHeyzer-Williams MG. Evolution of antigen-specific follicular helper T cell transcription from effector function to memory. *Sci Immunol*. 7 oct 2022;7(76):eabm2084.
 105. Weber JP, Fuhrmann F, Hutloff A. T-follicular helper cells survive as long-term memory cells. *Eur J Immunol*. 2012;42(8):1981-8.
 106. Lüthje K, Kallies A, Shimohakamada Y, Belz GT, Light A, Tarlinton DM, et al. The development and fate of follicular helper T cells defined by an IL-21 reporter mouse. *Nat Immunol*. mai 2012;13(5):491-8.
 107. Hale JS, Youngblood B, Latner DR, Mohammed AUR, Ye L, Akondy RS, et al. Distinct Memory CD4+ T Cells with Commitment to T Follicular Helper- and T Helper 1-Cell Lineages Are Generated after Acute Viral Infection. *Immunity*. 18 avr 2013;38(4):805-17.
 108. Shinnakasu R, Kurosaki T. Regulation of memory B and plasma cell differentiation. *Curr Opin Immunol*. 1 avr 2017;45:126-31.
 109. Nutt SL, Hodgkin PD, Tarlinton DM, Corcoran LM. The generation of antibody-secreting plasma cells. *Nat Rev Immunol*. mars 2015;15(3):160-71.

110. Smith KGC, Light A, Nossal GJV, Tarlinton DM. The extent of affinity maturation differs between the memory and antibody-forming cell compartments in the primary immune response. *EMBO J.* juin 1997;16(11):2996-3006.
111. Phan TG, Paus D, Chan TD, Turner ML, Nutt SL, Basten A, et al. High affinity germinal center B cells are actively selected into the plasma cell compartment. *J Exp Med.* 9 oct 2006;203(11):2419-24.
112. Manz RA, Hauser AE, Hiepe F, Radbruch A. Maintenance of serum antibody levels. *Annu Rev Immunol.* 2005;23:367-86.
113. Manz RA, Löhning M, Cassese G, Thiel A, Radbruch A. Survival of long-lived plasma cells is independent of antigen. *Int Immunol.* 1 nov 1998;10(11):1703-11.
114. Schroeder HW, Cavacini L. Structure and function of immunoglobulins. *J Allergy Clin Immunol.* 1 févr 2010;125(2):S41-52.
115. Zorn E, See SB. Antibody Responses to Minor Histocompatibility Antigens After Solid Organ Transplantation. *Transplantation.* avr 2022;106(4):749-53.
116. Reindl-Schwaighofer R, Heinzl A, Kainz A, van Setten J, Jelencsics K, Hu K, et al. Contribution of non-HLA incompatibility between donor and recipient to kidney allograft survival: genome-wide analysis in a prospective cohort. *The Lancet.* 2 mars 2019;393(10174):910-7.
117. Game DS, Lechler RI. Pathways of allorecognition: implications for transplantation tolerance. *Transpl Immunol.* 1 août 2002;10(2):101-8.
118. Afzali B, Lombardi G, Lechler RI. Pathways of major histocompatibility complex allorecognition. *Curr Opin Organ Transplant.* août 2008;13(4):438-44.
119. Archbold JK, Macdonald WA, Miles JJ, Brennan RM, Kjer-Nielsen L, McCluskey J, et al. Alloreactivity between Disparate Cognate and Allogeneic pMHC-I Complexes Is the Result of Highly Focused, Peptide-dependent Structural Mimicry*. *J Biol Chem.* 10 nov 2006;281(45):34324-32.
120. Villadangos JA, Galocha B, López de Castro JA. Unusual topology of an HLA-B27 allospecific T cell epitope lacking peptide specificity. *J Immunol Baltim Md 1950.* 1 mars 1994;152(5):2317-23.
121. Son ET, Faridi P, Paul-Heng M, Leong ML, English K, Ramarathnam SH, et al. The self-peptide repertoire plays a critical role in transplant tolerance induction. *J Clin Invest [Internet].* 1 nov 2021 [cité 16 mai 2022];131(21). Disponible sur: <https://www-jci-org.proxy.insermbiblio.inist.fr/articles/view/146771>
122. Suchin EJ, Langmuir PB, Palmer E, Sayegh MH, Wells AD, Turka LA. Quantifying the Frequency of Alloreactive T Cells In Vivo: New Answers to an Old Question. *J Immunol.* 15 janv 2001;166(2):973-81.
123. Herrera OB, Golshayan D, Tibbott R, Ochoa FS, James MJ, Marelli-Berg FM, et al. A Novel Pathway of Alloantigen Presentation by Dendritic Cells. *J Immunol.* 15 oct 2004;173(8):4828-37.
124. Russo V, Zhou D, Sartirana C, Rovere P, Villa A, Rossini S, et al. Acquisition of intact allogeneic human leukocyte antigen molecules by human dendritic cells. *Blood.* 1 juin 2000;95(11):3473-7.
125. Marino J, Babiker-Mohamed MH, Crosby-Bertorini P, Paster JT, LeGuern C, Germana S, et al. Donor exosomes rather than passenger leukocytes initiate alloreactive T cell responses after transplantation. *Sci Immunol.* 14 juill 2016;1(1):aaf8759-aaf8759.

126. Hughes AD, Zhao D, Dai H, Abou-Daya KI, Tieu R, Rammal R, et al. Cross-dressed dendritic cells sustain effector T cell responses in islet and kidney allografts. *J Clin Invest.* 2 janv 2020;130(1):287-94.
127. Scothorne RJ. Lymphatic Repair and the Genesis of Homograft Immunity. *Ann N Y Acad Sci.* 1958;73(3):673-5.
128. Málek P, Vrabel J, Kolc J. Lymphatic Aspects of Experimental and Clinical Renal Transplantation. *Bulletin de la Societe internationale de chirurgie.* 1969.
129. Lakkis FG, Arakelov A, Konieczny BT, Inoue Y. Immunologic 'ignorance' of vascularized organ transplants in the absence of secondary lymphoid tissue. *Nat Med.* juin 2000;6(6):686-8.
130. Dieu-Nosjean MC, Giraldo NA, Kaplon H, Germain C, Fridman WH, Sautès-Fridman C. Tertiary lymphoid structures, drivers of the anti-tumor responses in human cancers. *Immunol Rev.* mai 2016;271(1):260-75.
131. Pitzalis C, Jones GW, Bombardieri M, Jones SA. Ectopic lymphoid-like structures in infection, cancer and autoimmunity. *Nat Rev Immunol.* juill 2014;14(7):447-62.
132. Koenig A, Thaunat O. Lymphoid Neogenesis and Tertiary Lymphoid Organs in Transplanted Organs. *Front Immunol [Internet].* 2016 [cité 3 juin 2020];7. Disponible sur: <https://www.frontiersin.org/articles/10.3389/fimmu.2016.00646/full>
133. Thaunat O, Field AC, Dai J, Louedec L, Patey N, Bloch MF, et al. Lymphoid neogenesis in chronic rejection: Evidence for a local humoral alloimmune response. *Proc Natl Acad Sci.* 11 oct 2005;102(41):14723-8.
134. Kerjaschki D, Regele HM, Moosberger I, Nagy-Bojarski K, Watschinger B, Soleiman A, et al. Lymphatic Neoangiogenesis in Human Kidney Transplants Is Associated with Immunologically Active Lymphocytic Infiltrates. *J Am Soc Nephrol.* 1 mars 2004;15(3):603-12.
135. Wehner JR, Fox-Talbot K, Halushka MK, Ellis C, Zachary AA, Baldwin WMI. B Cells and Plasma Cells in Coronaries of Chronically Rejected Cardiac Transplants. *Transplantation.* 15 mai 2010;89(9):1141-8.
136. Sato M, Hirayama S, Hwang DM, Lara-Guerra H, Wagnetz D, Waddell TK, et al. The Role of Intrapulmonary De Novo Lymphoid Tissue in Obliterative Bronchiolitis after Lung Transplantation. *J Immunol.* 1 juin 2009;182(11):7307-16.
137. Aloisi F, Pujol-Borrell R. Lymphoid neogenesis in chronic inflammatory diseases. *Nat Rev Immunol.* mars 2006;6(3):205-17.
138. Thaunat O, Patey N, Caligiuri G, Gautreau C, Mamani-Matsuda M, Mekki Y, et al. Chronic Rejection Triggers the Development of an Aggressive Intragraft Immune Response through Recapitulation of Lymphoid Organogenesis. *J Immunol.* 1 juill 2010;185(1):717-28.
139. Thaunat O, Graff-Dubois S, Brouard S, Gautreau C, Varthaman A, Fabien N, et al. Immune Responses Elicited in Tertiary Lymphoid Tissues Display Distinctive Features. *PLOS ONE.* 30 juin 2010;5(6):e11398.
140. Celli S, Albert ML, Bousso P. Visualizing the innate and adaptive immune responses underlying allograft rejection by two-photon microscopy. *Nat Med.* juin 2011;17(6):744-9.

141. Zeng F, Chen Z, Chen R, Shufesky WJ, Bandyopadhyay M, Camirand G, et al. Graft-derived extracellular vesicles transported across subcapsular sinus macrophages elicit B cell alloimmunity after transplantation. *Sci Transl Med.* 17 mars 2021;13(585):eabb0122.
142. Liu Q, Rojas-Canales DM, Divito SJ, Shufesky WJ, Stolz DB, Erdos G, et al. Donor dendritic cell-derived exosomes promote allograft-targeting immune response. *J Clin Invest.* 01 2016;126(8):2805-20.
143. Conlon TM, Saeb-Parsy K, Cole JL, Motallebzadeh R, Qureshi MS, Rehakova S, et al. Germinal Center Alloantibody Responses Are Mediated Exclusively by Indirect-Pathway CD4 T Follicular Helper Cells. *J Immunol.* 15 mars 2012;188(6):2643-52.
144. Kwun J, Manook M, Page E, Burghuber C, Hong J, Knechtle SJ. Crosstalk Between T and B Cells in the Germinal Center After Transplantation. *Transplantation.* avr 2017;101(4):704-12.
145. Chen CC, Pouliquen E, Broisat A, Andreatta F, Racapé M, Bruneval P, et al. Endothelial chimerism and vascular sequestration protect pancreatic islet grafts from antibody-mediated rejection. *J Clin Invest.* 2 janv 2018;128(1):219-32.
146. Pouliquen E, Koenig A, Chen CC, Sicard A, Rabeyrin M, Morelon E, et al. Recent advances in renal transplantation: antibody-mediated rejection takes center stage. *F1000prime Rep.* 2015;7:51.
147. Hirohashi T, Chase CM, Della Pelle P, Sebastian D, Alessandrini A, Madsen JC, et al. A novel pathway of chronic allograft rejection mediated by NK cells and alloantibody. *Am J Transplant Off J Am Soc Transplant Am Soc Transpl Surg.* févr 2012;12(2):313-21.
148. Guidicelli G, Guerville F, Lepreux S, Wiebe C, Thauinat O, Dubois V, et al. Non-Complement-Binding De Novo Donor-Specific Anti-HLA Antibodies and Kidney Allograft Survival. *J Am Soc Nephrol JASN.* févr 2016;27(2):615-25.
149. Sicard A, Ducreux S, Rabeyrin M, Couzi L, McGregor B, Badet L, et al. Detection of C3d-binding donor-specific anti-HLA antibodies at diagnosis of humoral rejection predicts renal graft loss. *J Am Soc Nephrol JASN.* févr 2015;26(2):457-67.
150. Gaston RS, Cecka JM, Kasiske BL, Fieberg AM, Leduc R, Cosio FC, et al. Evidence for Antibody-Mediated Injury as a Major Determinant of Late Kidney Allograft Failure. *Transplantation.* juill 2010;90(1):68-74.
151. Sellarés J, de Freitas DG, Mengel M, Reeve J, Einecke G, Sis B, et al. Understanding the causes of kidney transplant failure: the dominant role of antibody-mediated rejection and nonadherence. *Am J Transplant Off J Am Soc Transplant Am Soc Transpl Surg.* févr 2012;12(2):388-99.
152. Elftman MD, Norbury CC, Bonneau RH, Truckenmiller ME. Corticosterone impairs dendritic cell maturation and function. *Immunology.* 2007;122(2):279-90.
153. Oh KS, Patel H, Gottschalk RA, Lee WS, Baek S, Fraser IDC, et al. Anti-Inflammatory Chromatinscape Suggests Alternative Mechanisms of Glucocorticoid Receptor Action. *Immunity.* 15 août 2017;47(2):298-309.e5.
154. Limon JJ, Fruman DA. Akt and mTOR in B Cell Activation and Differentiation. *Front Immunol.* 2012;3:228.
155. Zhang S, Readinger JA, DuBois W, Janka-Junttila M, Robinson R, Pruitt M, et al. Constitutive reductions in mTOR alter cell size, immune cell development, and antibody production. *Blood.* 27 janv 2011;117(4):1228-38.

156. Zhang S, Pruitt M, Tran D, Bois WD, Zhang K, Patel R, et al. B Cell–Specific Deficiencies in mTOR Limit Humoral Immune Responses. *J Immunol*. 15 août 2013;191(4):1692-703.
157. Aagaard-Tillery KM, Jelinek DF. Inhibition of Human B Lymphocyte Cell Cycle Progression and Differentiation by Rapamycin. *Cell Immunol*. 1 juill 1994;156(2):493-507.
158. Wicker LS, Boltz Jr. RC, Matt V, Nichols EA, Peterson LB, Sigal NH. Suppression of B cell activation by cyclosporin A, FK506 and rapamycin. *Eur J Immunol*. 1990;20(10):2277-83.
159. Kay JE, Kromwel L, Doe SE, Denyer M. Inhibition of T and B lymphocyte proliferation by rapamycin. *Immunology*. avr 1991;72(4):544-9.
160. Ersching J, Efeyan A, Mesin L, Jacobsen JT, Pasqual G, Grabiner BC, et al. Germinal Center Selection and Affinity Maturation Require Dynamic Regulation of mTORC1 Kinase. *Immunity*. 20 juin 2017;46(6):1045-1058.e6.
161. Li B, Li Z, Wang P, Huang Q, Xu L, He R, et al. Mammalian target of rapamycin complex 1 signalling is essential for germinal centre reaction. *Immunology*. 2017;152(2):276-86.
162. Chiu H, Jackson LV, Oh KI, Mai A, Ronai ZA, Ruggero D, et al. The mTORC1/4E-BP/eIF4E Axis Promotes Antibody Class Switching in B Lymphocytes. *J Immunol*. 15 janv 2019;202(2):579-90.
163. Domínguez Conde C, Xu C, Jarvis LB, Rainbow DB, Wells SB, Gomes T, et al. Cross-tissue immune cell analysis reveals tissue-specific features in humans. *Science*. 13 mai 2022;376(6594):eabl5197.
164. Uhlén M, Björling E, Agaton C, Szgyarto CAK, Amini B, Andersen E, et al. A Human Protein Atlas for Normal and Cancer Tissues Based on Antibody Proteomics. *Mol Cell Proteomics*. 1 déc 2005;4(12):1920-32.
165. Wadia PP, Herrera ND, Abecassis MM, Tambur AR. Mycophenolic acid inhibits maturation and function of human dendritic cells and B cells. *Hum Immunol*. 1 sept 2009;70(9):692-700.
166. Matz M, Lehnert M, Lorkowski C, Fabritius K, Unterwalder N, Doueiri S, et al. Effects of sotrastaurin, mycophenolic acid and everolimus on human B-lymphocyte function and activation. *Transpl Int*. 2012;25(10):1106-16.
167. Karnell JL, Karnell FG, Stephens GL, Rajan B, Morehouse C, Li Y, et al. Mycophenolic acid differentially impacts B cell function depending on the stage of differentiation. *J Immunol Baltim Md 1950*. 1 oct 2011;187(7):3603-12.
168. Xie A, Yan H, Fu J, He A, Xiao X, Li XC, et al. T follicular helper and memory cell responses and the mTOR pathway in murine heart transplantation. *J Heart Lung Transplant Off Publ Int Soc Heart Transplant*. févr 2020;39(2):134-44.
169. Zeng H, Cohen S, Guy C, Shrestha S, Neale G, Brown SA, et al. mTORC1 and mTORC2 Kinase Signaling and Glucose Metabolism Drive Follicular Helper T Cell Differentiation. *Immunity*. 20 sept 2016;45(3):540-54.
170. Yang J, Lin X, Pan Y, Wang J, Chen P, Huang H, et al. Critical roles of mTOR Complex 1 and 2 for T follicular helper cell differentiation and germinal center responses. *Rath S, éditeur. eLife*. 30 sept 2016;5:e17936.
171. Huang B, Phelan JD, Preite S, Gomez-Rodriguez J, Johansen KH, Shibata H, et al. In vivo CRISPR screens reveal a HIF-1 α -mTOR-network regulates T follicular helper versus Th1 cells. *Nat Commun*. 10 févr 2022;13(1):805.

172. Winslow MM, Gallo EM, Neilson JR, Crabtree GR. The Calcineurin Phosphatase Complex Modulates Immunogenic B Cell Responses. *Immunity*. 1 févr 2006;24(2):141-52.
173. Heidt S, Roelen DL, Eijsink C, Eikmans M, van Kooten C, Claas Fhj, et al. Calcineurin inhibitors affect B cell antibody responses indirectly by interfering with T cell help. *Clin Exp Immunol*. févr 2010;159(2):199-207.
174. Dutta D, Barr VA, Akpan I, Mittelstadt PR, Singha LI, Samelson LE, et al. Recruitment of calcineurin to the TCR positively regulates T cell activation. *Nat Immunol*. févr 2017;18(2):196-204.
175. Otsuka S, Melis N, Gaida MM, Dutta D, Weigert R, Ashwell JD. Calcineurin inhibitors suppress acute graft-versus-host disease via NFAT-independent inhibition of T cell receptor signaling. *J Clin Invest* [Internet]. 1 juin 2021 [cité 6 oct 2022];131(11). Disponible sur: <https://www-jci-org.proxy.insermbiblio.inist.fr/articles/view/147683>
176. Wallin EF, Hill DL, Linterman MA, Wood KJ. The Calcineurin Inhibitor Tacrolimus Specifically Suppresses Human T Follicular Helper Cells. *Front Immunol* [Internet]. 2018 [cité 19 sept 2022];9. Disponible sur: <https://www.frontiersin.org/articles/10.3389/fimmu.2018.01184>
177. Steines L, Poth H, Schuster A, Amann K, Banas B, Bergler T. Disruption of Tfh:B Cell Interactions Prevents Antibody-Mediated Rejection in a Kidney Transplant Model in Rats: Impact of Calcineurin Inhibitor Dose. *Front Immunol* [Internet]. 2021 [cité 6 oct 2022];12. Disponible sur: <https://www.frontiersin.org/articles/10.3389/fimmu.2021.657894>
178. Quéméneur L, Flacher M, Gerland LM, Ffrench M, Revillard JP, Bonnefoy-Berard N. Mycophenolic Acid Inhibits IL-2-Dependent T Cell Proliferation, But Not IL-2-Dependent Survival and Sensitization to Apoptosis. *J Immunol*. 1 sept 2002;169(5):2747-55.
179. Taves MD, Ashwell JD. Glucocorticoids in T cell development, differentiation and function. *Nat Rev Immunol*. avr 2021;21(4):233-43.
180. Kowalczyk A, D'Souza CA, Zhang L. Cell-extrinsic CTLA4-mediated regulation of dendritic cell maturation depends on STAT3. *Eur J Immunol*. avr 2014;44(4):1143-55.
181. Leibler C, Thiolat A, Héniqne C, Samson C, Pilon C, Tamagne M, et al. Control of Humoral Response in Renal Transplantation by Belatacept Depends on a Direct Effect on B Cells and Impaired T Follicular Helper-B Cell Crosstalk. *J Am Soc Nephrol*. 1 mars 2018;29(3):1049-62.
182. Sage PT, Paterson AM, Lovitch SB, Sharpe AH. The Coinhibitory Receptor CTLA-4 Controls B Cell Responses by Modulating T Follicular Helper, T Follicular Regulatory, and T Regulatory Cells. *Immunity*. 18 déc 2014;41(6):1026-39.
183. Wang CJ, Heuts F, Ovcinnikovs V, Wardzinski L, Bowers C, Schmidt EM, et al. CTLA-4 controls follicular helper T-cell differentiation by regulating the strength of CD28 engagement. *Proc Natl Acad Sci*. 13 janv 2015;112(2):524-9.
184. Young JS, Chen J, Miller ML, Vu V, Tian C, Moon JJ, et al. Delayed Cytotoxic T Lymphocyte-Associated Protein 4-Immunoglobulin Treatment Reverses Ongoing Alloantibody Responses and Rescues Allografts From Acute Rejection. *Am J Transplant*. 2016;16(8):2312-23.
185. Chen J, Yin H, Xu J, Wang Q, Edelblum KL, Sciammas R, et al. Reversing Endogenous Alloreactive B Cell GC Responses With Anti-CD154 or CTLA-4Ig. *Am J Transplant*. 2013;13(9):2280-92.

186. Ochsenbein AF, Pinschewer DD, Odermatt B, Ciurea A, Hengartner H, Zinkernagel RM. Correlation of T Cell Independence of Antibody Responses with Antigen Dose Reaching Secondary Lymphoid Organs: Implications for Splenectomized Patients and Vaccine Design. *J Immunol.* 15 juin 2000;164(12):6296-302.
187. Chen CC, Koenig A, Saison C, Dahdal S, Rigault G, Barba T, et al. CD4+ T Cell Help Is Mandatory for Naive and Memory Donor-Specific Antibody Responses: Impact of Therapeutic Immunosuppression. *Front Immunol.* 2018;9:275.
188. Harper IG, Ali JM, Harper SJF, Wlodek E, Alsughayyir J, Negus MC, et al. Augmentation of Recipient Adaptive Alloimmunity by Donor Passenger Lymphocytes within the Transplant. *Cell Rep.* 10 2016;15(6):1214-27.
189. Khoury DS, Cromer D, Reynaldi A, Schlub TE, Wheatley AK, Juno JA, et al. Neutralizing antibody levels are highly predictive of immune protection from symptomatic SARS-CoV-2 infection. *Nat Med.* juill 2021;27(7):1205-11.
190. Sahin U, Muik A, Derhovanessian E, Vogler I, Kranz LM, Vormehr M, et al. COVID-19 vaccine BNT162b1 elicits human antibody and TH1 T cell responses. *Nature.* oct 2020;586(7830):594-9.
191. Feng S, Phillips DJ, White T, Sayal H, Aley PK, Bibi S, et al. Correlates of protection against symptomatic and asymptomatic SARS-CoV-2 infection. *Nat Med.* 29 sept 2021;1-9.
192. Goldblatt D, Alter G, Crotty S, Plotkin SA. Correlates of protection against SARS-CoV-2 infection and COVID-19 disease. *Immunol Rev.* 2022;310(1):6-26.
193. Schwarz M, Torre D, Lozano-Ojalvo D, Tan AT, Tabaglio T, Mzoughi S, et al. Rapid, scalable assessment of SARS-CoV-2 cellular immunity by whole-blood PCR. *Nat Biotechnol.* 13 juin 2022;1-10.
194. Boyarsky BJ, Werbel WA, Avery RK, Tobian AAR, Massie AB, Segev DL, et al. Antibody Response to 2-Dose SARS-CoV-2 mRNA Vaccine Series in Solid Organ Transplant Recipients. *JAMA.* 1 juin 2021;325(21):2204-6.
195. Benotmane I, Gautier-Vargas G, Cognard N, Olagne J, Heibel F, Braun-Parvez L, et al. Low immunization rates among kidney transplant recipients who received 2 doses of the mRNA-1273 SARS-CoV-2 vaccine. *Kidney Int.* juin 2021;99(6):1498-500.
196. Marion O, Del Bello A, Abravanel F, Faguer S, Esposito L, Laure Hebral A, et al. Predictive Factors for Humoral Response After 2-dose SARS-CoV-2 Vaccine in Solid Organ Transplant Patients. *Transplant Direct.* janv 2022;8(1):e1248.
197. Chavarot N, Ouedrani A, Marion O, Leruez-Ville M, Vilain E, Baaziz M, et al. Poor Anti-SARS-CoV-2 Humoral and T-cell Responses After 2 Injections of mRNA Vaccine in Kidney Transplant Recipients Treated With Belatacept. *Transplantation.* 1 sept 2021;105(9):e94-5.
198. Ou MT, Boyarsky BJ, Chiang TPY, Bae S, Werbel WA, Avery RK, et al. Immunogenicity and Reactogenicity After SARS-CoV-2 mRNA Vaccination in Kidney Transplant Recipients Taking Belatacept. *Transplantation.* sept 2021;105(9):2119-23.
199. Caillard S, Thaunat O. COVID-19 vaccination in kidney transplant recipients. *Nat Rev Nephrol.* 27 sept 2021;
200. Caillard S, Chavarot N, Bertrand D, Kamar N, Thaunat O, Moal V, et al. Occurrence of severe COVID-19 in vaccinated transplant patients. *Kidney Int.* 23 mai 2021;S0085-2538(21)00509-3.

201. Caillard S, Thaunat O, Benotmane I, Masset C, Blancho G. Antibody Response to a Fourth Messenger RNA COVID-19 Vaccine Dose in Kidney Transplant Recipients: A Case Series. *Ann Intern Med* [Internet]. 11 janv 2022 [cité 20 janv 2022]; Disponible sur: <https://www.acpjournals.org/doi/full/10.7326/L21-0598>
202. Benschop RJ, Tuttle JL, Zhang L, Poorbaugh J, Kallewaard NL, Vaillancourt P, et al. The anti-SARS-CoV-2 monoclonal antibody, bamlanivimab, minimally impacts the endogenous immune response to COVID-19 vaccination. *Sci Transl Med*. 9 juin 2022;0(0):eabn3041.
203. Schrezenmeier E, Rincon-Arevalo H, Jens A, Stefanski AL, Hammett C, Osmanodja B, et al. Temporary antimetabolite treatment hold boosts SARS-CoV-2 vaccination-specific humoral and cellular immunity in kidney transplant recipients. *JCI Insight* [Internet]. 9 mai 2022 [cité 13 oct 2022];7(9). Disponible sur: <https://insight.jci.org/articles/view/157836>
204. Lee JH, Sutton HJ, Cottrell CA, Phung I, Ozorowski G, Sewall LM, et al. Long-primed germinal centres with enduring affinity maturation and clonal migration. *Nature*. sept 2022;609(7929):998-1004.
205. Röltgen K, Nielsen SCA, Silva O, Younes SF, Zaslavsky M, Costales C, et al. Immune imprinting, breadth of variant recognition, and germinal center response in human SARS-CoV-2 infection and vaccination. *Cell*. 17 mars 2022;185(6):1025-1040.e14.
206. Garrod KR, Liu FC, Forrest LE, Parker I, Kang SM, Cahalan MD. NK Cell Patrolling and Elimination of Donor-Derived Dendritic Cells Favor Indirect Alloreactivity. *J Immunol Baltim Md 1950*. 1 mars 2010;184(5):2329-36.
207. Laffont S, Seillet C, Ortaldo J, Coudert JD, Guéry JC. Natural killer cells recruited into lymph nodes inhibit alloreactive T-cell activation through perforin-mediated killing of donor allogeneic dendritic cells. *Blood*. 1 août 2008;112(3):661-71.
208. Koenig A, Chen CC, Marçais A, Barba T, Mathias V, Sicard A, et al. Missing self triggers NK cell-mediated chronic vascular rejection of solid organ transplants. *Nat Commun*. 25 nov 2019;10(1):5350.
209. Benveniste PM, Roy S, Nakatsugawa M, Chen ELY, Nguyen L, Millar DG, et al. Generation and molecular recognition of melanoma-associated antigen-specific human $\gamma\delta$ T cells. *Sci Immunol*. 14 déc 2018;3(30):eaav4036.
210. Couzi L, Lafarge X, Pitard V, Neau-Cransac M, Dromer C, Billes MA, et al. Gamma-delta T cell expansion is closely associated with cytomegalovirus infection in all solid organ transplant recipients. *Transpl Int Off J Eur Soc Organ Transplant*. mai 2011;24(5):e40-42.
211. Bachelet T, Couzi L, Pitard V, Sicard X, Rigotherier C, Lepreux S, et al. Cytomegalovirus-Responsive $\gamma\delta$ T Cells: Novel Effector Cells in Antibody-Mediated Kidney Allograft Microcirculation Lesions. *J Am Soc Nephrol*. 1 nov 2014;25(11):2471-82.

ANNEXES

1. Publication 1

Innate (and Innate-like) Lymphoid Cells: emerging immune subsets with multiple roles along transplant life.

Charmetant X*, Bachelet T*, Déchanet-Merville J, Walzer T, Thaunat O.

* : co-premier auteurs

Transplantation. 2021 Dec 1;105(12):e322-e336.

Innate (and Innate-like) Lymphoid Cells: Emerging Immune Subsets With Multiple Roles Along Transplant Life

Xavier Charmetant, MD,¹ Thomas Bachelet, MD, PhD,^{2,3} Julie Déchanet-Merville, PhD,⁴ Thierry Walzer, PhD,¹ and Olivier Thauinat, MD, PhD^{1,5,6}

Abstract. Transplant immunology is currently largely focused on conventional adaptive immunity, particularly T and B lymphocytes, which have long been considered as the only cells capable of allorecognition. In this vision, except for the initial phase of ischemia/reperfusion, during which the role of innate immune effectors is well established, the latter are largely considered as “passive” players, recruited secondarily to amplify graft destruction processes during rejection. Challenging this prevalent dogma, the recent progresses in basic immunology have unraveled the complexity of the innate immune system and identified different subsets of innate (and innate-like) lymphoid cells. As most of these cells are tissue-resident, they are overrepresented among passenger leukocytes. Beyond their role in ischemia/reperfusion, some of these subsets have been shown to be capable of allorecognition and/or of regulating alloreactive adaptive responses, suggesting that these emerging immune players are actively involved in most of the life phases of the grafts and their recipients. Drawing upon the inventory of the literature, this review synthesizes the current state of knowledge of the role of the different innate (and innate-like) lymphoid cell subsets during ischemia/reperfusion, allorecognition, and graft rejection. How these subsets also contribute to graft tolerance and the protection of chronically immunosuppressed patients against infectious and cancerous complications is also examined.

(*Transplantation* 2021;105: e322–e336).

INTRODUCTION

According to World Health Organization reports, terminal failure of a vital organ is the first cause of death in industrialized countries, accounting for approximately 25% of total health expenditures. Solid organ transplantation is the best (often the only) therapeutic option for these patients.

Transplantation procedure however implies exposing the grafts to ischemia/reperfusion, which not only creates damage to the tissues but also represents an immunogenic context^{1,2} favorable to allorecognition: the detection by the recipient’s adaptive immune system of polymorphic

determinants expressed by different individuals of the same species (such as donor-specific major histocompatibility complex [MHC] molecules). Allorecognition in turn results in the generation of immune effectors responsible for graft destruction, a process known as rejection, which represents the first cause of late failure in transplantation.^{3,4} To prevent rejection, transplanted patients are treated with immunosuppressive drugs. Because the latter therapies are nonspecific, they reduce immunosurveillance efficiency and increase the risk of infections and cancers.⁵⁻⁷

The prevalent dogma in transplant immunology is that only adaptive immune effectors (T and B lymphocytes

Received 3 February 2021. Revision received 9 March 2021.

Accepted 25 March 2021.

¹ CIRI, INSERM U1111, CNRS UMR5308, Ecole Normale Supérieure de Lyon, Université Claude Bernard Lyon I, Lyon, France.

² Clinique Saint-Augustin-CTMR, ELSAN, Bordeaux, France.

³ Department of Nephrology, Transplantation, Dialysis and Apheresis, Bordeaux University Hospital, Bordeaux, France.

⁴ CNRS, Immunoconcept, UMR 5164, University of Bordeaux, Bordeaux, France.

⁵ Department of Transplantation, Nephrology and Clinical Immunology, Edouard Herriot Hospital, Hospices Civils de Lyon, Lyon, France.

⁶ Lyon-Est Medical Faculty, Claude Bernard University (Lyon 1), Lyon, France.

X.C. and T.B. contributed equally to this work.

X.C. received funding for his PhD from the Société Francophone de Transplantation. O.T. is supported by the Agence Nationale pour la Recherche

(ANR-16-CE17-0007-01), the Fondation pour la Recherche Médicale (PME20180639518), and the Etablissement Français du Sang.

The authors declare no conflict of interest.

X.C., T.B., T.W., and O.T. wrote the first draft of the article. J.D.-M. participated in initial discussions and reviewed the first version of the article.

Supplemental Visual Abstract; <http://links.lww.com/TP/C208>.

Supplemental digital content (SDC) is available for this article. Direct URL citations appear in the printed text, and links to the digital files are provided in the HTML text of this article on the journal’s Web site (www.transplantjournal.com).

Correspondence: Olivier Thauinat, MD, PhD, CIRI, INSERM U1111, Université Lyon 1, 21 Ave Tony Garnier, 69365 Lyon Cedex 07, France. (olivier.thauinat@inserm.fr).

Copyright © 2021 Wolters Kluwer Health, Inc. All rights reserved.

ISSN: 0041-1337/20/10512-e322

DOI: 10.1097/TP.0000000000003782

equipped with clonal receptors) are capable of allorecognition (through the direct and the indirect pathways).⁸⁻¹⁰ In this vision, innate immune effectors are often overlooked, being only secondarily recruited by allospecific adaptive effectors to amplify graft destruction and accelerate rejection.

Over the last decades, considerable progress has been made in deciphering the complexity of the innate immune system, which consists in a myriad of not only molecular (complement system, for instance) but also cellular effectors belonging to both the myeloid and the lymphoid lineages.

Recent works from the Lakkis group have challenged the previous dogma by demonstrating that innate effectors from the myeloid lineage were capable of allorecognition independently of the adaptive immune system,¹¹⁻¹³ paving the way for the concept of “innate rejection.”

In this article, we synthesize published data on the very recently discovered innate (and innate-like) immune effectors from the lymphoid lineage (Figure 1). These cells are of particular interest in the field of transplant immunology because most of them are tissue-resident, and therefore overrepresented among passenger leukocytes.¹⁴ Furthermore, beyond their role in ischemia/reperfusion, some of these subsets have been shown to be capable of allorecognition and/or of regulating alloreactive adaptive responses, suggesting that these emerging immune players are actively involved in most of the life phases of the grafts and their recipients.

INNATE LYMPHOID CELLS, WHAT'S IN A NAME?

More than 40 y ago, lymphoid cells that could recognize and kill various tumor cell lines without prior stimulation

with cytokines or antigen were identified.¹⁵ These cells, named natural killer (NK) cells with respect to their innate properties, were devoid of antigen receptors encoded by somatically rearranged gene segments. This initial discovery was then followed many years later by the characterization of several other immune cell types capable of rapid cytokine production upon stimulation and with typical lymphoid morphology, despite the lack of a B- or T-cell antigen receptor. Because of their ontological relationships, these cell types were grouped under the name innate lymphoid cells (ILCs). ILCs are now subdivided into 3 groups corresponding to T-cell helper groups in terms of cytokine secretion patterns (Figure 2).

Group 1 ILCs

NK Cells

NK cells are defined by coexpression of T-bet and Eomes transcription factors in both mouse and human, whereas other group 1 ILCs (ie, ILC1s) only express 1 either factor.¹⁶ NK-cell activation is controlled by a series of inhibitory (NKiR) and activating (NKaR) receptors. NKiR mainly engage MHC-I molecules expressed by almost every healthy cell, ensuring tolerance. By contrast, NKaR interact with cellular ligands whose expression is increased upon cell transformation or infection. The relative engagement of NKaR versus NKiR determines NK-cell response: activation (cytokine secretion and cytotoxicity) or tolerance.¹⁷ As opposed to T lymphocytes, which require priming from antigen-presenting cells (APCs), NK cells are naturally poised to kill infected or tumor cells. Yet, NK-cell cytotoxic activity can be enhanced upon stimulation with various cytokines such as interleukin (IL)-2, IL-15, IL-12/IL-18, or IL-21.¹⁸

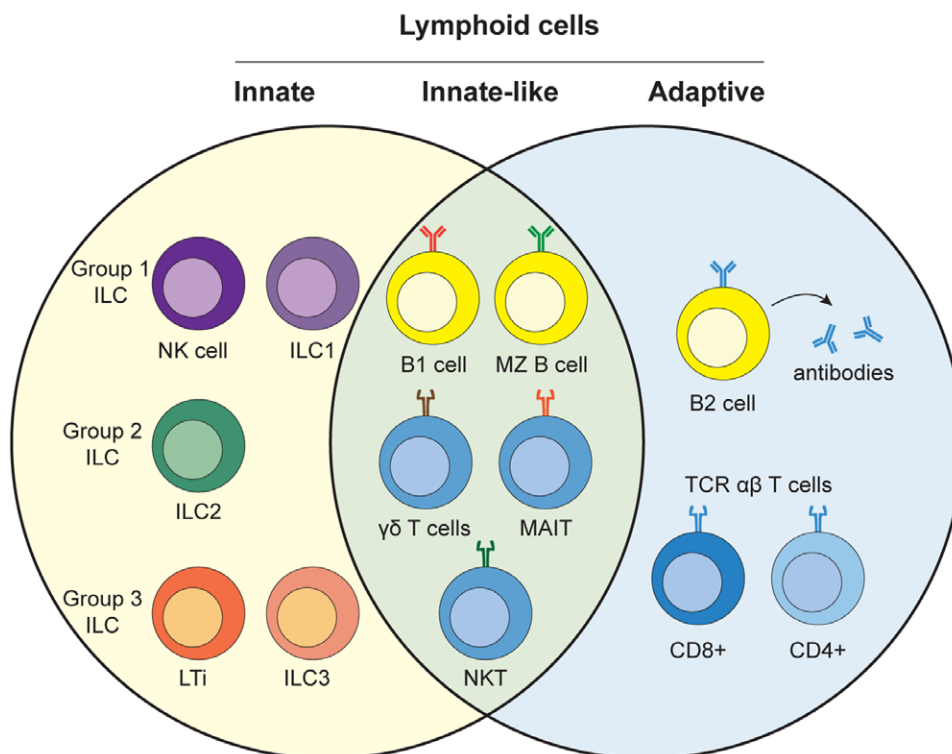


FIGURE 1. A simplified classification for lymphoid cells. ILC, innate lymphoid cell; LTi, lymphoid tissue inducer; MAIT, mucosal-associated invariant T; MZ, marginal zone; NK, natural killer; NKT, natural killer T; TCR, T-cell receptor.






	ILC	Transcription factors	Effectors molecules	Function	Disease association
Group 1	 ILC1	T-bet	IFN γ	Intracellular pathogens	
	 NK cell	T-bet Eomes	Perforin Granzyme IFN γ	Immunity to viruses and intracellular pathogens Tumor surveillance	Viral infection Cancer
Group 2	 ILC2	GATA3	IL-5 IL-13 Amphiregulin	Immunity to helminths	Allergy Asthma
Group 3	 LTi	ROR γ t	IL-17A IL-22 Lymphotoxin	Lymphoid tissue development Immunity to extracellular bacteria	
	 ILC3	ROR γ t	IL-17 IL-22	Homeostasis of epithelia Immunity to extracellular bacteria	Inflammatory bowel disease

FIGURE 2. Characteristics and functions of innate lymphoid cells. IFN, interferon; IL, interleukin; ILC, innate lymphoid cell; LTi, lymphoid tissue inducer; NK, natural killer.

In both mouse and human, immature NK cells express high levels of the CD94/NKG2A NKiR heterodimer, whereas mature NK cells express a higher frequency of inhibitory KIR (killer cell immunoglobulin-like receptor, human) or Ly49 (mouse) receptors allowing missing-self recognition.^{19,20} However, maturation is not sufficient to acquire responsiveness, and NK cells need to be educated to be able to gauge MHC-I surface expression.²¹ This education process involves continuous engagement and signaling through SHP1 of NKiR by their MHC-I ligands. In the absence of such signals, NK cells are hyporesponsive, unable to reject MHC-I-negative cells.

NK cells are the only ILCs known to circulate in the blood at steady state. They are strategically positioned in the lymph nodes (LNs) to rapidly respond to cytokines produced by dendritic cells (DCs) and monocytes upon pathogen infections.^{22,23} Many studies have documented the important role of NK cells in mice infected with various viruses or intracellular pathogens. In humans, a functional redundancy between NK cells and various T-cell subsets may compensate for decreased NK-cell responses. Yet, patients with selective NK-cell deficiencies suffer from recurrent infections, in particular from viruses of the herpes class.²⁴ Many NKaR expressed by NK cells can recognize some viral determinants,²⁵ which further supports this point.

The various and sophisticated evasion processes selected by many viruses to escape NK cells are also an indirect indication that these cells are important for the control of viral infections.²⁶ NK cells also contribute to antitumor

responses. This has been well demonstrated in mouse, where multiple studies have documented the impact of NK-cell depletion/deficiency on tumor growth. NK cells can not only directly recognize and kill tumor *in vivo* but also provide an essential source of interferon- γ (IFN- γ) to polarize and stimulate T-cell responses.²⁷

ILC1s

ILC1s are Eomes⁻/T-bet⁺ in mouse,^{28,29} but various phenotypes have been described in human, with some cells being Eomes⁺/T-bet⁻.¹⁶ ILC1s are tissue-resident and have low cytotoxic activity but have a strong capacity to produce IFN- γ and other inflammatory cytokines in response to cytokine stimulation.^{28,29}

The role of ILC1s in immunity recently came to light when it was found that mice deficient for the Hobit transcription factor had a relatively specific deficiency in ILC1s.³⁰ This new model showed that ILC1s responded very early during viral infections to IL-12 produced by DCs, by producing large amounts of IFN- γ .³¹ ILC1s can also expand and produce cytokines during infections by intracellular parasites.³² Moreover, recent analyses using Hobit-deficient mice have demonstrated that ILC1s and NK cells cooperate in antitumor responses.³³

Group 2 ILCs

Group 2 ILCs only comprise ILC2s that were initially discovered as an important source of type 2 cytokines IL-5 and IL-13 during parasitic infections.³⁴⁻³⁶ ILC2s are tissue-resident and widely distributed, but particularly abundant

at mucosal sites (lung and gastrointestinal tract).³⁷ ILC2s have been described in humans and are defined by their high expression of GATA3.³⁸ ILC2s have the capacity to expand in response to IL-25 and IL-33, upon local or systemic administration of these cytokines or during helminth infections.³⁴⁻³⁶ Moreover, despite the fact that tissue residency was considered a hallmark of helper ILCs, ILC2s were found to recirculate in the blood in response to IL-25 or helminth infection.³⁹

ILC2s are involved in protective immune responses against parasites.^{34,35} The cytokines they express activate multiple cell types, leading to parasite destruction or expulsion. Moreover, they can promote tissue remodeling and repair, notably through the production of amphiregulin, a member of the epithelial growth factor.⁴⁰ Finally, they are also involved in pathological immune responses in cases of allergy, and other types of inflammation at mucosal sites such as skin and airways.⁴¹ Moreover, a recent study reported that IL-33–induced activation of ILC2 suppressed NK-cell antitumor functions through IL-5–induced lung eosinophilia.⁴²

Group 3 ILCs: LTi and Other ILC3s

Group 3 ILC includes 3 main subsets: lymphoid tissue inducers (LTi), and other “non-LTi” ILC3s, including natural cytotoxicity receptors NCR+ and NCR– ILC3. These 3 subsets depend on the transcription factor ROR γ t⁴³ and have the capacity to secrete IL-17A and IL-22.⁴⁴⁻⁴⁶ ILC3s are particularly enriched in the gastrointestinal tract, and LTi are additionally located in lymphoid organs such as LNs and Peyer’s patches. LTi colonize fetal lymphoid structures and are essential for the development of secondary lymphoid organs (LNs and Peyer’s patches but also lymphoid structures associated with the intestinal mucosa called isolated lymphoid follicles).^{43,47,48} LTi induce lymphoid organogenesis through surface expression of lymphotoxin α 1 β 2 and interactions with stromal cells.^{43,47}

Group 3 ILCs participate in antimicrobial responses and maintenance of mucosal integrity. ILC3s are indeed the main source of IL-22 in the small intestine. ILC3-derived IL-22 acts directly on epithelial cells and induces the release of antimicrobial peptides,^{49,50} stimulates antiviral responses against rotavirus by activating IFN- λ pathways,⁵¹ and helps repair and heal the intestinal barrier after inflammation by promoting stem cell proliferation.⁵² LTi also produce IL-17A, an important proinflammatory mediator for antibacterial and antifungal responses that promotes neutrophil infiltration. IL-17–producing ILC3s have been shown to accumulate in the lamina propria of the colon of mice with bacterial-induced colitis and participate in inflammation.⁵³

BEYOND ILC: “INNATE-LIKE” LYMPHOID CELLS

Innate-like Lymphoid Cells

Innate-like lymphoid cells (ILLC) bridge innate and adaptive lymphoid cells (Figures 1 and 3).

Subsets of innate-like B cells have been identified (Figure 1), including B1 and marginal zone B cells.⁵⁴ They are characterized by semi-invariant (or germ-line–encoded) B cell receptor with limited diversity. Consequently, antibodies generated from B1 cells and marginal zone B cells

are polyreactive and autoreactive, with the capacity to recognize conserved structures across species. Following triggering by toll-like receptor agonists or microbial pathogens, innate-like B cells produce a large amount of natural IgM, providing a critical early defense against infections, and IL-10, a key regulatory cytokine that plays a crucial role in downmodulating immune responses.⁵⁵ As evidence of the involvement of innate-like B cells in transplant immunology is scarce, this review will focus on innate-like T cells (ILTCs).

ILTCs share several characteristics, including: (1) expression of a functional T-cell receptor (TCR) that monitors cell surfaces within tissues and acts as a rapid sensor of dysregulation, (2) generation during early life, (3) response that does not require prior clonal expansion, and (4) response that depends on the integration of TCR, cytokine-dependent signals, costimulation, and NK-cell receptor signaling, allowing for a large panel of effector responses depending on the context.

Based on the nature of the TCR, ILTCs can be divided in 3 main types, that is, natural killer T cells (NKT), mucosal-associated invariant T cells (MAIT), and gamma delta ($\gamma\delta$) T cells. In human, MAIT, NKT, and $\gamma\delta$ T cells represent 10%, 0.1%, and 0.5%–20% of circulating T cells, respectively. These proportions are increased among tissue-resident T cells, especially in liver and lung for MAIT and NKT and mucosal tissues for $\gamma\delta$ T cells.

ILTCs undergo thymic selection but are not restricted to MHC because they develop normally in β 2 microglobulin knock-out (KO) mice.⁵⁶ The TCR of NKT, MAIT, and V γ 9+V δ 2+ T cells is semi-invariant but is highly diverse for the other $\gamma\delta$ T cells (owing to RAG-mediated V(D)J recombination).

$\gamma\delta$ T Cells

$\gamma\delta$ T cells are the first T cells to develop in vertebrates. In humans, $\gamma\delta$ T-cell groups are functionally defined based on their γ and δ TCR chain expression: V γ 9+V δ 2+ T cells are usually opposed to V δ 2–negative $\gamma\delta$ T cells.

V γ 9+V δ 2+ T cells sense variations in cellular production of phosphorylated metabolites of the isoprenoid pathway (called phosphoantigens). The most active phosphoantigens are produced by microorganisms such as Gram-positive bacteria, *Mycobacterium tuberculosis*, *Plasmodium falciparum*, and *Toxoplasma gondii*. Less-active endogenous phosphoantigens can also accumulate in host cells upon activation or transformation. The recognition of ubiquitous microbial or stress signals by V γ 9+V δ 2+ TCR is reminiscent of the pattern recognition receptors process and is supported by the semi-invariant V-usage of these $\gamma\delta$ TCRs. Recent breakthroughs underline the importance of butyrophilins, which bind to phosphoantigens intracellularly⁵⁷ and to V γ 9 chain.^{58,59}

All the other $\gamma\delta$ T cells, collectively called V δ 2–negative $\gamma\delta$ T cells (mainly expressing the V δ 1 and V δ 3 chains), but to which the V γ 9–V δ 2+ population was recently integrated,⁶⁰ are considered to recognize a large panel of stress-induced antigens in the context of transformed or infected cells (especially by cytomegalovirus, CMV). Yet, most V δ 2–negative $\gamma\delta$ T-cell antigens remain to be identified. With a shorter CDR3g and a longer CDR3d carrying diversity, the TCR of V δ 2–negative $\gamma\delta$ T cells resembles

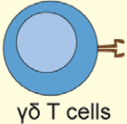
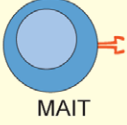
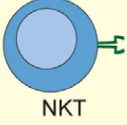
ILLC	TCR specificity	Effectors molecules	Function	Disease association
 γδ T cells	Vγ9+Vδ2+: Phospho-Ag/Butyrophilin Non Vγ9+Vδ2+: Stress-induced Ag	Perforin Granzyme IFNγ IL-17	Lymphoid stress surveillance	Vγ9+Vδ2+: Plasmodium/Toxoplasma/ Gram+ bacteria infections Cancer Non Vγ9+Vδ2+: CMV infection Cancer
 MAIT	Riboflavin metabolites bound to MR1	Perforin Granzyme IFNγ IL-17	Tissue homeostatis Interface immunity	Infections Inflammatory disease Cancer
 NKT	αGalCer (or glyco-/phospholipid Ag) bound to CD1d	Perforin Granzyme IFNγ IL-17 IL-4	Immune response regulation	Cancer Preeclampsia

FIGURE 3. Characteristics and functions of innate-like T cells. Ag, antigen; αGalCer, α-galactosylceramide; CMV, cytomegalovirus; IFN, interferon; IL, interleukin; ILLC, innate-like lymphoid cells; MAIT, mucosal-associated invariant T; NKT, natural killer T; TCR, T-cell receptor.

that of immunoglobulins and can therefore recognize conformational and sequential epitopes. Their ability to differentiate health and stress conditions relies on different mechanisms: differential expression of the TCR ligand upon stress, requirement of costimulatory molecules for full activation, conformational changes of the ligand (multi or monomerization), and differential glycosylation. Although the affinity of their TCR is low, Vδ2-negative γδ T cells interact with their cellular targets with high avidity due to the high density of TCR and ligand molecules on cell surfaces. Over the last decades, a plethora of structurally highly diverse TCR ligands have been identified, often restricted to 1 clone of Vδ2-negative γδ T cell, with no systematic generalization and uncertain physiological relevance.⁶¹ The multiplicity of presumed ligands for Vδ2-negative γδ T cells however illustrates the potentiality of what has been described as “beneficial self-immunogenicity.”⁶²

MAIT Cells

In contrast with mice, MAIT cells are the largest subset of unconventional T cells in human blood and tissue (up to 100 times more than NKTs).

The TCR of MAIT is composed of invariant TCR α chains (Vα7.2)Jα33/12/20) paired with a biased repertoire of Vβ chains (Vβ2 or Vβ13) that recognize a limited range of nonpeptide ligands (riboflavin) presented by monomorphic MHC-like molecules (MR1).^{63,64}

MAIT are CCR7-CD161^{high}CD26^{high} and CD8αα (80%) and constitute a homogeneous population with mixed Th1/Th17 functions and cytotoxic properties (perforin/granzyme), the development of which depends on a microbiota-derived metabolite.⁶⁵

NKT Cells

In contrast with MAIT, the development of NKT cells is conserved in germ-free mice. However, the transcription factor PLZF (promyelocytic leukemia zinc finger)

is important for both MAIT and NKT and governs the acquisition of innate-like characteristics with effector function and memory phenotype in both subsets.⁶⁶⁻⁶⁹

Although their TCR is specific for glycolipid/phospholipid antigens bound to the monomorphic MHC-like molecules CD1,⁷⁰ NKT cells are highly diverse and distributed into 2 subgroups:

Type I NKT or invariant (iNKT), the TCR of which, made of Vα24-Jα18 TCRα chain paired exclusively with Vβ11, is specific for CD1d-restricted α-galactosylceramide glycopeptide (αGalCer);

Type II NKT cells that are noninvariant and their TCR recognizes CD1-restricted diverse sulfatide and lysophosphatidylcholine antigens.

ISCHEMIA REPERFUSION INJURIES

The sequence of ischemia/reperfusion that strikes the transplanted organ is a model of violent sterile inflammation. Perisurgical procedure and each additional hour of ischemia increase the risk of graft failure and mortality.⁷¹

Ischemia/reperfusion injuries (IRI) cause mitochondrial damages due to variation of oxygen access with ATP depletion followed by the release of reactive oxygen species. The subsequent development of an inflammatory response leads to tissue damage and eventual cell death. Tissue-resident ILCs/ILTCs are prearmed effectors, prone to sense the danger signals and mount a rapid response to preserve tissue integrity. However, this response may also exacerbate necroinflammation and thereby promote allorecognition.²

Danger-associated Molecular Patterns and ILCs/ILTCs

IRI promotes the release of alarmins (in particular IL-33). IL-33 is a chromatin-associated nuclear cytokine from the IL-1 family, which is generated in an inflammatory

environment.⁷² In a mouse model of kidney transplantation, microvascular endothelial cells produce IL-33 that in turn signals on its receptor ST2 expressed on iNKT cells. This contributes to their recruitment and cytokine production (IFN- γ and IL-17), resulting in neutrophil infiltration and activation at the injury site.^{73,74} Contrary to their invariant counterparts, NKT may abrogate IRI through the secretion of IL-10.⁷⁵

IL-33 may also activate ILC2s. The expansion of ILC2s has a protective effect in mouse glomerulonephritis⁷⁶ and promotes tissue repair and metabolic homeostasis in adipose tissue.⁷⁷ Protection of IRI by ILC2s is also suggested in kidney and may be mediated by IL-25.⁷⁸

Other ILCs were reported to protect tissue from acute injury with mechanisms that could also intervene in IRI: ILC1s protect mice from acute liver injury after carbon tetrachloride injection via IFN- γ secretion and upregulation of Bcl-xl expression in hepatocytes.⁷⁹ ILC3s are potent producers of IL-22 after intestinal injury and target intestinal stem cell expansion and then intestinal regeneration through STAT3 phosphorylation.⁸⁰

In general, inflammation seems to induce dynamic changes in the balance of ILCs and ILTCs in tissue and in peripheral blood. Recently, ILC1s were reported to be significantly increased in the peripheral blood of patients with acute ST-segment elevation myocardial infarction and associated with poor outcome.⁸¹ If ILCs/ILTCs are sometimes associated with protection, they can also take part in an amplification loop of cell death and inflammation. In this regard, high-mobility group box-1, which is involved in IRI in liver⁸² and in kidney,⁸³ has been shown to exacerbate experimental mouse colitis through ILC3s.⁸⁴

NK Cells, ILC1s and IRI

NK cells promote apoptosis of stressed tubular epithelial cells (TEC).⁸⁵

IRI promote NK-cell recruitment by toll-like receptor 2 engagement^{86,87} or by reverse signaling of CD137L (also known as 4-1BBL and TNFSF9)⁸⁸ with the subsequent production of chemokines and maybe a special role for osteopontin.⁸⁹ However, peripheral NK cells might not be the most important in ischemic kidney injury. In mouse, ILC1s display a distinct phenotype. Compared with circulating NK cells, ILC1s have reduced expression of asialo-GM1 (AsGM1), and anti-AsGM1 antibody treatment therefore does not affect ILC1s. Because anti-AsGM1 antibody fails to protect against IRI, while anti-NK1.1 antibody does, Victorino et al⁹⁰ concluded that ILC1s rather than NK cells might have the prominent role in kidney IRI. Of note, kidney MAIT cells, which get activated in the presence of TECs cultured under hypoxic conditions and display upregulated expression of CD69 and cytotoxic molecules,⁹¹ might also be involved in IRI-induced kidney injury. These data suggest a potential role for passenger leukocytes (ie, originating from the donor, ILC1s and MAIT) in IRI. However, circulating recipient NK cells could also take part in this phenomenon.

The reason why NK cells get activated by ischemia/reperfusion could rely on their ability to sense the discontinuity of self-antigens.⁹² HLA-E is a nonclassical MHC-I molecule with a limited polymorphism that presents a restricted set of nonameric peptides, mainly derived

from the leader sequences of classical HLA-I proteins.⁹³ HLA-E is a major ligand for the NKIR CD94/NKG2A.⁹⁴ During cellular stress, an increased proportion of HLA-E molecules may bind the heat shock protein 60 signal peptide, leading to peptide interference that would gradually uncouple CD94/NKG2A inhibitory recognition and provide a mechanism for NK cells to detect stressed cells.⁹⁵ IRI also promote MHC-I polypeptide-related sequence A (MICA) expression during acute myocardial infarction⁹⁶ or in TEC through hypoxia-inducible factor as a response to hypoxia/reoxygenation.⁹⁷ NKG2D is the receptor for the stress-inducible MICA, and its engagement activates a cytolytic response in NK cells.⁹⁸ Cytotoxicity resulting from NK-cell activation through NKG2D may lead to allograft damage as already reported in the development of murine bronchiolitis obliterans.⁹⁹ Interestingly, MAIT,¹⁰⁰ iNKT,¹⁰¹ and $\gamma\delta$ T cells⁹⁸ also express NKG2D and could take part in this pathological process.

$\gamma\delta$ T Cells and IRI

Annexin A2 is unique among annexins in that it possesses redox-sensitive cysteine(s).¹⁰² Cells exposed to reactive oxygen species upregulate the expression of surface annexin A2, which is a ligand for a V γ 8V δ 3 TCR.¹⁰³ Annexin A2 can stimulate the proliferation of a fraction of (V δ 2-) T cells within peripheral blood mononuclear cells (PBMCs), and other annexin A2-specific $\gamma\delta$ T-cell clones could be derived from PBMCs.¹⁰³ The V γ 4V δ 5 TCR mediates recognition of broadly stressed human cells by engaging a stress-regulated self-antigen (endothelial protein C receptor) coexpressed with stress-induced costimulatory ligands.¹⁰⁴ β 2-microglobulin-free HLA-I heavy chain or open conformer can be recognized as a stress antigen by V γ 9V δ 3 T cells.¹⁰⁵ MIC-A/B are also directly recognized by the TCR of tumor-infiltrating $\gamma\delta$ T cells.¹⁰⁶

Finally, Guerville et al have demonstrated that TCR signaling sensitizes $\gamma\delta$ T cells to inflammatory mediators, and in particular IL-18, the receptor of which is upregulated at the cell surface after TCR engagement. Moreover, IL-18 secretion, which follows the caspase-1 inflammasome activation in stressed cells, could be a unified signal to alert $\gamma\delta$ T cells.¹⁰⁷

A mouse model of ischemic brain injury confirms the implication of IL-17 production by $\gamma\delta$ T cells in the delayed phase of ischemia-reperfusion,¹⁰⁸ with the implication of peroxiredoxin family proteins as key initiators.¹⁰⁹ Commensal microbiota affects ischemic stroke by regulating intestinal $\gamma\delta$ T cells.¹¹⁰ This implication of $\gamma\delta$ was found in other models of renal IRI.¹¹¹

At present, there are no data that would allow the responsibility of passenger $\gamma\delta$ versus recipient's $\gamma\delta$ T cells to be apportioned in the IRI mechanisms. It is conceivable that both populations are involved: the first one inside the graft and the second one at the blood/graft endothelium interface.

ALLORECOGNITION

Allorecognition designates the recognition by the recipient's adaptive immune system of donor-specific alloantigens. Several pathways of allorecognition have been evidenced.⁸⁻¹⁰ The direct pathway involves the recognition of intact allogeneic HLA molecules on the surface of

donor passenger APCs. The semidirect pathway resembles the direct pathway, but this time the intact allogeneic HLA molecules are on the surface of the recipient APCs after transfer via exosomes or extracellular vesicles.^{112,113} In contrast, the indirect pathway involves recognition by the recipient's T cells of peptides derived from allogeneic HLA molecules and presented within self-HLA molecules.^{114,115}

Because the TCRs of ILTCs (MAIT, $\gamma\delta$ T cells, and NKT) do not bind to MHC molecules, there is no evidence in the literature that these cell subsets can participate in allorecognition through any of the 3 pathways described above. However, there are other (TCR-independent) mechanisms by which ILCs/ILTCs may participate in allorecognition.

ILC3s Support Primary and Memory Adaptive Immune Responses

LTi are crucial for the development of secondary lymphoid organs, which are essential for building up an allo-immune response. Splenectomized, *aly^{-/-}* mice, which lack all secondary lymphoid organs, are unable to mount an adaptive response after allogeneic heart transplantation and “ignore” the graft that is therefore not rejected.¹¹⁶ It remains unclear whether LTi also participate in chronic rejection-associated lymphoid neogenesis and the formation of intragraft tertiary lymphoid structures.¹¹⁷⁻¹¹⁹

A study has reported that following stimulation with IL-1 β , ILC3s upregulate MHC-II and costimulation molecules (CD40, CD80, CD86) and that they are capable of processing protein antigens and eliciting a CD4 T response *in vitro*. *In vivo*, the cognate interaction between ILC3s and CD4 T leads to proliferation of the latter while its blockade inhibits thymo-dependent B responses.¹²⁰ However, the fact that ILCs may present antigens is not universally accepted and needs to be confirmed.

Finally, LTi that express high levels of tumor necrosis factor ligands (OX40L and CD30L) are important for the survival of CD4+ memory T lymphocytes in the secondary lymphoid organs¹²¹ and for secondary antibody responses.¹²²

The Elusive Role of $\gamma\delta$ T Cells in Alloimmune Responses

Studies published over a decade ago have reported that $\gamma\delta$ T cells can interact with B cells, promote the formation of germinal centers, and induce the production of switched antibodies of IgE and IgG1 isotypes in mouse models.¹²³⁻¹²⁵ The V γ 9+V δ 2+ cells express CXCR5, which allows their positioning in the B-cell areas of the secondary lymphoid organs. V γ 9+V δ 2+ cells have been shown to support the production of switched antibodies, in a way that is dependent on CD40L, ICOS, and ILs 4 and 10.¹²⁶ Beyond their “T follicular help (Tfh)-like” function, $\gamma\delta$ T cells could also act indirectly by inducing Tfh differentiation through (1) the secretion of Wnt agonists, which allow the Tfh program to be initiated under the control of *Ascl2*¹²⁷ and (2) the presentation of antigenic peptides within MHC-II.¹²⁸ Collectively, this literature supports the idea that recipient $\gamma\delta$ T cells could participate in humoral alloimmune response. However, in a recent set of experiments conducted in a murine model of heart transplantation, our group failed to show any defects in donor-specific

antibody (DSA) generation in recipient mice devoid of $\gamma\delta$ T cells or any generation of DSA in recipient mice with only $\gamma\delta$ T cells. Other evidence that $\gamma\delta$ T cells are incapable of allorecognition comes from the observation that they cannot induce graft-versus-host disease (GVHD) in mice.¹²⁹

Role of ILC and ILTCs in Tolerance to Allogeneic Transplants

NK Cells Control the Direct Allorecognition Pathway

Beilke et al¹³⁰ have reported that tolerance to allogeneic pancreatic islets in mice is dependent on the recipient's NK cells. Other studies using a skin graft model have proven that NK-cell-dependent tolerance results from the destruction of the donor's passenger APCs contained in the graft,¹³¹ which in turn prevents the priming of the recipient's T lymphocytes through the direct pathway.^{132,133} The same mechanism allows the recipient's NK cells to destroy donor's passenger CD4+ T cells and thereby block the activation of the recipient's B cells and the magnitude of the humoral response.¹³⁴ In all these studies, donor mice were of H-2^d genetic background, whereas recipient mice were H-2^b, and it was discovered that the H-2D^d molecules expressed on the surface of the graft cells constituted a ligand for the NKAR Ly49D.^{133,135} Of note, the recipient's NK cells could use the same mechanism to also destroy the syngeneic APCs involved in the semidirect pathway (after capture of the donor's intact MHC-I).

Nkp44 is another activating immunoglobulin-like receptor¹³⁶ expressed by activated NK lymphocytes (and a small number of T lymphocytes $\gamma\delta$).^{136,137} Niehrs et al¹³⁸ recently reported that Nkp44 binds to HLA-DP*0401,¹³⁹ a molecule highly expressed by activated APCs. Although no studies have been conducted so far to validate this hypothesis, it is tempting to speculate that Nkp44 could suppress the direct allorecognition pathway in humans, as Ly49D does in mice.

NKT and Tolerance

Although NKT deficiency does not modify the prognosis after allogeneic heart transplantation, this subset of ILLC seems to participate in the tolerance induced by the LFA-1 or CD28/B7 blockade. Indeed, tolerance to an allogeneic heart transplant induced by such immunosuppressive protocols is lost in the absence of NKT cells and restored after transfer of these cells in NKT KO mice.¹⁴⁰ Furthermore, in tolerant mice, NKT lymphocytes produce more IL-10, and this production is associated with the induction of IL-10-producing regulatory DCs and CD4+ T cells.¹⁴¹ Other teams have reported the involvement of NKT cells in islet graft tolerance but suggest that their role depends on TGF β in this context.¹⁴² How NKT cells are activated and acquire their tolerogenic functions after transplantation remains unknown.

$\gamma\delta$ T Cells and Tolerance to Liver Allograft

Alterations of the $\gamma\delta$ T lymphocyte compartment after viral (in particular CMV) infections have been frequently observed in liver and kidney transplant patients.^{143,144} Interestingly, CMV infections have been associated with decreased reactivity of allospecific T lymphocytes and a lower incidence of late cell rejection after liver transplantation. The virus-induced remodeling of the $\gamma\delta$ compartment

favors the V δ 1 subset,¹⁴⁵ a population identified in the signature of tolerant liver transplant patients,^{146,147} but absent in rejected organs.¹⁴⁸ Some authors have proposed using the V δ 1 signature as a diagnostic test of operational tolerance, a phenomenon commonly observed after liver transplantation.¹⁴⁷ Whether the V δ 1 T lymphocytes are only a marker or are also players (and through which mechanisms) of this tolerance remains to be clarified.

MAIT Cells Prevent GVHD of the Gut

Colonic MAIT cells locally suppress the presentation of alloantigens by a donor's DCs, thus limiting the expansion of effector alloreactive T and GVHD lesions in the gut.¹⁴⁹ These data suggest that further exploration of the role of MAIT cells in intestinal transplantation is needed.

ILCS AND ILTCS INFLUENCE ON THE MECHANISMS OF GRAFT DESTRUCTION

Missing Self-induced NK-Cell Activation and Chronic Vascular Rejection

In contrast to the adaptive alloimmune response, in which the priming (ie, allorecognition, see above) and effector phases are separated, both in time and space, innate immune cells sense the allogeneic nonself and react against it in the same movement.

More than a decade ago, Uehara et al¹⁵⁰ demonstrated that chronic vascular rejection lesions develop in cardiac allografts transplanted from parental to unmanipulated F1 hybrid mice, a transplant system that lacks specific antidonor T-cell reactivity but retains antidonor NK-cell responses. van Bergen et al¹⁵¹ reported that the existence of mismatches between NKiR of the recipient and MHC-I of the graft correlated with reduced graft survival after an HLA-A, B, and DR compatible kidney transplantation. A translational study recently shed light on the molecular mechanisms underlying these observations. Recipient's NK cells are equipped with surface NKiR, which have MHC-I molecules as ligands. Because the endothelium of a transplanted organ expresses the donor's MHC-I molecules, certain donor/recipient pairs create a "missing-self" situation, in which the endothelial cells of the graft are unable to deliver HLA-I-mediated inhibitory signals to recipient circulating NK cells. If the proportion of NK cells expressing the educated NKiR in the recipient are sufficient and following priming (by viral infection or IRI, for instance), the missing-self activates NK cells, which in turn promotes microvascular inflammation leading to reduced survival of the graft.^{152,153} This new type of "innate" chronic vascular rejection could account for a significant (30%–50%) fraction of patients with microvascular inflammation on graft biopsy but no detectable DSA in circulation.¹⁵² This is of importance because, in contrast with chronic (ie, complement-independent) antibody-mediated rejection (AMR), for which no efficient therapy is available, the mechanistic target of rapamycin (mTOR) inhibitor can prevent the development of "innate" chronic vascular rejection in a murine model.¹⁵² It is of note that an important proportion of $\gamma\delta$ T cells also express NKiR^{154,155} and could thereby also participate in the response to missing-self situations.

If a defect in inhibitory signals is sufficient to activate the NK cells within the microvascularization of the graft, it

is tempting to speculate that an excess of activation signals could do the same. MICA is a ligand of the NKaR NKG2D. MICA molecules are constitutively expressed on the surface of endothelial cells.^{156,157} This highly polymorphic protein^{158,159} can induce a humoral adaptive alloimmune response resulting in the production of anti-MICA DSA.^{157,160,161} Interestingly, MICA polymorphisms also affect its binding to NKG2D. In particular, the MICA-129/Met polymorphism induces stronger NKG2D signaling.¹⁶² It is therefore plausible that when the NK cells of a MICA-129/Met-negative recipient encounter MICA molecules on the surface of graft from a MICA-129/Met-positive donor, recipient's NK cells get activated, leading to "innate" chronic vascular rejection without "missing-self." Along the same line, Nkp44 is another NKaR that binds to HLA-DP*0401. Endothelial cells of the grafts express MHC-II molecules upon exposure to inflammatory cytokines.¹⁶³ It is therefore conceivable that the endothelium of the grafts from an HLA-DP*0401-positive donor could trigger activation of the recipient's NK cells.

Fc γ R-expressing ILCs and ILTCs Contribute to Chronic AMR Pathophysiology

AMR associated with acute dysfunction of the graft is due to activation of the classical complement pathway.¹⁶⁴ Lower titers of DSA fail to activate the complement but are still associated with reduced graft survival due to (complement-independent) chronic AMR.¹⁶⁵

Colvin's group was the first to demonstrate the crucial role of NK cells in the pathophysiology of chronic AMR. Using a murine model in which an allogeneic heart was transplanted to RAG-KO recipients (devoid of T and B cells) that were passively transfused with DSA, they showed that the recipient's NK cells infiltrate the intima of the arteries of chronically rejected grafts¹⁶⁶ and that NK-cell depletion abrogated the development of vascular lesions.¹⁶⁶⁻¹⁶⁸ DSA bound to the surface of graft endothelium, indeed recruits NK cells through their crystallizable fragment, which binds to the CD16 (Fc γ RIII) receptor^{169,170} and triggers ADCC (antibody-dependent cellular cytotoxicity) and microvascular inflammation lesions.^{167,171,172}

These experimental data were then confirmed in clinical studies. The humoral rejection biopsies of kidney grafts were enriched with specific transcripts of NK lymphocytes^{173,174} as a result of CD16-dependent signals.¹⁷⁵

Finally, our group recently demonstrated that the two mechanisms by which NK cells can get activated by an allogeneic transplant (ie, missing-self and ADCC) can synergize to accelerate kidney graft loss in patients with low DSA titers.¹⁷⁶

It has been shown that CMV infection in renal transplant recipients induces the expansion of a subpopulation of V δ 2-negative T cells, which represents a population as large as NK cells among CD16-expressing PBMCs¹⁷⁷ and maintains over time.¹⁴⁴ Interestingly, CD16-expressing V δ 2-negative T cells can perform ADCC *in vitro* against allogeneic target cells coated with DSA. The involvement of V δ 2-negative T cells in AMR pathophysiology is further suggested *in vivo* by: (1) the observation of V δ 2-negative T cells in contact with microvascular cells in AMR biopsies of kidney grafts, and (2) the fact that their frequency in circulation is inversely correlated with graft function in patients with DSA.¹⁷⁸

Some authors have proposed that $\gamma\delta$ T cells could also promote graft destruction by providing IL-17, which accelerates allograft rejection by locally increasing inflammation and preventing the expansion of regulatory T cells.^{179,180} This hypothesis is supported by data from murine heart transplantation models but remains to be confirmed in humans.

I(L)LCs-mediated Graft Protection

As suggested above, ILCs play a crucial role in the homeostasis of mucosal organs, particularly the lung and intestine, and participate in the repair of damaged epithelia. For instance, influenza virus triggers an IL-33–dependent response in the lungs leading in ILCs to the upregulation of genes involved in tissue repair, including amphiregulin, an essential mediator of functional recovery of the lungs after infection.⁴⁰ If intestine damage is present, ILC3 synthesizes IL-22 to promote regeneration of the epithelium by intestinal stem cells.⁸⁰ They also contribute to the maintenance of intestinal homeostasis via the secretion of IL-22, IL-17, and granulocyte-macrophage colony-stimulating factor, which participate in the maintenance of the equilibrium between antimicrobial defense and tolerance of commensal bacteria.¹⁸¹⁻¹⁸⁴

In the field of transplantation, emerging data seem to confirm the protective role of ILCs. In a murine model of lung transplantation, it has been reported that the production of IL-22 by intra-graft ILC3 (and $\gamma\delta$ T cells) allows for recruiting the recipient's B lymphocytes within the bronchus-associated lymphoid tissue and thereby promotes long-term lung graft tolerance.^{185,186} In accordance with this concept, a recent clinical study has established a correlation between lung graft dysfunction and a decrease in ILC2 in lung tissue.¹⁸⁷ In addition, NK and NKT cells could also protect allografts. Chronic lung rejection is associated with a decrease in the expression, by NK and NKT cells, of anti-inflammatory molecules, which (if increased by drug treatments) could potentially improve graft survival.^{188,189}

Donor chimerism is long lasting in the ILC compartment of intestinal transplant,^{190,191} and whether they originate from the recipient or the donor, ILC3s seem to be associated with the clinical outcome. A first study has indeed reported that early repopulation of intestinal grafts by IL-22–synthesizing ILC3 is associated with a better outcome,¹⁹² whereas a second work has shown that intestinal rejection is associated with a local decrease in ILC3 and IL-22 secretion.¹⁹³

ILCS AND ILTCS PROTECT TRANSPLANT RECIPIENTS OF THE SIDE EFFECTS OF THERAPEUTIC IMMUNOSUPPRESSION

Prevention of rejection in transplant recipients relies on nonspecific life-long immunosuppression, which increases the risk for infection and neoplasia.

Most immunosuppressive regimens include an induction followed by maintenance with a combination of drugs. Depleting agents used for induction (thymoglobulin, alemtuzumab, etc) are antibodies; they have limited ability to diffuse outside the circulation,¹⁹⁴ which suggests that tissue-resident cell subsets are relatively preserved. Maintenance immunosuppression principally relies on calcineurin inhibitors that target the signal

1 of activation, downstream from the T- or B-CR of lymphocytes. Classical immunosuppressive strategies could thus spare ILCs (and to a certain extent ILTCs, which can be activated through TCR-independent pathways).^{195,196} This specificity, together with the fact that ILCs or ILTCs have important roles in first-line defense against infections and tumors, suggests that these cells could play an important protective role in transplant recipients.

Roles of ILCs in Infections and Cancers

Gut ILCs have critical roles in cytokine-mediated regulation of intestinal epithelial cell barrier integrity. ILCs that express MHC class II, and can process and present antigen, also regulate CD4+ T cell and limit pathological adaptive immune cell responses to commensal bacteria.¹⁸²

ILC1s have been implicated in the response against 2 classical pathogens following transplantation: CMV³¹ and *Toxoplasma gondii*.¹⁹⁷ ILC1s also play a critical role for the maintenance of lung airway epithelial integrity, especially following infection with influenza virus,⁴⁰ a role they share with iNKT cells.¹⁹⁸

The role of NK cells and other ILCs in tumors has been extensively reviewed elsewhere.^{199,200} We will here only underlie the important graft-versus-leukemia effect of NK cells. The donor NK-cell alloreactivity is indeed effective in mismatched hematopoietic transplants in protecting the recipient.²⁰¹ Early NK-cell recovery is associated with better cancer-free survival after autologous hematopoietic stem cell transplantation.²⁰² In solid organ transplants, dysfunction of NK cells (decreased expression of NKP46, decreased number of IFN- γ –producing NK cells) is associated with posttransplant malignancy.^{203,204}

NK cells function also predicts severe infection in kidney transplant recipients.²⁰⁵ Interestingly, a more specific role for NK cells in anti-CMV response was recently highlighted. NK cells exhibit adaptive immune features after CMV infection in mouse (proliferation capacity, memory phenotype, and efficacy of adoptive transfer²⁰⁶). CMV reactivation after allogeneic transplantation promotes a long-lasting increase in adaptive NKG2C+ NK cells with more potent functions.²⁰⁷ Human CMV also imprints KIR repertoire towards activating KIR with the expansion of a unique NKG2C+CD57+ subset of NK cells.^{208,209} These CMV NKG2C+ NK cells were enriched in bronchoalveolar lavages of lung allograft and inversely correlated with CMV blood titers.²¹⁰ This subset may therefore represent a signature associated with reduced incidence of posttransplantation symptomatic CMV.²¹¹

Roles of ILTCs in Infections and Cancers

MAIT cells are involved in the maintenance of gut integrity and in the response to a large panel of bacteria,^{212,213} including the very common *Escherichia coli* that induces pyelonephritis, and viruses.^{214,215}

The role of V δ 2–negative $\gamma\delta$ T cells in CMV response was first demonstrated in immunocompromised solid organ transplant recipients.^{144,216} This seminal observation has since been extended to other settings of $\alpha\beta$ T-cell deficiencies: immaturity,²¹⁷ congenital immunodeficiency,²¹⁸ bone marrow transplantation,²¹⁹ and finally, also confirmed in healthy blood donors.²²⁰

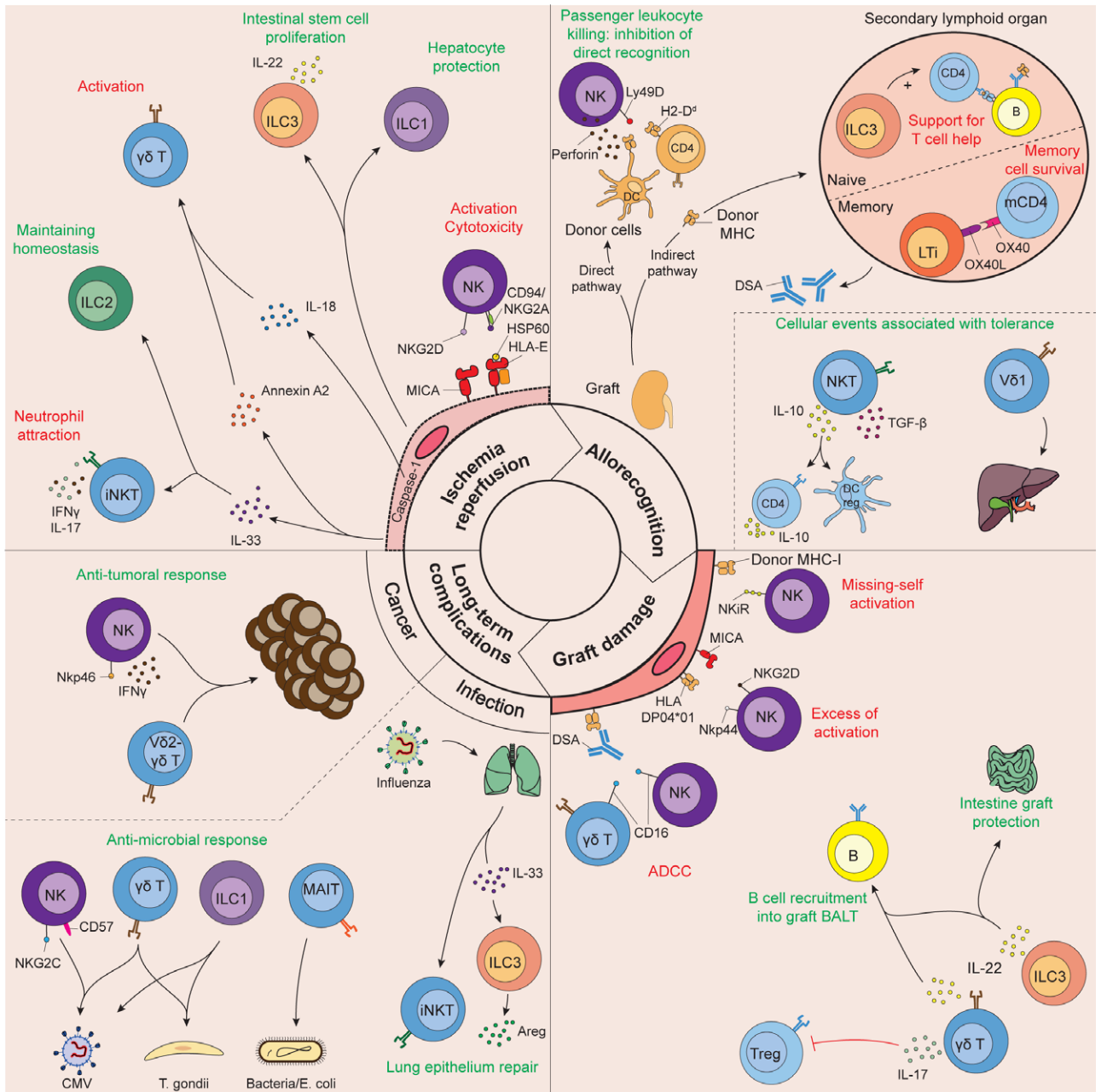


FIGURE 4. Graphical summary of the possible roles of innate (and innate-like) lymphoid cells in transplantation. ADCC, antibody-dependent cellular cytotoxicity; Areg, amphiregulin; BALT, bronchus-associated lymphoid tissue; CMV, cytomegalovirus; DSA, donor-specific antibody; IFN, interferon; IL, interleukin; ILC, innate lymphoid cell; iNKT, invariant natural killer T; LTi, lymphoid tissue inducer; MAIT, mucosal-associated invariant T; MHC, major histocompatibility complex; MICA, MHC-I polypeptide-related sequence A; NK, natural killer; NKT, natural killer T; TGF, transforming growth factor; Treg, regulatory T cell.

Anti-CMV Vδ2-negative γδ T cells display a late differentiated TEMRA (CD27-CD28-CD45RA+CCDR7-CD62L-) and activated (CD69+HLA-DR+) phenotype, cytotoxic ability (perforin+ granzyme B+), and expression of NKR (CD16+, NKG2D+, CD94/NKG2C/A+). CMV drives a presumed antigen-driven clonal selection with a repertoire restriction of the γδ TCR (CDR3 restriction for the Vδ chains). Longitudinal surveillance of non-Vγ9+Vδ2+ γδ T cells in kidney transplant recipients may predict CMV infection resolution and antiviral drug resistance.²²¹ Notably, γδ T lines/clones from CMV-infected patients kill both CMV-infected cells and several solid tumor cell lines in a TCR-dependent fashion.²²² In agreement with this TCR-dependent

cross-reactivity, an association between a high percentage of CMV-responsive γδ T lymphocytes in blood and a reduced cancer risk was observed in kidney recipients.²²³

CONCLUSION

Innate immune effectors are finally getting attention from transplant immunologists, and their many roles are starting to be recognized beyond the initial ischemia/reperfusion phase. Like their myeloid counterparts, which have been shown to be capable of allorecognition, ILCs (in particular NK cells through missing-self) can detect allogeneic nonself. Furthermore, convincing (direct or indirect) evidence suggests that almost all known ILC and ILLC subsets

can participate in rejection by accelerating or dampening graft destruction depending on the organ and the context. Finally, it should not be forgotten that ILCs and ILTCs contribute to the first line of defense against pathogens and cancers. Because these subsets might be less affected by immunosuppressive drugs, ILCs and ILTCs could play crucial roles in the protection of transplant recipients against these life-threatening complications (Figure 4).

Given the complexity of this field, intense efforts are still required to elucidate the exact role of each of these subsets in transplant immunology.

REFERENCES

1. Thauan O. Sterile inflammatory response to ischemia-reperfusion injury: immediate and long term consequences on graft function. *Bull Acad Natl Med.* 2011;195:847–59; discussion 859.
2. Zhao H, Alam A, Soo AP, et al. Ischemia-reperfusion injury reduces long term renal graft survival: mechanism and beyond. *Ebiomedicine.* 2018;28:31–42.
3. Gaston RS, Cecka JM, Kasiske BL, et al. Evidence for antibody-mediated injury as a major determinant of late kidney allograft failure. *Transplantation.* 2010;90:68–74.
4. Sellarés J, de Freitas DG, Mengel M, et al. Understanding the causes of kidney transplant failure: the dominant role of antibody-mediated rejection and nonadherence. *Am J Transplant.* 2012;12:388–399.
5. Buell JF, Gross TG, Woodle ES. Malignancy after transplantation. *Transplantation.* 2005;80(2 Suppl):S254–S264.
6. Chapman JR, Webster AC, Wong G. Cancer in the transplant recipient. *Cold Spring Harb Perspect Med.* 2013;3:a015677.
7. Fishman JA. Infection in solid-organ transplant recipients. *N Engl J Med.* 2007;357:2601–2614.
8. Siu JHY, Surendrakumar V, Richards JA, et al. T cell allorecognition pathways in solid organ transplantation. *Front Immunol.* 2018;9:2548.
9. Afzali B, Lombardi G, Lechler RI. Pathways of major histocompatibility complex allorecognition. *Curr Opin Organ Transplant.* 2008;13:438–444.
10. Lakkis FG, Lechler RI. Origin and biology of the allogeneic response. *Cold Spring Harb Perspect Med.* 2013;3:a014993.
11. Oberbarnscheidt MH, Zeng Q, Li Q, et al. Non-self recognition by monocytes initiates allograft rejection. *J Clin Invest.* 2014;124:3579–3589.
12. Dai H, Lan P, Zhao D, et al. PIRs mediate innate myeloid cell memory to nonself MHC molecules. *Science.* 2020;368:1122–1127.
13. Dai H, Friday AJ, Abou-Daya KI, et al. Donor SIRP α polymorphism modulates the innate immune response to allogeneic grafts. *Sci Immunol.* 2017;2:eaam6202.
14. Prosser AC, Kallies A, Lucas M. Tissue-resident lymphocytes in solid organ transplantation: innocent passengers or the key to organ transplant survival? *Transplantation.* 2018;102:378–386.
15. Kiessling R, Klein E, Pross H, et al. "Natural" killer cells in the mouse. II. Cytotoxic cells with specificity for mouse Moloney leukemia cells. Characteristics of the killer cell. *Eur J Immunol.* 1975;5:117–121.
16. Zhang J, Marotel M, Fauteux-Daniel S, et al. T-bet and Eomes govern differentiation and function of mouse and human NK cells and ILC1. *Eur J Immunol.* 2018;48:738–750.
17. Lanier LL. Up on the tightrope: natural killer cell activation and inhibition. *Nat Immunol.* 2008;9:495–502.
18. Marçais A, Viel S, Grau M, et al. Regulation of mouse NK cell development and function by cytokines. *Front Immunol.* 2013;4:450.
19. Björkström NK, Riese P, Heuts F, et al. Expression patterns of NKG2A, KIR, and CD57 define a process of CD56dim NK-cell differentiation uncoupled from NK-cell education. *Blood.* 2010;116:3853–3864.
20. Kim S, Iizuka K, Kang HS, et al. In vivo developmental stages in murine natural killer cell maturation. *Nat Immunol.* 2002;3:523–528.
21. Joncker NT, Raulet DH. Regulation of NK cell responsiveness to achieve self-tolerance and maximal responses to diseased target cells. *Immunity Rev.* 2008;224:85–97.
22. Kastenmüller W, Torabi-Parizi P, Subramanian N, et al. A spatially-organized multicellular innate immune response in lymph nodes limits systemic pathogen spread. *Cell.* 2012;150:1235–1248.
23. Fang V, Chaluvadi VS, Ramos-Perez WD, et al. Gradients of the signaling lipid S1P in lymph nodes position natural killer cells and regulate their interferon- γ response. *Nat Immunol.* 2017;18:15–25.
24. Orange JS. Human natural killer cell deficiencies. *Curr Opin Allergy Clin Immunol.* 2006;6:399–409.
25. Hammer Q, Rückert T, Romagnani C. Natural killer cell specificity for viral infections. *Nat Immunol.* 2018;19:800–808.
26. Mancini M, Vidal SM. Mechanisms of natural killer cell evasion through viral adaptation. *Annu Rev Immunol.* 2020;38:511–539.
27. Huntington ND, Cursons J, Rautela J. The cancer-natural killer cell immunity cycle. *Nat Rev Cancer.* 2020;20:437–454.
28. Daussy C, Faure F, Mayol K, et al. T-bet and Eomes instruct the development of two distinct natural killer cell lineages in the liver and in the bone marrow. *J Exp Med.* 2014;211:563–577.
29. Peng H, Jiang X, Chen Y, et al. Liver-resident NK cells confer adaptive immunity in skin-contact inflammation. *J Clin Invest.* 2013;123:1444–1456.
30. Mackay LK, Minnich M, Kragten NA, et al. Hobit and Blimp1 instruct a universal transcriptional program of tissue residency in lymphocytes. *Science.* 2016;352:459–463.
31. Weizman OE, Adams NM, Schuster IS, et al. ILC1 confer early host protection at initial sites of viral infection. *Cell.* 2017;171:795–808. e12.
32. Park E, Patel S, Wang Q, et al. Toxoplasma gondii infection drives conversion of NK cells into ILC1-like cells. *Elife.* 2019;8:e47605.
33. Ducimetière L, Lucchiari G, Litscher G, et al. Conventional NK cells and tissue-resident ILC1s join forces to control liver metastasis. *bioRxiv.* 2020.
34. Price AE, Liang H-E, Sullivan BM, et al. Systemically dispersed innate IL-13-expressing cells in type 2 immunity. *Proc Natl Acad Sci.* 2010;107:11489–11494.
35. Neill DR, Wong SH, Bellosi A, et al. Nuocytes represent a new innate effector leukocyte that mediates type-2 immunity. *Nature.* 2010;464:1367–1370.
36. Moro K, Yamada T, Tanabe M, et al. Innate production of T(H)2 cytokines by adipose tissue-associated c-Kit(+)Sca-1(+) lymphoid cells. *Nature.* 2010;463:540–544.
37. Kim CH, Hashimoto-Hill S, Kim M. Migration and tissue tropism of innate lymphoid cells. *Trends Immunol.* 2016;37:68–79.
38. Mjösberg JM, Trifari S, Crellin NK, et al. Human IL-25- and IL-33-responsive type 2 innate lymphoid cells are defined by expression of CCR2 and CD161. *Nat Immunol.* 2011;12:1055–1062.
39. Huang Y, Mao K, Chen X, et al. S1P-dependent interorgan trafficking of group 2 innate lymphoid cells supports host defense. *Science.* 2018;359:114–119.
40. Monticelli LA, Sonnenberg GF, Abt MC, et al. Innate lymphoid cells promote lung tissue homeostasis following acute influenza virus infection. *Nat Immunol.* 2011;12:1045–1054.
41. Halim TYF. Group 2 innate lymphoid cells in disease. *Int Immunol.* 2016;28:13–22.
42. Schuijs MJ, Png S, Richard AC, et al. ILC2-driven innate immune checkpoint mechanism antagonizes NK cell antimetastatic function in the lung. *Nat Immunol.* 2020;21:998–1009.
43. Eberl G, Marmon S, Sunshine MJ, et al. An essential function for the nuclear receptor ROR γ t in the generation of fetal lymphoid tissue inducer cells. *Nat Immunol.* 2004;5:64–73.
44. Satoh-Takayama N, Vosschenrich CA, Lesjean-Pottier S, et al. Microbial flora drives interleukin 22 production in intestinal NKp46+ cells that provide innate mucosal immune defense. *Immunity.* 2008;29:958–970.
45. Cella M, Fuchs A, Vermi W, et al. A human natural killer cell subset provides an innate source of IL-22 for mucosal immunity. *Nature.* 2009;457:722–725.
46. Sonnenberg GF, Monticelli LA, Elloso MM, et al. CD4(+) lymphoid tissue-inducer cells promote innate immunity in the gut. *Immunity.* 2011;34:122–134.
47. Mebius RE, Rennert P, Weissman IL. Developing lymph nodes collect CD4+CD3- LT β + cells that can differentiate to APC, NK cells, and follicular cells but not T or B cells. *Immunity.* 1997;7:493–504.
48. van de Pavert SA, Ferreira M, Domingues RG, et al. Maternal retinoids control type 3 innate lymphoid cells and set the offspring immunity. *Nature.* 2014;508:123–127.
49. Vaishnava S, Yamamoto M, Severson KM, et al. The antibacterial lectin RegIII γ promotes the spatial segregation of microbiota and host in the intestine. *Science.* 2011;334:255–258.
50. Cash HL, Whitham CV, Behrendt CL, et al. Symbiotic bacteria direct expression of an intestinal bactericidal lectin. *Science.* 2006;313:1126–1130.

51. Hernández PP, Mahlakoiv T, Yang I, et al. Interferon- λ and interleukin 22 act synergistically for the induction of interferon-stimulated genes and control of rotavirus infection. *Nat Immunol.* 2015;16:698–707.
52. Pickert G, Neufert C, Leppkes M, et al. STAT3 links IL-22 signaling in intestinal epithelial cells to mucosal wound healing. *J Exp Med.* 2009;206:1465–1472.
53. Buonocore S, Ahern PP, Uhlig HH, et al. Innate lymphoid cells drive interleukin-23-dependent innate intestinal pathology. *Nature.* 2010;464:1371–1375.
54. Kearney JF. Innate-like B cells. *Springer Semin Immunopathol.* 2005;26:377–383.
55. Zhang X. Regulatory functions of innate-like B cells. *Cell Mol Immunol.* 2013;10:113–121.
56. Correa I, Bix M, Liao NS, et al. Most gamma delta T cells develop normally in beta 2-microglobulin-deficient mice. *Proc Natl Acad Sci U S A.* 1992;89:653–657.
57. Sandstrom A, Peigné CM, Léger A, et al. The intracellular B30.2 domain of butyrophilin 3A1 binds phosphoantigens to mediate activation of human V γ 9V δ 2 T cells. *Immunity.* 2014;40:490–500.
58. Rigau M, Ostrouska S, Fulford TS, et al. Butyrophilin 2A1 is essential for phosphoantigen reactivity by $\gamma\delta$ T cells. *Science.* 2020;367:eaay5516.
59. Karunakaran MM, Willcox CR, Salim M, et al. Butyrophilin-2A1 directly binds germline-encoded regions of the V γ 9V δ 2 TCR and is essential for phosphoantigen sensing. *Immunity.* 2020;52:487–498.e6.
60. Davey MS, Willcox CR, Hunter S, et al. The human V δ 2+ T-cell compartment comprises distinct innate-like V γ 9+ and adaptive V γ 9- subsets. *Nat Commun.* 2018;9:1760.
61. Deseke M, Prinz I. Ligand recognition by the $\gamma\delta$ TCR and discrimination between homeostasis and stress conditions. *Cell Mol Immunol.* 2020;17:914–924.
62. Vantourout P, Hayday A. Six-of-the-best: unique contributions of $\gamma\delta$ T cells to immunology. *Nat Rev Immunol.* 2013;13:88–100.
63. Treiner E, Duban L, Bahram S, et al. Selection of evolutionarily conserved mucosal-associated invariant T cells by MR1. *Nature.* 2003;422:164–169.
64. Kjer-Nielsen L, Patel O, Corbett AJ, et al. MR1 presents microbial vitamin B metabolites to MAIT cells. *Nature.* 2012;491:717–723.
65. Legoux F, Bellet D, Daviaud C, et al. Microbial metabolites control the thymic development of mucosal-associated invariant T cells. *Science.* 2019;366:494–499.
66. Leeansyah E, Loh L, Nixon DF, et al. Acquisition of innate-like microbial reactivity in mucosal tissues during human fetal MAIT-cell development. *Nat Commun.* 2014;5:3143.
67. Dias J, Leeansyah E, Sandberg JK. Multiple layers of heterogeneity and subset diversity in human MAIT cell responses to distinct microorganisms and to innate cytokines. *Proc Natl Acad Sci U S A.* 2017;114:E5434–E5443.
68. Kovalovsky D, Uche OU, Eladad S, et al. The BTB-zinc finger transcriptional regulator PLZF controls the development of invariant natural killer T cell effector functions. *Nat Immunol.* 2008;9:1055–1064.
69. Mao AP, Constantinides MG, Mathew R, et al. Multiple layers of transcriptional regulation by PLZF in NKT-cell development. *Proc Natl Acad Sci U S A.* 2016;113:7602–7607.
70. Gapin L. Development of invariant natural killer T cells. *Curr Opin Immunol.* 2016;39:68–74.
71. Debout A, Foucher Y, Trébern-Launay K, et al. Each additional hour of cold ischemia time significantly increases the risk of graft failure and mortality following renal transplantation. *Kidney Int.* 2015;87:343–349.
72. Lefrançois E, Roga S, Gautier V, et al. IL-33 is processed into mature bioactive forms by neutrophil elastase and cathepsin G. *Proc Natl Acad Sci U S A.* 2012;109:1673–1678.
73. Li L, Huang L, Vergis AL, et al. IL-17 produced by neutrophils regulates IFN- γ -mediated neutrophil migration in mouse kidney ischemia-reperfusion injury. *J Clin Invest.* 2010;120:331–342.
74. Ferhat M, Robin A, Giraud S, et al. Endogenous IL-33 contributes to kidney ischemia-reperfusion injury as an Alarmin. *J Am Soc Nephrol.* 2018;29:1272–1288.
75. Yang SH, Lee JP, Jang HR, et al. Sulfatide-reactive natural killer T cells abrogate ischemia-reperfusion injury. *J Am Soc Nephrol.* 2011;22:1305–1314.
76. Riedel JH, Becker M, Kopp K, et al. IL-33-mediated expansion of type 2 innate lymphoid cells protects from progressive glomerulosclerosis. *J Am Soc Nephrol.* 2017;28:2068–2080.
77. Molofsky AB, Van Gool F, Liang HE, et al. Interleukin-33 and interferon- γ counter-regulate group 2 innate lymphoid cell activation during immune perturbation. *Immunity.* 2015;43:161–174.
78. Huang Q, Niu Z, Tan J, et al. IL-25 elicits innate lymphoid cells and multipotent progenitor type 2 cells that reduce renal ischemic/reperfusion injury. *J Am Soc Nephrol.* 2015;26:2199–2211.
79. Nabekura T, Riggan L, Hildreth AD, et al. Type 1 innate lymphoid cells protect mice from acute liver injury via interferon- γ secretion for upregulating Bcl-xL expression in hepatocytes. *Immunity.* 2020;52:96–108.e9.
80. Lindemans CA, Calafiore M, Mertelsmann AM, et al. Interleukin-22 promotes intestinal-stem-cell-mediated epithelial regeneration. *Nature.* 2015;528:560–564.
81. Li J, Wu J, Zhang M, et al. Dynamic changes of innate lymphoid cells in acute ST-segment elevation myocardial infarction and its association with clinical outcomes. *Sci Rep.* 2020;10:5099.
82. Kojima D, Mera T, Nishinakamura H, et al. Prevention of high-mobility group box 1-mediated early loss of transplanted mouse islets in the liver by antithrombin III. *Transplantation.* 2012;93:983–988.
83. Lee JY, Ismail OZ, Zhang X, et al. Donor kidney injury molecule-1 promotes graft recovery by regulating systemic necroinflammation. *Am J Transplant.* 2018;18:2021–2028.
84. Chen X, Li L, Khan MN, et al. HMGB1 exacerbates experimental mouse colitis by enhancing innate lymphoid cells 3 inflammatory responses via promoted IL-23 production. *Innate Immun.* 2016;22:696–705.
85. Zhang ZX, Wang S, Huang X, et al. NK cells induce apoptosis in tubular epithelial cells and contribute to renal ischemia-reperfusion injury. *J Immunol.* 2008;181:7489–7498.
86. Leemans JC, Stokman G, Claessen N, et al. Renal-associated TLR2 mediates ischemia/reperfusion injury in the kidney. *J Clin Invest.* 2005;115:2894–2903.
87. Kim HJ, Lee JS, Kim A, et al. TLR2 signaling in tubular epithelial cells regulates NK cell recruitment in kidney ischemia-reperfusion injury. *J Immunol.* 2013;191:2657–2664.
88. Kim HJ, Lee JS, Kim JD, et al. Reverse signaling through the costimulatory ligand CD137L in epithelial cells is essential for natural killer cell-mediated acute tissue inflammation. *Proc Natl Acad Sci U S A.* 2012;109:E13–E22.
89. Zhang ZX, Shek K, Wang S, et al. Osteopontin expressed in tubular epithelial cells regulates NK cell-mediated kidney ischemia reperfusion injury. *J Immunol.* 2010;185:967–973.
90. Victorino F, Sojka DK, Brodsky KS, et al. Tissue-resident NK cells mediate ischemic kidney injury and are not depleted by anti-asialo-GM1 antibody. *J Immunol.* 2015;195:4973–4985.
91. Law BMP, Wilkinson R, Wang X, et al. Human tissue-resident mucosal-associated invariant T (MAIT) cells in renal fibrosis and CKD. *J Am Soc Nephrol.* 2019;30:1322–1335.
92. Pradeu T, Jaeger S, Vivier E. The speed of change: towards a discontinuity theory of immunity? *Nat Rev Immunol.* 2013;13:764–769.
93. Braud V, Jones EY, McMichael A. The human major histocompatibility complex class Ib molecule HLA-E binds signal sequence-derived peptides with primary anchor residues at positions 2 and 9. *Eur J Immunol.* 1997;27:1164–1169.
94. Braud VM, Allan DS, O'Callaghan CA, et al. HLA-E binds to natural killer cell receptors CD94/NKG2A, B and C. *Nature.* 1998;391:795–799.
95. Michaëlsson J, Teixeira de Matos C, Achour A, et al. A signal peptide derived from HSP60 binds HLA-E and interferes with CD94/NKG2A recognition. *J Exp Med.* 2002;196:1403–1414.
96. Fu C, Shi Y, Yao Z. sMICA as novel and early predictors for acute myocardial infarction. *Eur J Med Res.* 2016;21:25.
97. Luo L, Lu J, Wei L, et al. The role of HIF-1 in up-regulating MICA expression on human renal proximal tubular epithelial cells during hypoxia/reoxygenation. *BMC Cell Biol.* 2010;11:91.
98. Bauer S, Groh V, Wu J, et al. Activation of NK cells and T cells by NKG2D, a receptor for stress-inducible MICA. *Science.* 1999;285:727–729.
99. Kawakami T, Ito K, Matsuda Y, et al. Cytotoxicity of natural killer cells activated through NKG2D contributes to the development of bronchiolitis obliterans in a murine heterotopic tracheal transplant model. *Am J Transplant.* 2017;17:2338–2349.
100. Dusseaux M, Martin E, Serriari N, et al. Human MAIT cells are xenobiotic-resistant, tissue-targeted, CD161hi IL-17-secreting T cells. *Blood.* 2011;117:1250–1259.

101. Kuylenstierna C, Björkström NK, Andersson SK, et al. NKG2D performs two functions in invariant NKT cells: direct TCR-independent activation of NK-like cytotoxicity and co-stimulation of activation by CD1d. *Eur J Immunol*. 2011;41:1913–1923.
102. Madureira PA, Hill R, Miller VA, et al. Annexin A2 is a novel cellular redox regulatory protein involved in tumorigenesis. *Oncotarget*. 2011;2:1075–1093.
103. Marlin R, Pappalardo A, Kaminski H, et al. Sensing of cell stress by human $\gamma\delta$ TCR-dependent recognition of annexin A2. *Proc Natl Acad Sci U S A*. 2017;114:3163–3168.
104. Willcox CR, Pitard V, Netzer S, et al. Cytomegalovirus and tumor stress surveillance by binding of a human $\gamma\delta$ T cell antigen receptor to endothelial protein C receptor. *Nat Immunol*. 2012;13:872–879.
105. Marlin R, Netzer S, Pitard V, et al. Key role of free heavy chain of HLA class I molecules in HCMV and tumor stress sensing by gamma-delta TCR. Available at https://www.frontiersin.org/10.3389/conf.fimmu.2013.02.00960/event_abstract. Accessed January 25, 2021.
106. Groh V, Rhinehart R, Secrist H, et al. Broad tumor-associated expression and recognition by tumor-derived $\gamma\delta$ T cells of MICA and MICB. *Proc Natl Acad Sci*. 1999;96:6879–6884.
107. Guerville F, Daburon S, Marlin R, et al. TCR-dependent sensitization of human $\gamma\delta$ T cells to non-myeloid IL-18 in cytomegalovirus and tumor stress surveillance. *Oncimmunology*. 2015;4:e1003011.
108. Shichita T, Sugiyama Y, Ooboshi H, et al. Pivotal role of cerebral interleukin-17-producing $\gamma\delta$ T cells in the delayed phase of ischemic brain injury. *Nat Med*. 2009;15:946–950.
109. Shichita T, Hasegawa E, Kimura A, et al. Peroxiredoxin family proteins are key initiators of post-ischemic inflammation in the brain. *Nat Med*. 2012;18:911–917.
110. Benakis C, Brea D, Caballero S, et al. Commensal microbiota affects ischemic stroke outcome by regulating intestinal $\gamma\delta$ T cells. *Nat Med*. 2016;22:516–523.
111. Hoehgegger K, Schätz T, Eller P, et al. Role of $\alpha\beta$ and $\gamma\delta$ T cells in renal ischemia-reperfusion injury. *Am J Physiol-Ren Physiol*. 2007;293:F741–F747.
112. Herrera OB, Golshayan D, Tibbott R, et al. A novel pathway of alloantigen presentation by dendritic cells. *J Immunol*. 2004;173:4828–4837.
113. Liu Q, Rojas-Canales DM, Divito SJ, et al. Donor dendritic cell-derived exosomes promote allograft-targeting immune response. *J Clin Invest*. 2016;126:2805–2820.
114. Lanzavecchia A. Antigen-specific interaction between T and B cells. *Nature*. 1985;314:537–539.
115. Conlon TM, Saeb-Parsy K, Cole JL, et al. Germinal center alloantibody responses are mediated exclusively by indirect-pathway CD4 T follicular helper cells. *J Immunol*. 2012;188:2643–2652.
116. Lakkis FG, Arakelov A, Konieczny BT, et al. Immunologic “ignorance” of vascularized organ transplants in the absence of secondary lymphoid tissue. *Nat Med*. 2000;6:686–688.
117. Thauinat O, Field AC, Dai J, et al. Lymphoid neogenesis in chronic rejection: evidence for a local humoral alloimmune response. *Proc Natl Acad Sci U S A*. 2005;102:14723–14728.
118. Thauinat O, Patey N, Caligiuri G, et al. Chronic rejection triggers the development of an aggressive intragraft immune response through recapitulation of lymphoid organogenesis. *J Immunol*. 2010;185:717–728.
119. Thauinat O, Nicoletti A. Lymphoid neogenesis in chronic rejection. *Curr Opin Organ Transplant*. 2008;13:16–19.
120. Burg N von, Chappaz S, Baerenwaldt A, et al. Activated group 3 innate lymphoid cells promote T-cell-mediated immune responses. *Proc Natl Acad Sci*. 2014;111:12835–12840.
121. Withers DR, Gaspal FM, Mackley EC, et al. Cutting edge: lymphoid tissue inducer cells maintain memory CD4 T cells within secondary lymphoid tissue. *J Immunol*. 2012;189:2094–2098.
122. Kim MY, Gaspal FM, Wiggert HE, et al. CD4(+)CD3(-) accessory cells costimulate primed CD4 T cells through OX40 and CD30 at sites where T cells collaborate with B cells. *Immunity*. 2003;18:643–654.
123. Wen L, Roberts SJ, Viney JL, et al. Immunoglobulin synthesis and generalized autoimmunity in mice congenitally deficient in $\alpha\beta$ (+) T cells. *Nature*. 1994;369:654–658.
124. Wen L, Pao W, Wong FS, et al. Germinal center formation, immunoglobulin class switching, and autoantibody production driven by “non alpha/beta” T cells. *J Exp Med*. 1996;183:2271–2282.
125. Horner AA, Jabara H, Ramesh N, et al. $\gamma\delta$ T lymphocytes express CD40 ligand and induce isotype switching in B lymphocytes. *J Exp Med*. 1995;181:1239–1244.
126. Caccamo N, Battistini L, Bonneville M, et al. CXCR5 identifies a subset of $V\gamma 9V\delta 2$ T cells which secrete IL-4 and IL-10 and help B cells for antibody production. *J Immunol*. 2006;177:5290–5295.
127. Liu X, Chen X, Zhong B, et al. Transcription factor achaete-scute homologue 2 initiates follicular T-helper-cell development. *Nature*. 2014;507:513–518.
128. Rezende RM, Lanser AJ, Rubino S, et al. $\gamma\delta$ T cells control humoral immune response by inducing T follicular helper cell differentiation. *Nat Commun*. 2018;9:3151.
129. Drobyski WR, Vodanovic-Jankovic S, Klein J. Adoptively transferred $\gamma\delta$ T cells indirectly regulate murine graft-versus-host reactivity following donor leukocyte infusion therapy in mice. *J Immunol*. 2000;165:1634–1640.
130. Beilke JN, Kuhl NR, Van Kaer L, et al. NK cells promote islet allograft tolerance via a perforin-dependent mechanism. *Nat Med*. 2005;11:1059–1065.
131. Yu G, Xu X, Vu MD, et al. NK cells promote transplant tolerance by killing donor antigen-presenting cells. *J Exp Med*. 2006;203:1851–1858.
132. Garrod KR, Liu FC, Forrest LE, et al. NK cell patrolling and elimination of donor-derived dendritic cells favor indirect alloreactivity. *J Immunol*. 2010;184:2329–2336.
133. Laffont S, Seillet C, Ortaldo J, et al. Natural killer cells recruited into lymph nodes inhibit alloreactive T-cell activation through perforin-mediated killing of donor allogeneic dendritic cells. *Blood*. 2008;112:661–671.
134. Harper IG, Ali JM, Harper SJ, et al. Augmentation of recipient adaptive alloimmunity by donor passenger lymphocytes within the transplant. *Cell Rep*. 2016;15:1214–1227.
135. Nabekura T, Lanier LL. Antigen-specific expansion and differentiation of natural killer cells by alloantigen stimulation. *J Exp Med*. 2014;211:2455–2465.
136. Cantoni C, Bottino C, Vitale M, et al. NKp44, a triggering receptor involved in tumor cell lysis by activated human natural killer cells, is a novel member of the immunoglobulin superfamily. *J Exp Med*. 1999;189:787–796.
137. Vitale M, Bottino C, Sivori S, et al. NKp44, a novel triggering surface molecule specifically expressed by activated natural killer cells, is involved in non-major histocompatibility complex-restricted tumor cell lysis. *J Exp Med*. 1998;187:2065–2072.
138. Niehrs A, Garcia-Beltran WF, Norman PJ, et al. A subset of HLA-DP molecules serve as ligands for the natural cytotoxicity receptor NKp44. *Nat Immunol*. 2019;20:1129–1137.
139. Wu C, Li XC. An unexpected partnership: MHC class II molecules as ligands for NK cells. *Transplantation*. 2020;104:229–230.
140. Seino KI, Fukao K, Muramoto K, et al. Requirement for natural killer T (NKT) cells in the induction of allograft tolerance. *Proc Natl Acad Sci U S A*. 2001;98:2577–2581.
141. Jiang X, Kojo S, Harada M, et al. Mechanism of NKT cell-mediated transplant tolerance. *Am J Transplant*. 2007;7:1482–1490.
142. Yang SH, Jin JZ, Lee SH, et al. Role of NKT cells in allogeneic islet graft survival. *Clin Immunol*. 2007;124:258–266.
143. Puig-Pey I, Bohne F, Benitez C, et al. Characterization of $\gamma\delta$ T cell subsets in organ transplantation. *Transpl Int*. 2010;23:1045–1055.
144. Déchanet J, Merville P, Lim A, et al. Implication of $\gamma\delta$ T cells in the human immune response to cytomegalovirus. *J Clin Invest*. 1999;103:1437–1449.
145. Shi XL, de Mare-Bredemeijer EL, Tapirdamaz Ö, et al. CMV primary infection is associated with donor-specific T cell hyporesponsiveness and fewer late acute rejections after liver transplantation. *Am J Transplant*. 2015;15:2431–2442.
146. Martínez-Llordella M, Puig-Pey I, Orlando G, et al. Multiparameter immune profiling of operational tolerance in liver transplantation. *Am J Transplant*. 2007;7:309–319.
147. Martínez-Llordella M, Lozano JJ, Puig-Pey I, et al. Using transcriptional profiling to develop a diagnostic test of operational tolerance in liver transplant recipients. *J Clin Invest*. 2008;118:2845–2857.
148. Zhao X, Li Y, Ohe H, et al. Intragraft $V\delta 1 \gamma\delta$ T cells with a unique T-cell receptor are closely associated with pediatric semiallogeneic liver transplant tolerance. *Transplantation*. 2013;95:192–202.
149. Varelias A, Bunting MD, Ormerod KL, et al. Recipient mucosal-associated invariant T cells control GVHD within the colon. *J Clin Invest*. 2018;128:1919–1936.
150. Uehara S, Chase CM, Kitchens WH, et al. NK cells can trigger allograft vasculopathy: the role of hybrid resistance in solid organ allografts. *J Immunol*. 2005;175:3424–3430.

151. van Bergen J, Thompson A, Haasnoot GW, et al. KIR-ligand mismatches are associated with reduced long-term graft survival in HLA-compatible kidney transplantation. *Am J Transplant.* 2011;11:1959–1964.
152. Koenig A, Chen CC, Marçais A, et al. Missing self triggers NK cell-mediated chronic vascular rejection of solid organ transplants. *Nat Commun.* 2019;10:5350.
153. Hamada S, Thauinat O, Koenig A. Un nouveau type de rejet de greffe induit par les lymphocytes naturel killer: le rejet chronique vasculaire "inné." *Médecine/Sciences.* 2020;36:984–987.
154. Couzi L, Pitard V, Netzer S, et al. Common features of gammadelta T cells and CD8(+) alphabeta T cells responding to human cytomegalovirus infection in kidney transplant recipients. *J Infect Dis.* 2009;200:1415–1424.
155. Halary F, Peyrat MA, Champagne E, et al. Control of self-reactive cytotoxic T lymphocytes expressing gamma delta T cell receptors by natural killer inhibitory receptors. *Eur J Immunol.* 1997;27:2812–2821.
156. Chauveau A, Tonnerre P, Pabois A, et al. Endothelial cell activation and proliferation modulate NKG2D activity by regulating MICA expression and shedding. *J Innate Immun.* 2014;6:89–104.
157. Sumitran-Holgersson S, Wilczek HE, Holgersson J, et al. Identification of the nonclassical HLA molecules, mica, as targets for humoral immunity associated with irreversible rejection of kidney allografts. *Transplantation.* 2002;74:268–277.
158. Visser CJ, Tilanus MG, Tatari Z, et al. Sequencing-based typing of MICA reveals 33 alleles: a study on linkage with classical HLA genes. *Immunogenetics.* 1999;49:561–566.
159. Choy MK, Phipps ME. MICA polymorphism: biology and importance in immunity and disease. *Trends Mol Med.* 2010;16:97–106.
160. Zwierner NW, Marcos CY, Mirbaha F, et al. Identification of MICA as a new polymorphic alloantigen recognized by antibodies in sera of organ transplant recipients. *Hum Immunol.* 2000;61:917–924.
161. Zou Y, Stastny P, Süsal C, et al. Antibodies against MICA antigens and kidney-transplant rejection. *N Engl J Med.* 2007;357:1293–1300.
162. Isernhagen A, Malzahn D, Viktorova E, et al. The MICA-129 dimorphism affects NKG2D signaling and outcome of hematopoietic stem cell transplantation. *EMBO Mol Med.* 2015;7:1480–1502.
163. Pober JS, Collins T, Gimbrone MA Jr, et al. Inducible expression of class II major histocompatibility complex antigens and the immunogenicity of vascular endothelium. *Transplantation.* 1986;41:141–146.
164. Sicard A, Ducreux S, Rabeyrin M, et al. Detection of C3d-binding donor-specific anti-HLA antibodies at diagnosis of humoral rejection predicts renal graft loss. *J Am Soc Nephrol.* 2015;26:457–467.
165. Guidicelli G, Guerville F, Lepreux S, et al. Non-complement-binding de novo donor-specific anti-HLA antibodies and kidney allograft survival. *J Am Soc Nephrol.* 2016;27:615–625.
166. Hirohashi T, Uehara S, Chase CM, et al. Complement independent antibody-mediated endarteritis and transplant arteriopathy in mice. *Am J Transplant.* 2010;10:510–517.
167. Hirohashi T, Chase CM, Della Pelle P, et al. A novel pathway of chronic allograft rejection mediated by NK cells and alloantibody. *Am J Transplant.* 2012;12:313–321.
168. Kohei N, Tanaka T, Tanabe K, et al. Natural killer cells play a critical role in mediating inflammation and graft failure during antibody-mediated rejection of kidney allografts. *Kidney Int.* 2016;89:1293–1306.
169. Aneón I, Cuturi MC, Trinchieri G, et al. Interaction of Fc receptor (CD16) ligands induces transcription of interleukin 2 receptor (CD25) and lymphokine genes and expression of their products in human natural killer cells. *J Exp Med.* 1988;167:452–472.
170. Parkes MD, Halloran PF, Hidalgo LG. Evidence for CD16a-mediated NK cell stimulation in antibody-mediated kidney transplant rejection. *Transplantation.* 2017;101:e102–e111.
171. Pouliquen E, Koenig A, Chen CC, et al. Recent advances in renal transplantation: antibody-mediated rejection takes center stage. *F1000Prime Rep.* 2015;7:51.
172. Miyairi S, Baldwin WM 3rd, Valujskikh A, et al. Natural killer cells: critical effectors during antibody-mediated rejection of solid organ allografts. *Transplantation.* 2021;105:284–290.
173. Hidalgo LG, Sis B, Sellares J, et al. NK cell transcripts and NK cells in kidney biopsies from patients with donor-specific antibodies: evidence for NK cell involvement in antibody-mediated rejection. *Am J Transplant.* 2010;10:1812–1822.
174. Yazdani S, Callemeyn J, Gazut S, et al. Natural killer cell infiltration is discriminative for antibody-mediated rejection and predicts outcome after kidney transplantation. *Kidney Int.* 2019;95:188–198.
175. Venner JM, Hidalgo LG, Famulski KS, et al. The molecular landscape of antibody-mediated kidney transplant rejection: evidence for NK involvement through CD16a Fc receptors. *Am J Transplant.* 2015;15:1336–1348.
176. Koenig A, Mezaache S, Callemeyn J, et al. Missing self-induced activation of NK cells combines with non-complement-fixing donor-specific antibodies to accelerate kidney transplant loss in chronic antibody-mediated rejection. *J Am Soc Nephrol.* 2021;32:479–494.
177. Couzi L, Pitard V, Sicard X, et al. Antibody-dependent anti-cytomegalovirus activity of human $\gamma\delta$ T cells expressing CD16 (Fc γ RIIIa). *Blood.* 2012;119:1418–1427.
178. Bachelet T, Couzi L, Pitard V, et al. Cytomegalovirus-responsive $\gamma\delta$ T cells: novel effector cells in antibody-mediated kidney allograft microcirculation lesions. *J Am Soc Nephrol.* 2014;25:2471–2482.
179. Itoh S, Nakae S, Axtell RC, et al. IL-17 contributes to the development of chronic rejection in a murine heart transplant model. *J Clin Immunol.* 2010;30:235–240.
180. Itoh S, Kimura N, Axtell RC, et al. Interleukin-17 accelerates allograft rejection by suppressing regulatory T cell expansion. *Circulation.* 2011;124(11 Suppl):S187–S196.
181. Zeng B, Shi S, Ashworth G, et al. ILC3 function as a double-edged sword in inflammatory bowel diseases. *Cell Death Dis.* 2019;10:315.
182. Hepworth MR, Monticelli LA, Fung TC, et al. Innate lymphoid cells regulate CD4+ T-cell responses to intestinal commensal bacteria. *Nature.* 2013;498:113–117.
183. Hepworth MR, Fung TC, Masur SH, et al. Group 3 innate lymphoid cells mediate intestinal selection of commensal bacteria-specific CD4+ T cells. *Science.* 2015;348:1031–1035.
184. Guo X, Qiu J, Tu T, et al. Induction of innate lymphoid cell-derived interleukin-22 by the transcription factor STAT3 mediates protection against intestinal infection. *Immunity.* 2014;40:25–39.
185. Li W, Bribriescio AC, Nava RG, et al. Lung transplant acceptance is facilitated by early events in the graft and is associated with lymphoid neogenesis. *Mucosal Immunol.* 2012;5:544–554.
186. Tanaka S, Gauthier JM, Fuchs A, et al. IL-22 is required for the induction of bronchus-associated lymphoid tissue in tolerant lung allografts. *Am J Transplant.* 2020;20:1251–1261.
187. Monticelli LA, Diamond JM, Saenz SA, et al. Lung innate lymphoid cell composition is altered in primary graft dysfunction. *Am J Respir Crit Care Med.* 2020;201:63–72.
188. Hodge G, Hodge S, Liu H, et al. BOS is associated with decreased SIRTI in peripheral blood proinflammatory T, NK, and NKT-like lymphocytes. *Transplantation.* 2019;103:2255–2263.
189. Hodge G, Hodge S, Yeo A, et al. BOS is associated with increased cytotoxic proinflammatory CD8 T, NKT-Like, and NK cells in the small airways. *Transplantation.* 2017;101:2469–2476.
190. Weiner J, Zuber J, Shonts B, et al. Long-term persistence of innate lymphoid cells in the gut after intestinal transplantation. *Transplantation.* 2017;101:2449–2454.
191. Gómez-Massa E, Lasa-Lázaro M, Gil-Etayo FJ, et al. Donor helper innate lymphoid cells are replaced earlier than lineage positive cells and persist long-term in human intestinal grafts—a descriptive study. *Transpl Int.* 2020;33:1016–1029.
192. Kang J, Loh K, Belyayev L, et al. Type 3 innate lymphoid cells are associated with a successful intestinal transplant. *Am J Transplant.* 2021;21:787–797.
193. Pucci Molineris M, González Polo V, Rumbo C, et al. Acute cellular rejection in small-bowel transplantation impairs NCR+ innate lymphoid cell subpopulation 3/interleukin 22 axis. *Transpl Immunol.* 2020;60:101288.
194. Chen CC, Pouliquen E, Broisat A, et al. Endothelial chimerism and vascular sequestration protect pancreatic islet grafts from antibody-mediated rejection. *J Clin Invest.* 2018;128:219–232.
195. Mentzel U, Vogt H, Rossol R, et al. Analysis of lymphocyte subsets in patients with aplastic anemia before and during immunosuppressive therapy. *Ann Hematol.* 1993;66:127–129.
196. Gómez-Massa E, Talayero P, Utrero-Rico A, et al. Number and function of circulatory helper innate lymphoid cells are unaffected by immunosuppressive drugs used in solid organ recipients - a single centre cohort study. *Transpl Int.* 2020;33:402–413.
197. Klose CSN, Flach M, Möhle L, et al. Differentiation of type 1 ILCs from a common progenitor to all helper-like innate lymphoid cell lineages. *Cell.* 2014;157:340–356.
198. Paget C, Ivanov S, Fontaine J, et al. Potential role of invariant NKT cells in the control of pulmonary inflammation and CD8+ T cell response during acute influenza A virus H3N2 pneumonia. *J Immunol.* 2011;186:5590–5602.

199. Chiossone L, Dumas PY, Vienne M, et al. Natural killer cells and other innate lymphoid cells in cancer. *Nat Rev Immunol.* 2018;18:671–688.
200. An Z, Flores-Borja F, Irshad S, et al. Pleiotropic role and bidirectional immunomodulation of innate lymphoid cells in cancer. *Front Immunol.* 2019;10:3111.
201. Ruggeri L, Capanni M, Urbani E, et al. Effectiveness of donor natural killer cell alloreactivity in mismatched hematopoietic transplants. *Science.* 2002;295:2097–2100.
202. Rueff J, Medinger M, Heim D, et al. Lymphocyte subset recovery and outcome after autologous hematopoietic stem cell transplantation for plasma cell myeloma. *Biol Blood Marrow Transplant.* 2014;20:896–899.
203. Peraldi MN, Berrou J, Venot M, et al. Natural killer lymphocytes are dysfunctional in kidney transplant recipients on diagnosis of cancer. *Transplantation.* 2015;99:2422–2430.
204. Baychelier F, Achour A, Nguyen S, et al; Study of Cancers After Solid Organs Transplants (K-GREF) Study Group. Natural killer cell deficiency in patients with non-Hodgkin lymphoma after lung transplantation. *J Heart Lung Transplant.* 2015;34:604–612.
205. Dendle C, Gan PY, Polkinghorne KR, et al. Natural killer cell function predicts severe infection in kidney transplant recipients. *Am J Transplant.* 2019;19:166–177.
206. Sun JC, Beilke JN, Lanier LL. Adaptive immune features of natural killer cells. *Nature.* 2009;457:557–561.
207. Foley B, Cooley S, Verneris MR, et al. Cytomegalovirus reactivation after allogeneic transplantation promotes a lasting increase in educated NKG2C+ natural killer cells with potent function. *Blood.* 2012;119:2665–2674.
208. Lopez-Vergès S, Milush JM, Schwartz BS, et al. Expansion of a unique CD57⁺NKG2Chi natural killer cell subset during acute human cytomegalovirus infection. *Proc Natl Acad Sci U S A.* 2011;108:14725–14732.
209. Béziat V, Liu LL, Malmberg JA, et al. NK cell responses to cytomegalovirus infection lead to stable imprints in the human KIR repertoire and involve activating KIRs. *Blood.* 2013;121:2678–2688.
210. Harpur CM, Stankovic S, Kanagarajah A, et al. Enrichment of cytomegalovirus-induced NKG2C+ natural killer cells in the lung allograft. *Transplantation.* 2019;103:1689–1699.
211. Ataya M, Redondo-Pachón D, Llinàs-Mallol L, et al. Pretransplant adaptive NKG2C+ NK cells protect against cytomegalovirus infection in kidney transplant recipients. *Am J Transplant.* 2020;20:663–676.
212. Le Bourhis L, Martin E, Péguillet I, et al. Antimicrobial activity of mucosal-associated invariant T cells. *Nat Immunol.* 2010;11:701–708.
213. Meierovics A, Yankelevich WJ, Cowley SC. MAIT cells are critical for optimal mucosal immune responses during in vivo pulmonary bacterial infection. *Proc Natl Acad Sci U S A.* 2013;110:E3119–E3128.
214. Loh L, Wang Z, Sant S, et al. Human mucosal-associated invariant T cells contribute to antiviral influenza immunity via IL-18-dependent activation. *Proc Natl Acad Sci U S A.* 2016;113:10133–10138.
215. van Wilgenburg B, Scherwitzl I, Hutchinson EC, et al; STOP-HCV consortium. MAIT cells are activated during human viral infections. *Nat Commun.* 2016;7:11653.
216. Déchanet J, Merville P, Bergé F, et al. Major expansion of gammadelta T lymphocytes following cytomegalovirus infection in kidney allograft recipients. *J Infect Dis.* 1999;179:1–8.
217. Vermijlen D, Brouwer M, Donner C, et al. Human cytomegalovirus elicits fetal gammadelta T cell responses in utero. *J Exp Med.* 2010;207:807–821.
218. Ehl S, Schwarz K, Enders A, et al. A variant of SCID with specific immune responses and predominance of gamma delta T cells. *J Clin Invest.* 2005;115:3140–3148.
219. Knight A, Madrigal AJ, Grace S, et al. The role of Vδ2-negative γδ T cells during cytomegalovirus reactivation in recipients of allogeneic stem cell transplantation. *Blood.* 2010;116:2164–2172.
220. Pitard V, Roumanes D, Lafarge X, et al. Long-term expansion of effector/memory Vdelta2-gammadelta T cells is a specific blood signature of CMV infection. *Blood.* 2008;112:1317–1324.
221. Kaminski H, Garrigue I, Couzi L, et al. Surveillance of γδ T cells predicts cytomegalovirus infection resolution in kidney transplants. *J Am Soc Nephrol.* 2016;27:637–645.
222. Halary F, Pitard V, Dlubek D, et al. Shared reactivity of V{delta}2(neg){gamma}{delta} T cells against cytomegalovirus-infected cells and tumor intestinal epithelial cells. *J Exp Med.* 2005;201:1567–1578.
223. Couzi L, Levaillant Y, Jamai A, et al. Cytomegalovirus-induced gammadelta T cells associate with reduced cancer risk after kidney transplantation. *J Am Soc Nephrol.* 2010;21:181–188.

2. Publication 2

Improved cell signaling analysis by biofunctionalized nanospheres and imaging flow cytometry.

Koenig A, Charmetant X, Barba T, Sicard A, Espi M, Dussurgey S, Thaunat O.

Cytometry Part A. 2021 Nov;99(11):1079-1090.



Improved cell signaling analysis by biofunctionalized nanospheres and imaging flow cytometry

Alice Koenig^{1,2,3} | Xavier Charmetant¹ | Thomas Barba^{1,2,3} | Antoine Sicard^{1,2,3} |
Maxime Espi^{1,2,3} | Sébastien Dussurgey⁴ | Olivier Thauinat^{1,2,3}

¹CIRI, INSERM U1111, Université Claude Bernard Lyon I, CNRS UMR5308, Ecole Normale Supérieure de Lyon, University of Lyon, Lyon, France

²Department of Transplantation, Nephrology and Clinical Immunology, Hospices Civils de Lyon, Edouard Herriot Hospital, Lyon, France

³Lyon-Est Medical Faculty, Claude Bernard University (Lyon 1), Lyon, France

⁴University of Lyon, ENS de Lyon, Inserm, CNRS SFR Biosciences US8 UMS3444, UCBL, Lyon, France

Correspondence

Olivier Thauinat, CIRI, INSERM U1111, Université Lyon 1, 21 Avenue Tony Garnier, 69365, Lyon cedex 07, France.
Email: olivier.thauinat@inserm.fr

Funding information

CoPoC INSERM, Grant/Award Number: 2018 grant; Hospices Civils de Lyon; INSERM, Grant/Award Number: 2015/1239/BT

Abstract

The analysis of immune cell signaling is critical for the understanding of the biology and pathology of the immune system, and thus a mandatory step for the development of efficient biomarkers and targeted therapies. Phosflow, which has progressively replaced the traditional western blot approach, relies on flow cytometry to analyze various signaling pathways at a single-cell level. This technique however suffers a lack of sensitivity largely due to the low signal/noise ratio that characterizes cell signaling analysis. In this study, we describe a new technique, which combines the use of biofunctionalized nanospheres (i.e., synthetic particulate antigens, SPAG) to stimulate the immune cells in suspension and imaging flow cytometry to identify homogeneously-stimulated cells and quantify the activity of the chosen signaling pathway in selected subcellular regions of interest. Using BCR signaling as model, we demonstrate that SIBERIAN (SPAG-assisted suB-cellulaR signaling ANALYSIS) allows assessing immune cell signaling with unprecedented sensitivity and specificity.

KEYWORDS

cell signaling, fluorescent nanoparticles, imaging flow cytometry, phosflow, phospho-proteins

1 | INTRODUCTION

Immune cell signaling, which is triggered in response to diverse stimuli, depends upon post-translational modification, in particular phosphorylation [1], of complex protein networks and aims at orchestrating the appropriate immune response. The study of the many signaling pathways is therefore critical to understand immune cell biology and pathology, and is considered as a crucial first step preceding the development of biomarkers and targeted therapies [2,3]. This concept is epitomized by the discovery in the mid 1990s' of the fusion protein kinase Bcr-Abl, which constitutive activation is responsible for the uncontrolled proliferation of tumoral cells during chronic myeloid leukemia. This observation led to the development of imatinib, a tyrosine kinase inhibitor, which revolutionized the treatment of this condition [4,5]. Inspired by this success story, many similar initiatives have since been conducted in a broad range of medical conditions [3].

Invented in the early 1980s', western blot has long remained the gold standard technique to study cell signaling [6,7]. Western blot indeed allows estimating the quantity of a given protein within complex mixtures generated from tissues or cellular extracts [8]. When the appropriate monoclonal antibodies are used, the technique can estimate the proportion of naïve versus phosphorylated form of the protein, hence the "activity" of the given signaling pathway. Despite its undisputable value, western blot technique have several limitations [8]. First, it is time-consuming and labor-intensive [9]. Second, the technique can affect the conformation of the protein making its subsequent detection by some monoclonal antibodies impossible [9]. Finally, because of its limited sensitivity, western blot technique requires a high quantity of the protein of interest, which can usually only be obtained by lysing many purified cells (i.e., bulk instead of single cell analysis) [9].

In order to circumvent these limitations, it has been proposed to study cell signaling by flow cytometry [10]. This new technique, called

phosflow, has rapidly gained interest over the last decade, based on the promise that it should allow tracking simultaneously multiple intracellular signaling molecules in the immune system at a single-cell level without the need for cell sorting or purification [11–13]. However, despite its many advantages, phosflow also have limitations. In particular, in the context of the typical low signal/noise ratio of cell signaling, it is not always easy to get accurate and valid results, even when the last technological evolutions, based on sandwich-labeling [14] or barcoding [15,16], are applied.

In the present manuscript, we describe a new technique, which combines the use of fluorescent synthetic particulate antigens (SPAg) [17] to stimulate immune cells and imaging flow cytometry to identify homogenously-stimulated cells and quantify the activity of the chosen signaling pathway in selected subcellular regions of interest. Using BCR signaling as model, we demonstrate that our approach allows assessing immune cell signaling with unprecedented sensitivity and specificity.

2 | MATERIALS AND METHODS

2.1 | Synthetic particulate antigens (SPAg)

2.1.1 | Nanospheres

Four hundred nano meter flash red (660/690) streptavidin nanospheres were purchased from Bangs laboratories (Indiana, USA). These nanospheres are composed primarily of polystyrene and are generated by an emulsion polymerization synthesis using a sulfate-based initiator. Flash red fluorescent dye is embedded within the core of the nanospheres. Following synthesis, streptavidin is covalently bound and a blocker is applied.

2.1.2 | SPAg quantification

The standard curve method was used to numerate SPAg. Briefly, SPAg samples and serial dilutions of uncoated nanospheres of known concentrations were pipetted into 96 wells black plates with transparent bottom (Greiner Bio One, Les Ulis, France) to establish a standard curve. Fluorescence was measured with a microplate reader (Infinite Reader M200, Tecan, Männedorf, Switzerland) at 660/690 nm. Data were analyzed with the i. control (v1.6) and Excel softwares.

2.1.3 | Protein biotinylation

Purified rat anti-mouse κ Light Chain (anti- κ mAb, clone 187.1, Becton Dickinson, Le Pont de Claix, France) and ovalbumin (Ova, Sigma, Saint-Quentin Fallavier, France) were monobiotinylated using the EZ-Link™ Sulfo-NHS-LC-LC-Biotin kit (ThermoFisher Scientific, Courtaboeuf, France) according to the manufacturer's instructions. A

Sulfo-NHS-LC-LC-Biotin form was chosen because it includes a long spacer arm, which allows minimizing steric hindrance on nanospheres surface. Briefly, anti- κ mAb suspended in phosphate-buffered saline (PBS) was incubated for 30 min at room temperature with Sulfo-NHS-LC-LC-Biotin at a 1:1 molar ratio. Excess nonreacted biotin was eliminated with Zeba Spin Desalting Columns, 7 K MWCO (ThermoFisher Scientific).

2.1.4 | Coupling procedure

Nanospheres were incubated for 30 min at room temperature with monobiotinylated anti-mouse κ mAb and monobiotinylated-ova with constant mixing.

Coated nanospheres (here after called Synthetic Particulate Antigen (SPAg)) were washed twice (PBS, 1% bovine serum albumin (BSA; Sigma), 0.0005% Tween 20 (Sigma)) with 100 nm pore size Ultrafree-MC DV Centrifugal Filters (2000G/2 min, Durapore, Merck Millipore, Molsheim, France). Then, they were filtrated with 650 nm pore size Ultrafree-MC DV Centrifugal Filters (2000G/2 min, Durapore, Merck Millipore) to get rid of SPAg aggregate.

2.1.5 | Evaluation of SPAg coating

The adequate coating of SPAgs with anti-mouse κ mAb was verified by flow cytometry or ELISA as follow.

SPAg coated with increasing amount of anti-mouse κ mAb were analyzed on a LSR II flow cytometer (BD Biosciences) after a staining with a mouse PE anti-rat IgG1 heavy chain antibody (clone G1 7E7, Abcam, Paris, France).

Alternatively, for each type of SPAg, the quantity of anti-mouse κ mAb coated on their surface was measured by ELISA in a sample of the initial mix of anti-mouse κ mAb and ova and a sample of the liquid collected after the first washing of SPAgs with 100 nm pore size Ultrafree-MC DV Centrifugal Filters. Maxisorp plates (Nunc, ThermoFisher Scientific) were coated with a κ light-chain positive mouse IgG2a isotype control (BD). Serially diluted samples were added for 1 h 30 at room temperature. Anti-mouse κ mAbs were detected using alkaline phosphatase conjugated goat anti-rat IgG antibody (Abcam, 1/2000 dilution) followed by phosphatase substrate (Sigma-Aldrich). The plates were then read at 405 nm/490 nm with an automatic reader (Zeiss VERSAmax). OD was converted to concentration based on a range made with an anti-mouse κ mAb of known concentration (So max Pro 5.3 so ware; Molecular Devices).

2.2 | Mice

Wild type C57BL/6 mice aged 8–15 weeks were purchased from Charles River Laboratories (Saint Germain sur l'Arbresle, France). All mice were maintained under EOPS condition in our animal facility (PBES, Lyon, France).

2.3 | Cell preparations and cultures

After spleen cells were harvested and erythrocytes lysed (ACK Lysing Buffer, Invitrogen, ThermoFisher Scientific), B cells were enriched to >95% purity by negative selection using magnetic enrichment kits (R&D system, Lille, France). After purification, cells were resuspended in complete media (RPMI 1640 media Glutamax (Invitrogen) supplemented with 10% FCS, 50 μ M β -mercaptoethanol (Sigma), 25 mM Hepes (Invitrogen), and 10 units/ml penicillin/streptomycin (Invitrogen).

2.4 | Cell staining

The phospho-epitopes exposure kit (Beckman Coulter, Villepinte, France) was used according to the manufacturer's instructions. Briefly, 1×10^6 prewarmed B cells were stimulated with soluble anti- κ mAb or SPAGs (100 SPAGs for 1 B cell) at 37°C for 3 min before being incubated 10 min at room temperature with fixative reagent and then 5 min at 37°C with permeabilizing reagent. Then, permeabilized cells were incubated for 15 min with κ light-chain positive mouse IgG isotype control (clone \times 40, Becton Dickinson) in order to avoid reactivity between anti- κ mAb present on SPAGs and mouse PE anti-p-BLNK mAb (clone J117-1278, Becton Dickinson). Finally, B cells were incubated with rat FITC anti- λ light chain (clone JC5-1, Abcam), rat APC-Cy7 anti-B220 (clone RA3-6B2, Becton Dickinson), and mouse PE anti-p-BLNK mAbs for 30 min at room temperature in the dark. Cells were washed prior to acquisition by flow cytometry or imaging flow cytometry. Single stained controls were prepared for spectral compensation.

2.5 | Flow cytometry acquisition and analysis

Data were collected on a LSR Fortessa flow cytometer (BD Biosciences). Samples were analyzed using the FlowJo software 10.0.8r1 (Tree Star, Ashland, OR). Briefly, cells were gated based on FSC-A versus SSC-A parameters. Doublets were removed by gating FSC-A versus FSC-H. B220+ λ negative cells were selected. When SPAGs were used as stimulators, the fluorescence of 1 SPAG was calculated in order to determine different B cells subsets according to the number of SPAGs coated. P-BLNK signal intensity was then assessed in these B cells subsets.

2.6 | Confocal microscopy acquisition and analysis

Fifteen 10^6 murine B cells were loaded with SPAGs coated with anti- κ mAb at a ratio of 1/100 for 5 min and fixed with phospho-epitopes exposure kit (Beckman coulter) according to the manufacturer's instructions. Fixed cell suspension then underwent cell sorting by using a BD FACS Aria cell sorter (BD Biosciences) to collect homogeneous populations of SPAG^{POS} B cells (low, medium, or high

populations). Sorted B cells were plated 30 min on 8 well μ -slides (Ibidi, Nanterre, France) preincubated 4 h with 0.01% poly-L-Lysine (Sigma-Aldrich). Cells were incubated for 30 min at room temperature with blocking solution (PBS 1 \times -5% BSA) and stained with Alexafluor488-conjugated anti-B220 (clone RA3-6B2, BD) for 45 min at room temperature. After five washes with PBS 1 \times -5% BSA, cells were stained with DAPI (10 μ g/ml) for 10 min. After five additional washes, μ -slides were mounted with fluoromount aqueous mounting medium (Sigma-Aldrich). Confocal 3D image stacks were acquired with Zeiss 800 inverse scanning confocal microscope. Quantification of SPAGs on the surface of B cells were performed with the FIJI software (<https://fiji.sc>).


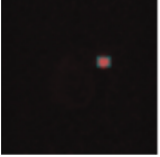


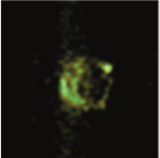
2.7 | Imaging flow cytometry acquisition and analysis

Samples were acquired on a 4-laser 12-Channel ImageStream X Mark II (Amnis-Luminex Corporation) with 60 \times magnification controlled by INSPIRE software and fully ASSIST calibrated (Amnis). Single stained controls were collected with bright-field (BF) illumination off, and with all necessary excitation lasers switched on (405, 488, 560, and 633 nm). A minimum of 10,000 total events was collected per sample. A compensation matrix was created using single stained raw image files (.rif) and the IDEAS 6.2 compensation wizard. The matrix was used to compensate sample .rif files. Briefly, single cell events were identified using the Area and Aspect ratio of channel 1 (BF) default mask (M01). Focused single cells were identified using the Gradient RMS of M01. B220 APC-Cy7, λ FITC, and Flash red nanospheres fluorescence were measured using the Intensity feature and the default M12, M02, and M11 masks, respectively. B cells were identified by B220 APC-Cy7 intensity. κ ^{POS} B cells coated with 1 SPAG were identified by λ FITC negativity and selecting the first peak of positivity on APC. M11 was adapted to be strictly restricted to the SPAG area and M03 was adapted to get rid of nonspecific p-BLNK PE signal (for details see Table 1). Then, a first intersection mask (Mask 1) between restricted adapted M11 and adapted M03 was created by Boolean combination. A feature spot count of Mask 1 was created to select only B cells in which SPAGs have triggered a specific signal. A spot count of 1 was in favor of a co-localization between 1 SPAG and sub-cellular p-BLNK expression Area and thus a specific p-BLNK signal. A result of 0 was in favor of an absence of co-localization between 1 SPAG and 1 spot of p-BLNK and thus of an absence of specific p-BLNK signal. After this first mask, M11 was adapted to cover the SPAG plus its close surroundings (for details see Table 1) and a second intersection between wider adapted M11 and adapted M03 mask (Mask 2) was designed by Boolean combination to measure p-BLNK signal intensity.

2.8 | Data analysis

Statistical analyses and graphs were performed using the Prism software (GraphPad, V8.0). *T*-test was used to compare quantitative

TABLE 1 Masking description

Mask	Description	Image
Adapted mask M11 used for Mask 1		
Peak (M11, SPAG, Bright, 5.5)	Peak mask used to identify B cells with focused SPAG	
Dilate (Peak (M11, SPAG, Bright, 5.5)1) = Mask 1A	Dilate mask adds pixels to edge of peak mask to mask entire SPAG area	
Adapted mask M11 used for Mask 2		
Peak (M11, SPAG, Bright, 5.5)	Peak mask used to identify B cells with focused SPAG	
Dilate (Peak (M11, SPAG, Bright, 5.5)4) = Mask 2A	Dilate mask adds pixels to edge of peak mask to mask entire SPAG area + its close surroundings	
Adapted mask M03 used for Mask 1 and 2		
Intensity (M03, p-BLNK, 65-4095) = Mask 1B & 2B	A threshold of 65, corresponding to the maximum raw max pixel obtained in the area of SPAG for PE FMO, was added to get rid of nonspecific signal in the area of the SPAG.	

variables; F-test was used to test if the slope of linear regression slope was significantly different from zero; *p* values <0.05 were considered significant.

3 | RESULTS

3.1 | Limits of the current gold standard technique: Analysis of the phosphorylation status of BLNK by phosflow

To develop an optimized protocol for the study of immune cell signaling, the well-known B cell receptor signaling pathway was chosen as model (Figure 1(A)). BCR pathway is typically triggered whenever the cognate antigen binds to and crosslinks surface immunoglobulins, which results in the assembly of a multimolecular complex at the cytosolic side of the plasma membrane. The B-cell linker protein (BLNK) is part of this complex and represents a central linker protein that

connects BCR stimulation to a multitude of downstream signaling pathways involved in selection, survival, proliferation, and differentiation of B cells [18]. The phosphorylation of the tyrosine residues of BLNK, which is necessary to its function, is therefore a widely used read-out for B cell receptor-associated signaling.

Although various chemical agents (such as phorbol myristate acetate/ionomycin for instance) can be used as activation signal, the crosslinking of surface immunoglobulins is generally considered as more physiological, and therefore as a more relevant method to study BCR signaling. It is not always possible or convenient to achieve BCR crosslinking by providing the cognate antigen to B cells. This indeed requires working with either the very little proportion of antigen-specific B cells or BCR transgenic models. To overcome this limitation and obtain BCR crosslinking of most polyclonal B cells in suspension, monoclonal antibodies (mAb) directed against a framework region of surface Ig are used (Figure 1(B)) [19].

BCR is composed of two pairs of polypeptides chains: two heavy chains and two light chains. Since more than 90% of murine B cells express κ light chain (the remaining 10% expressing the λ light chain, Figure 1(C)), we used soluble anti- κ mAb to activate purified polyclonal murine B cells in vitro (Figure 1(B), (C)). Three minutes after the addition of anti- κ mAb to the B cell suspension, the phosphorylation status of BLNK was assessed by the gold standard phosflow technique (Figure 1(C)). As expected, a higher p-BLNK signal was detected in κ^{pos} B cells than in both λ^{pos} B cells and negative controls (i.e., κ^{pos} B cells left unstimulated) (Figure 1(C)). However, the representative flow profile shown Figure 1(C), clearly illustrates the limitations of the phosflow approach. First, there is a significant overlap between the p-BLNK profiles of activated and resting κ^{pos} B cells, which indicates a low signal/noise ratio. Second, the overlap is even worse when considering κ^{pos} versus κ^{neg} (λ^{pos}) B cells, which demonstrates that some p-BLNK signal does not come from direct stimulation with the anti- κ mAb. Finally, the range of p-BLNK signal of κ^{pos} B cells is extremely wide (including some κ^{pos} B cells without detectable p-BLNK signal), suggesting a large variability in the signaling behavior of κ^{pos} B cells. In human samples, this feature could be explained by the fact that different patients have different proportions of naïve and memory subsets, which have distinct biochemical responses following BCR engagement [20]. However, in lab mice maintained in SOPF conditions, in which almost all B cells are naïve, this result rather indicates that it is the amount of stimulation of individual B cells in suspension which is not homogeneous and a source of variability.

3.2 | Overcoming inter-cellular stimulation heterogeneity using synthetic particulate antigens

Streptavidin-coated polystyrene nanospheres of 400 nm diameter (~ the size of a virus) were coated with biotinylated anti- κ mAb (Figure 2(A)) to generate synthetic particulate antigen (SPAG) [17]. Because SPAGs are fluorescent, we can take advantage of this characteristic to monitor the amount of BCR stimulation of any given B cells in suspension. From the fluorescence of 1 SPAG it is indeed possible

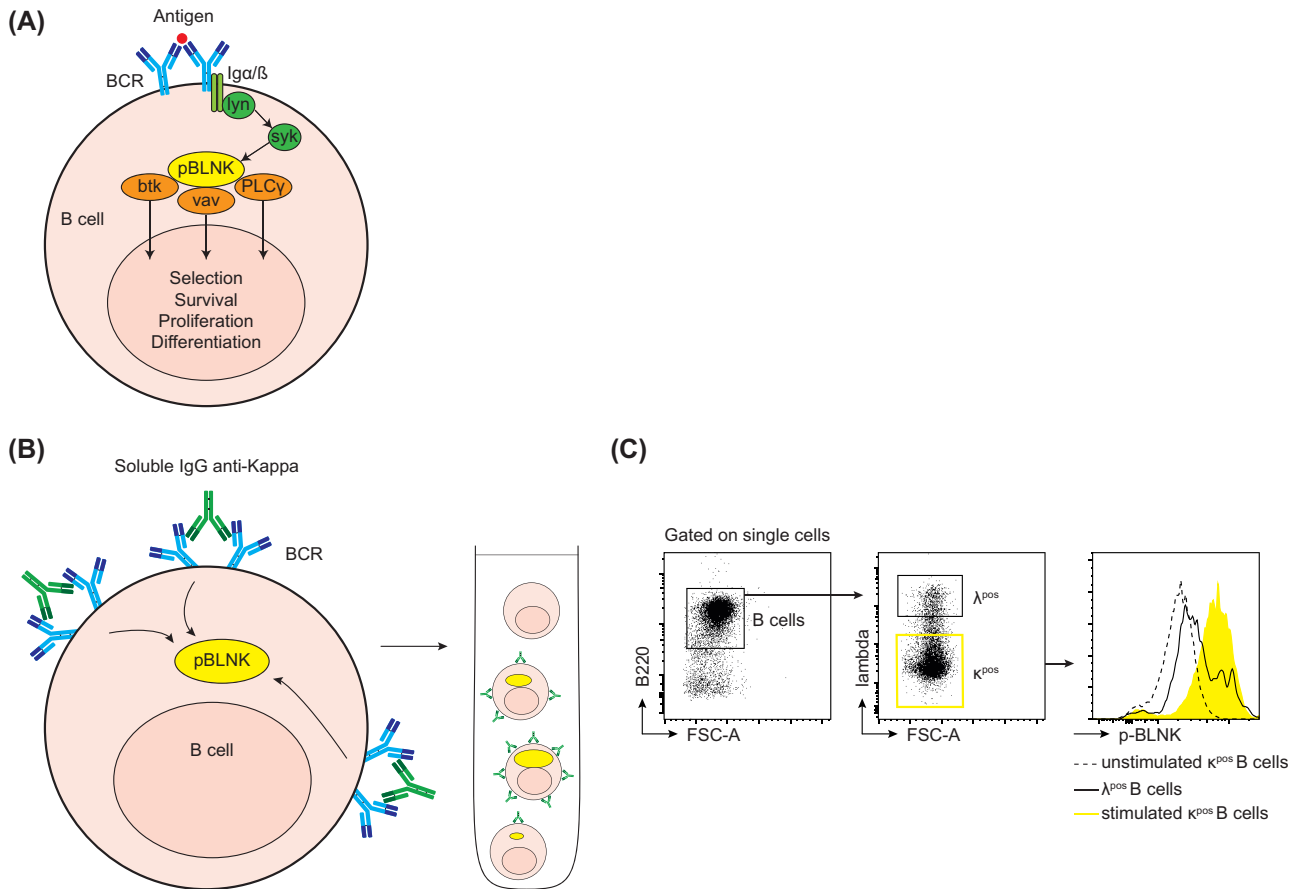


FIGURE 1 Analysis of the phosphorylation status of BLNK by phosflow. (A) Graphic representation of the signaling pathway triggered in a B lymphocyte by the binding of cognate antigen to its surface immunoglobulins (B Cell Receptor, BCR). (B, C) Murine B cells were stimulated for 3 min at 37°C with soluble anti-κ monoclonal antibody (anti-κ mAb) and the phosphorylated form of B-cell linker protein (p-BLNK) was quantified by flow cytometry. (B) Graphic representation of the experiment. (C) The gating strategy used to analyze p-BLNK signal is shown (dashed black line: negative control (unstimulated κ^{POS} B cells); solid black line: λ^{POS} B cells; solid yellow line: κ^{POS} B cells)

to determine how many SPAgs are bound to the surface of a B cell and therefore the quantity of BCR stimulation received by this particular cell (Figure 2(B)). In order to prove this point, we incubated B cells with anti-κ SPAg and FACS sorted three homogenous populations based on SPAg fluorescence (low, medium, and high MFI; Figures S1A,B and Movies S1–S3). As expected, confocal microscopy analyses of these three populations confirmed the tight correlation between the SPAg fluorescence quantified by flow cytometry and the number of SPAg effectively bound to the surface of B cells (Figure S1C).

We then went on analyzing the benefit of monitoring of BCR stimulation with the analysis of p-BLNK signal using conventional flow cytometry (Figure 2(B)). In line with our theory, the analyses revealed a direct positive correlation between the two variables. However, although the p-BLNK signal of homogeneously stimulated B cells was less spread than what was observed when all B cells (regardless their level of stimulation) were analyzed simultaneously (Figure 1(C)), there was still considerable overlap between the different categories of SPAg^{POS} B cells (Figure 2(B)). These results suggest that despite the fact that conventional flow cytometry is often considered as the most

sensitive method to analyze cell signaling [21], this technology does not provide a sufficient signal/noise ratio for accurate analysis.

3.3 | Improving signal/noise ratio by imaging flow cytometry

In cell signaling analysis, the specific signal is usually low and the results therefore heavily influenced by concurrent nonspecific signals. In this regard flow cytometry has several limitations because the technology measures all the fluorescence emitted in the intersection of laser beam and flow chamber at a given time point, which in addition to the specific signal of interest, also includes the signal emitted by free molecules of fluorochrome, autofluorescence of cellular debris and the cell itself, the nonspecific binding of the fluorescent mAb and the activity of the signaling pathway not directly related to the experimental stimulation (Figure 3(A)).

Imaging flow cytometry (IFC) has been developed over the last decade to combine the advantages of flow cytometry and microscopy. Like flow cytometry, IFC allows to simultaneously quantify several

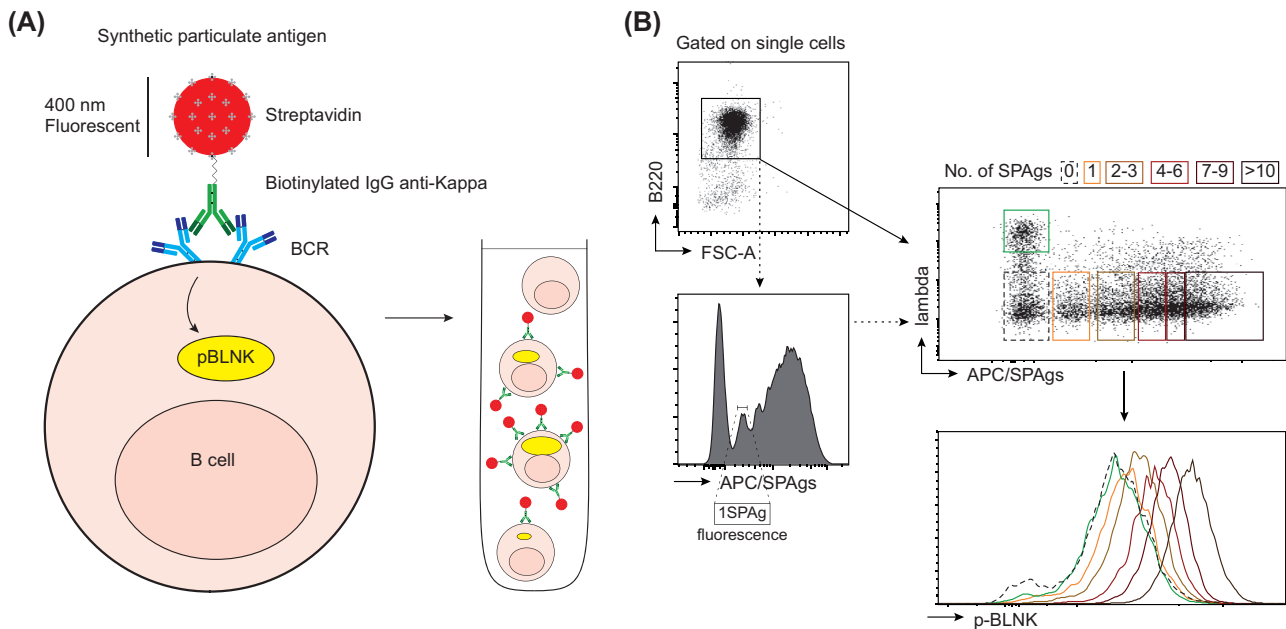


FIGURE 2 Overcoming inter-cellular stimulation heterogeneity using synthetic particulate antigens. (A, B) Murine B cells were stimulated for 3 min at 37°C with Synthetic Particulate Antigens (SPAg) that is, fluorescent nanospheres coated with anti- κ mAb and p-BLNK signal was assessed by flow cytometry. (A) Graphic representation of the experiment. (B) The gating strategy used to analyze p-BLNK signal in κ^{pos} B cells according to the number of SPAGs bound to cell surface is shown

fluorescent signals at a single cell-level in large numbers of cells in an objective and statistically robust manner. The first advantage of IFC technology is that it allows significant reduction of the noise. Dark current, which corresponds to the electric signal produced by a photodetector when it does not receive a photon, is indeed present in each pixel analyzed. As the total noise in a measure is the product of the noise of each pixel, restraining the analysis to a limited number of pixels (about 100 from the 10,000 of the image) results in massive reduction (by about 99%) of the electronic noise inherent to information processing. The signal resolution in IFC therefore is inversely proportional to the size of the area analyzed [22]. This advantage of IFC over conventional flow cytometry is clearly illustrated in the better definition of the successive peaks of SPAG fluorescence that corresponds to incremental binding of the nanospheres on the surface of κ^{pos} B cells (Figure 3(B)). Note that this advantage is mainly observed when a relatively low number of SPAGs are bound on B cell surface. This is explained by the fact that the relative difference in fluorescence between the peaks follows the rules of arithmetic progression: the fluorescence of B cells coated with n SPAG is defined as $F_n = F_{n-1} + 1/n$. Therefore, when the number of SPAGs on B cell surface increases, the change in fluorescence ($1/n$) represents a part less and less important which tends to zero (Figure 3(B)).

In addition, IFC relies on a CCD camera that provides spatial information allowing to localize the fluorescence at the subcellular level. This feature also provides a clear advantage over conventional flow cytometry regarding signal/noise performance. For instance, when analyzing B cells loaded with anti- κ SPAG by conventional flow cytometry, a weird population of B cells positive for both λ and SPAG was evidenced (Figure 2(B)). Analysis of the same cell suspension by

imaging flow cytometry (IFC) revealed that this λ^{pos} and SPAG $^{\text{pos}}$ population does not really exist. This observation was due to the fact that some SPAG $^{\text{pos}}$ (and therefore κ^{pos} B cells) were decorated with cell debris coming from λ^{pos} B cells (Figure 3(C)). This explanation is further supported by functional data, showing that λ^{pos} SPAG $^{\text{pos}}$ B cells have a p-BLNK signal similar to the κ^{pos} B cells loaded with the same number of SPAGs (Figure 3(D)).

3.4 | SPAG-assisted sub-cellular signaling analysis (SIBERIAN)

Since the spatial information provided by IFC also allows linking the signal measured to the experimental stimulation, we reasoned that a technique combining IFC with SPAG stimulation, which we named SIBERIAN (for SPAG-assisted sub-cellular signaling ANalysis), might help differentiating specific signaling signal from nonspecific noise in the context of immune cell signaling analysis (Figure 3(A)).

To test this theory, purified murine B cells were stimulated in vitro with SPAGs for 3 min and the phosphorylation status of BLNK was then assessed by IFC in κ^{pos} B cells that had bound 1 SPAG (i.e., homogeneous BCR stimulation) as explained Figure 4(A). Briefly, after gating on κ^{pos} B cells with 1 SPAG, a first (restrictive) mask of colocalization between the SPAG and p-BLNK signal (Mask 1) was applied in order to identify those κ^{pos} B cells in which the SPAG had effectively triggered a p-BLNK signal (Figure 4(A) and Table 1). To do so, we designed two masks (Masks 1A and 1B) that we co-localized (Mask1). The first (Mask 1A), based on SPAG fluorescence (Dilate (Peak [M11, SPAG, Bright, 5.5]1)), was made to select B cells with one

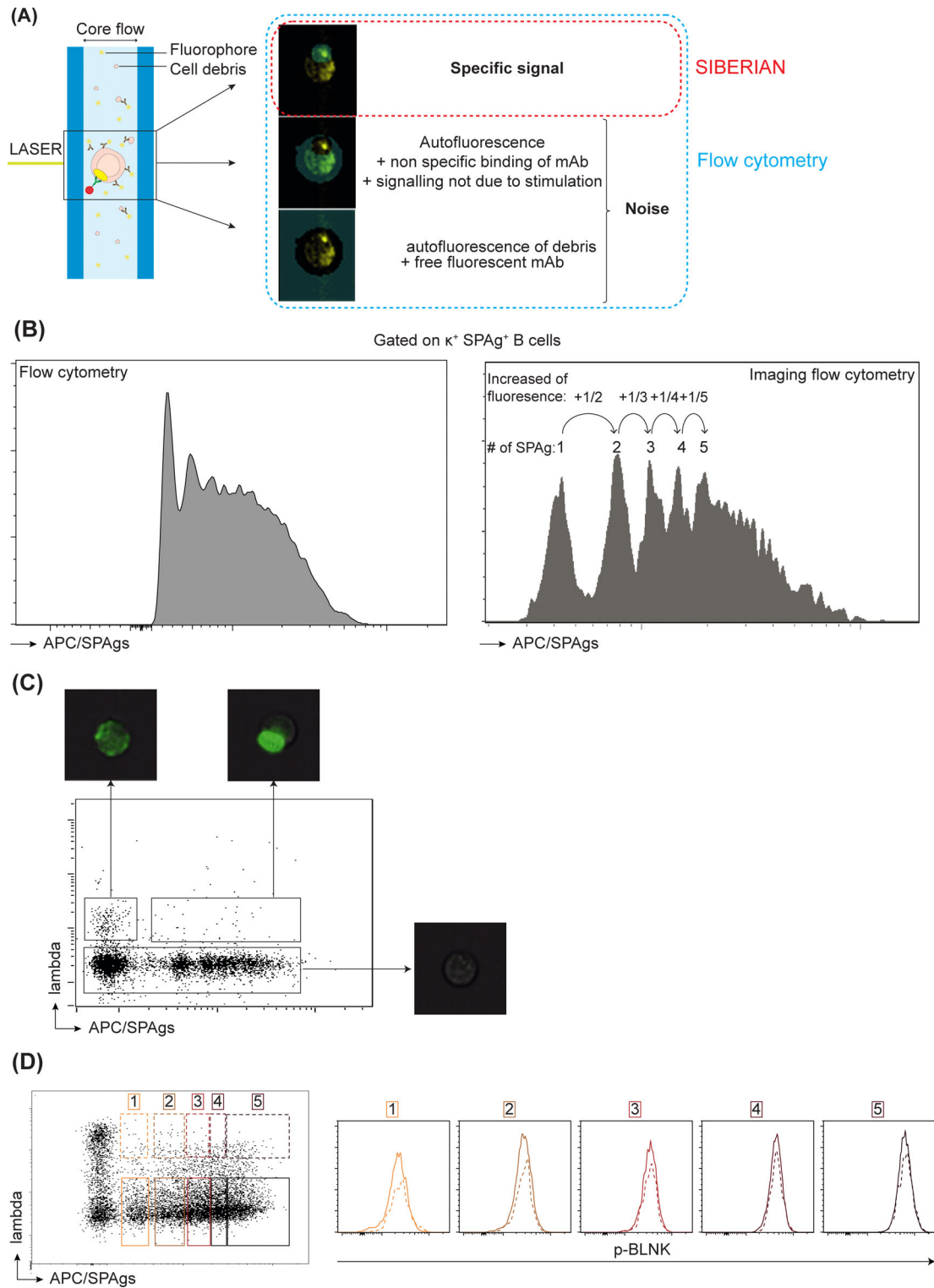
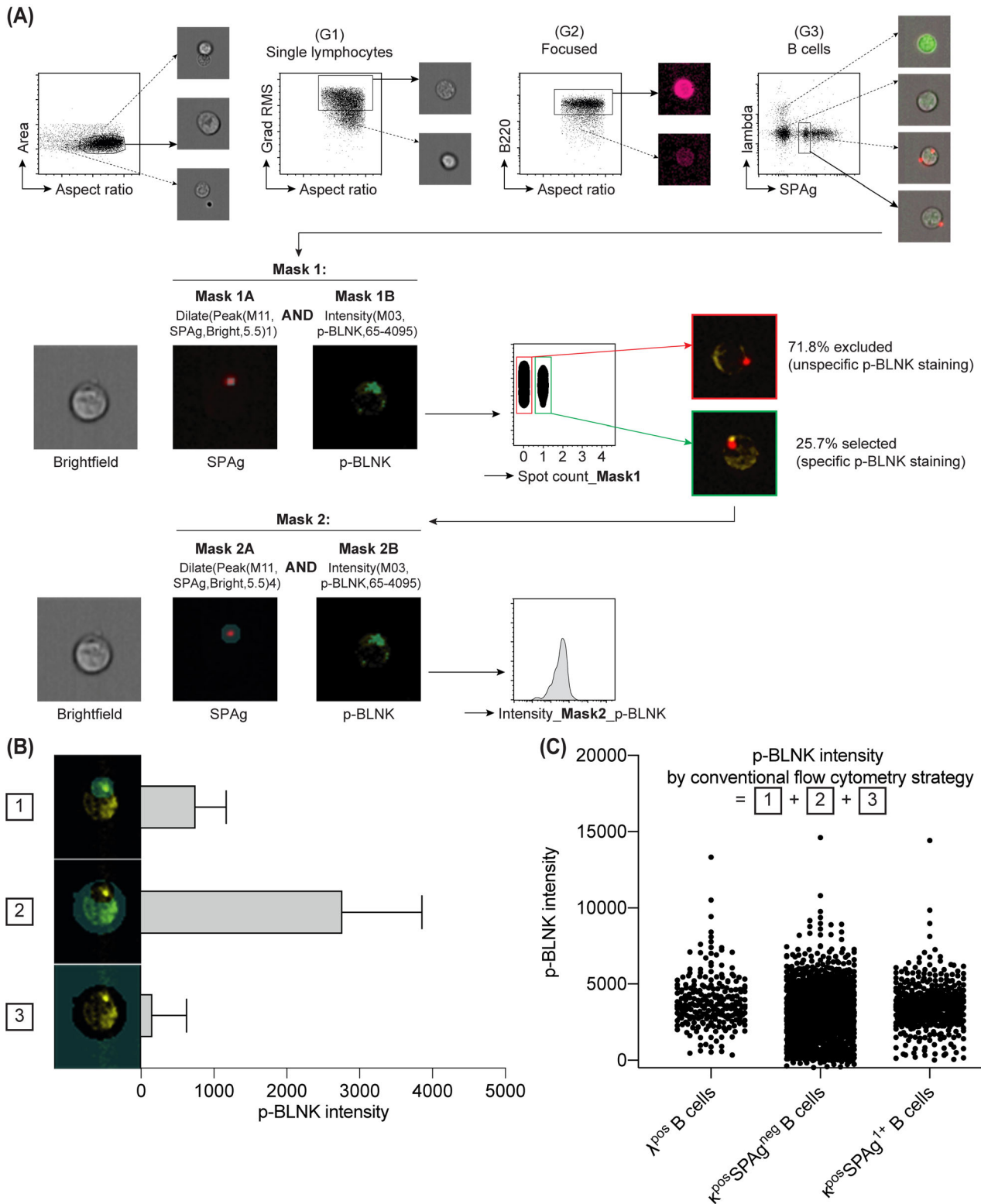


FIGURE 3 Improving signal/noise ratio by imaging flow cytometry. Murine B cells were stimulated for 3 min at 37°C with SPAGs and the phosphorylated form of B-cell linker protein (p-BLNK) was quantified by flow cytometry or imaging flow cytometry (IFC). The technique combining IFC with SPAG stimulation is named SIBERIAN (SPAG-assisted suB-cELLulaR signaling ANalysis). (A) Graphic representation of the experiment comparing the nature of the signals measured by SIBERIAN (red) versus conventional flow cytometry (blue). (B) Representative histograms of SPAG fluorescence for κ^{pos} B cells obtained by flow cytometry and IFC are shown. (C) Representative pictures of λ^{pos} SPAg $^{\text{pos}}$ B cells, λ^{pos} SPAg $^{\text{neg}}$ B cells, and κ^{pos} B cells obtained by IFC are shown. (D) The analysis of p-BLNK signal in λ^{pos} SPAg $^{\text{pos}}$ and κ^{pos} B cells according to the number of SPAGs bound to B cell surface is shown



SPAg in focus (Table 1). The second one (Mask 1B) based on p-BLNK fluorescence (Intensity [M03, p-BLNK, 65-4095]) relies on the addition of a threshold of 65, corresponding to the maximum raw max pixel obtained in the area of SPAg for PE FMO and allowed us getting rid of nonspecific p-BLNK signal in the area of the SPAg (Table 1). This step led to the exclusion of 71.8% of cells in which either no p-BLNK signal was detected at all or the p-BLNK signal detected did not localize where BCR crosslinking occurred (Figure 4(A)). Among the 25.7% of selected κ^{POS} B cells, a second (wider) mask (Mask 2) was designed based upon SPAg fluorescence (Mask 2A) (Dilate (Peak (M11, SPAg, Bright, 5.5)4) and p-BLNK fluorescence (Mask 2B) (Intensity (M03, p-BLNK, 65-4095)) and used to quantify the specific p-BLNK signal only in SPAg area and its close surroundings (Figure 4(A) and Table 1).

Figure 4(B) demonstrates that specific p-BLNK signal represents only a limited fraction of the total p-BLNK signal (20.4%) usually recorded by flow cytometry. It shall not be forgotten that this conclusion is reached when conventional phosflow is used to analyze homogeneously stimulated cells selected with the help of SPAg, a refinement usually not used in immune cell signaling analysis. The results generated with the current gold standard technique: phosflow analysis of B cells stimulated with anti- κ mAb in solution (as in Figure 1(B)) are even less reliable. Indeed, when a gating strategy similar to conventional flow cytometry was conducted on IFC data, some B cells that did not receive any BCR stimulation (λ^{POS} or κ^{POS} SPAg negative) displayed levels of p-BLNK signal similar to that of κ^{POS} SPAg¹⁺ B cells (Figure 4(C)).

3.5 | SIBERIAN provides exquisite specificity and sensitivity in immune cell signaling analysis

In order to demonstrate the superiority of the SIBERIAN approach over the current gold standard, we compared the ability of the two approaches to discriminate subtle differences in BCR signaling. Briefly, we generated four types of SPAg coated with increasing amount of anti- κ mAb molecules (Figure 5(A)). The amount of anti- κ mAb molecules coated on the different types of SPAgs was assessed by both ELISA and flow cytometry (Figure S2) and ranged between 8830 and 119,000 molecules per SPAg (Figure S2C).

Purified murine B cells in suspension were then stimulated with the various type of SPAg for 3 min before p-BLNK signal was measured by phosflow or SIBERIAN in homogeneously stimulated B cell populations (stimulated κ^{POS} B cells that had bound 1 SPAg). While phosflow could discriminate unstimulated κ^{POS} B cells (negative control) from κ^{POS} B cells stimulated through their BCR, this gold standard technique failed to evidence the difference in BCR signaling between κ^{POS} B cells stimulated with SPAg coated with low versus high density of anti- κ mAb (Figure 5(B), (C)). In contrast, SIBERIAN not only discriminated κ^{POS} B cells stimulated with SPAg coated with the lowest and highest density of anti- κ mAb, but also correctly classified κ^{POS} B cells stimulated with SPAg coated with two intermediate density of anti- κ mAb (Figure 5(B), (C)).

4 | DISCUSSION

In this study, we have illustrated the limits of phosflow, which is widely considered as the current gold standard technique to analyze immune cell signaling [21]. By analyzing a bulk of cells in suspension that did not receive the same amount of stimulation and without possibility to discriminate accurately the specific signal from the many sources of noise, phosflow technique is poised to limited performance, in particular when it comes to discriminate between subtle differences in signaling. To optimize immune cell signaling analyses, we instead propose to couple the use of SPAg with imaging flow cytometry, a technique that we named SIBERIAN (for SPAg-assisted subCellular signaling ANalysis).

SPAg [17] is a versatile, cheap, and handy tool, which allow stimulating virtually every kind of immune cells. Using the biotin/streptavidin system, the strongest noncovalent interactions known in nature [23], any mAb (or combination of mAbs) can be coated to the surface of the nanosphere: anti CD16 (for activation of NK cells), anti-CD3 + anti-CD28 (for T cells), ...and so on. In addition (as shown Figure 4), it is very simple to modify the density of mAb coated on SPAg surface, and therefore tune the intensity of immune cell stimulation. Finally, the fact that SPAg is fluorescent allows, not only the identification of the immune cells in suspension that have been stimulated, but also their categorization according to the intensity of stimulation they received (thereby suppressing inter-cellular heterogeneity). The present study was focusing on upstream events of BCR signaling cascade that take place close to the cytoplasmic membrane. We however believe that SPAg would be equally efficient for the analysis of downstream events of the signaling cascade. Following BCR crosslinking, the complex made of BCR and SPAg is internalized in endosomal compartment of activated B cells. Previous studies have shown that BCR signaling initiated at the plasma membrane continued after the BCR was endocytosed and trafficked through early TfR+ endosomes to late LAMP1+ endosomes and multivesicular compartments with the recruitment and phosphorylation of downstream kinases, initially cRaf and subsequently Erk, p38, and Jnk [24]. Because the fluorescence of SPAg is located in the core of the nanosphere it is protected from the proteolysis that occurs in endosomal compartment. Previous studies from our group have shown that this feature could be exploited to track SPAg for several days after internalization with the help of imaging flow cytometry [17,25].

Although using SPAg for the stimulation of immune cells would already represent a progress for conventional phosflow analysis (as shown Figure 1), it would however not solve the issue of the lack of sensitivity of flow cytometry, which results from the low signal/noise ratio that characterizes cell signaling analysis. In order to circumvent the later issue, we propose to take advantage of the development of imaging flow cytometry. This fairly recent technology combines features of flow cytometry and fluorescent microscopy with advances in data-processing algorithms. IFC allows multiparametric fluorescent and morphological analysis of thousands of cellular events and has the unique capability of identifying collected events by their

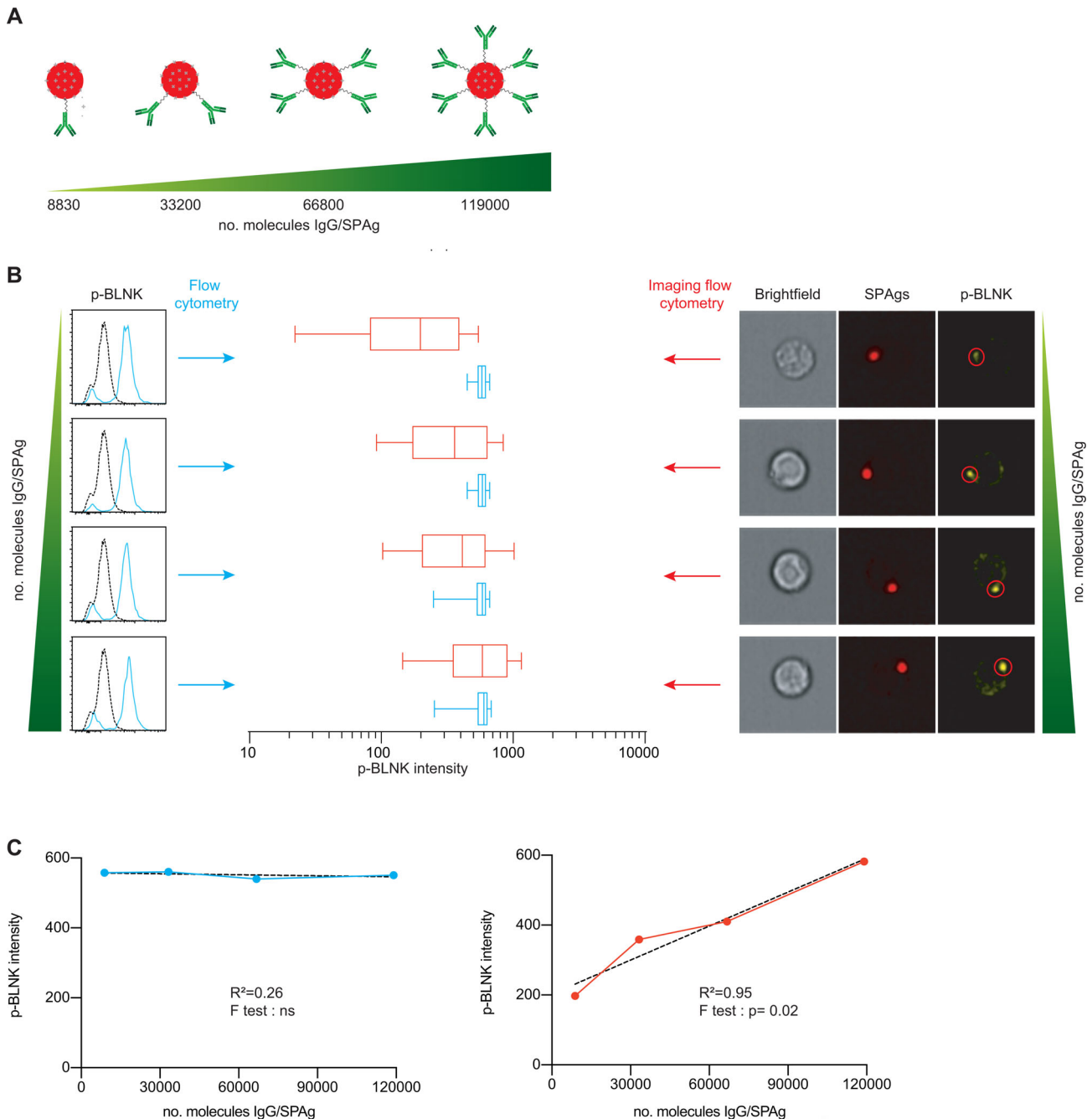


FIGURE 5 SIBERIAN provides exquisite specificity and sensitivity in immune cell signaling analysis. (A) SPAGs coated with increasing amount of anti- κ monoclonal antibody (8830–119,000 molecules of anti- κ mAb per SPAG; darker shades of green) were generated. (B) Purified murine B cells were simulated in vitro with the different types of SPAGs and p-BLNK signal was measured in SPAG¹⁺ κ^{pos} B cells using either conventional flow cytometry (left) or imaging flow cytometry (right). Left panel: representative histograms of p-BLNK signal obtained with flow cytometry for unstimulated κ^{pos} B cells (dashed black line) and for SPAG¹⁺ κ^{pos} B cells (solid blue line) are shown for each type of SPAG. Middle panel: comparison of p-BLNK signal intensity measured by conventional flow cytometry (blue) and imaging flow cytometry (red) for each type of SPAG. The center line shows the median; the box limits indicate the 25th and 75th percentiles, respectively. The whiskers indicate the 10th and 90th percentiles, respectively. Right panel: representative images of SIBERIAN analysis of p-BLNK signal in SPAG¹⁺ κ^{pos} B cells are shown for each type of SPAG. (C) Linear regression model was used to study the correlation between the number of anti- κ mAb at the surface of SPAGs (intensity of BCR cross-linking) in the x axis, and the intensity of the p-BLNK signal (Y axis) measured with conventional flow cytometry (gold standard, left panel) and SIBERIAN (right panel). *F* test

real images. These unique features make IFC the ideal technique to address the critical question of statistical analysis of subcellular distribution of proteins in a cell [26]. Taking advantage of SPAG

fluorescence, IFC can restrict the analysis of cell signaling to the subcellular region where the stimulation actually occurred, and by this mean eliminating most of the nonspecific signals responsible for the

noise. The gain in accuracy is such that SIBERIAN was able to discriminate the difference in cell signaling related to different intensity of stimulation, while conventional flow cytometry only discriminated activated from nonactivated B cells. This level of performance would be precious to anyone seeking to refine the understanding of signaling in immune cells or wishing to test therapeutic approaches to inhibit them.

Despite its many advantages, SIBERIAN technique also suffers limitations. In comparison to flow cytometry, less channels are currently available on imaging flow cytometers making it difficult to study more than 2 or 3 intracellular signaling molecules at the same time. For the same reason, it is also difficult to study intracellular signaling molecule in multiple populations at the same time [11]. Furthermore, imaging flow cytometer have been limited to analytical throughput speeds of 2000–3000 cells per second at 20× magnification, which is 10–100 times slower than traditional flow cytometers. Regarding the latter issue, it shall be mentioned that new developments in automated high-throughput imaging cytometers are now allowing researchers to analyze up to 60,000 cells per second [27]. Waiting for these progresses to be available in routine, it is already possible to partially overcome the problem by working with cell suspension enriched in the subset of interest. Finally, analysis of IFC data remains far more complex and time-consuming than flow cytometry data. Although this problem currently represents the most critical obstacle to the development of IFC it might soon be solved. Many researchers indeed currently develop advanced machine-learning software to mine IFC data and it has been recently reported that an open-source image processing software allows hundreds of morphological features to be measured and analyzed using machine learning, tree classification, neural networks and clustering [28].

In conclusion, our study describes a new technique, which combines the use of SPAG and imaging flow cytometry to analyze immune cell signaling with unprecedented specificity and sensibility.

ACKNOWLEDGMENT

Alice Koenig is supported by INSERM (poste accueil 2015/1239/BT) and the Hospices Civils de Lyon. The study was supported by a CoPoC INSERM transfer 2018 grant (SPAGETI).

CONFLICT OF INTEREST

The authors declare no potential conflict of interest.

AUTHOR CONTRIBUTIONS

Xavier Charmetant: Formal analysis; writing-original draft. **Thomas Barba:** Formal analysis. **Antoine Sicard:** Formal analysis. **Maxime Espi:** Formal analysis. **Sebastien Dussurgey:** Formal analysis.

ORCID

Alice Koenig  <https://orcid.org/0000-0003-4358-9719>

REFERENCES

- Nairn AC, Detre JA, Casnellie JE, Greengard P. Serum antibodies that distinguish between the phospho- and dephospho-forms of a phosphoprotein. *Nature*. 1982;299:734–6.
- Ding H, Wu T. Insulin-like growth factor binding proteins in autoimmune diseases. *Front Endocrinol (Lausanne)*. 2018;9:499.
- Baselga J, Arribas J. Treating cancer's kinase 'addiction'. *Nature Med*. 2004;10:786–7.
- Druker BJ, Tamura S, Buchdunger E, Ohno S, Segal GM, Fanning S, et al. Effects of a selective inhibitor of the Abl tyrosine kinase on the growth of Bcr-Abl positive cells. *Nature Med*. 1996;2:561–6.
- Druker BJ, Talpaz M, Resta DJ, Peng B, Buchdunger E, Ford JM, et al. Efficacy and safety of a specific inhibitor of the BCR-ABL tyrosine kinase in chronic myeloid leukemia. *N Engl J Med*. 2001;344:1031–7.
- Towbin H, Staehelin T, Gordon J. Electrophoretic transfer of proteins from polyacrylamide gels to nitrocellulose sheets: procedure and some applications. *Proc Natl Acad Sci U S A*. 1979;76:4350–4.
- Burnette WN. "Western blotting": electrophoretic transfer of proteins from sodium dodecyl sulfate–polyacrylamide gels to unmodified nitrocellulose and radiographic detection with antibody and radioiodinated protein A. *Anal Biochem*. 1981;112:195–203.
- Pillai-Kastoori L, Schutz-Geschwender AR, Harford JA. A systematic approach to quantitative Western blot analysis. *Anal Biochem*. 2020; 593:113608.
- Janes KA. An analysis of critical factors for quantitative immunoblotting. *Sci Signal*. 2015;8:rs2–2.
- Suni MA, Maino VC. Flow cytometric analysis of cell signaling proteins. *Methods Mol Biol*. 2011;717:155–69.
- Rip J, de Bruijn MJW, Kaptein A, Hendriks RW, Corneth OBJ. Phosphoflow protocol for signaling studies in human and murine B cell subpopulations. *The Journal of Immunology*. 2020;204:2852–63.
- Davies R, Vogelsang P, Jonsson R, Appel S. An optimized multiplex flow cytometry protocol for the analysis of intracellular signaling in peripheral blood mononuclear cells. *J Immun Methods*. 2016;436:58–63.
- Coppin E, Malergue F, Thibult M-L, Scifo C, Favre C, Nunès JA. Flow cytometric analysis of intracellular phosphoproteins in human monocytes. *Cytometry Part B: Clin Cytom*. 2017;92:207–10.
- Firaguay G, Nunès JA. Analysis of signaling events by dynamic phosphoflow cytometry. *Sci Signal*. 2009;2:pl3–3.
- Irish JM, Myklebust JH, Alizadeh AA, Houot R, Sharman JP, Czerwinski DK, et al. B-cell signaling networks reveal a negative prognostic human lymphoma cell subset that emerges during tumor progression. *Proc Natl Acad Sci U S A*. 2010;107:12747–54.
- Giudice V, Feng X, Kajigaya S, Young NS, Biancotto A. Optimization and standardization of fluorescent cell barcoding for multiplexed flow cytometric phenotyping. *Cytometry A*. 2017;91:694–703.
- Sicard A, Koenig A, Graff-Dubois S, Dussurgey S, Rouers A, Dubois V, et al. B cells loaded with synthetic particulate antigens: a versatile platform to generate antigen-specific helper T cells for cell therapy. *Nano Lett*. 2016;16:297–308.
- Fu C, Turck CW, Kurosaki T, Chan AC. BLNK: a central linker protein in B cell activation. *Immunity*. 1998;9:93–103.
- Defranco AL, Raveche ES, Asofsky R, Paul WE. Frequency of B lymphocytes responsive to anti-immunoglobulin. *J Exp Med*. 1982;155: 1523–36.
- Moens L, Kane A, Tangye SG. Naïve and memory B cells exhibit distinct biochemical responses following BCR engagement. *Immunol Cell Biol*. 2016;94:774–86.
- Krutzik PO, Irish JM, Nolan GP, Perez OD. Analysis of protein phosphorylation and cellular signaling events by flow cytometry: techniques and clinical applications. *Clin Immunol*. 2004;110:206–21.
- Ortyn WE, Hall BE, George TC, Frost K, Basiji DA, Perry DJ, et al. Sensitivity measurement and compensation in spectral imaging. *Cytometry A*. 2006;69:852–62.
- Weber PC, Ohlendorf DH, Wendoloski JJ, Salemme FR. Structural origins of high-affinity biotin binding to streptavidin. *Science*. 1989;243:85–8.
- Chaturvedi A, Martz R, Dorward D, Waisberg M, Pierce SK. Endocytosed BCRs sequentially regulate MAPK and Akt signaling pathways from intracellular compartments. *Nat Immunol*. 2011;12: 1119–26.

25. Thauinat O, Granja AG, Barral P, Filby A, Montaner B, Collinson L, et al. Asymmetric segregation of polarized antigen on B cell division shapes presentation capacity. *Science*. 2012;335:475–9.
26. Barteneva NS, Fasler-Kan E, Vorobjev IA. Imaging flow cytometry: coping with heterogeneity in biological systems. *J Histochem Cytochem*. 2012;60:723–33.
27. Holzner G, Mateescu B, Van Leeuwen D, Cereghetti G. Ultra high-throughput multiparametric imaging flow cytometry: towards diffraction-limited sub-cellular detection.
28. Hennig H, Rees P, Blasi T, Kamensky L, Hung J, Dao D, et al. An open-source solution for advanced imaging flow cytometry data analysis using machine learning. *Methods*. 2017;112:201–10.

SUPPORTING INFORMATION

Additional supporting information may be found online in the Supporting Information section at the end of this article.

How to cite this article: Koenig A, Charmetant X, Barba T, et al. Improved cell signaling analysis by biofunctionalized nanospheres and imaging flow cytometry. *Cytometry*. 2021; 1–12. <https://doi.org/10.1002/cyto.a.24354>

3. Publication 3

Predictive factors of a viral neutralizing humoral response after a third dose of COVID-19 mRNA vaccine.

Charmetant X*, Espi M*, Barba T, Ovize A, Morelon E, Mathieu C, Thaunat O.

* : co-premier auteurs

American Journal of Transplantation. 2022 May;22(5):1442-1450.

Predictive factors of a viral neutralizing humoral response after a third dose of COVID-19 mRNA vaccine

Xavier Charmetant¹  | Maxime Espi¹ | Thomas Barba¹ | Anne Ovize² | Emmanuel Morelon^{1,3,4} | Cyrille Mathieu¹ | Olivier Thauinat^{1,3,4} 

¹CIRI, INSERM U1111, Université Claude Bernard Lyon I, CNRS UMR5308, Ecole Normale Supérieure de Lyon, Univ. Lyon, Lyon, France

²Eurofins Biomnis Laboratory, Lyon, France

³Department of Transplantation, Nephrology and Clinical Immunology, Hospices Civils de Lyon, Edouard Herriot Hospital, Lyon, France

⁴Claude Bernard University (Lyon 1), Villeurbanne, France

Correspondence

Olivier Thauinat, Service de Transplantation, Néphrologie et Immunologie Clinique, Hôpital Edouard Herriot, 5 Place d'Arsonval, 69003 Lyon, France.
Email: olivier.thauinat@chu-lyon.fr

Funding information

Hospices Civils de Lyon; Société Francophone de Transplantation; Etablissement Français du Sang; Institut National de la Santé et de la Recherche Médicale; Fondation pour la Recherche Médicale, Grant/Award Number: PME20180639518

Kidney transplant recipients (KTRs) have reduced ability to mount adequate antibody response after two doses of the COVID-19 mRNA vaccine. French health authorities have allowed a third booster dose (D3) for KTRs, but their response is heterogeneous and tools able to discriminate the responders are lacking.

Anti-RBD IgG titers (chemiluminescence immunoassay), spike-specific cellular responses (IFN- γ -releasing assay, IGRA), and in vitro serum neutralization of the virus (the best available correlate of protection), were evaluated 7–14 days after the second dose (D2) of BNT162b2 vaccine in 93 KTRs. Among the 73 KTRs, whose serum did not neutralize SARS-CoV-2 in vitro after D2, 14 (19%) acquired this capacity after D3, and were considered as “responders.” Exploratory univariate analysis identified short time from transplantation and high maintenance immunosuppression as detrimental factors for the response to D3. In addition, any of the presence of anti-RBD IgGs and/or positive IGRA after D2 was predictive of response to D3. By contrast, none of the KTRs with both a negative serology and IGRA responded to D3. In summary, routinely available bioassays performed after D2 allow identifying KTRs that will respond to a booster D3. These results pave the way for the personalization of vaccination strategy in KTRs.

KEYWORDS

COVID-19, mRNA-vaccine, renal transplantation, SARS-CoV-2

1 | INTRODUCTION

Kidney transplant recipients (KTRs) carry a very high risk of death due to COVID-19 in case of infection by SARS-CoV-2.^{1–5} This vulnerable population has therefore been prioritized for vaccination. However, only 25% (range: 2.5%–48%) of KTRs develop adequate antibody response after the “standard” two doses of COVID-19 mRNA vaccine.^{6–14} These antibodies are responsible

for the neutralization of the virus, that can be assessed using in vitro functional assay, which currently represents the best available correlate of protection against severe COVID-19 for both the general population¹⁵ and KTRs.¹⁶ Accordingly the lack of adequate antibody response after vaccination in KTRs correlated with the occurrence of (sometime severe forms of) COVID-19 in vaccinated patients.^{17–19}

Preliminary reports suggest that a third dose (D3) of vaccine improves the humoral response in transplant recipients.^{20–25} In this prospective observational study, we aimed at describing the immune response of KTRs to D3 of mRNA vaccine and identifying the variables associated with response to this booster dose.

Abbreviations: BAU, binding antibody unit; CLIA, chemiluminescence immunoassay; D2, second dose; D3, third dose; IGRA, IFN- γ -releasing assay; KTRs, kidney transplant recipients; RBD, receptor binding domain.

Xavier Charmetant and Maxime Espi contributed equally to this study.

© 2022 The American Society of Transplantation and the American Society of Transplant Surgeons.

2 | METHODS

2.1 | Study population

The study protocol was approved by Institutional Review Board (approval number: 2020-A02918-31, Comité de Protection des Personnes Sud-Est I). All patients gave signed informed consent for the participation to the study. According to the French health authority's recommendations, a third vaccine injection was offered to all KTRs from Lyon University Hospital, whose serum showed no *in vitro* viral neutralization capacity after two doses of BNT162b2 mRNA vaccine (Pfizer-BioNtech).

Blood samples were collected the day of the first vaccine injection and between 7 and 14 days following D2 and D3.

Of note, we verified that none of the three assays (described below) that we used in this study was affected by the difference in sampling time across patients, as shown in Figure S1.

2.2 | Assessment of the tolerability and safety of vaccine injections

Local and systemic adverse events were collected retrospectively at each follow-up visit. Data collected correspond to adverse events within 7 days after D2 and D3, respectively. Data on allograft dysfunction were collected at the end of the follow-up.

2.3 | Anti-SARS-CoV-2 humoral response assessment

2.3.1 | Anti S-RBD IgG

The IgG antibodies directed against the Receptor Binding Domain (RBD) of the spike glycoprotein of the SARS-CoV-2 were detected by a chemiluminescence immunoassay (CLIA), using the Maglumi® SARS-CoV-2 S-RBD IgG test (Snibe Diagnostic, Shenzhen, China) on a Maglumi 2000® analyser (Snibe Diagnostic),²⁶ according to the manufacturer's instructions. This test displays clinical sensitivity and specificity of 100% and 99.6%, respectively. As recommended by the WHO, the obtained titer was then expressed as binding antibody units/mL (BAU/mL); correction factor for Maglumi®: 4.33.

2.3.2 | *In vitro* viral neutralization assay

The test was performed as previously reported.^{27,28} SARS-CoV-2 (BetaCoV/France/IDF0571/2020 virus [GISAID Accession ID = EPI_ISL_411218]) was isolated in Vero E6 from a nasal swab of one of the first COVID-19-positive patient in France and was kindly provided by Dr Olivier Terrier and the Virpath lab (CIRI-Lyon). To generate virus stocks, Vero E6 cells (kindly provided by Dr F-L. Cosset, CIRI-Lyon)

were inoculated with virus at an MOI of 0.01. Supernatant fluid was harvested at 72 h post-infection, clarified by low-speed centrifugation, aliquoted, and stored at -80°C . Virus stock was quantified by classic limiting dilution plaque assay on Vero E6 cells.

Two-fold dilutions of serum in 50 μl of Dulbecco's modified Eagle medium (DMEM), containing 2X penicillin/streptomycin, were incubated with 200 plaque-forming units (PFU) of SARS-CoV-2 in 50 μl of DMEM for 15 min at room temperature. Aliquots of 100 μl of DMEM +4% FBS containing 2.5×10^4 Vero E6 cells were added to achieve a final dilution of sera from 1:100 to 1:12,800 (4 wells per dilution). Cells were incubated for 5 days at 37°C , 5% CO_2 . After 15min of fixation in PFA4% in PBS1X, cytopathic effect was revealed by crystal violet staining and scored by a researcher (CM) blinded in the study design and sample identity. Neutralization endpoint titers were expressed as the log₁₀ value of the last serum dilution that completely inhibited virus-induced cytopathic effect.

2.4 | Anti-SARS-CoV-2 Spike cellular response assessment

Spike specific cellular response was quantified in the circulation of the KTRs using the QuantiFERON® SARS-CoV-2 test (Qiagen, Netherlands), a commercially available Interferon Gamma Releasing Assay (IGRA), according to the manufacturer's instructions.²⁹

Briefly, one milliliter blood was distributed in each tube of the assay: (i) uncoated tube: negative control/background noise, (ii) tube coated with mitogen: positive control, and (iii) tube coated with 13-mers peptides derived from the SARS-CoV-2 S1-Spike glycoprotein (thereafter designated as Ag1 tube). After 20 hours of culture at 37°C , tubes were centrifugated 15 minutes at 2500g, and stored at 4°C before IFN- γ quantification in the supernatant by ELISA. Although various cell types contribute to the production of IFN- γ in the IGRA, CD4+ T cells is the dominant subset (38% in the Ag1 tube, Figure S2A,B and Methods S1). Furthermore, the results of the IGRA correlate with the response of follicular helper T cells (the subset of CD4+ T cells specialized in B cell help for antibody production) evaluated by flow cytometry³⁰ (Figures S2A–D and Methods S1).

To be deemed analyzable, the IFN- γ concentration in the positive control tube had to exceed 0.5 IU/ml. The cellular assay value was the difference between the tube (iii) and the negative control (i). A test was considered positive if the value of IFN- γ concentration exceeded 0.07 IU/ml, a threshold which corresponds to the highest value obtained in a cohort of 13 controls (healthy volunteers naive for SARS-CoV-2, Figure S2E). To allow for log scale representations, negative and zero values were reported at 0.01 IU/ml.

2.5 | Statistical analysis

All the analyses were carried out using R software version 4.0.4 (R Foundation for Statistical Computing, Vienna, Austria, 2021, <https://www.R-project.org>) and or GraphPad Prism v8.0 (San Diego, CA).

Categorical variables were expressed as percentages and compared with a two-sided chi-square test or a two-sided Fisher's exact test when the conditions for a chi-square were not fulfilled. Since the results of the biological assays did not have a normal distribution, they were expressed as median and interquartile range (IQR) and compared using Mann-Whitney test. Wilcoxon test was used for paired data. Other continuous variables were expressed as mean \pm SD.

Logistic regression model was used for univariate analyses aiming at identifying potential differences between responders and non-responders to D3. No correction was applied for multiple tests in this exploratory analysis and the threshold for significance was set as $p < .05$.

3 | RESULTS

3.1 | Description of the cohort

Ninety-nine consecutive kidney transplant recipients (KTRs) from Lyon University Hospital were offered a two-doses scheme of an anti-SARS-CoV-2 mRNA vaccine (BNT162b2, Pfizer-BioNtech). Among them, two developed COVID-19 before receiving the second dose and four were lost during the follow-up (Figure 1).

The clinical characteristics of the 93 remaining patients are presented in Table 1. Mean age was 55.7 ± 12.4 years, 54% were male (50/93). Forty-one percent (38/93) of the patients had comorbidities, including 25% (23/93) with a cardiovascular disease and 23% (21/93) with diabetes mellitus. Enrolled patients were transplanted for 9.9 ± 8.8 years in mean. Seventy percent (65/93) were on a triple immunosuppression maintenance regimen (including a calcineurin inhibitors, an anti-proliferative and low-dose steroids).

Before vaccination, 16/93 KTRs (17%) had detectable titers of anti-RBD IgGs (Figure 2A), among which only five had a past positive

SARS-CoV-2 PCR. In the rest of the study, these 16 patients were all considered as having a past history of COVID-19.

3.2 | Spike-specific humoral and cellular responses after two doses of vaccine

The cellular and humoral responses against the spike protein of SARS-CoV-2 were measured between 7 and 14 days after D2 (mean sampling time: 9.6 ± 3.0 days).

Forty-seven percent (31/77) of naive patients developed detectable anti-RBD IgG after the D2 (Figure 2A), but only 3 of them (3%) had a serum with viral neutralization capacity in vitro (Figure 2B). Patients with a past history of COVID-19 developed higher titers of anti-RBD IgG after D2 (1801 BAU/mL, IQR [90; 3757]) in KTRs with a history of COVID-19 vs. 2 BAU/mL, IQR [1, 39] in naive KTRs; $p < .0001$) and as expected, a higher proportion (10/16, 62.5%) of the latter had serum with in vitro viral neutralization capacity (Figure 2B). Thus, a history of COVID-19 appeared to be a major determinant of serum neutralization capacity after two doses of vaccine (OR 41.1, 95%CI [8.9; 154.6], $p < .0001$).

Analyzing paired data from serology and viral neutralization assay, we confirmed the relation between high titers of anti-RBD IgG and viral neutralization capacity of the serum (Pearson's $R^2 = .7982$, $p = .0002$; Figure 2C). All sera with ≥ 1000 BAU/mL of anti-RBD IgG had viral neutralizing capacity in vitro. Of note, this relatively high threshold as compared with what published in the literature, is due to the fact that we determined virus neutralization capacity *in vitro* using live virus. This is considered as the gold standard for coronaviruses,³¹ but requires higher antibody titers than assays relying on pseudotyped virus-like particles or surrogate virus neutralization assays. We believe that this choice is justified by the fact that high antibody titers are necessary to

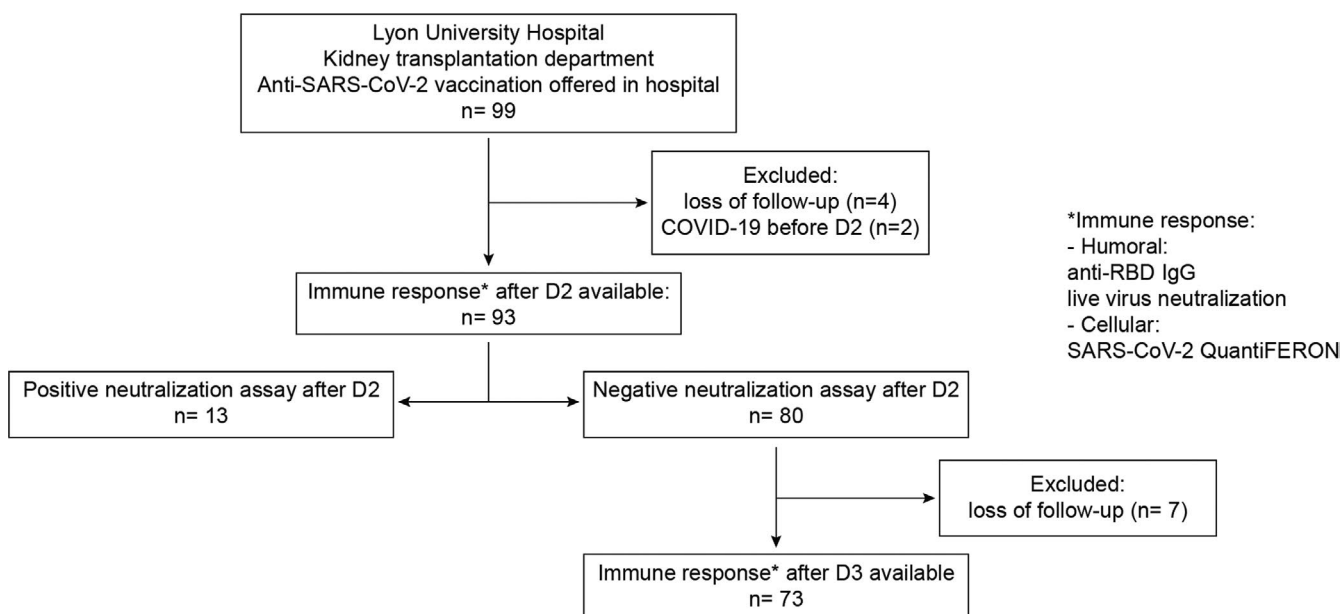


FIGURE 1 Flow chart of the study. D2, second dose of BNT162b2 vaccine; D3, third dose of BNT162b2 vaccine

TABLE 1 Characteristics of patients from Lyon University Hospital cohort

	Initial cohort (2 doses) n = 93	KTRs who received D3 (n=73)		p ^a
		Non-responders to D3 n = 59	Responders to D3 n = 14	
Age (y)	55.7 ± 12.4	57.7 ± 12.6	55.0 ± 12.2	.455
Male	50 (54)	33 (56)	7 (50)	.514
Comorbidities				
Cardiovascular disease	23 (25)	17 (29)		
Diabetes mellitus	21 (23)	11 (19)		
Time from transplantation (y)	9.9 ± 8.8	8.9 ± 6.9	17.6 ± 11.3	.002
Induction treatment				
Anti-thymocyte globulins	55 (59)	38 (64)	8 (57)	.374
Anti-CD25	32 (34)	20 (34)	2 (14)	
Maintenance immunosuppression				
Tacrolimus (vs no)	65 (70)	44 (75)	6 (43)	.027
MMF/MPA	71 (76)	50 (85)	5 (36)	.001
Steroids	80 (86)	50 (85)	12 (86)	.927
imTOR	8 (9)	6 (10)	3 (21)	.260
Biological data				
Lymphocytes (G/L)	1.6 ± 0.8	1.6 ± 0.8	1.6 ± 0.8	.859
Monocytes (G/L)	0.7 ± 0.2	0.6 ± 0.2	0.6 ± 0.1	.827
Creatinine (µmol/L)	126 ± 46	133 ± 48	117 ± 37	.241
COVID-19 history	16 (17)	5 (8)	1 (7)	.870
Biological results after the second dose				
Anti-RBD IgG	-	22 (35)	12 (86)	.004
IGRA	-	14 (24)	8 (57)	.021

Note: Data are provided as n (%) or mean ± SD.

Abbreviations: CNI, calcineurin inhibitor; IGRA, interferon γ releasing assay; imTOR, inhibitor of the mechanistic target of rapamycin; MMF/MPA, mycophenolate mofetil/mycophenolic acid; RBD, receptor-binding domain; y, years.

^aUnivariate logistic regression. *p* values < or = .05 are in bold.

retain neutralizing activity against the various emerging variants, and because of the rapid decay of antibody titers over time.³²

As the humoral response, the spike-specific cellular response of KTRs was also heterogeneous after D2. Only 23/76 (30%) of naive KTRs and 8/16 (50%) of patients with a past history of COVID-19 had a positive IGRA. However, in contrast with the humoral response, no significant difference was observed between these two groups regarding spike-specific cellular response (Figure 2D).

3.3 | Tolerability of a third dose of mRNA vaccine

Considering that these patients were not adequately protected against symptomatic COVID-19 and following French health authorities' recommendations, a third dose of BNT162b2 mRNA vaccine was offered to all 73 KTRs, whose serum had no viral neutralization capacity after D2 (7 patients were lost from follow-up after D2, Figure 1). The mean time between the second and third dose was 34.6 ± 5.3 days. Overall, the clinical tolerance of D3 was excellent and comparable to that of D2 (Figure 3). There were no serious

adverse events or graft dysfunction reported. The main side-effect was pain at the site of injection, which occurred with the same incidence after the second and the third dose (~50% of patients). Five patients had fever <39°C for a maximum of two days after D3.

3.4 | Efficacy of a third dose of mRNA vaccine

Spike-specific humoral and cellular immune responses of KTRs were monitored after D3 (mean sampling time: 12.3 ± 2.1 days). Administration of D3 resulted in a significant increase in anti-RBD IgG titers in non-responders to D2 (median IgG titer: 2.3, IQR [1.0; 40.6] after the second dose vs. 82.3, IQR [1.9; 464.9]; *p* < .0001, Figure 4A). Fourteen patients (14/73, 19%) developed viral neutralizing capacity after D3 (Figure 4B). In contrast, spike-specific cellular response after D3 was much more heterogeneous, with some patients increasing IFN- γ secretion in IGRA while the cellular response of others remained stable or even decreased (Figure 4C). Overall, spike-specific cellular responses after D2 and D3 were not statistically different (*p* = .205; Figure 4C).

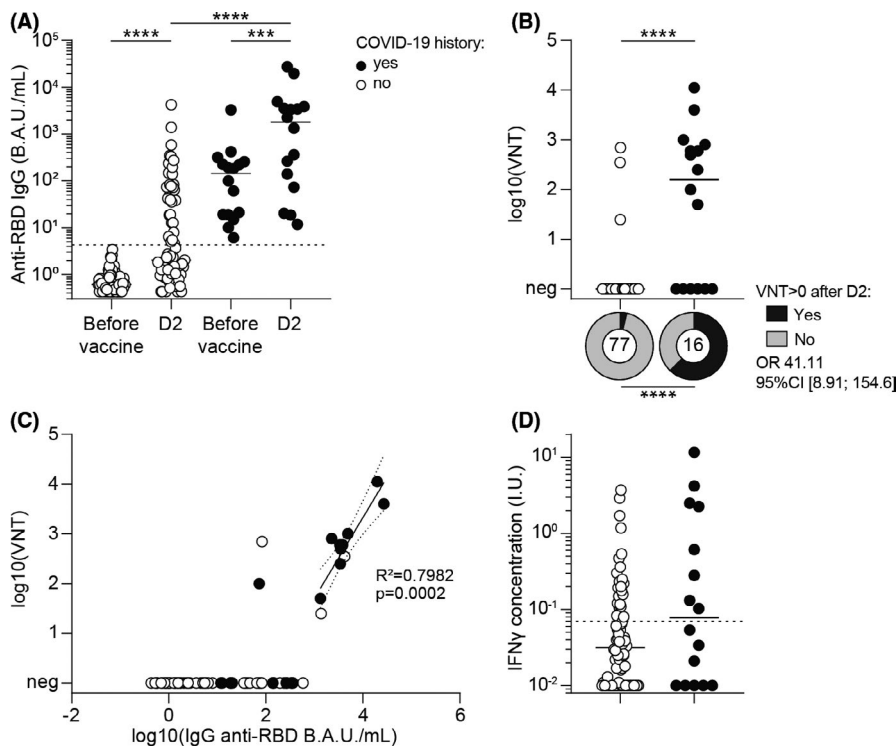
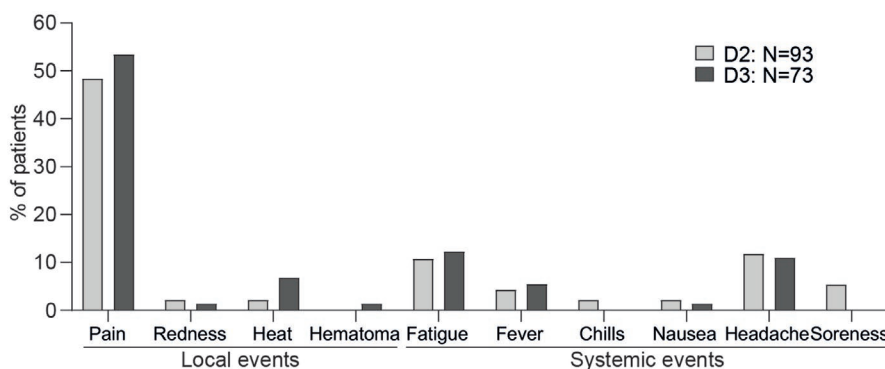


FIGURE 2 Spike-specific humoral and cellular responses after the second dose of BNT162b2 vaccine. Spike-specific humoral and cellular responses were measured 7–14 days after the D2 in kidney transplant recipients naïve for the SARS-CoV-2 (white circles) or with a previous history of COVID-19 (black circles). (A) Histogram showing the titers of anti-receptor binding domain (RBD) IgG before vaccination and after D2 of vaccine. Dashed line represents the limit of positivity of the assay. Wilcoxon test; ****p* < .001; *****p* < .0001. (B) Histogram showing the viral neutralization capacity of the serum in in vitro functional assay after D2. Mann-Whitney U test. Pie charts represent the proportion of patients with viral neutralization capacity. Fisher test; *****p* < .0001; VNT, viral neutralization titer. (C) The relationship between the anti RBD IgG titers and viral neutralization capacity was plotted. A linear regression was performed for patients with anti-RBD IgG titer above 1000 BAU/ml. R^2 : Pearson's coefficient. (D) Histogram showing the concentration of interferon gamma (IFN- γ) measured in IGRA (Quantiferon SARS-CoV-2) after D2. Dashed line represents the limit of positivity of the assay. IU, international units

FIGURE 3 Tolerability of the third dose of BNT162b2 vaccine. The proportion of kidney transplant recipients that developed local or systemic adverse events after the second and after the third dose of vaccine are plotted



3.5 | Clinical and biological variables predictive of response to D3

In order to identify which clinical and biological variables were associated with response to D3, KTRs were divided into responders and non-responders, according to whether or not they had acquired viral neutralizing capacity after the booster dose. Regarding clinical parameters, responders and non-responders had the same age and comorbid profile. Baseline biological parameters, including lymphocyte and monocyte counts and creatinine, were also similar (Table 1).

In contrast, responders to D3 had been transplanted for longer time than non-responders (17.6 ± 11.3 vs. 8.9 ± 6.9 years, $p = .002$), and were less frequently exposed to mycophenolate mofetil (5/14 vs. 50/59, $p = .001$) and tacrolimus (6/14 vs. 44/59, $p = .027$; Table 1).

In addition, the presence of non-neutralizing titers of anti-RBD IgG (Table 1, Figure 4D), or a positive IGRA (Table 1, Figure 4E) after D2, were both associated with a better response to D3 (OR 10.09, 95%CI [2.46; 68.85], $p = .004$ and OR 4.19, 95%CI [1.25; 14.82], $p = .021$, respectively). Furthermore, we observed that the probability to respond to D3 in KTRs was the highest in patients positive

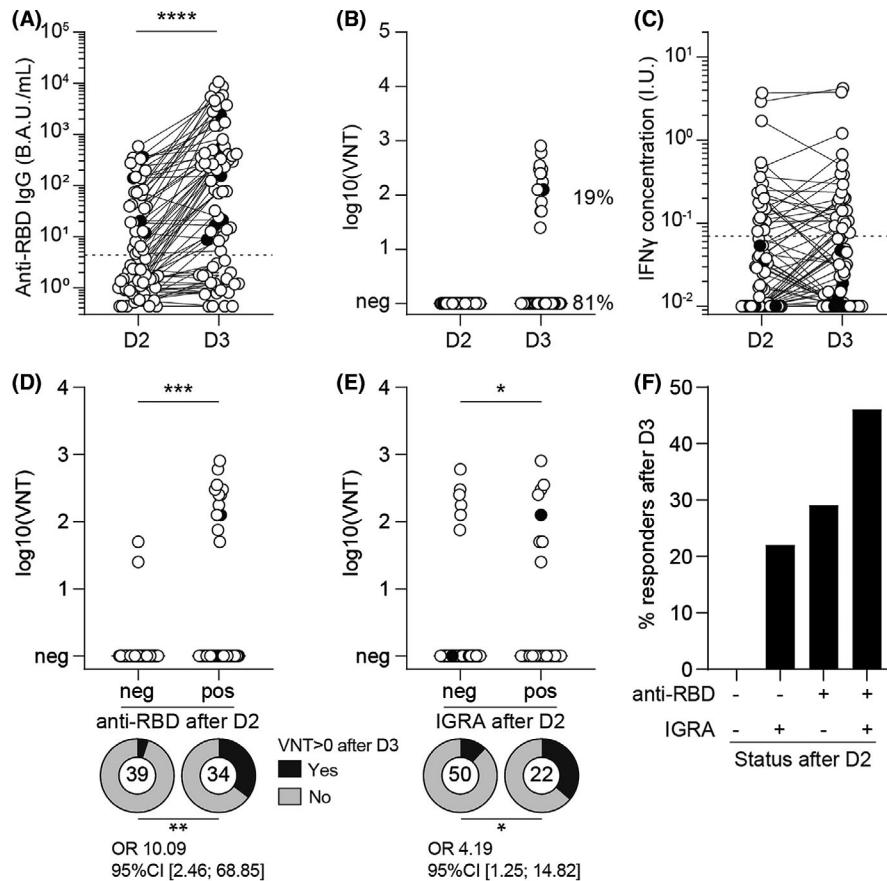


FIGURE 4 Spike-specific humoral and cellular responses after the third dose of BNT162b2 vaccine. Humoral and cellular responses were measured 7–14 days after the third dose of vaccine in kidney transplant recipients without viral neutralization capacity after D2. (A) Histogram showing the individual evolution of anti-receptor binding domain (RBD) IgG tiers (in binding antibody units, B.A.U.) after D2 and D3. Dashed line represents the limit of positivity of the test. Wilcoxon test; **** $p < .0001$. (B) Histogram showing the viral neutralization capacity of the serum in in vitro functional assay after D3. VNT, viral neutralization titer. (C) Histogram showing the evolution of the concentration of interferon gamma (IFN- γ) in IGRA (Quantiferon SARS-CoV-2) between D2 and D3. Dashed line represents the limit of positivity of the test. IU, international units. (D, E) Histogram showing the viral neutralization capacity after D3 according to the absence (neg) or the presence (pos) of anti-RBD IgG (D) or IFN- γ in IGRA (E) after D2. Mann-Whitney U test. Pie charts represent the proportion of patients with viral neutralization capacity after D3. Fisher test. VNT, viral neutralization titer; * $p < .05$; ** $p < .01$; *** $p < .001$. (F). Histogram showing the proportion of patients with viral neutralization capacity after D3 according to the presence (+) or the absence (-) of anti-RBD IgG and or positive IGRA after D2

for both tests (46%, Figure 4F). The response rate decreased to 29% in KTRs with only sub-optimal anti-RBD IgG titers after the second dose and 22% in those with only a positive IGRA. Finally, none of the KTRs in whom both assays were negative after D2 did develop a viral neutralization capacity after D3. These results suggest that combining the results of these two assays may allow refining the prediction of the response to D3 in KTRs.

4 | DISCUSSION

Our monocentric prospective observational study confirms that the “standard” scheme of vaccination, based on two doses of mRNA vaccine, induces a very heterogeneous response in KTRs.⁶⁻¹⁴ Administration of a third dose in non-responder patients was well tolerated and induced a significant increase in their anti-RBD IgG

titers, allowing 19% (14/73) of them to develop viral neutralization capacity, which is currently considered as the most reliable correlate of protection.^{15,33} Our results are in line with recent independent reports^{20,21,23-25} and provide original evidence that the response to this third dose of vaccine can be predicted after the second dose combining the results of simple and easily accessible biological assays.

An important finding of our study is the fact that the third dose of vaccine was very well tolerated, with no serious adverse events nor graft rejection reported. At a time when SARS-CoV-2 vaccine regimens are regularly updated with additional booster doses, the information that an additional dose is as well tolerated as the second dose of vaccine is reassuring for KTRs.

Identification of patients that would benefit from a third dose of vaccine is an important unmet medical need for physicians, who need to simultaneously optimize the protection of this vulnerable

population, while avoiding wasting time and precious vaccine doses. As previously reported by others, we observed that both a shorter time from transplantation and a higher level of maintenance immunosuppression were detrimental for the response to D3.^{21,23} However, we did not confirm the negative impact of age or renal function reported by Kamar et al.²¹ This discrepancy could be related to the fact that our study only enrolled KTR or explained by a lack of statistical power due to the relatively small number of patients enrolled ($n = 73$). Our study went deeper in the exploration of the predictive factors associated with the response to D3 and, beyond clinical variables, demonstrated that this prediction could be refined by the use of biological assays. We not only confirmed that a sub-optimal titer of anti-RBD IgG after D2 was a predictive factor for response to D3^{20,23} but provide original evidence that KTRs without antibodies but a detectable spike-specific cellular response in IGRA had similar chances to respond to D3. This is concordant with the fact that the results of the IGRA correlate with the response of follicular helper T cells, the subset specialized in providing help to B cells for antibody production³⁴ (Figure S2C,D).

An important, yet unsolved, question resulting from the total absence of response to D3 among KTRs with no detectable anti-RBD IgG and negative IGRA after D2 is how the latter vulnerable patients should be protected against COVID-19. Different strategies have been proposed to optimize response to vaccine. Reduction of maintenance immunosuppression³⁵ in KTRs may result in acute rejection and/or anti-HLA sensitization. Increasing vaccine immunogenicity by the use of heterologous prime-boost vaccination scheme seems an attractive option. However, when applied for the third vaccine dose in patients with immune-mediated inflammatory diseases or treated with Rituximab, this strategy did not increase response rates compared to an homologous 3D mRNA vaccine.^{36,37} An alternative option is the passive immunization with anti-SARS-CoV-2 monoclonal antibodies, a primary prevention strategy which was recently successfully tested in people with household exposure to SARS-CoV-2.³⁸

Our study has several limitations. First, we did not evaluate hard clinical endpoints (i.e., incidence of symptomatic COVID-19). Second, the analysis of the response to D3 has been performed without control group. This is due to the fact that in France, health authorities have strongly encouraged the rapid administration of a third dose of vaccine in vulnerable patients (including KTRs), making the randomization against a placebo deemed unethical by regulatory authorities. Although it is theoretically possible that the increase in viral neutralization capacity observed in patients' serum is due to time rather than D3, we consider this possibility as highly unlikely. A recent double-blind, randomized, controlled trial of a third dose of mRNA-1273 vaccine performed in Canada indeed demonstrated that serum neutralization capacity tended to decrease after D2 in patients that received a placebo while it significantly increased in those that received a third dose of vaccine.²² A third limitation of our study is the fact that the evaluation of the response to D2 and D3 was made at a single time point, 7-14 days after vaccine injection. One can argue that, although this time point is ideal for the

assessment of cellular responses, it could be too early to evaluate humoral responses, especially in KTRs in whom these responses may be delayed.^{39,40} However, delayed humoral response in vaccinated KTRs has not been observed by all investigators. Rincon-Arevalo et al reported that antibody titers after the second dose of COVID-19 vaccine peaked as early as 7 days and remained stable for several weeks thereafter in a cohort of KTRs.⁴¹ This unique time point had the advantage to allow the simultaneous evaluation of both the cellular and the humoral response of patients and was therefore chosen to optimize the chances that patients would participate to the study.

In conclusion, combining the results of the serology and IGRA after D2 could allow optimizing the personalization of the strategy of vaccination against COVID-19 in KTRs,³⁵ an approach that still requires independent validation.

ACKNOWLEDGMENTS

The authors are indebted to the members of the GRoupe de REcherche Clinique (GREC: Céline Dagot, Farah Pauwels, Fatiha M'Raiagh, and Daniel Sperandio) for excellent technical assistance during the collection of the samples, and to the clinicians (Fanny Buron, Charlène Lévi, Alice Koenig, Marion Delafosse, and Louis Manière) who recruited the patients. OT is thankful to Christine Bouz, Laurence Pellegrina, Emmanuelle Cart-Tanneur, Lise Siard, Claudine Lecuelle, and Philippe Favre from Eurofins Biomnis for their help during the conduction of the study. XC is supported by a funding from the Société Francophone de Transplantation. ME is supported by the Hospices civils de Lyon and currently holds a "poste accueil" position funded by INSERM. OT is supported by the Etablissement Français du Sang and the Fondation pour la Recherche Médicale (PME20180639518).

DISCLOSURE

The authors of this manuscript have no conflicts of interest to disclose as described by the *American Journal of Transplantation*.

DATA AVAILABILITY STATEMENT

The data that support the findings of this study are available from the corresponding author upon reasonable request.

ORCID

Xavier Charmetant  <https://orcid.org/0000-0002-2162-5873>

Olivier Thauat  <https://orcid.org/0000-0002-3648-8963>

REFERENCES

1. Thauat O, Legeai C, Anglicheau D, et al. IMPact of the COVID-19 epidemic on the moRTALity of kidney transplant recipients and candidates in a French Nationwide registry sTudy (IMPORTANT). *Kidney Int.* 2020;98(6):1568-1577. doi:10.1016/j.kint.2020.10.008
2. Caillard S, Chavarot N, Francois H, et al. Is COVID-19 infection more severe in kidney transplant recipients? *Am J Transplant.* 2021;21(3):1295-1303. doi:10.1111/ajt.16424
3. Jager KJ, Kramer A, Chesnaye NC, et al. Results from the ERA-EDTA Registry indicate a high mortality due to COVID-19 in dialysis

- patients and kidney transplant recipients across Europe. *Kidney Int.* 2020;98(6):1540-1548. doi:10.1016/j.kint.2020.09.006
4. Williamson EJ, Walker AJ, Bhaskaran K, et al. Factors associated with COVID-19-related death using OpenSAFELY. *Nature.* 2020;584(7821):430-436. doi:10.1038/s41586-020-2521-4
 5. Caillard S, Anglicheau D, Matignon M, et al. An initial report from the French SOT COVID Registry suggests high mortality due to COVID-19 in recipients of kidney transplants. *Kidney Int.* 2020;98(6):1549-1558. doi:10.1016/j.kint.2020.08.005
 6. Benotmane I, Gautier-Vargas G, Cognard N, et al. Low immunization rates among kidney transplant recipients who received 2 doses of the mRNA-1273 SARS-CoV-2 vaccine. *Kidney Int.* 2021;99(6):1498-1500. doi:10.1016/j.kint.2021.04.005
 7. Rozen-Zvi B, Yahav D, Agur T, et al. Antibody response to SARS-CoV-2 mRNA vaccine among kidney transplant recipients: a prospective cohort study. *Clin Microbiol Infect.* 2021;27(8):1173.e1-1173.e4. doi:10.1016/j.cmi.2021.04.028
 8. Grupper A, Rabinowich L, Schwartz D, et al. Reduced humoral response to mRNA SARS-CoV-2 BNT162b2 vaccine in kidney transplant recipients without prior exposure to the virus. *Am J Transplant.* 2021;21(8):2719-2726. doi:10.1111/ajt.16615
 9. Cucchiari D, Egri N, Bodro M, et al. Cellular and humoral response after mRNA-1273 SARS-CoV-2 vaccine in kidney transplant recipients. *Am J Transplant.* 2021;21(8):2727-2739. doi:10.1111/ajt.16701
 10. Husain SA, Tsapepas D, Paget KF, et al. Postvaccine Anti-SARS-CoV-2 spike protein antibody development in kidney transplant recipients. *Kidney Int Rep.* 2021;6(6):1699-1700. doi:10.1016/j.ekir.2021.04.017
 11. Korth J, Jahn M, Dorsch O, et al. Impaired humoral response in renal transplant recipients to SARS-CoV-2 vaccination with BNT162b2 (Pfizer-BioNTech). *Viruses.* 2021;13(5):756. doi:10.3390/v13050756
 12. Midtvedt K, Tran T, Parker K, et al. Low immunization rate in kidney transplant recipients also after dose 2 of the BNT162b2 vaccine: continue to keep your guard up! *Transplantation.* 2021;105(8):e80-e81. doi:10.1097/TP.0000000000003856
 13. Chavarot N, Ouedrani A, Marion O, et al. Poor Anti-SARS-CoV-2 humoral and T-cell responses after 2 injections of mRNA vaccine in kidney transplant recipients treated with belatacept. *Transplantation.* 2021;105(9):e94-e95. doi:10.1097/TP.0000000000003784
 14. Sattler A, Schrezenmeier E, Weber UA, et al. Impaired humoral and cellular immunity after SARS-CoV-2 BNT162b2 (tozinameran) prime-boost vaccination in kidney transplant recipients. *J Clin Invest.* 2021;131(14):150175. doi:10.1172/JCI150175
 15. Khoury DS, Cromer D, Reynaldi A, et al. Neutralizing antibody levels are highly predictive of immune protection from symptomatic SARS-CoV-2 infection. *Nat Med.* 2021;27(7):1205-1211. doi:10.1038/s41591-021-01377-8
 16. Charmetant X, Espi M, Benotmane I, et al. Comparison of infected and vaccinated transplant recipients highlights the role of Tfh and neutralizing IgG in COVID-19 protection. 2021. doi:10.1101/2021.07.22.21260852
 17. Caillard S, Chavarot N, Bertrand D, et al. Occurrence of severe COVID-19 in vaccinated transplant patients. *Kidney Int.* 2021;100(2):477-479. doi:10.1016/j.kint.2021.05.011
 18. Ali NM, Alnazari N, Mehta SA, et al. Development of COVID-19 infection in transplant recipients after SARS-CoV-2 vaccination. *Transplantation.* 2021;105(9):e104-e106.
 19. Wadei HM, Gonwa TA, Leoni JC, Shah SZ, Aslam N, Speicher LL. COVID-19 infection in solid organ transplant recipients after SARS-CoV-2 vaccination. *Am J Transplant.* 2021;21(10):3496-3499. doi:10.1111/ajt.16618
 20. Werbel WA, Boyarsky BJ, Ou MT, et al. Safety and Immunogenicity of a third dose of SARS-CoV-2 vaccine in solid organ transplant recipients: a case series. *Ann Intern Med.* 2021;174(9):1330-1332.
 21. Kamar N, Abravanel F, Marion O, Couat C, Izopet J, Del Bello A. Three doses of an mRNA Covid-19 vaccine in solid-organ transplant recipients. *N Engl J Med.* 2021;385(7):661-662.
 22. Hall VG, Ferreira VH, Ku T, et al. Randomized trial of a third dose of mRNA-1273 vaccine in transplant recipients. *N Engl J Med.* 2021;385(13):1244-1246. doi:10.1056/NEJMc2111462
 23. Benotmane I, Gautier G, Perrin P, et al. Antibody response after a third dose of the mRNA-1273 SARS-CoV-2 vaccine in kidney transplant recipients with minimal serologic response to 2 doses. *JAMA.* 2021;326(11):1063. doi:10.1001/jama.2021.12339
 24. Stumpf J, Tonnus W, Paliege A, et al. Cellular and humoral immune responses after 3 doses of BNT162b2 mRNA SARS-CoV-2 vaccine in kidney transplant. *Transplantation.* 2021;105(11):e267-e269. doi:10.1097/TP.0000000000003903
 25. Massa F, Cremoni M, Gérard A, et al. Safety and cross-variant immunogenicity of a three-dose COVID-19 mRNA vaccine regimen in kidney transplant recipients. *EBioMedicine.* 2021;73:103679. doi:10.1016/j.ebiom.2021.103679
 26. Padoan A, Bonfante F, Cosma C, et al. Analytical and clinical performances of a SARS-CoV-2 S-RBD IgG assay: comparison with neutralization titers. *Clinical Chemistry and Laboratory Medicine (CCLM).* 2021;59(8):1444-1452. doi:10.1515/cclm-2021-0313
 27. Weisberg SP, Connors TJ, Zhu Y, et al. Distinct antibody responses to SARS-CoV-2 in children and adults across the COVID-19 clinical spectrum. *Nat Immunol.* 2021;22(1):25-31. doi:10.1038/s41590-020-00826-9
 28. Espi M, Charmetant X, Barba T, et al. A prospective observational study for justification, safety, and efficacy of a third dose of mRNA vaccine in patients receiving maintenance hemodialysis. *Kidney Int.* 2021;. doi:10.1016/j.kint.2021.10.040
 29. QuantiFERON SARS-CoV-2. <https://www.qiagen.com/de/products/diagnostics-and-clinical-research/infectious-disease/quantiferon-sars-cov-2/>. Accessed January 3, 2022.
 30. Dahdal S, Saison C, Valette M, et al. Residual activatability of circulating Tfh17 predicts humoral response to thymodependent antigens in patients on therapeutic immunosuppression. *Front Immunol.* 2018;9:3178. doi:10.3389/fimmu.2018.03178
 31. Algaissi A, Hashem AM. Evaluation of MERS-CoV Neutralizing Antibodies in Sera Using Live Virus Microneutralization Assay. *Methods Mol Biol.* 2020;2099:107-116. doi:10.1007/978-1-0716-0211-9_9
 32. Collier AiY, Yu J, McMahan K, et al. Differential kinetics of immune responses elicited by Covid-19 vaccines. *N Engl J Med.* 2021;385(21):2010-2012. doi:10.1056/NEJMc2115596
 33. Feng S, Phillips DJ, White T, et al. Correlates of protection against symptomatic and asymptomatic SARS-CoV-2 infection. *Nat Med.* 2021;27(11):2032-2040.
 34. Chen CC, Koenig A, Saison C, et al. CD4+ T cell help is mandatory for naive and memory donor-specific antibody responses: impact of therapeutic immunosuppression. *Front Immunol.* 2018;9:275. doi:10.3389/fimmu.2018.00275
 35. Caillard S, Thaunat O. COVID-19 vaccination in kidney transplant recipients. *Nat Rev Nephrol.* 2021;17(12):785-787.
 36. Simon D, Tascilar K, Fagni F, et al. Efficacy and safety of SARS-CoV-2 revaccination in non-responders with immune-mediated inflammatory disease. *Ann Rheum Dis.* Published online November 24, 2021. doi:10.1136/annrheumdis-2021-221554
 37. Bonelli M, Mrak D, Tobudic S, et al. Additional Heterologous versus Homologous Booster Vaccination in Immunosuppressed Patients without SARS-CoV-2 Antibody Seroconversion after Primary mRNA Vaccination: A Randomized Controlled Trial. *Ann Rheum Dis.* 2021. doi:10.1101/2021.09.05.21263125
 38. O'Brien MP, Forleo-Neto E, Musser BJ, et al. Subcutaneous REGEN-COV antibody combination to prevent Covid-19. *New Engl J Med.* 2021;385(13):1184-1195.

39. Danthu C, Hantz S, Dahlem A, et al. Humoral response after SARS-CoV-2 mRNA vaccine in a cohort of hemodialysis patients and kidney transplant recipients. *J Am Soc Nephrol*. 2021. Published online June 16, 2021:ASN.2021040490. doi:10.1681/ASN.2021040490
40. Swai J, Gui M, Long M, Wei Z, Hu Z, Liu S. Humoral and cellular immune response to severe acute respiratory syndrome coronavirus-2 vaccination in haemodialysis and kidney transplant patients. *Nephrology*. 2022;27(1):7-24. doi:10.1111/nep.13974
41. Rincon-Arevalo H, Choi M, Stefanski AL, et al. Impaired humoral immunity to SARS-CoV-2 BNT162b2 vaccine in kidney transplant recipients and dialysis patients. *Sci Immunol*. 2021;6(60):eabj1031. doi:10.1126/sciimmunol.abj1031

SUPPORTING INFORMATION

Additional supporting information may be found in the online version of the article at the publisher's website.

How to cite this article: Charmetant X, Espi M, Barba T, et al. Predictive factors of a viral neutralizing humoral response after a third dose of COVID-19 mRNA vaccine. *Am J Transplant*. 2022;00:1–9. doi:[10.1111/ajt.16990](https://doi.org/10.1111/ajt.16990)

4. Publication 4

The ROMANOV study found impaired humoral and cellular immune responses to SARS-CoV-2 mRNA vaccine in virus-unexposed patients receiving maintenance hemodialysis.

Espi M*, Charmetant X*, Barba T, Koppe L, Pelletier C, Kalbacher E, Chalencon E, Mathias V, Ovize A, Cart-Tanneur E, Bouz C, Pellegrina L, Morelon E, Fouque D, Juillard L, Thauinat O.

*: co-premier auteurs

Kidney International. 2021 Oct;100(4):928-936.



The ROMANOV study found impaired humoral and cellular immune responses to SARS-CoV-2 mRNA vaccine in virus-unexposed patients receiving maintenance hemodialysis

Maxime Espi^{1,2,9}, Xavier Charmetant^{1,9}, Thomas Barba^{1,3,4}, Laetitia Koppe^{2,4}, Caroline Pelletier⁵, Emilie Kalbacher⁵, Elodie Chalencon², Virginie Mathias^{1,6}, Anne Ovize⁷, Emmanuelle Cart-Tanneur⁷, Christine Bouz⁷, Laurence Pellegrina⁷, Emmanuel Morelon^{4,8}, Denis Fouque^{2,4}, Laurent Juillard^{4,5} and Olivier Thauat^{1,4,8}

¹International Center for Infectiology Research (CIRI), French Institute of Health and Medical Research (INSERM) U1111, Université Claude Bernard Lyon I, National Center for Scientific Research (CNRS) Mixed Research Unit (UMR) 5308, Ecole Normale Supérieure de Lyon, University Lyon, Lyon, France; ²Department of Nephrology, Nutrition and Hemodialysis, Hospices Civils de Lyon, Centre Hospitalier Lyon Sud, Pierre-Bénite, France; ³Department of Internal Medicine, Hospices Civils de Lyon, Edouard Herriot Hospital, Lyon, France; ⁴Claude Bernard University (Lyon 1), Villeurbanne, France; ⁵Department of Nephrology, Hospices Civils de Lyon, Edouard Herriot Hospital, Lyon, France; ⁶Human Leukocyte Antigen Laboratory, French National Blood Service, Décines-Charpieu, France; ⁷Eurofins Biomnis Laboratory, Lyon, France; and ⁸Department of Transplantation, Nephrology and Clinical Immunology, Hospices Civils de Lyon, Edouard Herriot Hospital, Lyon, France

Patients on maintenance hemodialysis (MHD), which are at high risk of infection by SARS-CoV-2 virus and death due to COVID-19, have been prioritized for vaccination. However, because they were excluded from pivotal studies and have weakened immune responses, it is not known whether these patients are protected after the “standard” two doses of mRNA vaccines. To answer this, anti-spike receptor binding domain (RBD) IgG and interferon gamma-producing CD4⁺ and CD8⁺ specific-T cells were measured in the circulation 10–14 days after the second injection of BNT162b2 vaccine in 106 patients receiving MHD (14 with history of COVID-19) and compared to 30 healthy volunteers (four with history of COVID-19). After vaccination, most (72/80, 90%) patients receiving MHD naïve for the virus generated at least one type of immune effector, but their response was weaker and less complete than that of healthy volunteers. In multivariate analysis, hemodialysis and immunosuppressive therapy were significantly associated with absence of both anti-RBD IgGs and anti-spike CD8⁺ T cells. In contrast, previous history of COVID-19 in patients receiving MHD correlated with the generation of both types of immune effectors anti-RBD IgG and anti-spike CD8⁺ T cells at levels similar to healthy volunteers. Patients receiving MHD naïve for SARS-CoV-2 generate mitigated immune responses after two doses of mRNA vaccine. Thus, the good response to vaccine of patients receiving MHD with a history of COVID-19 suggest that these patients may benefit from a third vaccine injection.

Correspondence: Olivier Thauat, Service de Transplantation, Néphrologie et Immunologie Clinique, Hôpital Edouard Herriot, 5 Place d'Arsonval, 69003 Lyon, France. E-mail: olivier.thauat@chu-lyon.fr

⁹ME and XC contributed equally.

Received 9 April 2021; revised 24 June 2021; accepted 1 July 2021; published online 18 July 2021

Kidney International (2021) **100**, 928–936; <https://doi.org/10.1016/j.kint.2021.07.005>

KEYWORDS: BNT162b2; COVID-19; hemodialysis; mRNA vaccine; SARS-CoV-2
Copyright © 2021, International Society of Nephrology. Published by Elsevier Inc. All rights reserved.

Among the various alarms raised by the coronavirus disease 2019 (COVID-19) pandemic was its impact on the population of patients with end-stage renal disease,^{1,2} particularly those requiring in-center hemodialysis. Logistical aspects of maintenance hemodialysis (MHD), including frequent encounters at health care facilities with other patients and staff, the physical proximity of patients during sessions, and transportation to and from center in shared vehicles, increase the risk for disease transmission.³ As a result, the reported incidence of COVID-19 in hemodialysis centers was high, particularly during the peaks of the pandemic.^{1,4,5} Furthermore, because of their comorbid profile and chronic kidney disease–induced immunosuppression,^{6–8} the risk of death due to COVID-19 was consistently and dramatically higher in MHD patients infected with severe acute respiratory syndrome coronavirus 2 (SARS-CoV-2) than in the general population.^{9–11}

Because of their higher risk for both infection by SARS-CoV-2 and death due to COVID-19, MHD patients were prioritized for vaccination in France.¹² Pivotal studies using lipid nanoparticle-encapsulated mRNA-based vaccines that encode the full-length spike protein of SARS-CoV-2 showed excellent efficacy (~95%) at preventing COVID-19 illness in the general population after 2 doses of the vaccine administered i.m. 3 weeks apart.^{13,14} However, whether these good results are generalizable to individuals living with kidney disease, in particular those on MHD, is not certain because the latter were not enrolled in these studies.¹⁵ Furthermore,

several lines of evidence suggest that in MHD patients, immune response (in particular after vaccination) may be blunted.^{7,8}

Aiming at evaluating the immunogenicity of the SARS-CoV-2 mRNA vaccine BNT162b2 in MHD individuals, the Response Of heModialyzed pATieNts to cOvid-19 Vaccination (ROMANOV) study prospectively quantified the humoral and cellular responses after the second dose of vaccines in 106 patients on MHD in Lyon University Hospital and compared these results with those of a cohort of 30 healthy volunteers (HVs).

METHODS

Study population

According to the recommendations of the French health authority,¹² vaccination with mRNA BNT162b2 COVID-19 vaccine was offered to all patients on MHD in the 2 centers of Lyon University Hospital (France) who did not have any of the following contraindications: diagnosis of COVID-19 within the last 3 months, organ transplantation within the last 3 months, rituximab injection within the last 3 months, ongoing flare of vasculitis, acute sepsis, or major surgery within the last 2 weeks.

All adult patients who received a standard (prime + boost 3 to 5 weeks apart, depending on availability of the dose) vaccination with BNT162b2 vaccine and gave consent for the use of their blood, collected at the time of a routine biological evaluation, for analysis of the postvaccinal immune response were enrolled in ROMANOV study.

In the absence of validated correlates of vaccine-induced protection against SARS-CoV-2 (i.e., measurable parameter indicating that a person is protected against becoming infected and/or developing COVID-19 disease),¹⁴ we reasoned that hemodialyzed patients would have the same excellent level of protection as the general population¹⁴ if they were able to generate similar amount of specific humoral (antibodies) and cellular (helper and cytotoxic T lymphocytes) effectors. We therefore compared the amount of anti-spike receptor-binding domain (RBD) IgG and interferon- γ -

producing cluster of differentiation (CD) 4⁺ and CD8⁺ T cells measured 10 to 14 days after the second injection in MHD patients with the values measured at the same time point in a cohort of 30 HVs. This timing was selected on the basis of previous reports demonstrating that both cellular and antibody responses are at their peak at this time point.¹⁶

History of COVID-19 was defined as a positive polymerase chain reaction test in nasopharyngeal swab. The screening for infection was performed in patients in the presence of symptoms or because the patient had contact with a positive case. The same detection strategy was applied to MHD patients and HVs.

The ROMANOV study was conducted in accordance with the French legislation on biomedical research and the Declaration of Helsinki, and the protocol was evaluated by a national ethical research committee (ID-RCB 2021-A00325-36). The French National Commission for the Protection of Digital Information authorized the conduction of the study.

Anti-SARS-CoV-2 spike-RBD (S-RBD) humoral response assessment

The IgG antibodies directed against the RBD of the spike glycoprotein of the SARS-CoV-2 were detected by a chemiluminescence technique, using the Maglumi SARS-CoV-2 S-RBD IgG test (Snibe Diagnostic) on a Maglumi 2000 analyzer (Snibe Diagnostic), according to the manufacturer's instructions.

Briefly, 10 μ l of serum was incubated in the appropriate buffer with magnetic microbeads covered with S-RBD recombinant antigen, to form immune complexes. After precipitation in a magnetic field and washing, N-(4-aminobutyl)-N-ethylisoluminol-stained anti-human IgG antibodies were added to the samples. After a second magnetic separation and washing, the appropriate reagents were added to initiate a chemiluminescence reaction. When necessary, sera were diluted sequentially up to 1:1000.

Anti-SARS-CoV-2 spike cellular response assessment

Spike-specific CD4⁺ and CD8⁺ T-cell response was quantified in the circulation of the HVs and hemodialyzed patients using the QuantiFERON SARS-CoV-2 test (Qiagen), a commercially available

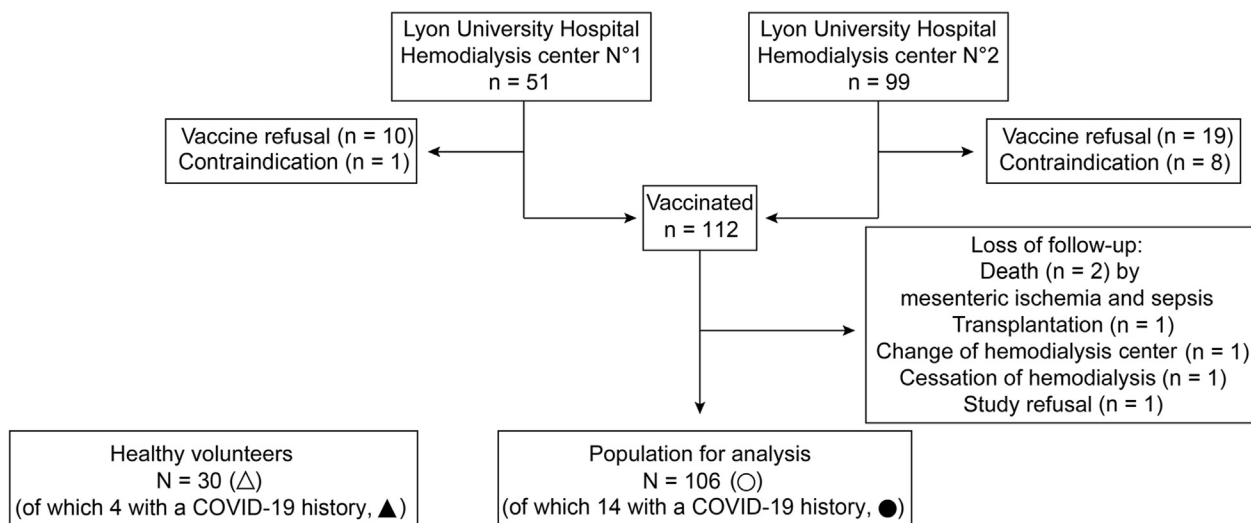


Figure 1 | Flowchart of the study. COVID-19, coronavirus disease 2019.

interferon- γ releasing assay, according to the manufacturer's instructions.

Briefly, after collection, 1 ml blood was distributed in each tube of the assay: (i) uncoated tube: negative control/background noise, (ii) tube coated with mitogen: positive control, (iii) tube coated with human leukocyte antigen-II restricted 13-mer peptides derived from the entire SARS-CoV-2 spike glycoprotein used to stimulate CD4⁺ T cells, and (iv) tube coated with human leukocyte antigen-II and human leukocyte antigen-I 8- and 13-mer derived from the entire SARS-CoV-2 spike glycoprotein used to stimulate both CD4⁺ and CD8⁺ T cells. After 20 hours of culture at 37 °C, tubes were centrifuged for 15 minutes at 2500g, and stored at 4 °C before interferon- γ quantification by enzyme-linked immunosorbent assay.

The CD4⁺ T-cell assay value was the difference between tube (iii) and the negative control. The CD8⁺ T-cell assay value was the value obtained for tube (iv), with subtraction of the CD4 tube (iii) and the negative control (i).

Statistical analysis

All the analyses were performed using R software version 4.0.4 (R Foundation for Statistical Computing; 2021; <https://www.R-project.org>) and/or GraphPad Prism v8.0. Categorical variables were expressed as percentages and compared with the χ^2 test. Continuous variables were expressed as mean \pm SD and compared using 1-way analysis of variance and multiple *t*-test *post hoc* analyses or as median \pm interquartile range and compared using Mann-Whitney test for variables with nonnormal distribution.

Logistic regression models were used in both univariate and multivariate analyses. Noncolinear explanatory variables associated with outcomes (i.e., optimal humoral and cellular responses) in univariate analysis ($P < 0.1$) were included in multivariate models. The Firth bias-correction method was used in cases of complete separation.¹⁷ Stepwise regression analyses with bidirectional elimination were then performed, using Aikake information criterion to select the most fitting final multivariate models.

Venn diagrams were computed using R with the “ggplot2” and “ggVennDiagram” packages.

RESULTS

Study design and characteristics of the population

Among the 150 MHD patients dialyzing at Lyon University Hospital, 38 refused the vaccine or had contraindications to the injection. Of the 112 who were vaccinated, 1 declined participating in the study and 5 were lost during the follow-up (Figure 1). The general characteristics of the 106 MHD patients available for analysis, including 14 with a previous history of COVID-19 dating >3 months (black circles), are summarized in Table 1. Mean age was 65 years, and most of them were male (65%) and had a high burden of comorbid conditions (including cardiovascular disease in 45% and diabetes in 44%). In addition, 22% had a history of kidney transplantation and 12% were on immunosuppressive drugs (crossed circles).

These 106 MHD patients were compared with a cohort of 30 unmatched HVs, 4 of whom had a history of COVID-19 dating of >3 months (black triangles; Figure 1). The general characteristics of HVs are presented in Table 1.

Table 1 | Clinical description of HVs and MHD patients

Variable	MHD patients (N = 106)	HVs (N = 30)
Age, yr	64.9 \pm 15.2	46.6 \pm 14.8
Male sex	69 (65)	14 (47)
BMI, kg/m ²	26.5 \pm 6.5	24.1 \pm 3.8
Cause of renal failure		NA
Vascular	19 (18)	
Diabetes mellitus	37 (35)	
Glomerulonephritis	15 (14)	
Hereditary	3 (3)	
Uropathy	0 (0)	
Others	32 (30)	
Comorbidities		
Cardiovascular disease	46 (43)	1 (3)
Respiratory disease	13 (12)	1 (3)
Liver disease	5 (5)	0 (0)
Diabetes mellitus	47 (44)	0 (0)
History of COVID-19	14 (13)	4 (13)
Asymptomatic	3 (21)	1 (25)
Mild or moderate	7 (50)	3 (75)
Critical	4 (29)	0 (0)
Previous SOT	23 (22)	0 (0)
Time in HD, d	1520 \pm 1822	NA
HD parameters		NA
HD time per week, min	691 \pm 85	
Kt/V ^a	1.58 \pm 0.41	
IS drugs	13 (12)	0 (0)
Tacrolimus	8 (8)	
Anti-metabolite	4 (4)	
Steroids >5 mg/d	3 (3)	
Rituximab	1 (1)	
Chemotherapy	4 (4)	
Biological data		NA
Hemoglobin, g/L	109 \pm 14	
Lymphocytes, G/L	1.18 \pm 0.53	
Monocytes, G/L	0.63 \pm 0.25	
CRP, mg/L	12.6 \pm 21.0	
Albumin, g/L	35.8 \pm 5.2	
Prealbumin, g/L	0.34 \pm 0.27	
Phosphorus, mmol/L	1.58 \pm 0.50	

BMI, body mass index; COVID-19, coronavirus disease 2019; CRP, C-reactive protein; G, giga; HD, hemodialysis; HV, healthy volunteer; IS, immunosuppressive; MHD, maintenance hemodialysis; NA, not available; SOT, solid organ transplantation. Data are given as n (%) or mean \pm SD.

^aKt/V was used for the quantification of dialysis adequacy by the following formula: dialysis clearance of urea (K) multiplied by dialysis time (t), divided by the volume of distribution of urea (V).

Humoral response against SARS-CoV-2 mRNA vaccine

According to the manufacturer, the threshold of detection of the assay for anti-RBD IgG is 1 arbitrary unit (Figure 2a; dashed line). In contrast with all 30 HVs, who exhibited a homogeneous IgG response against RBD, 19 MHD patients (18%) did not develop any detectable antibody after 2 doses of vaccine (nonresponders; Figure 2a). To identify predictors of seroconversion following anti-SARS-CoV-2 vaccination, a first multivariate analysis was performed to compare these 19 nonresponders with the responders (87 MHD patients and 30 HVs). Only 2 variables were found independently associated with a lack of seroconversion: (i) being on hemodialysis (odds ratio [OR], 0.11; 95% confidence interval [CI], 0.01–0.93; $P = 0.041$) or (ii) being on immunosuppressive treatment (OR, 0.09; 95% CI, 0.02–0.312; $P = 0.001$; Figure 2b and Supplementary Table S1). In contrast, a history of COVID-19

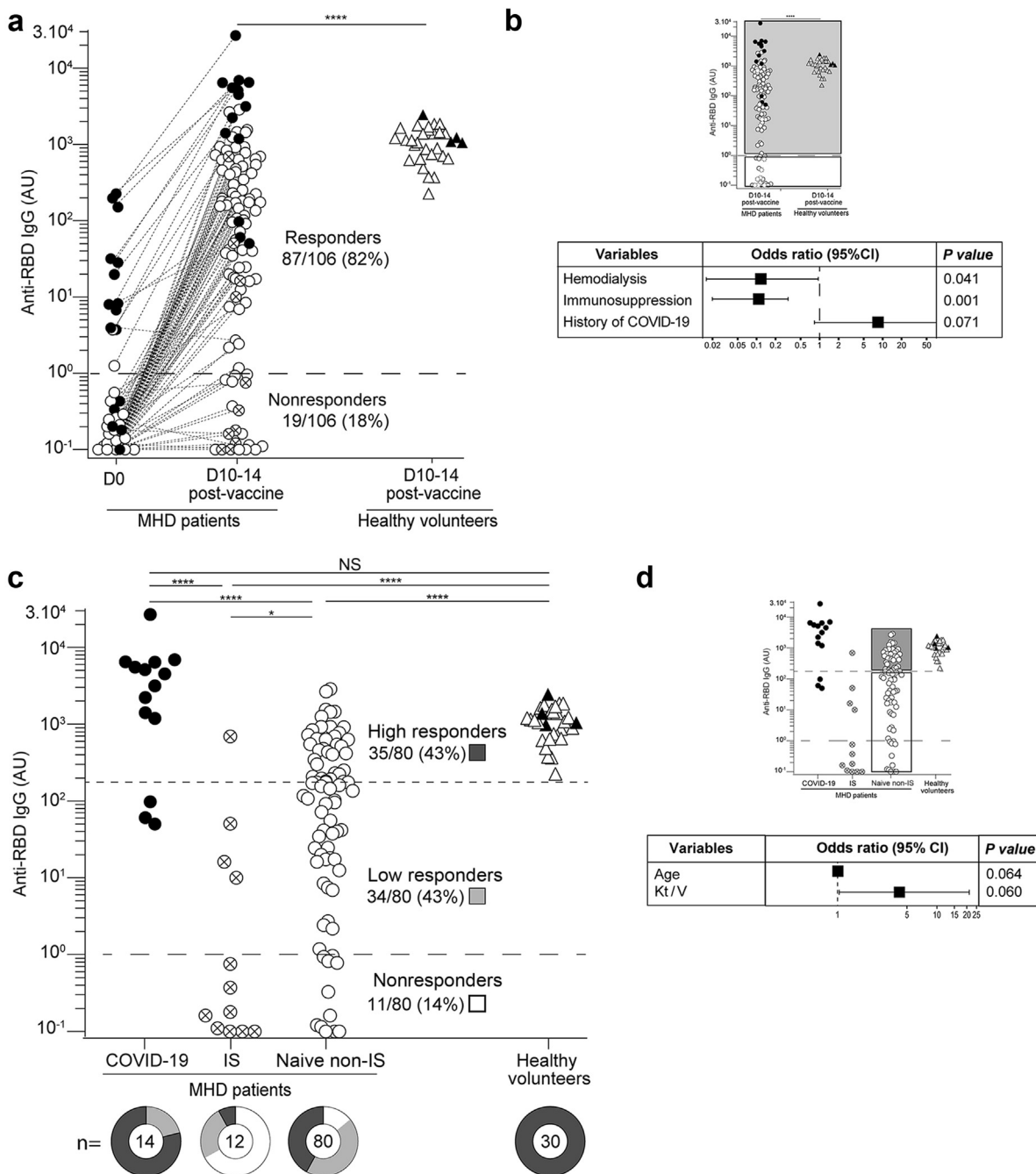


Figure 2 | Humoral response of maintenance hemodialysis (MHD) patients to the BNT162b2 vaccine. (a) The titer of IgG anti-receptor-binding domain of the severe acute respiratory syndrome coronavirus 2 spike protein (RBD) was determined by a chemoluminescence assay in 30 healthy volunteers (HVs; triangles) and 106 hemodialyzed patients (HDs; circles) before vaccination (day [D] 0) and 10 to 14 days after the second injection of vaccine. The dashed line represents the limit of detection of the test. Black symbols represent patients with a history of coronavirus disease 2019 (COVID-19) (HVs, n = 4; HDs, n = 14). Crossed circles represent patients on immunosuppressive (IS) drugs. Mann-Whitney test; ****P < 0.0001. (b) A multivariate analysis was conducted to identify the variables independently associated with seroconversion in the whole cohort (gray square vs. white square). For each variable with a P < 0.10 in multivariate analysis, a forest plot shows the odds ratio and the 95% confidence interval (CI). (c) Comparison of anti-RBD IgG titers in HVs (n = 30), MHD patients with COVID-19 history (n = 14; black circles), MHD patients with IS drugs (n = 12; crossed circles), and naïve MHD patients (n = 80; white circles). The upper dotted line represents the median IgG titer of responder naïve MHD patients. Donuts represent proportions of nonresponders (white), low responders (light gray), and high responders (dark gray). (d) A multivariate analysis was conducted to identify the variables independently associated with a high IgG response to vaccine in naïve MHD patients without IS drugs (gray square vs. white square). For each variable with a P < 0.10 in multivariate analysis, a forest plot shows the odds ratio and the 95% CI. AU, arbitrary unit; Kt/V, dialysis clearance of urea (K) multiplied by dialysis time (t), divided by the volume of distribution of urea (V); NS, not significant.

correlated with higher chances of seroconversion after vaccination (OR, 8.31; 95% CI, 0.87–1145; $P = 0.071$; Figure 2b).

The median titer of anti-RBD IgG (176 arbitrary units; Figure 2b; dotted line) was used to further divide naïve responder MHD patients without immunosuppressive therapy into low responders (34/80 [43%]) and high responders (35/80 [43%]).

The clinical and biological characteristics of the 3 categories of naïve MHD patients without immunosuppressive therapy are compared in Table 2. A second multivariate analysis, conducted among naïve MHD patients without immunosuppressive therapy only (Figure 2c and Supplementary Table S2), identified 2 independent characteristics associated with a better antibody response after vaccination in this group: (i) younger age (OR, 0.97; 95% CI, 0.93–1.00; $P = 0.064$) and (ii) better dialysis quality (OR, 4.19; 95% CI, 1.04–21.15; $P = 0.060$).

Spike-specific CD4⁺ T-cell response correlates with anti-RBD IgG response

The generation of IgG against a target protein requires a cognate interaction between antigen-specific B cells and antigen-specific CD4⁺ T cells.^{18,19}

In line with their strong anti-RBD IgG response, all HVs (30/30 [100%]) and MHD patients with history of COVID-19 (14/14 [100%]) had detectable spike-specific CD4⁺ T cells in their circulation (Figure 3a). This percentage was 70% (48/69) for responders but decreased to 18% (2/11) for non-responders among naïve MHD patients without immunosuppressive therapy (Figure 3a). As expected, MHD patients on immunosuppressive therapy had almost never detectable spike-specific CD4⁺ T cells (Figure 3a). A correlation was therefore established between the presence of spike-specific CD4⁺ T cells and the titer of anti-RBD IgG (Figure 3b).

Spike-specific CD8⁺ T-cell response in MHD patients

Complementing the role of antibodies, virus-specific CD8⁺ T cells are involved in the elimination of infected cells (virus “factories”). Like the humoral response, CD8⁺ T-cell response of MHD patients appeared more heterogeneous than that of HVs (Figure 4a). Spike-specific CD8⁺ T cells could be detected in the large majority of HVs (21/30 [70%]) and MHD patients with history of COVID-19 (12/14 [86%]; Figure 4b). This percentage was 43% (30/69) for responders but only 18% (2/11) for nonresponders among naïve MHD patients without immunosuppressive therapy (Figure 4b). Again, MHD patients on immunosuppressive therapy had

Table 2 | Description of clinical and biological characteristics of naïve MHD patients without immunosuppressive therapy, according to their anti-RBD IgG response

Variables	Non-R (N = 11)	Low-R (N = 34) ^a	High-R (N = 35) ^a	P value
Age, yr	67.8 ± 10.5	71.6 ± 13.2	61.4 ± 15.5	0.013
Male sex	7 (64)	25 (74)	28 (80)	0.165
BMI, kg/m ²	25.0 ± 6.1	28.6 ± 7.2	26.2 ± 6.2	0.201
Comorbidities				
Cardiovascular	8 (73)	19 (56)	13 (37)	0.080
Respiratory disease	4 (36)	2 (6)	4 (11)	0.028
Diabetes mellitus	5 (45)	16 (47)	14 (40)	0.833
Previous SOT	4 (36)	2 (6)	9 (26)	0.029
Cause of renal failure				0.965
Vascular	3 (27)	6 (18)	9 (26)	
Diabetes mellitus	3 (27)	14 (41)	12 (34)	
Glomerulonephritis	1 (9)	5 (15)	4 (11)	
Hereditary	1 (9)	1 (3)	1 (3)	
Uropathy	0 (0)	0 (0)	0 (0)	
Others	3 (27)	8 (24)	9 (26)	
Time in HD, d	1772 ± 1420	1345 ± 1693	2037 ± 2406	0.977
HD parameters				
HD time per week, min	665 ± 86	699 ± 56	711 ± 64	0.123
Kt/V ^b	1.59 ± 0.39	1.45 ± 0.30	1.69 ± 0.36	0.022
Biological data				
Hemoglobin, g/L	106 ± 12	109 ± 12	112 ± 14	0.446
Lymphocytes, G/L	0.84 ± 0.52	1.19 ± 0.46	1.36 ± 0.55	0.015
Monocytes, G/L	0.62 ± 0.41	0.64 ± 0.17	0.63 ± 0.21	0.964
CRP, mg/L	20.4 ± 20.9	10.8 ± 10.9	6.2 ± 7.4	0.003
Albumin, g/L	33.4 ± 4.3	36.6 ± 4.7	35.9 ± 5.6	0.206
Prealbumin, g/L	0.25 ± 0.08	0.34 ± 0.10	0.39 ± 0.45	0.387
Phosphorus, mmol/L	1.32 ± 0.39	1.58 ± 0.61	1.55 ± 0.50	0.299

BMI, body mass index; CRP, C-reactive protein; G, giga; HD, hemodialysis; High-R, high responders; Low-R, low responders; MHD, maintenance hemodialysis; Non-R, non-responders; RBD, receptor-binding domain; SOT, solid organ transplantation.

Data are given as n (%) or mean ± SD. Qualitative variables are compared by χ^2 test, and quantitative variables are compared by 1-way analysis of variance.

^aLow-R and High-R are defined by the median titer value of responder MHD patients without immunosuppressive therapy and naïve for the virus.

^bKt/V was used for the quantification of dialysis adequacy by the following formula: dialysis clearance of urea (K) multiplied by dialysis time (t), divided by the volume of distribution of urea (V).

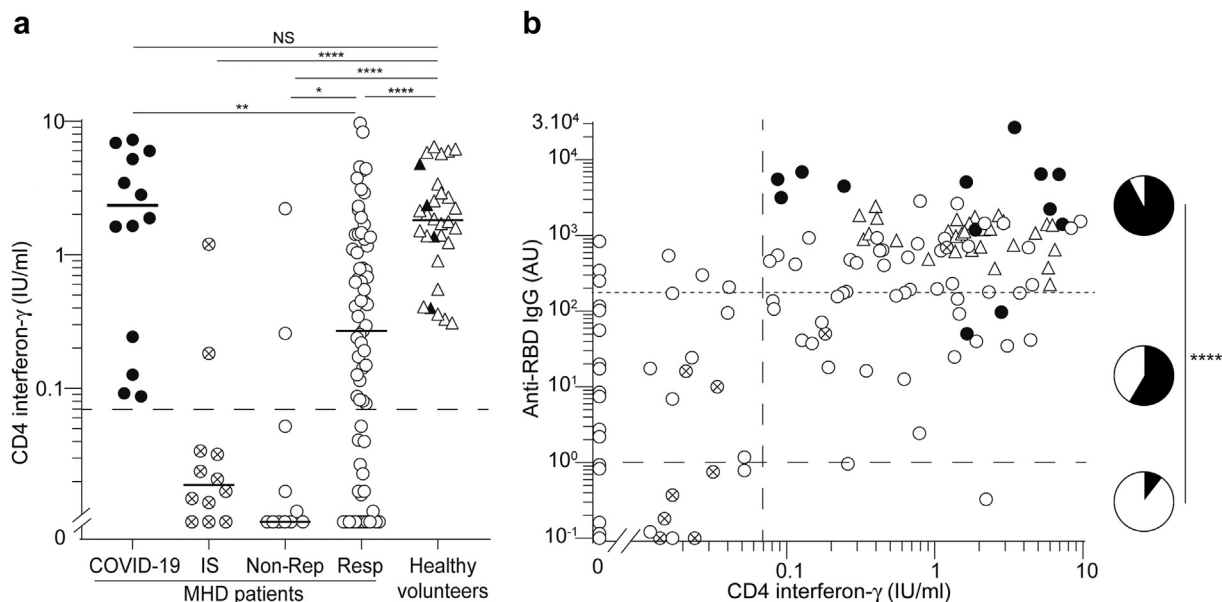


Figure 3 | Cluster of differentiation (CD) 4⁺ T-cell response of maintenance hemodialysis (MHD) patients to the BNT162b2 vaccine correlates with humoral response. (a) The secretion of interferon- γ by circulating spike protein-specific CD4⁺ T cells was measured *in vitro* in healthy volunteers (HVs; n = 30; triangles), MHD patients with coronavirus disease 2019 (COVID-19) history (n = 14; black circles), MHD patients with immunosuppressive (IS) drugs (n = 12; crossed circles), and naïve MHD patients (n = 80; white circles) 10 to 14 days after the second injection of vaccine. Naïve MHD patients were divided into 2 groups according to the absence (nonresponders [Non-Resp]; n = 11) or presence (responders [Resp]; n = 69) of humoral response. The dashed line represents the threshold of positivity of the test. Mann-Whitney test; **P* < 0.05, ***P* < 0.01, *****P* < 0.0001. (b) The correlation between the titer of anti-receptor-binding domain of the severe acute respiratory syndrome coronavirus 2 spike protein (RBD) IgG and the secretion of interferon- γ by spike-specific CD4⁺ T cells is shown for HVs (n = 30), MHD patients with COVID-19 history (n = 14; black circles), MHD patients with IS drugs (n = 12; crossed circles), and naïve MHD patients (n = 80; white circles). The lower dashed line represents the limit of detection for anti-RBD IgG. The upper dotted line represents the median IgG titer of responder naïve MHD patients. Pie charts represent the percentage of patients with a positive (black) and negative (white) CD4⁺ T-cell response in each stratum of anti-RBD IgG response. χ^2 Test; *****P* < 0.0001. AU, arbitrary unit; NS, not significant (*P* > 0.05).

almost never (1/12 [8%]) detectable spike-specific CD8⁺ T cells (Figure 4b).

The multivariate analysis conducted to identify the variable independently associated with the presence of spike-specific CD8⁺ T cells in the circulation after vaccination identified 3 variables: (i) being on hemodialysis (OR, 0.33; 95% CI, 0.13–0.81; *P* = 0.018), (ii) being on immunosuppression therapy (OR, 0.20; 95% CI, 0.03–0.89; *P* = 0.062), and (iii) a history of COVID-19 (OR, 12.26; 95% CI, 3.11–83.59; *P* = 0.002; Figure 4c and Supplementary Table S3). Among naïve MHD patients without immunosuppressive therapy, there were no differences in clinical and biological characteristics between patients who had or had not generated specific CD8⁺ T cells (Supplementary Table S4).

Profiling the immune response against SARS-CoV-2 mRNA vaccine

Color-coded Venn diagrams were used to analyze the logical relation between the individual components of the immune response (IgG, CD4⁺ T cells, and CD8⁺ T cells) induced by SARS-CoV-2 mRNA vaccine. Because immunosuppressive therapy has been shown above to strongly impair the response to the vaccine, these patients were analyzed separately (Figure 5a). The profiles of the 3 remaining populations (HVs and MHD patients with and without medical history of COVID-19) were compared (Figure 5b).

Two doses of BNT162b2 vaccine were sufficient to induce the generation of a high number of all types of immune

effectors in HVs (Figure 5b; left panel). However, although the same complete profile was observed in most (12/14 [86%]) MHD patients with a medical history of COVID-19 (Figure 5b; middle panel), most (52/80 [65%]) MHD patients naïve for the virus showed some defect in their anti-spike immune response (Figure 5b; right panel). The defective immune response of naïve MHD patients predominated for cellular response (i.e., CD4⁺ T cells detectable in only 50% of naïve MHD patients vs. 100% in HVs, and CD8⁺ T cells detectable in only 31% of naïve MHD patients vs. 70% in HVs).

Of note, only 3 naïve MHD patients had detectable spike-specific T cells in absence of anti-RBD IgG.

DISCUSSION

The ROMANOV study prospectively quantified the anti-RBD IgG and the helper and cytotoxic T lymphocytes generated after 2 doses of BNT162b2 vaccine in MHD patients. Comparing these results with those of a cohort of unmatched HVs, we observed that if most MHD patients naïve for the virus develop some immune effectors after vaccination, their numbers remain below those observed in HVs, raising a question about the level of protection of vaccinated MHD patients. The facts that (i) hemodialysis was an independent predictor of lack of seroconversion after vaccination and (ii) the quality of the dialysis estimated by the Kt/V (dialysis clearance of urea [K] multiplied by dialysis time [t], divided by the volume of distribution of urea

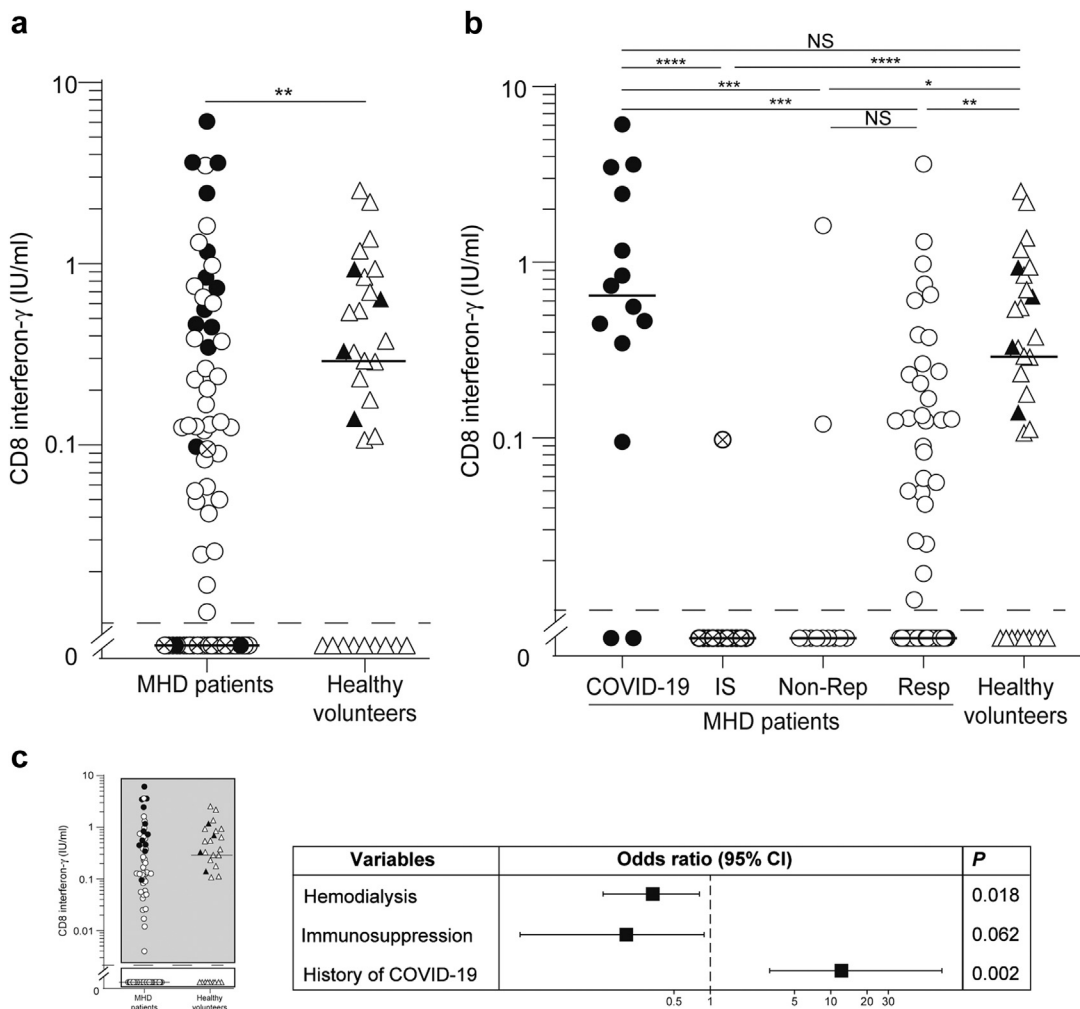


Figure 4 | Cluster of differentiation (CD) 8⁺ T-cell response of maintenance hemodialysis (MHD) patients to the BNT162b2 vaccine. (a) The secretion of interferon- γ by circulating spike protein-specific CD8⁺ T cells was measured *in vitro* in healthy volunteers (HVs; n = 30; triangles) and hemodialyzed patients (n = 106; circles) 10 to 14 days after the second injection of the vaccine. Black symbols represent patients with a history of coronavirus disease 2019 (COVID-19). The dashed line represents the threshold of positivity of the test. Mann-Whitney test; ** $P < 0.01$. (b) Spike-specific CD8⁺ responses in MHD patients were represented for patients with a COVID-19 history (n = 14; black circles), MHD patients with immunosuppressive (IS) drugs (n = 12; crossed circles), and naïve MHD patients (n = 80; white circles), according to the absence (nonresponders [Non-resp]; n = 11) or presence (responders [Resp]; n = 69) of humoral response. Mann-Whitney test; * $P < 0.05$, ** $P < 0.01$, *** $P < 0.001$, **** $P < 0.0001$. (c) A multivariate analysis was conducted to identify the variables independently associated with a CD8⁺ T-cell response to the vaccine in the whole cohort (30 HVs and 106 MHD patients) (gray square as reference group vs. white square). A forest plot shows the odds ratio and the 95% confidence interval (CI) for a variable with $P < 0.10$ in the multivariate analysis. NS, not significant ($P > 0.05$).

[V]) was associated with a better response to vaccine in naïve nonimmunosuppressed MHD suggest that uremic toxins could potentially play a detrimental role on the development of a humoral response.⁷ Furthermore, it has also been suggested that uremic milieu of end-stage renal disease may be associated with antibody dysfunction.²⁰ It is therefore tempting to speculate that one could improve immune function (and therefore response to vaccine) of MHD patients by optimizing uremic toxin elimination. This theory is in line with the data reported by Kovacic *et al.*, demonstrating that higher Kt/V values were associated with better antibody response to hepatitis B virus vaccine.²¹

The parameter that predicted the best optimal response to vaccination of MHD patients was a history of COVID-19. Indeed, although history of COVID-19 did not significantly

impact the generation of any of the 3 types of immune effectors in vaccinated HVs, this parameter had a massive impact in MHD patients. In contrast with MHD patients naïve for the virus, those with a history of COVID-19 had a response to vaccine, which was indistinguishable from that of HVs. This result may indicate that increasing the exposure to viral antigens could circumvent the immune dysfunction of hemodialyzed patients. It is therefore tempting to speculate that naïve MHD patients with suboptimal immune response after 2 doses of vaccine might benefit from a third injection. This theory is in line with the better vaccine responses consistently reported in MHD populations following adaptation (i.e., increase in the dose and/or the number of injections) of vaccinal schemes.²²

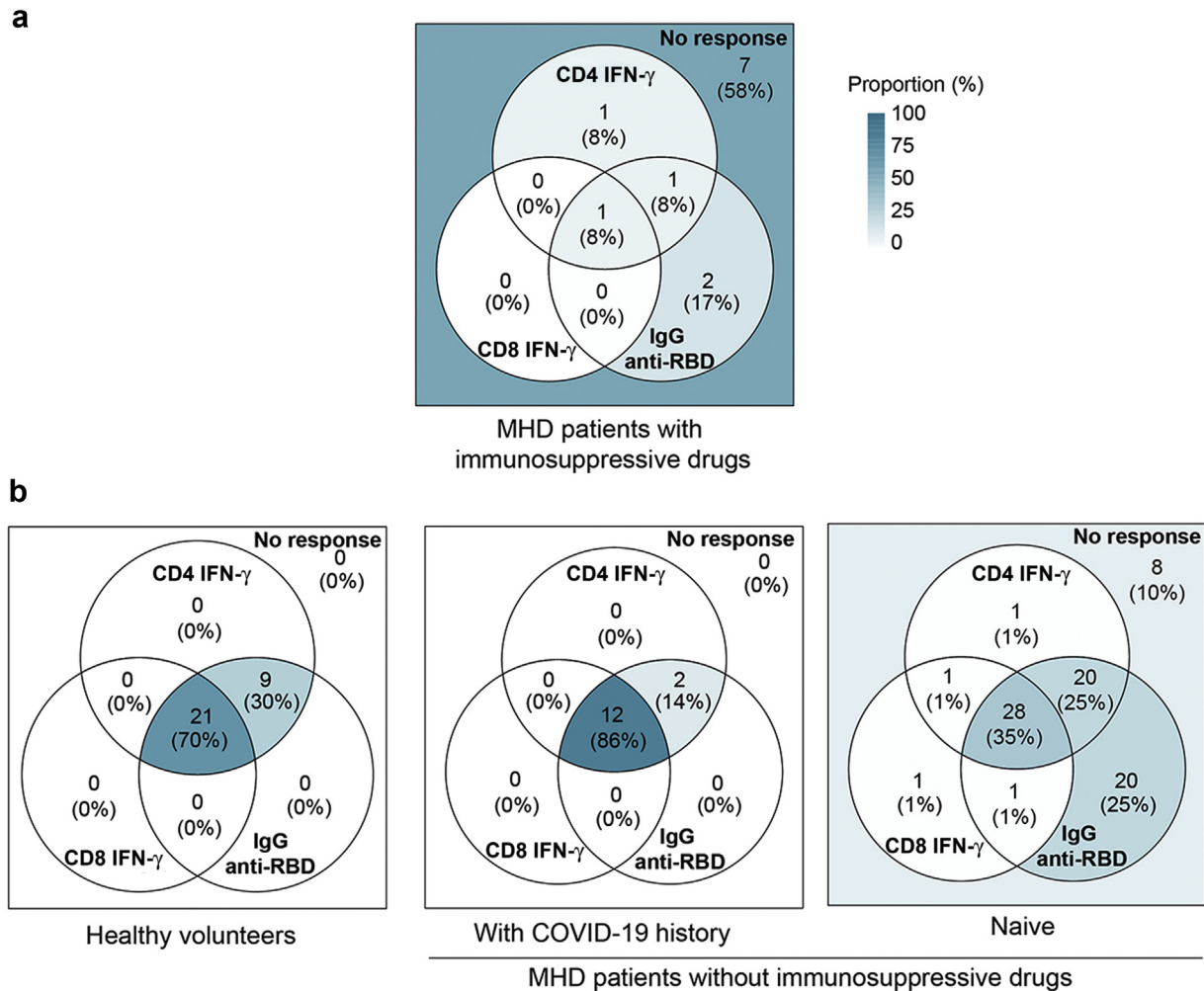


Figure 5 | Profiling the immune response of maintenance hemodialysis (MHD) patients to the standard BNT162b2 vaccination. Color-coded Venn diagrams were used to analyze the logical relation between the individual components of the immune response (IgG, cluster of differentiation [CD] 4⁺ T cells, and CD8⁺ T cells) induced by the severe acute respiratory syndrome coronavirus 2 (SARS-CoV-2) mRNA vaccine. (a) Profile of immune response in MHD patients with immunosuppressive drugs. (b) Comparison of the profiles of 3 populations: healthy volunteers (n = 30) and MHD patients with (n = 14) and without (n = 80) a medical history of coronavirus disease 2019 (COVID-19). IFN- γ , interferon- γ ; RBD, receptor-binding domain of the SARS-CoV-2 spike protein.

In conclusion, MHD patients naïve for SARS-CoV-2 are particularly vulnerable to SARS-CoV-2 and would greatly benefit from vaccine protection. However, the standard 2 doses scheme seems insufficient to induce in naïve MHD patients the same intensity of immune response as in HVs. In addition to optimization of dialysis therapy, which could improve immune function, naïve MHD patients might require additional injections of SARS-CoV-2 mRNA vaccine. Prospective studies are urgently needed to validate this hypothesis.

DISCLOSURE

All the authors declared no competing interests.

ACKNOWLEDGMENTS

The authors are indebted to the members of the Groupe de REcherche Clinique (Céline Dagot, Farah Pauwels, Fatiha M'Raiagh, and Daniel Sperandio), and Lise Siard, Claudine Lecuelle, and Philippe Favre from Eurofins Biomnis, for their precious help during the

conduction of the study. ME is supported by the Hospices Civils de Lyon. XC is supported by funding from the Société Francophone de Transplantation. OT is supported by Fondation pour la Recherche Médicale (PME20180639518).

SUPPLEMENTARY MATERIAL

[Supplementary File \(PDF\)](#)

Table S1. Univariate analysis relating characteristics of responders versus nonresponders in the whole cohort (106 maintenance hemodialysis [MHD] patients + 30 healthy volunteers [HV]).

Table S2. Univariate analysis relating comparisons between high responders and low + no responders in naïve maintenance hemodialysis (MHD) patients without immunosuppressive (IS) drugs.

Table S3. Univariate analysis relating characteristics of CD8 responders versus CD8⁺ nonresponders in the whole cohort (106 maintenance hemodialysis [MHD] patients + 30 healthy volunteers [HV]).

Table S4. Univariate analysis relating comparisons between CD8 responders and CD8 nonresponders in naïve maintenance hemodialysis (MHD) patients without immunosuppressive (IS) drugs.

REFERENCES

1. Thauinat O, Legeai C, Anglicheau D, et al. IMPact of the COVID-19 epidemic on the moRTALity of kidney transplant recipients and candidates in a French Nationwide registry sTudy (IMPORTANT). *Kidney Int.* 2020;98:1568–1577.
2. Williamson EJ, Walker AJ, Bhaskaran K, et al. Factors associated with COVID-19-related death using OpenSAFELY. *Nature.* 2020;584:430–436.
3. Weiner DE, Watnick SG. Hemodialysis and COVID-19: an Achilles' heel in the pandemic health care response in the United States. *Kidney Med.* 2020;2:227–230.
4. Quintaliani G, Reboldi G, Di Napoli A, et al. Exposure to novel coronavirus in patients on renal replacement therapy during the exponential phase of COVID-19 pandemic: survey of the Italian Society of Nephrology. *J Nephrol.* 2020;33:725–736.
5. Creput C, Fumeron C, Toledano D, et al. COVID-19 in patients undergoing hemodialysis: prevalence and asymptomatic screening during a period of high community prevalence in a large Paris center. *Kidney Med.* 2020;2:716–723.e1.
6. Caillard S, Chavarot N, Francois H, et al. Is COVID-19 infection more severe in kidney transplant recipients? *Am J Transplant.* 2021;21:1295–1303.
7. Espi M, Koppe L, Fouque D, Thauinat O. Chronic kidney disease-associated immune dysfunctions: impact of protein-bound uremic retention solutes on immune cells. *Toxins.* 2020;12:300.
8. Betjes MGH. Immune cell dysfunction and inflammation in end-stage renal disease. *Nat Rev Nephrol.* 2013;9:255–265.
9. Ng JH, Hirsch JS, Wanchoo R, et al. Outcomes of patients with end-stage kidney disease hospitalized with COVID-19. *Kidney Int.* 2020;98:1530–1539.
10. Jager KJ, Kramer A, Chesnaye NC, et al. Results from the ERA-EDTA Registry indicate a high mortality due to COVID-19 in dialysis patients and kidney transplant recipients across Europe. *Kidney Int.* 2020;98:1540–1548.
11. Hilbrands LB, Duivenvoorden R, Vart P, et al. COVID-19-related mortality in kidney transplant and dialysis patients: results of the ERACODA collaboration. *Nephrol Dial Transplant.* 2020;35:1973–1983.
12. Haute Autorité de Santé. Vaccins Covid-19: quelle stratégie de priorisation à l'initiation de la campagne?. Available at: https://www.has-sante.fr/jcms/p_3221237/fr/vaccins-covid-19-quelle-strategie-de-priorisation-a-l-initiation-de-la-campagne. Accessed April 2, 2021.
13. Baden LR, El Sahly HM, Essink B, et al. Efficacy and safety of the mRNA-1273 SARS-CoV-2 vaccine. *N Engl J Med.* 2021;384:403–416.
14. Polack FP, Thomas SJ, Kitchin N, et al. Safety and efficacy of the BNT162b2 mRNA Covid-19 vaccine. *N Engl J Med.* 2020;383:2603–2615.
15. Glenn DA, Hegde A, Kotzen E, et al. Systematic review of safety and efficacy of COVID-19 vaccines in patients with kidney disease. *Kidney Int Rep.* 2021;6:1407–1410.
16. Sahin U, Muik A, Derhovanessian E, et al. COVID-19 vaccine BNT162b1 elicits human antibody and T H 1 T cell responses. *Nature.* 2020;586:594–599.
17. Firth D. Bias reduction of maximum likelihood estimates. *Biometrika.* 1993;80:27–38.
18. Lanzavecchia A. Antigen-specific interaction between T and B cells. *Nature.* 1985;314:537–539.
19. Chen C-C, Koenig A, Saison C, et al. CD4+ T cell help is mandatory for naive and memory donor-specific antibody responses: impact of therapeutic immunosuppression. *Front Immunol.* 2018;9:275.
20. Canas JJ, Starr MC, Hooks J, et al. Longitudinal SARS-CoV-2 seroconversion and functional heterogeneity in a pediatric dialysis unit. *Kidney Int.* 2021;99:484–486.
21. Kovacic V, Sain M, Vukman V. Efficient haemodialysis improves the response to hepatitis B virus vaccination. *Intervirology.* 2002;45:172–176.
22. Vaccinating_Dialysis_Patients_and_patients_dec2012.pdf. Available at: https://www.cdc.gov/dialysis/PDFs/Vaccinating_Dialysis_Patients_and_patients_dec2012.pdf. Accessed April 2, 2021.

5. Publication 5

A prospective observational study for justification, safety, and efficacy of a third dose of mRNA vaccine in patients receiving maintenance hemodialysis.

Espi M*, Charmetant X*, Barba T, Mathieu C, Pelletier C, Koppe L, Chalencon E, Kalbacher E, Mathias V, Ovize A, Cart-Tanneur E, Bouz C, Pellegrina L, Morelon E, Juillard L, Fouque D, Couchoud C, Thaunat O; REIN Registry.

*: co-premier auteurs

Kidney International. 2022 Feb;101(2):390-402.



A prospective observational study for justification, safety, and efficacy of a third dose of mRNA vaccine in patients receiving maintenance hemodialysis

Maxime Espi^{1,2,11}, Xavier Charmetant^{1,11}, Thomas Barba^{1,3,4}, Cyrille Mathieu¹, Caroline Pelletier⁵, Laetitia Koppe^{2,4}, Elodie Chalencon², Emilie Kalbacher⁵, Virginie Mathias^{1,6}, Anne Ovize⁷, Emmanuelle Cart-Tanneur⁷, Christine Bouz⁷, Laurence Pellegrina⁷, Emmanuel Morelon^{4,8}, Laurent Juillard^{4,5}, Denis Fouque^{2,4}, Cécile Couchoud^{9,10} and Olivier Thauinat^{1,4,8}; in collaboration with the REIN Registry¹²

¹Centre International de Recherche en Infectiologie, Institut National de la Santé et de la Recherche Médicale U1111, Université Claude Bernard Lyon I, Centre National de la Recherche Scientifique Unité Mixte de Recherche 5308, Ecole Normale Supérieure de Lyon, Université Lyon, Lyon, France; ²Department of Nephrology, Nutrition, and Hemodialysis, Centre Hospitalier Lyon Sud, Hospices Civils de Lyon, Pierre-Bénite, France; ³Department of Internal Medicine, Edouard Herriot Hospital, Hospices Civils de Lyon, Lyon, France; ⁴Medical School, Claude Bernard University (Lyon 1), Villeurbanne, France; ⁵Department of Nephrology, Edouard Herriot Hospital, Hospices Civils de Lyon, Lyon, France; ⁶Human Leukocyte Antigen Laboratory, French National Blood Service, Décines-Charpieu, France; ⁷Eurofins Biomnis Laboratory, Lyon, France; ⁸Department of Transplantation, Nephrology, and Clinical Immunology, Edouard Herriot Hospital, Hospices Civils de Lyon, Lyon, France; ⁹REIN Registry, Agence de la Biomédecine, Saint-Denis La Plaine, France; and ¹⁰Biostatistique Santé Department, Laboratoire de Biométrie et Biologie Evolutive, Centre National de la Recherche Scientifique Unité Mixte de Recherche 5558, Université Lyon I, Villeurbanne, France

The level of protection achieved by the standard two doses of COVID-19 mRNA vaccines in patients receiving maintenance hemodialysis (MHD) remains unclear. To study this we used the French Renal Epidemiology and Information Network (REIN) Registry to compare the incidence and severity of 1474 cases of COVID-19 diagnosed in patients receiving MHD after none, one or two doses of vaccine. Vaccination significantly reduce COVID-19 incidence and severity, but 11% of patients infected after two doses still died. Lack of vaccinal protection in patients naïve for SARS-CoV-2 could be due to defective Tfh response [38% of patients with negative spike-specific CD4⁺ T-cell interferon gamma release assay] and failure to generate viral neutralizing titers of anti-spike receptor binding domain (RBD) IgGs (63% of patients with titer at or under 997 BAU/ml, defining low/no responders) after two doses of vaccine. To improve protection, a third dose of vaccine was administered to 75 patients [57 low/no responders, 18 high responders after two doses] from the ROMANOV cohort that prospectively enrolled patients receiving MHD vaccinated with BNT162b2 (Pfizer). Tolerance to the third dose was excellent. High responders to two doses did not generate more anti-RBD IgGs after three doses but had more side effects. Importantly, 31

(54%) of low/no responders to two doses reached neutralizing titers of anti-RBD IgGs after three doses. A positive interferon gamma release assay and/or suboptimal titer of anti-RBD IgGs after two doses were the only predictive variables for response to three doses in multivariate analysis. Thus, the standard scheme of vaccination insufficiently protects patients receiving MHD. Anti-RBD IgG and specific CD4⁺ T-cell response after two doses can guide personalized administration of the third dose, which improves the humoral response of SARS-CoV-2-naïve patients receiving MHD.

Kidney International (2022) **101**, 390–402; <https://doi.org/10.1016/j.kint.2021.10.040>

KEYWORDS: BNT162b2; COVID-19; hemodialysis; mRNA vaccine; SARS-CoV-2
Copyright © 2022, International Society of Nephrology. Published by Elsevier Inc. All rights reserved.

Among the various alarms raised by the coronavirus disease 2019 (COVID-19) pandemic was its impact on the population of patients with end-stage kidney disease,^{1,2} particularly those requiring in-center hemodialysis. The logistical aspects of the technique indeed increase the risk of severe acute respiratory syndrome coronavirus 2 (SARS-CoV-2) infections,³ which on the highly comorbid profile of patients on maintenance hemodialysis (MHD) then translates into a high rate of COVID-19–related death.^{1,4–6}

Aiming at protecting this vulnerable population, French health authorities prioritized patients on MHD for vaccination.⁷ However, while 2 doses (2Ds) administered i.m. 3 weeks apart of BNT162b2, a lipid nanoparticle-encapsulated mRNA-based vaccine, induced both strong humoral and cellular immune responses against the spike protein of SARS-

Correspondence: Olivier Thauinat, Service de Transplantation, Néphrologie et Immunologie Clinique, Hôpital Edouard Herriot, 5 Place d'Arsonval, 69003 Lyon, France. E-mail: olivier.thauinat@chu-lyon.fr

¹¹ME and XC are co-first authors.

¹²The list of collaborators from the REIN registry are listed in the Appendix.

Received 9 July 2021; revised 20 October 2021; accepted 26 October 2021; published online 29 November 2021

CoV-2 in the general population,⁸ our group⁹ and others^{10–14} have recently reported that patients on MHD, particularly those that were naïve for SARS-CoV-2, generated weaker responses than did healthy volunteers after this “standard” scheme of vaccination, raising questions about the actual level of protection provided by the vaccine.

The prospective observational Response of Hemodialyzed Patients to COVID-19 Vaccination (ROMANOV-II) study compared the severity of COVID-19 disease in patients on MHD according to their vaccination status and evaluated whether a third dose (3D) of BNT162b2 vaccine was safe and efficient to increase the generation of immune effectors.

METHODS

Epidemiologic study

The Renal Epidemiology and Information Network (REIN) is the French national registry of all patients being treated by renal replacement therapy.¹⁵ Clinical, demographic, and laboratory data are collected at the start of renal replacement therapy along with dialysis modalities and are updated annually. Events such as death, transfer, withdrawal from dialysis, placement on a transplant waiting list, and kidney transplantation (from living or deceased donors), as well as COVID-19 diagnosis and severity are systematically reported in real time. Interrogation of the REIN registry was made on June 18, 2021, on the period from the February 1 to May 18, 2021.

To estimate the cumulative incidence of COVID-19 in patients on MHD, data from the REIN registry were cross-referenced with those of the Caisse Nationale d'Assurance Maladie (CNAM),¹⁶ which collects each week the cumulative number of patients on MHD that had received their first and second doses of mRNA vaccine.

Because protection of a vaccine dose was previously reported to be efficient from the 10th day following injection onward,¹⁷ patients were considered as “not vaccinated” until the 10th day after the first dose and remained in the group “1 dose of vaccine” until the 10th day after the second dose.

Severity of COVID-19 was graded as asymptomatic, mild, moderate, severe, critical, or death following the World Health Organization's recommendations.¹⁸

The ROMANOV-II prospective observational study

In line with the French health authority's recommendations,¹⁹ a third vaccine injection of mRNA BNT162b2 COVID-19 vaccine was proposed to all patients on MHD in the 2 centers of Lyon University Hospital who already received 2Ds of mRNA BNT162b2 and did not have any of the following contraindications: diagnosis of COVID-19 within the last 3 months, organ transplantation within the last 3 months, rituximab injection within the last 3 months, ongoing flare of vasculitis, acute sepsis, or major surgery within the last 2 weeks. Before the third injection, patients were informed of their serological status after 2Ds.

History of COVID-19 was defined as a positive polymerase chain reaction test in nasopharyngeal swab. The screening for infection was performed in patients in the presence of symptoms or because the patient had contact with a positive case. The same detection strategy was applied to patients on MHD and healthy volunteers (HVs).

All adult patients who received a third vaccine injection (within 3 months after the second vaccine injection) with BNT162b2 vaccine and who gave consent for the use of their blood were enrolled in this study. The samples were collected 10 to 14 days after the second and after the third vaccine injection for analysis of the postvaccinal

immune response. This timing was selected based on previous reports demonstrating that both cellular and antibody responses are at their peak at this time point.⁸

Postvaccinal immune responses of patients on MHD were compared after the 2D and the 3D to those of a cohort of HVs, with blood sample collected at the same time point after the 2D of BNT162b2 for patients on MHD.

The ROMANOV-II study was conducted in accordance with the French legislation on biomedical research and the Declaration of Helsinki, and the protocol was evaluated by a national ethical research committee (ID-RCB 2021-A00325-36) and registered on clinicaltrials.gov as NCT04881396. The French national commission for the protection of digital information (Commission Nationale de l'Informatique et des Libertés) authorized the conduction of the study.

Assessment of the tolerability and safety of vaccine injections

Local and systemic adverse events and use of anti-pyretic medications were collected retrospectively, based on a self-assessment questionnaire. Data collected correspond to adverse events within 7 days after the 2D and 3D, respectively.

As previously described,¹⁷ pain at the injection site was assessed according to the following scale: mild, does not interfere with activity; moderate, interferes with activity; severe, prevents daily activity; and critical, emergency department visit or hospitalization. Redness and swelling were measured according to the following scale: mild, 2.0 to 5.0 cm in diameter; moderate, >5.0 to 10.0 cm in diameter; severe, >10.0 cm in diameter; and critical, necrosis or exfoliative dermatitis (for redness) and necrosis (for swelling). Fever categories were mild, 38.0 °C to 38.4 °C; moderate >38.4 °C to 38.9 °C; severe, >38.9 °C to 40 °C; and critical, >40 °C. Medication use was not graded. Additional scales were as follows: fatigue, headache, chills, new or worsened muscle pain, new or worsened joint pain (mild: does not interfere with activity; moderate: some interference with activity; or severe: prevents daily activity), vomiting (mild: 1 to 2 times in 24 hours; moderate: >2 times in 24 hours; or severe: requires intravenous hydration), and diarrhea (mild: 2 to 3 loose stools in 24 hours; moderate: 4 to 5 loose stools in 24 hours; or severe: 6 or more loose stools in 24 hours); critical for all events indicated an emergency department visit or hospitalization.

Assessment of anti-SARS-CoV-2 humoral response

In vitro neutralization assay. SARS-CoV-2 (BetaCoV/France/IDF0571/2020 virus [Global Initiative on Sharing Avian Influenza Data Accession ID = EPI_ISL_411218]) was isolated in Vero E6 from a nasal swab of one of the first patients who was found to be COVID-19-positive in France and was kindly provided by Dr. Olivier Terrier and the Virpath lab (Centre International de Recherche en Infectologie–Lyon). To generate virus stocks, Vero E6 cells were inoculated with virus at a multiplicity of infection of 0.01. Supernatant fluid was harvested at 72 hours postinfection, clarified by low-speed centrifugation, aliquoted, and stored at –80 °C. Virus stock was quantified by classic limiting dilution plaque assay on Vero E6 cells (kindly provided by Dr. F-L. Cosset, Centre International de Recherche en Infectologie–Lyon).

Two-fold dilutions of serum in 50 µl of Dulbecco's modified Eagle's medium, containing 2X penicillin/streptomycin, were incubated with 200 plaque-forming units of SARS-CoV-2 in 50 µl of Dulbecco's modified Eagle's medium for 15 minutes at room temperature. Aliquots of 100 µl of Dulbecco's modified Eagle's medium + 4% fetal bovine serum containing 2.5×10^4 Vero E6 cells

were added to achieve a final dilution of sera from 1:100 to 1:12,800 (4 wells per dilution). Cells were incubated for 5 days at 37 °C, 5% CO₂. After 15 minutes of fixation in paraformaldehyde 4% in phosphate buffered saline 1X, cytopathic effect was revealed by crystal violet staining and scored by a researcher (CM) blinded to the study design and sample identity. Neutralization endpoint titers were expressed as the value of the last serum dilution that completely inhibited a virus-induced cytopathic effect.

Anti-RBD IgG response. The IgG antibodies directed against the receptor binding domain (RBD) of the spike glycoprotein of the SARS-CoV-2 were detected by a chemiluminescence technique, using the Maglumi SARS-CoV-2 S-RBD IgG test (Snibe Diagnostic) on a Maglumi 2000 analyzer (Snibe Diagnostic), according to the manufacturer's instructions. Briefly, 10 µl of serum were incubated in the appropriate buffer with magnetic microbeads covered with spike RBD recombinant antigen to form immune complexes. After precipitation in a magnetic field and washing, N-(4-aminobutyl)-N-ethylisoluminol-stained anti-human IgG antibodies were added to the samples. After a second magnetic separation and washing, the appropriate reagents were added to initiate a chemiluminescence reaction. When necessary, sera were diluted sequentially up to 1:1000.

As recommended by the World Health Organization,²⁰ the titers are expressed as binding arbitrary units/ml (BAU/ml).

Assessment of the anti-SARS-CoV-2 spike cellular immune responses

Enumeration of SARS-CoV-2 spike-specific T CD4+, Tfh, and CD8+ cytotoxic cells. Peripheral blood mononuclear cells were collected and isolated by centrifugation on a Ficoll density gradient. The cells were then frozen in fetal calf serum supplemented with 10% dimethylsulfoxide (Sigma).

CD8+ and CD4+ T cells specific for SARS-CoV-2 spike protein were enumerated using the technique reported by Grifoni et al.²¹ SARS-CoV-2 spike-specific T follicular helper (Tfh) cells were enumerated according to a technique developed by our team and previously published.²² Briefly, after thawing, cells were concentrated at 10⁷ cells/ml in Roswell Park Memorial Institute complete medium and left to rest overnight at 37 °C and 5% CO₂ in a 96-well round-bottom plate, 10⁶ cells/well. The next day, the Roswell Park Memorial Institute medium was changed, and the cells were cultured for 24 hours in the presence of a pool of overlapping peptides covering the entire sequence of the spike protein of SARS-CoV-2 (PepMix™, JPT Peptides Technologies GmbH). The final concentration of the peptides was 1 µg/ml. Cells cultured with dimethylsulfoxide (Sigma) alone (1/250) were used as negative controls. Cells were then rinsed and incubated at room temperature with a Fixable Viability Dye (eBiosciences) and 1 of the 2 following fluorescent antibodies panels for 30 minutes. Panel 1: CD3 (UHCT1), CD8 (SK1), from BD Biosciences; CD4 (SK3), CD69 (FN50), CD137 (4B4-1), CD134 (OX-86) from BioLegend. Panel 2: CD4 (SK3) from BioLegend, CD3 (UHCT1) CXCR5 (RF8B2), CD25 (2A3), from BD Biosciences. Cells were fixed with 2% methanol-free formaldehyde. Sample acquisitions were made on a BD LSR Fortessa 4L flow cytometer (BD Biosciences). The gating strategies used for these analyses are shown in [Supplementary Figure S1A to C](#).

Interferon-γ release assay. Spike-specific CD4+ T-cell responses were quantified in the circulation of the HVs and patients on MHD using the QuantiFERON SARS-CoV-2 test (Qiagen), a

commercially available interferon-γ release assay (IGRA), according to the manufacturer's instructions.

Briefly, 1 ml blood was distributed in each tube of the assay: (i) uncoated tube: negative control/background noise, (ii) tube coated with mitogen: positive control, (iii) tube coated with human leukocyte antigen II-restricted 13-mers peptides derived from the entire SARS-CoV-2 spike glycoprotein used to stimulate CD4+ T cells. After 20 hours of culture at 37 °C, tubes were centrifuged 15 minutes at 2500g and stored at 4 °C before interferon-γ quantification in the supernatant by enzyme-linked immunosorbent assay.

The CD4+ T-cell assay value was the difference between tube (iii) and the negative control (i).

Statistical analysis

All the analyses were carried out using R software version 4.0.4 (R Foundation for Statistical Computing) and or GraphPad Prism version 8.0 (GraphPad Software). Categorical variables were expressed as percentages and compared with the chi-squared test. Continuous variables were expressed as mean ± SD and compared using one-way analysis of variance and multiple *t*-tests post hoc analyses or as median and interquartile range (IQR) and compared using Mann-Whitney *U* test for variables with nonnormal distribution.

Logistic regression models were used in both univariate and multivariate analyses. All the explanatory variables significantly associated with outcomes in univariate analyses (*P* < 0.10) were included in multivariate models. Stepwise regression analyses with bidirectional elimination were then performed, using Akaike information criterion to select the most fitting final multivariate models.

RESULTS

Patients on MHD are insufficiently protected against COVID-19 after 2 doses of mRNA vaccine

To evaluate the level of protection conferred by COVID-19 mRNA vaccination to patients on MHD who are naïve for the virus the French national registry Renal Epidemiology and Information Network (REIN)²³ was interrogated to identify all the cases of COVID-19 diagnosed in patients on MHD from February 1 to May 18, 2021, the period during which MHD population was prioritized for vaccination in France ([Figure 1a](#)). During this period, the virus circulation rate in France was moderate (estimated ~200 cases/week per 100,000 people) and the large majority of COVID-19 cases were related to either to the original coronavirus strain detected in Wuhan, or the alpha variant ([Supplementary Figure S2](#)).²⁴

The cumulative incidence of COVID-19 at 28 days was 1.98% in patients on MHD who are virus-naïve and non-vaccinated. Although vaccination reduced this number to, respectively, 0.65% after the first dose (1D) and to 0.25% after the 2D (log-rank *P* < 0.0001) ([Figure 1b](#)), this level of protection remains largely inferior to what was reported in the general population.^{17,25}

Over the study period, a total of 1474 cases of COVID-19 were reported. For the 1439 patients on MHD who were infected (97.6%), for whom the information was available, the severity of disease was analyzed according to whether the diagnosis of COVID-19 was made before vaccination (not

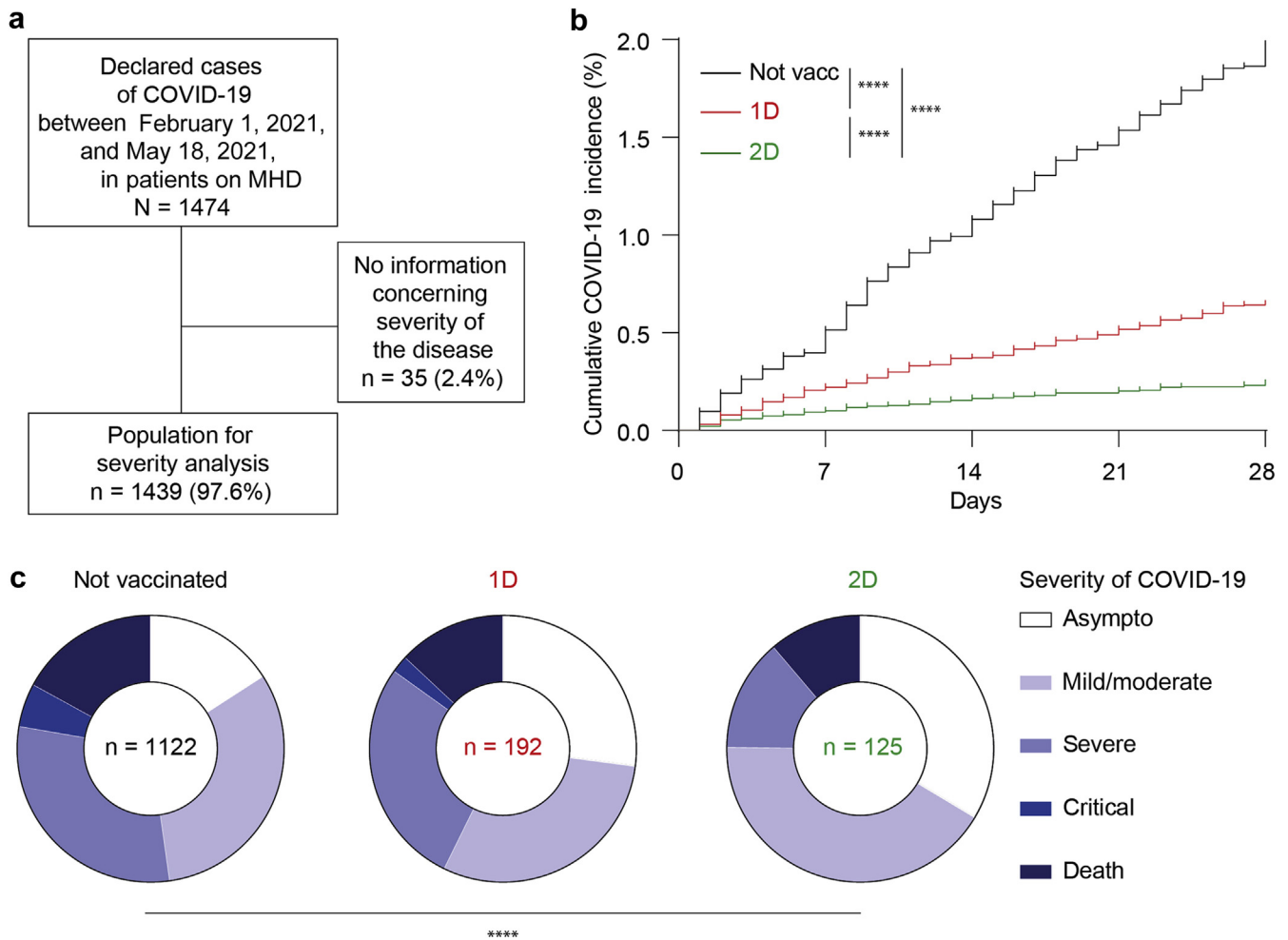


Figure 1 | Severity of coronavirus disease 2019 (COVID-19) in patients on maintenance hemodialysis (MHD) according to their vaccination status. (a) Flowchart of the epidemiologic study conducted through the Renal Epidemiology and Information Network (REIN) network. (b) Cumulative incidence of the cases of COVID-19 that occurred over the study period in patients on MHD before vaccination or up to 10 days after the first dose (Not vacc, black curve), from 10 days after the first dose to 10 days after the second dose (1D, red curve), or more than 10 days after the second dose of vaccine (2D, green curve). Log-rank test, **** $P < 0.0001$. (c) Severity of COVID-19 was color coded and the distribution was compared between the groups of patients on MHD defined according to their vaccination status. Chi-square test; **** $P < 0.0001$. Asympto, asymptomatic; Not vacc, not vaccinated.

vaccinated, $n = 1122$; Figure 1b, black), 10 days after the 1D ($n = 192$; Figure 1b, red), or 10 days after the 2D ($n = 125$; Figure 1b, green) of vaccine. The characteristics of the population are presented in Table 1. Patients' characteristics were similar in the 3 groups with exception of age, cardiopathy, and time in MHD, which were all higher in patients who developed COVID-19 after the 2D of vaccine, probably because the patients with the more comorbid profile were vaccinated with the highest priority (Table 1).

The distribution of patients across the 5 stages of severity (asymptomatic, mild, severe, critical, or death²⁶) of COVID-19 as defined by the World Health Organization was statistically different among the 3 groups (Figure 1c). However, despite an increased proportion of less severe forms (asymptomatic or mild or moderate) of COVID-19 in patients who were vaccinated, 11% of patients on MHD that had received 2Ds of mRNA vaccine still died from COVID-19 (Figure 1c). The

latter result is drastically different from that reported in the pivotal studies conducted in the general population¹⁷ and demonstrates that vaccination with the 2D "standard" scheme is insufficient to protect all patients on MHD.

Standard 2D scheme of vaccination induces flawed humoral immune responses in patients on MHD who are virus-naïve

Among the 150 patients on MHD who were dialyzing at Lyon University Hospital, 38 (25.3%) refused the vaccine or had contraindications. Of the 112 who received 2Ds of BNT162b2 mRNA vaccine, 106 (14 of whom had a previous history of COVID-19, black circle) gave consent for analysis of the postvaccinal immune response and were enrolled in ROMANOV study (Figure 2). To understand why patients on MHD who were virus-naïve and were insufficiently protected by COVID-19 mRNA vaccination, the humoral and cellular immune responses of the latter were compared to that of 30

Table 1 | Characteristics of COVID-19-infected patients on MHD according to their vaccination status

Variables	Whole cohort (N = 1439)	Not vaccinated (n = 1122)	1D (n = 192)	2D (n = 125)	P
Sex ratio, M/F	1.37 (833/606)	1.32 (639/483)	1.49 (115/77)	1.72 (79/46)	0.338
Age, yr	69.6 ± 15.0	68.5 ± 15.2	71.7 ± 14.3	74.0 ± 13.5	<0.0001
BMI, kg/m ²	27.4 ± 6.30	27.5 ± 6.24	27.0 ± 6.48	27.3 ± 6.52	0.676
Comorbidities					
Diabetes	732 (51)	581 (52)	89 (46)	62 (50)	0.364
Cardiopathy	572 (40)	420 (37)	84 (44)	68 (54)	0.0006
Vascular disease	380 (26)	280 (25)	58 (30)	42 (34)	0.051
Respiratory disease	269 (19)	204 (18)	42 (22)	23 (18)	0.477
Malignancy	148 (10)	108 (10)	25 (13)	15 (12)	0.289
HD parameters					
Time in HD, mo	5.5 ± 6.6	5.2 ± 6.2	6.4 ± 7.7	6.0 ± 7.6	0.046
Time HD/wk, h	11.6 ± 1.63	11.6 ± 1.62	11.8 ± 1.70	11.7 ± 1.60	0.196

1D, first dose; 2D, second dose; BMI, body mass index; COVID-19, coronavirus disease 2019; HD, hemodialysis; MHD, maintenance hemodialysis. Values are n (%) or mean ± SD.

HVs (4 of whom had a previous history COVID-19, black triangle).

Enumeration of SARS-CoV-2 spike-specific CD8+ T cells was made after 2Ds by flow cytometry using the activation induced marker technique²¹ (Figure 3a). Although the percentage of circulating spike-specific CD8+ T cells was more heterogeneous and slightly reduced in patients on MHD as compared with in HVs (median: 0.15 [IQR: 0.05–0.57] vs. 0.31 [IQR: 0.21–0.45]; P = 0.042; Figure 3b), this mild difference was unlikely to be the sole explanation to the major difference in protection against COVID-19 observed in the 2 vaccinated populations.

We next went on analyzing the viral-neutralizing capacity of patients' sera after 2Ds using an *in vitro* functional assay (Figure 3c). While the serum of patients on MHD with previous history of COVID-19 (Figure 3d, black circles) had similar viral neutralizing capacity as the sera of HVs, this serum characteristic was profoundly depressed in patients on MHD who were vaccinated and naïve for the virus (Figure 3d, open circles).

Viral neutralization capacity of serum depends on the presence of high titers of IgGs directed against the spike protein. The generation of IgGs against a protein antigen requires a particular subset of CD4+ T cells, the Tfh cells, which are specialized in providing the help to B cells and are necessary to B cells' differentiation into antibody-producing plasma cells.^{27,28} Enumeration of SARS-CoV-2 spike-specific CD4+ T and Tfh cells was performed in the circulation after the 2D using 2 distinct techniques.^{21,22} In contrast to patients on MHD who developed neutralizing IgG titers (neutral+), patients on MHD whose serum lacks viral neutralizing capacity (neutral-) had reduced levels of both spike-specific CD4+ T cells (Supplementary Figure S1D and E) and spike-specific Tfh cells in their circulation (Figure 3f).

Surrogate assays to monitor neutralizing antibodies and spike-specific Tfh cells in routine clinical practice

Viral-neutralizing antibodies, the generation of which depends on spike-specific Tfh cells, seem important to provide protection against COVID-19 after vaccination. Monitoring of these immune effectors after vaccination could therefore be

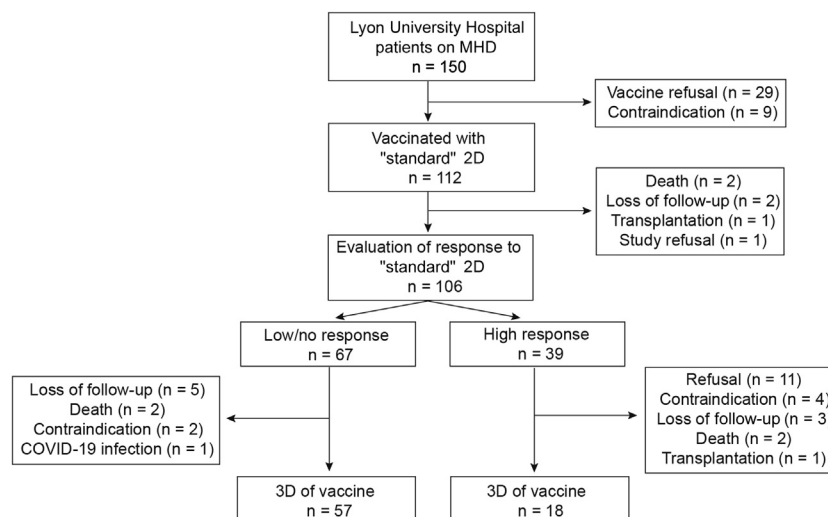


Figure 2 | Flowchart of the Response of Hemodialyzed Patients to COVID-19 Vaccination (ROMANOV) prospective study. 2Ds, 2 doses; 3Ds, 3 doses; COVID-19, coronavirus disease 2019; MHD, maintenance hemodialysis.

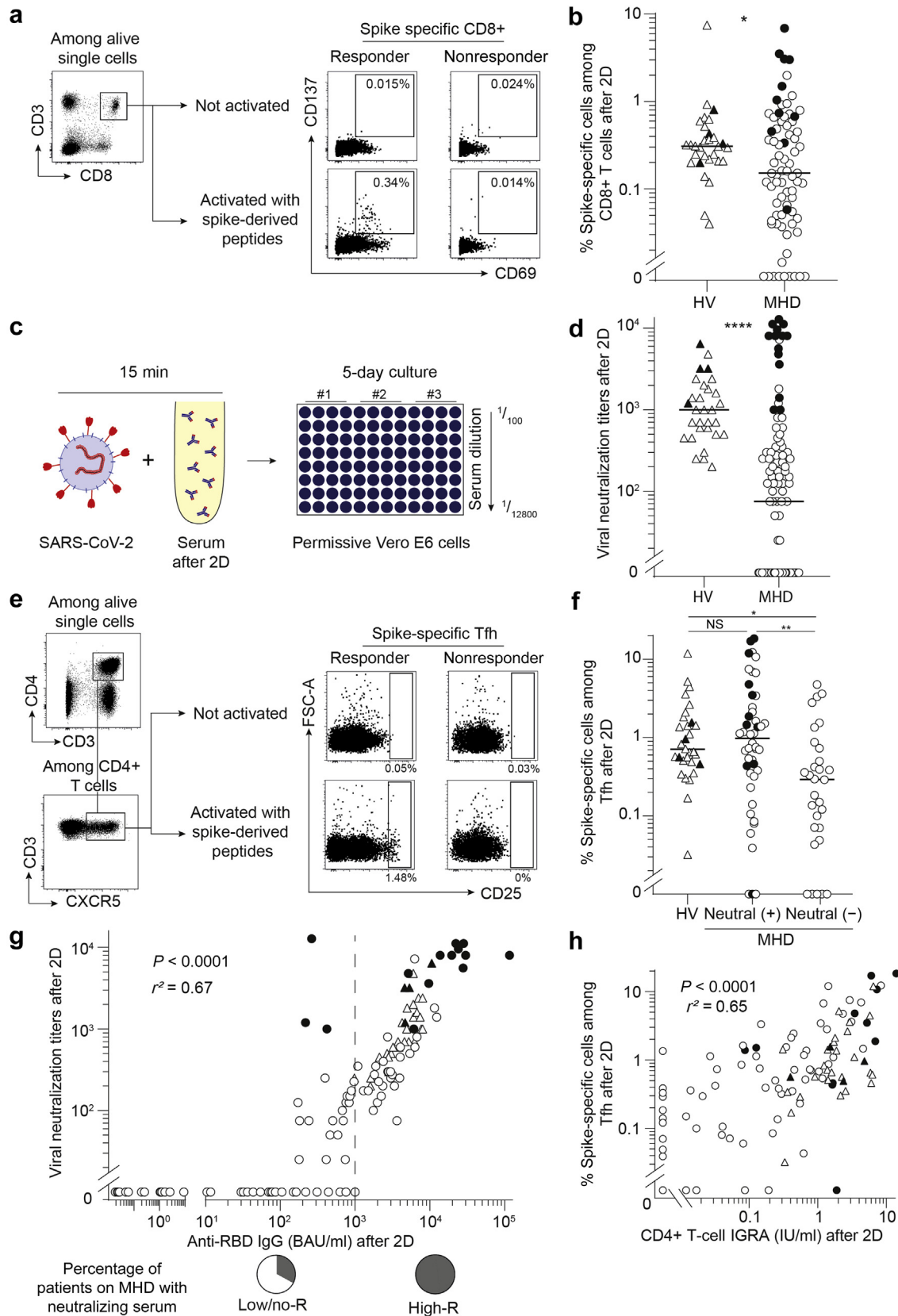


Figure 3 | Comparison of the immune responses of patients on maintenance hemodialysis (MHD) and healthy volunteers (HVs) after 2 doses (2Ds) of BNT162b2. Spike-specific cellular and humoral immune responses were evaluated 10 to 14 days after the 2D of vaccine in the circulation of 77 patients on MHD (circles; among which 14 had a previous history of coronavirus disease 2019, black circles) and 30 HVs (triangles; among which 4 had a previous history of coronavirus disease 2019, black triangles). (a,b) Enumeration of spike-specific (continued)

interesting to identify patients on MHD who are insufficiently protected. Unfortunately, neither *in vitro* neutralizing assay, nor the enumeration of spike-specific Tfh cells in the circulation can be performed in routine clinical practice.

Antigen-binding assays are convenient and widely used in routine clinical care for monitoring of antibody response. Comparing the titer of IgG directed against the RBD of the spike glycoprotein of the SARS-CoV-2 (anti-RBD IgG) measured with chemoluminescence assay and the neutralizing capacity of the serum, we observed a highly significant ($P < 0.0001$) and strong ($r^2 = 0.67$) positive correlation (Figure 3g). Hence, we could establish that a titer of anti-RBD IgGs ≥ 997 BAU/ml (Figure 3g, vertical dashed line) was systematically associated with viral neutralizing capacity of the serum. This threshold was therefore used in the rest of the study to define “high” (anti-RBD IgG ≥ 997 BAU/ml; $n = 39$ of 106, 36.8%) vs. “low or no” (anti-RBD IgG < 997 BAU/ml; $n = 67$ of 106, 63.2%) response to vaccine (Figure 2). An indirect validation of this functional threshold is provided by the fact that almost all HVs, who are efficiently protected against COVID-19 by the vaccination, had anti-RBD IgG titers ≥ 997 BAU/ml after 2Ds of vaccine (Figure 3d and g).

IGRAs are already used in clinical practice to monitor the T-cell response against *Mycobacterium tuberculosis*.²⁹ The results obtained with a commercially available SARS-CoV-2 CD4+ T-cell IGRA were compared to the enumeration of antigen-specific Tfh cells by flow cytometry (Figure 3h). The highly significant ($P < 0.0001$) and strong ($r^2 = 0.65$) positive correlation observed suggests that CD4+ T-cell IGRA can be used as a surrogate assay to flow cytometry for the monitoring of spike-specific Tfh-cell response.

Prospective observational study on the third dose of mRNA vaccine in patients on MHD

In an attempt to improve vaccine protection against COVID-19 in patients on MHD, French health officials authorized the administration of a 3D of vaccine in this population from mid-April 2021 onward.¹⁹

A 3D of BNT162b2 mRNA vaccine was therefore offered to all 67 patients on MHD in the ROMANOV study with low or no anti-RBD IgG response and was effectively administered to 57 of them (85.1%) (Figure 2). In absence of clear consensus, the administration of the 3D of vaccine was not limited to

Table 2 | Clinical and biological characteristic of patients on MHD who were injected with a 3D of BNT162b2

Variables	Whole cohort (N = 75)
Male	48 (64)
Age, yr	65.8 ± 14.4
BMI, kg/m ²	26.8 ± 6.4
Comorbidities	
Diabetes	35 (47)
Cardiopathy	36 (48)
Respiratory disease	6 (8)
Hepatic disease	4 (5)
Cause of renal failure	
Vascular	17 (23)
Diabetes	27 (36)
Glomerulonephritis	7 (9)
Hereditary	3 (4)
Uropathy	0 (0)
Others	21 (28)
Previous SOT	16 (21)
IS therapy	8 (11)
History of COVID-19	3 (4)
Time in HD, mo	56 ± 69
HD parameters	
Time HD/wk, h	10.6 ± 2.77
Kt/V	1.56 ± 0.43
Biological characteristics	
Hemoglobinemia, g/l	106 ± 16
C-reactive protein, mg/l	13.4 ± 20.9
Albuminemia, g/l	36.4 ± 6.7

3D, third dose; BMI, body mass index; COVID-19, coronavirus disease 2019; HD, hemodialysis; IS, immunosuppressive; Kt/V, quantification of dialysis adequacy by the formula: dialysis clearance of urea (K) multiplied by t (dialysis time) divided by the volume of distribution of urea (V); MHD, maintenance hemodialysis; SOT, solid organ transplantation. Values are n (%) or mean ± SD.

patients on MHD with low or no anti-RBD IgG titers, and 18 of 39 patients on MHD with high IgG response (46.2%; $P < 0.0001$) also accepted a 3D of vaccine (Figure 2). The characteristics of the 75 patients on MHD that received 3Ds of vaccine are presented Table 2.

Reactogenicity to the 3D of mRNA vaccine in patients on MHD

Among included patients on MHD, tolerability data were available for 82 of 106 patients after the 2D and 63 of 75 after the 3D. Overall tolerance to the 3D of BNT162b2 mRNA vaccine was good in patients on MHD (Figure 4a and b). No patients developed critical side effects requiring hospitalization. Forty percent of these patients with a 3D (25 of 63)

Figure 3 | (continued) CD8+ T cells by the activation-induced markers technique. (a) Gating strategy is shown on representative flow cytometry profiles. (b) Histogram showing individual values for HVs and patients on MHD. (c,d) Evaluation of viral neutralization capacity of the serum by *in vitro* functional assay. (c) Schematic representation of the methodology. (d) Histogram showing individual values for HVs and patients on MHD. (e,f) Enumeration of spike-specific CD4+ T follicular helper (Tfh) cells. (e) Gating strategy is shown on representative flow cytometry profiles. (f) Histogram showing individual values for HVs and patients on MHD, the latter being distributed in 2 groups (Neutral[+] or Neutral[-]) according to the viral neutralization capacity of their serum. Mann-Whitney U test; not significant (NS), $P > 0.05$; * $P \leq 0.05$; ** $P < 0.01$; **** $P < 0.0001$. (g) The relation between the titers of anti-receptor binding domain (RBD) IgG measured in antigen-binding assay and the viral neutralization capacities evaluated in the *in vitro* functional assay shown in c was analyzed by linear regression. The threshold of anti-RBD IgG titer (997 binding arbitrary units [BAU]/ml) above which all sera had viral neutralization capacity is indicated by a vertical dashed line and was used to defined high responders (High-R) versus low or no responders (Low- or no-R) to 2Ds of vaccine. (h) The relation between the result of spike-specific CD4+ T-cell interferon- γ release assay (IGRA) and the percentage of spike-specific CD4+ Tfh cells enumerated as shown in e was analyzed by linear regression. FSC-A, forward scatter area; SARS-CoV-2, severe acute respiratory syndrome coronavirus 2.

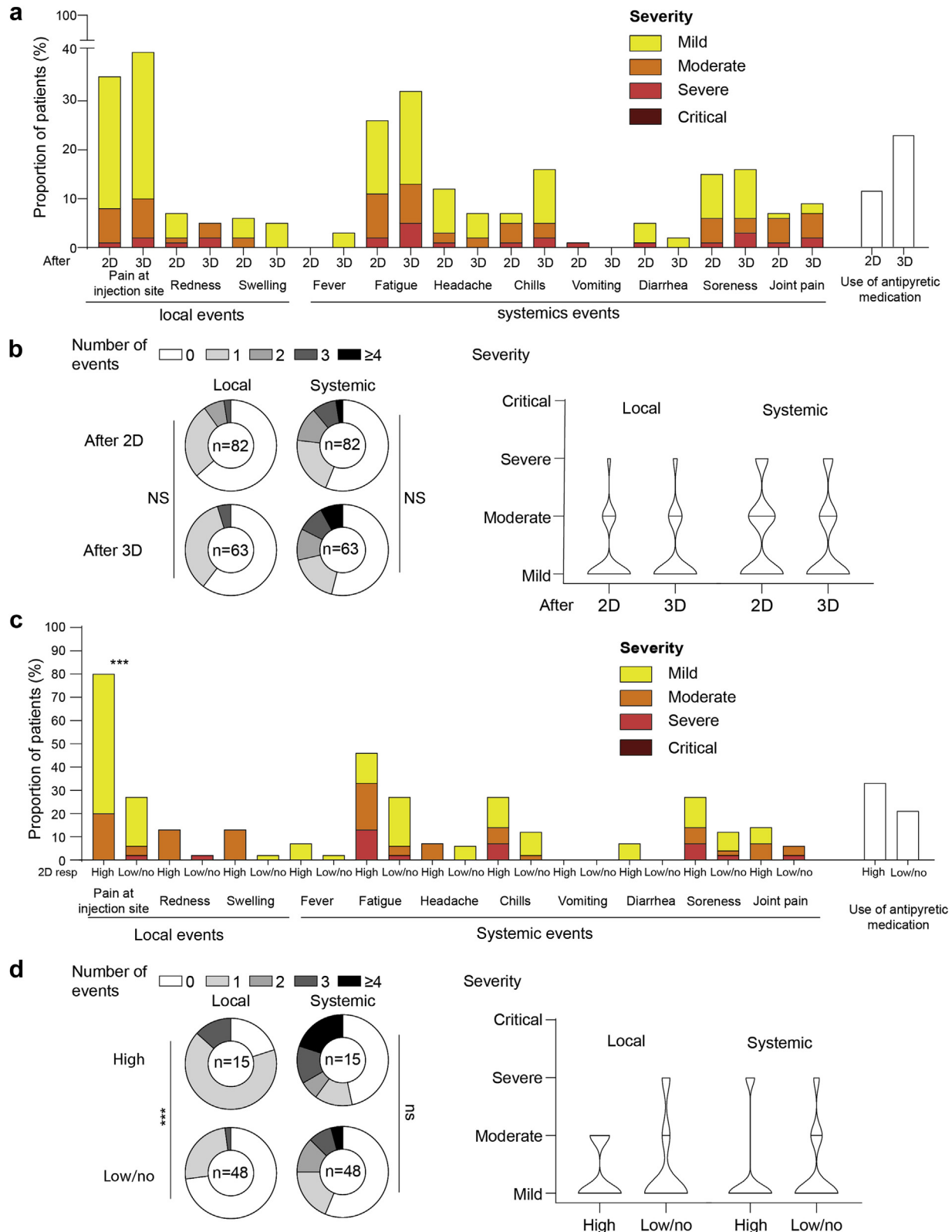


Figure 4 | Reactogenicity to the third dose (3D) of mRNA vaccine in patients on maintenance hemodialysis (MHD). (a) Proportion of patients on MHD who developed local and systemic adverse events after the second dose (2D) and the 3D of vaccine are represented. Severity of the adverse event is color-coded (0–4) according to the scale detailed in the Methods section. (b) The number and the severity of local and systemic adverse events that occurred after the 2D and 3D of vaccine are compared. Chi-square test. (c) Proportion of patients on MHD who developed local and systemic adverse events after the 3D of vaccine according to the viral neutralization capacity of their serum after the 2D (high: neutralization+ vs. low or no: neutralization–). (d) The number and the severity of local and systemic adverse events that occurred after 3D of vaccine were compared between patients who were high responders and those who were low or no responders. Chi-square test. *** $P < 0.0001$. NS, not significant.

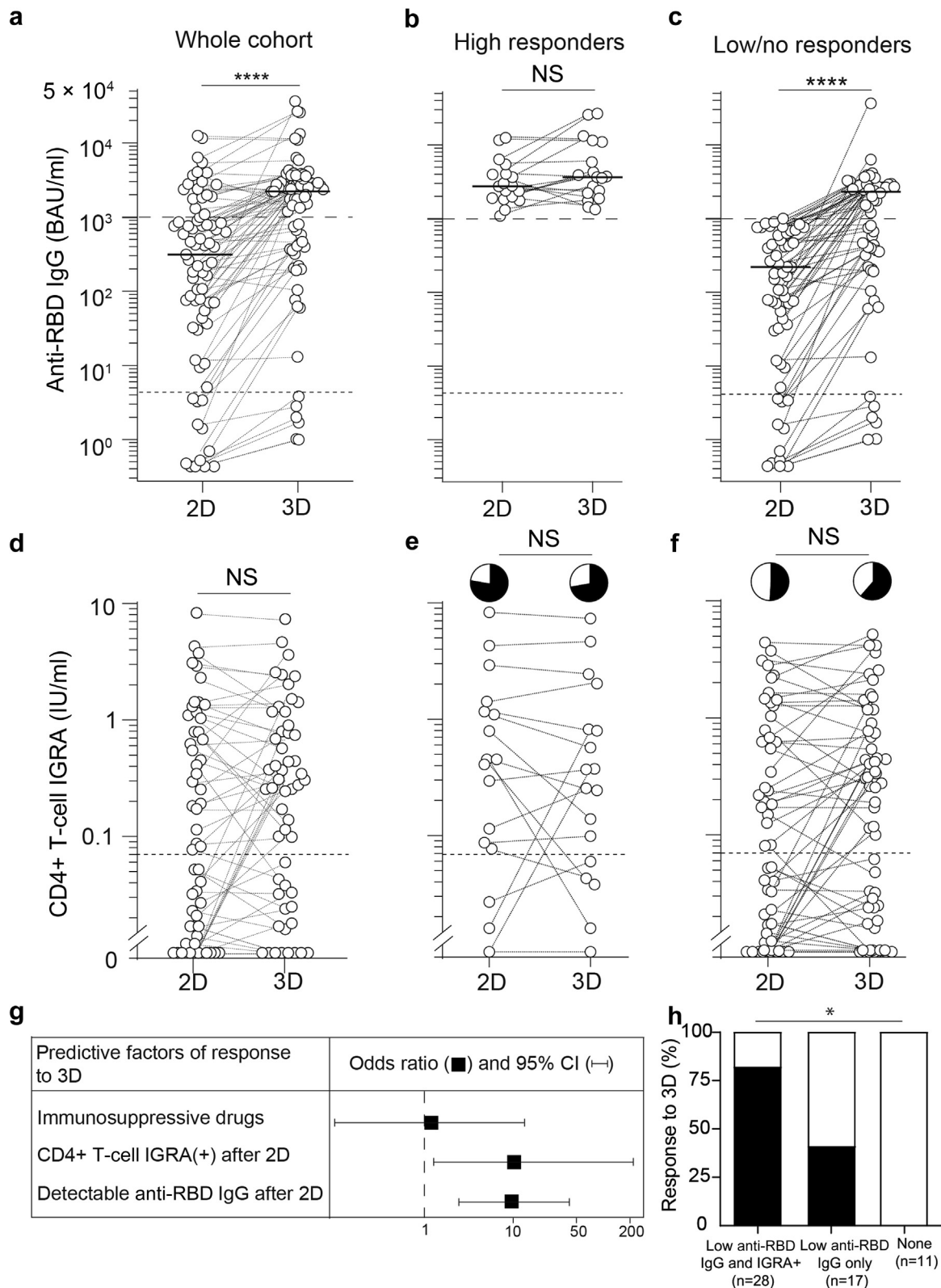


Figure 5 | Evolution of anti-receptor binding domain (RBD) IgG titers and the results of spike-specific CD4+ T-cell interferon-γ release assay (IGRA) between the second dose (2D) and the third dose (3D) of vaccine in patients on maintenance hemodialysis (MHD). (a–c) Anti-RBD IgG titers expressed in binding arbitrary units (BAU/ml) were measured 10 to 14 days after the 2D and 3D of vaccine. Upper dashed line represents the threshold (997 BAU/ml) above which all sera have viral neutralization capacity. This limit was used to define high versus low or no responders to the 2D. Lower dotted line indicates the limit of detection of the assay. (a) Results of the whole cohort of patients on MHD are plotted. (b,c) Evolution of anti-RBD IgG titers between the 2D and 3D of vaccine were compared for high (continued)

developed local side effects, the most frequently reported being pain at the injection site (40%). Forty-six percent of these patients with a 3D (29 of 63) reported systemic side effects, including fatigue (32%), chills (16%), and soreness (16%). In almost all cases (74 of 83, 89%), the intensity of the symptoms was mild or moderate (Figure 4a and b).

When local and systemic side effects of vaccine were compared between the 2D and the 3D, no significant difference was found, neither regarding the frequency nor severity of symptoms (Figure 4a and b). However, when the profile of tolerance was compared between patients on MHD according to the intensity of the humoral response after 2Ds of vaccine, a significant trend for more side effects was observed in patients with high response (Figure 4c and d).

Impact of the 3D of mRNA vaccine on humoral response of patients on MHD

When the whole cohort of patients on MHD ($n = 75$) was considered, a significant increase in the median titer of anti-RBD IgG was observed after the 3D of vaccine (309.8 [IQR: 36.5–996.3 vs. 2212 [IQR: 394.9–3247] BAU/ml after the 2D and 3D, respectively; $P < 0.0001$; Figure 5a). However, this global positive result hides major interindividual heterogeneity.

Patients on MHD with high humoral response after 2Ds of vaccine ($n = 18$), all maintained high levels of anti-RBD IgG after the 3D but without significant increase of their titer (median: 2757 [IQR: 1869–4365] vs. 3619 [IQR: 2127–11035] BAU/ml after the 2D and 3D, respectively; $P = 0.154$; Figure 5b). In contrast, patients on MHD with low or no humoral response after 2Ds experienced a significant increase of anti-RBD IgG after the 3D (median: 10.5 [IQR: 1.05–69.9] vs. 353.1 [IQR: 36.2–2592] BAU/ml; $P < 0.0001$; Figure 5c). However, there was again significant interindividual heterogeneity in the response and only 31 of 57 of low or no responders to 2Ds (54.4%) reached optimal titer (i.e., ≥ 997 BAU/ml; Figure 5c, dashed line) of anti-RBD IgG after a 3D.

Impact of the 3D of mRNA vaccine on cellular response of patients on MHD

The impact of a 3D on antigen-specific Tfh-cell response was indirectly monitored using spike-specific CD4+ T-cell IGRA. Globally, the 3D of vaccine did not result in a significant increase in spike-specific Tfh-cell response in the circulation of patients on MHD neither when the amount of interferon- γ (median: 0.127 [IQR: 0.014–1.040] vs. 0.261 [IQR: 0.025–0.820] IU/ml; $P = 0.517$) nor the proportion of patients on MHD with positive IGRA (57% vs. 64%; $P = 0.50$) were

considered (Figure 5d). The result remained unchanged when the analysis was made within the subpopulations of patients on MHD with high versus low or no humoral response after 2Ds of vaccine (Figure 5e and f).

Unexpectedly, we noticed that some patients on MHD experienced a reduction in their CD4+ T-cell IGRA result between the 2D and 3D (Figure 5d–f). This proportion was not different between high and low or no responders to 2Ds (8 of 18, 44% vs. 24 of 57, 42%; $P > 0.99$). Although we do not have definitive explanation for this observation, it could be due to technical limitations of the assay and/or it could indicate interindividual heterogeneity in the durability of the CD4+ T-cell response.

Defining the subpopulation of patients on MHD that should receive a 3D of vaccine

Because it was less well tolerated in these patients (Figure 4c and d) and did not improve their immune response (Figure 5b and f), we concluded that the subpopulation of patients on MHD with already high humoral response after 2Ds should not receive a 3D of vaccine.

To identify among the patients on MHD with low or no response after the standard scheme of vaccination those who would benefit from a 3D of vaccine, the characteristics of the patients on MHD who reached high titer of anti-RBD IgG after the 3D (responders to the 3D: $n = 31$ of 57, 54.4%) were compared to that of the rest of the cohort (nonresponders to 3D: $n = 26$ of 57, 45.6%). The former group was less exposed to immunosuppressive drugs and had more often detectable anti-RBD IgG and positive spike-specific CD4+ T-cell IGRA after 2Ds (Table 3). In multivariate analysis, the only variables that predicted an immune response to the 3D was the presence of low titers of anti-RBD IgG (odds ratio: 10.1 [95% confidence interval: 1.3–216.5]; $P = 0.054$) and a positive spike-specific CD4+ T-cell IGRA (odds ratio: 9.25 [95% confidence interval: 2.44–40.7]; $P = 0.002$) after 2Ds (Figure 5g). Furthermore, combining this information, we observed that the probability to respond to the 3D in patients on MHD that were low or no responders to 2Ds was the highest in patients positive for both tests (82%) (Figure 5h). The response rate decreased to 41% in patients on MHD with only low anti-RBD IgG after the 2D and dropped to 0% in those in whom both tests were negative after the 2D (Figure 5h).

DISCUSSION

This prospective observational study demonstrates that, in contrast with what reported in the general population,¹⁷ the

Figure 5 | (continued) responders ($n = 18$; **b**) and low or no responders ($n = 57$; **c**) only. Wilcoxon test. (**d–f**) Result of spike-specific CD4+ T-cell IGRA were measured 10 to 14 days after the 2D and 3D of vaccine. Lower dashed line indicates the limit of positivity of the assay. (**d**) Results of the whole cohort of patients on MHD are plotted. (**e,f**) Evolution of the results of spike-specific CD4+ T-cell IGRA between the 2D and 3D of vaccine were compared for high responders ($n = 18$; **e**) and low or no responders ($n = 57$; **f**) only. Wilcoxon test. The proportion of positive IGRA is indicated in the pie chart. (**g**) Forest plot of the results of the multivariate analysis conducted to identify the variables independently associated with the generation of anti-RBD IgG titers ≥ 997 BAU/ml after the 3D. (**h**) The proportion of patients on MHD that generated anti-RBD IgG titers ≥ 997 BAU/ml after the 3D is shown according to the presence of anti-RBD IgG and the result of spike-specific CD4+ T-cell IGRA after the 2D. Chi-square test. NS, not significant: $P > 0.05$; * $P \leq 0.05$; **** $P < 0.0001$. CI, confidence interval.

Table 3 | Univariate and multivariate analysis used to identify predictive factors of response to the 3D

Variables	No response to 3D (n = 26)	Response to 3D (n = 31)	OR univariate (95% CI; P)	OR multivariate (95% CI; P)
Male	21 (81)	19 (61)	0.38 (0.10–1.22; 0.115)	
Age, yr	69.2 ± 13	66.6 ± 14	0.99 (0.95–1.02; 0.455)	
BMI, kg/m ²	25.8 ± 4.7	27.7 ± 7.3	1.06 (0.97–1.18; 0.256)	
Comorbidities				
Diabetes	13 (50)	15 (48)	0.94 (0.33–2.67; 0.903)	
Cardiopathy	16 (62)	13 (42)	0.45 (0.15–1.29; 0.143)	
Respiratory disease	2 (8)	3 (10)	1.29 (0.20–10.4; 0.792)	
Hepatic disease	3 (12)	1 (3)	0.26 (0.01–2.14; 0.251)	
Previous SOT	6 (23)	3 (10)	0.36 (0.07–1.52; 0.179)	
IS drug	6 (23)	2 (6)	0.23 (0.03–1.11; 0.090)	1.18 (0.10–13.2; 0.890)
History of COVID-19	1 (4)	2 (6)	1.72 (0.16–38.4; 0.664)	
Time in HD, d	1135 ± 1022	1266 ± 1511	1.00 (1.00–1.00; 0.705)	
HD parameters				
Time HD/wk, h	683 ± 94	685 ± 78	1.00 (0.99–1.01; 0.926)	
Kt/V	1.5 ± 0.3	1.4 ± 0.5	0.74 (0.20–2.63; 0.644)	
Biological				
Hemoglobinemia, g/l	108 ± 10	107 ± 16	1.00 (0.96–1.04; 0.940)	
C-reactive protein, mg/l	19.0 ± 30.1	9.0 ± 8.4	0.97 (0.93–1.00; 0.124)	
Albuminemia, g/l	34.6 ± 4.5	36.6 ± 5.7	1.08 (0.97–1.20; 0.167)	
Anti-SARS-CoV-2 response after 2Ds				
Detectable anti-RBD IgG	15 (58)	30 (97)	22.0 (3.8–421.7; 0.005)	10.1 (1.3–216.5; 0.054)
CD4+ T-cell IGRA (+)	5 (19)	24 (77)	14.4 (4.26–57.6; <0.001)	9.25 (2.44–40.7; 0.002)

2Ds, 2 doses; 3D, third dose; BMI, body mass index; CI, confidence interval; COVID-19, coronavirus disease 2019; HD, hemodialysis; IGRA, interferon-γ release assay; IS, immunosuppressive; Kt/V, the quantification of dialysis adequacy by the formula: dialysis clearance of urea (K) multiplied by t (dialysis time) divided by the volume of distribution of urea (V); OR, odd ratio; RBD, receptor binding domain; SOT, solid organ transplantation. Values are n (%) or mean ± SD.

“standard” 2D scheme with BNT162b2 vaccine provides insufficient protection against the severe forms of COVID-19 in patients on MHD who are naïve for the virus.

This problem could be due to the fact that patients on MHD develop a flawed humoral response after 2Ds of vaccine, as illustrated by the very limited viral neutralizing capacity of their serum as compared with that of HVs. This could be the consequence of the deleterious impact of uremic toxins^{30,31} on the generation of spike-specific Tfh cells, a crucial subset to generate high titer of IgGs²⁷ that was detected in reduced number in patients on MHD who fail to respond to the vaccination. These conclusions are in line with recent studies that reported that patients on MHD who are naïve for SARS-CoV-2 develop impaired humoral and cellular immune responses after 2Ds of BNT162b2.^{9–14}

Based on the observations that (i) patients on MHD with a previous history of COVID-19 had a response to vaccine indistinguishable from that of HVs,⁹ and (ii) previous studies with protein-based vaccine (such as hepatitis B vaccine) reported acceptable response rates when dosing and/or number of administrations were increased,³² a 3D of BNT162b2 vaccine was offered to patients on MHD in France.¹⁹ Although, the safety of the 3D of BNT162b2 vaccine was excellent and comparable to that of the 2D with no critical local or systemic side-effect reported, the tolerance was worst in patients with already high humoral response, who did not improve significantly their immune response against the spike protein of SARS-CoV-2 after this additional injection. Furthermore, while not identified in our cohort, some cases

of (re)activation of autoimmune disorders have been reported after mRNA vaccines in the literature.^{33–35} This threat further supports avoiding useless additional vaccine injection in patients already protected after 2Ds.

In contrast, after a 3D, 91% of patients on MHD who are virus-naïve with low or no response after 2Ds experienced an increase of anti-RBD-IgG titer, 54% of whom up to an optimal (≥997 BAU/ml) level that was associated with viral neutralization. This latter subgroup could be identified after 2Ds (preemptively) by the fact that they had a positive CD4+ T-cell IGRA (a surrogate for the presence of spike-specific Tfh cells) and/or suboptimal titers (detectable but <997 BAU/ml) of anti-RBD IgGs in antigen-binding assay. Importantly, both assays are commercially available and easy to implement in routine clinical practice, which could pave the way for the personalization of the vaccination strategy in patients on MHD.

Our study has some limitations. Even if the size of the ROMANOV cohort is at least comparable to what is currently reported in the literature,^{10,11,14} our observations were made on a limited number of patients from a single university hospital. Furthermore, all these patients were receiving in-center MHD and were therefore characterized by a highly comorbid profile (Table 2). This shall be kept in mind because this bias may limit the generalizability of our conclusions.

Based on the findings presented herein, we propose the following strategy to optimize the protection of patients on MHD who are naïve for SARS-CoV-2. All these vulnerable patients should be offered the standard scheme of vaccination

in priority. Anti-RBD IgG and spike-specific CD4+ T cells should be monitored in their circulation 10 to 14 days after the 2D, resulting in the definition of 3 subgroups with distinct needs: (i) patients with high anti-RBD IgG titer (≥ 997 BAU/ml) do not require further intervention; (ii) patients with low or no anti-RBD IgG titer but positive CD4+ T-cell IGRA, whom are the most likely to respond, should be offered a 3D of vaccine; and (iii) patients with neither detectable anti-RBD IgG nor positive CD4+ T-cell IGRA after 2Ds, whom will not respond to a 3D, might rather receive infusion of monoclonal antibodies as means to induce passive immunization. Future prospective studies are urgently needed to confirm the validity of such personalized anti-COVID-19 vaccination strategy in patients on MHD who are naïve for SARS-CoV-2.

APPENDIX

List of collaborators from the REIN Registry: Chantrel François, Reydit Mathilde, Tiple Aurélien, Bechade Clémence, Bemrah Abdelkader, Vigneau Cécile, Sautenent Bénédicte, Kazes Isabelle, Courivaud Céline, Gabriel Jean-Marc, Edet Stéphane, Mercadal Lucile, Moranne Olivier, Toure Fatouma, Laurain Emmanuelle, Ranlin Alex, Longlune Nathalie, Glowacki François, Tivollier Jean-Michel, Brunet Philippe, Lavainne Frédéric, Berard Etienne, Sarraj Ayman, Bauwens Marc, Testevuide Pascale, Vacher Coponat Henri, Galland Roula, Schauder Nicole, Salmi Louis -Rachid, Cerasuolo Damiano, Tendron-Franzin Anaïs, Bayat Sahar, Halimi Jean Michel, Wolak Aurore, Gentile Stéphanie, Devictor Bénédicte, Monnet Elisabeth, Boucaut Maitre Denis, Nacher Mathieu, Merle Véronique, Jais Jean-Philippe, Daures Jean-Pierre, Vergnenegre Alain, Loos-Ayav Carole, Merle Sylvie, Hazzan Marc, Gervolino Shirley, Nguyen Jean-Michel, and Iacobelli Silvia.

DISCLOSURE

All the authors declared no competing interests.

ACKNOWLEDGMENTS

The authors are indebted to the members of the Groupe de Recherche Clinique (GREC: Céline Dagot, Farah Pauwels, Fatiha M'Raiagh, and Daniel Sperandio) and Lise Siard, Claudine Lecuelle, and Philippe Favre from Eurofins Biomnis for their precious help during the conduction of the study.

ME is supported by the Hospices Civils de Lyon (Année Médaille d'Or) and by Institut National de la Santé et de la Recherche Médicale (Poste Accueil). XC is supported by the Société Française de Transplantation. OT is supported by Fondation pour la Recherche Médicale (PME20180639518) and the Etablissement Français du Sang.

ME, XC, TB, EM, and OT are members of the Lyon Immunopathology Federation of the Hospices Civils de Lyon.

SUPPLEMENTARY MATERIAL

Supplementary File (PDF)

Figure S1. Flow cytometry analyses of anti-spike T-cell responses.

Figure S2. Epidemiology of coronavirus disease 2019 pandemic in France during the study period.

REFERENCES

1. Thaanat O, Legeai C, Anglicheau D, et al. IMPact of the COVID-19 epidemic on the moRTAlity of kidney transplant recipients and candidates in a French Nationwide registry sTudy (IMPORTANT). *Kidney Int.* 2020;98:1568–1577.
2. Williamson EJ, Walker AJ, Bhaskaran K, et al. Factors associated with COVID-19-related death using OpenSAFELY. *Nature.* 2020;584:430–436.
3. Quintaliani G, Reboldi G, Di Napoli A, et al. Exposure to novel coronavirus in patients on renal replacement therapy during the exponential phase of COVID-19 pandemic: survey of the Italian Society of Nephrology. *J Nephrol.* 2020;33:725–736.
4. Ng JH, Hirsch JS, Wanchoo R, et al. Outcomes of patients with end-stage kidney disease hospitalized with COVID-19. *Kidney Int.* 2020;98:1530–1539.
5. Jager KJ, Kramer A, Chesnaye NC, et al. Results from the ERA-EDTA Registry indicate a high mortality due to COVID-19 in dialysis patients and kidney transplant recipients across Europe. *Kidney Int.* 2020;98:1540–1548.
6. Hilbrands LB, Duivenvoorden R, Vart P, et al. COVID-19-related mortality in kidney transplant and dialysis patients: results of the ERACODA collaboration. *Nephrol Dial Transplant.* 2020;35:1973–1983.
7. Haute Autorité de Santé. Vaccins Covid-19: quelle stratégie de priorisation à l'initiation de la campagne?. https://www.has-sante.fr/jcms/p_3221237/fr/vaccins-covid-19-quelle-strategie-de-priorisation-a-l-initiation-de-la-campagne. Accessed April 2, 2021.
8. Sahin U, Muik A, Derhovanessian E, et al. COVID-19 vaccine BNT162b1 elicits human antibody and T_H1 T cell responses. *Nature.* 2020;586:594–599.
9. Espi M, Charmetant X, Barba T, et al. The ROMANOV study found impaired humoral and cellular immune responses to SARS-CoV-2 mRNA vaccine in virus unexposed patients receiving maintenance hemodialysis. *Kidney Int.* 2021;100:928–936.
10. Bertrand D, Hamzaoui M, Lemée V, et al. Antibody and T cell response to SARS-CoV-2 messenger RNA BNT162b2 vaccine in kidney transplant recipients and hemodialysis patients. *J Am Soc Nephrol.* 2021;32:2147–2152.
11. Danthu C, Hantz S, Dahlem A, et al. Humoral response after SARS-CoV-2 mRNA vaccine in a cohort of hemodialysis patients and kidney transplant recipients. *J Am Soc Nephrol.* 2021;32:2153–2158.
12. Speer C, Göth D, Benning L, et al. Early humoral responses of hemodialysis patients after COVID-19 vaccination with BNT162b2. *Clin J Am Soc Nephrol.* 2021;16:1073–1082.
13. Grupper A, Sharon N, Finn T, et al. Humoral response to the Pfizer BNT162b2 vaccine in patients undergoing maintenance hemodialysis. *Clin J Am Soc Nephrol.* 2021;16:1037–1042.
14. Rincon-Arevalo H, Choi M, Stefanski A-L, et al. Impaired humoral immunity to SARS-CoV-2 BNT162b2 vaccine in kidney transplant recipients and dialysis patients. *Sci Immunol.* 2021;6:eabj1031.
15. Couchoud C, Stengel B, Landais P, et al. The renal epidemiology and information network (REIN): a new registry for end-stage renal disease in France. *Nephrol Dial Transplant.* 2006;21:411–418.
16. L'Assurance Maladie. Données vaccination par pathologie et département/région. <https://datavaccin-covid.ameli.fr/explore/dataset/donnees-vaccination-par-pathologie/explore/information>. Accessed September 9, 2021.
17. Polack FP, Thomas SJ, Kitchin N, et al. Safety and efficacy of the BNT162b2 mRNA Covid-19 vaccine. *N Engl J Med.* 2020;83:2603–2615.
18. World Health Organization. COVID-19 Clinical management: living guidance. <https://www.who.int/publications/i/item/WHO-2019-nCoV-clinical-2021-2>. Accessed December 15, 2021.
19. DGS-Urgent. Précisions sur la vaccination COVID-19: modalités d'administration des rappels et vaccination des personnes immunodéprimées et de leurs proches. https://solidarites-sante.gouv.fr/IMG/pdf/dgs_urgent_52_precisions_sur_la_vaccination_imd.pdf. Accessed May 17, 2021.
20. Mattiuzzo G, Bentley EM, Hassall M, et al. Establishment of the WHO International Standard and Reference Panel for anti-SARS-CoV-2 antibody. <https://www.who.int/publications/m/item/WHO-BS-2020.2403>. Accessed December 12, 2021.
21. Grifoni A, Weiskopf D, Ramirez SI, et al. Targets of T cell responses to SARS-CoV-2 coronavirus in humans with COVID-19 disease and unexposed individuals. *Cell.* 2020;181:1489–1501.e15.
22. Dahdal S, Saison C, Valette M, et al. Residual activatability of circulating Tfh17 predicts humoral response to thymodependent antigens in patients on therapeutic immunosuppression. *Front Immunol.* 2018;9:3178.
23. Agence de la Biomédecine. R.E.I.N. (Réseau Epidémiologique et Information en Néphrologie). <https://www.agence-biomedecine.fr/R-E-I-N-Reseau-Epidemiologique-et-Information-en-Nephrologie>. Accessed June 25, 2021.

24. Santé Publique France. Coronavirus: circulation des variants du SARS-CoV-2. <https://www.santepubliquefrance.fr/dossiers/coronavirus-covid-19/coronavirus-circulation-des-variants-du-sars-cov-2>. Accessed September 9, 2021.
25. Baden LR, El Sahly HM, Essink B, et al. Efficacy and safety of the mRNA-1273 SARS-CoV-2 vaccine. *N Engl J Med*. 2021;384:403–416.
26. National Institutes of Health. COVID-19 Treatment Guidelines: clinical spectrum of SARS-CoV-2 Infection. <https://www.covid19treatmentguidelines.nih.gov/overview/clinical-spectrum/>. Accessed June 25, 2021.
27. Chen C-C, Koenig A, Saison C, et al. CD4+ T cell help is mandatory for naive and memory donor-specific antibody responses: impact of therapeutic immunosuppression. *Front Immunol*. 2018;9:275.
28. Crotty S. T follicular helper cell biology: a decade of discovery and diseases. *Immunity*. 2019;50:1132–1148.
29. Lalvani A. Diagnosing tuberculosis infection in the 21st century: new tools to tackle an old enemy. *Chest*. 2007;131:1898–1906.
30. Espi M, Koppe L, Fouque D, Thauinat O. Chronic kidney disease-associated immune dysfunctions: impact of protein-bound uremic retention solutes on immune cells. *Toxins*. 2020;12:300.
31. Betjes MGH. Immune cell dysfunction and inflammation in end-stage renal disease. *Nat Rev Nephrol*. 2013;9:255–265.
32. Mast EE, Weinbaum CM, Fiore AE, et al. A comprehensive immunization strategy to eliminate transmission of hepatitis B virus infection in the United States: recommendations of the Advisory Committee on Immunization Practices (ACIP) Part II: immunization of adults. *MMWR Recomm Rep*. 2006;55:1–33. quiz CE1–4.
33. Masset C, Kervella D, Kandel-Aznar C, et al. Relapse of IgG4-related nephritis following mRNA COVID-19 vaccine. *Kidney Int*. 2021;100:465–466.
34. D'Agati VD, Kudose S, Bombardieri AS, et al. Minimal change disease and acute kidney injury following the Pfizer-BioNTech COVID-19 vaccine. *Kidney Int*. 2021;100:461–463.
35. Hanna C, Hernandez LPH, Bu L, et al. IgA nephropathy presenting as macroscopic hematuria in 2 pediatric patients after receiving the Pfizer COVID-19 vaccine. *Kidney Int*. 2021;100:705–706.









6. Publication 6

SARS-CoV-2-specific serological and functional T cell immune responses during acute and early COVID-19 convalescence in solid organ transplant patients.

Favà A, Donadeu L, Sabé N, Pernin V, González-Costello J, Lladó L, Meneghini M, Charmetant X, García-Romero E, Cachero A, Torija A, Rodríguez-Urquía R, Crespo E, Teubel I, Melilli E, Montero N, Manonelles A, Preyer R, Strecker K, Ovize A, Lozano JJ, Sidorova J, Cruzado JM, Le Quintrec M, Thaunat O, Bestard O.

American Journal of Transplantation. 2021 Aug;21(8):2749-2761.

SARS-CoV-2-specific serological and functional T cell immune responses during acute and early COVID-19 convalescence in solid organ transplant patients

Alexandre Favà^{1,2}  | Laura Donadeu² | Nuria Sabé³ | Vincent Pernin⁴  | José González-Costello⁵ | Laura Lladó⁶  | Maria Meneghini^{1,2} | Xavier Charmetant⁷ | Elena García-Romero⁵ | Alba Cachero⁶ | Alba Torija² | Ronny Rodriguez-Urquia¹ | Elena Crespo² | Iris Teubel² | Edoardo Melilli¹  | Nuria Montero¹  | Anna Manonelles¹ | Rosemarie Preyer⁸ | Kevin Strecker⁸ | Anne Ovize⁹ | Juan J. Lozano¹⁰ | Julia Sidorova¹¹ | Josep M. Cruzado^{1,2}  | Moglie Le Quintrec⁴ | Olivier Thauat⁷  | Oriol Bestard^{1,2} 

¹Kidney Transplant Unit, Bellvitge University Hospital, Barcelona, Spain

²Nephrology and Transplantation Experimental Laboratory, IDIBELL, Barcelona, Spain

³Infectious disease department, Bellvitge University Hospital, Barcelona, Spain

⁴Kidney Transplant Unit, Hospital de Montpellier, Montpellier, France

⁵Heart Transplant Unit, Bellvitge University Hospital, Barcelona, Spain

⁶Liver Transplant unit, Bellvitge University Hospital, Barcelona, Spain

⁷Department of Transplantation, Nephrology and Clinical Immunology, Edouard Herriot Hospital Lyon, Hospices Civils de Lyon, Lyon, France

⁸GenID GmbH, Strassberg, Germany

⁹Eurofins Biomnis Laboratory, Lyon, France

¹⁰Bioinformatics Platform, Centro de Investigación Biomédica en Red de Enfermedades Hepáticas y Digestivas (CIBEREHD), Barcelona, Catalonia, Spain

¹¹Instituto de Tecnología del Conocimiento (ITC), Campus de Somosaguas, Universidad Complutense de Madrid (UCM), Madrid, Spain

Correspondence

Oriol Bestard, Kidney Transplant Unit, Bellvitge University Hospital, Barcelona, Spain.

Email: obestard@bellvitgehospital.cat

Funding information

This work was supported by the Instituto de Salud Carlos III (ISCIII) (grant number COV20/00324).

The description of protective humoral and T cell immune responses specific against SARS-CoV-2 has been reported among immunocompetent (IC) individuals developing COVID-19 infection. However, its characterization and determinants of poorer outcomes among the at-risk solid organ transplant (SOT) patient population have not been thoroughly investigated. Cytokine-producing T cell responses, such as IFN- γ , IL-2, IFN- γ /IL-2, IL-6, IL-21, and IL-5, against main immunogenic SARS-CoV-2 antigens and IgM/IgG serological immunity were tracked in SOT ($n = 28$) during acute infection and at two consecutive time points over the following 40 days of convalescence and were compared to matched IC ($n = 16$) patients admitted with similar moderate/severe COVID-19. We describe the development of a robust serological and functional T cell immune responses against SARS-CoV-2 among SOT patients, similar to IC patients during early convalescence. However, at the infection onset, SOT displayed lower IgG seroconversion rates (77% vs. 100%; $p = .044$), despite no differences on

Alexandre Favà and Laura Donadeu equally contributed as first authors to this work.

© 2021 The American Society of Transplantation and the American Society of Transplant Surgeons

IgG titers, and a trend toward decreased SARS-CoV-2-reactive T cell frequencies, especially against the membrane protein (7 [0–34] vs. 113 [15–245], $p = .011$, 2 [0–9] vs. 45 [5–74], $p = .009$, and 0 [0–2] vs. 13 [1–24], $p = .020$, IFN- γ , IL-2, and IFN- γ /IL-2 spots, respectively). In summary, our data suggest that despite a certain initial delay, SOT population achieve comparable functional immune responses than the general population after moderate/severe COVID-19.

KEYWORDS

adaptive immunity, basic (laboratory) research / science, clinical research / practice, COVID-19 infection, heart transplantation / cardiology, infection and infectious agents, kidney transplantation / nephrology, liver transplantation / hepatology, solid organ transplantation, T cell biology

1 | INTRODUCTION

A novel coronavirus, designated as SARS-CoV-2, emerged in Wuhan, China, at the end of 2019 and has spread all over the globe in a logarithmic manner. The increasing number of fatal outcomes related to the Coronavirus Disease-2019 (COVID-19) has put global health institutions on high alert.

While most people remain asymptomatic or develop only mild symptoms during COVID-19,^{1,2} some specific group of patients seem to be at significantly higher risk of fatal outcomes,³ and among them recipients of solid organ transplants (SOT) most likely because they receive chronic immunosuppressive therapy that predominantly targets T cell adaptive immunity.⁴ Importantly, SOT patients represent an important prevalent high-risk population in whom the biology of the adaptive immunity specific to SARS-CoV-2 during COVID-19 has not yet been thoroughly investigated.

First studies evaluating immunocompetent (IC) convalescent individuals have shown the induction of neutralizing antibodies after primary infection^{5–8} which seem to be detectable essentially among patients with more severe forms of COVID-19.^{9,10} Conversely, robust anti-viral T cell responses have been described after SARS-CoV-2 infection, which seem to correlate with the magnitude of SARS-CoV-2-specific IgG and IgA titers during the initial phase of convalescence¹¹ and with the severity of COVID-19 infection.¹² Interestingly, SARS-CoV-2-reactive T cell immunity seems to last for a longer period of time, even among seronegative convalescent patients¹³ and can discriminate those patients with the poorest outcomes.¹⁴

In this study, we aimed at investigating the IgM and IgG serological antibody responses as well as the SARS-CoV-2-reactive T cell responses against main four different structural viral proteins, Spike (S), Nucleocapsid (N), Membrane (M), and Envelope (E), in SOT recipients as compared to matched hospitalized IC healthy individuals due to COVID-19, both at the time of the acute infection phase and over the convalescent clinical course after infection, in order to provide mechanistic insights that could explain the recent epidemiological observations of a higher risk of poorer outcomes in SOT as compared to IC-infected patients.

2 | MATERIAL AND METHODS

2.1 | Patients of the study and clinical definitions

In this study, we evaluated 44 consecutive patients hospitalized between March 15 and April 18, 2020, at Bellvitge University Hospital (Barcelona, Spain) and Montpellier University Hospital (Montpellier, France) due to COVID-19 infection, and in whom peripheral blood mononuclear cells (PBMCs) and serum samples were available. All patients had been tested positive for SARS-CoV-2 infection by a RT-PCR analysis on nasopharyngeal swab samples. Among these 44 patients, 28 were SOT recipients and 16 IC patients, who were matched for age, gender, and severity of COVID-19 at study inclusion (Figure 1; Table 1).

A total of 113 serially collected peripheral blood samples at three different time points of the disease were analyzed in this study—during the acute phase of infection (T1; median 16, IQR 12–19 days after symptom onset) and at two convalescence periods (T2; median 32, IQR 25–37 days, and T3; 49 days, IQR 43–53), which represented a median of 7 days, IQR 4–11 and 23 days, IQR 20–27 and 40 days, and IQR 37–44, after first positive PCR, respectively.

Additionally, PBMC samples from 16 non-immunosuppressed patients on the waiting list for kidney transplantation that were obtained 2 years before the COVID-19 outbreak (November 2018) and were stored in our biobank facilities were used as healthy controls (HC).

All clinical, demographic, and immunological patient characteristics as well as the main outcomes, such as mortality, or the need of invasive/non-invasive mechanical ventilation (MV) were recorded. COVID-19 disease severity was defined according to the level of oxygen support during hospitalization according to the World Health Organization interim guidance to define Acute Respiratory Distress Syndrome (bilateral opacities not explained by volume overload with an oxygen saturation/fraction of inspired oxygen ratio <315).¹⁵

The study was approved by the Ethical Review Boards (PR115/20) at each center and patients were recruited in the study after providing a signed informed consent.

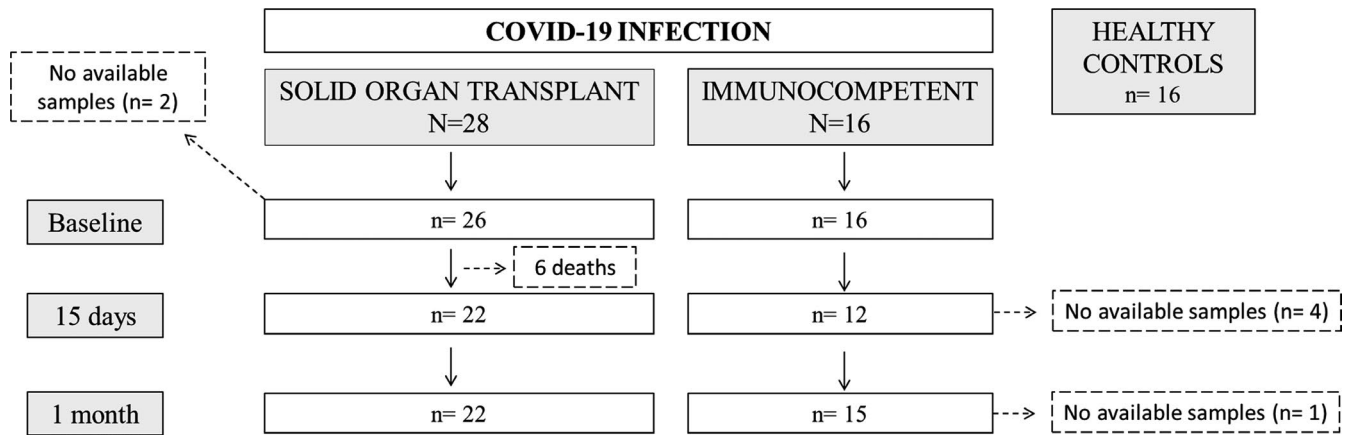


FIGURE 1 Flowchart of the study

2.2 | Collection and management of serum and PBMC samples

Detailed description is depicted in Data S1.

2.3 | Assessment of SARS-CoV-2-specific antibodies

IgM and IgG antibodies against SARS-CoV-2 were detected by a chemiluminescence technique, using the MaglumiTM 2019 nCov-IgM and the MaglumiTM 2019 nCov-IgG tests (Snibe Diagnostic) on a Maglumi 2000® analyzer (Snibe Diagnostic), according to the manufacturer's instructions. Detailed information is provided in Data S1.

2.4 | Assessment of cytokine-producing SARS-CoV-2-reactive T cell responses

SARS-CoV-2-reactive T cell responses were evaluated using a multicolor FluoroSpot Immune assay kit (AID® GmbH). Distinct cytokine-producing T cell frequencies were assessed: effector (IFN- γ), proliferative (IL-2) and central (IFN- γ /IL-2) memory Th1 responses, IL-5 and IL-21 Th2 responses, and IL-6 pro-inflammatory T cell responses. The main four structural SARS-CoV-2 proteins, Spike Glycoprotein (S), Membrane Protein (M), Nucleoprotein (N), and Envelope Small Membrane Protein (E) (JPT®), were used for stimulation in the multicolor FluoroSpot Immune assay individually. Overlapping peptide pools covering the whole Influenza virus antigen length (AID® GmbH) were also tested. In each test, complete medium alone and Pokeweed (PWM) mitogen were used as negative and positive controls, respectively. Any antigen-specific ELISPOT test with less than 5 spots/ 2×10^5 PBMC was considered as negative when assessed in a qualitative manner. Precise information is provided in Data S1.

2.5 | Statistics

Continuous variables were expressed as mean \pm SD or median and IQR and categorical variables as number of total (n) and percentage (%). A comparison between groups was performed using Pearson's χ^2 test for categorical data. Continuous measurements were compared among groups using Kruskal-Wallis and Mann-Whitney U test for non-normally distributed data, while ANOVA and t tests were used when data were normally distributed. *p*-values $<.05$ were considered statistically significant. SARS-CoV-2-reactive cellular and humoral responses were centered and scaled and heatmap was built by means of the pheatmap R package¹⁶ using Euclidean distance and complete method as agglomeration method. R package version 1.0.12 was used <https://CRAN.R-project.org/package=pheatmap>. All other analyses were performed using SPSS version 26 software, and graphs were generated using GraphPad Prism version 8.0 software (GraphPad Software).

3 | RESULTS

3.1 | Patients of the study

Forty-four hospitalized patients with COVID-19 disease confirmed by reverse transcriptase-polymerase chain reaction (RT-PCR) were included: 28 SOT recipients and 16 IC patients. Eighteen (64.3%) kidney, five (17.9%) heart, and five (17.9%) liver transplants composed the SOT group, with a median time after transplantation of 9 ± 7 years (IQR 3–14) and were receiving a calcineurin inhibitor (CNI)-based immunosuppressant scheme (67.9%). Also, 16 individuals in whom PBMC samples were retrieved and stored at our biobank facilities in 2018 were included in the study (Figure 1).

Main clinical, demographic, and immunological characteristics are depicted in Table 1. As shown, SOT and IC patients of the study were matched for age, sex, and main comorbidities, but IC patients were less diabetic. The degree of COVID-19 severity and time of

TABLE 1 Demographic and clinical characteristics of patients infected by SARS-CoV-2

	SOT (N = 28)	IC (N = 16)	HC (n = 16)	P value
Age (years, mean ± SD)	59.4 ± 13.6	59.4 ± 11.3	63.4 ± 10	0.531
Sex (Female) (n, %)	7 (25)	7 (44)	5 (31.3)	0.437
Comorbidities (n, %)				
Diabetes	11 (39.3)	1 (6.3)	N/A	0.032
Arterial hypertension	19 (67.9)	6 (37.5)	N/A	0.051
Obesity ^a	6 (21.4)	3 (18.8)	N/A	0.868
Pulmonary disease ^b	2 (7.1)	2 (12.5)	N/A	0.614
Heart disease ^c	6 (21.4)	2 (12.5)	N/A	0.689
Active neoplasm	4 (14.3)	1 (6.3)	N/A	0.638
ACEi/ARB use	10 (35.7)	2 (12.5)	N/A	0.116
Previous Influenza vaccine (yes)	22 (78.6)	7 (43.8)	12 (75)	0.082
Clinical symptoms at onset (n, %)				
Cough	18 (64.3)	13 (81.3)	N/A	0.314
Dyspnea	10 (35.7)	7 (43.8)	N/A	0.749
Diarrhea	14 (50)	6 (37.5)	N/A	0.534
Myalgias	11 (39.3)	7 (43.8)	N/A	1.000
Fever	23 (82.1)	16 (100)	N/A	0.141
Disease severity at enrollment (n, %)				
No oxygen therapy needed	5 (17.9)	1 (6.2)	N/A	0.276
Oxygen requirement (NO ARDS)	8 (28.6)	6 (37.5)	N/A	0.738
ARDS	15 (53.6)	9 (56.3)	N/A	1.000
Outcomes at the end of follow-up (n, %)				
Death	6 (21.4)	0 (0)	N/A	0.072
MV or Death	9 (32.1)	1 (6.2)	N/A	0.05
Sampling time points (days)				
Days from symptom onset to first time-point PBMC collection (median, IQR)	15 (12–20)	17 (10–18)	N/A	0.794
Days from symptom onset to second time-point PBMC collection (median, IQR)	31 (25–40)	32 (26–37)	N/A	0.711
Days from symptom onset to third time-point PBMC collection (median, IQR)	48 (42–53)	50 (44–54)	N/A	0.225
Days from positive PCR to first time-point collection (median, IQR)	7 (5–12)	6 (4–10)	N/A	0.15
Days from positive PCR to second time-point collection (median, IQR)	23 (20–28)	24 (20–26)	N/A	0.762
Days from positive PCR to third time-point collection (median, IQR)	40 (36–44)	41 (38–44)	N/A	0.556

Abbreviations: ACEi, angiotensin-converting enzyme inhibitor; ARB, angiotensin II receptor blocker; ARDS, acute respiratory distress syndrome; HC, healthy controls; IC, immunocompetent; MV, mechanical ventilation (invasive or non-invasive); PBMC, peripheral blood mononuclear cells; PCR, polymerase chain reaction; SOT, solid organ transplant.

^aObesity: body mass index >30.

^bPulmonary disease: chronic obstructive pulmonary disease, asthma, bronchiectasis, or sleep apnea-hypopnea syndrome.

^cHeart disease: congestive heart failure, coronary artery disease, atrial fibrillation, or valvular heart disease.

assessment were not different between groups. After a follow-up of 40 days (37–44), six (13.6%) patients passed away, they were all SOT (three liver, two kidney, and one heart transplant recipient). The composite outcome depicted as requirement of MV or death did also occur more frequently among SOT (9 [32.1%] SOT vs. 1 [6.2%] IC;

$p = .05$). First time-point blood samples were retrieved prior to this composite outcome.

We further evaluated 16 healthy control (HC) individuals in whom PBMC samples had been retrieved in 2018, before the SARS-CoV-2 pandemic, and were also matched for age and gender with the

other two study groups. As expected, previous influenza vaccination rate was lower among the IC group (43.8%) as compared to SOT (78.6%) and HC (75%) groups ($p = .082$).

3.2 | Circulating lymphocytes and functional adaptive immunity during acute and convalescent COVID-19 infection

Our first analysis showed that while both SOT and IC patients displayed abnormally low total lymphocyte counts, this lymphopenia was more pronounced for SOT recipients (866 ± 427 vs. 1531 ± 490 in IC; $p < .001$). Total lymphocyte counts in HC were 1564 ± 427 and were significantly higher than SOT at T1 ($p < .001$) (Figure S2).

As shown in Figure 2A and Figure S3A, during acute infection (T1), SARS-CoV-2-reactive T cell responses against four main viral antigens were more predominantly detected among IC patients than within SOT and especially among those with higher severity index. Notably, no SARS-CoV-2-reactive responses were observed among HC. IgG and IgM serological immunity against SARS-CoV-2 was detected within both SOT and IC. At the last convalescent period (T3) (Figure 2B and Figure S3B), SARS-CoV-2-reactive T cell immune responses were now detectable within the SOT group while they had faded in IC patients. Likewise, more predominant IgM responses were observed among SOT than IC, whereas IgG-specific antibodies were similarly detected.

Conversely, non-SARS-CoV-2-reactive T cell immune responses against influenza and a polyclonal stimuli (PWM) were significantly weaker within both SOT and IC as compared to HC at baseline, which persisted during the convalescence period.

3.3 | SARS-CoV-2-reactive T cell immunity during acute and early convalescent COVID-19 infection

No correlation was observed between absolute lymphocyte counts and SARS-CoV-2-reactive T cell frequencies for each antigen-specific cytokine-producing T cell (IFN- γ , IL-2, IFN- γ /IL-2, IL-6, IL-21, and IL-5) at any time point of the study (Table S1).

3.3.1 | SARS-CoV-2-reactive T cell function during acute COVID-19 infection

A strong correlation was observed between all four SARS-CoV-2 antigen responses (Table S2), showing a wide and different range of T cell frequencies.

As illustrated in Figure 3A and described in Table S3, as compared to IC individuals, SOT displayed numerically lower IFN- γ , IL-2, and IFN- γ /IL-2-producing T cell frequencies, although being statistically significant only for antigen M (7 [0–34] vs. 113 [15–245], $p = .011$; 2 [0–9] vs. 45 [5–74], $p = .009$, and 0 [0–2] vs. 13 [1–24], $p = .020$, for IFN- γ , IL-2, and IFN- γ /IL-2 spots in SOT and IC, respectively). A certain detectable IL-6 stimulation was widely detected in all evaluated

patients, including HC thus suggesting a general non-antigen-specific immune response. Notably, IL-21 and IL-5-producing T cells against SARS-CoV-2 were barely detectable in both SOT and IC patients at this time point. As also illustrated, the highest frequencies were observed for T cells only producing IFN- γ , whereas the lowest for those polyfunctional IFN- γ /IL-2-producing T cells.

While IC patients showed similarly high T cell immune responses against both antigens S and M, the highest immune response among SOT was only against antigen S. Of note, T cell responses against antigen E were barely detectable in all infected patients (Figure S4A).

As illustrated in Figure S5A, a higher proportion of SARS-CoV-2 T cell non-responders was observed among SOT as compared to IC, and especially those IFN- γ /IL-2-producing T cells.

3.3.2 | Progression of SARS-CoV-2-reactive T cell immunity during COVID-19 convalescence

We next sequentially monitored these patients at two consecutive time points during convalescence periods: at T2; 32 (IQR 25–37) and T3; 49 (IQR 43–53) days after symptom onset, which represents a median of 11 (IQR 3–16) and 27 (IQR 22–30) days after discharge, respectively. Similar to T1, a strong correlation of T cell responses was observed between the different SARS-CoV-2 antigens at both time points (Tables S4–S5).

Unlike during acute infection, there were in general no longer differences between SOT and IC regarding the distinct SARS-CoV-2-reactive T cell responses (Figure 3B; Tables S6–S7). However, at T3, while no statistically significant differences were noted between groups, numerically higher SARS-CoV-2-reactive T cell responses in SOT as compared to IC patients were observed, and particularly against antigen S for IL-2 and IL-21 (425 [242–606] vs. 181 [58–289], $p = .07$ and 107 [36–212] vs. 10 [2–83], $p = .025$, respectively) (Figure 3C). Similarly, as during the acute infection phase, while the strongest T cell responses among IC were driven against SARS-CoV-2 antigens S and M, the predominant T cell response among SOT was against antigen S but not to antigen M (Figure S4B,C). Also, almost no detectable T cell responses were observed against SARS-CoV-2 antigen E. As also illustrated in Figures S5B,C, now at T2 and T3, the great majority of both SOT and IC patients showed detectable SARS-CoV-2-reactive T cell frequencies.

To examine the kinetics of SARS-CoV-2-reactive T cell responses over time in the two groups, we assessed the global SARS-CoV-2-reactive T cell immune responses by means of the median T cell frequencies against the three main immunogenic antigens (S, M, and N) in each patient and at each time point. As shown in Figure 4, both SOT and IC developed a rapid increase of global SARS-CoV-2-reactive T cell responses until T3. Notably, these functional changes were more evident among SOT as compared to IC patients, which fundamentally occurred between T1 and T2. As previously described at the single antigen level, SOT displayed weaker global SARS-CoV-2-reactive T cell frequencies at baseline than IC patients (11 [1–42] vs. 90 [26–143] spots, $p = .003$ and; 6 [0–15] vs. 30 [4–60] spots, $p = .049$; 1 [0–2] vs. 9 [0–16], $p = .050$; for IFN- γ , IL-2, and IFN- γ /IL-2, respectively).

FIGURE 2 Heatmaps generated by hierarchical clustering of SARS-CoV-2-specific and non-specific immune responses for SOT, IC patients, and HC, according to the COVID-19 disease severity (0 = no oxygen need; 1 = oxygen need; 2 = acute respiratory distress syndrome, 3 = death). Immune responses used for clustering were differentially expressed (fold change >2, false discovery rate $p < .05$). Gray fields indicate missing values. (A) Heatmap performed at first time point during acute COVID-19 infection (7; 4–11 days after the diagnosis) among 26 SOT, 16 IC, and 16 HC. (B). Heatmap performed during the early convalescent period (40; 37–44 days after the diagnosis) of COVID-19 disease in 22 SOT, 15 IC, and 16 HC

3.4 | SARS-CoV-2-specific serological immunity in SOT and IC with severe COVID-19

All infected patients showed detectable SARS-CoV-2-specific IgM titers at baseline (Figure 5A) and remained detectable in the following two time points. Conversely, while all 16 IC patients showed detectable virus-specific IgG titers already at T1, 6/26 (23%) SOT did not ($p = .044$). All SOT seroconverted at T2 and remained positive until T3. Nevertheless, while no differences were observed regarding quantitative IgG titers between the two groups at any time point, IgM titers, albeit detectable, seemed to be cleared from the circulation much faster among IC than in SOT over time (Figure 5B). Indeed, at T2 and T3, IC showed significantly lower IgM titers than SOT patients (1.6 [0.75–3.1] vs. 5.3 [3.7–7.7] UA/ml, $p = .001$ at T2 and 0.8 [0.6–1.6] vs. 3.5 [1.9–5.3] UA/ml; $p < .001$ at T3).

Of note, patients without IgG class-switch seroconversion displayed lower SARS-CoV-2-reactive IL-2-producing T cell frequencies against antigens S and M than patients with IgG serology (6 [1–9] vs. 28 [4–98], $p = .073$ and 1 [0–5] vs. 7 [2–63], $p = .067$ for IL-2-producing T cells against antigens S and M, respectively).

3.5 | T cell immunity against influenza and polyclonal stimulation during COVID-19

To investigate the degree of general immune impairment in patients developing moderate/severe COVID-19 infection, we assessed non-SARS-CoV-2-reactive T cell responses to influenza peptides and to a strong polyclonal T cell stimulation with PWM. To note, a correlation was found between these antigens, mainly for IFN- γ -producing T cells at the two first time points of evaluation, T1 ($r = .403$, $p = .015$) and T2 ($r = .403$, $p = .015$). No differences were observed between SOT and IC patients regarding both influenza and PWM T cell responses at any time point. Remarkably, both SOT and IC individuals displayed significantly lower IFN- γ , IL-2, IFN- γ /IL-2, and IL-21 T cell responses against both stimuli as compared to HC, which lasted in some cases until T3 (Figure 6), despite significant vaccination rates.

3.6 | Baseline SARS-CoV-2-reactive T cell immunity and clinical outcomes among SOT

In our study, 10 (22.7%) patients required MV or died during the follow-up, being nine SOT. As depicted in Table S8, we did not find any

differences regarding main clinical or demographic within the whole study population. Likewise, no differences were observed when analyzing SARS-CoV-2-reactive T cell responses and outcomes (data not shown). However, and since almost no fatal events occurred within the IC group in our study, we then focused on the SOT group. Also, no clinical nor demographical variables discriminated a poorer clinical evolution. Nevertheless, while no differences were observed regarding most SARS-CoV-2-reactive T cell responses, SOT with the poorest outcomes displayed lower IL-2-producing T cell frequencies against main three immunogenic SARS-CoV-2 antigens as compared to those with better clinical results (0 [0–3] vs. 10 [4–60] $p = .003$; 6 [0–13] vs. 28 [4–110] $p = .085$; and 0 [0–3] vs. 4 [0–22] $p = .075$ for antigens N, S, and M, respectively) (Figure 7A). Intriguingly, the only patient of the IC group who required MV showed robust IL-2-producing T cell frequencies against the three viral antigens (Figure 7B). Furthermore, the proportion of IgG seroconversion was numerically lower among those with worse outcomes (80% vs. 62.5%, $p = .245$).

In terms of immunosuppression, while mycophenolate was broadly withdrawn in our cohort (Table S9), no differences were found between patients with or without CNI-based immunosuppressive regimens at T1. Also, no differences were observed at the successive time points for those patients who had the CNI withdrawn during the infection phase (data not shown).

4 | DISCUSSION

In this study, we investigated the magnitude and kinetics of adaptive immunity, both serological and specific T cell responses to main four immunogenic SARS-CoV-2 antigens among chronically immunocompromised SOT recipients and compared them to matched IC individuals developing the same moderate/severe COVID-19 infection. Here, we show that SOT patients achieve a similarly robust serological and functional T cell immune response comparable to that of IC patients during early COVID-19 convalescence. Nonetheless, a certain delay achieving such strong immune responses was observed among SOT, depicted by lower IgG seroconversion rates and cytokine-producing T cell frequencies, especially against the membrane antigen, as compared to IC patients during the acute infection onset. Moreover, we also describe that among SOT, those patients developing the worst clinical outcomes displayed more deprived SARS-CoV-2-reactive IL-2-producing T cell immune responses as compared to patients with better clinical results.

A widely reported viral-related effect is the severe peripheral lymphopenia observed during COVID-19 infection.^{17–19} Indeed, it

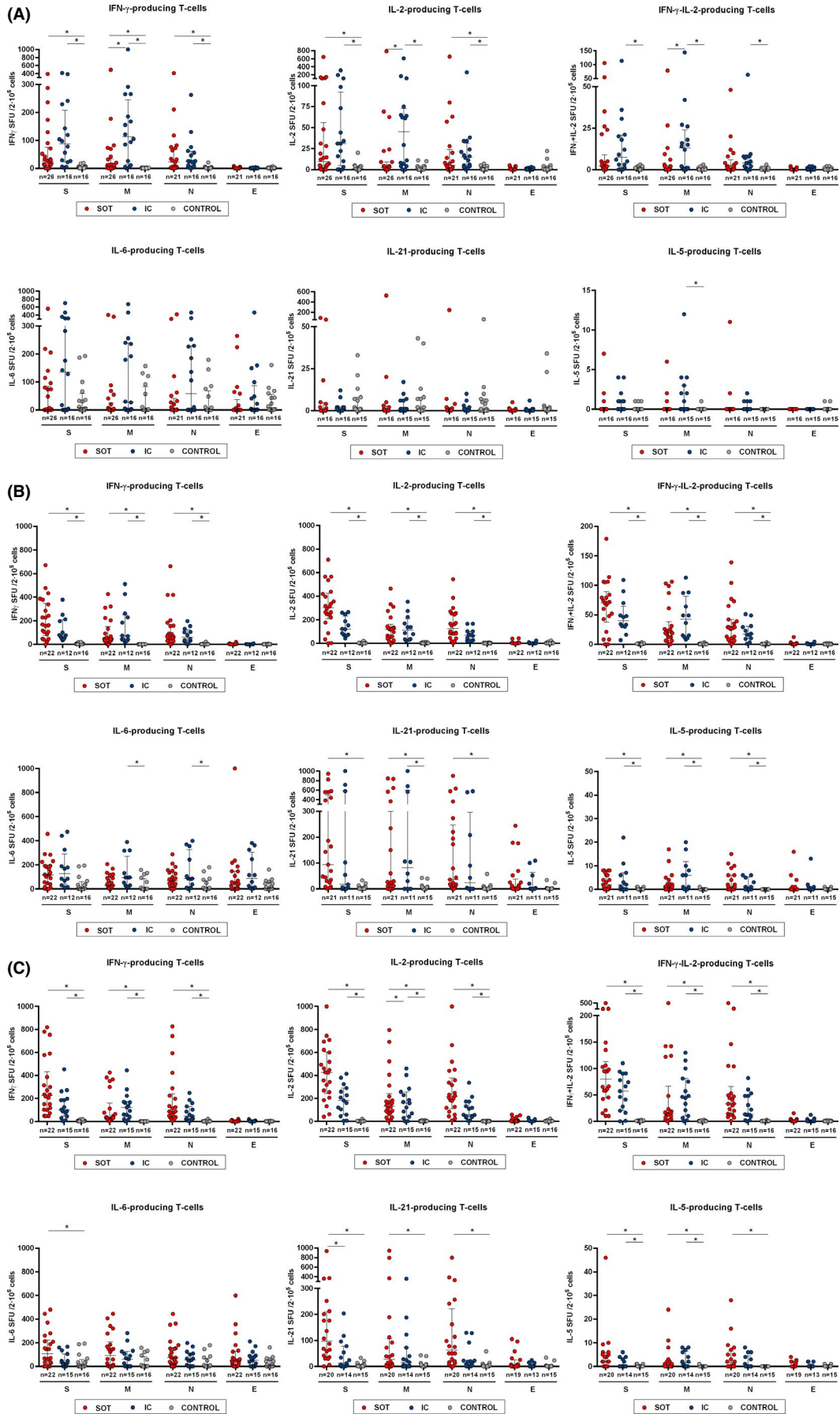


FIGURE 3 Cytokine profile of T cell responses against main structural SARS-CoV-2 proteins Spike (S), Membrane (M), Nucleoprotein (N), and Envelope (E). Frequencies of IFN- γ , IL-2, IFN- γ /IL-2, IL-6, IL-5, and IL-21-producing T cells were assessed among the three study group samples at different time points. * $p < .05$, calculated with Kruskal-Wallis test. (A) T1 = 16; 12–19 days. (B) T2 = 32; 25–37 days. (C) T3 = 49; 43–53 days after symptom onset

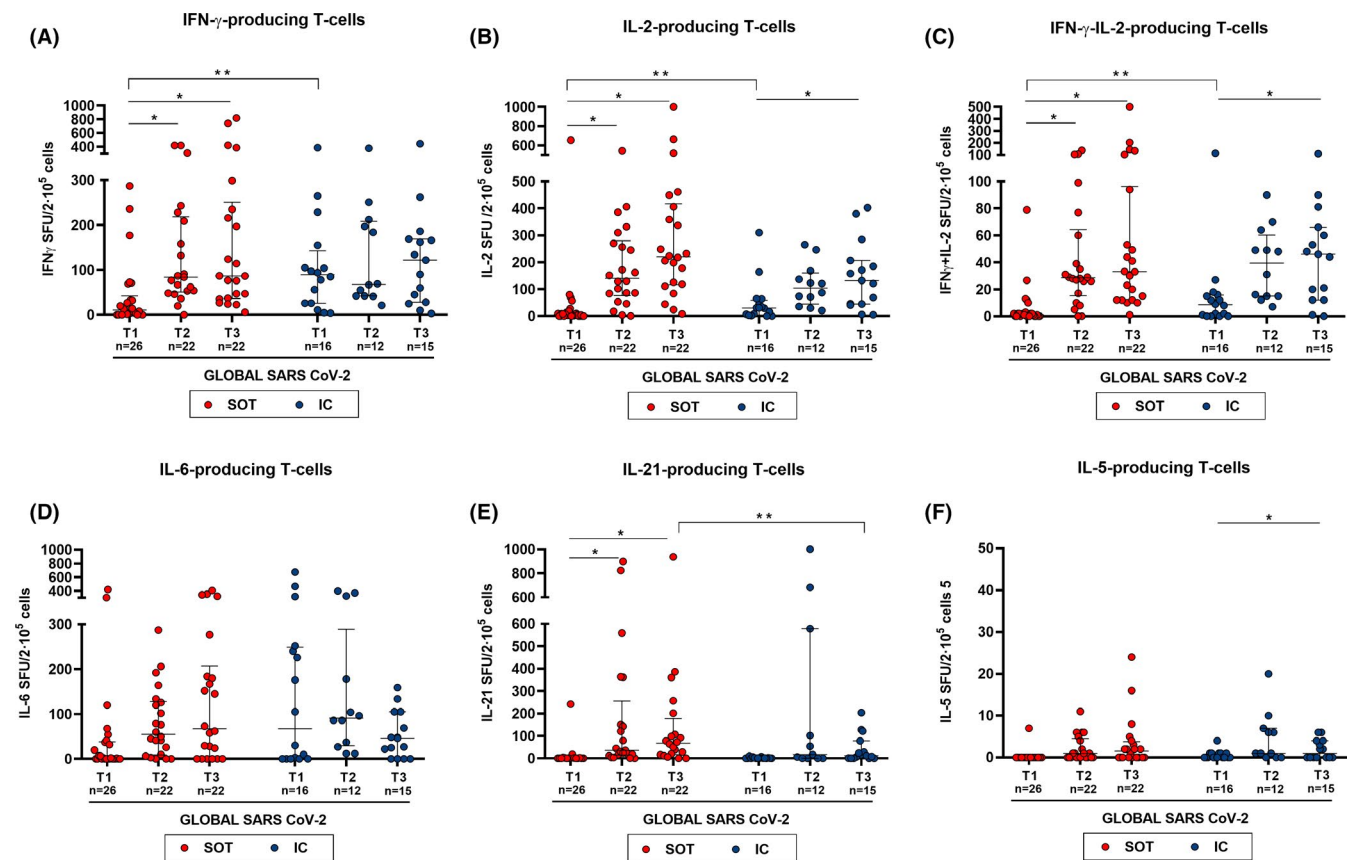


FIGURE 4 Global T cell responses specific to SARS-CoV-2 at different time points (median T cell frequencies against the three SARS-CoV-2 immunogenic antigens: S, M, and N). At T1, N = 42 (SOT = 26, IC = 16); T2, N = 34 (SOT = 22, IC = 12), and T3, N = 37 (SOT = 22, IC = 15). Median and IQR are shown. Intragroup paired analysis; * $p < .05$ evaluated with Friedman's test. Significant intergroup differences (IC vs. SOT) are also shown; ** $p < .05$ (analyzed by Mann-Whitney U test)

was particularly severe among SOT as compared to IC patients, a finding that would seem to be most likely favored in this group of patients by the chronic immunosuppressive therapy these patients follow. However, we did not observe any correlation between total lymphocyte counts and the different SARS-CoV-2-reactive T cell responses, thus illustrating the importance of not only measuring total cell numbers but also their antigen-specific function.

So far, a number of studies have shown the contribution of T cell immunity specific to SARS-CoV-2 in COVID-19 patients.²⁰ However, most of them have exclusively focused in patients without previous underlying immune condition such as SOT, and have not assessed the magnitude and relevance of different peripheral T cell immune subsets against the distinct viral antigens both during the acute infection phase as well as during the convalescence period.^{11,13,21} Herein, we first show that an important proportion of patients, both SOT and IC, display a wide range of SARS-CoV-2-reactive T

cell responses, already in a very early phase of the disease. Globally, and as previously reported, main functional T cell responses were observed against three viral antigens: Spike (S), Membrane (M), and Nucleocapsid (N),^{11,22-24} but not against Envelope (E).

Different studies have described the significantly higher risk of fatal outcomes among SOT developing COVID-19 infection as compared to healthy population.^{4,25-27} While the main hypothesis for these poorer outcomes is sustained on their T cell immunocompromised status, no evaluation of their anti-viral immune response, both at the time of acute infection and during convalescence, has been reported yet. In our study, the lower IFN- γ , IL-2, and IFN- γ /IL-2-producing T cell frequencies against SARS-CoV-2, especially against antigen M, along with the higher proportion of patients with no detectable SARS-CoV-2-reactive T cell responses and the lower IgG seroconversion rates at the infection onset in SOT as compared to IC patients, suggest a certain delay of SOT to achieve a similarly robust

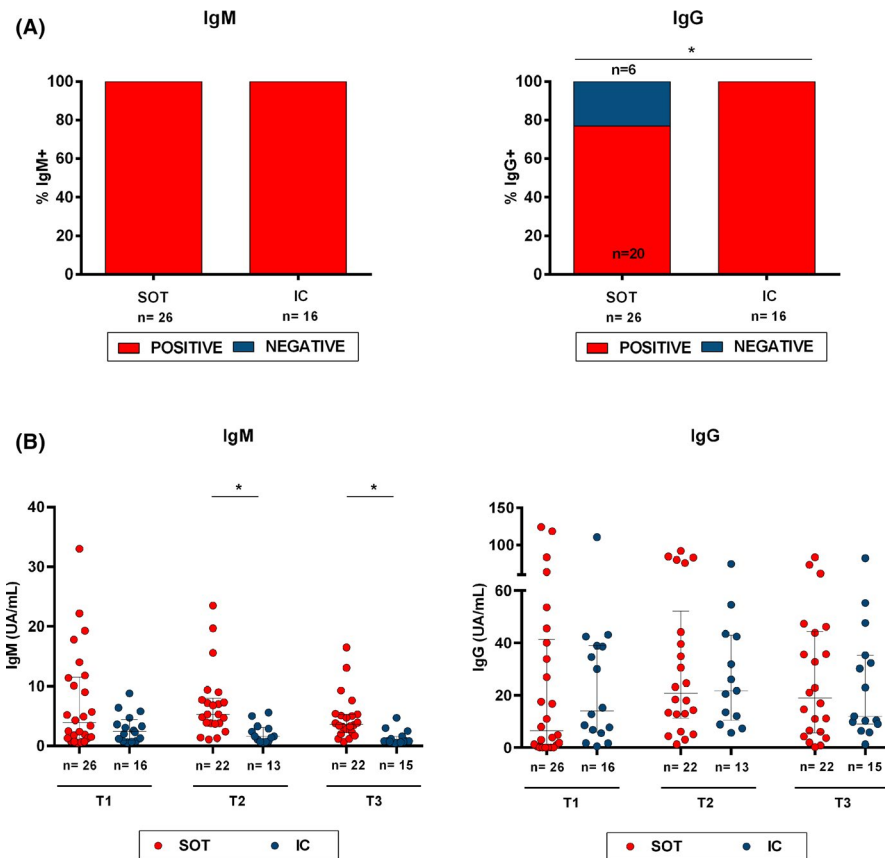


FIGURE 5 IgM and IgG antibody responses to SARS-CoV-2. (A) Percentage at T1 of SOT and IC patients with detectable SARS-CoV-2-specific IgM and IgG class-switching. * $p < .05$ (Chi-square test). (5B) IgM and IgG titers for every time point and study group (SOT and IC). * $p < .05$ (Mann-Whitney test analysis)

initial adaptive immune response than IC patients, most likely due to their chronic immunosuppressive therapy. Nonetheless, a rapid increase of such adaptive T cell immunity, similar to that of IC, is achieved by SOT during early COVID-19 convalescence.

Interestingly, a progressive emergence of both IL-5- and IL-21-producing T cells was detected during the convalescent period in both groups. Although we did not phenotypically characterize these immune cells due to the lack of viable cell samples, these data suggest the fact that for an optimal B-cell activation, cognate T cell help, most likely through antigen-specific follicular helper T cells, is needed.²¹

As similarly described in a recent published report,²⁸ we did not find any specific clinical, demographic, or immunological factors influencing worse clinical outcomes within the whole study group. Nonetheless, among the SOT group, significantly lower IL-2-producing T cell frequencies were observed in patients with the poorest clinical evolution. Conversely, the sole IC patient also needing MV support exhibited significantly more robust IL-2-specific T cell responses than SOT with the same severe outcome, a finding in line with a recent report¹⁴ suggesting that patients with advanced age and higher comorbidity index showed higher IL-2 but decreasing portions of IFN- γ -secreting cells, in particular against antigen N. This different biological observation between SOT and IC may most likely rely in the chronic immunosuppressive effect of transplant immunotherapies, which abrogate IL-2 production on T cells.²⁹

Importantly, SARS-CoV-2-reactive T cell responses and antibody titers progressively increased over time, during the convalescent

period. Interestingly, this enhancement was more pronounced among SOT, who reached similar or even higher functional T cell and serological immune responses than IC patients. Interestingly, longer SARS-CoV-2 viral shedding has been reported among immunosuppressed patients,^{30,31} which might account to some extent for a longer persistence of antigen stimulation ultimately leading to higher SARS-CoV-2-reactive T cell frequencies among SOT at later time points. This is of importance, since these data show that SOT patients may develop an optimal and sustained adaptive immune response, despite receiving chronic immunosuppressive therapy. Thus, vaccination against SARS-CoV-2 should be highly encouraged also among this prevalent high-risk population.³²

In line with previous works,^{33,34} non-specific T cell immune assessment did also reveal a severe global immune impairment of moderate/severe COVID-19, which was similarly depressed both in SOT and IC patients. Indeed, influenza and PWM-derived T cell responses were significantly abrogated at the acute phase of the infection, displaying a progressive restoration over time. In fact, influenza-specific memory T cell responses did not reach the same frequencies as those observed among healthy controls at the end of the follow-up, thus highlighting that recovery of adaptive immunity in some individuals was not fully achieved yet. These results underscore the difference between inflammation and adaptive immunity, which may raise concern about the hypothesis of potential therapeutic effects of some immunosuppressive agents, such as cyclosporine, aiming at reducing systemic inflammatory state in these patients.^{35,36}

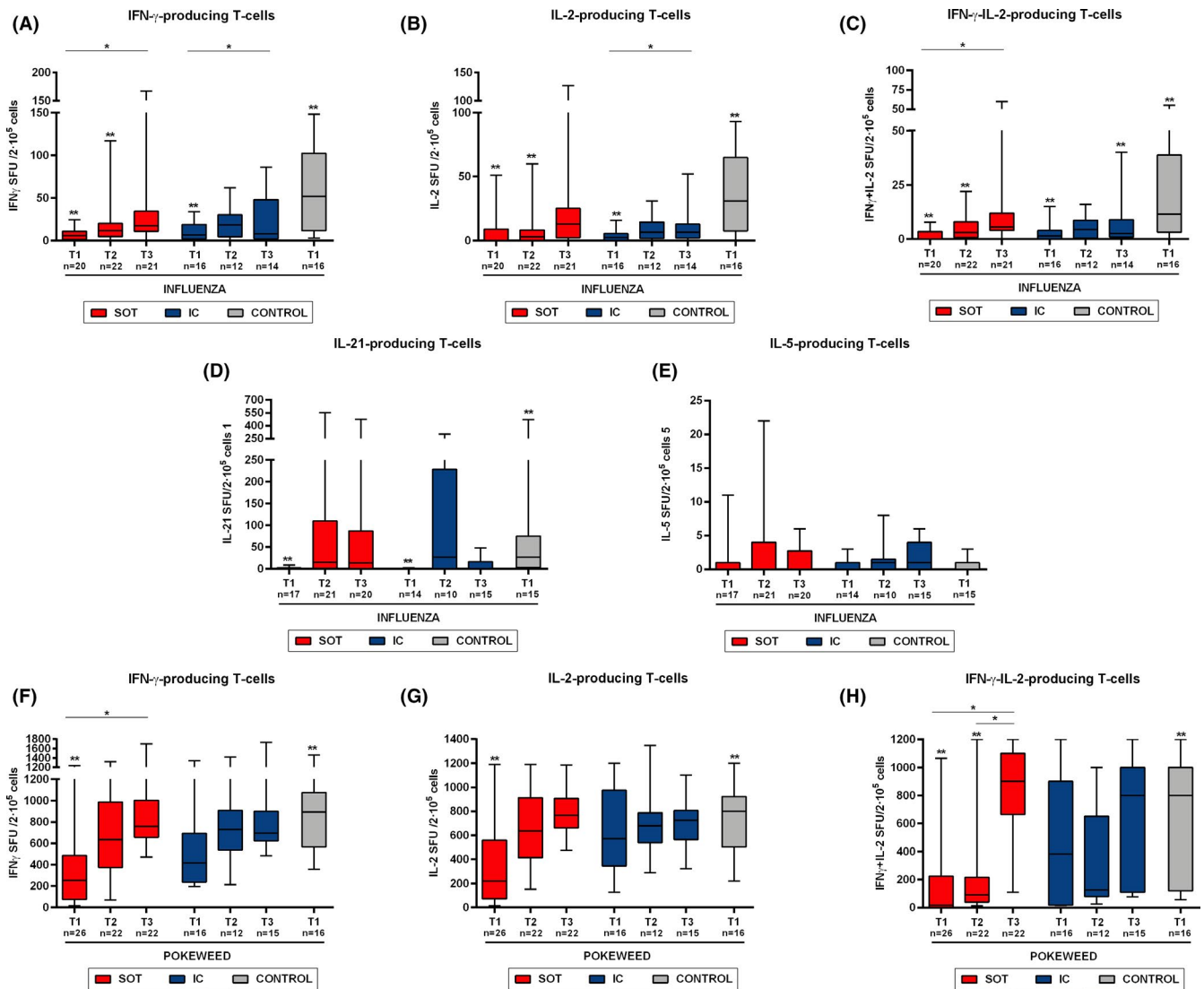


FIGURE 6 T cell responses against non-specific SARS-CoV-2 antigens (influenza and PWM) at the different time points of study. Percentile 5–95 represented by whiskers; median and IQR inside the boxes. Intragroup paired analysis; * $p < .05$ evaluated with Friedman's test. Significant differences with healthy controls are shown by ** $p < .05$ (analyzed by Mann-Whitney U test). No differences were found between IC and SOT

Finally, we did not find SARS-CoV-2-reactive T cell responses against any of the four viral antigens in any HC thus, no evidence for T cell immune cross-reactivity was observed in our cohort, at least in vitro. Despite the presence of IL-6-producing T cell responses against SARS-CoV-2 in HC suggesting unspecific T cell stimulation, the assessment of SARS-CoV-2-reactive IL-6-producing T cell frequencies over time showed a similar pattern than that also observed in other T cell compartments.

There are some limitations in this study such as the small sample size evaluated, which was directly influenced by the difficulty in obtaining biological samples during acute COVID-19 infection. While our FluoroSpot assay allowed us to investigate in a functional manner the frequencies of different cytokine-producing T cells reactive to distinct SARS-CoV-2 antigens at single cell level, we could not describe the predominant T cell subset compartment, either CD4+ or CD8+ T cells, responsible of these SARS-CoV-2-reactive T

cells. Although previous reports have shown a predominant role of SARS-CoV-2-reactive CD4+ T cells, CD8+ T cells do also account for a robust anti-viral T cell immunity.¹¹

In summary, this study describes that despite the strong general immune impairment occurring in patients with severe acute COVID-19 infection, SARS-CoV-2 elicits robust adaptive immune responses also in SOT recipients, both at the cellular and humoral level, although with a certain functional immune delay as compared to IC individuals. Notably, the robust immune response against the virus during convalescence strongly supports the need of active immunization with the up-coming vaccines also in SOT patients.

ACKNOWLEDGMENTS

We thank CERCA Program / Generalitat de Catalunya for their institutional support. We want to particularly acknowledge the patients

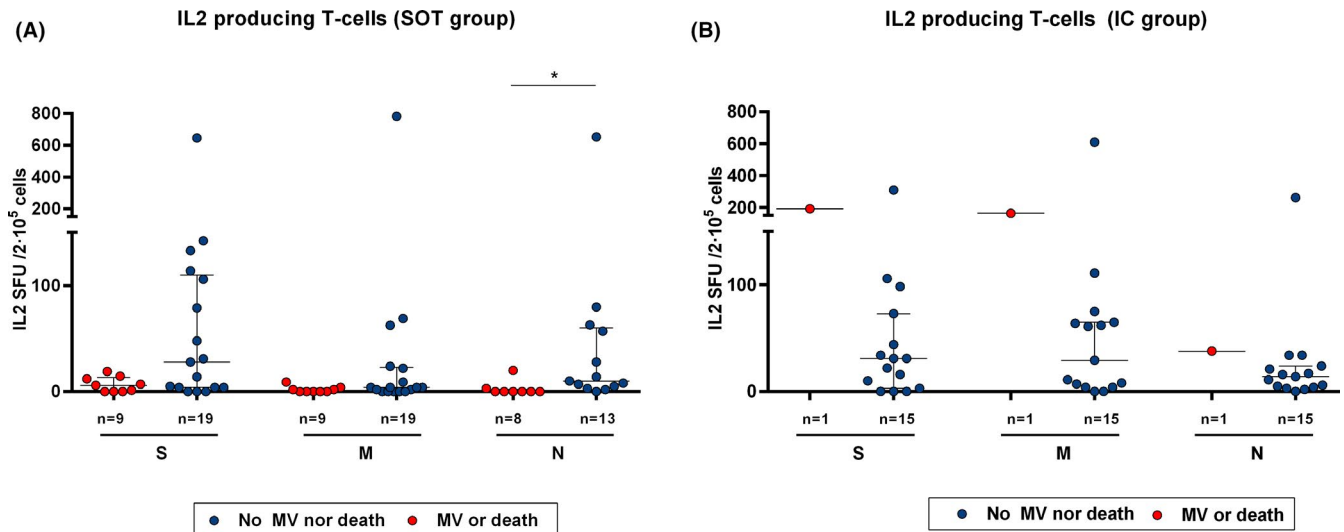


FIGURE 7 Baseline SARS-CoV-2-specific IL-2-producing T cell frequencies and clinical outcomes in SOT and IC patients with severe COVID-19 infection. IL-2-producing frequencies between patients with a poor outcome (VM or death) and those with a favorable clinical evolution. (A) SOT patients $**p < .05$ (analyzed by Mann-Whitney U test). (B) IC patients. Only one IC patient required mechanical ventilation

and the Biobank HUB-ICO-IDIBELL (PT17/0015/0024) integrated in the Spanish National Biobanks Network for their collaboration. The authors acknowledge Ms Gema Cerezo and Ms Iris Alvarez Teubel for careful management of all biological samples, and all kidney transplant unit staff for their support and care of the patients, especially in the context of this pandemic.

DISCLOSURE

The authors of this manuscript have no conflicts of interest to disclose as described by the *American Journal of Transplantation*.

AUTHOR CONTRIBUTIONS

A.F.: Designed the study, collected the data, performed experiments, analyzed the data, drafted the article, and revised the article critically. L.D.: Designed the study, collected the data, performed experiments, analyzed the data, drafted the article, and revised the article critically. I.T.: Performed experiments. N.S.: Collected the data and revised the article critically. V.P.: Collected the data and revised the article critically. J.C.: Revised the article critically. L.L.L.: Revised the article critically. M.M.: Collected the data and revised the article critically. J.J.L.: Performed statistical analyses, J.A.S.: Performed statistical analyses. E.R.: Revised the article critically. A.C.: Revised the article critically. A.T.: Performed research and revised the article critically. R.U.: Collected the data and revised the article critically. E.C.: Designed the study, performed research, collected the data, analyzed the data and revised the article critically. E.M.: Revised the article critically. N.M.: Revised the article critically. A.M.: Revised the article critically. A.O.: Revised the article critically. J.M.C.: Revised the article critically. M.L.Q.: Revised the article critically. O.T.: Revised the article critically. O.B.: Conceived and designed the study, analyzed the data, drafted the article, and revised the article critically.

DATA AVAILABILITY STATEMENT

The data that support the findings of this study are available from the corresponding author upon reasonable request.

ORCID

Alexandre Favà [ID https://orcid.org/0000-0003-1664-6001](https://orcid.org/0000-0003-1664-6001)
 Vincent Pernin [ID https://orcid.org/0000-0003-4983-0139](https://orcid.org/0000-0003-4983-0139)
 Laura Lladó [ID https://orcid.org/0000-0002-3717-3306](https://orcid.org/0000-0002-3717-3306)
 Edoardo Melilli [ID https://orcid.org/0000-0001-6965-3745](https://orcid.org/0000-0001-6965-3745)
 Nuria Montero [ID https://orcid.org/0000-0002-5123-4603](https://orcid.org/0000-0002-5123-4603)
 Josep M. Cruzado [ID https://orcid.org/0000-0003-1388-8558](https://orcid.org/0000-0003-1388-8558)
 Olivier Thauinat [ID https://orcid.org/0000-0002-3648-8963](https://orcid.org/0000-0002-3648-8963)
 Oriol Bestard [ID https://orcid.org/0000-0001-9468-7920](https://orcid.org/0000-0001-9468-7920)

REFERENCES

- Guan W-J, Ni Z-Y, Hu YU, et al. Clinical characteristics of coronavirus disease 2019 in China. *N Engl J Med*. 2020;382(18):1708-1720.
- He XI, Lau EHY, Wu P, et al. Temporal dynamics in viral shedding and transmissibility of COVID-19. *Nat Med*. 2020. <https://doi.org/10.1038/s41591-020-0869-5>
- Wu Z, McGoogan JM. Characteristics of and important lessons from the coronavirus disease 2019 (COVID-19) outbreak in China: summary of a report of 72314 cases from the chinese center for disease control and prevention. *JAMA - J Am Med Assoc*. 2020;323(13):1239-1242.
- Williamson EJ, Walker AJ, Bhaskaran K, et al. Factors associated with COVID-19-related death using OpenSAFELY. *Nature*. 2020;584(7821):430-436.
- Hotez PJ, Corry DB, Strych U, Bottazzi ME. COVID-19 vaccines: neutralizing antibodies and the alum advantage. *Nat Rev Immunol*. 2020;20(7):399-400.
- Robbiani DF, Gaebler C, Muecksch F, et al. Convergent antibody responses to SARS-CoV-2 in convalescent individuals. *Nature*. 2020;584(7821):437-442.

7. Seydoux E, Homad LJ, MacCamy AJ, et al. Analysis of a SARS-CoV-2-infected individual reveals development of potent neutralizing antibodies with limited somatic mutation. *Immunity*. 2020;53(1):98-105.e5.
8. Iyer AS, Jones FK, Nodoushani A, et al. Persistence and decay of human antibody responses to the receptor binding domain of SARS-CoV-2 spike protein in COVID-19 patients. *Sci Immunol*. 2020;5(52):1-13.
9. Long Q-X, Tang X-J, Shi Q-L, et al. Clinical and immunological assessment of asymptomatic SARS-CoV-2 infections. *Nat Med*. 2020;26(8):1200-1204.
10. Chen X, Pan Z, Yue S, et al. Disease severity dictates SARS-CoV-2-specific neutralizing antibody responses in COVID-19. *Sig Transduct Target Ther*. 2020;5(1):180.
11. Grifoni A, Weiskopf D, Ramirez SI, et al. Targets of T cell responses to SARS-CoV-2 coronavirus in humans with COVID-19 disease and unexposed individuals. *Cell*. 2020;181(7):1489-1501.e15.
12. Zhang F, Gan R, Zhen Z, et al. Adaptive immune responses to SARS-CoV-2 infection in severe versus mild individuals. *Sig Transduct Target Ther*. 2020;5(1):156.
13. Sekine T, et al. Robust T cell immunity in convalescent individuals with asymptomatic or mild COVID-19. *Cell*. 2020;183(1):158-168.e14.
14. Sattler A, Angermair S, Stockmann H, et al. SARS-CoV-2 specific T-cell responses and correlations with COVID-19 patient predisposition. *J Clin Invest*. 2020;130(12):6477-6489. <https://doi.org/10.1172/JCI140965>. Published August 24, 2020.
15. Clinical management of COVID-19. WHO Information Web Site. [https://www.who.int/publications/i/item/clinical-management-of-severe-acute-respiratory-infection-when-novel-coronavirus-\(ncov\)-infection-is-suspected](https://www.who.int/publications/i/item/clinical-management-of-severe-acute-respiratory-infection-when-novel-coronavirus-(ncov)-infection-is-suspected). Updated May 27, 2020. Accessed November 3, 2020.
16. Kolde R. Pheatmap: Pretty Heatmaps [Software]. 2019.
17. Zhou F, Yu T, Du R, et al. Clinical course and risk factors for mortality of adult inpatients with COVID-19 in Wuhan, China: a retrospective cohort study. *Lancet*. 2020;395(10229):1054-1062.
18. Wu C, Chen X, Cai Y, et al. Risk factors associated with acute respiratory distress syndrome and death in patients with coronavirus disease 2019 pneumonia in Wuhan, China. *JAMA Intern Med*. 2020;180(7):934-943.
19. Mazzoni A, Salvati L, Maggi L, et al. Impaired immune cell cytotoxicity in severe COVID-19 is IL-6 dependent. *J Clin Invest*. 2020;130(9):4694-4703.
20. Le Bert N, Tan AT, Kunasegaran K, et al. SARS-CoV-2-specific T cell immunity in cases of COVID-19 and SARS, and uninfected controls. *Nature*. 2020;584(7821):457-462.
21. Ni L, Ye F, Cheng M-L, et al. Report detection of SARS-CoV-2-specific humoral and cellular immunity in COVID-19 convalescent individuals II report detection of SARS-CoV-2-specific humoral and cellular immunity in COVID-19 convalescent individuals. *Immunity*. 2020;52(6):971-977.e3.
22. Poland GA, Ovsyannikova IG, Kennedy RB. Review SARS-CoV-2 immunity: review and applications to phase 3 vaccine candidates. *Lancet*. 2020;6736(20).
23. Babel N, Anft M, Blazquez-Navarro A, et al. Immune monitoring facilitates the clinical decision in multifocal COVID-19 of a pancreas-kidney transplant patient. *Am J Transplant*. 2020;20(11):3210-3215.
24. Candon S, et al. T cell and antibody responses to SARS-CoV-2: experience from a French transplantation and hemodialysis center during the COVID-19 pandemic. *Am J Transplant*. 2020;00:1-10.
25. Favà A, Cucchiari D, Montero N, et al. Clinical characteristics and risk factors for severe COVID-19 in hospitalized kidney transplant recipients: a multicentric cohort study. *Am J Transplant*. 2020;20(11).
26. Akalin E, Azzi Y, Bartash R, et al. Covid-19 and kidney transplantation. *N Engl J Med*. 2020;382:2475-2477.
27. Alberici F, Delbarba E, Manenti C, et al. A single center observational study of the clinical characteristics and short-term outcome of 20 kidney transplant patients admitted for SARS-CoV2 pneumonia. *Kidney Int*. 2020;97(6):1083-1088.
28. Thieme JC, Anft M, Paniskaki K, et al. Robust T cell response toward spike, membrane, and nucleocapsid SARS-CoV-2 proteins is not associated with recovery in critical COVID-19 patients. *Cell Reports Medicine*. 2020;1(6):100092.
29. Halloran PF. Immunosuppressive drugs for kidney transplantation. *N Engl J Med*. 2004;351(26):2715-2729.
30. Caillard S, Benotmane I, Gautier Vargas G, Perrin P, Fafi-Kremer S. SARS-CoV-2 viral dynamics in immunocompromised patients. *Am J Transplant*. 2020;ajt.16353.
31. Aydilto T, Gonzalez-Reiche AS, Aslam S, et al. Shedding of viable SARS-CoV-2 after immunosuppressive therapy for cancer. *N Engl J Med*. 2020;383(26):2586-2588.
32. Peiris M, Leung GM. What can we expect from first-generation COVID-19 vaccines? *Lancet*. 2020.
33. Remy KE, Mazer M, Striker DA, et al. Severe immunosuppression and not a cytokine storm characterizes COVID-19 infections. *JCI Insight*. 2020;5(17):e140329.
34. Wilk AJ, Rustagi A, Zhao NQ, et al. A single-cell atlas of the peripheral immune response in patients with severe COVID-19. *Nat Med*. 2020;26(7):1070-1076.
35. Willicombe M, Thomas D, McAdoo S. COVID-19 and calcineurin inhibitors: should they get left out in the storm? *J Am Soc Nephrol*. 2020;31(6):1145-1146.
36. Schoot TS, Kerckhoffs APM, Hilbrands LB, van Marum RJ. Immunosuppressive drugs and COVID-19: a review. *Front Pharmacol*. 2020;11:1333.

SUPPORTING INFORMATION

Additional supporting information may be found online in the Supporting Information section.

How to cite this article: Favà A, Donadeu L, Sabé N, et al. SARS-CoV-2-specific serological and functional T cell immune responses during acute and early COVID-19 convalescence in solid organ transplant patients. *Am J Transplant*. 2021;00:1-13. <https://doi.org/10.1111/ajt.16570>

7. Publication 7

Hamster organotypic kidney culture model of early-stage SARS-CoV-2 infection highlights a two-step renal susceptibility.

Shyfrin SR, Ferren M, Perrin-Cocon L, Espi M, Charmetant X, Brailly M, Decimo D, Iampietro M, Canus L, Horvat B, Lotteau V, Vidalain PO, Thauinat O, Mathieu C.

Journal of Tissue Engineering. 2022 Sep 6;13:20417314221122130. eCollection 2022 Jan-Dec.

Hamster organotypic kidney culture model of early-stage SARS-CoV-2 infection highlights a two-step renal susceptibility

Journal of Tissue Engineering
Volume 13: 1–15
© The Author(s) 2022
Article reuse guidelines:
sagepub.com/journals-permissions
DOI: 10.1177/20417314221122130
journals.sagepub.com/home/tej



Sophie R Shyfrin^{1,2}, Marion Ferren^{1,2}, Laure Perrin-Cocon³,
Maxime Espi⁴, Xavier Charmetant⁴, Manon Brailly²,
Didier Decimo^{1,2}, Mathieu Iampietro², Lola Canus¹,
Branka Horvat², Vincent Lotteau³, Pierre-Olivier Vidalain³,
Olivier Thauinat^{4,5} and Cyrille Mathieu^{1,2}

Abstract

Kidney pathology is frequently reported in patients hospitalized with COVID-19, the pandemic disease caused by the Severe acute respiratory coronavirus 2 (SARS-CoV-2). However, due to a lack of suitable study models, the events occurring in the kidney during the earliest stages of infection remain unknown. We have developed hamster organotypic kidney cultures (OKCs) to study the early stages of direct renal infection. OKCs maintained key renal structures in their native three-dimensional arrangement. SARS-CoV-2 productively replicated in hamster OKCs, initially targeting endothelial cells and later disseminating into proximal tubules. We observed a delayed interferon response, markers of necroptosis and pyroptosis, and an early repression of pro-inflammatory cytokines transcription followed by a strong later upregulation. While it remains an open question whether an active replication of SARS-CoV-2 takes place in the kidneys of COVID-19 patients with AKI, our model provides new insights into the kinetics of SARS-CoV-2 kidney infection and can serve as a powerful tool for studying kidney infection by other pathogens and testing the renal toxicity of drugs.

Keywords

SARS-CoV-2, kidney, organotypic cultures

Received: 1 May 2022; accepted: 11 August 2022

¹CIRI, Centre International de Recherche en Infectiologie, Team Neuro-Invasion, TROPism and VIRal Encephalitis, Univ Lyon, Inserm, U1111, CNRS, UMR5308, Université Claude Bernard Lyon 1, Ecole Normale Supérieure de Lyon, Lyon, France

²CIRI, Centre International de Recherche en Infectiologie, Team Immunobiology of the Viral infections, Univ Lyon, Inserm, U1111, CNRS, UMR5308, Université Claude Bernard Lyon 1, Ecole Normale Supérieure de Lyon, Lyon, France

³CIRI, Centre International de Recherche en Infectiologie, Team Viral Infection, Metabolism and Immunity, Univ Lyon, Inserm, U1111, CNRS, UMR5308, Université Claude Bernard Lyon 1, Ecole Normale Supérieure de Lyon, Lyon, France

⁴CIRI, Centre International de Recherche en Infectiologie, Team Normal and pathogenic B cell responses, Univ Lyon, Inserm, U1111, CNRS, UMR5308, Université Claude Bernard Lyon 1, Ecole Normale Supérieure de Lyon, Lyon, France

⁵Hospices Civils de Lyon, Edouard Herriot Hospital, Department of Transplantation, Nephrology and Clinical Immunology, Lyon, France

Corresponding author:

Cyrille Mathieu, CIRI, Centre International de Recherche en Infectiologie, Team Neuro-Invasion, TROPism and VIRal Encephalitis, Univ Lyon, Inserm, U1111, CNRS, UMR5308, Université Claude Bernard Lyon 1, Ecole Normale Supérieure de Lyon, 21 avenue Tony Garnier, Tour CERVI, Lyon 69364, France.
Email: cyrille.mathieu@inserm.fr



Introduction

Severe acute respiratory syndrome coronavirus 2 (SARS-CoV-2) is the causative agent of Coronavirus Disease 2019 (COVID-19),¹ a pandemic disease that in January 2022 has counted at least 454.5 million cases and claimed 6 million lives worldwide,² leading to devastating personal, social, and economic consequences. Pulmonary failure is the most common symptom of severe COVID-19. However, COVID-19 can also involve cardiovascular, neurological, gastrointestinal, hepatic and renal complications potentially resulting in multiorgan failure.³ While being rare in the mild and moderate form of the disease, acute kidney injury (AKI) is frequently reported in hospitalized patients, reaching 50% for patients in critical care units. In such cases, AKI is a significant predictor of poor outcome.^{4–10} Furthermore, a persistent decline in renal function has been documented in discharged COVID-19 patients, including a proportion of those not presenting with AKI during the acute phase of the disease, for at least 6 months of follow-up.¹¹ An increased risk of AKI and chronic kidney disease development in post-acute COVID-19 has also been reported.¹² As long-term COVID-19 sequelae affect millions of recovered patients, such complications may become a significant public health concern.^{13,14}

Studies of kidney autopsy samples from COVID-19 patients with AKI reveal signs of acute tubular necrosis, collapsing glomerulopathy and thrombotic microangiopathy. Knowledge of the precise mechanisms underlying renal pathology in acute and post-acute COVID-19 remain scarce.^{5,7,15} AKI could be a consequence of microangiopathy, thrombosis, rhabdomyolysis, inflammatory cytokine expression and complement activation. It may also be related to ventilation-induced alterations in blood flow, hemodynamic failure and to the nephrotoxicity of drugs used to treat the patients. Moreover, SARS-CoV-2 particles have been detected in renal biopsies, suggesting direct infection and viral replication may cause cytopathic effects in the kidney.^{9,16–22} Further investigation is required to confirm whether the virus can replicate in renal tissue, identify its initial cellular targets and dissemination pattern, and elucidate the organ's response to infection.

To date, the vast majority of samples used to study renal involvement in COVID-19 were obtained via autopsy or biopsy from patients with advanced disease, and do not provide information regarding the early stages of renal infection.⁷ As in the case of other nephrotropic pathogens, studying SARS-CoV-2 kidney infection is challenging due to the lack of relevant *in vitro* models and the difficulties in monitoring an *in vivo* infection in a non-invasive way.^{23,24} In order to gain insight into the early stages of SARS-CoV-2 infection of kidney, we turned to organotypic culture systems. In this *ex vivo* model, 350–500 μm thick slices of organs are cultured on an air-liquid interface. Organotypic cultures represent the only model

containing all cell types from an organ of interest in their native three-dimensional arrangement.^{25,26} Organotypic cultures prepared from mouse and hamster brain have been used successfully to study the infection of the central nervous system by Measles virus²⁶ and Nipah virus,²⁷ or, together with lung organotypic cultures, by SARS-CoV-2.²⁵ Organotypic cultures from human and mouse kidney slices have been described previously but have never been used to study SARS-CoV-2 or other viral infections.^{28–31}

Live samples of human kidneys are very difficult to obtain for obvious ethical reasons. Golden Syrian hamsters (*Mesocricetus auratus*) are a representative and economical model for SARS-CoV-2 infection. When challenged with SARS-CoV-2, they develop symptoms mimicking mild disease in humans and accumulate a viral load in various organs, including kidney.³² Recently, our group has developed and characterized hamster organotypic lung, brainstem and cerebellum cultures as models for studying SARS-CoV-2 infection and platforms for testing antiviral drugs.²⁵ To study SARS-CoV-2 infection in renal tissue, we have now developed hamster organotypic kidney cultures (OKCs). SARS-CoV-2 infection of these organotypic cultures was effective, thus supporting the possibility of active viral replication in human kidneys. Our OKC models proved particularly valuable for investigating the tropism and dissemination of SARS-CoV-2 in renal tissue and analyzing its innate immune response to infection.

Materials and methods

Animals and ethical authorization. Syrian golden hamsters (*Mesocricetus auratus*) used in this study were obtained from Janvier Labs (Le Genest-Saint-Isle, France) with clean health monitoring report. K18-hACE2 mice were obtained from the Jackson laboratory. The sex of the animals was random and dependent on the litter throw by the mother. Animals were euthanized at 7 days old. This study was performed according to French ethical committee (CECCAPP) regulations (accreditation CECCAPP_ENS_2014_034).

Preparation of organotypic cultures. The procedure for Organotypic Kidney Cultures (OKC) was adapted from the protocol for Organotypic Brain Cultures (OBC) described previously.³³ A day before the dissection, Millicell[®] cell culture inserts with PTFE membranes (Merck) were pre-activated with OKC medium. The OKC medium contains 375 mL of Minimal Essential Medium GlutaMAX (ThermoFisher Scientific), 125 mL of heat-inactivated horse serum (Gibco), 2.5 g of D-glucose (Sigma-Aldrich) and 1 mL of human recombinant insulin (10 mg/mL) (Sigma-Aldrich), and was sterilized with a 0.22 μm filter. The OKC medium is identical to the OBC medium described by Welsch³³ and used by Ferren et al.²⁵ for organotypic lung,

brainstem and cerebellum cultures. Seven to nine-day suckling hamsters were sacrificed and their abdominal cavity was opened. Kidneys were collected and placed into a solution of Hibernate[®]-A medium (Sigma-Aldrich), 1X kynurenic acid solution (for a 10X solution: 378 mg of kynurenic acid (Sigma-Aldrich) in 170 mL of H₂O, 20 mL of 1 M MgCl₂ (Sigma-Aldrich) adjusted to pH 7.4 with 0.1 M NaOH (Sigma-Aldrich), 1 mL HEPES (Sigma-Aldrich), adjusted to a final volume of 200 mL) and 1X penicillin/streptomycin solution (Corning). Kidneys were placed on six layers of Whatman paper with their longitudinal axis perpendicular to the tissue chopper blade and sliced transversely using the McIlwain[®] tissue chopper (Campden Instruments) at 500 μ m thickness for all experiments except the Seahorse XF Analyzer Respiratory Assay that required 400 μ m slices. The slices were dissociated under a dissection microscope. Undamaged and homogenous slices were selected and maintained on an air-liquid interface provided by PTFE membranes pre-activated with OKC medium. Organotypic lung cultures were prepared using the protocol described by Ferren et al.²⁵

Viruses and infection of organotypic kidney cultures. Viral stocks have been produced and titrated at 37°C in Vero E6 cells. Briefly, cells were infected at a Multiplicity Of Infection (MOI) of 0.01 in DMEM. After 90 min of incubation at 37°C, the medium was replaced with DMEM-2% FBS and the cells were incubated at 37°C in 5% CO₂ atmosphere for 2 days. Viral supernatants were collected and centrifuged (400 \times g, 5 min), aliquoted, and titrated as plaque-forming units using a classic dilution limit assay. A 2 μ L drop containing the required amount of viral plaque-forming units (pfu) was placed on each organotypic kidney slice. Infected slices were incubated at 37°C until collection. Slices were infected with wild-type SARS-CoV-2 (2019-nCoV/USA_WA1/2020) or a recombinant strain icSARS-CoV-2-mNG expressing the mNeonGreen reporter gene inserted into its ORF7.³⁴

Seahorse XF analyzer respiratory assay. Organotypic kidney slices were prepared and sliced in Neurobasal[®]-A Medium 1X (Gibco) at 400 μ m and assayed on the day of preparation (day 0) or following 1 or 4 days of culture at air-liquid interface with OKC medium at 37°C. OKCs were washed in 1X phosphate buffer saline (Gibco). 1 mm punches were prepared from the renal cortex and 1 punch/well was placed in a 24-wells islet capture microplate (Agilent). Punches were washed twice with 1 mL Seahorse XF DMEM medium (pH 7.4) supplemented with glucose (10 mM), pyruvate (1 mM) and L-glutamine (2 mM) and incubated 1 h at 37°C in a non-CO₂ incubator. 500 μ L of fresh Seahorse medium were added to each well before the respiration assay. The oxygen consumption rate (OCR) was measured using the MitoStress test (Agilent), optimized for tissue assay according to the method described

by Underwood et al.³⁵ Seahorse running program: injection Port A—3 μ M Oligomycin; Injection Port B—3 μ M FCCP with 0.7 mM Pyruvate and injection Port C—6 μ M Rotenone and 6 μ M Antimycin A. Results were analyzed using the Seahorse Wave software.

Quantitative RT-PCR. Each organotypic kidney slice was collected in 350 μ L of RA1 buffer (NucleoSpin RNA, Macherey-Nagel) and 3.5 μ L of 2-Mercaptoethanol (Sigma-Aldrich), and lysed using a pestle mixer (Argos Technologies). RNA was extracted from the lysates with the NucleoSpin RNA kit (Macherey-Nagel). 200 ng of RNA was reverse transcribed with the iScript cDNA Synthesis Kit (Bio-Rad) according to the manufacturers' protocols. cDNA was diluted 1:10 to avoid inhibition between mix with the following step. Gene transcription was quantified via qPCR using the Platinum SYBR Green qPCR SuperMix-UDG (Invitrogen), according to the manufacturer's protocol. Readings were made with the StepOne-Plus Quantitative PCR System (Applied Biosystems) and viewed in the StepOne version 2.3 software (Applied Biosystems). The primers for measuring the expression of the mRNA of the cytokines IL-4, IL-10, IL-13, and IL-22 were designed for this study (Supplemental Table 1). Other primers were designed by Ferren et al.²⁵ The efficacy (*E*) of the primers was calculated as $10^{-1/\text{slope}}$ based on the slope of the standard curve. The copy number of mRNA per μ g of total RNA was calculated using the $E^{-\Delta\Delta CT}$ model³⁶ (for each gene and normalized by the standard deviation in the expression of glyceraldehyde-3-phosphate dehydrogenase (GAPDH), a housekeeping gene (UniProtKB P04406), from the mean of its expression level across all days.³⁷

Immunofluorescence staining. Organotypic kidney slices were fixed overnight at 4°C in 4% paraformaldehyde (16% paraformaldehyde, methanol-free; ThermoFisher Scientific) diluted in phosphate buffer saline (PBS 1X; Gibco). Slices were washed with PBS 1X (here and later: 4 times, 5 min each wash) and placed into a sucrose (Sigma-Aldrich) gradient (5%, 15%, 20%) solution overnight at 4°C. Slices were embedded in the Optimal Cutting Temperature (OCT) solution (ThermoFisher Scientific) and sectioned along the horizontal plane with the Leica CM3050 S cryostat-microtome (Leica Biosystems). 10 μ m sections were placed on Superfrost Gold Plus adhesion slides (Fisher Scientific), washed in PBS 1X, permeabilized and blocked in permeabilization and blocking solution (1X DPBS; ThermoFisher Scientific, 3% BSA; Sigma-Aldrich, 0.3% Triton-X100; Sigma-Aldrich) for 30 min at 4°C. Slices were incubated overnight with primary antibodies diluted in permeabilization and blocking solution, washed in PBS 1X, stained for 1 h with secondary antibodies diluted in permeabilization and blocking solution, washed with PBS 1X and mounted in Fluoromount-G[®] aqueous mounting medium (SouthernBiotech).

Anti-SARS-CoV-2 nucleoprotein (NP) antibodies (SinoBiological, Cat# 40143-MM05 mouse, 1:200 dilution) were used to detect the presence of virus. Endothelial cells were stained with anti-CD34 antibodies (abcam, Cat# ab81289 rabbit, 1:100 dilution), proximal tubular epithelial cells with anti-aquaporin-1 (ThermoFisher Scientific, Cat# PA5-53954 rabbit, 1:100 dilution), and podocytes with anti-nephrin (abcam, Cat# ab216341, rabbit, 1:100 dilution). Alexa Fluor™ 488 donkey anti-rabbit (ThermoFisher Scientific, Cat# A21206, 1:500 dilution) and Alexa Fluor™ 555 donkey anti-mouse (ThermoFisher Scientific, Cat# A31570, 1:500 dilution) secondary antibodies were used. Cell nuclei were stained with 4',6-diamidino-2-phenylindole (DAPI) (ThermoFisher Scientific, Cat# 62248, 1:1000 dilution).

Imaging. OKCs infected with icSARS-CoV-2-mNG were photographed using the Nikon Eclipse Ts2R optical microscope and stitched using the Stitching plugin in ImageJ.³⁸ Immunostained OKCs were examined and photographed using the Zeiss Axio Observer.Z1 microscope with confocal unit LSM 980 (Zeiss). Images were edited and analyzed using the ImageJ software 1.52p FiJi package³⁹ and assembled in Inkscape.

Statistical analysis. Statistical analysis was performed in GraphPad Prism version 9.3.0.⁴⁰ For the Seahorse XF metabolic activity assay, day 1 and day 4 OCRs of punches were compared to the day 0 OCR using ordinary one-way ANOVA. For the gene expression analysis, differences between normalized mRNA copy numbers per μg RNA in infected and non-infected samples were compared using a Mann-Whitney *U*-test. *= $p < 0.05$; **= $p < 0.01$; ***= $p < 0.001$.

Results

Organotypic kidney cultures maintain key renal native structures for at least 4 days in culture

Kidneys were collected from 7-day-old suckling hamsters, sliced on a tissue chopper into 500 μm thick slices and maintained on an air-liquid interface provided by polytetrafluoroethylene membranes. The renal capsule, cortex and medulla were clearly identifiable in hamster OKCs (Figure 1(a)). A nephron (Figure 1(b)) is a functional unit of the kidney. Blood is filtered in the renal glomerulus (Figure 1(c)). Through the afferent arteriole, it enters under high pressure a capillary bundle known as the glomerulus and passes the filtration barrier consisting of the glomerular endothelium, basement membrane and podocytes. The filtration barrier retains blood cells, large particles and proteins but not nutrients or ions. Glucose, amino acids, water and salts are re-absorbed into capillaries from the filtrate in the proximal convoluted tubule, loop of Henle and distal convoluted tubule. Following reabsorption, the filtrate becomes urine and flows into the collecting duct

leading to the renal pelvis and, eventually, the ureter.⁴¹ We confirmed the presence of essential functional elements of nephrons in our OKCs via immunofluorescence staining of aquaporin-positive proximal tubules, nephrin-positive podocytes and CD34-positive endothelial cells of the renal vasculature. Reflecting their native arrangement, proximal tubules and renal glomeruli were localized in the cortex (Figure 1(d)). However, we then further determined whether organotypic kidney slices survive in culture and maintain metabolic activity for up to 4 days after preparation. To measure the mitochondrial respiratory activity of OKCs, 1 mm large punches prepared from the cortical zone of 400 μm -thick slices were analyzed on a Seahorse XF Analyzer using the MitoStress Test with procedures adapted for tissue.³⁵ Oxygen Consumption Rate (OCR) was monitored at basal stage and after addition of mitochondrial modulators to determine the basal and maximal respiratory capacity of OKCs. The maximal metabolic rate was monitored following disruption of the mitochondrial proton gradient by FCCP. Non-mitochondrial OCR measured after complete inhibition of mitochondrial respiration by rotenone and antimycin A was subtracted to basal and maximal OCR to calculate basal and maximal respiration (Figure 2(a)). The basal metabolic activity of punches from OKC cortices was maintained after 1 day of culture and remained at more than 60% of its initial level on day 4 (Figure 2(a) and (b)). As shown in Figure 2(c), maximal respiration remained stable after 1 day of culture and decreased by only 20% at day 4. According to the immunofluorescent staining, the arrangement of the OKC structure was preserved even after 4 days of culture (Figure 3(d) and (e)).

Total RNA was extracted from slices and quantified as another measure of their viability. Over the duration of the experiment, its amount did not decrease (Figure 2(d)). The expression of glyceraldehyde-3-phosphate dehydrogenase (GAPDH), a key enzyme in the glycolysis pathway and a housekeeping gene (UniProtKB P04406), also remained stable (Figure 2(e)), reflecting the ability of OKCs to maintain steady glycolytic activity in culture. Such results indicate that, despite a progressive reduction in mitochondrial respiration, organotypic kidney cultures remain viable on an air-liquid interface for at least 4 days.

Organotypic kidney cultures are highly permissive to SARS-CoV-2 infection

SARS-CoV-2 mainly enters cells via the binding of the Spike glycoprotein to one of its target receptors such as angiotensin converting enzyme 2 (ACE2) or Neuropilin-1. The fusion of the viral envelope with the cell membrane is enhanced by the cleavage of the Spike by host proteases such as TMPRSS2 on the cell surface or cathepsins B and L in endosomes.^{42,43} These proteins are all expressed in the kidney,⁴⁴ especially ACE2 which is critically involved in

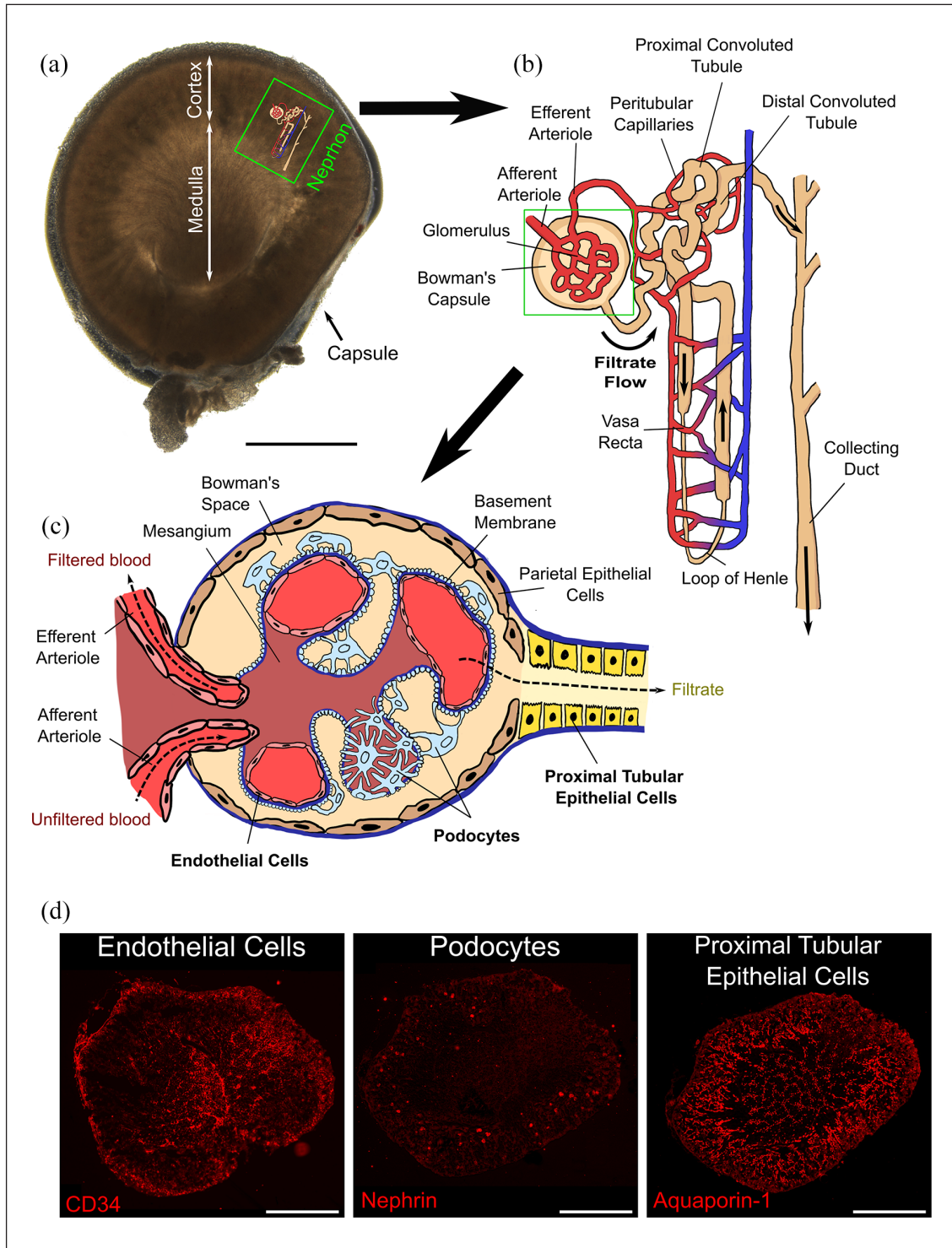


Figure 1. Schematic representation of the anatomy of hamster organotypic kidney cultures. (a) A 500- μm thick organotypic kidney slice maintained on an air-liquid interface provided by a PTFE membrane was photographed in brightfield using a Nikon Eclipse Ts2R epifluorescence microscope. Scalebar = 1 mm. The renal capsule, cortex and medulla are identified and labeled. A nephron schematic is positioned in its physiological location and highlighted with a green rectangle. (b) The structure of a nephron, a functional unit of the kidney, showing the flow of the filtrate. (c) The structure of a renal corpuscle. The schematic was rendered in-house using Procreate[®] and Inkscape 1.1. (d) Organotypic kidney cultures were fixed in 4% paraformaldehyde, embedded in OCT solution and cryosectioned at 10 μm thickness. Sections were immunostained to visualize endothelial cells, podocytes and proximal tubular epithelial cells with anti-CD34 (endothelial cells; left panel), anti-nephrin (podocytes; middle panel) and anti-aquaporin I (proximal tubular epithelial cells) primary antibodies (right panel). Scalebar = 1 mm. Images were reconstructed using the Stitching plugin in ImageJ.³⁸

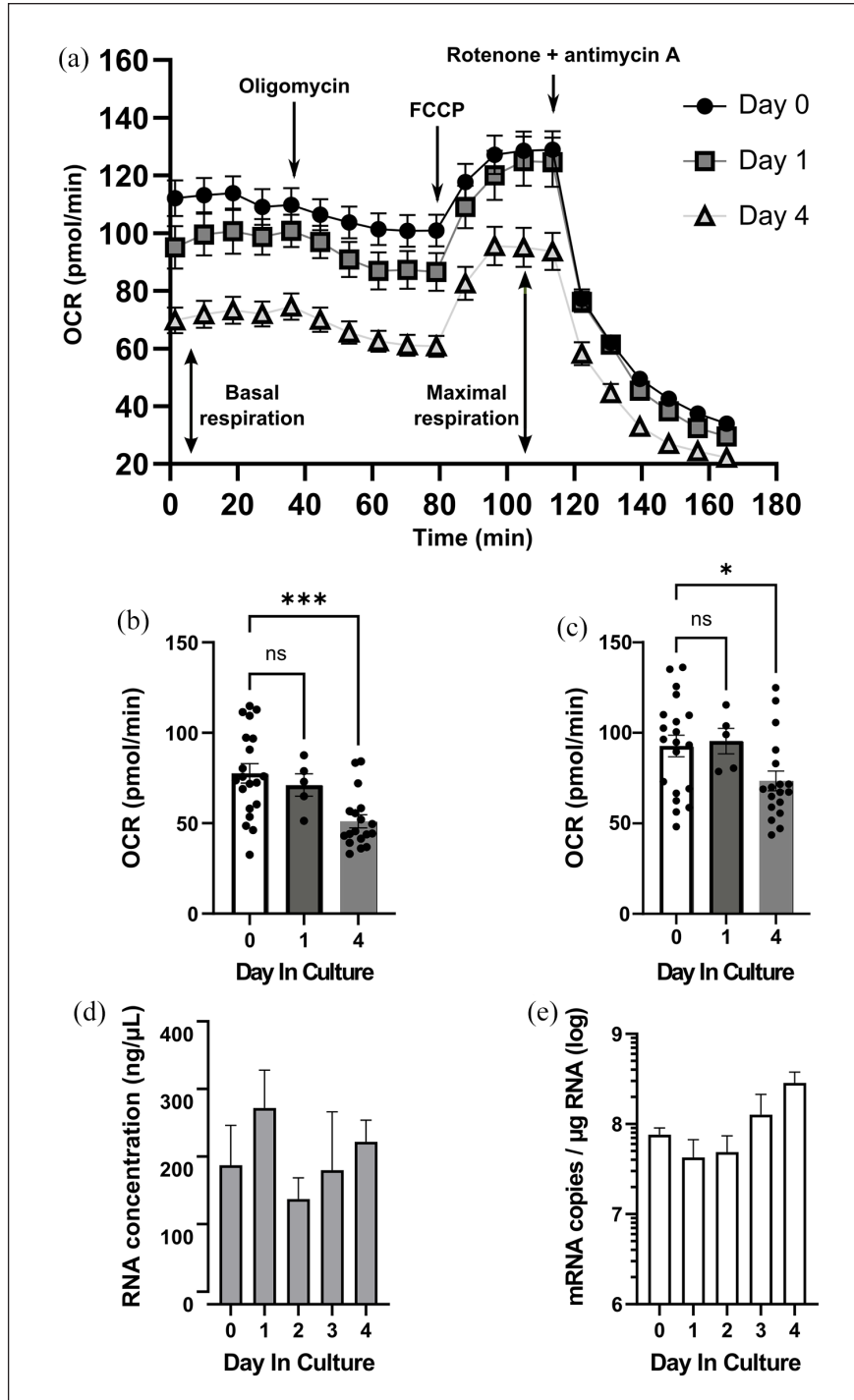


Figure 2. Viability of hamster organotypic slices in culture. The Seahorse XF Analyzer was used to analyze the metabolic activity of OKCs. Briefly, 400- μm thick OKCs were maintained at an air-liquid interface in the OKC medium for 0, 1 or 4 days prior to measurement. One punch per slice was cut in the cortical zone and basal and maximal respiration of each punch was determined using the MitoStress test. The oxygen consumption rate (OCR) was measured according to time. Punches received successive additions of respiratory modulators indicated by arrows, ATP synthase inhibitor oligomycin ($3\ \mu\text{M}$), uncoupling agent FCCP ($3\ \mu\text{M}$) with pyruvate supplement ($0.7\ \text{mM}$), and then rotenone + antimycin A ($6\ \mu\text{M}$) to completely inhibited mitochondrial respiration. (a) For each experiment, mean OCR \pm SEM is plotted. Determination of the basal and maximal respiration is indicated with green arrows on the mean OCR curve obtained at day 4. (b) Basal and (c) maximal respiration rates of OKCs. Mean respiration rates obtained at day 1 and 4 were compared to that of day 0 using ordinary one-way ANOVA. *, $p < 0.05$; **, $p < 0.01$; ***, $p < 0.001$. (d) Concentration of RNA extracted from non-infected OKCs collected after 0 to 4 days of culture. (e) Expression of GAPDH in non-infected OKCs collected after 0 to 4 days of culture.

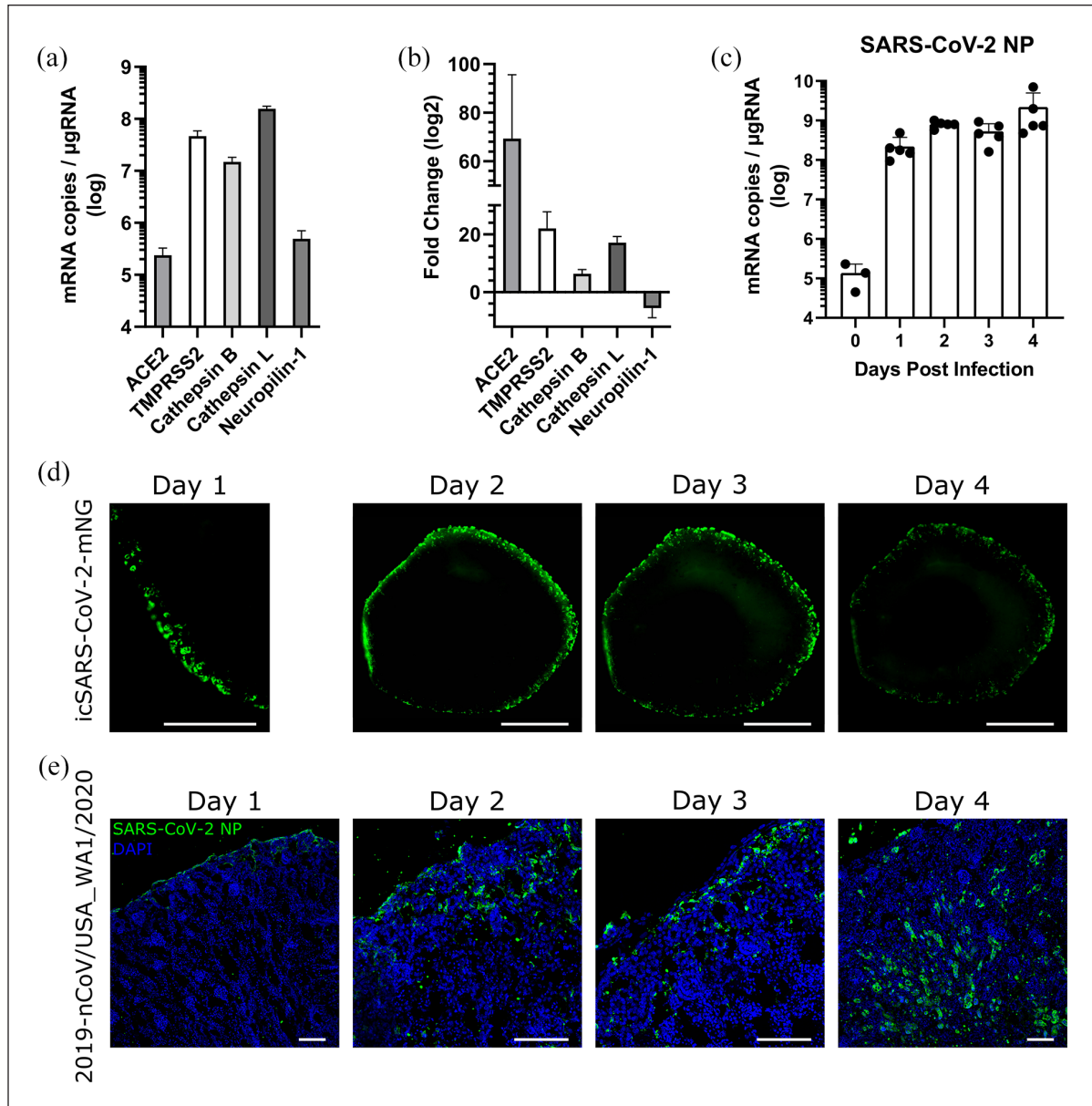


Figure 3. SARS-CoV-2 permissiveness of and progression in hamster organotypic kidney cultures. (a and b) Gene expression was quantified in non-infected organotypic kidney cultures (OKCs) and hamster organotypic lung cultures collected on the day of dissection via RT-qPCR as the number of mRNA copies per μg of total RNA and normalized by the standard deviation in GAPDH expression. (a) mRNA copy numbers of candidate SARS-CoV-2 entry factors per μg of total RNA. (b) Fold change of SARS-CoV-2 entry factor mRNA copy numbers per μg of total RNA in OKCs compared to organotypic lung cultures. (c) Hamster organotypic cultures were infected with 1000 pfu of wild-type SARS-CoV-2 (2019-nCoV/USA_WA1/2020) and collected every day from day 0 (90 min post-infection) to day 4 post-infection. SARS-CoV-2 replication was measured by quantifying the amount of SARS-CoV-2 nucleocapsid (NP) mRNA per μg of total mRNA via RT-qPCR and normalizing it by the expression of a housekeeping gene (GAPDH). (d) Hamster OKCs infected with 10,000 pfu of SARS-CoV-2_mNeon Green (icSARS-CoV-2-mNG) were imaged from day 0 to day 4 post-infection using a Nikon Eclipse Ts2R epifluorescence microscope. Scalebar = 1 mm. (e) Hamster OKCs were infected with 1000 pfu of wild-type SARS-CoV-2 and fixed in 4% paraformaldehyde every day from 1 to 4 days post infection. OKC sections were stained against SARS-CoV-2 nucleoprotein (NP). Cell nuclei were stained with 4',6-diamidino-2-phenylindole (DAPI). Pictures were obtained by confocal microscopy. Scalebar = 100 μm .

the renin-angiotensin system responsible for controlling blood pressure and vascular resistance.^{45,46} The global expression of SARS-CoV-2 entry factors in hamster OKCs

was quantified via RT-qPCR. The entry receptors ACE2 and neuropilin-1, as well as the proteases TMPRSS2 and cathepsins B and L were highly expressed in the slices

(Figure 3(a)). The mRNA expression of all entry factors except neuropilin-1 was significantly enriched compared to lung organotypic cultures (Figure 3(b)).

In order to probe the susceptibility of hamster OKCs to SARS-CoV-2, five slices from five animals ($n=5$) were infected with wild-type SARS-CoV-2 (2019-nCoV/USA_WA1/2020) while maintained in culture on an air-liquid interface. The number of copies of mRNA encoding the viral nucleocapsid protein (NP) was quantified via RT-qPCR in slices from day 0 to day 4 post-infection, starting 90 min post-infection. Similarly to the pattern observed in hamster organotypic lung cultures,²⁵ viral mRNA expression increased by four logs in infected OKCs, approaching a plateau at 1 day post-infection (Figure 3(c)). In slices infected with a recombinant SARS-CoV-2 strain encoding a mNeonGreen reporter (icSARS-CoV-2-mNG), infected cells were observable from day 1 post-infection, thus mirroring the RT-qPCR data (Figure 3(d)). Infection started in the capsular zone (Figure 3(d) and (e)) and propagated toward the center of the slice when using the wild-type virus expressing ORF7 (Figure 3(d) and (e)). Indeed, ORF7 is a known virulence factor that promotes viral growth by controlling the innate antiviral response. The fact that the infection starts in the capsular zone is unexpected. However, the same phenomenon was observed when infecting OKCs from K18-hACE2 mice, which express the entry receptor ubiquitously, with 500 pfu of icSARS-CoV-2-mNG (Supplemental Figure S1). This suggests that SARS-CoV-2 preferentially infects and replicates cells in the capsular zone independently of the expression of the entry receptor. In parallel, we infected the OKCs with a pan-tropic Vesicular Stomatitis Virus expressing GFP (VSV-GFP) (Supplemental Figures S1 and S2). As opposed to icSARS-CoV-2-mNG, VSV extensively infected the medullar area of the cultures from day 1 post-infection. We have also confirmed that the infection of the OKC was productive by plaque assay with the production of pfu peaking 2 days after infection both in the cultures and the culture medium (Supplemental Figure S1C).

In hamster organotypic kidney cultures, SARS-CoV-2 targets endothelial cells and proximal tubules but not podocytes

To investigate the early tropism and subsequent propagation of SARS-CoV-2 in hamster OKCs further, cells serving as the primary targets of the virus were identified via immunofluorescence. 10 μ m thick cryosections of OKCs were stained with antibodies against the SARS-CoV-2 nucleoprotein (NP) and markers of endothelial cells (CD34), proximal tubular epithelial cells (aquaporin-1) and podocytes (nephrin) (Figure 4, Supplemental Figures S3 and S4).

In line with observations of slices infected with icSARS-CoV-2-mNG, infection initiated in the subcapsular zone

(Figure 4(a)) and propagated toward the center of the slice (Figure 4(b)). Colocalization of CD34 and SARS-CoV-2 NP was observed on day 1 (Figure 4(a)) and day 2 (Fig. S4A) post-infection. At later timepoints, colocalization with CD34⁺ cells was restricted to peripheral blood vessels (Supplemental Figures S4A and S4B) and was limited compared to day 1 (Figure 4(a)). Infection of podocytes was not detected over the 4 days of the experiment (Supplemental Figure S3). Proximal tubular epithelial cells positive for viral nucleoprotein were observed on day 4 post-infection (Figure 4(c)), but not at earlier timepoints (Supplemental Figure S4B). These results suggest that early targets of SARS-CoV-2 in hamster OKCs include CD34⁺ endothelial cells and other subcapsular parietal cells, while proximal tubular epithelial cells serve as later sites of viral dissemination.

Gene expression analysis of organotypic kidney cultures infected with SARS-CoV-2

In order to evaluate how organotypic kidney cultures respond to infection, the expression of immune-related genes was measured and compared in infected and non-infected OKCs. No substructures of the OKCs were isolated and entire slices were compared. In particular, we measured the expression of inflammatory cytokines genes (IL-6, IL-1 β , IL-18, TNF α), selected genes associated with highly inflammatory types of programmed cell death (MLKL and gasdermin D), and interferon-stimulated genes that hallmark the antiviral response (CXCL10, MX1). We also monitored the expression of SARS-CoV-2 receptor ACE2 and the entry-associated protease TMPRSS2.

Infected OKCs display a limited expression of TNF α and a repression of IL-1 β (Figure 5(a) and (b)), IL-18 (Figure 5(c)), and IL-6 (Figure 5(d)) on days 1 and 2 post-infection, followed by strong induction from day 3 onward, preceding closely the infection of proximal tubular epithelial cells shown in Figure 4(c). This effect was particularly pronounced for IL-1 β (Figure 5(b)), which was upregulated approximately 2500-fold between day 2 and 3 post-infection. Although TNF α (Figure 5(a)) was not particularly repressed initially, it displayed a statistically significant upregulation only on day 4. The expression of IL-1 β dropped dramatically on day 4, reaching levels equivalent to those of non-infected samples, while the expression of IL-18 and IL-6 was maintained. Necroptosis and pyroptosis are highly inflammatory cell death programs which play a role in the innate antiviral response in parallel to immune mediators.⁴⁷ Moreover, cytokines such as TNF α and members of the IL-1 family have been demonstrated to regulate necroptosis and pyroptosis, respectively.^{48,49} An upregulation of mixed lineage kinase domain-like pseudokinase (MLKL), a marker of necroptosis, was observed at day 4 post-infection in OKCs, suggesting that necroptosis had

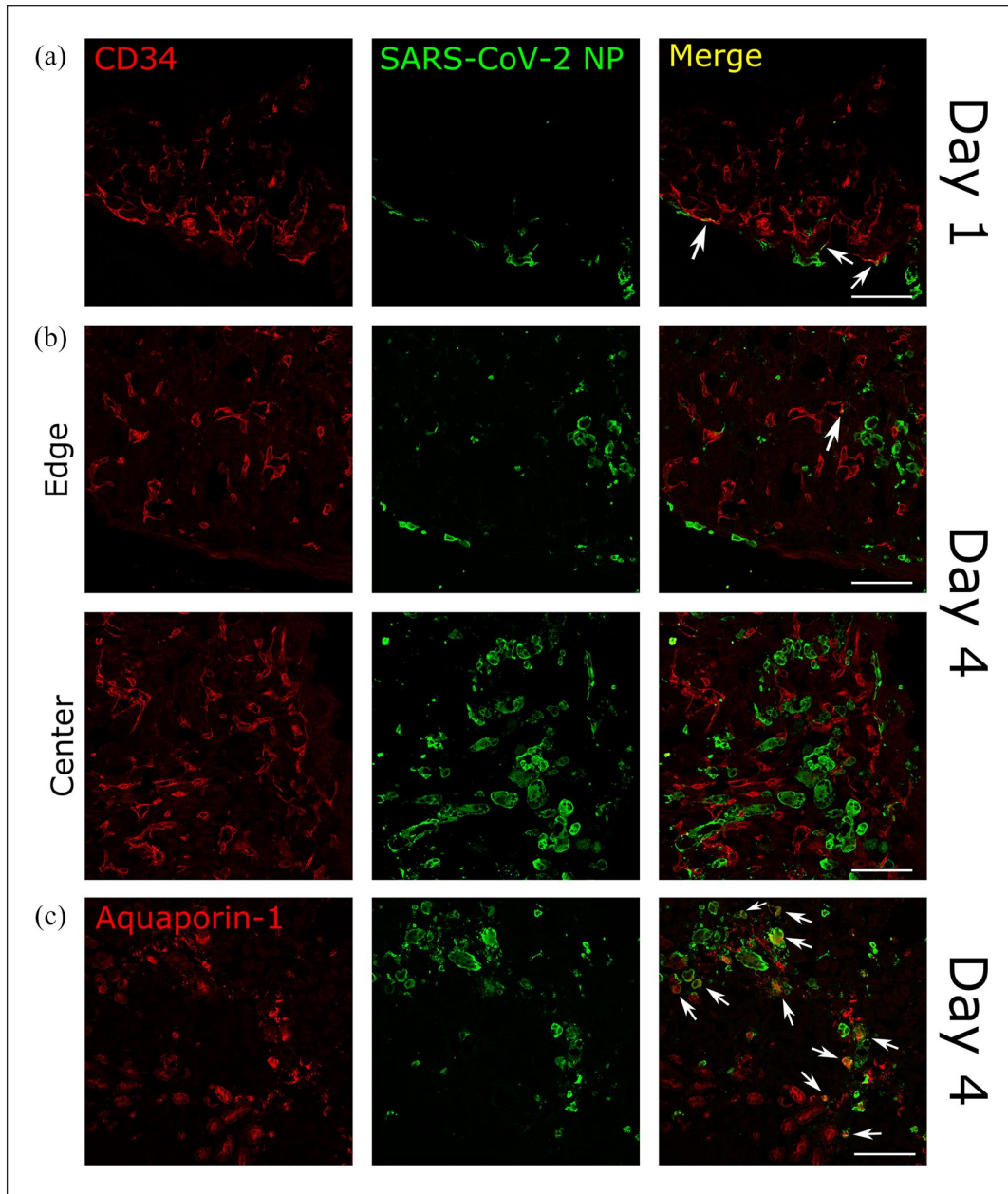


Figure 4. Tropism and dissemination of SARS-CoV-2 in hamster organotypic kidney cultures. Organotypic kidney cultures (OKC) were infected with 1000 pfu of wild-type SARS-CoV-2 and fixed in 4% paraformaldehyde at 1 or 4 days post infection (dpi). (a and b) OKC sections stained against SARS-CoV-2 nucleoprotein (NP) and CD34 (marker of endothelial cells) at day 1 and 4 post infection ((a and b), respectively). (a) is showing the edge of the slice. (b) is showing both the edge and the center of the slice, demonstrating the spread of infection toward the center. (c) OKC sections stained against SARS-CoV-2 NP and (c) aquaporin-1 (marker of proximal tubular epithelial cells). Immunofluorescence images were acquired using confocal microscopy and is representative of three independent experiments. Colocalization of cell type markers (red) with SARS-CoV-2 NP (green) is denoted with arrows. Scalebar = 100 μ m.

likely been induced at this stage of infection (Figure 5(e)). The expression of gasdermin D, a key mediator of pyroptosis, was raised throughout the experiment, peaking at day 2 post-infection (Figure 5(f)).

The expression of ISGs such as CXCL10 (Figure 5(g)) of the chemokine family and myxovirus resistance 1

(MX1) (Figure 5(h)) were measured as a proxy for an efficient IFN response to SARS-CoV-2 challenge. CXCL10 expression was only induced on day 4, whereas MX1 expression increased 13-fold on day 2 post-infection and continued to rise up to day 4, reaching a 24-fold level compared to non-infected cultures. Thus, it mirrored the

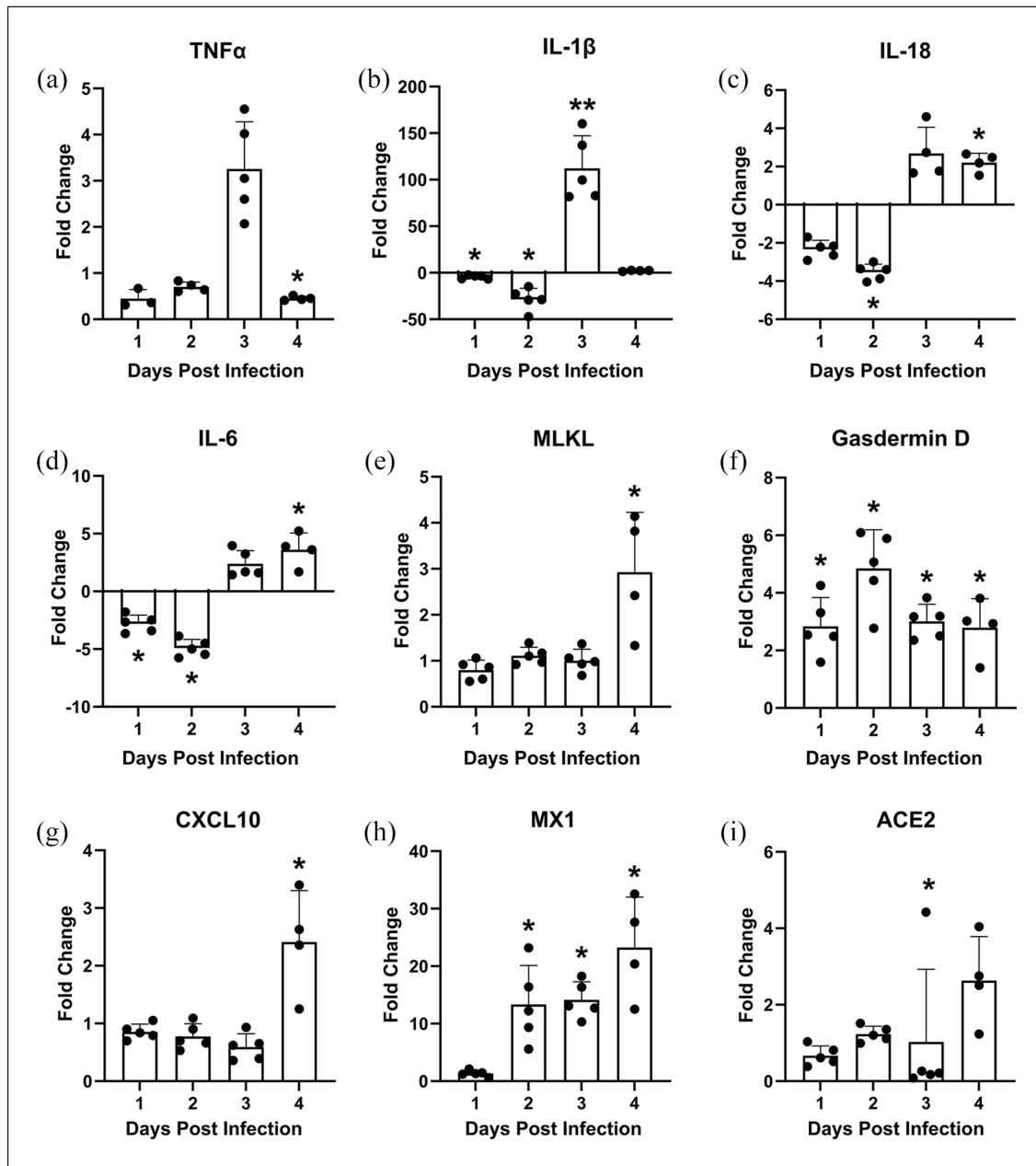


Figure 5. Gene expression analysis of hamster organotypic kidney cultures challenged with SARS-CoV-2. Hamster organotypic kidney cultures were cultured uninfected or infected with 1000 pfu of wild-type SARS-CoV-2 (2019-nCoV/USA_WA/2020) and collected every day from day 1 to day 4 post-infection. In both infected and non-infected slices, gene expression was measured via RT-qPCR as the number of mRNA copies per μg of total RNA and normalized by the standard deviation of GAPDH expression from its average across all days. To calculate the fold changes, values from infected slices were divided by the average values of non-infected slices from the corresponding day. (a–i) Fold change in the expression of (a) TNF α , (b) IL-1 β , (c) IL-18, (d) IL-6, (e) MLKL, (f) gasdermin D, (g) CXCL10, (h) MX1, (i) ACE2 from day 1 to day 4 post-infection. For each day, mRNA copy numbers per $1 \mu\text{g}$ of RNA of infected and non-infected samples were compared using the Mann-Whitney U-test. * = $p < 0.05$; ** = $p < 0.01$.

infection kinetics observed (Figure 3(c)) with a 24-h delay. Studies in primary and immortalized human cell lines indicate that the expression of ACE2, one of the main candidate SARS-CoV-2 entry receptors, may be inducible by interferons^{50,51} and/or IL-10.⁵² Since the expression of numerous cytokines was delayed (or repressed) during the

first days, we also tried to follow four canonical repressive cytokines (i.e. IL-4, IL-10, IL-13, and IL-22) (Supplemental Figure S5). IL-4 and IL-22 mRNA levels remained too low to be appropriately quantified. Fold variations of IL-10 and IL-13 mRNA in infected OKCs remained lower than 2-fold compared to the non-infected ones, suggesting that

they could not be considered significant at the global organ scale. We extended our gene expression analysis to observe how infection may impact the transcription of ACE2 and other putative viral entry factors such as the receptor neuropilin-1 and the proteases TMPRSS2 and cathepsin B. A slight tendency toward the upregulation over the course of infection was detected for ACE2 (Figure 5(i)). Neuropilin-1 (Supplemental Figure S6A), TMPRSS2 (Supplemental Figure S6B), and cathepsin B (Supplemental Figure S6C) also tended toward overexpression in infected slices.

Discussion

It remains an open question whether an active replication of SARS-CoV-2 takes place in the kidneys of COVID-19 patients with AKI. Several groups have detected the presence of a significant viral load in the kidney via methods such as RT-qPCR, in situ hybridization, immunohistochemistry, transmission electron microscopy and isolation of live virus.^{16,18–22,53} Others have failed to find viral particles or RNA in autopsy samples,^{54–56} thus questioning the actual replication of SARS-CoV-2 in the kidneys and the relevance of measuring viral load post-mortem, and bringing to light the heterogeneity of the samples and quantification methods used. In humans, SARS-CoV-2 infection tends to progress asymptotically or with mild symptoms before deteriorating into a severe form.^{3,57} Therefore, only late samples which do not provide the possibility to pinpoint the starting point of renal infection are available. Recent studies showed progress on organoids obtained from human induced pluripotent stem cells,⁵⁸ which present the advantage of enabling work with human tissue, as we have shown elsewhere for human brain organoids and Measles virus.⁵⁹ However, their main limitation, apart from the impossibility to model fluid circulation, remains that such organoids still allow working only with one or two tissues at a time, which restricts the number of questions that such models can address. The absence of an appropriate model is the principal reason for the lack of knowledge on SARS-CoV-2 replication in the kidneys.⁷ Here, we present hamster OKCs as a relevant ex vivo model for studying the infection of the kidney by SARS-CoV-2. Hamster OKCs conserved the native structure of renal tissue (Figure 1) and could be maintained in culture for at least 4 days (Figure 2). While their mitochondrial metabolic activity progressively decreased by day 4, it remained compatible with cell viability (Figure 2(a)–(c)) as confirmed by the stable quantity of RNA extracted from OKCs and their GAPDH expression pattern at later timepoints (Figure 2(d) and (e)). We further demonstrated by immunostaining that all cell types were still present after 4 days of culture, confirming that the decrease of viability was not selective for one cell type (Figure 4, Supplemental Figures S3 and S4). Hence, these cultures thus provide a relevant ex vivo culture model for studying renal infections.

SARS-CoV-2 was found in the kidneys of experimentally infected hamsters, but its ability to replicate in them was not confirmed.³² In this study, organotypic kidney culture modeling showed that hamster renal tissue is highly permissive to SARS-CoV-2 infection and allows for efficient viral replication. The viral load peaked on day 1 post-infection, similarly to the dynamics observed in organotypic lung cultures but distinctly from those observed in organotypic cerebellum and brainstem cultures, where infection peaked on day 2.²⁵ To go further, we confirmed these observations in OKCs from K18-hACE2 mice, which showed very similar infection dynamics, as assessed by the production of PFUs both in tissue and culture medium (Supplemental Figure S1). We have also confirmed that the tendency of SARS-CoV-2 infection to start in the cortical area was not an artifact of the infection technique by demonstrating that the pan-tropic Vesicular Stomatitis Virus extensively infected the medullar area from day 1 post-infection (Supplemental Figures S1 and S2). Immunostainings revealed the predominant infection of CD34⁺ endothelial cells on day 1 post-infection (Figure 4(a)). Indeed, SARS-CoV-2 infection can provoke endotheliitis in a range of organs, including the kidney. The presence of viral particles in glomerular endothelial cells in a kidney autopsy sample has also been confirmed via transmission electron microscopy.⁶⁰ Thus, in hamster OKCs, SARS-CoV-2 could first target endothelial cells and later disseminate to other sites, including proximal tubules (Figure 4(c)). In contrast, we did not observe any infection in podocytes. Whether hamster podocytes lack an essential viral entry or replication factor remains to be deciphered. Endothelial cells would be the first renal cells to encounter viral particles in case of viremia in a living organism and interestingly, this sequence of infection seems to be conserved in organotypic cultures.

Acute tubular injury is the most common renal pathology observed in kidney autopsy samples of COVID-19 patients.^{5,7,18,20,53,61} Although organotypic cultures are inoculated by placing a virus-containing droplet on top of the entire slice, infection of proximal tubular epithelial cells did not occur before day 4 post-infection (Supplemental Figure S4B). This was confirmed not to be a technical artifact (Supplemental Figures S1 and S2). In contrast, they became the main infected cell population on day 4 post-infection (Figure 4(c)). This suggests that the susceptibility and permissiveness of tubular epithelia is favored by additional factors, most likely produced by the infection of other cell populations. Our results may reflect the fact that tubular damage is a late event in SARS-CoV2 pathogenesis, which makes it difficult to predict.

Despite the viral load peaking on day 1 post-infection, pro-inflammatory cytokine upregulation was not observed in hamster OKCs until day 3 for IL-1 β (Figure 5(b)), IL-18 (Figure 5(c)), IL-6 (Figure 5(d)), and TNF α (Figure 5(a)) and day 4 for CXCL10 (Figure 5(g)). Moreover, a strong

repression of IL-1 β , IL-18, and IL-6 was observed on days 1 and 2 post-infection. Such a delay in mounting a strong pro-inflammatory response may be explained by the dominance of anti-inflammatory cytokines released early in the course of the infection. Indeed, a previously described role of IL-10 secreted by infected endothelial cells,⁶² the primary targets of SARS-CoV-2 in OKCs (Figure 4(a)), in repressing pro-inflammatory responses has to be considered here. Furthermore, resident monocyte-derived macrophages could potentially be present in high amounts in organotypic cultures and serve as a major source of IL-10 production following interaction with SARS-CoV-2.^{63,64} As the initially infected subcapsular parietal cells die, they may relay the infection to proximal tubular epithelial cells from day 2 to day 3, where the repression of pro-inflammatory cytokines and IFN no longer occurs. Indeed, the late transcriptional upregulation of the pro-inflammatory cytokines IL-1 β , IL-18, and IL-6 observed on day 3 post-infection (Figure 5(b)–(d)) correlated with dissemination of the virus into proximal tubular epithelial cells (Figure 4(c)). Once again, a two-step model of infection could be the result of an initial strong release of a repressor, which could dampen the expression of inflammatory cytokines at early timepoints but also promote the expression of SARS-CoV-2 receptor ACE-2 in bystander cells.⁵² This could favor viral spreading to additional cell populations within the tissue. However, the expression of the four canonical repressive cytokines (IL-4, IL-10, IL-13, IL-22) did not vary significantly at the global culture scale (Supplemental Figure S5). Thus, further investigation via global transcriptomic analysis or single-cell approaches is required to determine what causes the delay in the pro-inflammatory cytokine response and whether specific cells are expressing IL-10 or its equivalent locally, but not in a way detectable at the organ scale. Furthermore, the virus itself could be at the origin of this repression, especially in the kidney, via a mechanism that also remains to be determined.

In parallel to pro-inflammatory cytokines, MX1 and CXCL10, two interferon-stimulated genes,^{65,66} were induced. MX1 was only induced only on day 2 post-infection (Figure 5(h)), which could indicate a potential delay in the IFN response. Indeed, numerous SARS-CoV-2 factors were reported to interfere with innate immunity pathways, including IFN signaling.^{67–72} Interestingly, the peak IFN response mounted by OKCs challenged with SARS-CoV-2 was significantly less pronounced in comparison to that observed in organotypic lung and brainstem cultures,²⁵ potentially supporting an important role of a repressor in viral spread or simply fewer cells capable of IFN production. Whether the relatively attenuated interferon response of the kidney contributes to pathogenesis in COVID-19 patients should be further investigated further.

While MX1 was strongly upregulated on day 2 post-infection (Figure 5(h)), CXCL10 expression did not increase markedly until day 4 (Figure 5(g)), suggesting its independence from the interferon pathway in this specific

context. However, CXCL10 can also be induced directly by IL-6. It has been reported that in the lungs SARS-CoV-2 infection leads to the overexpression of IL-6, which then stimulates CXCL10 production.⁷³ The late induction of CXCL10 may, therefore, reflect the two-step susceptibility of the model, where induction of IL-6 eventually leading to the late overexpression of CXCL10 mRNA only occurs when the infection of proximal tubular cells reaches a certain threshold.

The upregulation of MLKL (Figure 5(e)) associated with cell death via necroptosis occurred concomitantly with the increase of TNF α transcription on day 3 post-infection (Figure 5(a)). TNF α binding to tumor necrosis factor receptors (TNFR) is known to trigger necroptosis.⁷⁴ In addition, necroptosis can be activated via direct sensing of PAMPs by TLRs⁷⁵ and cytosolic nucleic acid sensors.⁷⁶ Day 4 post-infection is also the time where immunofluorescence staining reveals significant virus propagation into proximal tubules (Figure 4(c)). Possibly, proximal tubular epithelia are more susceptible to necroptosis due to elevated levels of TNF α , and its receptors compared to the initial targets of SARS-CoV-2.

Pyroptosis is another form of inflammatory programmed cell death. It is induced by inflammasome sensors responsive to activation by nuclear factor kappa B (NF- κ B) following TLR, TNFR and interleukin-1 receptor (IL-1R) sensing.⁴⁹ Interestingly, while the expression of the pyroptosis mediator gasdermin D mRNA was elevated throughout the 4 days of infection in OKCs, IL-1 β and IL-18 mRNA levels remained repressed for the first 2 days of infection before strongly increasing on day 3 post-infection (Figure 5(b), (c) and (f)). As discussed by Ferren et al.²⁵ such discrepancy may result from the involvement of another cytokine belonging to the IL-1 family. Indeed, a prolonged secretion of IL-33 following infection in OKCs could be triggering pyroptosis within the tissue through the ST2 receptor activity⁷⁷ for the first 2 days. Then, once SARS-CoV-2 spreads to proximal tubules on day 3 post-infection, IL-1 β and IL-18 mRNA levels may increase and contribute to pyroptosis from this point.⁴⁹ Moreover, pyroptosis itself leads to the amplification of inflammation via the cleavage of cytosolic pro-IL-1 β and pro-IL-18 into their active forms and their release from the cell.^{78–80}

To which extent the observations made in hamster OKCs reflect SARS-CoV-2 infection of human kidneys remains to be investigated. However, OKCs offer for the first time a window on the early events of infection at the organ level. Understanding these events is essential for elucidating the pathogenesis of later stage renal dysfunction and of long-term renal sequelae alike, and provides the basis for developing adequate treatments. The poor annotation of hamster genomes and the lack of molecular biology tools adapted to hamsters begin to be inverted, allowing for a better characterization of host-pathogen interactions. The use of OKCs could be extended to studying other human nephrotropic

pathogens such as the Nipah virus, for which golden Syrian hamsters are an established model⁸¹ as well as other emergent viruses including feline morbillivirus (FeMV)^{82,83} and bat nephrotropic viruses.⁸⁴ Other human viruses capable of infecting the kidney include polyomavirus, cytomegalovirus, parvovirus, Epstein-Barr virus, adenovirus. Such infections are especially common in immunocompromised hosts, including renal transplant recipients and HIV-infected patients.^{85,86} OKCs could also be of interest for early drug screening, and this will be investigated in the near future. Therefore, OKCs represents a general platform for studying kidney infections by SARS-CoV-2, that could be extended to other viruses and pathogens with a potential for drug discovery.

Acknowledgements

We acknowledge World Reference Center for Emerging Viruses and Arboviruses (WRCEVA) and UTMB investigator, Dr. Pei Yong Shi for kindly providing recombinant icSARS-CoV-2-mNG virus based on 2019-nCoV/USA_WA1/2020 isolate. We acknowledge the contribution of the AniRA-ImmOs metabolic phenotyping platform of the SFR Biosciences (UMS3444/CNRS, US8/Inserm, ENS de Lyon, UCBL) and we gratefully thank Laurence Canaple for technical assistance. We thank the Plateau Technique d'Imagerie/Microscopie (PLATIM) facility, where confocal microscopy experiments were conducted.

Declaration of conflicting interests

The author(s) declared no potential conflicts of interest with respect to the research, authorship, and/or publication of this article.

Funding

The author(s) disclosed receipt of the following financial support for the research, authorship, and/or publication of this article: The authors disclosed receipt of the following financial support for the research, authorship, and/or publication of this article: this work was supported by ANR-CoronaPepStop (ANR-20-COVI-000) and Fondation de France to BH, ANRS-COV8-SARSRhinCell to CM and CIRI-Intramural grant to LPC and CM.

ORCID iDs

Sophie R Shyfrin  <https://orcid.org/0000-0002-5512-8664>

Marion Ferren  <https://orcid.org/0000-0003-4117-7411>

Xavier Charmetant  <https://orcid.org/0000-0002-2162-5873>

Cyrille Mathieu  <https://orcid.org/0000-0002-6682-2029>

Supplemental material

Supplemental material for this article is available online.

References

- Zhou P, Yang X, Lou, et al. A pneumonia outbreak associated with a new coronavirus of probable bat origin. *Nature* 2020; 579: 270–273.
- Worldometer. Coronavirus cases, <https://www.worldometers.info/coronavirus/> (2022, accessed 11 March 2022).
- Xie J, Wu W, Li S, et al. Clinical characteristics and outcomes of critically ill patients with novel coronavirus infectious disease (COVID-19) in China: a retrospective multicenter study. *Intensive Care Med* 2020; 46: 1863–1872.
- Chan L, Chaudhary K, Saha A, et al. AKI in hospitalized patients with COVID-19. *J Am Soc Nephrol* 2021; 32: 151–160.
- George JA and Khoza S. SARS-CoV-2 infection and the kidneys: an evolving picture. *Adv Exp Med Biol* 2021; 1327: 107–118.
- Hirsch JS, Ng JH, Ross DW, et al. Acute kidney injury in patients hospitalized with COVID-19. *Kidney Int* 2020; 98: 209–218.
- Nadim MK, Forni LG, Mehta RL, et al. COVID-19-associated acute kidney injury: consensus report of the 25th Acute Disease Quality Initiative (ADQI) Workgroup. *Nat Rev Nephrol* 2020; 16: 747–764.
- Nimkar A, Naaraayan A, Hasan A, et al. Incidence and risk factors for acute kidney injury and its effect on mortality in patients hospitalized from COVID-19. *Mayo Clin Proc Innov Qual Outcomes* 2020; 4: 687–695.
- Svetitsky S, Shuaib R, McAdoo S, et al. Long-term effects of Covid-19 on the kidney. *QJM An Int J Med* 2021; 114: 621–622.
- Fisher M, Neugarten J, Bellin E, et al. AKI in hospitalized patients with and without COVID-19: a comparison study. *J Am Soc Nephrol* 2020; 31: 2145–2157.
- Huang C, Huang L, Wang Y, et al. 6-month consequences of COVID-19 in patients discharged from hospital: a cohort study. *Lancet* 2021; 397: 220–232.
- Al-Aly Z, Xie Y and Bowe B. High-dimensional characterization of post-acute sequelae of COVID-19. *Nature* 2021; 594: 259–264.
- Wu L, Wu Y, Xiong H, et al. Persistence of symptoms after discharge of patients hospitalized due to COVID-19. *Front Med* 2021; 8: 761314.
- Copur S, Berkkan M, Basile C, et al. Post-acute COVID-19 syndrome and kidney diseases: what do we know? *J Nephrol* 2022; 35: 795–805.
- Khan S, Chen L, Yang CR, et al. Does SARS-cov-2 infect the kidney? *J Am Soc Nephrol* 2020; 31: 2746–2748.
- Braun F, Lütgehetmann M, Pfeffeler S, et al. SARS-CoV-2 renal tropism associates with acute kidney injury. *Lancet* 2020; 396: 597–598.
- Brienza N, Puntillo F, Romagnoli S, et al. Acute kidney injury in Coronavirus disease 2019 infected patients: a meta-analytic study. *Blood Purif* 2021; 50(1): 35–41.
- Diao B, Wang C, Wang R, et al. Human kidney is a target for novel severe acute respiratory syndrome coronavirus 2 infection. *Nat Commun* 2021; 12: 2506.
- Puelles VG, Lütgehetmann M, Lindenmeyer MT, et al. Multiorgan and renal tropism of SARS-CoV-2. *N Engl J Med* 2020; 383: 590–592.
- Su H, Yang M, Wan C, et al. Renal histopathological analysis of 26 postmortem findings of patients with COVID-19 in China. *Kidney Int* 2020; 98: 219–227.
- Hanley B, Naresh KN, Roufosse C, et al. Histopathological findings and viral tropism in UK patients with severe fatal

- COVID-19: a post-mortem study. *Lancet Microbe* 2020; 1: e245–e253.
22. Liu J, Li Y, Liu Q, et al. SARS-CoV-2 cell tropism and multiorgan infection. *Cell Discov* 2021; 7: 17.
 23. Alpers CE and Kowalewska J. Emerging Paradigms in the renal pathology of viral diseases. *Clin J Am Soc Nephrol* 2007; 2: S6–S12.
 24. Prasad N and Patel MR. Infection-induced kidney diseases. *Front Med* 2018; 5: 327.
 25. Ferren M, Favède V, Decimo D, et al. Hamster organotypic modeling of SARS-CoV-2 lung and brainstem infection. *Nat Commun* 2021; 12(1): 5809.
 26. Welsch JC, Charvet B, Dussurgey S, et al. Type I interferon receptor signaling drives selective permissiveness of astrocytes and microglia to measles virus during brain infection. *J Virol* 2019; 93: e00618-19.
 27. Bloyet L-M, Welsch J, Enchery F, et al. HSP90 chaperoning in addition to phosphoprotein required for folding but not for supporting enzymatic activities of measles and Nipah virus L polymerases. *J Virol* 2016; 90: 6642–6656.
 28. Poosti F, Pham BT, Oosterhuis D, et al. Precision-cut kidney slices (PCKS) to study development of renal fibrosis and efficacy of drug targeting ex vivo. *Dis Model Mech* 2015; 8: 1227–1236.
 29. Genovese F, Kárpáti ZS, Nielsen SH, et al. Precision-Cut kidney slices as a tool to understand the dynamics of extracellular matrix remodeling in renal fibrosis. *Biomark Insights* 2016; 11: 77–84.
 30. Zhang S, Liu Q, Xiao J, et al. Molecular validation of the precision-cut kidney slice (PCKS) model of renal fibrosis through assessment of TGF- β 1-induced Smad and p38/ERK signaling. *Int Immunopharmacol* 2016; 34: 32–36.
 31. Bigaeva E, Puerta Cavanzo N, Stribos EGD, et al. Predictive value of Precision-Cut kidney slices as an ex vivo screening platform for therapeutics in human renal fibrosis. *Pharmaceutics* 2020; 12: 459.
 32. Chan JFW, Zhang AJ, Yuan S, et al. Simulation of the clinical and pathological manifestations of Coronavirus disease 2019 (COVID-19) in a Golden Syrian hamster model: implications for disease pathogenesis and transmissibility. *Clin Infect Dis* 2020; 71: 2428–2446.
 33. Welsch J, Lionnet C, Terzian C, et al. Organotypic brain cultures: a framework for studying CNS infection by neurotropic viruses and screening antiviral drugs. *Bio Protoc* 2017; 7: e2605.
 34. Xie X, Muruato A, Lokugamage KG, et al. An infectious cDNA clone of SARS-CoV-2. *Cell Host Microbe* 2020; 27: 841–848.e3.
 35. Underwood E, Redell JB, Zhao J, et al. A method for assessing tissue respiration in anatomically defined brain regions. *Sci Rep* 2020; 10: 13179.
 36. Pfaffl MW. A new mathematical model for relative quantification in real-time RT-PCR. *Nucleic Acids Res* 2001; 29: e45.
 37. Mathieu C, Pohl C, Szecsi J, et al. Nipah virus uses leukocytes for efficient dissemination within a host. *J Virol* 2011; 85: 7863–7871.
 38. Preibisch S, Saalfeld S and Tomancak P. Globally optimal stitching of tiled 3D microscopic image acquisitions. *Bioinformatics* 2009; 25: 1463–1465.
 39. Schneider CA, Rasband WS and Eliceiri KW. NIH image to ImageJ: 25 years of image analysis. *Nat Methods* 2012; 9: 671–675.
 40. GraphPad. GraphPad Software, www.graphpad.com (2021).
 41. Kurts C, Panzer U, Anders HJ, et al. The immune system and kidney disease: Basic concepts and clinical implications. *Nat Rev Immunol* 2013; 13: 738–753.
 42. Hoffmann M, Kleine-Weber H, Schroeder S, et al. SARS-CoV-2 cell entry depends on ACE2 and TMPRSS2 and is blocked by a clinically proven protease inhibitor. *Cell* 2020; 181: 271–280.e8.
 43. Ou X, Liu Y, Lei X, et al. Characterization of spike glycoprotein of SARS-CoV-2 on virus entry and its immune cross-reactivity with SARS-CoV. *Nat Commun* 2020; 11: 1620.
 44. Uhlén M, Fagerberg L, Hallström BM, et al. Tissue-based map of the human proteome. *Science* 2015; 347: 1260419.
 45. Gkogkou E, Barnasas G, Vougas K, et al. Expression profiling meta-analysis of ACE2 and TMPRSS2, the putative anti-inflammatory receptor and priming protease of SARS-CoV-2 in human cells, and identification of putative modulators. *Redox Biol* 2020; 36: 101615.
 46. Paul M, Poyan Mehr A and Kreutz R. Physiology of local renin-angiotensin systems. *Physiol Rev* 2006; 86: 747–803.
 47. Bertheloot D, Latz E and Franklin BS. Necroptosis, pyroptosis and apoptosis: an intricate game of cell death. *Cell Mol Immunol* 2021; 18: 1106–1121.
 48. Christofferson DE and Yuan J. Necroptosis as an alternative form of programmed cell death. *Curr Opin Cell Biol* 2010; 22: 263–268.
 49. Bergsbaken T, Fink SL and Cookson BT. Pyroptosis: host cell death and inflammation. *Nat Rev Microbiol* 2009; 7: 99–109.
 50. Busnadiego I, Fernbach S, Pohl MO, et al. Antiviral activity of type i, ii, and iii interferons counterbalances ace2 inducibility and restricts sars-cov-2. *mBio* 2020; 11: 1–10.
 51. Ziegler CGK, Allon SJ, Nyquist SK, et al. SARS-CoV-2 receptor ACE2 is an interferon-stimulated gene in human airway epithelial cells and is detected in specific cell subsets across tissues. *Cell* 2020; 181: 1016–1035.e19.
 52. Albin A, Calabrone L, Carlini V, et al. Preliminary evidence for IL-10-Induced ACE2 mRNA expression in lung-derived and endothelial cells: implications for SARS-Cov-2 ARDS pathogenesis. *Front Immunol* 2021; 12: 718136.
 53. Farkash EA, Wilson AM and Jentzen JM. Ultrastructural evidence for direct renal infection with SARS-CoV-2. *J Am Soc Nephrol* 2020; 31: 1683–1687.
 54. Gaillard F, Ismael S, Sannier A, et al. Tubuloreticular inclusions in COVID-19-related collapsing glomerulopathy. *Kidney Int* 2020; 98: 241.
 55. Peleg Y, Kudose S, D’Agati V, et al. Acute kidney injury due to collapsing glomerulopathy following COVID-19 infection. *Kidney Int Rep* 2020; 5: 940–945.
 56. Santoriello D, Khairallah P, Bombardieri AS, et al. Postmortem kidney pathology findings in patients with COVID-19. *J Am Soc Nephrol* 2020; 31: 2158–2167.

57. Wang Y, Wang Y, Chen Y, et al. Unique epidemiological and clinical features of the emerging 2019 novel coronavirus pneumonia (COVID-19) implicate special control measures. *J Med Virol* 2020; 92: 568–576.
58. Monteil V, Kwon H, Prado P, et al. Inhibition of SARS-CoV-2 infections in engineered human tissues using clinical-grade soluble human ACE2. *Cell* 2020; 181: 905–913.e7.
59. Mathieu C, Bovier FT, Ferren M, et al. Molecular features of the measles virus viral fusion complex that favor infection and spread in the brain. *mBio* 2021; 12(3): e0079921.
60. Varga Z, Flammer AJ, Steiger P, et al. Endothelial cell infection and endotheliitis in COVID-19. *Lancet* 2020; 395: 1417–1418.
61. Bouquegneau A, Erpicum P, Grosch S, et al. COVID-19-associated nephropathy includes tubular necrosis and capillary congestion, with evidence of SARS-CoV-2 in the nephron. *Kidney360* 2021; 2: 639–652.
62. Azizan A, Sweat J, Espino C, et al. Differential proinflammatory and angiogenesis-specific cytokine production in human pulmonary endothelial cells, HPMEC-ST1.6R infected with dengue-2 and dengue-3 virus. *J Virol Methods* 2006; 138: 211–217.
63. Daviaud N, Garbayo E, Schiller PC, et al. Organotypic cultures as tools for optimizing central nervous system cell therapies. *Exp Neurol* 2013; 248: 429–440.
64. Islam H, Chamberlain TC, Mui AL, et al. Elevated interleukin-10 levels in COVID-19: potentiation of pro-inflammatory responses or impaired anti-inflammatory action? *Front Immunol* 2021; 12: 677008.
65. Haller O, Staeheli P and Kochs G. Interferon-induced Mx proteins in antiviral host defense. *Biochimie* 2007; 89: 812–818.
66. Majumder S, Zhou LZ, Chaturvedi P, et al. P48/STAT1alpha-containing complexes play a predominant role in induction of IFN-gamma-inducible protein, 10 kDa (IP-10) by IFN-gamma alone or in synergy with TNF-alpha. *J Immunol* 1998; 161: 4736–4744.
67. Perrin-Cocon L, Diaz O, Jacquemin C, et al. The current landscape of coronavirus-host protein-protein interactions. *J Transl Med* 2020; 18: 319.
68. Sa Ribero M, Jouvenet N, Dreux M, et al. Interplay between SARS-CoV-2 and the type I interferon response. *PLoS Pathog* 2020; 16: e1008737.
69. Pawlica P, Yario TA, White S, et al. SARS-CoV-2 expresses a microRNA-like small RNA able to selectively repress host genes. *Proc Natl Acad Sci U S A* 2021; 118: e2116668118.
70. Wu J, Shi Y, Pan X, et al. SARS-cov-2 ORF9b inhibits RIG-I-MAVS antiviral signaling by interrupting k63-linked ubiquitination of NEMO. *Cell Rep* 2021; 34: 108761.
71. Chen K, Xiao F, Hu D, et al. SARS-CoV-2 nucleocapsid protein interacts with RIG-I and represses RIG-Mediated IFN- β production. *Viruses* 2020; 13: E47.
72. Mu J, Fang Y, Yang Q, et al. SARS-CoV-2 N protein antagonizes type I interferon signaling by suppressing phosphorylation and nuclear translocation of STAT1 and STAT2. *Cell Discov* 2020; 6: 65.
73. Coperchini F, Chiovato L and Rotondi M. Interleukin-6, CXCL10 and infiltrating macrophages in COVID-19-related cytokine storm: not one for all but all for one! *Front Immunol* 2021; 12: 668507.
74. Holler N, Zaru R, Micheau O, et al. Fas triggers an alternative, caspase-8-independent cell death pathway using the kinase RIP as effector molecule. *Nat Immunol* 2000; 1: 489–495.
75. He S, Liang Y, Shao F, et al. Toll-like receptors activate programmed necrosis in macrophages through a receptor-interacting kinase-3-mediated pathway. *Proc Natl Acad Sci U S A* 2011; 108: 20054–20059.
76. Schock SN, Chandra NV, Sun Y, et al. Induction of necroptotic cell death by viral activation of the RIG-I or STING pathway. *Cell Death Differ* 2017; 24: 615–625.
77. Cohen ES, Scott IC, Majithiya JB, et al. Oxidation of the alarmin IL-33 regulates ST2-dependent inflammation. *Nat Commun* 2015; 6: 1–10.
78. Baroja-Mazo A, Martín-Sánchez F, Gomez AI, et al. The NLRP3 inflammasome is released as a particulate danger signal that amplifies the inflammatory response. *Nat Immunol* 2014; 15: 738–748.
79. Kanneganti TD, Body-Malapel M, Amer A, et al. Critical role for cryopyrin/nalp3 in activation of caspase-1 in response to viral infection and double-stranded RNA. *J Biol Chem* 2006; 281: 36560–36568.
80. Wang K, Sun Q, Zhong X, et al. Structural Mechanism for GSDMD targeting by autoprocessed caspases in pyroptosis. *Cell* 2020; 180: 941–955.e20.
81. Wong KT, Grosjean I, Brisson C, et al. A golden hamster model for Human Acute Nipah virus infection. *Am J Pathol* 2003; 163: 2127–2137.
82. Choi EJ, Ortega V and Aguilar HC. Feline Morbillivirus, a new paramyxovirus possibly associated with feline kidney disease. *Viruses* 2020; 12: E501.
83. De Luca E, Sautto GA, Crisi PE, et al. Feline Morbillivirus infection in domestic cats: what have we learned so far? *Viruses* 2021; 13: 683.
84. de Souza WM, Fumagalli MJ, Carrera JP, et al. Paramyxoviruses from neotropical bats suggest a novel genus and nephrotropism. *Infect Genet Evol* 2021; 95: 105041.
85. Mikulak J and Singhal PC. HIV-1 and kidney cells: better understanding of viral interaction. *Nephron Exp Nephrol* 2010; 115: e15–e21.
86. Singh HK and Nickleleit V. Kidney disease caused by viral infections. *Curr Diagn Pathol* 2004; 10: 11–21.